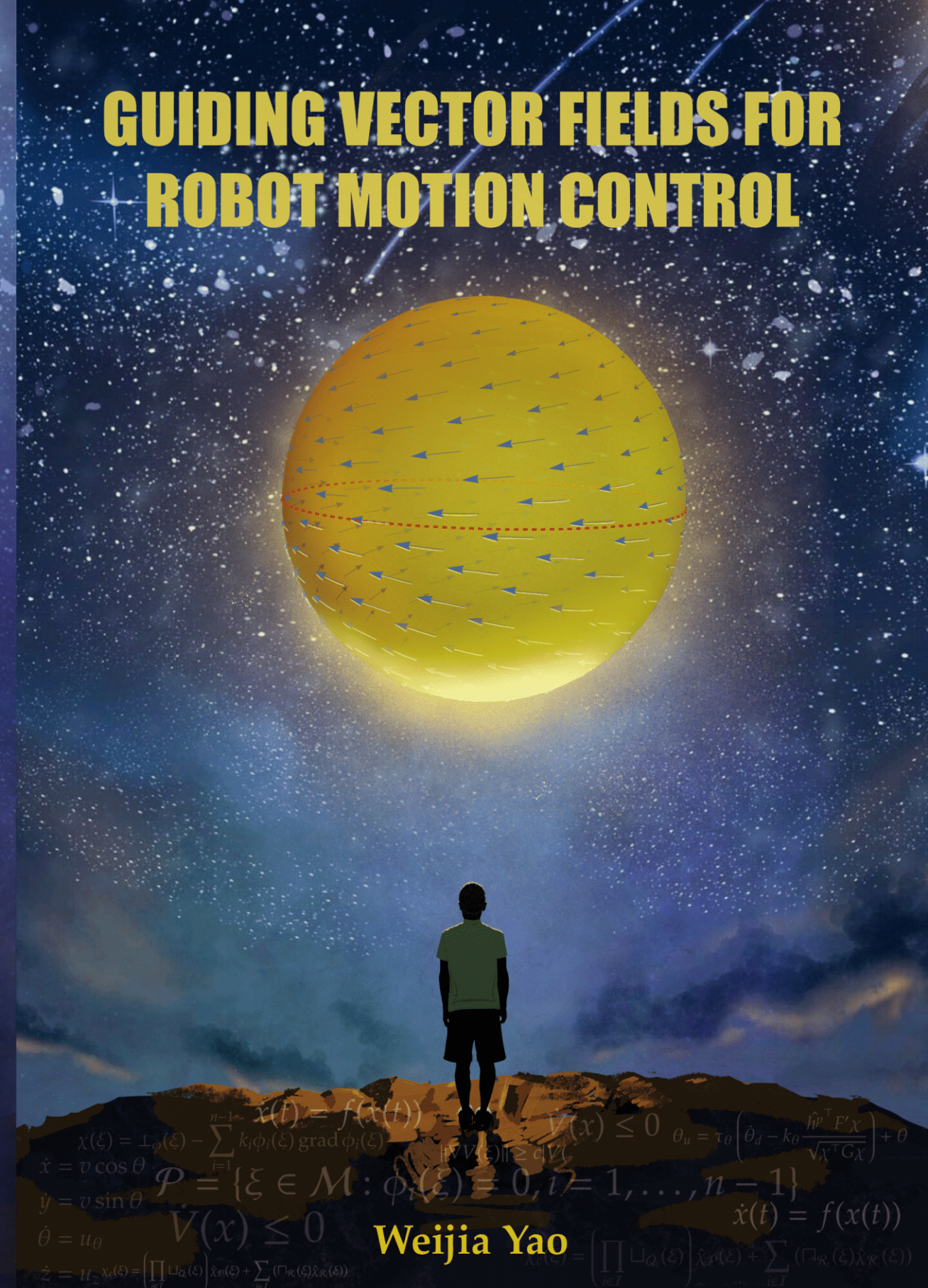




Guiding Vector Fields for Robot Motion Control Weijia Yao



Guiding Vector Fields for Robot Motion Control

Weijia Yao
姚伟嘉



university of
groningen

The research described in this dissertation has been carried out at the Faculty of Science and Engineering, University of Groningen, the Netherlands.

disc

The research reported in this dissertation is part of the research program of the Dutch Institute of Systems and Control (DISC). The author has successfully completed the education program of the Graduate School DISC.

Cover design by Qian Wang

The thesis style is based on André Miede and Ivo Pletikosić's Classisc Thesis.



/ university of
groningen

Guiding Vector Fields for Robot Motion Control

PhD thesis

to obtain the degree of PhD at the
University of Groningen
on the authority of the
Rector Magnificus Prof. C. Wijmenga
and in accordance with the decision by the College of Deans.

This thesis will be defended in public on

Friday 8 October 2021 at 12.45 hours

by

Weijia Yao

born on 14 November, 1992
in Guangdong, China

Supervisors

Prof. M. Cao

Prof. J.M.A. Scherpen

Assessment committee

Prof. A.J. van der Schaft

Prof. K.Y. Pettersen

Prof. M.B. Egerstedt

To my family

献给我的家人

ACKNOWLEDGMENTS

As I am writing the acknowledgments, I cannot help reflecting on the four years of my PhD journey. Perhaps one of the most unexpected events is the COVID-19 pandemic, and no one would predict that we have been socially distancing with each other for more than a year since the lock-down of the Netherlands in March, 2020. We also experienced the first nationwide curfew since World War II for more than three months. Nevertheless, I managed to keep advancing on the PhD journey, and I am finally reaching the destination! This would not have been possible without the help from many people, to whom I would like to pay my special regards.

First of all, I would like to express my eternal gratitude to my primary supervisor Prof. Ming Cao. Thank you for offering me the opportunity to pursue my PhD degree at the prestigious University of Groningen, and for helping me grow to be an independent researcher. In particular, I always enjoy being an audience of your group meetings, where everyone is encouraged to ask the speaker any kind of questions. On the other hand, it is never easy to be a speaker at the group meetings! When I gave a presentation at one of the meetings for the first time, I received perhaps more than sixty questions, and my presentation lasted for literally two hours! Thank you also for your valuable academic and life advice, as well as honest and helpful criticism. I have learned to clearly see both my strengths and weaknesses. In addition, I am particularly grateful for your detailed guidance when we were preparing the presentation to compete for the ICRA best conference paper award in 2021, and I could not appreciate it more when I saw you present during my (online) talk at 2:30 AM! (By the way, that is my first and last time sleeping in my office in Groningen.)

I would also like to express my heartfelt appreciation to my secondary supervisor Prof. Jacquelin M.A. Scherpen for her generous support and encouragement. Thank you for suggesting courses for my personal development, and for helping me out when I was in need. I appreciate the Dutch specialty “nieuwjaarsrolletjes” with cream you bring to the group at the beginning of every year (except 2021 due to COVID-19), and the annual (physical and virtual) group outings that you and many others organized.

My profound gratitude also goes to my collaborators, including Bohuan Lin, Prof. Brian D. O. Anderson, Dr. Yuri A. Kapitanyuk, Dr. Hector G. de Marina, Dr. Zhiyong Sun, LuLu Gong, and Binbin Hu. In particular, I owe my deepest gratitude to Bohuan Lin, who is not only my closest collaborator, but also my good friend, my mathematics mentor and my paranymphe. Bohuan, thank you so much for spending a huge amount of time discussing the research conducted

in this thesis with me, and for sharing the happiness and bitterness of pursuing a PhD. Additionally, I am constantly inspired by your thought-provoking ideas regarding academia, mathematics and also life. I would also like to show my gratitude to Brian. Brian, you are always a role model for me. I admire your persistent passion for research, your work ethic and your encyclopedic knowledge. It is a great pleasure working with you and I have benefited enormously from the technical and non-technical discussions, and the meticulous comments on my manuscripts. I would like to recognize the invaluable assistance that Yuri provided during my first year. Thank you, Yuri, for leading me to this research topic and working with me on my first academic paper. Hector, thank you for the technical discussions and for conducting fixed-wing aircraft experiments. I also enjoy many late-night Google chats with you on different aspects of academia. Zhiyong, thank you for spending time on our technical discussions and for giving me tips on academic writing. Thank you, Lulu, for inviting me to the wonderful world of evolutionary game theory, and Binbin, for extending the guiding vector field to the ordering-free case.

My special thanks go to the reading committee: Prof. Arjan J. van der Schaft, Prof. Kristin Y. Pettersen and Prof. Magnus B. Egerstedt. I greatly appreciate your spending precious time reading my thesis and providing valuable comments, especially during the summer break. I also received generous support from Sha Luo, Bohuan Lin, Marco A. Vasquez Beltran, Rafael F. Cunha and Zhiyuan Liu for proofreading chapters of my thesis. The advice and comments from you helped me improve the thesis significantly. I am particularly grateful to Dr. Nelson Chan for translating the English summary to Dutch and Matthijs C. de Jong for proofreading it.

I thank all my colleagues from the ENTEG institute and the Bernoulli Institute. Specifically, I am deeply grateful to Marco A. Vasquez Beltran for agreeing to be my paronymph, and for the joyful and fruitful discussions on DISC homework. On top of that, Marco, thank you for letting me distract you whenever you were concentrating on your research. I am thankful to my office-mates, Carlo Cenedese, Lulu Gong, Fangzhou Liu, Lanlin Yu, Anja Schmerbauch, Amirreza Silani, Tinghua Li, Rafael F. Cunha, Miao Guo, Ningbo Li and Agung Prawira Negara, for accompanying me and discussing interesting topics. Moreover, I cannot forget the days I spent with Carlo and Yuri on preparing a robotics demonstration for the royal family on King's day in 2018. Neither can I forget the time we worked together as a TA team for the robotics course. In addition, I would like to express my gratitude to our thoughtful, courteous secretary Frederika G. Fokkens, and our kind and helpful technicians Simon Busman and Martin Stokroos for everything that they helped me.

During the preparation of my ICRA talk for the best paper award, I have received valuable feedback from many people in addition to my collaborators of the ICRA paper. These people include Prof. Paolo Robuffo Giordano, Prof. Guido de Croon, Prof. Vinícius M. Gonçalves, Prof. Kristin Y. Pettersen, Dr. Chen Wang,

Dr. Mengbin Ye, Dr. Fabrizio Schiano, Dr. Qingkai Yang, Dr. Lorenzo Zino, Sha Luo, Rafael F. Cunha, Kathinka Frieswjik, Zhiyuan Liu and Emin Martirosyan. I greatly appreciate your help in improving the quality of my talk.

Finally, I want to thank my friends and family. My PhD life would not have been so special without the company of my friends in Groningen, especially those once stayed in the SSH student apartment on Plutolaan. Special thanks go to Qian Wang for designing the amazing cover of this thesis. I would also like to address some words to my beloved girlfriend Sha Luo. You are being supportive, thoughtful and understanding, especially when I was diving into the boundless ocean of scientific exploration. I always enjoy every second with you, and I appreciate your company these years!

Last but not least, I owe my beloved family members a deep debt of gratitude for their selfless and endless love and support!

Weijia Yao
Groningen, the Netherlands
30 August, 2021

CONTENTS

1	INTRODUCTION	1
1.1	Background	1
1.1.1	Path-following navigation	1
1.1.2	An example of a 2D guiding vector field	3
1.1.3	Vector-field guided path-following (VF-PF) navigation problem on general spaces	4
1.1.4	Review of guiding vector fields in the literature	5
1.1.5	Guiding vector fields studied in this thesis	7
1.1.6	Comparison with potential energy shaping for path planning	7
1.2	Research challenges and contributions	8
1.3	Thesis outline	10
1.4	List of publications	13
1.5	General notations	15
2	PRELIMINARIES	17
2.1	Nonlinear systems and control	17
2.1.1	Existence and uniqueness of system trajectories	17
2.1.2	Lyapunov stability	18
2.1.3	LaSalle's invariance principle, Barbalat's lemma and an invariance-like theorem	19
2.1.4	Local input-to-state stability (ISS)	20
2.1.5	Nagumo's theorem	20
2.1.6	Poicaré-Bendixson theorem	21
2.1.7	Index theorem	22
2.2	Point-set topology	22
2.3	Topological and differential manifolds	23
I	THEORETICAL FOUNDATION	
3	VANISHING LEVEL VALUE AND CONVERGENCE TO ZERO-LEVEL SET	27
3.1	Introduction	28
3.2	Background and problem formulation	29
3.3	Main results	30
3.3.1	Preliminaries	30
3.3.2	Metrical convergence and topological convergence	30
3.3.3	Convergence characterized by different level functions	36
3.4	Conclusions	37
4	PATH FOLLOWING CONTROL IN 3D USING A VECTOR FIELD	39
4.1	Introduction	40
4.2	Problem formulation	41

4.2.1	The guiding vector field and assumptions	41
4.3	Analysis of the vector field	44
4.3.1	Bounded desired path	44
4.3.2	Unbounded desired path	47
4.4	Normalization and perturbation of the vector field	52
4.5	Control algorithm for a fixed-wing aircraft	55
4.6	Simulations	60
4.7	Conclusions	63
5	TOPOLOGICAL ANALYSIS OF VECTOR-FIELD GUIDED PATH FOLLOWING ON MANIFOLDS	65
5.1	Introduction	66
5.1.1	Contributions	67
5.1.2	Chapter structure	68
5.2	Guiding vector field for path following	69
5.2.1	Guiding vector fields on Riemannian manifolds	69
5.2.2	Standing assumptions	72
5.3	Computation of guiding vector fields on manifolds	73
5.4	Dichotomy convergence and stability analysis	78
5.5	Singular points and non-path-converging trajectories	85
5.5.1	Existence of singular points	85
5.5.2	The existence of non-path-converging trajectories	89
5.6	Numerical simulations	93
5.7	Conclusions	98
6	THE DOMAIN OF ATTRACTION OF THE DESIRED PATH IN VECTOR-FIELD GUIDED PATH FOLLOWING	99
6.1	Introduction	100
6.2	Problem formulation	100
6.2.1	VF-PF on Riemannian manifolds	101
6.2.2	Assumptions and problem statement	101
6.3	Further characterization of the DOA	103
6.3.1	A property near a compact regular level set	103
6.3.2	DOA of the desired path	104
6.4	Conclusions	114
7	REFINED DICHOTOMY CONVERGENCE IN VECTOR-FIELD GUIDED PATH-FOLLOWING ON \mathbb{R}^n	117
7.1	Introduction	118
7.2	Background and problem formulation	119
7.2.1	Guiding vector fields on \mathbb{R}^n	119
7.2.2	Assumptions	120
7.3	Refined dichotomy convergence	120
7.4	Simulations	125
7.5	Conclusions	126

II APPLICATIONS WITH FORMAL GUARANTEES

8	GUIDING VECTOR FIELDS FOR FOLLOWING OCCLUDED PATHS	129
8.1	Introduction	130
8.1.1	Contributions	131
8.1.2	Chapter structure	133
8.2	Problem formulation	134
8.2.1	Preliminaries	134
8.2.2	Desired paths	134
8.2.3	Obstacles, reactive areas and repulsive areas	134
8.2.4	Problem formulation	136
8.3	Composite vector field	137
8.3.1	Path-following vector field and reactive vector field	137
8.3.2	Behavior with a single vector field	138
8.3.3	Smooth zero-in and zero-out functions	140
8.3.4	Composite vector field	141
8.4	Analysis of the composite vector field	143
8.5	Switching vector field	151
8.6	Discussions	156
8.6.1	Moving obstacles	156
8.6.2	Higher-dimensional spaces	158
8.6.3	Complicated robot models	159
8.7	Simulations	160
8.7.1	Smooth zero-in and zero-out functions	160
8.7.2	2D composite vector field	160
8.7.3	Switching vector field to overcome the deadlock	161
8.7.4	Moving obstacles and 2D Dubins car model	162
8.7.5	3D composite vector field and 3D Dubins car model	163
8.8	Conclusions	164
9	A SINGULARITY-FREE GUIDING VECTOR FIELD FOR ROBOT NAVIGATION	167
9.1	Introduction	168
9.1.1	Contributions	170
9.2	Guiding vector fields for path following	172
9.2.1	Guiding vector fields on \mathbb{R}^n	172
9.2.2	Assumptions	174
9.3	Issues on the global convergence to desired paths	175
9.4	Extended dynamics and convergence results	177
9.5	High-dimensional singularity-free guiding vector fields	180
9.5.1	Construction of a singularity-free guiding vector field	182
9.5.2	Features of the approach	184
9.6	Experiments with an autonomous aircraft	185
9.6.1	The autonomous aircraft and airfield	185
9.6.2	Aircraft's guidance system design	186

9.6.3	Accommodating the guidance to the aircraft's dynamics	189
9.6.4	The 2D trefoil curve	190
9.6.5	The 3D Lissajous curve	194
9.7	Discussion: Path following or trajectory tracking?	194
9.8	An alternative proof	197
9.9	Conclusions	200
10	GUIDING VECTOR FIELDS FOR MULTI-ROBOT COORDINATED NAVIGATION	201
10.1	Introduction	202
10.1.1	Related work	202
10.1.2	Contributions	203
10.2	Preliminaries	204
10.2.1	Notations	204
10.2.2	Graph theory	205
10.2.3	Guiding vector field with a virtual coordinate for a single robot	205
10.3	Distributed motion coordination on desired paths	206
10.3.1	Mathematical problem formulation	207
10.3.2	Time-invariant and time-varying coordination components and convergence analysis	210
10.4	Distributed coordinated maneuvering on surfaces	217
10.4.1	Coordinated motion in a desired set	218
10.4.2	Mathematical problem formulation	219
10.4.3	Time-invariant coordination component	223
10.5	Extending the vector field to incorporate collision avoidance	229
10.6	Saturated controller for a Dubins-car-like model	232
10.7	Simulations and experiments	237
10.7.1	Simulations	237
10.7.2	Experiments with multiple fixed-wing aircraft	240
10.8	Conclusions	240
11	CONCLUSIONS AND FUTURE RESEARCH	247
11.1	Conclusions	247
11.2	Future research	249
III APPENDIX		
A	CONTROL ALGORITHMS FOR A 3D UAV MODEL AND A DYNAMICS MODEL	255
A.1	3D UAV model	255
A.2	A control algorithm design example for a dynamics model	257
BIBLIOGRAPHY		261
SUMMARY		275
SAMENVATTING		279

LIST OF FIGURES

Figure 1.1	Robot navigation tasks	2
Figure 1.2	The common control structure.	2
Figure 1.3	Thesis structure and relationships among chapters	11
Figure 3.1	Metrical and topological convergence	31
Figure 3.2	Vanishing level value does not imply convergence to the zero-level set.	35
Figure 4.1	The illustration of the proof of Proposition 4.14.	50
Figure 4.2	A fixed-wing aircraft follows a 3D bounded desired path .	61
Figure 4.3	The path-following errors for the first simulation	61
Figure 4.4	A fixed-wing aircraft follows a 3D unbounded desired path	62
Figure 4.5	The path-following errors for the second simulation	62
Figure 5.1	Different convergence results corresponding to the same desired path with different level functions $\phi_i, i = 1, 2$	74
Figure 5.2	The guiding vector field χ on the sphere $\mathcal{M} = S^2$	77
Figure 5.3	A non-real-analytic vector field	84
Figure 5.4	Relationships of continuous maps in Theorem 5.30	92
Figure 5.5	Streamlines of the first example	93
Figure 5.6	The second and third simulation examples	94
Figure 5.7	The fourth simulation example	96
Figure 5.8	The motions of the coordinate frames	97
Figure 6.1	The illustration of Proposition 6.5	104
Figure 6.2	The illustration of Corollary 6.7	105
Figure 6.3	Illustration of \mathcal{W} , \mathcal{W}° and \mathcal{W}^- in \mathcal{M}	106
Figure 6.4	A schematic diagram for the continuity of the function Λ in the proof of Proposition 6.14	112
Figure 6.5	A schematic diagram for the continuity of the function Λ' in the proof of Proposition 6.14	113
Figure 7.1	Simulation example 1: a real analytic level function	125
Figure 7.2	Simulation example 2: a non-real-analytic level function .	126
Figure 8.1	Concepts for collision avoidance	135
Figure 8.2	Smooth zero-in and zero-out bump functions	141
Figure 8.3	Construction of the composite vector field	144
Figure 8.4	The common limitation is removed	148
Figure 8.5	Notations for the switching vector field	152
Figure 8.6	The discrete transitions of the switching signal σ	154
Figure 8.7	Simulation I	161
Figure 8.8	Simulation II	162

Figure 8.9	Simulation III	163
Figure 8.10	Simulation IV	165
Figure 9.1	Two <i>normalized</i> vector fields	169
Figure 9.2	Opterra 1.2m	186
Figure 9.3	Flight results I	191
Figure 9.4	The ground control station of Flight I	192
Figure 9.5	Flight results II	193
Figure 9.6	The ground control station of Flight II	194
Figure 9.7	Layers of a 3D vector field	197
Figure 9.8	The projected 2D vector field	198
Figure 10.1	Simulation results of two robots coordinating their motions on a sphere	220
Figure 10.2	The signed angle $\sigma^{[i]}$	234
Figure 10.3	The first simulation results of robots following a 3D bent “ ∞ ”-shaped curve.	238
Figure 10.4	The second simulation results of robots covering a cube	242
Figure 10.5	The third simulation results of robots following different desired paths	243
Figure 10.6	The fourth simulation results of robots maneuvering on a torus	244
Figure 10.7	Two aircraft follow a 3D bent “ ∞ ”-shaped path	245
Figure 10.8	Path-following errors and coordinating errors of the experiment with two aircraft	245
Figure A.1	Simulation results of a controller for a 3D UAV model	257

ACRONYMS

VF-PF	Vector-Field Guided Path-Following
VF-CAPF	Vector-Field Guided Path-Following with Collision-Avoidance
UAV	Unmanned Aerial Vehicle
LOS	Line-of-sight
NLGL	Nonlinear Guidance Law
LQR	Linear Quadratic Regulator
ISS	Input-to-state Stable/Stability
GAS	Globally Asymptotically Stable / Global Asymptotic Stability
DOA	Domain of Attraction

1

INTRODUCTION

In this chapter, we first present the background of the thesis on the path-following (navigation) problem. Then we detail the research challenges this thesis deals with and our contributions addressing these challenges. Finally, the thesis outline is illustrated.

1.1 BACKGROUND

1.1.1 Path-following navigation

Several robot navigation tasks, such as highway traffic monitoring, underwater pipeline inspection and border patrolling (see Fig. 1.1), require the fundamental functionality of mobile robots to *follow a desired path* [130], and new applications are emerging, such as using drones to probe atmospheric phenomena along prescribed paths [71]. The *path-following* (navigation) problem is a classic problem, and has attracted the attention from both the robotics community [32], [50], [81], [89], [119] and the control community [15], [21], [64], [72], [90], [156]. In a path-following algorithm, the desired path is usually given in the form of a single connected curve *without temporal information*, and then robots are guided to converge to and move along it with sufficient accuracy. In [5], it is shown that, treating the desired path as a *geometric object* rather than a time-dependent point, path-following algorithms sometimes are able to overcome a number of performance limitations rooted in trajectory tracking, such as inaccuracy due to unstable zero dynamics [126] and difficulty to maintain constant tracking speed [63]. In fact, it is claimed in [5] that path-following algorithms enable robots to accurately follow a path with a constant speed or fixed orientation. Moreover, comparing with trajectory tracking algorithms, there is separate interest for the study of path-following algorithms since they are more suitable for some applications, such as fixed-wing aircraft guidance and control [74], [119], [137].

To our knowledge, most of path-following algorithms work on the kinematics level of a robot model; namely, path-following algorithms usually give guidance signals such as desired linear velocities v_d or desired angular velocities ω_d to guide a robot such that a desired path can be followed eventually. This high-level of kinematics control enables a specific path-following control algorithm to be applicable to a wide range of robots which can be described by the same kinematics model but might correspond to drastically different dynamics models.

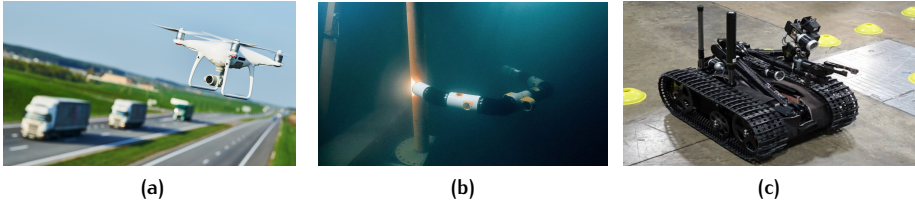


Figure 1.1: (a) UAV highway traffic monitoring [105]. (b) Snake robots underwater pipeline inspection [1]. (c) A robot employed for border patrolling [2].

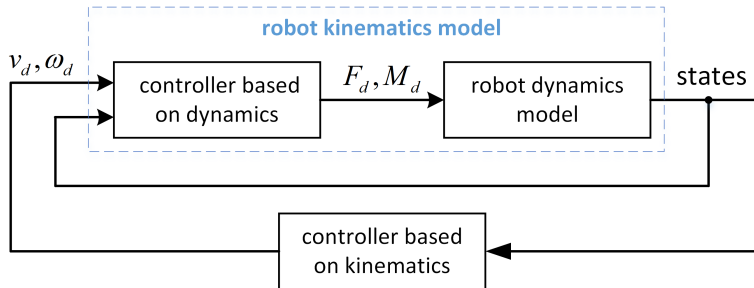


Figure 1.2: The common control structure.

Depending on these different dynamics models, the low-level dynamics control involving, e.g., computing the corresponding forces F_d or moments M_d , is usually accomplished by open-source or commercially available controllers (e.g., autopilots for UAVs), possibly using classic control methods such as PID control or model predictive control. To be more specific, in practice, a widely used control structure of robots are shown in Fig. 1.2, which can be roughly divided into an inner loop and an outer loop. In the inner loop, the robot dynamics model is considered and a dynamics controller takes the desired linear velocities v_d , the desired angular velocities ω_d and the robot states as inputs and computes the corresponding forces F_d or moments M_d using the dynamics model. If this inner loop control is fast and accurate, then the two components enclosed by the dashed rectangle in the figure can be seen as a robot kinematics model. Therefore, in the outer loop, a kinematics controller takes the robot states as input and computes the desired linear velocities v_d and the desired angular velocities ω_d . Many path-following algorithms, including those that are studied in this thesis, act as the kinematics controller.

There are many existing path-following algorithms, many of which have been surveyed in [137] and [121]. In [137], path-following algorithms are generally classified into two categories: geometric algorithms and control theoretic algorithms. Geometric algorithms include pure pursuit [29], Line-of-sight (LOS) [40], [122], Vector-Field Guided Path-Following (VF-PF) algorithms [50], [63], [104],

etc. Control theoretic algorithms include Nonlinear Guidance Law (NLGL) [111], Linear Quadratic Regulator (LQR) [79], sliding mode control [104], backstepping control [80] algorithms, etc.

Among different path-following algorithms, VF-PF algorithms have been studied widely [50], [64], [72], [89], [90], [119]. The *guidance* feature of the guiding vector fields is justified as follows: usually robot *kinematics models* (e.g., single-integrator and double-integrator models [50], [74]) are considered, and the guiding vector fields, as their names suggest, provide *guidance signals* to the models. This is valid based on the aforementioned assumption that the *robot-specific inner-loop dynamics control* can track these guidance signal inputs effectively [63], [113], [121]. Thus, one can simply focus on the guidance layer (i.e., designing a guiding vector field), and consider other control layers separately. Specifically, the guiding vector field is designed such that its integral curves are guaranteed to converge to a predefined geometric desired path. Utilizing the convergence property of the vector field, one can then derive suitable control laws. It is reported in [137] that VF-PF algorithms demonstrate the lowest cross-track error while they require the least control effort among several other path-following algorithms. In addition, [22] shows that VF-PF algorithms achieve better path-following accuracy than the integral line-of-sight (ILOS) method [15].

1.1.2 An example of a 2D guiding vector field

To understand what a guiding vector field is, we introduce the 2D guiding vector field in [63] as a simple example. To derive the guiding vector field, first we suppose that the desired path \mathcal{P} is described by the zero-level set of an implicit function:

$$\mathcal{P} = \{(x, y) \in \mathbb{R}^2 : \phi(x, y) = 0\}, \quad (1.1)$$

where $\phi : \mathbb{R}^2 \rightarrow \mathbb{R}$ is twice continuously differentiable. In this setting, \mathcal{P} is a subset of \mathbb{R}^2 . The description is different from some other works where the desired path is a parameterized differentiable curve (e.g., [5]); that is, a differentiable map $f : I \rightarrow \mathbb{R}^n$ of an open interval $I = (a, b)$ of the real line \mathbb{R} into \mathbb{R}^n [35]. From the definition, one observes that the mathematical object in (1.1) is actually the *trace* of a parameterized curve f [35], or the image of a mapping f . Note that this description of the desired path without any parametrization is common in the VF-PF navigation problem [24], [28], [36], [50], [89], [98], [119], [156], [157], which will be formally defined later. One of the advantages is that the vector field can be derived directly from the function $\phi(\cdot)$, independent of the specific parametrization of the desired path. Another advantage is that one can replace the calculation of the Euclidean distance¹ $\text{dist}(\xi, \mathcal{P}) := \inf\{\|\xi - p\| : p \in \mathcal{P}\}$ between a point $\xi \in \mathbb{R}^2$ and the desired path \mathcal{P} simply by the value of $|\phi(\xi)|$

¹ This calculation is generally difficult since one needs to find the closest point on the desired path to ξ ; e.g., it is not trivial for even an ellipse.

under some assumptions to be explained in later chapters. For simplicity, rather than referring to \mathcal{P} in (1.1) as “the trace of a parameterized curve”, we call \mathcal{P} the *desired path* throughout the thesis. In fact, one feature of the VF-PF navigation problem is that the desired path \mathcal{P} is a *one-dimensional connected submanifold*, so we have the extra freedom of choosing different analytic expressions (i.e., ϕ) for the same desired path.

If the desired path is non-self-intersecting, then a valid 2D guiding vector field $\chi : \mathbb{R}^2 \rightarrow \mathbb{R}^2$ to solve the VF-PF navigation problem is [63]:

$$\chi(x, y) = E\nabla\phi(x, y) - k\psi(\phi(x, y))\nabla\phi(x, y), \quad (1.2)$$

where $E \in SO(2)$ is the 90° rotation matrix² $\begin{bmatrix} 0 & -1 \\ 1 & 0 \end{bmatrix}$, and $\psi : \mathbb{R} \rightarrow \mathbb{R}$ is a strictly increasing function satisfying $\psi(0) = 0$. For simplicity, one can choose $\psi(\phi(x, y)) = \phi(x, y)$. The first term of the vector field is “tangential” to the desired path, thus enables a robot to propagate/traverse/move along the desired path, while the second term of the vector field is perpendicular to the first term, helping the robot move closer to the desired path. Therefore, intuitively, the vector field guides the robot to move along and towards the desired path at the same time. For simplicity, we call the first term the *propagation term*, and the second term the *convergence term*. A *singular point* $p \in \mathbb{R}^2$ of the vector field χ is the point where the vector field becomes zero (i.e., $\chi(p) = 0$). The set of all singular points is called the *singular set* of the vector field. Recall that an integral curve of the vector field is a trajectory of the following autonomous system:

$$\dot{\xi}(t) = \chi(\xi(t)), \quad (1.3)$$

given some initial condition $\xi(t = 0) = \xi_0$, where $\dot{\xi}(t)$ denotes the time derivative of $\xi(t)$.

1.1.3 Vector-field guided path-following (VF-PF) navigation problem on general spaces

In this thesis, we will mainly study the properties of a guiding vector field defined on an n -dimensional general smooth Riemannian manifold \mathcal{M} (in particular, on an n -dimensional Euclidean space for $n \geq 3$), by investigating the integral curves of the guiding vector field. Therefore, we can unify the definition of the VF-PF navigation problem by considering the smooth Riemannian manifold \mathcal{M} . Before we formally present the definition, we first need to define the desired path on \mathcal{M} as a counterpart of (1.1):

$$\mathcal{P} = \{\xi \in \mathcal{M} : \phi_i(\xi) = 0, i = 1, \dots, n - 1\}, \quad (1.4)$$

² In fact, the matrix is $-E$ in [63], but we use E for conventional simplicity. This only affects the direction of the motion (forward or backward) on the desired path.

where $\phi_i : \mathcal{M} \rightarrow \mathbb{R}$ are twice continuously differentiable functions. Assumptions will be introduced in Chapter 5 to make sure that (1.4) defines a “practical” desired path (e.g., it is nonempty and connected). Therefore, the VF-PF navigation problem on \mathcal{M} , where recall that \mathcal{M} can be Euclidean spaces, is formally defined below

Problem 1.1 (VF-PF navigation problem on \mathcal{M}). Given a desired path $\mathcal{P} \subseteq \mathcal{M}$ defined in (1.4), the VF-PF navigation problem is to design a continuously differentiable vector field $\chi : \mathcal{M} \rightarrow T\mathcal{M}$, where $T\mathcal{M}$ denotes the tangent bundle of \mathcal{M} , for the differential equation $\dot{\xi}(t) = \chi(\xi(t))$ such that the two conditions below are satisfied:

- 1) There exists a neighborhood $\mathcal{D} \subseteq \mathcal{M}$ of the desired path \mathcal{P} such that for all initial conditions $\xi(0) \in \mathcal{D}$, the distance $\text{dist}(\xi(t), \mathcal{P})$ between the trajectory $\xi(t)$ and the desired path \mathcal{P} approaches zero as time $t \rightarrow \infty$; that is, $\lim_{t \rightarrow \infty} \text{dist}(\xi(t), \mathcal{P}) = 0$;
- 2) If a trajectory starts from the desired path, then the trajectory stays on the desired path for $t \geq 0$ (i.e., $\xi(0) \in \mathcal{P} \implies \xi(t) \in \mathcal{P}$ for all $t \geq 0$). In addition, the vector field on the desired path is non-zero (i.e., $0 \notin \chi(\mathcal{P})$).

We will study guiding vector fields and the autonomous system (1.3), where the right-hand-side is a guiding vector field defined on \mathcal{M} , throughout the thesis.

1.1.4 Review of guiding vector fields in the literature

In this thesis, we focus on VF-PF algorithms for the path-following control problem. The essential differences among different VF-PF algorithms are the guiding vector fields. In this subsection, we review some of the guiding vector fields in the literature and point out the major differences among them and those studied in this thesis.

- ([89]) If the desired path in \mathbb{R}^2 is defined by (1.1), then the guiding vector field $\chi : \mathbb{R}^2 \rightarrow \mathbb{R}^2$ is

$$\chi(\xi) = v_d \frac{R \nabla \phi(\xi)}{\|\nabla \phi(\xi)\|} - k_p \phi(\xi) \frac{\nabla \phi(\xi)}{\|\nabla \phi(\xi)\|} \quad (1.5)$$

for $\xi \in \mathbb{R}^2$, where $R = \begin{bmatrix} 0 & 1 \\ -1 & 0 \end{bmatrix}$, $v_d > 0$ and $k_p > 0$ are constants. The major difference from (1.2) is the state-dependent scaling coefficient $1/\|\nabla \phi(\xi)\|$.

- ([81]) If the desired path in \mathbb{R}^2 is defined by (1.1), then the guiding vector field $\chi : \mathbb{R}^2 \rightarrow \mathbb{R}^2$ is

$$\chi(\xi) = s V_g \operatorname{sech}(\kappa \phi(\xi)) \frac{R \nabla \phi(\xi)}{\|\nabla \phi(\xi)\|} - V_g \tanh(\kappa \phi(\xi)) \frac{\nabla \phi(\xi)}{\|\nabla \phi(\xi)\|} \quad (1.6)$$

for $\xi \in \mathbb{R}^2$, where $R = \begin{bmatrix} 0 & 1 \\ -1 & 0 \end{bmatrix}$, $\kappa > 0$, $V_g > 0$ are constants, and $s = \pm 1$, which determines the direction of following the desired path. The major differences from (1.2) are the state-dependent scaling coefficients $\operatorname{sech}(\kappa\phi(\xi))/\|\nabla\phi(\xi)\|$ and $\tanh(\kappa\phi(\xi))/\|\nabla\phi(\xi)\|$.

If the desired path in \mathbb{R}^3 is defined by (1.4), where $\mathcal{M} = \mathbb{R}^3$, then the guiding vector field $\chi : \mathbb{R}^3 \rightarrow \mathbb{R}^3$ is

$$\begin{aligned}\chi(\xi) = sV_g \operatorname{sech}(\kappa r(\xi)) &\frac{\nabla\phi_1(\xi) \times \nabla\phi_2(\xi)}{\|\sum_{i=1}^2 \phi_i(\xi) \nabla\phi_i(\xi)\|} \\ &- V_g \tanh(\kappa r(\xi)) \frac{\sum_{i=1}^2 \phi_i(\xi) \nabla\phi_i(\xi)}{\|\sum_{i=1}^2 \phi_i(\xi) \nabla\phi_i(\xi)\|} \quad (1.7)\end{aligned}$$

for $\xi \in \mathbb{R}^3$, where $r(\xi) = \|(\phi_1(\xi), \phi_2(\xi))\|$. Similarly, the major differences from the 3D counterpart of (1.2), which will be studied in detail later in Chapter 4, are the state-dependent scaling coefficients $\operatorname{sech}(\kappa r(\xi))/\|\sum_{i=1}^2 \phi_i(\xi) \nabla\phi_i(\xi)\|$ and $\tanh(\kappa r(\xi))/\|\sum_{i=1}^2 \phi_i(\xi) \nabla\phi_i(\xi)\|$.

- ([72]) If the desired path in \mathbb{R}^3 is defined by (1.4), where $\mathcal{M} = \mathbb{R}^3$, then the guiding vector field $\chi : \mathbb{R}^3 \rightarrow \mathbb{R}^3$ is:

$$\chi(\xi) = u_s \sigma \frac{\nabla\phi_1(\xi) \times \nabla\phi_2(\xi)}{\|\nabla\phi_1(\xi)\| \|\nabla\phi_2(\xi)\|} - k_p \left(\phi_1(\xi) \frac{\nabla\phi_1(\xi)}{\|\nabla\phi_1(\xi)\|} + \phi_2(\xi) \frac{\nabla\phi_2(\xi)}{\|\nabla\phi_2(\xi)\|} \right)$$

for $\xi \in \mathbb{R}^3$, where σ determines the direction of movement along the desired path and $u_s \in \mathbb{R}$, $k_p > 0$ are constants. The major differences from the 3D counterpart of (1.2), which will be studied in detail later in Chapter 4, are the state-dependent scaling coefficients $1/\|\nabla\phi_i(\xi)\|$, $i = 1, 2$, and $1/(\|\nabla\phi_1(\xi)\| \|\nabla\phi_2(\xi)\|)$.

- ([50]) If the desired path is defined by (1.4), where $\mathcal{M} = \mathbb{R}^n$, then the guiding vector field $\chi : \mathbb{R}^n \rightarrow \mathbb{R}^n$ is:

$$\chi(\xi) = H(t, \xi) \wedge_{i=1}^{n-1} \nabla\phi_i(\xi) - G(t, \xi) \nabla V(\phi_1(\xi), \dots, \phi_{n-1}(\xi)) + \rho(t, \xi) \quad (1.8)$$

for $\xi \in \mathbb{R}^n$, where $V : \mathbb{R}^{n-1} \rightarrow \mathbb{R}$ is a differentiable positive-definite function (i.e., $V = 0$ if and only if $\phi_i = 0$ for all $i = 1, \dots, n-1$), $G : \mathbb{R} \times \mathbb{R}^n \rightarrow \mathbb{R}_{\geq 0}$ is a non-negative function which only becomes zero at points where $\bar{\nabla}V = 0$, $H : \mathbb{R} \times \mathbb{R}^n \rightarrow \mathbb{R}_{\geq 0}$ is a continuous function which is strictly positive or negative on \mathcal{P} , and \wedge is the wedge product. If the desired path is static (i.e., independent of time t), then $\rho(\cdot) = 0$; otherwise, $\rho : \mathbb{R} \times \mathbb{R}^n \rightarrow \mathbb{R}^n$ is a term to guarantee the convergence to the moving desired path (i.e., \mathcal{P} is dependent on time t). The guiding vector field defined in [74] is similar.

The major differences from the \mathbb{R}^n counterpart of (1.2), which will be studied in detail later in Chapter 9, are the state-dependent scaling functions $G(\cdot)$, $H(\cdot)$, and the time-varying terms. If the desired path is independent of time t (hence $\rho(\cdot) = 0$), and let $G(\cdot) = H(\cdot) = 1$, $V = 1/2 \sum_{i=1}^{n-1} \phi_i^2$, then (1.8) is of the same form as (9.2) in Chapter 9.

1.1.5 Guiding vector fields studied in this thesis

In this thesis, we specifically study guiding vector fields of the same structure as that in (1.2); namely, each of them consists of a propagation term and a convergence term. More specifically, the counterpart of (1.2) defined on \mathbb{R}^3 is studied in Chapter 4 (i.e., (4.2)); the one defined on \mathbb{R}^n is studied in Chapter 9 (i.e., (9.2)) and the one defined on an n -dimensional smooth Riemannian manifold is studied in Chapter 5 (i.e., (5.6)) and Chapter 6 (i.e., (6.3)). Here, we emphasize the significance of studying these guiding vector fields.

Firstly, different from many existing studies which restrict consideration to simple desired paths such as a circle or a straight line (or a combination of them) [21], [104], [137], the guiding vector fields studied in this thesis are designed for any *general* sufficiently smooth desired path in the form of (1.4). Secondly, many guiding vector fields in the literature are essentially *variants* of guiding vector fields in this thesis. For example, as discussed in Section 1.1.4, some variants are obtained by adding ϕ_i -dependent gains to the convergence terms or (and) the propagation terms [63], [81], [89], and some by adding time-varying gains or an additional time-varying component [50], [74]. Thus, the guiding vector fields in [63], [81], [89], [162] can be regarded as 2D specializations of the guiding vector fields studied in this thesis (e.g., (5.3)), and those in [65], [72], [81], [156], [157] as 3D specializations of the guiding vector fields studied in this thesis (e.g., (5.3)). In some cases, the ϕ_i -dependent gains to the convergence terms or (and) the propagation terms would not change the phase portraits [25, Proposition 1.14], and thus the convergence properties of the guiding vector fields remain unchanged. Therefore, the study of the guiding vector fields in this thesis (e.g., (5.3) and (5.6)) is of great significance. In addition, to clearly observe the topological properties of the guiding vector fields, we do not consider time-varying components, and thus we focus on the *autonomous* differential equation (1.3).

1.1.6 Comparison with potential energy shaping for path planning

The guiding vector field approach has one major component in common with the potential energy shaping approach for path planning (e.g., [68], [120]); that is, they all use (feedback) vector fields for path following or motion planning. In addition, similar to the potential energy shaping approach, the guiding vector

field can be used for control algorithm design for both the purely kinematic, first-order integrator, and the dynamic, second-order integrator [50].

However, there are also major differences listed as follows:

1. (Problem formulations) The potential energy shaping approach aims to plan a path between two given points (in the presence of obstacles), while in the path-following problem, one does not aim to find such a path and there are no given two points either. More specifically, in the path following formulation, a geometric desired path is given, and one aims to design a vector field such that the integral curves converge to and traverse along the path. One also does not restrict consideration to a compact workspace, while those works in [68], [120] only consider a compact workspace (i.e., a sphere world).
2. (Vector fields) Guiding vector fields are usually *not* the gradients of any potential functions, while the potential energy shaping approach relies on designing a potential/navigation function, and the corresponding vector field is the (negative) gradient of the potential/navigation function.
3. (Topological results) We prove a general result showing a *common* limitation of combining two vector fields (see Lemma 8.20). This result gives a theoretical explanation of the common phenomenon that singular points exist when two vector fields are blended. The result may be regarded as a counterpart of the well-known limitation of motion-planning algorithms based on the negative gradient of a potential/navigation function [68], [120], both issues being fundamentally topological. However, in our case, the limitation can sometimes be removed, and thereby, global convergence of trajectories to the desired path with the collision-avoidance guarantee is possible (see Remark 8.21).

1.2 RESEARCH CHALLENGES AND CONTRIBUTIONS

Equilibrium points are usually the central subject of study in the systems and control field. However, in this thesis, since the desired path is not a singleton, we aim to let trajectories of (1.3), where the right-hand side can be guiding vector fields on high dimensional spaces, converge to a closed invariant set (i.e., the desired path). The difficulty of the analysis of guiding vector fields arises due to two facts. First, the guiding vector fields are nonlinear and not the gradient of any potential functions. Second, there are usually singular points in the vector field, where the vector field vanishes. We recognize these challenges and make the first contribution as stated below, which is detailed in Chapters 3, 4, and 7.

Contribution I

We derive new theoretical results (e.g., the refined dichotomy convergence property, the exponential convergence of path-following errors, the input-to-state stability of path-following error dynamics) for guiding vector fields on \mathbb{R}^n , where $n \geq 2$.

Moreover, most, if not all, of the existing literature only studies the guiding vector fields on Euclidean spaces, while the generalization to a smooth manifold has not been investigated thoroughly. Our second contribution is to generalize guiding vector fields to a smooth Riemannian manifold, and provide theoretical results including the topological analysis. The contribution is elaborated in Chapters 5 and 6.

Contribution II

We generalize guiding vector fields to a general smooth Riemannian manifold, and derive new theoretical results including the dichotomy convergence result and the stability of the desired path. In particular, we derive some topological results regarding the existence of singular points and trajectories not converging to the desired path. In addition, we characterize the domain of attraction of the desired path.

We have shown that on Euclidean spaces, the guiding vector field corresponding to a compact desired path (precisely, homeomorphic to the unit circle S^1) cannot have global convergence of trajectories of (1.3) to the desired path. However, in practical applications, this global convergence property is desirable. Yet, it is challenging, if not impossible, to remove this topological obstruction to global convergence. In addition, the traditional guiding vector field is not applicable to a self-intersecting desired path since the self-intersecting point is itself a singular point of the vector field. It is unclear how to remove this limitation in the existing literature. It is our third contribution to resolve these problems, which is detailed in Chapter 9.

Contribution III

We propose an approach to generate singularity-free higher-dimensional guiding vector fields on Euclidean spaces such that the topological obstruction of global convergence of trajectories to the desired path is removed, and thereby it becomes possible to follow self-intersecting desired paths.

Most of the VF-PF algorithms have been designed for one single robot, but it was unclear how to extend these algorithms for a multi-robot system to accomplish some coordination tasks. In addition, when considering obstacle avoidance,

many existing algorithms cannot provide mathematical guarantees. As the fourth contribution, we have successfully achieved the extension of guiding vector fields for multi-robot systems, and derive a variation of the guiding vector field to rigorously guarantee both path-following and obstacle-avoidance capabilities. This contribution is reported in Chapters 8 and 10.

Contribution IV

We extend guiding vector fields having been designed for a single robot to those for a multi-robot system to achieve distributed coordinated motion control. In addition, we extend guiding vector fields such that path-following and obstacle-avoidance behaviors are achieved simultaneously with mathematical guarantees.

1.3 THESIS OUTLINE

The remainder of the thesis is structured as follows, and the relationships among different chapters are illustrated in Fig. 1.3.

In Chapter 2, preliminaries on nonlinear systems and control, point-set topology, topological and differentiable manifolds are briefly introduced. These preliminary results underpin the subsequent theoretical findings in the thesis.

After Chapter 2, the thesis is divided into two parts. Part I establishes the theoretical foundation of vector-field guided path-following (VF-PF) algorithms, and it consists of Chapters 3 to 7. Part II extends Part I, and presents variations of the guiding vector fields and their applications in following occluded desired paths, global robot navigation and multi-robot coordinated maneuvering. This part consists of Chapters 8 to 10 (see the two shaded areas in Fig. 1.3).

Chapter 3 studies the relationship between level values and level sets. The zero level set of a specific smooth function, called *level function*, is usually the central object of study (e.g., the zero level set of a Lyapunov function is usually the singleton containing an equilibrium of a dynamical system). Therefore, we investigate the question whether the convergence of the value of the level function, called the *level value*, to zero along a trajectory implies the convergence of the trajectory to the zero level set. This is not generally true, but some conditions or assumptions are identified in the chapter to make this implication hold. These conditions or assumptions are then used throughout the rest of the thesis (see the arrows starting from Ch. 3 in Fig. 1.3). This chapter is based on our work in [160].

In Chapter 4, we study the properties of a general 3D guiding vector field for path following, which is an extension of the 2D guiding vector field in Section 1.1.2. We derive conditions under which the path-following error converges

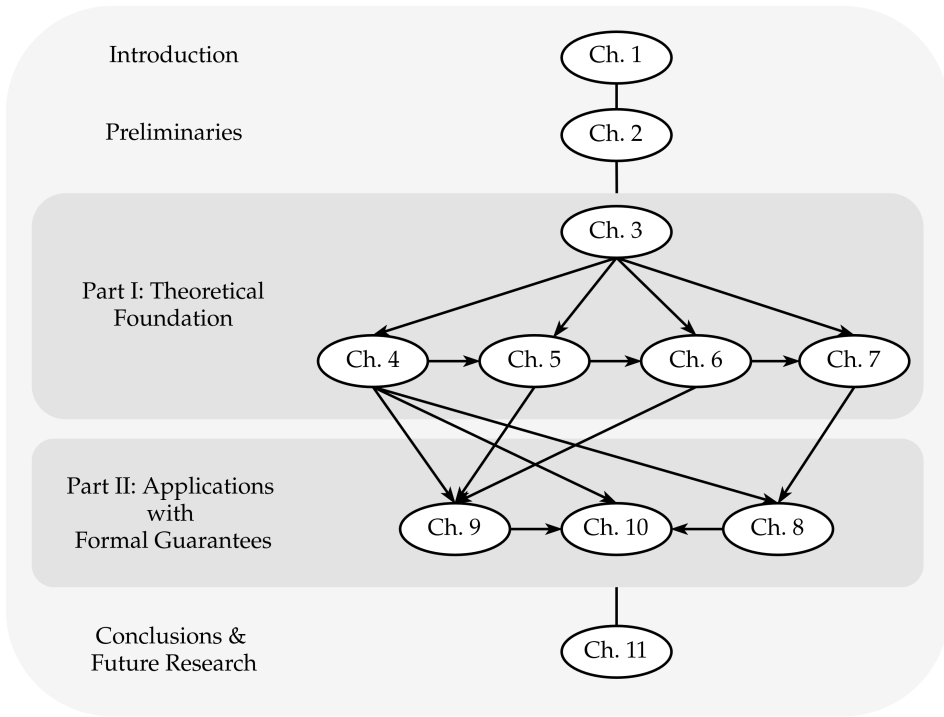


Figure 1.3: The structure of the thesis and relationships among chapters.

exponentially to zero in the vicinity of the desired path, and show the local input-to-state stability (ISS) property of the path-following error dynamics. Thanks to this ISS property, we propose a control algorithm design principle for robot models of which the motions are determined by their headings. This chapter is the basis for the design of higher-dimensional guiding vector fields, for which some of the results in the chapter can be generalized straightforwardly. The control algorithm design principle is adopted in Chapters 8, 9 and 10 (see the arrows starting from Ch. 4 in Fig. 1.3). This chapter is based on our work in [157] and [156].

Chapter 5 focuses on the analysis of vector-field guided path-following algorithms from a topological perspective. Based on Chapter 4, we derive guiding vector fields on n -dimensional Euclidean spaces \mathbb{R}^n and n -dimensional smooth Riemannian manifolds \mathcal{M} . In this chapter, we only take into account desired paths that are homeomorphic to the unit circle S^1 . For the guiding vector field on Riemannian manifolds, we show the dichotomy convergence result, the asymptotic stability of the desired path and the non-attractiveness of the singular set under some conditions. Then we conclude that the domain of attraction of the desired path is homotopy equivalent to S^1 . This further leads to results about

the existence of singular points and the impossibility of global convergence in the Euclidean spaces. Furthermore, we also demonstrate a topological result regarding the existence of trajectories not converging to the desired path. The results of the chapter are the main motivations for Chapter 9, which aims to remove the topological obstruction to global convergence to the desired path (see the arrow starting from Ch. 5 to Ch. 9). This Chapter is based on our work in [161].

Chapter 6 is an extension of Chapter 5 (see the arrow starting from Ch. 5 to Ch. 6 in Fig. 1.3); it further characterizes the domain of attraction of the desired path, which is generally a compact asymptotically stable regular level set in a finite-dimensional Riemannian manifold \mathcal{M} . The central result is that the domain of attraction of the desired path is homeomorphic to $\mathbb{R}^{n-1} \times S^1$, where n is the dimension of the ambient manifold \mathcal{M} . As in Chapter 5, the results of this chapter motivate the studies in Chapter 9 (see the arrow starting from Ch. 6 to Ch. 9 in Fig. 1.3). This chapter is based on our work in [158].

In Chapter 7, we consider guiding vector fields on Euclidean spaces \mathbb{R}^n for $n \geq 2$ (illustrated by an arrow from Ch. 6, which inherits from Ch. 4 and Ch. 5, to Ch. 7 in Fig. 1.3), and refine the dichotomy convergence result. Specifically, we provide conditions under which a trajectory converging to the singular set implies that it converges to a single point of the set. This refined conclusion is used in Chapter 8 (see the arrow starting from Ch. 7 to Ch. 8 in Fig. 1.3). This chapter is based on our work in [160].

Chapter 8 considers the practical scenario where a planar desired path is partly occupied by a finite number of static and moving obstacles of arbitrary shapes. In this case, it is no longer possible to persistently follow the desired path, and temporarily deviating from the desired path to avoid collision with obstacles is crucial. To address this problem, we propose to use smooth bump functions to integrate two guiding vector fields while the negative effect due to the integration is mitigated. Technical conditions are derived to guarantee the effective path-following and obstacle-avoidance behavior simultaneously. We also propose a switching mechanism to avoid possible deadlocks, and discuss several extensions, including obstacle-avoidance in higher-dimensional spaces, nonholonomic robot models and moving obstacles. The results in this chapter can be adopted in Chapter 10 to avoid collisions among robots (see the arrow starting from Ch. 8 to Ch. 10 in Fig. 1.3). This chapter is based on our work in [162] and [159].

Due to the topological obstruction of global convergence of trajectories to the desired path in Euclidean spaces as shown in Chapters 5 and 6, Chapter 9 investigates how to remove this topological obstruction. Using parametric equations of desired paths, we propose an approach to change the topology of the desired paths and extend the dimensions of the space that the desired paths live in. Thanks to this approach, we can guarantee the global convergence of trajectories to desired paths that are homeomorphic to the unit circle S^1 or are self-intersecting, which was initially not possible. We also discuss the differences between our

proposed vector-field guided path-following algorithm and a traditional trajectory tracking algorithm, along with the practical implementation of the proposed algorithm on a fixed-wing aircraft. This chapter is based on our work in [164] and [165].

The previous chapters all deal with the single-robot path-following problem, while the last chapter, Chapter 10, further extends the guiding vector field to enable multiple robots to follow possibly different desired paths in a distributed and coordinated way. The new guiding vector field proposed in this chapter utilizes the additional dimension of the guiding vector field proposed in Chapter 9 to reach consensus on a virtual coordinate, and thus coordinated motions (i.e., robots maintaining desired parametric distances while maneuvering) is achieved; see the arrow starting from Ch. 9 to Ch. 10 in Fig. 1.3. We also extend the path-following algorithm to enable coordinated maneuvering on two-dimensional surfaces. This chapter is based on our work in [166] and [167].

Chapter 11 concludes the thesis and provides recommendations for future research.

1.4 LIST OF PUBLICATIONS

JOURNAL PUBLICATIONS

- [1] W. Yao and M. Cao, "Path following control in 3D using a vector field," *Automatica*, vol. 117, p. 108 957, 2020. (Chapter 4)
- [2] W. Yao, H. G. de Marina, B. Lin, and M. Cao, "Singularity-free guiding vector field for robot navigation," *IEEE Transactions on Robotics (TRO)*, vol. 37, no. 4, 2021. (Chapter 9)
- [3] W. Yao, B. Lin, B. D. O. Anderson, and M. Cao, "Topological analysis of vector-field guided path following on manifolds," *IEEE Transactions on Automatic Control (TAC)*, 2021, *Conditionally accepted*. (Chapter 5)
- [4] W. Yao, B. Lin, B. D. O. Anderson, and M. Cao, "Guiding vector fields for following occluded paths," *IEEE Transactions on Automatic Control (TAC)*, 2021, *Under review*. (Chapter 8)
- [5] L. Gong, W. Yao, J. Gao, and M. Cao, "Limit cycles analysis and control of evolutionary game dynamics with environmental feedback," *Automatica*, 2020, *Under review*.
- [6] W. Yao, H. G. de Marina, Z. Sun, and M. Cao, "Guiding vector fields for multi-robot coordinated navigation," 2021, *Submitted*. (Chapter 10)

- [7] W. Yao, B. Lin, B. D. O. Anderson, and M. Cao, "The domain of attraction of the desired path in vector-field guided path following," 2021, *Submitted*. (Chapter 6)
- [8] B. Lin, W. Yao, and M. Cao, "On Wilson's theorem about domains of attraction and tubular neighborhoods," 2021, *Under preparation*. (Chapter 6)
- [9] H. G. de Marina, J. J. Castellanos, and W. Yao, "Collective motions in affine formation control," 2021, *Under preparation*.

CONFERENCE PUBLICATIONS

- [1] W. Yao, H. G. de Marina, Z. Sun, and M. Cao, "Distributed coordinated path following using guiding vector fields," in *IEEE International Conference on Robotics and Automation (ICRA)*, 2021. (**Best Conference Paper Finalist**). (Chapter 10)
- [2] W. Yao, B. Lin, B. D. O. Anderson, and M. Cao, "Refining dichotomy convergence in vector-field guided path following control," in *European Control Conference (ECC)*, 2021. (Chapters 3, 7)
- [3] H. G. de Marina, J. J. Castellanos, and W. Yao, "Leaderless collective motions in affine formation control," 2021 *IEEE 60th Conference on Decision and Control (CDC)*, IEEE, 2021.
- [4] W. Yao, H. G. de Marina, and M. Cao, "Vector field guided path following control: Singularity elimination and global convergence," in *2020 59th IEEE Conference on Decision and Control (CDC)*, IEEE, 2020, pp. 1543–1549. (Chapter 9)
- [5] L. Gong, W. Yao, J. Gao, and M. Cao, "Limit cycles in replicator-mutator dynamics with game-environment feedback," in *21st IFAC World Congress*, 2020.
- [6] W. Yao, B. Lin, and M. Cao, "Integrated path following and collision avoidance using a composite vector field," in *2019 IEEE 58th Conference on Decision and Control (CDC)*, IEEE, 2019, pp. 250–255. (Chapter 8)
- [7] W. Yao, Y. A. Kapitanyuk, and M. Cao, "Robotic path following in 3D using a guiding vector field," in *2018 IEEE 57th Conference on Decision and Control (CDC)*, IEEE, 2018, pp. 4475-4480. (Chapter 4)

CONFERENCE ABSTRACTS

- [1] W. Yao, M. Cao. "Mobile robot path following control: singularity elimination." *39th Benelux Meeting on Systems and Control*, 2020, p. 25. (Chapter 9)

- [2] W. Yao, Y. A. Kapitanyuk, M. Cao. "High-dimensional vector field for path following." *38th Benelux Meeting on Systems and Control*, 2019, p. 115. (Chapter 9)
- [3] W. Yao, Y. A. Kapitanyuk, M. Cao. "3D path-following using a guiding vector field." *37th Benelux Meeting on Systems and Control*, 2018, p. 130. (Chapter 4)

1.5 GENERAL NOTATIONS

In this section we define notations that are used throughout the thesis, while notations specific to chapters are defined within the chapters themselves.

The set of natural numbers (including 0), integers and real numbers are denoted by \mathbb{N} , \mathbb{Z} and \mathbb{R} , respectively. We use $\mathbb{R}_{\geq 0}$ to denote the non-negative real numbers. The notation “ \coloneqq ” means “defined to be”. If $\mathcal{A} \subsetneq \mathcal{B}$, then \mathcal{A} is a *proper* subset of \mathcal{B} . If $\mathcal{A} \subseteq \mathcal{B}$, then \mathcal{A} is a (proper or non-proper) subset of \mathcal{B} . The notations $\mathcal{A} \setminus \mathcal{B}$ or $\mathcal{A} - \mathcal{B}$ denote the set of elements which belong to \mathcal{A} but not \mathcal{B} ; i.e., $\mathcal{A} \setminus \mathcal{B} = \mathcal{A} - \mathcal{B} := \{x \in \mathcal{A} : x \notin \mathcal{B}\}$.

Given a positive integer n , if a mapping $f : \mathbb{R} \rightarrow \mathbb{R}^n$ is a differentiable function in time t , then $f(t)$ denotes the function’s derivative with respect to t . Suppose there is a function $\rho : \mathcal{C} \rightarrow \mathcal{D}$, where the sets \mathcal{C} and \mathcal{D} are nonempty. The image of a subset $\mathcal{F} \subseteq \mathcal{C}$ under ρ is the subset $\rho(\mathcal{F}) \subseteq \mathcal{D}$ defined by $\rho(\mathcal{F}) := \{\rho(x) \in \mathcal{D} : x \in \mathcal{F}\}$. Given two functions $f : X \rightarrow Y, g : Y \rightarrow Z$, the composition of these two functions is denoted by $g \circ f : X \rightarrow Z$. A function is said to be of class C^r , $r \geq 1$, if it is r times differentiable, and its r -th derivative is continuous. A function is of class C^0 if it is continuous, and C^∞ if it is smooth (i.e., infinitely differentiable).

Suppose (\mathcal{X}, d) is a metric space with a metric d and \mathcal{A} is a subset in \mathcal{X} . The *distance* between a point $p \in \mathcal{X}$ and the set \mathcal{A} is $\text{dist}(\mathcal{A}, p) = \text{dist}(p, \mathcal{A}) := \inf\{d(p, q) : q \in \mathcal{A}\}$, and if $\mathcal{A} = \emptyset$, then $\text{dist}(p, \mathcal{A}) = \inf\{\emptyset\} = +\infty$. The distance between two subsets $\mathcal{A}, \mathcal{B} \subseteq \mathcal{X}$ is $\text{dist}(\mathcal{B}, \mathcal{A}) = \text{dist}(\mathcal{A}, \mathcal{B}) = \inf\{d(a, b) : a \in \mathcal{A}, b \in \mathcal{B}\}$. If we consider the n -dimensional Euclidean space $\mathcal{X} = \mathbb{R}^n$, then we use the Euclidean metric by default unless otherwise mentioned³; i.e., $\text{dist}(p, \mathcal{A}) = \inf\{d_{l^2}(p, q) : q \in \mathcal{A}\}$, where $d_{l^2}(p, q) = \|p - q\|$ and $\|\cdot\|$ is the Euclidean norm.

If M is a matrix, $\|M\|$ denotes the induced matrix two-norm of M . The transpose of a vector or a matrix v is denoted by v^\top . The determinant of a matrix M is denoted by $\det(M)$ or $\det M$.

³ Other metrics in \mathbb{R}^n include but not limit to the taxi-cab metric and the sup norm metric [140, Examples 1.1.7, 1.1.9].

2 | PRELIMINARIES

This chapter provides preliminaries for subsequent theoretical derivation.

2.1 NONLINEAR SYSTEMS AND CONTROL

For a comprehensive introduction to nonlinear systems and control theory, see [66], [107], [124], [142], [149]. In what follows, we select some results from [66] that will be used in subsequent chapters.

2.1.1 Existence and uniqueness of system trajectories

Consider the following initial-value problem

$$\dot{x}(t) = f(t, x(t)), \quad x(t_0) = x_0 \quad (2.1)$$

where t_0 is the initial time instant, $x \in \mathbb{R}^n$ for some positive integer n , and $f : \mathbb{R}^n \rightarrow \mathbb{R}^n$ is a function. The first question to ask is the existence and uniqueness of solutions to (2.1) (i.e., trajectories of (2.1)). This is stated in the following theorem.

Theorem 2.1 (Local existence and uniqueness, [66, Theorem 3.1]). *If $f(t, x)$ in (2.1) is piecewise continuous in t and satisfies the Lipschitz condition*

$$\|f(t, x) - f(t, y)\| \leq L\|x - y\| \quad (2.2)$$

for all $x, y \in \mathcal{B} := \{x \in \mathbb{R}^n : \|x - x_0\| \leq r\}$, and for all $t \in [t_0, t_1]$, then there exists some $\delta > 0$ such that (2.1) has a unique solution over $[t_0, t_0 + \delta]$.

If $f(t, x)$ satisfies (2.2) locally (i.e., for all x, y in a ball \mathcal{B}), then it is said to be *locally Lipschitz in x* .

Theorem 2.2 (Global existence and uniqueness, [66, Theorem 3.2]). *If $f(t, x)$ in (2.1) is piecewise continuous in t and satisfies the Lipschitz condition*

$$\|f(t, x) - f(t, y)\| \leq L\|x - y\|$$

for all $x, y \in \mathbb{R}^n$, and for all $t \in [t_0, t_1]$, then (2.1) has a unique solution over $[t_0, t_1]$.

Note that for a nonlinear system, a trajectory may not be well defined on $t \in [t_0, \infty)$; namely, it cannot be prolonged to infinity. The following theorem gives a sufficient condition under which the trajectory of (2.1) is well-defined on $t \in [t_0, \infty)$.

Theorem 2.3 ([66, Theorem 3.3]). *Let $f(t, x)$ in (2.1) be piecewise continuous in t and locally Lipschitz in x for all $t > t_0$ and all x in a domain $\mathcal{D} \subseteq \mathbb{R}^n$. Let \mathcal{W} be a compact subset of \mathcal{D} , $x_0 \in \mathcal{W}$, and suppose every solution of (2.1) lies entirely in \mathcal{W} . Then there is a unique solution defined for all $t > t_0$.*

2.1.2 Lyapunov stability

We review some definitions and theorems on Lyapunov stability. In particular, we restrict our attention to the following *autonomous system*

$$\dot{x}(t) = f(x(t)), \quad (2.3)$$

where $f : \mathcal{D} \subseteq \mathbb{R}^n \rightarrow \mathbb{R}^n$ is a locally Lipschitz function. This guarantees the existence and uniqueness of the trajectory of (2.3) given an initial condition $x(t_0)$. Suppose, without loss of generality, that 0 is an equilibrium point of (2.3); that is, $f(0) = 0$, and the initial time instant $t_0 = 0$.

Definition 2.4 ([66, Definition 4.1]). The equilibrium point $x = 0$ of (2.3) is

1. *stable* if $\forall \epsilon > 0$, $\exists \delta(\epsilon) > 0$ such that $\|x(0)\| < \delta(\epsilon) \implies \|x(t)\| < \epsilon, \forall t \geq 0$.
2. *unstable* if it is not stable.
3. *asymptotically stable* if it is stable and δ can be chosen such that $\|x(0)\| < \delta \implies \lim_{t \rightarrow \infty} x(t) = 0$.

Now we present below one of the celebrated Lyapunov stability theorems.

Theorem 2.5 ([66, Theorem 4.1]). *Suppose $x = 0$ is an equilibrium point for (2.3) and $\mathcal{D} \subseteq \mathbb{R}^n$ is a domain containing the equilibrium point. Let $V : \mathcal{D} \rightarrow \mathbb{R}$ be a continuously differentiable function such that*

$$V(0) = 0 \quad \text{and} \quad V(x) > 0 \text{ in } \mathcal{D} \setminus \{0\}$$

$$\dot{V}(x) \leq 0 \text{ in } \mathcal{D}$$

Then, $x = 0$ is stable. Moreover, if

$$\dot{V}(x) < 0 \text{ in } \mathcal{D} \setminus \{0\}$$

then $x = 0$ is asymptotically stable.

2.1.3 LaSalle's invariance principle, Barbalat's lemma and an invariance-like theorem

A frequently used result is the LaSalle's invariance principle for autonomous systems. (2.3).

Theorem 2.6 ([66, Theorem 4.4]). *Let $\Omega \subseteq \mathcal{D}$ be a compact set that is positively invariant with respect to (2.3). Let $V : \mathcal{D} \rightarrow \mathbb{R}$ be a continuously differentiable function such that $\dot{V} \leq 0$ in Ω . Define the set $\mathcal{E} := \{x \in \Omega : \dot{V}(x) = 0\}$. Then every solution starting in Ω approaches the largest invariant set \mathcal{L} in \mathcal{E} as $t \rightarrow \infty$.*

The following lemma is known as Barbalat's lemma, which is frequently utilized in the literature to prove convergence of some error signals to zero. It also lies at the core of the proof of Theorem 2.8.

Lemma 2.7 ([66, Lemma 8.2]). *Let $\phi : \mathbb{R} \rightarrow \mathbb{R}$ be a uniformly continuous function on $[0, \infty)$. If $\lim_{t \rightarrow \infty} \int_0^t \phi(\tau) d\tau$ exists and is finite, then*

$$\phi(t) \rightarrow 0 \text{ as } t \rightarrow \infty.$$

The following theorem is an invariance-like theorem for non-autonomous systems. We consider the following general form of a non-autonomous system:

$$\dot{x} = f(t, x), \quad (2.4)$$

where $f(t, x)$ is piecewise continuous in t and locally Lipschitz in x , uniformly in t , on $[0, \infty) \times \mathcal{D}$ with \mathcal{D} being a domain containing $x = 0$, and $f(t, 0) = 0$ for $t \geq 0$. Let $\mathcal{B}_r := \{x \in \mathbb{R}^n : \|x\| \leq r\}$ for a positive constant r .

Theorem 2.8 ([66, Theorem 8.4]). *Suppose $f(t, 0)$ in (2.4) is uniformly bounded for all $t \geq 0$. Let $V : [0, \infty) \times \mathcal{D} \rightarrow \mathbb{R}$ be a continuously differentiable function such that*

$$\begin{aligned} W_1(x) &\leq V(t, x) \leq W_2(x) \\ \dot{V}(t, x) &= \frac{\partial V}{\partial t} + \frac{\partial V}{\partial x} f(t, x) \leq -W(x) \end{aligned}$$

$\forall t \geq 0, \forall x \in \mathcal{D}$, where $W_1(x)$ and $W_2(x)$ are continuous positive definite functions and $W(x)$ is a continuous positive semidefinite function on \mathcal{D} . Choose $r > 0$ such that $\mathcal{B}_r \subseteq \mathcal{D}$ and let $\rho < \min_{\|x\|=r} W_1(x)$. Then, all solutions of (2.4) with $x(t_0) \in \{x \in \mathcal{B}_r : W_2(x) \leq \rho\}$ are bounded and satisfy

$$W(x(t)) \rightarrow 0 \text{ as } t \rightarrow \infty.$$

Moreover, if all the assumptions hold globally and $W_1(x)$ is radially unbounded, the statement is true for all $x(t_0) \in \mathbb{R}^n$.

2.1.4 Local input-to-state stability (ISS)

Consider the system

$$\dot{x} = f(t, x, u) \quad (2.5)$$

where $f : [0, \infty) \times \mathbb{R}^n \times \mathbb{R}^m \rightarrow \mathbb{R}^n$ is piecewise continuous in t and locally Lipschitz in x and u . The input $u(t)$ is a piecewise continuous, bounded function of t for all $t \geq 0$.

Definition 2.9 ([66, Definitions 4.2, 4.3]). A continuous function $\alpha : [0, a) \rightarrow [0, \infty)$ is a class \mathcal{K} function if it is strictly increasing and $\alpha(0) = 0$. A continuous function $\beta : [0, a) \times [0, \infty) \rightarrow [0, \infty)$ is a class \mathcal{KL} function if, for each fixed s , the mapping $\beta(r, s)$ is a class \mathcal{K} function with respect to r and, for each fixed r , the mapping $\beta(r, s)$ is decreasing with respect to s and $\beta(r, s) \rightarrow 0$ as $s \rightarrow 0$.

Definition 2.10 (local ISS). The system (2.5) is said to be locally ISS if there exists a class \mathcal{KL} function β , a class \mathcal{K} function γ and positive constants k_1 and k_2 such that for initial state $\|x(t_0)\| < k_1$ and bounded input $\sup_{t \geq t_0} \|u(t)\| < k_2$, the solution $x(t)$ exists for all $t \geq t_0$ and satisfies $\|x(t)\| \leq \beta(\|x(t_0)\|, t - t_0) + \gamma \left(\sup_{t_0 \leq \tau \leq t} \|u(\tau)\| \right)$.

Lemma 2.11. Let $V : [0, \infty) \times \mathbb{R}^n \rightarrow \mathbb{R}$ be a continuously differentiable function such that

$$\alpha_1(\|x\|) \leq V(t, x) \leq \alpha_2(\|x\|) \quad (2.6)$$

$$\frac{\partial V}{\partial t} + \frac{\partial V}{\partial x} f(t, x, u) \leq -W_3(x), \quad \forall \|x\| \geq \rho(\|u\|) > 0 \quad (2.7)$$

$\forall (t, x, u) \in [0, \infty) \times \mathcal{B}_r \times \mathcal{B}_{r_u}^{-1}$, where α_1, α_2 are class \mathcal{K} functions, ρ is a class \mathcal{K} function, and $W_3(x)$ is a continuous positive definite function on \mathbb{R}^n . Then, the system (2.5) is locally ISS with $\gamma = \alpha_1^{-1} \circ \alpha_2 \circ \rho$ in Definition 2.10.

2.1.5 Nagumo's theorem

This section explains the Nagumo's theorem based on [13].

Definition 2.12 (Bouligand's tangent cone, [13, Definition 4.6]). Given a closed set $\mathcal{S} \subseteq \mathbb{R}^n$, the tangent cone to \mathcal{S} at $x \in \mathbb{R}^n$ is defined as follows:

$$\mathcal{T}_{\mathcal{S}}(x) = \left\{ z \in \mathbb{R}^n : \liminf_{\tau \rightarrow 0} \frac{\text{dist}(x + \tau z, \mathcal{S})}{\tau} = 0 \right\}.$$

The tangent cone is nontrivial (i.e., non-identical to \mathbb{R}^n) only on the boundary of \mathcal{S} .

¹ Given $a > 0$, the (open) ball $\mathcal{B}_a \subseteq \mathbb{R}^n$ is defined as $\mathcal{B}_a := \{\xi \in \mathbb{R}^n : \|\xi\| < a\}$.

Theorem 2.13 (Nagumo's theorem, [13, Corollary 4.8]). *Consider the system (2.3) and assume that for each initial condition $x(0)$ in an open set $\mathcal{O} \subseteq \mathbb{R}^n$, it admits a unique solution defined for all $t \geq 0$. Let $\mathcal{S} \subseteq \mathcal{O}$ be a closed set. Then, \mathcal{S} is positively invariant for the system if and only if the velocity vector $f(x)$ satisfies the Nagumo's condition:*

$$f(x) \in \mathcal{T}_{\mathcal{S}}(x), \text{ for all } x \in \partial\mathcal{S},$$

where $\partial\mathcal{S}$ denotes the boundary of \mathcal{S} .

The readers are recommended to read the clear explanation and intuitive interpretation of the Bouligand's tangent cone and the Nagumo's theorem in [13, pp. 102-103].

2.1.6 Poicaré-Bendixson theorem

This subsection is based on Chapter 9 of [149]. The Poicaré-Bendixson theorem is a celebrated result since it completely determines the asymptotic behavior of flows on the plane, cylinder, and two-sphere.

We consider C^r , $r \geq 1$, vector fields

$$\begin{aligned}\dot{x} &= f(x, y), \\ \dot{y} &= g(x, y),\end{aligned}\tag{2.8}$$

for $\xi = (x, y) \in \mathcal{N}$, where \mathcal{N} denotes the state space that can be the plane, cylinder, or two-sphere. The flow $\phi : \mathbb{R} \times \mathbb{R}^2 \rightarrow \mathbb{R}^2$ generated by (2.8) is denoted by $\phi(t, \xi)$. Namely, for $\xi \in \mathbb{R}^2$, $t \mapsto \phi(t, \xi)$ is the solution of (2.8) such that² $\phi(0, \xi) = \xi$.

Definition 2.14 ([149, Definition 8.1.1 and 8.1.2]). A point $\xi_0 \in \mathbb{R}^n$ is called an ω limit point of $\xi \in \mathbb{R}^n$, denoted by $\omega(\xi)$, if there exists a sequence $\{t_i\}$, $t_i \rightarrow \infty$, such that $\phi(t_i, \xi) \rightarrow \xi_0$. An α limit point is defined analogously by taking a sequence $\{t_i\}$ as $t_i \rightarrow -\infty$. The set of all ω limit points of a flow or map is called the ω limit set. The α limit set is defined analogously.

Theorem 2.15 ([149, Theorem 9.0.6]). *Let \mathcal{L} be a positively invariant region for the vector field in (2.8) containing a finite number of equilibrium points. Let $p \in \mathcal{L}$, and consider the ω limit set of p , denoted by $\omega(p)$. Then one of the following possibilities holds.*

1. $\omega(p)$ is an equilibrium point;
2. $\omega(p)$ is a closed orbit;

² For simplicity, suppose that solutions of (2.8) exist for all time; namely, solutions are *complete*. Then ϕ defines a one-parameter group expressed concisely as follows: $\phi(t+s, \xi) = \phi(t, \phi(s, \xi))$ for $t \geq 0, s \geq 0$. [25, Chapter 1.4].

3. $\omega(p)$ consists of a finite number of equilibrium points p_1, \dots, p_n and orbits γ with $\alpha(\gamma) = p_i$ and $\omega(\gamma) = p_j$, where $\alpha(\cdot)$ denotes the α limit set.

2.1.7 Index theorem

This subsection explains the index theorem based on [66].

Definition 2.16 (Poincaré index, [66, p. 68]). Consider the second-order autonomous system (2.8). Let C be a *simple closed* curve *not* passing through any equilibrium point of (2.8). Consider the orientation of the vector field $f(x)$ at a point $p \in C$. Letting p traverse C in the *counterclockwise* direction, the vector $f(x)$ rotates continuously and, upon returning to the original position, must have rotated an angle $2k\pi$ for some integer k , where the angle is measured *counterclockwise*. The integer k is called the *index* of the closed curve C . If C is chosen to encircle a single isolated equilibrium point \bar{x} , then k is called the *index* of \bar{x} .

Theorem 2.17 (Index theorem, [66, Lemma 2.3]).

1. The index of a node, a focus, or a center is +1.
2. The index of a (hyperbolic) saddle is -1.
3. The index of a closed orbit is +1.
4. The index of a closed curve not encircling any equilibrium point is 0.
5. The index of a closed curve is equal to the sum of the indices of the equilibrium points within it.

2.2 POINT-SET TOPOLOGY

This section presents some basic knowledge of point-set topology based on [101]. For more detailed discussion, one may refer to [101].

Definition 2.18 ([101, p. 76]). A *topology* on a set X is a collection \mathcal{T} of subsets of X satisfying the following properties:

1. \emptyset and X are in \mathcal{T} ;
2. Arbitrary unions of elements of \mathcal{T} are in \mathcal{T} ;
3. Finite intersections of elements of \mathcal{T} are in \mathcal{T} .

A set X for which a topology \mathcal{T} has been defined is called a *topological space*. A subset \mathcal{U} of X is called an *open set* of X if \mathcal{U} belongs to \mathcal{T} .

Definition 2.19 ([101, p. 88]). Let X be a topological space with topology \mathcal{T} . If Y is a subset of X , the collection $\mathcal{T}_Y := \{Y \cap U : U \in \mathcal{T}\}$ is a topology on Y , called the *subspace topology*. With this topology, Y is called a *subspace* of X .

Definition 2.20 ([101, p. 102]). Let X and Y be topological spaces. A function $f : X \rightarrow Y$ is *continuous* if for each open subset V of Y , the preimage $f^{-1}(V)$ is an open subset of X .

2.3 TOPOLOGICAL AND DIFFERENTIAL MANIFOLDS

Some basic concepts about topological and differential manifolds [76], [77], [107] are explained here.

Suppose \mathcal{X}, \mathcal{Y} are topological spaces. A *component* of \mathcal{X} is a maximal nonempty connected subset of \mathcal{X} (i.e., a nonempty connected subset that is not properly contained in any other connected subset of \mathcal{X}). A subset of \mathcal{X} is *precompact* in \mathcal{X} if its closure in \mathcal{X} is compact. A *homeomorphism* (*diffeomorphism* resp.) $f : \mathcal{X} \rightarrow \mathcal{Y}$ is a continuous (smooth resp.) bijection that has a continuous (smooth resp.) inverse. If there exists a homeomorphism between \mathcal{X} and \mathcal{Y} , then \mathcal{X} and \mathcal{Y} are *homeomorphic*, denoted by $\mathcal{X} \approx \mathcal{Y}$. If \mathcal{V} and \mathcal{W} are vector spaces, a bijective linear map $T : \mathcal{V} \rightarrow \mathcal{W}$ is called an *isomorphism*. If this isomorphism exists, then \mathcal{V} and \mathcal{W} are called *isomorphic*, denoted by $\mathcal{V} \cong \mathcal{W}$. An *open cover* of \mathcal{X} is a collection of open subsets of \mathcal{X} whose union is \mathcal{X} .

Let $f, g : \mathcal{X} \rightarrow \mathcal{Y}$ be continuous maps. A *homotopy* from f to g is a continuous map $H : \mathcal{X} \times [0, 1] \rightarrow \mathcal{Y}$ such that $H(x, 0) = f(x)$ and $H(x, 1) = g(x)$ for all $x \in \mathcal{X}$. If there exists such a homotopy, then f and g are *homotopic*, denoted by $f \simeq g$. Let $h : \mathcal{Y} \rightarrow \mathcal{X}$ be another continuous map. If $f \circ h \simeq \text{id}_{\mathcal{Y}}$ and $h \circ f \simeq \text{id}_{\mathcal{X}}$, where $\text{id}_{(\cdot)}$ is the identity map, then h is a *homotopy inverse* for f , and f is called a *homotopy equivalence*. In this case, \mathcal{X} is *homotopy equivalent* to \mathcal{Y} .

Let $\mathcal{A} \subseteq \mathcal{X}$. The *inclusion map* of \mathcal{A} in \mathcal{X} is $\iota_{\mathcal{A}} : \mathcal{A} \rightarrow \mathcal{X}$ defined by $\iota_{\mathcal{A}}(x) = x$ for $x \in \mathcal{A}$. A continuous map $r : \mathcal{X} \rightarrow \mathcal{A}$ is a *retraction* if the restriction of r to \mathcal{A} is the identity map of \mathcal{A} , or equivalently if $r \circ \iota_{\mathcal{A}} = \text{id}_{\mathcal{A}}$, where $\iota_{\mathcal{A}} : \mathcal{A} \rightarrow \mathcal{X}$ is the inclusion map and $\text{id}_{\mathcal{A}}$ is the identity map of \mathcal{A} . In this case, \mathcal{A} is called a *retract* of \mathcal{X} . Furthermore, if $\iota_{\mathcal{A}} \circ r$ is homotopic to the identity map of \mathcal{X} (i.e., $\iota_{\mathcal{A}} \circ r \simeq \text{id}_{\mathcal{X}}$), then r is a *deformation retraction* and \mathcal{A} is called a *deformation retract* of \mathcal{X} . Equivalently, \mathcal{A} is a deformation retract of \mathcal{X} if there exists a homotopy $H : \mathcal{X} \times [0, 1] \rightarrow \mathcal{X}$ that satisfies $H(x, 0) = x$, $H(x, 1) \in \mathcal{A}$ for all $x \in \mathcal{X}$ and $H(a, 1) = a$ for all $a \in \mathcal{A}$. In addition, if the homotopy H is stationary on \mathcal{A} ; that is, the last equation is replaced by $H(a, t) = a$ for all $a \in \mathcal{A}$ and all $t \in [0, 1]$, then r is a *strong deformation retraction* and \mathcal{A} is called a *strong deformation retract* of \mathcal{X} . The space \mathcal{X} is called *contractible* if the identity map of \mathcal{X} is homotopic to a constant map, or equivalently, if any point of \mathcal{X} is a deformation retract of \mathcal{X} .

Intuitively, this means that the whole space \mathcal{X} can be continuously shrunk to a point.

Let \mathcal{M} and \mathcal{N} be smooth manifolds. A (*coordinate*) *chart on \mathcal{M}* is a pair (\mathcal{U}, φ) , where the *coordinate neighborhood* \mathcal{U} is an open subset of \mathcal{M} and the (*local*) *coordinate map* $\varphi : \mathcal{U} \rightarrow \hat{\mathcal{U}} \subseteq \mathbb{R}^n$ is a homeomorphism for some integer n . The component functions of φ are called *local coordinates on \mathcal{U}* . The *tangent space* $T_p\mathcal{M}$ to \mathcal{M} at $p \in \mathcal{M}$ is a vector space consisting of maps (called *derivations*) $X_p : C^\infty(p) \rightarrow \mathbb{R}$ which satisfy the linearity and product rules, where $C^\infty(p)$ is the set of smooth real-valued functions defined on an open neighborhood of p . Other alternative definitions of the tangent space are summarized in [77, pp. 71-73]. Given a sufficiently smooth map $F : \mathcal{M} \rightarrow \mathcal{N}$, the *tangent (or differential) map of F at $p \in \mathcal{M}$* is denoted by $F_{*p} : T_p\mathcal{M} \rightarrow T_{F(p)}\mathcal{N}$ and satisfies $F_{*p}(X_p)(f) = X_p(f \circ F)$ for $X_p \in T_p\mathcal{M}$ and $f \in C^\infty(F(p))$. The notation F_{*p} is used interchangeably with dF_p or $dF|_p$. If the subscript p is omitted, then it is a map $F_* : T\mathcal{M} \rightarrow T\mathcal{N}$ defined at any $p \in \mathcal{M}$, where the *tangent bundle* $T\mathcal{M}$ is the disjoint union of the tangent spaces at all points of \mathcal{M} (i.e., $T\mathcal{M} := \coprod_{p \in \mathcal{M}} T_p\mathcal{M}$), and $T\mathcal{N}$ is defined analogously. The map F is a *submersion on \mathcal{M}* if for any $p \in \mathcal{M}$, the tangent map F_{*p} at p is surjective. If the tangent map F_{*p} at p is surjective, then p is called a *regular point* of F . If for every $p \in F^{-1}(q)$, the tangent map F_{*p} at p is surjective, then $q \in \mathcal{N}$ is called a *regular value* of F . The definition of a tubular neighborhood is in [77, pp. 137-139], and that of an embedded submanifold is in [77, pp. 98-99]. For an introduction to *fundamental groups* and homomorphisms of fundamental groups induced by continuous maps, see [76, Chapter 7].

Part I

THEORETICAL FOUNDATION

3

VANISHING LEVEL VALUE AND CONVERGENCE TO ZERO-LEVEL SET

In the vector-field guided path-following problem, the desired path is described by the zero-level set of a sufficiently smooth real-valued function and to follow this path, a (guiding) vector field is designed, which is not the gradient of any potential function. The value of the aforementioned real-valued function at any point in the ambient space is called the *level value* at this point. In this chapter, we show that the vanishing of the level value does not necessarily imply the convergence of a trajectory to the zero-level set, while additional conditions or assumptions identified in the chapter are needed to make this implication hold. The results in this chapter, although obtained in the context of the vector-field guided path-following problem, are widely applicable in many control problems, where the desired sets to converge to (in particular, a singleton constituting a desired equilibrium point) form the zero-level set of a Lyapunov(-like) function, and the system is not necessarily a gradient system.

This chapter is based on

- W. Yao, B. Lin, B. D. O. Anderson, and M. Cao, “Refining dichotomy convergence in vector-field guided path following control,” in *European Control Conference (ECC)*, 2021.

3.1 INTRODUCTION

Although equilibrium points of a dynamical system have often been the subject of study in the control literature, it is important to recognize that the convergence of trajectories of a dynamical system to a *closed invariant set* is also of intense research interest in many control problems, which include the geometric path-following problem [50], [74], [104] and the formation maneuvering problem [33], [143]. Note in particular that in the path-following problem, the trajectories of a system are required to converge to and traverse along a desired path, which is usually a geometric object like a closed curve rather than an equilibrium point [121], [137].

The closed invariant set can sometimes be described by the zero-level set of a continuous real-valued non-negative function, such as a Lyapunov(-like) function [59] or (the norm of) an error signal, while convergence of trajectories to the set is usually characterized by the distance of points on a trajectory to the set with respect to a metric (e.g., the Euclidean metric) [11], [54], [63], [66]. For convenience, such a continuous non-negative function is referred to as the *level function* and its value at a point is called the point's *level value*. Therefore, one natural idea is to use the level value, instead of the distance to the set, along a system trajectory to characterize the convergence to the zero-level set. This idea is utilized in vector-field guided path-following algorithms [50], [63], [74], [157], [161], and in some applications of Barbalat's lemma (e.g., Lemma 2.7, Theorem 2.8, [74, Theorem 1], [50, Theorem 1]). Now a central set-theoretic issue is whether the vanishing of the level value entails the convergence to the zero-level set of the level function: as clarified by examples later, a trajectory might diverge to infinity and the associated level value can still converge to zero. An associated issue arises from the fact that convergence with respect to a topology is a stronger notion than that with respect to a metric, while the former is relatively less studied in the control literature. This stronger notion is especially needed when a system evolves in some topological space rather than a Euclidean space, or when there are different metrics in a metric space but a metric-independent convergence result is required.

Contributions: In this chapter, we discuss the relationship between vanishing of the level value and the convergence of trajectories to the zero-level set. This issue is motivated by, but independent of, the vector-field guided path-following scenario. We show that as the level value evaluated at an infinite sequence of points converges to zero, this sequence might not converge to the (possibly compact) zero-level set in the Euclidean space. Specifically, we prove that the sequence converges (with respect to a topology) to the union of the zero-level set and infinity. This result is of interest in many control problems where the desired set forms the zero-level set of a Lyapunov(-like) function or (the norm of) an error signal. Additional conditions or assumptions are suggested such that the vanishing of the level value does imply the convergence to the zero-level set,

which is the intuitive idea behind many of the results in the literature (e.g., [32], [50], [63], [74], [157]).

The rest of the chapter is organized as follows. Section 3.2 introduces the vector-field guided path-following problem and formulate the problem. Then the main results are presented in Section 3.3. Finally, Section 3.4 concludes the chapter.

3.2 BACKGROUND AND PROBLEM FORMULATION

In the vector-field guided path-following problem, the desired path \mathcal{P} is a set-theoretic object in \mathbb{R}^n , and it is the intersection of several hyper-surfaces described by the zero-level sets of sufficiently smooth functions [24], [28], [36], [50], [89], [98], [119], [156], [157]:

$$\mathcal{P} = \{\xi \in \mathbb{R}^n : \phi_i(\xi) = 0, i = 1, \dots, n - 1\}, \quad (3.1)$$

where $\phi_i : \mathbb{R}^n \rightarrow \mathbb{R}$ are twice continuously differentiable functions. Some conditions will be adopted in subsequent chapters to ensure that the ϕ_i functions define a genuine path \mathcal{P} , but now we only need to treat \mathcal{P} as a non-empty set-theoretic object. Let $f = \|(\phi_1, \dots, \phi_{n-1})\|$, then \mathcal{P} is the zero-level set of f ; i.e., $\mathcal{P} = f^{-1}(0)$. For convenience, we call the non-negative real-valued function f the *level function*, and for any point $\xi \in \mathbb{R}^n$, the value $f(\xi)$ is called the *level value* of f at the point ξ . Since $f(\xi) = 0 \iff (\phi_1(\xi), \dots, \phi_{n-1}(\xi)) = \mathbf{0} \iff \xi \in \mathcal{P}$ for a point $\xi \in \mathbb{R}^n$, one may use $f(\xi) = \|(\phi_1(\xi), \dots, \phi_{n-1}(\xi))\|$ to roughly represent the distance from a point ξ to the desired path \mathcal{P} . The following question arises naturally:

Q1. Suppose $f(\xi(t)) = \|(\phi_1(\xi(t)), \dots, \phi_{n-1}(\xi(t)))\| \rightarrow 0$ as $t \rightarrow \infty$ along a continuous trajectory $\xi(t)$ defined on $[0, \infty)$, which can be an arbitrary continuous function or a trajectory of an autonomous system. Does it hold that the trajectory $\xi(t)$ will converge to the set \mathcal{P} with respect to a metric or a topology (called *metrical convergence* and *topological convergence* respectively, and to be discussed later)?

Note that this question **Q1** does *not* depend on the path-following setting, but is relevant to any problem where a set is described by the zero-level set of a level function, and the convergence to the set is an indispensable requirement of the problem. For **Q1**, one might be inclined to give a positive answer based on intuition, but as shown later, the answer is negative even if the set \mathcal{P} is compact.

3.3 MAIN RESULTS

3.3.1 Preliminaries

Suppose (\mathcal{M}, d) is a metric space with a metric d , and its topology is induced by the metric d . An (open) neighborhood of $\mathcal{A} \subseteq \mathcal{M}$ is an open set $\mathcal{U} \subseteq \mathcal{M}$ such that $\mathcal{A} \subseteq \mathcal{U}$. An ϵ -neighborhood \mathcal{U}_ϵ of $\mathcal{A} \subseteq \mathcal{M}$, where $\epsilon > 0$ is a constant, is an open neighborhood of \mathcal{A} defined by $\mathcal{U}_\epsilon := \{p \in \mathcal{M} : \text{dist}(p, \mathcal{A}) < \epsilon\}$. Note that an ϵ -neighborhood is an open neighborhood, but the converse is not necessarily true. In particular, there can exist an open neighborhood \mathcal{U} such that no ϵ -neighborhood \mathcal{U}_ϵ is a subset of \mathcal{U} . For example, let \mathcal{A} be the x -axis in the plane; i.e., $\mathcal{A} = \{(x, 0) \in \mathbb{R}^2 : x \in \mathbb{R}\}$ and choose an open neighborhood of \mathcal{A} as $\mathcal{U} = \{(x, y) \in \mathbb{R}^2 : x \in \mathbb{R}, |y| < \exp(-x)\}$ (see Fig. 3.1). Intuitively, the neighborhood \mathcal{U} is “shrinking” infinitely close to the set \mathcal{A} as x increases. Then there does not exist an $\epsilon > 0$ such that $\mathcal{U}_\epsilon \subseteq \mathcal{U}$. However, as will be shown in Lemma 3.2, if \mathcal{A} is compact, then (unsurprisingly perhaps) for any open neighborhood of \mathcal{A} , there always exists an epsilon neighborhood \mathcal{U}_ϵ that is a subset of \mathcal{U} .

3.3.2 Metrical convergence and topological convergence

Suppose (\mathcal{M}, d) is a metric space with a metric d . One can regard \mathcal{M} as a topological space with the topology induced by its metric d . Suppose a set $\mathcal{A} \subseteq \mathcal{M}$, called the *desired set*, is a level set of a function $g : \mathcal{M} \rightarrow \mathbb{R}^n$; that is, $\mathcal{A} = g^{-1}(\mathbf{c})$ for some constant $\mathbf{c} \in \mathbb{R}^n$. One can define a (non-negative) *level function* $e(\cdot) = \|g(\cdot) - \mathbf{c}\|$, where $\|\cdot\| = \sqrt{d(\cdot, \cdot)}$, such that $\mathcal{A} = e^{-1}(0)$. Namely, \mathcal{A} is the zero-level set of the level function e . Therefore, every point in the desired set \mathcal{A} renders the level value $e = 0$. When we consider convergence to a set, it is important to clarify if this convergence is with respect to a metric or a topology, which correspond to the notions *metrical convergence* and *topological convergence* respectively defined below.

Definition 3.1 (Metrical and topological convergence). Consider a metric space (\mathcal{M}, d) and the topology induced by the metric d . Suppose $\mathcal{A} \subseteq \mathcal{M}$ is a closed and nonempty set, and let $(\xi_i)_{i=0}^\infty \in \mathcal{M}$ be an infinite sequence of points. The sequence converges to \mathcal{A} *metrically* if for any $\epsilon > 0$, there exists $I > 0$ such that $\xi_i (i \geq I) \subseteq \mathcal{U}_\epsilon$ (or equivalently, $\text{dist}(\xi_i, \mathcal{A}) \leq \epsilon$ for $i \geq I$), where $\xi_i (i \geq I) := \{\xi_i \in \mathcal{M} : i \geq I\}$. The sequence $(\xi_i)_{i=0}^\infty$ converges to \mathcal{A} *topologically* if for any open neighborhood \mathcal{U} of \mathcal{A} , there exists $I' > 0$ such that $\xi_i (i \geq I') \subseteq \mathcal{U}$.

In the sequel, we will clarify the relationship between level value convergence (to a constant), metrical convergence (to a set) and topological convergence (to a set). The notion of metrical convergence has been used in many, if not most,

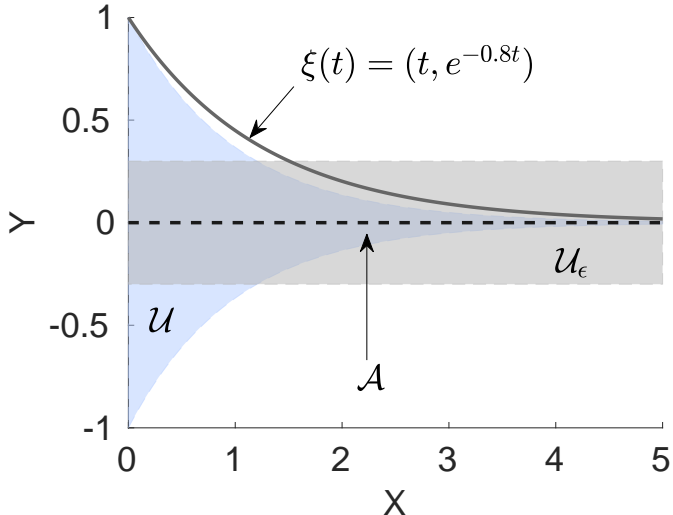


Figure 3.1: The non-compact desired set $\mathcal{A} \subseteq \mathbb{R}^2$ is the x -axis, $\mathcal{U} = \{(x, y) \in \mathbb{R}^2 : |y| < \exp(-x)\}$ is an open neighborhood of \mathcal{A} and \mathcal{U}_ϵ is an ϵ -neighborhood of \mathcal{A} for $\epsilon = 0.3$. It is obvious that there does not exist an $\epsilon > 0$ such that $\mathcal{U}_\epsilon \subseteq \mathcal{U}$. Also note that the continuous trajectory $\xi(t) = (t, \exp(-0.8t))$ converges metrically but *not* topologically to the desired set \mathcal{A} , since $\text{dist}(\xi(t), \mathcal{A}) \rightarrow 0$ as $t \rightarrow \infty$ but $\xi(t) \notin \mathcal{U}$ for sufficiently large $t > 0$.

of the control-related textbooks (e.g., [11], [54], [66], [124]). However, the notion of topological convergence is more general and is necessary when a topological space is considered, or when there are different metrics to choose but one wants the convergence results to be independent of which metric to use. From the definition, if a trajectory converges topologically to the desired set \mathcal{A} , then it also converges to \mathcal{A} metrically, but the converse is not true in general (see Fig. 3.1). Nevertheless, if the set \mathcal{A} is compact, then metrical convergence also implies topological convergence. To prove this, we first present the following lemma, which is a standard result in topology (see [101, p.177, Exercise 2(d)]). For completeness, we present a brief proof.

Lemma 3.2. *Let \mathcal{A} be nonempty and compact in the metric space (\mathcal{M}, d) . For any open neighborhood \mathcal{U} of \mathcal{A} , there exists an ϵ -neighborhood \mathcal{U}_ϵ of \mathcal{A} , such that $\mathcal{U}_\epsilon \subseteq \mathcal{U}$.*

Proof. Since \mathcal{U} is an open neighborhood of \mathcal{A} , the complement $\mathcal{K} = \mathcal{M} \setminus \mathcal{U}$ is closed in \mathcal{M} . Define a function $f : \mathcal{A} \rightarrow \mathbb{R}_{\geq 0}$ by $f(x) = \text{dist}(x, \mathcal{K})$, which is continuous with respect to x . Since $x \notin \mathcal{K}$ and \mathcal{K} is closed, we have $f(x) > 0$ for any $x \in \mathcal{A}$. Since \mathcal{A} is compact, f has a positive lower bound on \mathcal{A} ; that is, there exists a positive constant δ such that $f(x) = \text{dist}(x, \mathcal{K}) \geq \delta$. Let $\epsilon = \delta/2$, then it is obvious that the epsilon neighborhood $\mathcal{U}_\epsilon \cap \mathcal{K} = \emptyset$, and it follows that $\mathcal{U}_\epsilon \subseteq \mathcal{U}$. \square

We can now prove the following proposition.

Proposition 3.3. *Suppose the desired set \mathcal{A} is nonempty and compact. Then an infinite sequence of points converges metrically to the desired set \mathcal{A} if and only if it converges topologically to \mathcal{A} .*

Proof. If a sequence of points converges topologically to \mathcal{A} , then it is obvious that it converges metrically to \mathcal{A} . Now we prove the necessity. For any open neighborhood \mathcal{U} of \mathcal{A} , there exists an epsilon neighborhood $\mathcal{U}_\epsilon \subseteq \mathcal{U}$ from Lemma 3.2. Since the sequence $(\xi_i)_{i=0}^\infty$ converges metrically to \mathcal{A} , there exists $I > 0$, such that $\xi_i (i \geq I) \subseteq \mathcal{U}_\epsilon \subseteq \mathcal{U}$. \square

In much of the literature, an isolated equilibrium point of a system is studied, often taken as the origin for convenience, and thus in these cases, the desired set $\mathcal{A} = \{\mathbf{0}\}$ is a singleton, which is obviously compact in the Euclidean space \mathbb{R}^n . Therefore, metrical convergence automatically implies the stronger notion of topological convergence, and the existing results about convergence can directly be applied to general topological spaces. However, in the study of, e.g., path-following control, the desired set is usually not a singleton. If the desired set is non-compact, then it is necessary to clarify which convergence notions are used¹.

For simplicity, we mostly consider Euclidean space in the sequel. *If we do not specify which convergence notion we use throughout the thesis, then by default it is the metrical convergence, but the notion of topological convergence will still be used wherever this stronger notion is applicable.*

Perhaps surprisingly, the convergence of the level value to zero for an infinite sequence of points in \mathcal{M} does *not* imply that the sequence converges (metrically or topologically) to the desired set \mathcal{A} . As shown later, the sequence may even converge to infinity, even if the desired set \mathcal{A} is compact in \mathcal{M} . Before proceeding to this result, we clarify the meaning of a sequence converging to ∞ or $\mathcal{A} \cup \{\infty\}$, where \mathcal{A} is a nonempty set, in the following definition.

Definition 3.4. Consider a metric space (\mathcal{M}, d) and a nonempty closed subset $\mathcal{A} \subseteq \mathcal{M}$. A sequence $(x_i)_{i \in \mathbb{N}} \in \mathcal{M}$ converges *metrically* to ∞ if for any $b > 0$, there exists $N \geq 0$, such that $\|x_i\| = \sqrt{d(x_i, x_i)} > b$ for $i \geq N$. Consider the topology induced by the metric d , then $(x_i)_{i \in \mathbb{N}} \in \mathcal{M}$ converges *topologically* to ∞ if for any compact set \mathcal{U} in \mathcal{M} , there exists $N \geq 0$, such that $x_i \in \mathcal{M} \setminus \mathcal{U}$ for $i \geq N$. The sequence converges *metrically (topologically)* to $\mathcal{A} \cup \{\infty\}$ if there exists a subsequence $(x_{i_k})_{k \in \mathbb{N}}$ of $(x_i)_{i \in \mathbb{N}}$ such that the subsequence $(x_{i_k})_{k \in \mathbb{N}}$ converges *metrically (topologically)* to \mathcal{A} or ∞ .

The sequence in Definition 3.4 can analogously be replaced by a continuous trajectory. This definition is motivated by the *one-point compactification* of \mathcal{M}

¹ One can similarly define stability with respect to a metric or a topology (e.g. , Definition 5.16).

that is used in the proofs of Theorems 3.6 and 3.7. To ensure that the one-point compactification of \mathcal{M} exists², we impose the following assumption:

Assumption 3.5. The metric space \mathcal{M} is *locally compact*³.

This assumption is satisfied if \mathcal{M} is a smooth manifold or a Euclidean space \mathbb{R}^n for some $n \in \mathbb{N}$. Theorem 3.6 follows.

Theorem 3.6. Define the (closed) set $\mathcal{A} := \{\xi \in \mathcal{M} : \|\phi(\xi)\| = 0\}$, where $\phi : \mathcal{M} \rightarrow \mathbb{R}^m$ is a continuous function and $m \in \mathbb{N}$. If $(\xi_i)_{i=0}^\infty \in \mathcal{M}$ is an infinite sequence of points such that $\|\phi(\xi_i)\| \rightarrow 0$ as $i \rightarrow \infty$, then the sequence converges topologically to the set $\mathcal{B} := \mathcal{A} \cup \{\infty\}$ as $i \rightarrow \infty$.

Proof. The closedness of \mathcal{A} in \mathcal{M} is due to the continuity of $\|\phi\|$ and the closedness of $\{0\} \subseteq \mathbb{R}$. We can consider the problem in the one-point compactification [101, p. 185] of \mathcal{M} . In other words, \mathcal{M} can be embedded in a compact Hausdorff space \mathcal{N} , and ∞ is regarded as a particular point, denoted by p , in \mathcal{N} . Let this embedding be denoted by $f : \mathcal{M} \rightarrow \mathcal{N} \setminus \{p\}$. We prove by contradiction. Suppose the sequence $(\xi_i)_{i=0}^\infty$ does not converge topologically to the set $\mathcal{B} = \mathcal{A} \cup \{\infty\}$, then the sequence $(\zeta_i)_{i=0}^\infty$, where $\zeta_i = f(\xi_i) \in \mathcal{N}$, does not converge topologically to the set $\mathcal{B}' := f(\mathcal{A}) \cup \{p\} \subseteq \mathcal{N}$. Therefore, there exists an open neighborhood $\mathcal{U} \subseteq \mathcal{N}$ of \mathcal{B}' and a subsequence $(\zeta_{i_k})_{k=0}^\infty$ of $(\zeta_i)_{i=0}^\infty$ such that $\zeta_{i_k} \notin \mathcal{U}$ for all $k \geq 0$. Since \mathcal{N} is sequentially compact [101, p. 179], the sequence $(\zeta_{i_k})_{k=0}^\infty$ has a convergent subsequence $(\zeta_{i_{k_l}})_{l=0}^\infty$, which converges to a point $\zeta' \in \overline{\mathcal{N} \setminus \mathcal{U}}$, where $\overline{(\cdot)}$ represents the closure of a set. Now turn to the original metric space \mathcal{M} . This means that the corresponding subsequence $(\xi_{i_{k_l}})_{l=0}^\infty$ converges to a point $\xi' \in f^{-1}(\overline{\mathcal{N} \setminus \mathcal{U}}) \subseteq \mathcal{M} \setminus \mathcal{B}$. Since ϕ is continuous, we have $\phi(\xi') = \lim_{l \rightarrow \infty} \phi(\xi_{i_{k_l}}) = \lim_{i \rightarrow \infty} \phi(\xi_i) = 0$, which implies that $\xi' \in \mathcal{A} \subseteq \mathcal{B}$. But this is a contradiction since $(\mathcal{M} \setminus \mathcal{B}) \cap \mathcal{B} = \emptyset$. \square

Note that the sequence converging topologically to the set $\mathcal{B} := \mathcal{A} \cup \{\infty\}$ implies four mutually exclusive possibilities: 1) The sequence converges to \mathcal{A} ; 2) The sequence converges to ∞ ; 3) The sequence converges to both \mathcal{A} and ∞ (in which case the set \mathcal{A} is unbounded); 4) The sequence converges neither to \mathcal{A} nor ∞ . The fourth case happens if the sequence has a subsequence converging to \mathcal{A} and another subsequence converging to ∞ , but the whole sequence is not convergent. However, if the set \mathcal{A} is compact and a continuous trajectory is considered, then only the first two cases are possible, as shown in the following theorem.

² There always exists the one-point compactification of a locally compact Hausdorff space [101, Chapter 3, Section 29].

³ The space \mathcal{M} is *locally compact* at $x \in \mathcal{M}$ if there is a compact subspace $\mathcal{N} \subseteq \mathcal{M}$ that contains a neighborhood of x . If \mathcal{M} is locally compact at every point, then \mathcal{M} is said to be locally compact.

Theorem 3.7. Define the (closed) set $\mathcal{A} := \{\xi \in \mathcal{M} : \|\phi(\xi)\| = 0\}$, where $\phi : \mathcal{M} \rightarrow \mathbb{R}^m$ is continuous and $m \in \mathbb{N}$. If \mathcal{A} is compact, and $\xi : \mathbb{R}_{\geq 0} \rightarrow \mathcal{M}$ is continuous and $\|\phi(\xi(t))\| \rightarrow 0$ as $t \rightarrow \infty$, then $\xi(t)$ converges topologically to the set \mathcal{A} or to ∞ exclusively as $t \rightarrow \infty$.

To prove this theorem, we need Lemma 3.8 below. This lemma extends [156, Lemma 7] as it considers a general metric space and the topological convergence instead of a Euclidean space and the metrical convergence.

Lemma 3.8. Consider a metric space (\mathcal{M}, d) , where d is a metric. Define two nonempty sets $\mathcal{A}_1, \mathcal{A}_2 \subseteq \mathcal{M}$ such that $\text{dist}(\mathcal{A}_1, \mathcal{A}_2) > 0$, and let $\mathcal{D} := \mathcal{A}_1 \cup \mathcal{A}_2$. If a continuous trajectory $p : \mathbb{R}_{\geq 0} \rightarrow \mathcal{M}$ converges topologically to \mathcal{D} as $t \rightarrow \infty$, then $p(t)$ converges topologically to either \mathcal{A}_1 or \mathcal{A}_2 exclusively as $t \rightarrow \infty$.

Proof of Lemma 3.8. Suppose $\text{dist}(\mathcal{A}_1, \mathcal{A}_2) = \beta > 0$. First, it is obvious that the continuous trajectory $p(t)$ cannot converge to both \mathcal{A}_1 and \mathcal{A}_2 simultaneously. Now we show that $p(t)$ converges to either \mathcal{A}_1 or \mathcal{A}_2 exclusively. We can let $\epsilon = \beta/4$, implying that the ϵ -neighborhoods \mathcal{U}_ϵ of \mathcal{A}_1 and \mathcal{V}_ϵ of \mathcal{A}_2 satisfy $\text{dist}(\mathcal{U}_\epsilon, \mathcal{V}_\epsilon) > 2\epsilon$. Also note that $\mathcal{W}_\epsilon := \mathcal{U}_\epsilon \cup \mathcal{V}_\epsilon$ is the ϵ -neighborhood of $\mathcal{D} = \mathcal{A}_1 \cup \mathcal{A}_2$, and \mathcal{W}_ϵ is a disconnected set. Since the continuous trajectory $p(t)$ converges topologically to \mathcal{D} , there exists $T > 0$ such that $p(t \geq T) \subseteq \mathcal{W}_\epsilon = \mathcal{U}_\epsilon \cup \mathcal{V}_\epsilon$. If $p(t = T) \in \mathcal{U}_\epsilon$, then due to the continuity of $p(t)$ and $\text{dist}(\mathcal{U}_\epsilon, \mathcal{V}_\epsilon) > 2\epsilon$, there holds $\xi(t \geq T) \subseteq \mathcal{U}_\epsilon$, and thereby $p(t)$ converges topologically to \mathcal{A}_1 . The same argument applies to the case where $p(t = T) \in \mathcal{V}_\epsilon$. Therefore, $p(t)$ converges topologically to either \mathcal{A}_1 or \mathcal{A}_2 exclusively as $t \rightarrow \infty$, dependent on the initial condition. \square

Proof of Theorem 3.7. As in the proof in Theorem 3.6, we consider the one-point compactification [101, p. 185] of \mathcal{M} . Thus, \mathcal{M} can be embedded in the compact space \mathcal{N} , and ∞ is regarded as a point p in \mathcal{N} . Let this embedding be denoted by $f : \mathcal{M} \rightarrow \mathcal{N} \setminus \{p\}$. Since \mathcal{A} is compact, the image $\mathcal{A}' = f(\mathcal{A}) \subseteq \mathcal{N}$ is also compact, and it is obvious that⁴ $\text{dist}(\mathcal{A}', p) > 0$. According to Theorem 3.6, $\xi(t)$ converges topologically to $\mathcal{A} \cup \{\infty\}$ as $t \rightarrow \infty$. Therefore, $\zeta(t) = f(\xi(t)) \in \mathcal{N}$ converges topologically to $\mathcal{D} := \mathcal{A}' \cup \{p\}$ as $t \rightarrow \infty$. According to Lemma 3.8, $\zeta(t)$ converges topologically to either \mathcal{A}' or $\{p\}$ exclusively as $t \rightarrow \infty$. Turn to the original metric space \mathcal{M} ; then this implies that $\xi(t)$ converges topologically to \mathcal{A} or ∞ exclusively as $t \rightarrow \infty$. \square

Note that Theorem 3.6 is independent of whether the desired set \mathcal{A} is compact or not, and it does *not* depend on the path-following setting either, but for convenience, we use path-following examples to illustrate the result of convergence to ∞ permitted in Theorem 3.6. One example is presented in Example 5.8 in

⁴ The conclusion that $\text{dist}(\mathcal{A}', p) > 0$ is independent of which metric one chooses. This is because in a metric space, there is always a positive distance between any two disjoint nonempty compact sets (see, e.g., [136, Lemma 3.1]).

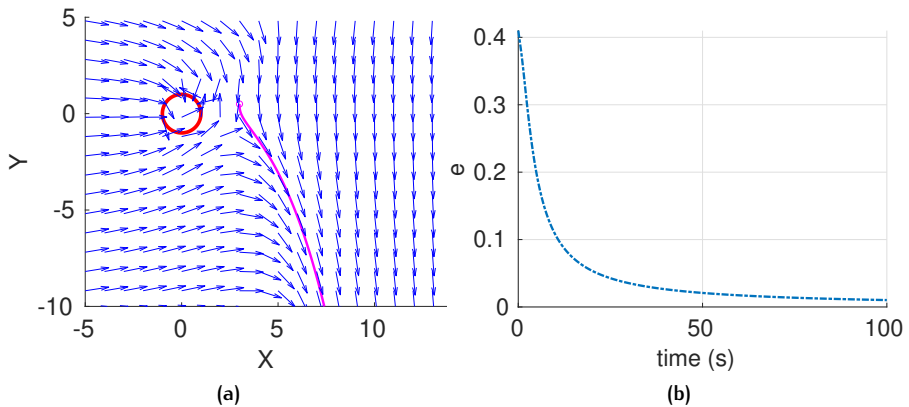


Figure 3.2: The desired set \mathcal{A} is a unit circle illustrated by a red curve in (a), and in this subfigure, the arrows represent the *normalized* vector field computed by (1.2). Although the level value $e = \phi = (x^2 + y^2 - 1) \exp(-x)$ converges to 0 in (b), the trajectory given by the magenta curve in (a) escapes to infinity.

Chapter 5 where the desired set \mathcal{A} (i.e., the desired path \mathcal{P}) is non-compact and a trajectory converges to infinity even when the level value converges to 0. A perhaps more surprising example is when the desired set \mathcal{A} is a compact set as in the following example.

Example 3.9. Suppose the desired set \mathcal{A} (i.e., the desired path \mathcal{P}) is a unit circle, which is obviously compact. The ϕ function to describe the desired set $\mathcal{A} = \mathcal{P}$ is chosen as $\phi(x, y) = (x^2 + y^2 - 1) \exp(-x)$ in (3.1), where $n = 2$, and the vector field is constructed as in (1.2). As illustrated in Fig. 3.2, even though the level value $e = \phi$ converges to 0, the trajectory does not converge to the circle but rather escapes to infinity. This undesirable behavior does not appear if $\exp(-x)$ is removed from ϕ (see Remarks 3.11 and 3.14 for a “good” choice of ϕ). Note that since the desired path is compact, it is proved in Proposition 4.8 in Chapter 4 that if a trajectory starts *sufficiently close* to the desired path, it will converge to the desired path or the singular set, regardless of the relationship between the level value and the level function. \triangleleft

Remark 3.10. Besides the theoretical interest in its own right, the importance of Theorem 3.6 is also due to its close relevance to many control problems where an error signal $e : \mathbb{R}^n \rightarrow \mathbb{R}^m$ is defined and the system's desired states correspond to $\|e\| = 0$; namely, if $f(x) = \|e(x)\|$, then the system's desired states form the zero-level set $f^{-1}(0)$. Often, a Lyapunov or Lyapunov-like function V which takes the error signal as the argument is involved, and a typical case is the quadratic form $V(e) = e^\top Pe$, where $P \in \mathbb{R}^{m \times m}$ is a positive definite matrix. Therefore, the desired states (e.g., an equilibrium of the system) form the zero-level set $V^{-1}(0)$ of V . In general, as shown by Theorem 3.6, the Lyapunov function value

$V \rightarrow 0 \implies \|e\| \rightarrow 0$ along the system trajectory does not necessarily mean that the trajectory will converge to the desired states $V^{-1}(0) = e^{-1}(\mathbf{0})$, since the trajectory might also diverge to infinity. Nevertheless, as shown in many control textbooks (e.g., [66], [124]), the desired state is often an equilibrium point (i.e., $V^{-1}(0) = e^{-1}(\mathbf{0}) = \{\mathbf{0}\}$), and extra detailed analysis (e.g., [66, Theorem 4.1]) guarantees that once a trajectory starts close enough to the equilibrium point, the trajectory will stay in a compact set containing the equilibrium point, and thus the possibility of divergence to infinity is excluded. However, if the desired states form a non-compact set, then it is more involved to exclude this divergence possibility, or extra assumptions are necessary.

Theorem 3.6 is also relevant when the desired set convergence is proved by using Barbalat's lemma (e.g., Lemma 2.7, [133, Lemma 4.2]). Take Theorem 2.8 as an example, which is an invariance-like theorem for non-autonomous systems. This theorem states that under some conditions, we have $W(x(t)) \rightarrow 0$ and hence $x(t) \rightarrow W^{-1}(0)$, where $x(t)$ is a trajectory of a non-autonomous system $\dot{x}(t) = f(t, x)$ and $W(\cdot)$ is a continuous positive semidefinite function. This does not contradict Theorem 3.6 because the assumptions in Theorem 2.8 guarantee that the trajectory $x(t)$ is bounded. \triangleleft

Remark 3.11. Theorem 3.6 gives a negative answer to **Q1**. If the desired set \mathcal{A} is compact, to exclude the possibility of trajectories escaping to infinity such that $\|\phi(\xi_i)\| \rightarrow 0$ implies topological convergence to \mathcal{A} , one may retreat to one of the following two strategies:

1) Prove that trajectories are bounded. For example, one can find a Lyapunov-like function V and a compact set $\Omega_\alpha := \{x : V(x) \leq \alpha\}$, and prove that $\dot{V} \leq 0$ in this compact set Ω_α . One might also retreat to the LaSalle's invariance principle (Theorem 2.6).

2) Modify $\phi(\cdot)$, if feasible, such that $\|\phi(x)\|$ tends to a non-zero constant (possibly infinity) as $\|x\|$ tends to infinity. In other words, $\phi(\cdot)$ is modified to be *radially non-vanishing*.

Furthermore, regardless of whether the desired set \mathcal{A} is compact or not, one could impose the verifiable assumption introduced in Lemma 3.12 below. \triangleleft

3.3.3 Convergence characterized by different level functions

The following result is a generalization of [156, Lemma 5].

Lemma 3.12. *Suppose there are two non-negative continuous functions $h_i : \mathcal{M} \rightarrow \mathbb{R}_{\geq 0}$, $i = 1, 2$. If for any given constant $\kappa > 0$, it holds that*

$$\inf\{h_1(p) : p \in \mathcal{M}, h_2(p) \geq \kappa\} > 0, \quad (3.2)$$

then there holds

$$\lim_{k \rightarrow \infty} h_1(p_k) = 0 \implies \lim_{k \rightarrow \infty} h_2(p_k) = 0,$$

where $(p_k)_{k=1}^\infty$ is an infinite sequence of points in \mathcal{M} .

Proof. We prove this by contradiction. If $h_2(p_k)$ does not converge to 0 as $k \rightarrow \infty$, then

$$(\exists \epsilon > 0)(\forall L > 0)(\exists k' \geq L) h_2(p_{k'}) \geq \epsilon. \quad (3.3)$$

Replacing κ by ϵ in the assumption of this theorem, we have

$$\inf\{h_1(p) : p \in \mathcal{M}, h_2(p) \geq \epsilon\} = \beta > 0, \quad (3.4)$$

where β is some positive constant. Since $\lim_{k \rightarrow \infty} h_1(p_k) = 0$, it follows that

$$(\exists L' > 0)(\forall k \geq L') h_1(p_k) < \beta. \quad (3.5)$$

Let L be chosen as L' in (3.3), then there exists $k' \geq L'$ such that $h_2(p_{k'}) \geq \epsilon$. Then due to (3.4), $h_1(p_{k'}) \geq \beta$, which contradicts (3.5). Therefore, $\lim_{k \rightarrow \infty} h_2(p_k) = 0$. \square

Based on Lemma 3.12 and Proposition 3.3, we have the following corollary, which is a specialization of Theorem 3.6.

Corollary 3.13. Suppose $\mathcal{A} := \{\xi \in \mathcal{M} : \|\phi(\xi)\| = 0\}$, where $\phi : \mathcal{M} \rightarrow \mathbb{R}^m$ is a continuous function. Let $h_1(\cdot) = \|\phi(\cdot)\|$ and $h_2 = \text{dist}(\cdot, \mathcal{A})$ in Lemma 3.12, and suppose the condition (3.2) holds. If $(\xi_i)_{i=0}^\infty$ is a sequence of points $\xi_i \in \mathcal{M}$ such that $\|\phi(\xi_i)\| \rightarrow 0$ as $i \rightarrow \infty$, then the sequence converges metrically to \mathcal{A} (i.e., $\text{dist}(\xi_i, \mathcal{A}) \rightarrow 0$). Moreover, if \mathcal{A} is compact, then the convergence is also topological.

Remark 3.14. One can verify that the ϕ function in Example 3.9 does not satisfy the condition in (3.2) with h_1 and h_2 defined as in Corollary 3.13, but the condition is met if the ϕ function is changed to $\phi(x, y) = x^2 + y^2 - 1$, and thus Corollary 3.13 holds. Note also that this modification renders ϕ radially non-vanishing. \triangleleft

Corollary 3.13 underpins some proposed assumptions in the subsequent chapters to facilitate the vector-field guided path-following algorithms.

3.4 CONCLUSIONS

This chapter is motivated by the recent interest in the vector-field guided path-following control problem, where one important issue is the convergence with respect to a metric or a topology to a compact or non-compact desired set. The desired set is the zero-level set of a non-negative continuous level function. We show that the convergence of the level value to zero does not necessarily imply the convergence of an infinite sequence of points to the compact or non-compact desired set. This result is closely related to many control problems, where the desired set is the zero-level set of a Lyapunov(-like) function.

4

PATH FOLLOWING CONTROL IN 3D USING A VECTOR FIELD

Using a designed vector field to control a mobile robot to follow a given desired path has found a range of practical applications, and it is in great need to further build a rigorous theory to guide its implementation. In this chapter, we study the properties of a general 3D vector field for robotic path following. We derive conditions under which the local path-following error vanishes exponentially in a sufficiently small neighborhood of the desired path, which is key to show the local input-to-state stability (local ISS) property of the path-following error dynamics. The local ISS property then justifies the control algorithm design for a fixed-wing aircraft model. Our approach is effective for any sufficiently smooth desired path in 3D, bounded or unbounded; the results are particularly relevant since unbounded desired paths have not been sufficiently discussed in the literature. Simulations are conducted to verify the theoretical results.

This chapter is based on

- W. Yao, Y. A. Kapitanyuk, and M. Cao, "Robotic path following in 3D using a guiding vector field," in *2018 IEEE 57th Conference on Decision and Control (CDC)*, IEEE, 2018, pp. 4475-4480.
- W. Yao and M. Cao, "Path following control in 3D using a vector field," *Automatica*, vol. 117, p. 108 957, 2020.

4.1 INTRODUCTION

There are already many existing methods for path following [9], [28], [37]. Notably, it is shown in [137] that vector-field guided path-following algorithms achieve the smallest cross-track error while they require the least control efforts among several tested algorithms. In this context, a (guiding) vector field is carefully designed such that its integral curves are proven to converge to and traverse the desired path.

Many of the vector-field guided path-following algorithms are only applicable to simple desired paths, such as circles and straight lines [104]. In addition, convergence to the desired path is often guaranteed locally in a small vicinity of the desired path. This is partly due to the fact that usually there are singular points¹ in the vector field. Recently, the work [63] analyzes in details the properties of a 2D vector field for any desired path that is sufficiently smooth.

The previous study [63], as well as many other existing works [31], [104], [137], only consider planar desired paths, while the 3D counterpart is less studied. In [50], given that the desired path is described by the intersection of several hyper-surfaces, a general vector field is proposed for robot navigation in the n -dimensional Euclidean space. However, strictly speaking, the analysis of this approach is only valid for (bounded) closed curves, such as circles, while the analysis cannot be directly applied to unbounded desired paths such as a straight line. Moreover, the assumption regarding the repulsiveness of the set of singular points is perhaps conservative. For example, this assumption is valid for a circle, but not for a Cassini oval or some other desired paths. In some literature, for ease of analysis, it is assumed that the workspace is free of singular points, but usually this is only guaranteed locally near the desired path.

In this chapter, we justify and employ a 3D guiding vector field for path following with rigorous analysis. Firstly, the convergence results and the maximal extensibility of solutions are analyzed rigorously. In addition, the conditions under which the local path-following error vanishes exponentially in a neighborhood of the desired path are provided, which is typically not available in the related literature. Secondly, we show the local input-to-state stability (ISS) of the path-following error dynamics, which justifies the control algorithm design for a nonholonomic model: a fixed-wing aircraft. In comparison to many methods which only consider standard paths such as circles and straight lines, our method is applicable to any 3D desired path that can be described by the intersection of the zero-level sets of two implicit functions. And we specifically analyze rigorously the case of unbounded desired paths. Note that the analysis for the 3D vector field in this chapter can be easily extended to any higher dimensional vector field (see Chapter 9).

¹ A point where a vector field becomes zero is called a *singular point* of the vector field [77, p. 219]. The set of singular points of a vector field is called the *singular set* of the vector field.

The rest of this chapter is organized as follows. Section 4.2 presents the problem formulation. Then the analysis of the proposed vector field and its normalized and perturbed counterparts are elaborated in Section 4.3 and 4.4 respectively. The control algorithm for a fixed-wing aircraft model is provided in Section 4.5. Finally, Section 4.7 concludes the chapter.

4.2 PROBLEM FORMULATION

Suppose the desired path \mathcal{P} is characterized by two functions $\phi_i : \mathbb{R}^3 \rightarrow \mathbb{R}, i = 1, 2$, which are twice continuously differentiable:

$$\mathcal{P} := \{\xi \in \mathbb{R}^3 : \phi_1(\xi) = 0, \phi_2(\xi) = 0\}. \quad (4.1)$$

It is natural to assume that \mathcal{P} is nonempty, connected and one-dimensional. We will further require the regularity of the desired path as stated later in Assumption 4.3. One of the advantages of definition (4.1) is that the vector field can be derived directly from the function $\phi_i(\cdot)$ independent of the specific parametrization of the path. Another advantage is that the distance between a point $\xi \in \mathbb{R}^3$ and the path $\text{dist}(\xi, \mathcal{P}) = \inf\{\|\xi - p\| : p \in \mathcal{P}\}$ can be approximated by the value of $\|(\phi_1(\xi), \phi_2(\xi))\|$ under some assumptions presented later.

The vector-field guided path-following problem is formally defined in Problem 1.1, where the manifold \mathcal{M} is changed to \mathbb{R}^3 .

4.2.1 The guiding vector field and assumptions

The 3D guiding vector field $\chi \in C^1 : \mathbb{R}^3 \rightarrow \mathbb{R}^3$ is as follows:

$$\chi(\xi) = n_1(\xi) \times n_2(\xi) - k_1 e_1(\xi) n_1(\xi) - k_2 e_2(\xi) n_2(\xi), \quad (4.2)$$

where $n_i(\xi) = \nabla \phi_i(\xi)$ is the gradient of ϕ_i , $k_i > 0$ are constant gains and the error function $e_i = \phi_i(\xi)$ can be simply treated as the signed “distance” to the surfaces $\{\xi \in \mathbb{R}^3 : \phi_i(\xi) = 0\}$ for $i = 1, 2$. For notational simplicity, we define $k_{\min} = \min\{k_1, k_2\}$ and $k_{\max} = \max\{k_1, k_2\}$ throughout the chapter.

Remark 4.1. The vector field (4.2) can be interpreted intuitively. The first term, $n_1(\xi) \times n_2(\xi)$, is the “translational velocity”, being perpendicular to the two gradient vectors. The latter term, $k_1 e_1(\xi) n_1(\xi) + k_2 e_2(\xi) n_2(\xi)$, acts as two signed “forces” to pull the trajectory to get closer to the respective surfaces $\phi_i(\xi) = 0$. Therefore, roughly speaking, when $\xi(0) \in \mathcal{P}$, the vector field only has the first term, thus the trajectory moves tangential to the path and evolves along it; when $\xi(0) \notin \mathcal{P}$, the latter term of the vector field enables the trajectory to converge to the path in the meanwhile. The formal analysis is presented later. \triangleleft

To write (4.2) in a compact form, let $\tau(\xi) = n_1(\xi) \times n_2(\xi) \in \mathbb{R}^3$, $N(\xi) = (n_1(\xi), n_2(\xi)) \in \mathbb{R}^{3 \times 2}$, $K = \text{diag}(k_1, k_2) \in \mathbb{R}^{2 \times 2}$ and $e(\xi) = (e_1(\xi), e_2(\xi))^{\top} \in \mathbb{R}^2$. Then the vector field (4.2) is rewritten to

$$\chi(\xi) = \tau(\xi) - N(\xi)Ke(\xi). \quad (4.3)$$

To study the properties of the vector field, we investigate trajectories of the following nonlinear autonomous ordinary differential equation (ODE):

$$\frac{d}{dt}\xi(t) = \chi(\xi(t)), \quad t \geq 0. \quad (4.4)$$

We aim to let the integral curves of the vector field converge (metrically) to and move along the desired path. Namely, $\text{dist}(\xi(t), \mathcal{P}) \rightarrow 0$ as $t \rightarrow \infty$. Note that once the trajectory is on the desired path, the vector field degenerates to a set of *tangent vectors* of the desired path (precisely, $\chi(\xi) = \tau(\xi)$), thus the trajectory stays on the desired path and moves along it.

Remark 4.2. In the 2D case [63], the vector field is $\chi = E\nabla\phi - k\phi\nabla\phi$, where $E \in SO(2)$ is a constant rotational matrix. This vector field can be further simplified to $\chi = (E - k\phi I)\nabla\phi$. However, for the 3D vector field (4.2), due to the introduction of the cross product, this vector field *cannot* be further simplified, which complicates the analysis. This is the reason why the analysis of the extension from the 2D vector field to 3D vector field is nontrivial. However, after investigating the 3D case, the extension to a higher dimensional vector field becomes straightforward (see Chapters 5, 7 and 9). \triangleleft

As explained in Chapter 3, to carry out the analysis and to exclude some pathological cases, some assumptions are necessary. First we define the *invariant set* \mathcal{H} (its invariance will be shown later):

$$\mathcal{H} := \{\xi \in \mathbb{R}^3 : N(\xi)Ke(\xi) = 0\}, \quad (4.5)$$

and the *singular set* \mathcal{C} :

$$\mathcal{C} = \{\xi \in \mathbb{R}^3 : \chi(\xi) = 0\} = \{\xi \in \mathcal{H} : \text{rank}(N(\xi)) \leq 1\}. \quad (4.6)$$

The equivalence of the two expressions in (4.6) can be seen as follows: if $n_1(\xi)$ and $n_2(\xi)$ are linearly independent, then they are also linearly independent with $n_1(\xi) \times n_2(\xi)$. Since the coefficient of $n_1(\xi) \times n_2(\xi)$ is non-zero, it is obvious that $\chi(\xi) \neq 0$. Therefore, the linear dependence of $n_1(\xi)$ and $n_2(\xi)$, which is equivalent to $\text{rank}(N(\xi)) \leq 1$, is a necessary condition for $\chi = 0$. Also note that in the second expression, we restrict the elements to be in \mathcal{H} . The elements of the singular set are *singular points* of the vector field. Now we present the main assumptions in this chapter.

Assumption 4.3. There are no singular points on the desired path. More precisely, \mathcal{C} is empty or otherwise there holds $\text{dist}(\mathcal{C}, \mathcal{P}) > 0$.

Assumption 4.4. For any given constant $\kappa > 0$, we have

$$\inf\{\|e(\xi)\| : \text{dist}(\xi, \mathcal{P}) \geq \kappa\} > 0.$$

Assumption 4.5. For any given constant $\kappa > 0$, we have

$$\inf\{\|N(\xi)Ke(\xi)\| : \text{dist}(\xi, \mathcal{H}) \geq \kappa\} > 0.$$

Assumption 4.3 is needed for the “regularity” of the desired path. In view of the definition of the critical set \mathcal{C} in (4.6), and noting that $\mathcal{P} \supseteq \{\xi \in \mathcal{H} : \text{rank}(N(\xi)) = 2\}$, it follows that $\mathcal{P} \cup \mathcal{C} = \mathcal{H}$, but the intersection of \mathcal{P} and \mathcal{C} can be nonempty. That is to say, singular points may exist on the desired path. In this case, the robot will get “stuck” on the path, since the “translational velocity” is zero at a critical point c (i.e., $\tau(c) = 0$). This issue can be avoided by making Assumption 4.3. Moreover, since $\phi_i \in C^2$ and \mathcal{P} is the intersection of $\phi_i = 0$, $i = 1, 2$, a natural question arises regarding the “smoothness” of \mathcal{P} . Under Assumption 4.3, the next lemma can answer this question.

Lemma 4.6. *Under Assumption 4.3, \mathcal{P} is a C^2 embedded submanifold in \mathbb{R}^3 .*

Proof. Denote $\Phi(\xi) = (\phi_1(\xi), \phi_2(\xi))^\top$. So $\Phi : \mathbb{R}^3 \rightarrow \mathbb{R}^2$, and $\mathcal{P} = \Phi^{-1}(0)$ is the preimage of Φ due to the definition in (4.1). Under Assumption 4.3, for any $\xi \in \mathcal{P}$, the Jacobian matrix $\frac{d\Phi}{d\xi} = N^\top(\xi)$ is of full rank. Therefore, 0 is a regular value of Φ and \mathcal{P} is a C^2 embedded submanifold in \mathbb{R}^3 [77, Corollary 5.14]. \square

Remark 4.7. Note that Assumption 4.3 implies that $\mathcal{C} \cap \mathcal{P} = \emptyset$, but not vice versa. However, using the fact that \mathcal{C} and \mathcal{P} are closed subsets in \mathbb{R}^3 , if either \mathcal{C} or \mathcal{P} is bounded (and thus compact), one has $\mathcal{C} \cap \mathcal{P} = \emptyset \iff \text{dist}(\mathcal{C}, \mathcal{P}) > 0$. In many practical applications, roughly speaking, the desired path is a simple closed curve, and hence a bounded path. In this case, if $\mathcal{C} \cap \mathcal{P} = \emptyset$, then Assumption 4.3 is held. \triangleleft

Assumption 4.4 is motivated by observing that the desired path \mathcal{P} can be equivalently defined as

$$\mathcal{P} = \{\xi \in \mathbb{R}^3 : e(\xi) = 0\}.$$

This inspires one to use $\|e(\xi)\|$, the Euclidean norm of the vector function e , rather than the more complicated quantity $\text{dist}(\xi, \mathcal{P})$, to quantify the distance between a point $\xi \in \mathbb{R}^3$ and the desired path. Although it is usually assumed that $\|e(\xi)\|$ approximates the distance to the desired path $\text{dist}(\xi, \mathcal{P})$, this is not always the case if Assumption 4.4 is not verified, as shown in Chapter 3 (see Corollary 3.13). Thus, Assumption 4.4 is crucial in the sense that it enables one to

use a Lyapunov function candidate related to $\|e(\xi)\|$ and the decreasing property to prove the convergence to the desired path conveniently. Therefore, under Assumption 4.4, we call $e(\xi)$ the *path-following error*, or simply the *error*, of a point $\xi \in \mathbb{R}^3$ to the desired path \mathcal{P} throughout the chapter.

Similarly, Assumption 4.5 enables one to use $\|N(\xi)Ke(\xi)\|$ to measure the distance to the invariant set $\mathcal{H} = \mathcal{P} \cup \mathcal{C}$. It is suggestive to regard $\|N(\xi)Ke(\xi)\|$ as an “error” since when it equals 0, the point ξ is in \mathcal{H} , in view of the definition of \mathcal{H} in (4.5). As detailed in Chapter 3, under Assumption 4.5, it can be similarly concluded that the vanishing of the “invariant set error” $\|N(\xi(t))Ke(\xi(t))\|$ implies the convergence of the trajectory to the set \mathcal{H} , and hence to the desired path \mathcal{P} or the singular set \mathcal{C} exclusively as $t \rightarrow \infty$.

4.3 ANALYSIS OF THE VECTOR FIELD

4.3.1 Bounded desired path

Since the desired path is sufficiently smooth, a bounded desired path is the trace of a simple closed curve (i.e., it is homeomorphic to the unit circle S^1)². It is proved below that the integral curves of (4.4) asymptotically converge to either the desired path or the singular set.

Proposition 4.8. *Let $\xi(t)$ be the solution of (4.4). If the desired path \mathcal{P} is bounded, then $\xi(t)$ will (locally) asymptotically converge to the desired path or the singular set exclusively as $t \rightarrow \infty$. Namely, the trajectory will converge to either the desired path or the singular set but not to both of them.*

Proof. The time derivative of e with respect to t is:

$$\begin{aligned}\dot{e}(\xi(t)) &= N^\top(\xi(t))\dot{\xi}(t) \\ &= N^\top(\xi(t))\chi(\xi(t)) \\ &= -N^\top(\xi(t))N(\xi(t))Ke(\xi(t)).\end{aligned}\tag{4.7}$$

Note that the above result has utilized the property that $N^\top(\xi(t))\tau(\xi(t)) = 0$. Now we define a continuously differentiable function:

$$V(\xi(t)) = 1/2 e^\top(\xi(t))Pe(\xi(t)),\tag{4.8}$$

where P is a symmetric positive definite matrix. Then $V > 0$ on $\mathbb{R}^3 \setminus \mathcal{P}$. Note that the Lyapunov function candidate $V(\cdot)$ is regarded as a function of $\xi(t)$ rather

² Due to Lemma 4.6, desired paths can be conveniently classified into two categories: those homeomorphic to the unit circle S^1 if they are compact and those homeomorphic to the real line \mathbb{R} otherwise [76, Theorem 5.27].

than $e(\xi(t))$. Thus LaSalle's invariance principle (Theorem 2.6) is valid to use in the sequel. Taking the derivative of V with respect to t , we obtain:

$$\begin{aligned}\dot{V}(\xi(t)) &= 1/2 (\dot{e}^\top(\xi(t))Pe(\xi(t)) + e^\top(\xi(t))P\dot{e}(\xi(t))) \\ &= -\frac{1}{2}e^\top(\xi(t))Qe(\xi(t)),\end{aligned}\tag{4.9}$$

where

$$Q = K^\top N^\top(\xi(t))N(\xi(t))P + PN^\top(\xi(t))N(\xi(t))K.$$

Let $P = K$, which is positive definite, then $\dot{V}(\xi(t)) = -\|N(\xi(t))Ke(\xi(t))\|^2 \leq 0$ for $\xi \in \mathbb{R}^3$.

To use LaSalle's invariance principle (Theorem 2.6), we need to construct a compact set that is positively invariant with respect to (4.4). Given $r > 0$, a closed ball is defined by $\bar{\mathcal{B}}_r = \{\xi \in \mathbb{R}^3 : \|\xi\| \leq r\} \subseteq \mathbb{R}^3$. Since \mathcal{P} is bounded, r can be chosen sufficiently large such that $\mathcal{P} \subseteq \bar{\mathcal{B}}_r$, and $\alpha := \min_{\|\xi\|=r} V(e(\xi)) > 0$. Take $\beta \in (0, \alpha)$ and let

$$\Omega_\beta = \{\xi \in \bar{\mathcal{B}}_r : V(e(\xi)) \leq \beta\}.\tag{4.10}$$

Obviously, Ω_β is in the interior of $\bar{\mathcal{B}}_r$, and hence it is compact. In addition, since $\dot{V}(\xi(t)) \leq 0$, the set Ω_β is also positively invariant. Therefore, (4.4) has a unique solution defined for all $t \geq 0$ whenever $\xi(0) \in \Omega_\beta$. Let $\mathcal{A} = \{\xi \in \Omega_\beta : \dot{V}(\xi) = 0\} = \{\xi \in \Omega_\beta : N(\xi)Ke(\xi) = 0\} \subseteq \mathcal{H}$. Next we are going to prove that the largest invariant set in \mathcal{A} is itself. Note that \mathcal{A} is the union of two sets; i.e., $\mathcal{A} = \mathcal{A}_1 \cup \mathcal{A}_2$, where $\mathcal{A}_1 = \{\xi \in \mathcal{A} : \text{rank}(N(\xi)) \leq 1\}$ and $\mathcal{A}_2 = \{\xi \in \mathcal{A} : \text{rank}(N(\xi)) = 2\}$. We consider the solutions of (4.4) starting from these two sets respectively.

1. When the trajectory starts from \mathcal{A}_1 ; i.e., $\xi(0) \in \mathcal{A}_1$, $n_1(\xi(0))$ and $n_2(\xi(0))$ are linearly dependent (this includes the case where either of them is zero). Thus (4.4) indicates that $\dot{\xi}(t)|_{t=0} = 0$. Since the solution of (4.4) exists and is unique, $\xi(0) \in \mathcal{A}_1 \Rightarrow \xi(t) \equiv \xi(0) \in \mathcal{A}_1$, $t \geq 0$.
2. When the trajectory starts from \mathcal{A}_2 ; i.e., $\xi(0) \in \mathcal{A}_2$, $n_1(\xi(0))$ and $n_2(\xi(0))$ are linearly independent. Then (4.4) becomes $\dot{\xi}(t)|_{t=0} = \tau$, which is the tangent vector of \mathcal{P} at $\xi(0)$. According to Lemma 4.6 and the existence and uniqueness of solutions of ordinary differential equations on manifolds (e.g. [35]), the trajectory $\xi(t)$ will not leave \mathcal{P} , or \mathcal{A}_2 . That is, $\xi(0) \in \mathcal{A}_2 \Rightarrow \xi(t) \in \mathcal{A}_2$, $t \geq 0$.

The above discussion concludes that \mathcal{A} is itself the largest invariant set. Then according to LaSalle's invariance principle (with respect to the autonomous ODE (4.4)) (Theorem 2.6), every solution $\xi \in \mathbb{R}^3$ starting in Ω_β approaches $\mathcal{A} \subseteq \mathcal{H}$ as $t \rightarrow \infty$. Since $\mathcal{A}_1 \subseteq \mathcal{C}$, $\mathcal{A}_2 \subseteq \mathcal{P}$ and $\text{dist}(\mathcal{C}, \mathcal{P}) > 0$ (by Assumption 4.3), it follows that $\text{dist}(\mathcal{A}_1, \mathcal{A}_2) > 0$ and in particular, the solution converges either to the desired path or the singular set as $t \rightarrow \infty$. \square

Asymptotic convergence is not quite appealing compared to exponential convergence. For this reason, we show as follows the exponential convergence result. We will use the Lyapunov function candidate in (4.8), and the compact set Ω_β in the proof of Proposition 4.8, which is proved to be positively invariant. Moreover, we define two more sets:

$$\mathcal{E}_\alpha = \{\xi \in \mathbb{R}^3 : \|e(\xi)\| \leq \alpha\}, \quad (4.11)$$

which is the set of points at which the error is less than some positive number α . This set can be treated as the (closed) neighborhood of the desired path \mathcal{P} . Now the theorem is stated below:

Theorem 4.9. *Let $\xi(t)$ be the solution to (4.4) and suppose that the desired path \mathcal{P} is bounded. There exists $\delta > 0$ such that \mathcal{E}_δ defined in (4.11) is compact, and $\|\tau(\xi)\| \neq 0$ for every point $\xi \in \mathcal{E}_\delta$. Furthermore, the error $\|e(\xi(t))\|$ (locally) exponentially converges to 0 as $t \rightarrow \infty$, given that the initial condition $\xi(0) \in \mathcal{E}_{\delta'}$, where $0 < \delta' \leq \delta\sqrt{k_{\min}/k_{\max}}$.*

Proof. Since K is positive definite, from (4.8), we have

$$\|e(\xi)\|^2 \geq 2V(e(\xi))/k_{\max}.$$

Taking the derivative of (4.8) with respect to time, we have (t is omitted for simplicity):

$$\dot{V}(e(\xi)) = -e^\top(\xi)Q(\xi)e(\xi) = -\|N(\xi)Ke(\xi)\|^2,$$

where

$$Q(\xi) = KN^\top(\xi)N(\xi)K \quad (4.12)$$

is positive semidefinite. Note that $\det(Q(\xi)) = k_1^2 k_2^2 \|\tau(\xi)\|^2$. Therefore, $\det(Q(\xi)) \neq 0$ if and only if n_1 and n_2 are linearly independent.

By Assumption 4.3, $\|\tau(\xi)\|$ has a non-zero minimum on \mathcal{P} (i.e., there exists $\min_{\xi \in \mathcal{P}} \|\tau(\xi)\| > 0$). By the continuity of $\|\tau(\xi)\|$, the compactness of the desired path \mathcal{P} and Assumption 4.4, there exists $\delta > 0$ such that for any point $\xi \in \mathcal{E}_\delta$ as defined in (4.11), we have $\|\tau(\xi)\| \neq 0$. Note that δ can be chosen sufficiently small such that \mathcal{E}_δ is bounded, hence compact³.

Let $\iota = k_{\min}\delta^2/2$, then⁴ $\Omega_\iota \subseteq \mathcal{E}_\delta$. Therefore, in the compact and positively invariant set Ω_ι , we have $\|\tau(\xi)\| \neq 0$, implying that $Q(\xi)$ does not loose rank, and further implying that $Q(\xi)$ is positive definite. Let $\Lambda := \min_{\xi \in \Omega_\iota} \{\lambda_{\min}(Q(\xi))\}$, where $\lambda_{\min}(\cdot)$ denotes the minimum eigenvalue. It can be observed that $\Lambda > 0$.

³ This is justified as follows: one can choose a set Ω_β as defined in (4.10), which is compact. Then there exists $\gamma' > 0$ such that $\mathcal{E}_{\gamma'} \subseteq \Omega_\beta$ (this is true because by choosing $\gamma' \leq \sqrt{2\beta/k_{\max}}$, $\forall \xi \in \mathcal{E}_{\gamma'}, \|e(\xi)\| \leq \gamma' \implies V(\xi) \leq k_{\max}\|e(\xi)\|^2/2 \leq k_{\max}\gamma'^2/2 \leq \beta \implies \xi \in \Omega_\beta$). Therefore, $\mathcal{E}_{\gamma'}$ is compact. Finally, by selecting $0 < \delta < \min\{\gamma, \gamma'\}$, it can be guaranteed that \mathcal{E}_δ is compact as desired (since $\mathcal{E}_\delta \subseteq \mathcal{E}_{\gamma'} \subseteq \Omega_\beta$).

⁴ Since $\forall \xi \in \Omega_\iota, k_{\min}\|e(\xi)\|^2/2 \leq V(e(\xi)) \leq \iota \implies \|e(\xi)\| \leq \delta \implies \xi \in \mathcal{E}_\delta$.

Note that Λ always exists because the eigenvalues of a matrix continuously depends on its entries, and the minimum is obtained over a compact set. Therefore,

$$\dot{V}(e(\xi)) \leq -\Lambda \|e(\xi)\|^2 \leq -2\Lambda V(e(\xi))/k_{\max},$$

which implies that

$$V(e(\xi)) \leq V(e_0) \exp(-2\Lambda t/k_{\max}),$$

and furthermore,

$$\|e(\xi)\| \leq c \|e_0\| \exp(-\Lambda t/k_{\max}),$$

where $e_0 = e(\xi(0))$ and $c = \sqrt{k_{\max}/k_{\min}}$. Therefore, $\|e(\xi(t))\|$ exponentially approaches 0 as t approaches infinity. Lastly, note that $\mathcal{E}_{\delta'} \subseteq \Omega_t$; thus $\xi(0) \in \mathcal{E}_{\delta'} \implies \xi(0) \in \Omega_t$. \square

4.3.2 Unbounded desired path

The analysis presented above for bounded desired paths cannot be directly applied to an unbounded desired path. This is partly because for any (closed) ball $\bar{\mathcal{B}}_r$ containing part of the desired path, $\alpha = \min_{\|\xi\|=r} V(e(\xi)) = 0$. Therefore, $\beta \in (0, \alpha)$ is not valid in the definition of Ω_β in (4.10). The key issue is that LaSalle's invariance principle is no longer effective regarding an unbounded desired path, since there is not a compact set containing the desired path. In addition, the solution to (4.4) may not be extended infinitely. Therefore, we need to analyze this case differently.

4.3.2.1 Extensibility of solutions

Assuming that $\|\tau\| = \|n_1 \times n_2\|$ is upper bounded on some set, it can still be proved that solutions exist for all $t \geq 0$. We consider the following unbounded set:

$$\Xi_\beta = \{\xi \in \mathbb{R}^3 : V(e(\xi)) \leq \beta\}, \quad (4.13)$$

where $\beta > 0$. The definition is similar to that of Ω_β in (4.10), except that Ξ_β is unbounded since $\mathcal{P} \subseteq \Xi_\beta$ and \mathcal{P} is unbounded.

Lemma 4.10. Suppose $\|\tau\|$ is upper bounded in \mathcal{E}_α for some $\alpha > 0$. Let $\xi(t)$ be the trajectory with respect to (4.4) with the initial condition $\xi(0) \in \mathcal{E}_{\alpha'}$, where $0 < \alpha' \leq \alpha\sqrt{k_{\min}/k_{\max}}$. Then the trajectory $\xi(t)$ can be extended to infinity; namely, the trajectory $\xi(t)$ exists for $t \geq 0$.

Proof. Suppose the maximum extended time t^* of the solution is finite; i.e., $t^* < \infty$. Let $\beta = k_{\min}\alpha^2/2$. First one observes that $\Xi_\beta \subseteq \mathcal{E}_\alpha$ (since $\forall x \in \Xi_\beta, k_{\min}\|x\|^2/2 \leq V(x) \leq \beta \implies \|x\| \leq \sqrt{2\beta/k_{\min}} \leq \alpha \implies x \in \mathcal{E}_\alpha$). Using the

same Lyapunov function as in (4.8), its derivative with respect to t is $\dot{V}(e(\xi(t))) = -\|N(\xi(t))Ke(\xi(t))\|^2 \leq 0$. Therefore, Ξ_β is positively invariant (note that in this case Ξ_β is not bounded). This means that $\xi(0) \in \Xi_\beta \implies \xi(t) \in \Xi_\beta \subseteq \mathcal{E}_\alpha$ for $t \in [0, t^*]$, where $\xi(t)$ is the trajectory with respect to (4.4). In other words, $\|\tau(\xi(t))\|$ is upper bounded by some positive number denoted by κ_b for all $t \in [0, t^*]$.

Since $V(\xi(t)) \geq 0$, it follows that

$$\int_0^{t^*} \|N(\xi(t))Ke(\xi(t))\|^2 dt = - \int_0^{t^*} \dot{V}(\xi(t)) dt = V(\xi(0)) - V(\xi(t^*)) < \infty.$$

Therefore, for all $0 \leq \tilde{t} < t^*$,

$$\begin{aligned} \|\xi(\tilde{t}) - \xi(0)\| &\leq \int_0^{\tilde{t}} \|\dot{\xi}(t)\| dt \leq \int_0^{\tilde{t}} \|\tau(\xi(t))\| dt + \int_0^{\tilde{t}} \|N(\xi(t))Ke(\xi(t))\| dt \\ &\leq \kappa_b \tilde{t} + \sqrt{t^* \int_0^{t^*} \|N(\xi(t))Ke(\xi(t))\|^2 dt} := R < \infty. \end{aligned}$$

The last inequality is due to Hölder's inequality. Therefore, the trajectory $\xi(t)$ remains in a compact set $\{p \in \mathbb{R}^3 : \|p - \xi(0)\| \leq R\}$, and hence the trajectory can be extended to infinity (i.e., the trajectory exists for $t \geq 0$). Lastly, note that $\mathcal{E}_{\alpha'} \subseteq \Xi_\beta$; thus $\xi(0) \in \mathcal{E}_{\alpha'} \implies \xi(0) \in \Xi_\beta$. \square

Corollary 4.11. *Suppose the assumptions of Lemma 4.10 are satisfied. Then along the trajectory $\xi(t)$ with respect to (4.4), we have*

$$\int_0^\infty \|N(\xi(t))Ke(\xi(t))\|^2 dt = - \int_0^\infty \dot{V}(\xi(t)) dt < +\infty. \quad (4.14)$$

4.3.2.2 Convergence Results

We can draw a similar conclusion for the case of an unbounded desired path. To this end, we present the absolute continuity of the Lebesgue integral first.

Lemma 4.12 (Absolute continuity of Lebesgue integrals [62]). *If f is Lebesgue integrable on \mathbb{R}^n , then for any $\epsilon > 0$, there exists $\delta > 0$ such that for all measurable sets $\mathcal{D} \subseteq \mathbb{R}^n$ with measure $m(\mathcal{D}) < \delta$, it follows that $\int_{\mathcal{D}} |f| dm < \epsilon$.*

Now we are ready to prove the following result.

Corollary 4.13. *For any $\epsilon > 0$, there exists $0 < \delta \leq \epsilon$ such that for all intervals with length $|\Delta| < \delta$,*

$$\int_{\Delta} \|N(\xi(t))Ke(\xi(t))\| dt < 2\epsilon.$$

Proof. For any function $f : \mathbb{R} \rightarrow \mathbb{R}^n$, we define a new function $f(t)_{>1}$ as below:

$$f(t)_{>1} = \begin{cases} f(t), & \|f(t)\| > 1, \\ 0, & \text{otherwise.} \end{cases}$$

Another function $f(t)_{\leq 1}$ is similarly defined. It follows that

$$\begin{aligned} \int_0^\infty \|N(\xi(t))Ke(\xi(t))\|_{>1} dt &\leq \int_0^\infty \|N(\xi(t))Ke(\xi(t))\|_{>1}^2 dt \\ &\leq \int_0^\infty \|N(\xi(t))Ke(\xi(t))\|^2 dt < \infty, \end{aligned}$$

where the last inequality is due to Corollary 4.11. Therefore, $\|N(\xi(t))Ke(\xi(t))\|_{>1}$ is Lebesgue integrable. Thus, for any $\epsilon > 0$, there exists $\gamma > 0$ as the length of the interval such that Lemma 4.12 holds. In addition, taking $\delta = \min\{\gamma, \epsilon\}$, then $|\Delta|$ can be chosen sufficiently small such that $|\Delta| < \delta \leq \epsilon$, and $\int_\Delta \|N(\xi(t))Ke(\xi(t))\|_{>1} dt < \epsilon$. Finally,

$$\begin{aligned} \int_\Delta \|N(\xi(t))Ke(\xi(t))\| dt &= \int_\Delta \|N(\xi(t))Ke(\xi(t))\|_{>1} dt \\ &\quad + \int_\Delta \|N(\xi(t))Ke(\xi(t))\|_{\leq 1} dt \leq \epsilon + \epsilon = 2\epsilon. \end{aligned}$$

□

The following proposition for an unbounded desired path is the counterpart of Proposition 4.8.

Proposition 4.14. *Let $\xi(t)$ be the solution of (4.4). If \mathcal{P} is unbounded and the assumptions of Lemma 4.10 are satisfied (i.e., $\|\tau\|$ is upper bounded by $\kappa_b > 0$ in \mathcal{E}_α for some $\alpha > 0$), then the trajectory $\xi(t)$ will asymptotically converge to the desired path or the singular set exclusively as $t \rightarrow \infty$.*

Proof. Define the Lyapunov function candidate $V(\xi(t))$ as in Proposition 4.8 and denote $\eta(\xi(t)) = \|N(\xi(t))Ke(\xi(t))\|$. Suppose $\xi(t)$ does not converge to \mathcal{H} , then there exists an increasing time sequence $\{t_k\}$, and $t_k \rightarrow \infty$ as $k \rightarrow \infty$, such that (due to Assumption 4.5)

$$\text{dist}(\xi(t_k), \mathcal{H}) > \delta > 0 \Rightarrow \eta(\xi(t_k)) > \epsilon > 0.$$

Therefore, $\dot{V}(\xi(t_k)) = -\eta^2(\xi(t_k)) < -\epsilon^2$. According to Assumption 4.5, there exists $\epsilon' > 0$ such that when $\text{dist}(\xi, \mathcal{H}) > \delta/2$, one has $\|\eta(\xi)\| > \epsilon'$. Since $\text{dist}(\xi(t_k), \mathcal{H}) > \delta$, given a ball $\mathcal{B}(\xi(t_k), \delta/4)$, then for any $y \in \mathcal{B}(\xi(t_k), \delta/4)$, it follows that (see Fig. 4.1)

$$\text{dist}(y, \mathcal{H}) > \delta/2 \Rightarrow \dot{V}(y) < -\epsilon'^2.$$

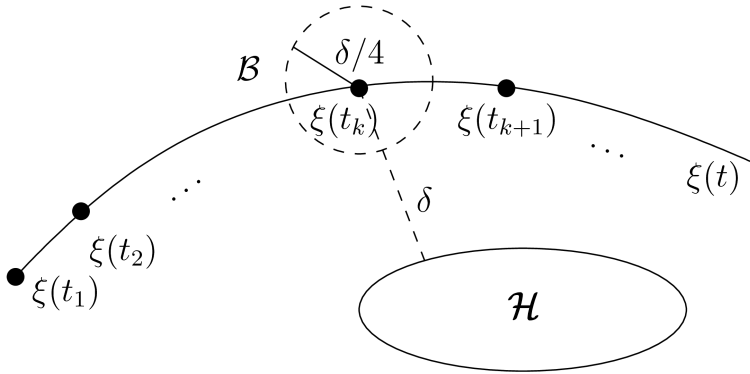


Figure 4.1: The illustration of the proof of Proposition 4.14.

Taking $\epsilon = \delta/(2(2 + \kappa_b))$ in Corollary 4.13, there exists an interval Δ with the length $|\Delta| < \epsilon$ such that

$$\begin{aligned} \int_{\Delta} \|\dot{\xi}(t)\| dt &= \int_{\Delta} \|\tau(\xi(t)) - N(\xi(t))K\epsilon(\xi(t))\| dt \\ &\leq \int_{\Delta} \|\tau(\xi(t))\| dt + \int_{\Delta} \|N(\xi(t))K\epsilon(\xi(t))\| dt \leq (\kappa_b + 2)\epsilon < \delta/2. \end{aligned}$$

Then it follows that

$$\xi[t_k - \Delta/2, t_k + \Delta/2] \subseteq \mathcal{B}(\xi(t_k), \delta/4).$$

Therefore,

$$\int_{t_k - \Delta/2}^{t_k + \Delta/2} \dot{V}(\xi(t)) dt < -\epsilon'^2 \Delta.$$

This leads to⁵

$$\int_0^{\infty} \dot{V}(\xi(t)) dt \leq \sum_{k=1}^{\infty} \int_{t_k - \Delta/2}^{t_k + \Delta/2} \dot{V}(\xi(t)) dt \leq -\sum_{k=1}^{\infty} \epsilon'^2 \Delta \leq -\infty, \quad (4.15)$$

which contradicts Corollary 4.11. Therefore, $\xi(t)$ converges to \mathcal{H} as $t \rightarrow \infty$. Then due to Assumption 4.3, the solution converges either to the desired path or the singular set. \square

For unbounded desired paths, we also have the following exponential convergence result. Before presenting the result, we say that a function $f : \Omega \subseteq \mathbb{R}^m \rightarrow$

⁵ The first inequality of (4.15) is justified since one can always choose the sequence $\{t_k\}$ such that $t_{k+1} - t_k > \Delta$ for all $k \geq 1$.

\mathbb{R}^n is bounded away from zero in Ω if there exists a real number $c > 0$, such that $\|f(x)\| > c$ for all $x \in \Omega$.

Theorem 4.15. *Let $\xi(t)$ be the solution to (4.4) and the desired path \mathcal{P} be unbounded. Define \mathcal{E}_α as in (4.11) for some $\alpha > 0$. Suppose both $\|n_1(\xi)\|$ and $\|n_2(\xi)\|$ are upper bounded in \mathcal{E}_α , and $\|\tau(\xi)\|$ is bounded away from zero on \mathcal{P} , then there exists $0 < \gamma \leq \alpha$ such that $\inf_{\xi \in \mathcal{E}_\gamma} \|\tau(\xi)\| > 0$. Furthermore, the error $\|e(\xi)\|$ (locally) exponentially converges to 0 as $t \rightarrow \infty$, given that the initial condition $\xi(0) \in \mathcal{E}_{\gamma'}$, where $0 < \gamma' \leq \sqrt{k_{\min}/k_{\max}}$.*

Proof. It is obvious that the assumptions of Lemma 4.10 are satisfied. Thus the solution $\xi(t)$ with respect to (4.4) can be prolonged to infinity. Since the desired path is unbounded, we cannot find a compact set Ω_β as in Theorem 4.9. Instead, we consider Ξ_β defined in (4.13). Since $\|\tau\|$ is bounded away from zero on \mathcal{P} , and due to the continuity of $\tau(\xi)$ with respect to its argument, there exists $0 < \gamma \leq \alpha$ such that $\inf_{\xi \in \mathcal{E}_\gamma} \|\tau(\xi)\| > 0$. That is, $\|\tau\|$ is bounded away from zero in the subset $\mathcal{E}_\gamma \subseteq \mathcal{E}_\alpha$. It can be shown that there exists a positively invariant set $\Xi_\beta \subseteq \mathcal{E}_\gamma$ by choosing $\beta = k_{\min}\gamma^2/2$ (see the proof in Lemma 4.10), where Ξ_β is defined in (4.13). Next we consider the case where the solution $\xi(t)$ starts from this invariant set Ξ_β . Since $\|\tau\|$ is bounded away from zero in the subset $\mathcal{E}_\gamma \supset \Xi_\beta$ as shown previously, there are no singular points in Ξ_β , and thus we do not need to consider the case where the solution converges to the singular set, and thus the remaining proof is similar to that of Theorem 4.9. It follows that

$$\inf_{\xi \in \Xi_\beta} \lambda_1(Q(\xi))\lambda_2(Q(\xi)) = \inf_{\xi \in \Xi_\beta} \det(Q(\xi)) = k_1^2 k_2^2 \inf_{\xi \in \Xi_\beta} \|\tau(\xi)\|^2 > 0,$$

where $\lambda_1(Q(\xi))$ and $\lambda_2(Q(\xi))$ are two eigenvalues of $Q(\xi)$. Note that the sum of the two eigenvalues $\lambda_1(Q(\xi)) + \lambda_2(Q(\xi)) = \text{tr}(Q(\xi)) = k_1^2 \|n_1\|^2 + k_2^2 \|n_2\|^2$. Since $\|n_1\|$ and $\|n_2\|$ are upper bounded in $\Xi_\beta \subseteq \mathcal{E}_\alpha$, the two eigenvalues are finite. Therefore, we have $\Lambda' := \inf_{\xi \in \Xi_\beta} \{\lambda_{\min}(Q(\xi))\} > 0$. This leads to

$$\dot{V}(e(\xi)) \leq -\Lambda' \|e(\xi)\|^2 \leq 2\Lambda' V(e(\xi))/k_{\max}.$$

Therefore,

$$V(e(\xi)) \leq V(e_0) \exp(-2\Lambda' t/k_{\max}) \implies \|e(\xi)\| \leq c \|e_0\| \exp(-\Lambda' t/k_{\max}),$$

where $e_0 = e(\xi(0))$ and $c = \sqrt{k_{\max}/k_{\min}}$. Consequently, the error $\|e(\xi)\|$ will exponentially approach 0 as t approaches infinity. Lastly, note that $\mathcal{E}_{\gamma'} \subseteq \Xi_\beta$, thus $\xi(0) \in \mathcal{E}_{\gamma'} \implies \xi(0) \in \Xi_\beta$. \square

Remark 4.16. For an unbounded desired path, the result presented above is valid under the condition that $\|\tau\| = \|n_1 \times n_2\|$ is upper bounded. This seems restrictive. However, by introducing a *smooth bounding operator* $f_b : \mathbb{R}^n \rightarrow \mathbb{R}^n$,

$\|f_b(\tau)\|$ can be guaranteed to be bounded and additionally, $f_b(\tau)$ is smooth. For example, $f_b(\xi) = \frac{\xi}{1+\|\xi\|^2}$, where $\xi \in \mathbb{R}^3$ and the upper bound is 1/2. However, $\|f_b(\xi)\|$ vanishes as $\|\xi\| \rightarrow \infty$. Another better choice of the smooth bounding operator contains a bump function. For example,

$$f_b(\xi) = \frac{\xi}{1 + \varphi(\|\xi\|)\|\xi\|},$$

where $\varphi : \mathbb{R} \rightarrow \mathbb{R}$ is a bump function chosen as

$$\varphi(x) = \begin{cases} 0, & x \in [-1, 1] \\ \exp\left(\frac{-1}{x-1}\right), & x \in [1, \infty) \\ \exp\left(\frac{1}{x+1}\right), & x \in (-\infty, -1] \end{cases}$$

and the upper bound is 1. Therefore, the original guiding vector field can be modified to $\chi(\xi) = f_b(n_1 \times n_2) - k_1 e_1 n_1 - k_2 e_2 n_2$. Note that the smooth bounding operator neither changes the direction of $n_1 \times n_2$ nor affects the speed of the convergence to the desired path, which is dominated by the unmodified latter term as can be seen from the time derivative of the Lyapunov function in Proposition 4.8. Nevertheless, for practical reasons, it is desirable to normalize the original vector field, but undesirably compromise the maximal extensibility of the solutions. This will be discussed in the next section. \triangleleft

4.4 NORMALIZATION AND PERTURBATION OF THE VECTOR FIELD

In this section, based on the results presented above, we study the properties of the normalized 3D guiding vector field. We show that the essential feature of the vector field is the direction rather than the amplitude at each point in \mathbb{R}^3 . Then the robustness of the vector field against perturbation is also analyzed.

For notational simplicity, we define the *normalization operator* $\hat{\cdot} : \mathbb{R}^n \rightarrow \mathbb{R}^n$, which normalizes a given non-zero vector a such that $\hat{a} := a/\|a\|$. Therefore, the desired direction of velocity at location $\xi \in \mathbb{R}^3$ is represented by $\hat{\chi}(\xi)$, where $\chi(\xi)$ is the vector field in (4.2). This vector field is well defined in the open set $\mathbb{R}^3 \setminus \mathcal{C}$, where $\|\chi\| \neq 0$. The integral curves of the normalized vector field correspond to the solution to the following autonomous ODE:

$$\frac{d}{dt} \xi(t) = \hat{\chi}(\xi(t)), \quad (4.16)$$

where $\xi : \mathbb{R}_{\geq 0} \rightarrow \mathbb{R}^3 \setminus \mathcal{C}$. The existence and uniqueness of solutions of the ODE can be guaranteed since the right-hand side of (4.16) is continuously differentiable in $\mathbb{R}^3 \setminus \mathcal{C}$. Note that the vector field in (4.16) differs from that in (4.4) by a positive scalar function that only depends on the states ξ . Therefore, these two vector fields have the same direction of each vector at the same point. This fact implies that there is a bijection between non-equilibrium solutions of the two differential equations (4.4) and (4.16). Recall that a *phase portrait* or *phase diagram* is a geometric picture of all the orbits of an autonomous differential equation [25, p. 9].

Lemma 4.17. *The ODE (4.16) with a normalized vector field and the ODE (4.4) with the original vector field have the same phase portrait in $\mathbb{R}^3 \setminus \mathcal{C}$.*

Proof. The right-hand side of (4.16) can be written as $\hat{\chi}(\xi) = \chi(\xi) / \|\chi(\xi)\|$, where the original vector field $\chi(\xi)$ is scaled down by a positive and continuously differentiable function $1/\|\chi(\xi)\|$ in $\mathbb{R}^3 \setminus \mathcal{C}$. Therefore, the ODE (4.16) with a normalized vector field is obtained from the ODE (4.4) by a re-parametrization of time [25, Proposition 1.14]. Thus, they have the same phase portrait in $\mathbb{R}^3 \setminus \mathcal{C}$ [25]. \square

Since the differential equation (4.16) is defined in $\mathbb{R}^3 \setminus \mathcal{C}$, the maximal interval to which a solution can be extended is finite when the solution is approaching \mathcal{C} .

Lemma 4.18. *Let $\xi(t)$ be a solution to (4.16). If the solution is only maximally extended to $t^* < \infty$, then it will converge to the singular set; that is, $\lim_{t \rightarrow t^*} \text{dist}(\xi(t), \mathcal{C}) = 0$.*

Proof. Since $\|\dot{\xi}(t)\|$ is bounded, $\xi^* := \lim_{t \rightarrow t^*} \xi(t) = \xi(0) + \int_0^{t^*} \dot{\xi}(t) dt$ exists. To show that $\|\chi(\xi^*)\| = 0$, suppose $\|\chi(\xi^*)\| > 0$. Since χ continuously depends on ξ , the same holds in the vicinity of ξ^* , and hence the right-hand side of (4.16) is well defined and bounded in the vicinity of ξ^* . This enables one to define the solution at $t = t^*$ and, by the existence theorem [66], extend to $[t^*, t^* + \epsilon]$ for some $\epsilon > 0$. We arrive at the contradiction with the definition of t^* , which proves that $\|\chi(\xi^*)\| = 0$. Thus the solution will converge to the singular set. \square

Due to Lemma 4.18, the solution to (4.16) will possibly converge to the singular set in finite time. However, it can still be similarly proved that the trajectory will either converge to the desired path or the singular set by Lemma 4.17. Furthermore, the exponential convergence results still hold under the conditions of Theorem 4.9 for bounded desired paths or Theorem 4.15 for unbounded desired paths. The corresponding results are straightforward and thus not presented here.

Now we consider a system with a perturbed vector field

$$\dot{\xi}(t) = \chi(\xi(t)) + d(t), \quad (4.17)$$

where χ is the vector field in (4.2) and $d : \mathbb{R}_{\geq 0} \rightarrow \mathbb{R}^n$ is a piecewise continuous and bounded function of time t for all $t \geq 0$. Therefore, the dynamics for the path-following error with respect to (4.17) is

$$\dot{e}(t) = N(\xi(t))^\top (\chi(\xi(t)) + d(t)). \quad (4.18)$$

It will be proved subsequently that the path-following error dynamics (4.18) is locally ISS (see Section 2.1.4). We will use the definition of an open ball: given $a > 0$, the open ball $\mathcal{B}_a \subseteq \mathbb{R}^n$ is defined as $\mathcal{B}_a := \{\xi \in \mathbb{R}^n : \|\xi\| < a\}$.

Theorem 4.19. *Suppose that the desired path \mathcal{P} is bounded. Then the path-following error (4.18) is locally ISS.*

Proof. From Theorem 4.9, there exists $\delta > 0$ such that \mathcal{E}_δ defined in (4.11) is compact, and $\|\tau(\xi)\| \neq 0$ for every point $\xi \in \mathcal{E}_\delta$, and thus the eigenvalue

$$\Lambda' := \min_{\xi \in \mathcal{E}_\delta} \{\lambda_{\min}(Q(\xi))\} > 0,$$

where the matrix Q is defined in (4.12). We use the same Lyapunov function in (4.8) and take the time derivative:

$$\dot{V} = -\|NKe\|^2 + d^\top NKe \quad (4.19)$$

$$\leq -\frac{1}{2}\|NKe\|^2 + \frac{1}{2}\|d\|^2 \quad (4.20)$$

$$\stackrel{(4.12)}{=} -\frac{1}{2}e^\top Qe + \frac{1}{2}\|d\|^2 \quad (4.21)$$

$$\leq -\frac{1}{2}\Lambda'\|e\|^2 + \frac{1}{2}\|d\|^2 \quad (4.22)$$

$$\leq -\frac{\epsilon}{2}\Lambda'\|e\|^2, \quad \forall \|e\| \geq \rho(\|d\|) > 0, \quad (4.23)$$

for all $(t, e, d) \in [0, \infty) \times \mathcal{B}_\delta \times \mathcal{B}_r$, where $r = \delta\sqrt{(1-\epsilon)\Lambda'}$ with $0 < \epsilon < 1$, and $\rho(\|d\|) = \|d\|/\sqrt{(1-\epsilon)\Lambda'}$ is a class \mathcal{K} function. Note that (4.20) is due to Young's inequality (i.e., $d^\top NKe \leq \|d\|^2/2 + \|NKe\|^2/2$). Also note that (4.22) is verified since we have restricted $e \in \mathcal{B}_\delta$. The disturbance is also restricted to $d \in \mathcal{B}_r$ such that $\rho(\|d\|) < \delta$ is satisfied and (4.23) is valid. Therefore, the path-following error in (4.18) is locally ISS by Lemma 2.11. \square

Remark 4.20. This theorem indicates that the error satisfies

$$\|e(\xi(t))\| \leq \beta(\|e(\xi(0))\|, t) + \gamma \left(\sup_{s \in [0, t]} \|d(s)\| \right)$$

for a class \mathcal{KL} function β and a class \mathcal{K} function γ . If the disturbance $d(t)$ is vanishing as $t \rightarrow \infty$, then the error $\|e(\xi(t))\| \rightarrow 0$ as $t \rightarrow \infty$; if the disturbance $d(t)$

is bounded but non-vanishing with respect to time t , then the error $\|e(\xi(t))\|$ will be uniformly ultimately bounded by a class \mathcal{K} function of $\sup_{s \in [0, \infty)} \|d(s)\|$. \triangleleft

Remark 4.21. This theorem can be easily adapted for unbounded desired paths if the assumptions of Theorem 4.15 are satisfied. The significance of this theorem is that it justifies the design of control algorithms: one can focus on designing a control algorithm such that the direction of the robot's velocity converges to that of the vector field. \triangleleft

4.5 CONTROL ALGORITHM FOR A FIXED-WING AIRCRAFT

We use the following fixed-wing aircraft kinematics model discussed in [119]:

$$\dot{x} = s \cos \theta \quad (4.24a)$$

$$\dot{y} = s \sin \theta \quad (4.24b)$$

$$\dot{z} = \tau_z^{-1}(-z + z_u) \quad (4.24c)$$

$$\dot{\theta} = \tau_\theta^{-1}(-\theta + \theta_u) \quad (4.24d)$$

$$\dot{s} = \tau_s^{-1}(-s + s_u), \quad (4.24e)$$

where (x, y, z) is the position of the center of mass of the aircraft, $s > 0$ is the airspeed, θ is the yaw angle, $\tau_z > 0$, $\tau_\theta > 0$ and $\tau_s > 0$ are the time constants, and z_u , θ_u and s_u are the control inputs. The control of the z coordinate in (4.24c) and the airspeed s in (4.24e) are independent from the other variables. Therefore, we can first consider the planar orientation control. Denote the orientation of the aircraft on the X - Y plane and that of the normalized vector field $\hat{\chi}$ on the X - Y plane by $h^p(\theta)$ and χ^p respectively; that is,

$$h^p(\theta) := (\cos \theta, \sin \theta)^\top$$

and

$$\chi^p := (\hat{\chi}_1, \hat{\chi}_2)^\top,$$

where $\hat{\chi}_1$ and $\hat{\chi}_2$ are the first two entries of $\hat{\chi}$. Note that the superscript p implies that the vector is the projection on the X - Y plane. To utilize the vector field designed and analyzed before, it is desirable that h^p is steered to align with χ^p . In other words, we want to achieve $\hat{h}^p \rightarrow \hat{\chi}^p$, where $\hat{\cdot}$ is the normalization operator defined before. For convenience, we call \hat{h}^p and $\hat{\chi}^p$ the *planar orientations* of the aircraft and of the vector field respectively. It can be observed that $\hat{h}^p = h^p$ and

$$\hat{\chi}^p = \frac{\chi^p}{\|\chi^p\|} = \frac{1}{\sqrt{\hat{\chi}_1^2 + \hat{\chi}_2^2}} \begin{bmatrix} \hat{\chi}_1 \\ \hat{\chi}_2 \end{bmatrix} = \frac{1}{\sqrt{\chi_1^2 + \chi_2^2}} \begin{bmatrix} \chi_1 \\ \chi_2 \end{bmatrix}.$$

Before presenting the control algorithm, we first state a lemma regarding some calculations involved. We consider a vector function $r : \mathbb{R}^n \rightarrow \mathbb{R}^m$, where m, n are positive integers, defined as $x := (x_1, \dots, x_n)^\top \mapsto r(x) := (r_1(x), \dots, r_m(x))^\top$. In addition, each x_i is a function of time $t \mapsto x_i(t)$. The *Jacobian matrix* with respect

to x is denoted by $J(r)$; that is, $J(r) = \begin{bmatrix} \frac{\partial r_1}{\partial x_1} & \dots & \frac{\partial r_1}{\partial x_n} \\ \vdots & \vdots & \vdots \\ \frac{\partial r_m}{\partial x_1} & \dots & \frac{\partial r_m}{\partial x_n} \end{bmatrix}$. We define $E \in SO(2)$ as

the (90°) rotation matrix $E = \begin{bmatrix} 0 & -1 \\ 1 & 0 \end{bmatrix}$.

Lemma 4.22. *Given a vector function $r : \mathbb{R}^n \rightarrow \mathbb{R}^m$ defined above, it holds that*

$$\frac{d}{dt} \hat{r}(x(t)) = \frac{1}{\|r\|} (I - \hat{r}\hat{r}^\top) J(r) \frac{d}{dt} x, \quad (4.25)$$

where I is the identity matrix of suitable dimensions, and $J(r)$ is the Jacobian matrix with respect to x . If $m = 2$, then the above equation can be transformed to

$$\frac{d}{dt} \hat{r}(x(t)) = \left(\frac{-1}{\|r\|} \hat{r}^\top E J(r) \frac{d}{dt} x \right) E \hat{r}. \quad (4.26)$$

Proof. For notational simplicity, we denote $\partial r_{x_1} := \frac{\partial r}{\partial x_1} = (\frac{\partial r_1}{\partial x_1}, \dots, \frac{\partial r_m}{\partial x_1})^\top$. The calculation is shown below:

$$\frac{\partial}{\partial x_1} \|r\| = \frac{1}{2} (r^\top r)^{-\frac{1}{2}} (2 \partial r_{x_1}^\top r) = \frac{\partial r_{x_1}^\top r}{\|r\|}. \quad (4.27a)$$

$$\frac{\partial}{\partial x_1} \frac{1}{\|r\|} = -\|r\|^{-2} \frac{\partial}{\partial x_1} \|r\| \stackrel{(4.27a)}{=} -\frac{\partial r_{x_1}^\top r}{\|r\|^3}. \quad (4.27b)$$

$$\partial \hat{r}_{x_1} = \frac{\partial}{\partial x_1} \frac{r}{\|r\|} = \frac{\partial}{\partial x_1} r \cdot \frac{1}{\|r\|} + r \cdot \frac{\partial}{\partial x_1} \frac{1}{\|r\|} \stackrel{(4.27b)}{=} \frac{1}{\|r\|} (I - \hat{r}\hat{r}^\top) \partial r_{x_1}. \quad (4.27c)$$

$$\begin{aligned} J(\hat{r}) &= \begin{bmatrix} \partial \hat{r}_{x_1} & \dots & \partial \hat{r}_{x_n} \end{bmatrix} \\ &\stackrel{(4.27c)}{=} \frac{1}{\|r\|} (I - \hat{r}\hat{r}^\top) \begin{bmatrix} \partial r_{x_1} & \dots & \partial r_{x_n} \end{bmatrix} \\ &= \frac{1}{\|r\|} (I - \hat{r}\hat{r}^\top) J(r). \end{aligned} \quad (4.27d)$$

$$\frac{d}{dt}\hat{r} = J(\hat{r})\dot{x} \stackrel{(4.27d)}{=} \frac{1}{\|r\|}(I - \hat{r}\hat{r}^\top)J(r)\frac{d}{dt}x. \quad (4.27e)$$

Note that $\hat{r}\hat{r}^\top$ is a projection matrix [51]. If this matrix is multiplied from the right by a non-zero vector v of suitable dimensions, then it orthogonally projects v onto \hat{r} . Similarly, $I - \hat{r}\hat{r}^\top$ is also a projection matrix, while it orthogonally projects the vector v to the *orthogonal complement* of \hat{r} . Given that $\hat{r} \in \mathbb{R}^2$, since $E\hat{r}$ is orthogonal to \hat{r} , it is now easy to observe that $I - \hat{r}\hat{r}^\top = (E\hat{r})(E\hat{r})^\top = -E\hat{r}\hat{r}^\top E$. Substituting this equation into (4.25), one obtains (4.26). \square

Remark 4.23. It is known that the derivative of a unit vector is perpendicular to itself. Since $E\hat{r}$ in (4.26) is already perpendicular to \hat{r} , one observes that the “rotation rate” of the unit vector \hat{r} is $\frac{-1}{\|r\|}\hat{r}^\top EJ(r)\frac{d}{dt}x$. This “rotation rate” is useful as it is related to the “course rate” in flight control. \triangleleft

The following theorem gives the angle control input θ_u which can steer the planar orientation of the aircraft to that of the vector field asymptotically.

Theorem 4.24. *Let the angle directed from $\hat{\chi}^p$ to \hat{h}^p be denoted by $\beta \in (-\pi, \pi]$. When the control input in (4.24d) takes the form*

$$\theta_u = \tau_\theta(\dot{\theta}_d - k_\theta \hat{h}^p \top E \hat{\chi}^p) + \theta, \quad (4.28)$$

$$\dot{\theta}_d = \frac{-1}{\|\hat{\chi}^p\|} \hat{\chi}^p \top E J(\hat{\chi}^p) \dot{\xi}, \quad (4.29)$$

where $E = \begin{bmatrix} 0 & -1 \\ 1 & 0 \end{bmatrix}$ is the rotation matrix of angle $\pi/2$, k_θ is a positive gain, $\dot{\xi} = (\dot{x}, \dot{y}, \dot{z})$ is the aircraft’s actual velocity and $J(\hat{\chi}^p)$ is the Jacobian matrix of $\hat{\chi}^p$ with respect to $\dot{\xi}$, then the angle $\beta(t) \rightarrow 0$ as $t \rightarrow \infty$ whenever $\beta(0) \in (-\pi, \pi)$.

Proof. Substituting (4.28) into (4.24d), one has

$$\dot{\theta} = \dot{\theta}_d - k_\theta \hat{h}^p \top E \hat{\chi}^p. \quad (4.30)$$

First, one can calculate that

$$\frac{d}{dt} \hat{h}^p = (-\sin \theta, \cos \theta)^\top \dot{\theta} = \dot{\theta} E \hat{h}^p,$$

and

$$\frac{d}{dt} \hat{\chi}^p = (-\hat{\chi}^p \top E J(\hat{\chi}^p) \dot{\xi} / \|\hat{\chi}^p\|) E \hat{\chi}^p = \dot{\theta}_d E \hat{\chi}^p.$$

Note that

$$\cos \beta = \hat{h}^p \top \hat{\chi}^p.$$

Taking the time derivative of both sides of the previous equation, we have:

$$\begin{aligned} -\sin \beta \cdot \dot{\beta} &= (\dot{\theta} E \hat{h}^p)^\top \hat{\chi}^p + \hat{h}^p^\top \dot{\theta}_d E \hat{\chi}^p \\ &= (\dot{\theta}_d - \dot{\theta}) \hat{h}^p^\top E \hat{\chi}^p \stackrel{(4.30)}{=} k_\theta (\hat{h}^p^\top E \hat{\chi}^p)^2 = k_\theta \sin^2 \beta, \end{aligned}$$

where the last equality is due to $\hat{h}^p^\top E \hat{\chi}^p = \sin \beta$. Therefore, the dynamics of the angle β is simply

$$\dot{\beta} = -k_\theta \sin \beta.$$

Since $\beta \in (-\pi, \pi]$, there are two equilibria $\beta = 0$ and $\beta = \pi$ in the previous differential equation. Using linearization [66, Theorem 4.7], one can easily observe that the equilibrium $\beta = \pi$ is unstable while the other equilibrium $\beta = 0$ is asymptotically stable. One also observes that $\dot{\beta} < 0$ when $\beta \in (0, \pi)$ and $\dot{\beta} > 0$ when $\beta \in (-\pi, 0)$. Therefore, whenever $\beta(0) \in (-\pi, \pi)$, the trajectory of the angle $\beta(t)$ will asymptotically converge to 0, inferring that $\hat{h}^p \rightarrow \hat{\chi}^p$ asymptotically as $t \rightarrow \infty$. \square

Remark 4.25. In view of (4.29), it is required that $\|\chi^p\| \neq 0$. This implies that pure vertical lifting is not allowed. This condition is satisfied if we employ the path-following algorithm during the cruise flight of the aircraft; that is, the phase when the aircraft levels after climbing and before landing. This flight phase accounts for the majority of the flight time. \triangleleft

Remark 4.26. To simplify computation, terms related to χ^p can be replaced by χ

in (4.28) and (4.29). First we define several matrices. Let $F = \begin{bmatrix} 1 & 0 & 0 \\ 0 & 1 & 0 \end{bmatrix}$, $F' = EF = \begin{bmatrix} 0 & -1 & 0 \\ 1 & 0 & 0 \end{bmatrix}$, $G = F^\top F = \begin{bmatrix} 1 & 0 & 0 \\ 0 & 1 & 0 \\ 0 & 0 & 0 \end{bmatrix}$ and $G' = F^\top EF = \begin{bmatrix} 0 & -1 & 0 \\ 1 & 0 & 0 \\ 0 & 0 & 0 \end{bmatrix}$.

Therefore, we have $\chi^p = F\hat{\chi}$, $\|\chi^p\|^2 = \frac{\chi^\top G\chi}{\|\chi\|^2}$, $\hat{\chi}^p = \frac{Fv}{\sqrt{\chi^\top G\chi}}$, and $J(\chi^p) = FJ(\hat{\chi}) = F(I - \hat{\chi}\hat{\chi}^\top)J(\chi)/\|\chi\|$ (by (4.27d) in Lemma 4.22). Then the simplified forms of (4.28) and (4.29) are as follows

$$\begin{aligned} \theta_u &= \tau_\theta \left(\dot{\theta}_d - k_\theta \frac{\hat{h}^p^\top F'\chi}{\sqrt{\chi^\top G\chi}} \right) + \theta, \\ \dot{\theta}_d &= \frac{-1}{\chi^\top G\chi} \chi^\top G'(I - \hat{\chi}\hat{\chi}^\top)J(\chi)\dot{\zeta}. \end{aligned}$$

\triangleleft

Remark 4.27. To improve the convergence speed, the following angle control input is preferred:

$$\theta_u = \tau_\theta \left(\dot{\theta}_d - k_\theta \frac{1 - \hat{h}^p^\top \hat{\chi}^p}{\hat{h}^p^\top E \hat{\chi}^p} \right) + \theta.$$

Using this control input, it can be easily calculated that $\dot{\theta} = \dot{\theta}_d - k_\theta \frac{1 - \hat{h}^p^\top \hat{\chi}^p}{\hat{h}^p^\top E \hat{\chi}^p}$, and hence $\dot{V} = -k_\theta(1 - \hat{h}^p^\top \hat{\chi}^p) = -k_\theta V$. This shows that \hat{h}^p will exponentially converge to $\hat{\chi}^p$. However, note that

$$\frac{1 - \hat{h}^p^\top \hat{\chi}^p}{\hat{h}^p^\top E \hat{\chi}^p} = \frac{1 - \cos \beta}{\sin \beta} = \tan \frac{\beta}{2}.$$

Thus when $\beta = \pi$ (i.e., $\hat{h}^p = -\hat{\chi}^p$), the control input becomes infinitely large. Therefore, this control input is adopted when $\beta(0) \neq \pi$. In addition, similar to Remark 4.26, the above control input can be simplified to

$$\theta_u = \tau_\theta \left(\dot{\theta}_d - k_\theta \frac{\sqrt{\chi^\top G \chi} - \hat{h}^p^\top F \chi}{\hat{h}^p^\top F' \chi} \right) + \theta.$$

△

This theorem implies that the planar orientation of the robot \hat{h}^p will asymptotically converge to that of the vector field $\hat{\chi}^p$ (i.e., $\hat{h}^p \rightarrow \hat{\chi}^p$) almost globally with respect to the initial angle difference $\beta(0)$. The altitude and airspeed control are more straightforward. Since the planar orientation of the aircraft $\hat{h}^p = (\dot{x}, \dot{y})^\top / s$ will approach that of the vector field $\hat{\chi}^p$ using the control input θ_u developed in the previous part, it is desirable that \dot{z} equals the third component of the vector field χ_3 . However, in view of (4.24a) and (4.24b), since $\|(\dot{x}, \dot{y})\| = s$, \dot{z} should be scaled accordingly to $\dot{z} = s \chi_3 / \sqrt{\chi_1^2 + \chi_2^2}$. Therefore, it can be computed from (4.24d) that the altitude control input is

$$z_u = z + \tau_z s \chi_3 / \sqrt{\chi_1^2 + \chi_2^2}. \quad (4.31)$$

The idea of scaling is the same as that in [119]. Next, to let the aircraft fly at the constant nominal speed (cruise speed) s^* , the airspeed control input in (4.24e) is simply

$$s_u = s^*. \quad (4.32)$$

Therefore, the control inputs θ_u, z_u and s_u result in the asymptotic convergence of the orientation difference between the aircraft and the 3D vector field to zero. If this orientation error is regarded as a vanishing disturbance, then according to

the local ISS property in Theorem 4.19, the path-following error will also vanish, and thus the path-following behavior is successfully realized.

4.6 SIMULATIONS

The first simulation considers a bounded desired path in 3D. It is described by the intersection of two cylindrical surfaces, $\phi_1 = 0$ and $\phi_2 = 0$. Specifically,

$$\phi_1(\xi) = (x - a)^2 + (z - b)^2 - r^2, \quad \phi_2(\xi) = y^2 + z^2 - R^2,$$

where $a, b, R, r \in \mathbb{R}$ are parameters. We choose $R = 2, r = 1, a = 0, b = 1.5$. The desired path is shown in Fig. 4.2. Then the vector field $\chi(\xi)$ is readily obtained according to (4.2) with $k_1 = k_2 = 2$. It can be calculated that there are only three isolated singular points in this vector field (cross marks in Fig. 4.2). The control inputs in (4.28), (4.31) and (4.32) are used to guide the aircraft to follow this path. The other parameters are: $\tau_z = \tau_\theta = \tau_s = 1, k_\theta = 1$ and $s^* = 1$. The initial value of the kinematics model (4.24) is $(x(0), y(0), z(0), \theta(0), s(0)) = (1.8, 1, 2, \pi/4, 0)$. The aircraft trajectory is the solid line shown in Fig. 4.2, and the error $\|e\|$ is plotted in Fig. 4.3. As can be seen from the figure, the error $\|e\|$ is not monotonically decreasing. The initial increase of the error is due to the fact that the robot cannot move in any arbitrary direction; it first needs to steer its orientation towards that of the vector field, resulting in movement further away from the desired path in the beginning (see the beginning segment of the trajectory in Fig. 4.2). However, the aircraft successfully follows the desired bounded path as the error eventually converges to zero.

For the 3D unbounded path, we choose a helix described by

$$\phi_1(\xi) = x - \cos z, \quad \phi_2(\xi) = y - \sin z.$$

It can be easily calculated that $n_1 = (1, 0, \sin z)^\top$, $n_2 = (0, 1, -\cos z)^\top$ and $\tau = n_1 \times n_2 = (-\sin z, \cos z, 1)^\top$. It is interesting to note that there are no singular points in this case as $\tau \neq 0$ in \mathbb{R}^3 . In addition, since $\|n_1\| \leq \sqrt{2}$, $\|n_2\| \leq \sqrt{2}$ and $\|\tau\| = \sqrt{2}$, the assumptions in Theorem 4.15 are satisfied (globally). Therefore, the control inputs in (4.28), (4.31) and (4.32) can be used to guide the aircraft to follow this path. The other parameters are: $\tau_z = \tau_\theta = \tau_s = 1, k_1 = k_2 = k_\theta = 1$ and $s^* = 1$. The initial value is $(x(0), y(0), z(0), \theta(0), s(0)) = (0.1, 0, -5, \pi, 0)$. The aircraft's trajectory is the solid line shown in Fig. 4.4, and the error $\|e\|$ is plotted in Fig. 4.3. As can be seen from the figures, the aircraft successfully follows the desired unbounded path.

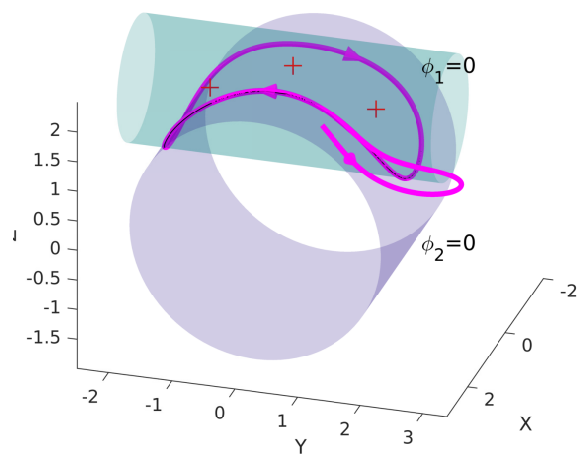


Figure 4.2: The fixed-wing aircraft successfully follows a 3D bounded desired path. The actual trajectory and the desired path overlaps. The arrows indicate the orientation of the aircraft.

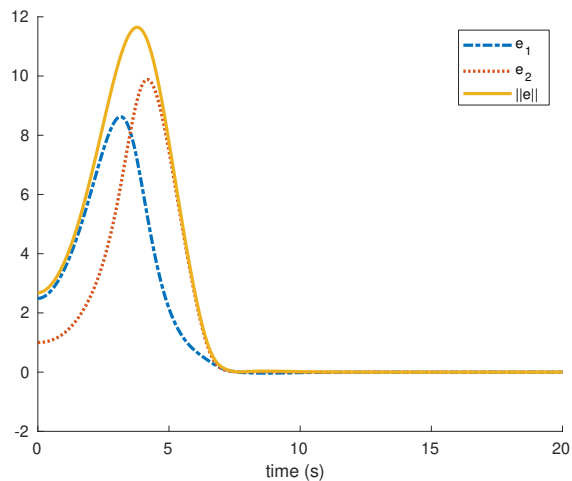


Figure 4.3: The path-following errors for the first simulation.

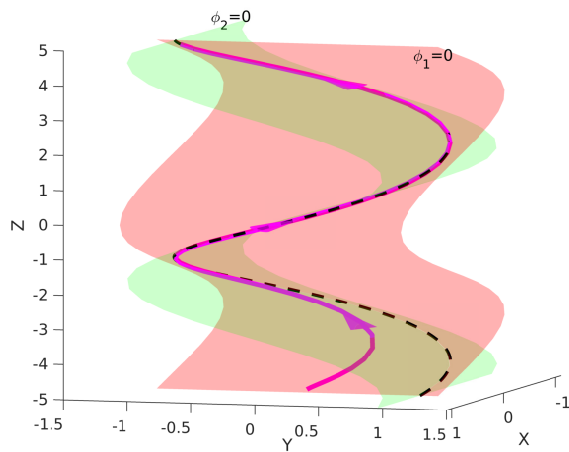


Figure 4.4: The trajectory of the fixed-wing aircraft (the solid line) gradually overlaps the 3D unbounded desired path (the dashed line). The arrows indicate the orientation of the aircraft.

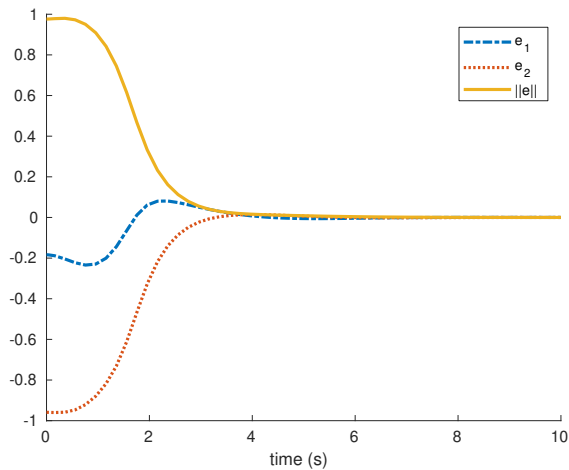


Figure 4.5: The path-following errors for the second simulation.

4.7 CONCLUSIONS

We have provided rigorous theoretical results for path-following control using a 3D vector field. Crucial assumptions are presented and elaborated. Based on this, we have shown the asymptotic and exponential convergence of the path-following error for both bounded and unbounded desired paths. Furthermore, the local ISS property of the path-following error dynamics is proved, which justifies the control algorithm designed for a nonholonomic model: a fixed-wing aircraft. Our vector field method is flexible in the sense that it is valid for any general desired path that is sufficiently smooth, and its extension to higher-dimension is straightforward.

5

TOPOLOGICAL ANALYSIS OF VECTOR-FIELD GUIDED PATH FOLLOWING ON MANIFOLDS

A path-following control algorithm enables a system's trajectories under its guidance to converge to and evolve along a given geometric desired path. There exist various such algorithms, but many of them can only guarantee local convergence to the desired path in its neighborhood. In contrast, the control algorithms using a well-designed guiding vector field can ensure almost global convergence of trajectories to the desired path; here, "almost" means that in some cases, a measure-zero set of trajectories converge to the singular set where the vector field becomes zero (with all other trajectories converging to the desired path). In this chapter, we first generalize the guiding vector field from the Euclidean space to a general smooth Riemannian manifold. This generalization can deal with path-following in some abstract configuration space (such as robot arm joint space). Then we show several theoretical results from a topological viewpoint. Specifically, we are motivated by the observation that singular points of the guiding vector field exist in many examples where the desired path is homeomorphic to the unit circle, but it is unknown whether the existence of singular points always holds in general (i.e., is inherent in the topology of the desired path). In the n -dimensional Euclidean space, we provide an affirmative answer, and conclude that it is not possible to guarantee global convergence to desired paths that are homeomorphic to the unit circle. Furthermore, we show that there always exist *non-path-converging trajectories* (i.e., trajectories that do not converge to the desired path) starting from the boundary of a ball containing the desired path in an n -dimensional Euclidean space where $n \geq 3$. Examples are provided to illustrate the theoretical results.

This chapter is based on

- W. Yao, B. Lin, B. D. O. Anderson, and M. Cao, "Topological analysis of vector-field guided path following on manifolds," *IEEE Transactions on Automatic Control (TAC)*, 2021, *Conditionally accepted*.

5.1 INTRODUCTION

Among various path-following algorithms, the vector-field guided path-following algorithms have been investigated extensively [50], [65], [72], [104], [172]. In these algorithms, the desired path is usually implicitly or explicitly assumed to be a sufficiently smooth *one-dimensional connected submanifold* in \mathbb{R}^n for regularity reasons. Thus, desired paths can be conveniently classified into two categories: those homeomorphic to the unit circle S^1 if they are compact and those homeomorphic to the real line \mathbb{R} otherwise [76, Theorem 5.27]. These algorithms utilize a sufficiently smooth vector field of which the integral curves are proved to converge to the desired path at least asymptotically. Moreover, once any point of a trajectory is on the desired path, the integral curves will keep evolving on the desired path [50], [74].

Note that most, if not all, of the studies assume that the Euclidean space \mathbb{R}^n is the configuration space of the considered ordinary differential equation where the right-hand side is the designed vector field. Although the explicit expressions of vector fields χ vary in different studies (c.f. [44], [50], [63], [72], [74], [81], [89], [172]), they generally consist of two components: a *convergence component* and a *propagation component*. The convergence component enables the integral curves of the vector field to approach the desired path, while the propagation component, orthogonal to the convergence component, provides a tangential direction to the desired path, and thus helps the integral curves propagate along the desired path. The two-component structure of the vector field is intuitive and effective in solving the path-following problem. In [50], a time-varying component is added to the vector field to deal with a time-varying desired path.

There are several advantages of the vector-field guided path-following algorithms. One of them is the removal of the condition requiring the initial point to be sufficiently close to the desired path, as otherwise commonly required by algorithms such as LOS [40], [93], [122], among others [137]. In addition, the vector-field guided algorithms are shown to achieve the highest path-following accuracy with the least control efforts among several algorithms in benchmark tests to follow a circle and a straight line [137]. However, their major drawback is the existence of *singular points* where the vector field becomes zero, and the consequences are: i) the integral curves of the vector field might only be extended in a finite time interval [63]; ii) normalization of the vector field, which is common in many practical applications [63], [156], at the singular point is not well defined; iii) if there are singular points, then the algorithm does not have the desirable property of *global convergence* to the desired path from any initial conditions, and the analysis becomes more difficult. Therefore, some existing studies either impose conservative assumptions ruling out attractive singular points or avoid providing detailed analysis for singular points [50], [72], [81], [98], [119]. The study in [63] does not use these assumptions and shows that the integral curves

of a 2D guiding vector field either converge to the desired path or the singular set, which consists of all singular points of the vector field. This dichotomy convergence result has been extended to a 3D vector field in Chapter 4. However, it is unknown whether this dichotomy convergence property holds for guiding vector fields defined on general manifolds, including \mathbb{R}^m for $m > 3$.

In the literature and in practice, vector-field guided path-following examples are typically illustrated with a desired path homeomorphic to the unit circle, such as a circle, an ellipse or a Cassini oval [63], [74]. In these examples, singular points of the guiding vector field exist, which implies that global convergence to the desired path cannot be guaranteed. Therefore, a natural question arises: *do singular points of the guiding vector field always exist when the desired path is homeomorphic to the unit circle, and thus global convergence to the desired path is not guaranteed?* This question is simple when the configuration space is the two-dimensional Euclidean space (i.e., $\mathcal{M} = \mathbb{R}^2$). Since the desired path is a closed orbit by construction, the Poincaré-Bendixson theorem (see Theorem 2.15) concludes that there is at least one singular point of the vector field¹ in the region enclosed by the desired path. Therefore, once a trajectory starts from the singular point, it stays there and thus global convergence to the desired path is not possible. However, the Poincaré-Bendixson theorem is only applicable for the planar case \mathbb{R}^2 , while the conclusion for the higher-dimensional case \mathbb{R}^n , where $n > 2$, and general manifolds is still untreated.

5.1.1 Contributions

This chapter extends the vector-field guided path-following algorithms to a general smooth Riemannian manifold \mathcal{M} , which is the first contribution (see Sections 5.2.1 and 5.3). One reason to consider smooth manifolds \mathcal{M} rather than the Euclidean space is the immediate relevance to potential applications, especially when one deals with mechanical systems [19]. For example, the control of revolute joint angles of a two-joint robot arm corresponds to the case where the manifold is a torus (i.e., $\mathcal{M} = \mathbb{T}^2 = S^1 \times S^1$) in the joint space (see the fourth example in Section 5.6). We show that global convergence from any point in the torus \mathbb{T}^2 to the desired path $\mathcal{P} \subseteq \mathbb{T}^2$ homeomorphic to the unit circle S^1 is not possible, but this issue can be solved by lifting the torus \mathbb{T}^2 to its covering space \mathbb{R}^2 (see Section 5.6).

The second contribution of this study arises from the analysis related to convergence, stability and attractiveness for the vector field defined on general manifolds (see Section 5.4). Specifically, we show that the dichotomy convergence property still holds for the vector-field guided path-following algorithms defined on the general smooth manifold \mathcal{M} . This means that trajectories either

¹ Here, a singular point of the vector field happens to be an equilibrium point of the ordinary differential equation where the right-hand side is the vector field.

converge to the desired path on \mathcal{M} or the singular set. This result is not only an extension of [63] which only considers \mathbb{R}^2 , but also plays an important role in the subsequent theoretical development (e.g., Corollary 5.17, Lemma 5.18, Corollary 5.19, Theorem 5.27). We also prove, under some mild conditions, the asymptotic stability of the desired path \mathcal{P} (i.e., Corollary 5.17) and the non-attractiveness² of the singular set \mathcal{C} (i.e., Corollary 5.19), which are highly desirable properties in any path-following algorithms. However, we show by an example that these two properties alone cannot guarantee the almost-global convergence property of the desired path (i.e., Example 5.22). All such analysis motivates the subsequent topological analysis.

The third contribution is to answer with respect to initial conditions the question proposed above regarding the existence of singular points and the possibility of global convergence (see Section 5.5). We first revisit a topological result (i.e., Lemma 5.23) revealing the relationship between a compact asymptotically stable embedded submanifold and its domain of attraction, and provide some interpretations along with an outline of our independent proof of this result (i.e., Remark 5.24). This reveals two essential elements behind the result: the regularity of the desired path (a compact asymptotically stable embedded submanifold) and the continuity of the *first hitting time*. Notably, we show that when the configuration space is the n -dimensional Euclidean space (i.e., $\mathcal{M} = \mathbb{R}^n$) and the desired path is homeomorphic to the unit circle, singular points of the vector field always exist, and it is impossible to enable trajectories to converge globally to the desired path from all initial conditions in \mathbb{R}^n (i.e., Theorem 5.27).

This impossibility result further motivates us to show the existence of *non-path-converging trajectories* (i.e., trajectories that do not converge to the desired path), which is the fourth contribution. It turns out that every ball containing the desired path has at least one non-path-converging trajectory starting from its boundary in \mathbb{R}^n for $n \geq 3$ (i.e., Theorem 5.30). This topological result is related to the impossibility of global convergence to the destination point of integral curves of a feedback motion planner [70, Chapter 8] in an obstacle-populated environment [68] (see Conjectures 5.33 and 5.34).

5.1.2 Chapter structure

Section 5.2 introduces the guiding vector field on a smooth n -dimensional Riemannian manifold for path following, and a concrete computation procedure of the vector field defined on manifolds is presented in Section 5.3. Section 5.4 elaborates on the preliminary analysis of the convergence issues. The main results are given in Section 5.5 regarding the existence of singular points, global convergence

² A formal definition is provided subsequently, but note that it is possible for some trajectories starting outside a non-attractive set to approach that set in the limit, a fact which is perhaps counter-intuitive. Consider in \mathbb{R}^2 the system $\dot{x}_1 = x_1, \dot{x}_2 = -x_2$, with the origin as the singular set.

to the desired path and the existence of non-path-converging trajectories. Several examples are provided in Section 5.6 to verify the theoretical results.

In this chapter, unless otherwise specified, all the manifolds have no boundaries.

5.2 GUIDING VECTOR FIELD FOR PATH FOLLOWING

In the literature of path-following problems using a guiding vector field, usually the guiding vector field is defined on the Euclidean space \mathbb{R}^n . In this section, we generalize the discussion to Riemannian manifolds and introduce notions (e.g., the distance) as generalized counterparts of those on the Euclidean space \mathbb{R}^n for the subsequent analysis. In other words, given a sufficiently smooth guiding vector field $\chi : \mathcal{M} \rightarrow T\mathcal{M}$, where \mathcal{M} is a Riemannian manifold that also satisfies some regularity conditions presented later and $T\mathcal{M}$ is the tangent bundle [77], we investigate the solutions to the following autonomous ordinary differential equation:

$$\dot{\xi}(t) = \chi(\xi(t)), \quad (5.1)$$

where $\xi(t) \in \mathcal{M}$ usually corresponds to a physical quantity such as the position of a mobile robot, and $\chi(\xi(t))$ corresponds to the desired velocity of the robot. The manifold \mathcal{M} is called the *configuration space*. The guiding vector field defined on a Riemannian manifold is introduced in Section 5.2.1 and some standard assumptions are presented in Section 5.2.2.

5.2.1 Guiding vector fields on Riemannian manifolds

We introduce some concepts first. A Riemannian manifold is denoted by (\mathcal{M}, g) , where g is the Riemannian metric [78]. The distance between a point $p \in \mathcal{M}$ and a submanifold $\mathcal{N} \subseteq \mathcal{M}$ is defined by $\text{dist}(p, \mathcal{N}) = \text{dist}(\mathcal{N}, p) := \inf\{d(p, q) : q \in \mathcal{N}\}$, where $d(\cdot, \cdot)$ is the Riemannian distance of two points in \mathcal{M} [78, p. 36]. The distance between \mathcal{N} and another submanifold $\mathcal{N}' \subseteq \mathcal{M}$ is defined by $\text{dist}(\mathcal{N}, \mathcal{N}') = \text{dist}(\mathcal{N}', \mathcal{N}) := \inf\{d(r, q) : r \in \mathcal{N}, q \in \mathcal{N}'\}$. The tangent space of \mathcal{M} at a point $p \in \mathcal{M}$ is denoted by $T_p\mathcal{M}$, and the length or norm of a tangent vector $v \in T_p\mathcal{M}$ is denoted by $\|v\|$ and defined by $\|v\| = \langle v, v \rangle_g^{1/2}$, where $\langle \cdot, \cdot \rangle_g$ is the inner product of tangent vectors in $T_p\mathcal{M}$. As a special case, if $\mathcal{M} = \mathbb{R}^n$, then the Riemannian metric is replaced by the canonical Riemannian metric (i.e., Euclidean metric) on \mathbb{R}^n , the Riemannian distance by the Euclidean distance and the inner product by the dot product.

Suppose the configuration space of (5.1) is an n -dimensional smooth Riemannian manifold (\mathcal{M}, g) , which is oriented, connected and complete [77, p. 340].

Suppose a desired path $\mathcal{P} \subseteq \mathcal{M}$ is described by the intersection of $(n - 1)$ zero-level sets; that is,

$$\mathcal{P} = \{\xi \in \mathcal{M} : \phi_i(\xi) = 0, i = 1, \dots, n - 1\}, \quad (5.2)$$

where $\phi_i : \mathcal{M} \rightarrow \mathbb{R}$, $i = 1, \dots, n - 1$, called *level functions* for convenience, are of differentiability class C^2 . Such a geometric description of the desired path without explicit parametric form is common in the literature when $\mathcal{M} = \mathbb{R}^n$ [24], [50], [89], [119], [157]. However, the set description of \mathcal{P} might not be desirable if no further restrictions are imposed; e.g., the set \mathcal{P} might be disconnected or even empty. Therefore, one usually needs to assume that \mathcal{P} is a connected one-dimensional submanifold in \mathcal{M} such that it corresponds to a desired path in practice. One advantage of the level-set description (5.2) is that the distance of a point $\xi \in \mathcal{M}$ to the desired path \mathcal{P} can be *approximated* by the value of $\|(\phi_1, \dots, \phi_{n-1})\|$ under some mild assumptions to be proposed later. Thus one could avoid the computation of the distance $\text{dist}(\xi, \mathcal{P})$, which is difficult even if the desired path is as standard as an ellipse in \mathbb{R}^2 .

For simplicity, we first briefly introduce the guiding vector field on \mathbb{R}^n , and later extend it to the general manifold \mathcal{M} . The n -dimensional vector field $\chi : \mathbb{R}^n \rightarrow \mathbb{R}^n$ is (see Chapter 9):

$$\chi(\xi) = \wedge(\nabla\phi_1(\xi), \dots, \nabla\phi_{n-1}(\xi)) - \sum_{i=1}^{n-1} k_i \phi_i(\xi) \nabla\phi_i(\xi), \quad (5.3)$$

for $\xi \in \mathbb{R}^n$, where $\nabla\phi_i : \mathbb{R}^n \rightarrow \mathbb{R}^n$ is the gradient of ϕ_i , $k_i > 0$ are constant gains, and $\wedge : \underbrace{\mathbb{R}^n \times \dots \times \mathbb{R}^n}_{n-1} \rightarrow \mathbb{R}^n$ is the wedge product [77, p. 355]. In the

Euclidean space, the wedge product can be calculated as follows: suppose we have vectors $p_i = (p_{i1}, \dots, p_{in})^\top \in \mathbb{R}^n$, $i = 1, \dots, n - 1$, then the k -th component of $\wedge(p_1, \dots, p_{n-1})$ is $(-1)^{k-1}$ multiplying the determinant of the submatrix obtained by deleting the k -th column of the $(n - 1)$ by n matrix which is formed by placing the vectors $p_1^\top, \dots, p_{n-1}^\top$ row by row. Note that $\wedge(\nabla\phi_1(\xi), \dots, \nabla\phi_{n-1}(\xi))$ is orthogonal to each of the gradients $\nabla\phi_i(\xi)$ for $i = 1, \dots, n - 1$ [45, Proposition 7.2.1].

We explain the physical interpretation of the vector field in (5.3). As mentioned before, the vector field generally consists of two terms: the *propagation term* and the *convergence term*. The propagation term $\wedge(\nabla\phi_1, \dots, \nabla\phi_{n-1})$ is orthogonal to each gradient vector $\nabla\phi_i$, and thus is tangent to each c -level surface described by $\{p \in \mathbb{R}^n : \phi_i(p) = c\}$. This enables the trajectory to move along the intersection of these level surfaces, and especially move along the desired path when $c = 0$. The forward or backward direction of the movement with regard to the desired path can be changed by switching the order of any two of the gradient vectors in the wedge product. The convergence term $-\sum_{i=1}^{n-1} k_i \phi_i \nabla\phi_i$ is a linear combination of

the gradient vectors, with the state dependent “weight” $-k_i\phi_i$. Thus it provides a direction towards the intersection of the zero-level surfaces, which is the desired path \mathcal{P} .

Now we show how to generalize the former discussion from the Euclidean space \mathbb{R}^n to the Riemannian manifold \mathcal{M} . Specifically, the gradient $\nabla\phi_i(\xi)$ and the term $\wedge(\nabla\phi_1(\xi), \dots, \nabla\phi_{n-1}(\xi))$ for $\xi \in \mathbb{R}^n$ will be replaced by their counterparts denoted by $\text{grad } \phi_i(\xi)$ and $\perp_\phi(\xi)$ respectively for $\xi \in \mathcal{M}$. The Riemannian gradient $\text{grad } \phi_i(\xi) \in T_\xi \mathcal{M}$ is the tangent vector to \mathcal{M} at $\xi \in \mathcal{M}$ such that for all tangent vectors $v \in T_\xi \mathcal{M}$, there holds

$$\langle \text{grad } \phi_i(\xi), v \rangle_g = d\phi_i|_\xi(v), \quad (5.4)$$

where $d\phi_i|_\xi : T_\xi \mathcal{M} \rightarrow \mathbb{R}$ is the *differential* of ϕ_i at $\xi \in \mathcal{M}$ [77, p. 281]. The other term $\perp_\phi(\xi) \in T_\xi \mathcal{M}$ is the tangent vector such that for all tangent vectors $v \in T_\xi \mathcal{M}$, there holds

$$\langle \perp_\phi(\xi), v \rangle_g = \omega_g(\text{grad } \phi_1(\xi), \dots, \text{grad } \phi_{n-1}(\xi), v), \quad (5.5)$$

where ω_g is the *volume form*³ associated with \mathcal{M} [78, p. 30]. The existence and uniqueness of $\text{grad } \phi_i(\xi)$ and $\perp_\phi(\xi)$ are guaranteed by the Riesz representation theorem [7, Theorem 6.42]. The calculations of these two terms are deferred until Section 5.3. Therefore, the guiding vector field defined on \mathcal{M} becomes

$$\chi(\xi) = \perp_\phi(\xi) - \sum_{i=1}^{n-1} k_i \phi_i(\xi) \text{grad } \phi_i(\xi). \quad (5.6)$$

with $k_i > 0$. In addition, as in the Euclidean case, the term $\perp_\phi(\xi)$ is also orthogonal to each of the gradients $\text{grad } \phi_i(\xi)$, as formally stated in the following lemma:

Lemma 5.1 (Orthogonality). *With definitions as above, there holds*

$$\langle \perp_\phi(\xi), \text{grad } \phi_i(\xi) \rangle_g = 0$$

for $i = 1, \dots, n-1$ and $\xi \in \mathcal{M}$.

Proof. This is an immediate consequence of the skew-symmetric property of the volume form ω_g . \square

Remark 5.2. In view of (5.4) and (5.5), although different Riemannian metrics would result in different gradients $\text{grad } \phi_i(\cdot)$ and orthogonal terms $\perp_\phi(\cdot)$, they would not affect the convergence properties of the guiding vector field (5.6). Nevertheless, a natural choice of the Riemannian metric is the one determined by the kinetic energy of a robot. \triangleleft

³ The volume form exists since the manifold \mathcal{M} is assumed to be oriented.

We define $e : \mathcal{M} \rightarrow \mathbb{R}^{n-1}$ by stacking ϕ_i ; that is,

$$e(\xi) = (\phi_1(\xi), \dots, \phi_{n-1}(\xi))^\top. \quad (5.7)$$

Using this notation, the desired path is equivalent to

$$\mathcal{P} = \{\xi \in \mathcal{M} : e(\xi) = \mathbf{0}\}. \quad (5.8)$$

This definition of the desired path suggests that $e(\xi)$ can be taken as the *path-following error* between the point $\xi \in \mathcal{M}$ and the desired path \mathcal{P} . The *singular set* is defined by

$$\begin{aligned} \mathcal{C} &= \{\xi \in \mathcal{M} : \chi(\xi) = \mathbf{0}\} \\ &= \left\{ \xi \in \mathcal{M} : \perp_\phi(\xi) = \sum_{i=1}^{n-1} k_i \phi_i(\xi) \operatorname{grad} \phi_i(\xi) = \mathbf{0} \right\}, \end{aligned} \quad (5.9)$$

with the second equality following from Lemma 5.1. Note that the singular set \mathcal{C} may be empty or nonempty. To illustrate this, we provide two examples respectively below.

Example 5.3 (Non-empty \mathcal{C}). Consider that the desired path is a 2D unit circle in the Euclidean space \mathbb{R}^2 described by $\phi(x, y) = x^2 + y^2 - 1 = 0$; then one can obtain the vector field by (5.3) and calculate that the singular set \mathcal{C} is a singleton consisting of the origin; that is, $\mathcal{C} = \{(0, 0)\}$. \triangleleft

Example 5.4 (Empty \mathcal{C}). A simple example is a straight line in the Euclidean space \mathbb{R}^2 described by $\phi(x, y) = y = 0$, which is the X-axis. One can calculate that the propagation term is a non-zero constant vector (i.e., $E \nabla \phi = (-1, 0)^\top$, where $E = \begin{bmatrix} 0 & -1 \\ 1 & 0 \end{bmatrix}$ is the 90° rotation matrix). Due to the orthogonality of the propagation term and the convergence term of (5.3), this implies that the vector field $\chi(x, y) \neq \mathbf{0}$ in \mathbb{R}^2 , and thus the singular set \mathcal{C} is empty. \triangleleft

Whether or not the singular set is empty may not be straightforward to determine, since one needs to obtain the analytic expression of the vector field and check if any point on the manifold renders it zero.

5.2.2 Standing assumptions

In the remainder of the chapter, the following assumptions will be made:

Assumption 5.5. There are no singular points on the desired path. More precisely, \mathcal{C} is empty or otherwise there holds $\operatorname{dist}(\mathcal{C}, \mathcal{P}) > 0$.

Assumption 5.6. For any given constant $\kappa > 0$, there holds $\inf\{|e(\xi)| : \operatorname{dist}(\xi, \mathcal{P}) \geq \kappa\} > 0$.

Assumption 5.5 ensures the “regularity” of the desired path \mathcal{P} stated in Lemma 5.7 below.

Lemma 5.7 (Regularity of \mathcal{P}). *The zero vector $\mathbf{0} \in \mathbb{R}^{n-1}$ is a regular value of the map e in (5.7), and hence the desired path \mathcal{P} is a C^2 (properly) embedded submanifold in \mathcal{M} .*

Proof. This is a direct application of the regular level set theorem [77, Corollary 5.14]. \square

Assumption 5.6 implies that as the norm of the path-following error $\|e(\xi)\|$ approaches zero, the trajectory $\xi(t)$ approaches the desired path \mathcal{P} (see Corollary 3.13). These assumptions are vital in the sense that if either of these assumptions is not satisfied, then different choices of level functions ϕ_i for the same desired path may lead to opposite convergence results, as the next example shows.

Example 5.8 (Opposite convergence results). We consider a straight line in the 3D Euclidean space \mathbb{R}^3 . One can choose the level functions $\phi_i, i = 1, 2$, as $\phi_1(x, y, z) = y, \phi_2(x, y, z) = z$, and the integral curves of the corresponding vector field (5.3) converge to the desired straight line (see Fig. 5.1a). Another design of level functions ϕ_i is $\phi_1(x, y, z) = ye^{-x}, \phi_2(x, y, z) = z$. In this case, however, as shown in Fig. 5.1b, the trajectory diverges from the desired path, although the norm of the path-following error $\|e\|$ for this case is also approaching zero along the trajectory (see Fig. 5.1c). The reason is that the second case violates Assumption 5.6. This can be observed by considering a straight line L parallel to the desired path but keeping a positive distance $\text{dist}(L, \mathcal{P}) > 0$. For example, let $L := \{(x, 1, 0) : x \in \mathbb{R}\}$. Then the fact that $\inf\{\|e(\xi)\| : \xi \in L\} = 0$ violates Assumption 5.6. \triangleleft

5.3 COMPUTATION OF GUIDING VECTOR FIELDS ON MANIFOLDS

The definitions of the gradient $\text{grad } \phi_i$ in (5.4) and the orthogonal term \perp_ϕ in (5.5) for the guiding vector field on the manifold \mathcal{M} are too abstract for direct computations. In this section, we present some general methods to compute these terms and hence the guiding vector field in coordinates. To this end, we suppose that the manifold \mathcal{M} considered in (5.2) is an n -dimensional smooth submanifold embedded in the Euclidean space \mathbb{R}^{n+k} , where n is the dimension of the manifold \mathcal{M} and k is some positive integer⁴, and the manifold \mathcal{M} is a regular level set of a smooth function $F : \mathbb{R}^{n+k} \rightarrow \mathbb{R}^k$. Specifically, we assume

$$\mathcal{M} = F^{-1}(a) = \{x \in \mathbb{R}^{n+k} : f_i(x) = a_i, i = 1, \dots, k\}, \quad (5.10)$$

⁴ This is always possible according to the Whitney embedding theorem [77, Theorem 6.15], which concludes that every smooth n -manifold admits a proper smooth embedding into \mathbb{R}^{2n+1} .

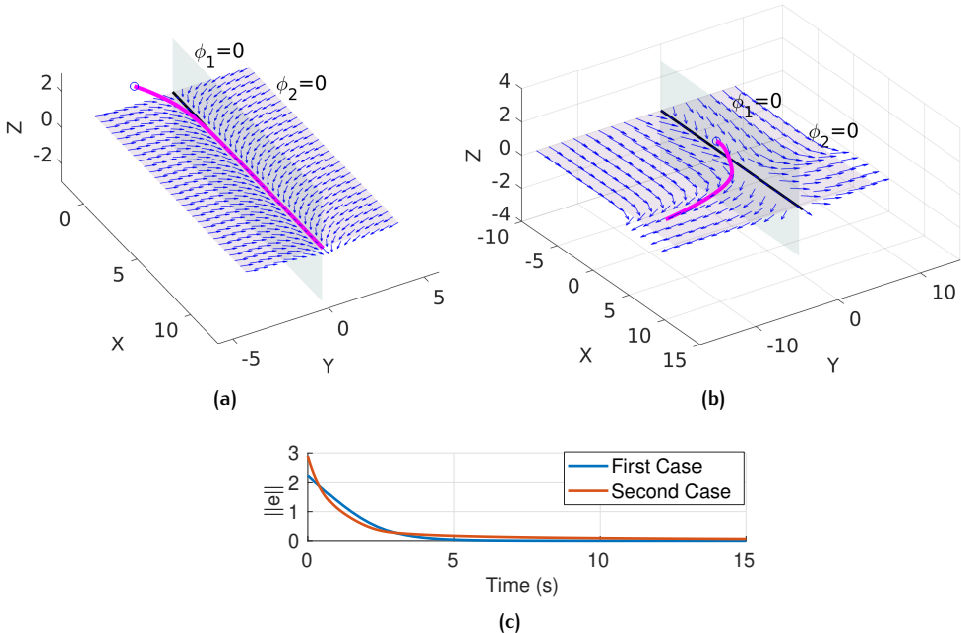


Figure 5.1: The same desired path (X -axis) with different level functions $\phi_i, i = 1, 2$. Magenta lines are trajectories, starting from the positions represented by blue points. (a) The trajectory converges to the desired path. (b) The trajectory diverges from the desired path. (c) Both of the norms of the path-following error converge to zero.

where $f_i : \mathbb{R}^{n+k} \rightarrow \mathbb{R}$ are smooth component functions of F and $a = (a_1, \dots, a_k) \in \mathbb{R}^k$ is a regular value of F . For example, if the manifold \mathcal{M} is the sphere S^2 , then it is a two-dimensional manifold embedded in \mathbb{R}^3 and can be described by $S^2 = \{x = (x_1, x_2, x_3) \in \mathbb{R}^3 : f_1(x) = x_1^2 + x_2^2 + x_3^2 = 1\}$. In this case, $n = 2, k = 1$, $F = f_1$ and $a = 1$ is a regular value of F . Similar examples can be found for some other common manifolds, such as the special orthogonal group $SO(3)$ and the torus $\mathbb{T} = S^1 \times S^1$.

For notational simplicity, let $m := n + k$. In addition, to distinguish the Riemannian metrics in the Euclidean space \mathbb{R}^m and in the manifold \mathcal{M} , we adopt the following notations. For $x \in \mathbb{R}^m$, the Riemannian metric in the Euclidean space \mathbb{R}^m is the canonical one, denoted by $\langle \cdot, \cdot \rangle_x^{\mathbb{R}^m} : T_x \mathbb{R}^m \times T_x \mathbb{R}^m \rightarrow \mathbb{R}$, while for $y \in \mathcal{M}$, the Riemannian metric is denoted by $\langle \cdot, \cdot \rangle_y^{\mathcal{M}} : T_y \mathcal{M} \times T_y \mathcal{M} \rightarrow \mathbb{R}$. Let $\tilde{\phi}_i : \mathcal{U} \rightarrow \mathbb{R}$, where $\mathcal{U} \subseteq \mathbb{R}^m$ is a neighborhood of $\mathcal{M} \subseteq \mathbb{R}^m$, be an extension of the level function $\phi_i : \mathcal{M} \rightarrow \mathbb{R}$ in (5.2) [77, Lemma 5.34]; that is, the restriction of $\tilde{\phi}_i$ on \mathcal{M} is ϕ_i , or $\tilde{\phi}_i|_{\mathcal{M}} = \phi_i$.

The following result shows that the gradient defined on the manifold \mathcal{M} is just the orthogonal projection of the “usual” gradient in the Euclidean space onto the tangent space to the manifold \mathcal{M} at some point.

Proposition 5.9. *For $x \in \mathcal{M} \subseteq \mathbb{R}^m$, define the orthogonal projection function $Pr_{T_x\mathcal{M}} : T_x\mathbb{R}^m \rightarrow T_x\mathcal{M}$. Then we have*

$$\text{grad } \phi_i(x) = Pr_{T_x\mathcal{M}}(\nabla \tilde{\phi}_i(x)), \quad (5.11)$$

where $\text{grad } \phi_i(x) \in T_x\mathcal{M}$ and $\nabla \tilde{\phi}_i(x) \in T_x\mathbb{R}^m$. In particular,

$$\text{grad } \phi_i(x) = \nabla \tilde{\phi}_i(x) - \sum_{j=1}^k \frac{\langle \nabla \tilde{\phi}_i(x), \nabla f_j(x) \rangle_x^{\mathbb{R}^m}}{\|\nabla f_j(x)\|^2} \nabla f_j(x), \quad (5.12)$$

where $f_j, j = 1, \dots, k$, are functions in (5.10).

Proof. The equation (5.11) is a standard result (see, e.g., [55, pp. 360-362]). Since the manifold \mathcal{M} is described by (5.10), we have that $(T_x\mathcal{M})^\perp = \text{span}(\nabla f_1(x), \dots, \nabla f_k(x))$, hence (5.12). \square

Using these computable gradients $\text{grad } \phi_i, i = 1, \dots, n-1$, as in Proposition 5.9, we can now derive a computable form for the orthogonal term \perp_ϕ in (5.5). Before that, recall that for $p_i = (p_{i1}, p_{i2}, p_{i3})^\top \in \mathbb{R}^3, i = 1, 2$, the cross product $p_1 \times p_2$ is calculated by the following intuitive *formal expression* involving the matrix determinant [42, pp. 241-242]:

$$p_1 \times p_2 = \begin{vmatrix} \mathbf{b}_1 & \mathbf{b}_2 & \mathbf{b}_3 \\ p_{11} & p_{12} & p_{13} \\ p_{21} & p_{22} & p_{23} \end{vmatrix} \quad (5.13)$$

$$= \begin{vmatrix} p_{12} & p_{13} \\ p_{22} & p_{23} \end{vmatrix} \mathbf{b}_1 - \begin{vmatrix} p_{11} & p_{13} \\ p_{21} & p_{23} \end{vmatrix} \mathbf{b}_2 + \begin{vmatrix} p_{11} & p_{12} \\ p_{21} & p_{22} \end{vmatrix} \mathbf{b}_3 \quad (5.14)$$

$$= \begin{vmatrix} p_{11} & p_{21} & \mathbf{b}_1 \\ p_{12} & p_{22} & \mathbf{b}_2 \\ p_{13} & p_{23} & \mathbf{b}_3 \end{vmatrix}, \quad (5.15)$$

where $\mathbf{b}_j \in \mathbb{R}^3, j = 1, 2, 3$, are the standard basis vectors and $|\cdot|$ is the determinant of a square matrix. Equation (5.14) is obtained using the cofactor expansion along the first row of (5.13), where in evaluating the determinant, the \mathbf{b}_i should initially be regarded as scalars, and in the final evaluation replaced by the basis vectors which they are. This formal expression can be naturally extended to Euclidean spaces of any dimension, a fact utilized below.

Proposition 5.10. For $x \in \mathcal{M} \subseteq \mathbb{R}^m$, the orthogonal term \perp_ϕ defined in (5.5) can be computed by the following formal form:

$$\perp_\phi(x) = \det \begin{bmatrix} \mathbf{b}_1 \\ \nabla f_1(x), \dots, \nabla f_k(x), \text{grad } \phi_1(x), \dots, \text{grad } \phi_{n-1}(x), \vdots \\ \mathbf{b}_m \end{bmatrix}, \quad (5.16)$$

where $\mathbf{b}_i \in \mathbb{R}^m, i = 1, \dots, m$, are standard basis vectors, and $\text{grad } \phi_i, i = 1, \dots, n-1$, are calculated from Proposition 5.9.

Proof. We first consider the case for the Euclidean space \mathbb{R}^m , and then extend to that for the manifold \mathcal{M} . For any $x \in \mathbb{R}^m$, we can pick a volume form $\omega_x : \underbrace{T_x \mathbb{R}^m \times \dots \times T_x \mathbb{R}^m}_m \rightarrow \mathbb{R}$, which is a skew-symmetric and non-degenerate linear function, such that ω_x is smooth with respect to x . Note that the general form of ω_x is $\omega_x = c(x) \cdot dx_1 \wedge \dots \wedge dx_m$, where $c : \mathbb{R}^m \rightarrow \mathbb{R}$ is a non-zero and smooth function. Specifically, for the column vectors $a_i = (a_{i,1}, \dots, a_{i,m})^\top \in \mathbb{R}^m, i = 1, \dots, m$, it holds that

$$dx_1 \wedge \dots \wedge dx_m (a_1, \dots, a_m) = \det \begin{bmatrix} a_{1,1} & \cdots & a_{1,m} \\ \vdots & \ddots & \vdots \\ a_{m,1} & \cdots & a_{m,m} \end{bmatrix}. \quad (5.17)$$

Let $\omega_x(a_1, \dots, a_m) := dx_1 \wedge \dots \wedge dx_m (a_1, \dots, a_m)$. We can calculate the volume form on the manifold \mathcal{M} , denoted by $\omega^{\mathcal{M}} : \underbrace{T_x \mathcal{M} \times \dots \times T_x \mathcal{M}}_n \rightarrow \mathbb{R}$, as follows:

$$\begin{aligned} \omega_x^{\mathcal{M}}(v_1, \dots, v_n) &:= \omega_x(\nabla f_1(x), \dots, \nabla f_k(x), v_1, \dots, v_n) \\ &= \det [\nabla f_1(x), \dots, \nabla f_k(x), v_1, \dots, v_n], \end{aligned}$$

where $v_j \in T_x \mathcal{M}, j = 1, \dots, n$. Hence, by (5.5), we have

$$\langle \perp_\phi(\xi), \cdot \rangle_x^{\mathcal{M}} = \omega_x^{\mathcal{M}}(\text{grad } \phi_1(x), \dots, \text{grad } \phi_{n-1}(x), \cdot) = \langle \Delta, \cdot \rangle_x^{\mathcal{M}},$$

where Δ is the right-hand side of (5.16). So (5.16) holds. \square

The above results serve collectively as a general procedure to compute the guiding vector field on \mathcal{M} . Note that in some particular examples, one might not necessarily need to compute all quantities appearing in these propositions. For example, (5.12) is not necessary if the tangent space $T_x \mathcal{M}$ is explicitly known (e.g., the tangent space of $SO(3)$).

Example 5.11 (Guiding vector field on S^2). Suppose the sphere S^2 is the manifold \mathcal{M} on which the guiding vector field is defined. It is a two-dimensional manifold

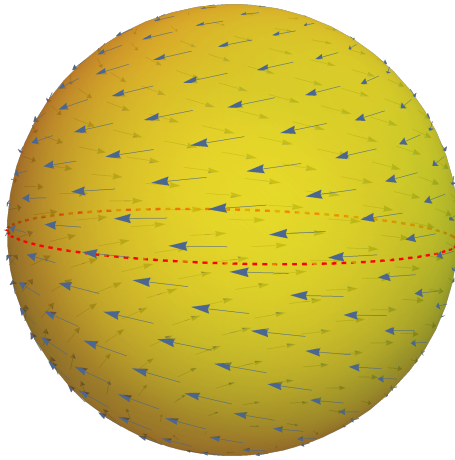


Figure 5.2: The guiding vector field χ on the sphere $\mathcal{M} = \mathbb{S}^2$ in Example 5.11. The red dashed line is the desired path \mathcal{P} , which is a circle on the sphere.

that can be naturally embedded in the Euclidean space \mathbb{R}^3 , and then (5.10) becomes

$$\mathcal{M} = \mathbb{S}^2 = \{(x, y, z) \in \mathbb{R}^3 : f_1(x, y, z) = x^2 + y^2 + z^2 = 1\}.$$

The desired path $\mathcal{P} \subseteq \mathcal{M}$ is the unit circle with $z = 0$. Therefore, we can let $\tilde{\phi}_1 : \mathbb{R}^3 \rightarrow \mathbb{R}$ be defined by $\tilde{\phi}_1(x, y, z) = z$, and then $\phi_1 : \mathcal{M} \rightarrow \mathbb{R}$ is just $\phi_1 = \tilde{\phi}_1|_{\mathcal{M}}$ in (5.2). We can calculate the gradient term $\text{grad } \phi_1$ and the orthogonal term \perp_{ϕ} by Proposition 5.9 and Proposition 5.10 respectively. First, we have $\nabla \tilde{\phi}_1 = (0, 0, 1)^{\top}$ and $\nabla f_1 = (2x, 2y, 2z)^{\top}$. For any point $\xi \in \mathcal{M}$, it follows from (5.12) that

$$\text{grad } \phi_1(\xi) = \nabla \tilde{\phi}_1(\xi) - \frac{\langle \nabla \tilde{\phi}_1(\xi), \nabla f_1(\xi) \rangle}{\|\nabla f_1(\xi)\|^2} \nabla f_1(\xi) = \begin{bmatrix} -xz \\ -yz \\ 1-z^2 \end{bmatrix},$$

and from (5.16) that

$$\perp_{\phi}(\xi) = \det \begin{bmatrix} & b_1 \\ \nabla f_1(\xi), \text{grad } \phi_1(\xi), b_2 \\ & b_3 \end{bmatrix} = \begin{bmatrix} 2y \\ -2x \\ 0 \end{bmatrix}.$$

Finally, the “computable” guiding vector field on the sphere is obtained by putting these two terms into (5.6) as follows:

$$\chi(\xi) = \perp_\phi(\xi) - k_1 \phi_1(\xi) \operatorname{grad} \phi_1(\xi) = \begin{bmatrix} 2y + k_1 xz^2 \\ -2x + k_1 yz^2 \\ k_1 z(z^2 - 1) \end{bmatrix} \quad (5.18)$$

for any point $\xi = (x, y, z) \in S^2 \subseteq \mathbb{R}^3$. The vector field is shown in Fig. 5.2. Interestingly, there are two singular points in this vector field (5.18): the north pole and the south pole (i.e., $(0, 0, \pm 1)$). However, as shown in Example 5.3, if we consider the Euclidean space $\mathcal{M} = \mathbb{R}^2$, then there is only one singular point: the origin $(0, 0)$. Similarly, if we consider the 3D Euclidean space $\mathcal{M} = \mathbb{R}^3$, and use the functions $\phi_1(x, y, z) = x^2 + y^2 - 1 = 0$ and $\phi_2(x, y, z) = z = 0$ to characterize the same unit circle as the desired path, there is now only one singular point and it is at the origin $(0, 0, 0)$. This example shows that corresponding to the same desired path, guiding vector fields (and singular sets) defined on different manifolds are possibly quite different. \triangleleft

5.4 DICHOTOMY CONVERGENCE AND STABILITY ANALYSIS

It is important to analyze the convergence results of the integral curves of the vector field (5.6); that is, the trajectories of the differential equation (5.1), where the vector field $\chi(\cdot)$ is defined in (5.6). It turns out that the dichotomy convergence property holds not only for the vector field on the Euclidean space $\mathbb{R}^n, n \geq 2$ (see Chapter 4), but also for that on the Riemannian manifold \mathcal{M} . First we define the function $V : \mathcal{M} \rightarrow \mathbb{R}$ as

$$V(\xi) = e^\top(\xi) K e(\xi), \quad (5.19)$$

where $K := \operatorname{diag}\{k_1, \dots, k_{n-1}\}$ is the diagonal matrix with all the positive gains $k_i, i = 1, \dots, n-1$. The function V is non-negative and attains zero if and only if $\xi \in \mathcal{P}$. This function is utilized as a Lyapunov-like function in the analysis subsequently. We assume in this chapter until further notice that the desired path \mathcal{P} is homeomorphic to the unit circle (hence compact):

Assumption 5.12. The desired path \mathcal{P} is homeomorphic to the unit circle S^1 (i.e., $\mathcal{P} \approx S^1$).

Then we can choose $r > 0$ sufficiently large such that the open ball $\mathcal{B}_r := \{x \in \mathcal{M} : \|x\| < r\}$ contains the desired path \mathcal{P} (i.e., $\mathcal{P} \in \operatorname{int} \mathcal{B}_r$). Let $\alpha' := \min_{p \in \partial \mathcal{B}_r} V(p) > 0$, where the minimum is attained on the compact sphere $\partial \mathcal{B}_r$ (i.e., the boundary of the ball \mathcal{B}_r), and it is positive since $\partial \mathcal{B}_r \cap \mathcal{P} = \emptyset$. We can

choose a positive constant α such that $0 < \alpha < \alpha'$, and the set Ω_α defined below is compact:

$$\Omega_\alpha := \{\xi \in \mathcal{B}_r : V(\xi) \leq \alpha\}. \quad (5.20)$$

Note that $\mathcal{P} \subseteq \Omega_\alpha$ for any $\alpha > 0$. Now we can present the dichotomy convergence result as follows:

Theorem 5.13 (Dichotomy convergence). *Consider the autonomous system (5.1), where the vector field $\chi : \mathcal{M} \rightarrow T\mathcal{M}$ is in (5.6). Then the compact set Ω_α in (5.20) is positively invariant. In addition, every trajectory of (5.1) starting from Ω_α converges to either the desired path \mathcal{P} , or the singular set \mathcal{C} as $t \rightarrow \infty$ (i.e., the dichotomy convergence property holds).*

Proof. The proof for a special case $\mathcal{M} = \mathbb{R}^3$ (but easily generalizable to $\mathcal{M} = \mathbb{R}^n$) is presented in Chapter 4. It can be further generalized to the case of a Riemannian manifold \mathcal{M} by modifying the involved calculations related to the Riemannian metric. First note that

$$\begin{aligned} \langle \text{grad } \phi_i, \chi \rangle_g &\stackrel{(5.6)}{=} \left\langle \text{grad } \phi_i, \perp_\phi(\xi) - \sum_{j=1}^{n-1} k_j \phi_j(\xi) \text{grad } \phi_j(\xi) \right\rangle_g \\ &= \left\langle \text{grad } \phi_i, - \sum_{j=1}^{n-1} k_j \phi_j(\xi) \text{grad } \phi_j(\xi) \right\rangle_g, \end{aligned} \quad (5.21)$$

for $i = 1, \dots, n-1$, where we have used the orthogonality property (Lemma 5.1) in the last equation. Now we can calculate the time derivative of the path-following error e :

$$\begin{aligned} \frac{d}{dt} e(\xi(t)) &= \frac{d}{dt} \begin{bmatrix} \phi_1(\xi(t)) \\ \vdots \\ \phi_{n-1}(\xi(t)) \end{bmatrix} = \begin{bmatrix} \langle \text{grad } \phi_1, \chi \rangle_g \\ \vdots \\ \langle \text{grad } \phi_{n-1}, \chi \rangle_g \end{bmatrix} \\ &\stackrel{(5.21)}{=} \begin{bmatrix} \langle \text{grad } \phi_1, - \sum_{j=1}^{n-1} k_j \phi_j \text{grad } \phi_j \rangle_g \\ \vdots \\ \langle \text{grad } \phi_{n-1}, - \sum_{j=1}^{n-1} k_j \phi_j \text{grad } \phi_j \rangle_g \end{bmatrix}. \end{aligned} \quad (5.22)$$

Therefore, the time derivative of the Lyapunov function (5.19) is

$$\begin{aligned}
 \frac{d}{dt} V &= 2 \left(\frac{d}{dt} e \right)^T K e \\
 &\stackrel{(5.22)}{=} 2 \begin{bmatrix} \langle \text{grad } \phi_1, -\sum_{j=1}^{n-1} k_j \phi_j \text{ grad } \phi_j \rangle_g \\ \vdots \\ \langle \text{grad } \phi_{n-1}, -\sum_{j=1}^{n-1} k_j \phi_j \text{ grad } \phi_j \rangle_g \end{bmatrix}^T \begin{bmatrix} k_1 \phi_1 \\ \vdots \\ k_{n-1} \phi_{n-1} \end{bmatrix} \\
 &= -2 \left\langle \sum_{j=1}^{n-1} k_j \phi_j \text{ grad } \phi_j, \sum_{j=1}^{n-1} k_j \phi_j \text{ grad } \phi_j \right\rangle_g \leq 0.
 \end{aligned} \tag{5.23}$$

Due to the negative semi-definiteness of (5.23), the compact set Ω_α is positively invariant. Next we will use the LaSalle's invariance principle (Theorem 2.6) to conclude the convergence results. First, we have the following equivalent sets

$$\mathcal{I} := \left\{ \xi \in \mathcal{M} : \frac{d}{dt} V(\xi) = 0 \right\} = \left\{ \xi \in \mathcal{M} : \sum_{j=1}^{n-1} k_j \phi_j(\xi) \text{ grad } \phi_j(\xi) = 0 \right\} = \mathcal{P} \cup \mathcal{C}.$$

The last equality is justified as follows. If a point $p \in \mathcal{P} \cup \mathcal{C}$, then it is obvious that p is contained in the set on the left-hand side of the equality, and thus $\mathcal{P} \cup \mathcal{C}$ is a subset of the set on the left-hand side. If a point p is in the set of the left-hand side, then we have $\sum_{j=1}^{n-1} k_j \phi_j(p) \text{ grad } \phi_j(p) = 0$. This implies that either all gradients $\text{grad } \phi_j(p)$ are linearly independent and $\phi_j(p) = 0$ for all $j = 1, \dots, n-1$, or the gradients $\text{grad } \phi_j(p)$ are linearly dependent and hence $\perp_\phi(p) = 0$. In the former case, $p \in \mathcal{P}$, and in the latter case, $p \in \mathcal{C}$. Therefore, the set on the left-hand side is a subset of $\mathcal{P} \cup \mathcal{C}$. Combining these two arguments, the last equality holds.

It is easy to see that the largest invariant set in $\mathcal{I} \cap \Omega_\alpha$ is itself: every trajectory of (5.1) starting from $\mathcal{C} \cap \Omega_\alpha$ will remain in $\mathcal{C} \cap \Omega_\alpha$ because $\mathcal{C} \cap \Omega_\alpha$ consists of equilibrium points of (5.1), and every trajectory of (5.1) starting from $\mathcal{P} \cap \Omega_\alpha = \mathcal{P}$ will remain in \mathcal{P} because the guiding vector field in (5.6) degenerates to $\chi(\xi) = \perp_\phi(\xi)$ on \mathcal{P} . Therefore, according to the LaSalle's invariance principle (Theorem 2.6), all trajectories starting from the compact and positively invariant set Ω_α will converge to the largest invariant set $\mathcal{I} \cap \Omega_\alpha$. By Assumption 5.5, this implies that trajectories either converge to the desired path \mathcal{P} or the singular set \mathcal{C} , hence the dichotomy convergence property still holds. \square

Remark 5.14. This Lemma relies on LaSalle's invariance principle for autonomous systems (Theorem 2.6), but to partially extend the result for non-autonomous systems, we can utilize the invariance principle for (non-autonomous) periodic systems [124, Theorem 5.26], [54, Theorem 55.1]. Consider the Euclidean space \mathbb{R}^n . We can modify the vector field (5.3) to $\chi = \wedge(\nabla \phi_1, \dots, \nabla \phi_{n-1}) -$

$\sum_{i=1}^{n-1} k_i(t) \phi_i(I_n - P_i) \nabla \phi_i$, where the matrix P_i is the projector in \mathbb{R}^n onto the subspace spanned by $\nabla \phi_j$, $\forall j \neq i$, and $k_i(t)$, $i = 1, \dots, n-1$, are piecewise constant and periodic. Then Theorem 5.13 is still applicable in this case. However, it is generally difficult to conduct topological analysis on non-autonomous systems, and thus we restrict to autonomous systems with the vector field (5.6) for the subsequent analysis. \triangleleft

We have shown by Theorem 5.13 that some undesirable phenomena in nonlinear systems, such as chaos, finite-time escape, cannot occur for the system (5.1) with the vector field (5.6). Now we show another desirable property: the desired path \mathcal{P} is attractive, while the singular set \mathcal{C} is not.

Definition 5.15. A nonempty closed positively invariant set $\mathcal{A} \subseteq \mathcal{M}$ is *attractive* with respect to (5.1), if there exists an open neighborhood \mathcal{U} of \mathcal{A} such that every trajectory $\xi(t)$ of (5.1) that starts within \mathcal{U} (i.e., $\xi(0) \in \mathcal{U}$) converges (topologically) to \mathcal{A} in the sense that for any neighborhood \mathcal{V} of \mathcal{A} , there exists a $T > 0$, such that $\xi(t \geq T) \subseteq \mathcal{V}$ when $\xi(0) \in \mathcal{U}$ (this implies that $\text{dist}(\xi(t), \mathcal{A}) \rightarrow 0$ as $t \rightarrow \infty$). If the set \mathcal{A} is not attractive, then it is called *non-attractive*. The set of all points for which trajectories start from and converge (topologically) to \mathcal{A} is the domain of attraction of \mathcal{A} (obviously, \mathcal{U} is a subset of the domain of attraction of \mathcal{A}).

Note that in the definition above, \mathcal{A} is not required to be compact. Note also that a set can be non-attractive and yet trajectories from outside the set can converge to the set; consider for example a time-invariant linear system $\dot{x} = Ax$, where some eigenvalues of A are in the left half plane and some are in the right half plane, resulting in the origin being non-attractive. We can also define the (Lyapunov) stability and asymptotic stability of the set \mathcal{A} [53, Definition 4.10] as below.

Definition 5.16. A nonempty closed positively invariant set \mathcal{A} is (*Lyapunov*) *stable* with respect to (5.1), if for every open neighborhood \mathcal{U}_1 of \mathcal{A} , there exists an open neighborhood $\mathcal{U}_2 \subseteq \mathcal{U}_1$ of \mathcal{A} , such that every trajectory of (5.1) stays in \mathcal{U}_1 once it starts from \mathcal{U}_2 (i.e., $\xi(t) \in \mathcal{U}_1$ for $t \geq 0$ with $\xi(0) \in \mathcal{U}_2$). Furthermore, if \mathcal{A} is both Lyapunov stable and attractive, then it is called *asymptotically stable*.

Corollary 5.17 (Asymptotic stability of \mathcal{P}). *The desired path \mathcal{P} is asymptotically stable.*

Proof. Due to Assumptions 5.5 and 5.6, there always exists a sufficiently small positive constant α such that $\Omega_\alpha \cap \mathcal{C} = \emptyset$. Therefore, by Theorem 5.13, the desired path \mathcal{P} is attractive. To prove that \mathcal{P} is asymptotically stable, we need to additionally show that it is (Lyapunov) stable. Define the set $\Gamma_a := \{p \in \mathcal{M} : \|e(p)\| < a\}$ for some positive constant $a > 0$, and it is obvious that $\mathcal{P} \subseteq \Gamma_a$. By the Lyapunov argument in (5.23) and Theorem 4.8 in [66], the equilibrium point $e = 0$ of the non-autonomous system (5.22) is uniformly stable. That is, for any $\epsilon > 0$, there is $\delta > 0$ (independent of the initial time instant t_0), such that

$\xi(t_0) \in \Gamma_\delta \implies \xi(t) \in \Gamma_\epsilon$ for all $t \geq t_0 \geq 0$. For any open neighborhood \mathcal{U}_1 of \mathcal{P} , we can choose a positive constant ϵ sufficiently small⁵, such that Γ_ϵ is contained in \mathcal{U}_1 (i.e., $\Gamma_\epsilon \subseteq \mathcal{U}_1$). Due to the uniform stability of $e = 0$, there exists $0 < \delta < \epsilon$, such that $\xi(t) \in \Gamma_\epsilon$ for $t \geq 0$ whenever $\xi(0) \in \Gamma_\delta$. By letting $\mathcal{U}_2 = \Gamma_\delta$ in Definition 5.16, \mathcal{P} is asymptotically stable. \square

Lemma 5.18. *Suppose every trajectory starting at any point in \mathcal{M} converges to either the desired path \mathcal{P} or the singular set \mathcal{C} as $t \rightarrow \infty$. Then the desired path \mathcal{P} and the singular set \mathcal{C} cannot be both attractive.*

Proof. If $\mathcal{C} = \emptyset$, then \mathcal{C} is non-attractive, and the claim is vacuously true. Thus we assume that $\mathcal{C} \neq \emptyset$. We first show that the domain of attraction of a nonempty closed attractive set \mathcal{A} of a dynamical system is open⁶, as a generalization of the standard result where this attractive set is replaced by an equilibrium point [124, Proposition 5.44]. Since \mathcal{A} is attractive, by Definition 5.15, there exists some open neighborhood \mathcal{U} of \mathcal{A} such that for any $x \in \mathcal{U}$, the trajectory starting from x converges (topologically) to \mathcal{A} . Therefore, for any point y in the domain of attraction of \mathcal{A} , there exists a time $T > 0$ such that $\Psi(T, y) \in \mathcal{U}$ (because we choose $\mathcal{V} = \mathcal{U}$ in Definition 5.16), where $\Psi : \mathbb{R}_{\geq 0} \times \mathcal{M} \rightarrow \mathcal{M}$ denotes the flow of the dynamical system. By the continuity of $\Psi(T, \cdot)$ with respect to the second argument, there is some open neighborhood \mathcal{B} of y such that $\Psi(T, \mathcal{B}) \subseteq \mathcal{U}$. Therefore, for all points $b \in \mathcal{B}$, any trajectory starting from b will go through $\Psi(T, b) \in \mathcal{U}$ and converge to \mathcal{A} (by the existence and uniqueness of trajectory; i.e., Theorem 2.1), implying that \mathcal{B} is an open subset of the domain of attraction of \mathcal{A} . Therefore, the domain of attraction of the attractive set \mathcal{A} is indeed open.

We show by contradiction by assuming that both \mathcal{C} and \mathcal{P} are attractive. Thus, their domains of attraction are both open. Therefore, the whole configuration space \mathcal{M} consists of only two kinds of points, those converging to \mathcal{C} and those to \mathcal{P} by the global dichotomy convergence property in Theorem 5.13. This means that the configuration space \mathcal{M} is a union of two disjoint open subsets, which is not possible since \mathcal{M} is assumed to be connected. \square

Corollary 5.19 (Non-attractiveness of \mathcal{C}). *Under the hypotheses of Lemma 5.18, the singular set \mathcal{C} is non-attractive.*

Proof. By Corollary 5.17, the desired path \mathcal{P} is attractive. Under the hypotheses of Lemma 5.18, the desired path \mathcal{P} and the singular set \mathcal{C} cannot be both attractive. Therefore, the singular set \mathcal{C} is non-attractive. \square

⁵ The existence of ϵ is guaranteed by the compactness of \mathcal{P} and Assumption 5.6. In fact, Assumption 5.6 can be dropped, but the set Γ_ϵ should be changed to its component (i.e., the maximal connected subset of Γ_ϵ) that contains \mathcal{P} , and similarly, the set Γ_δ used in the subsequent part of the proof should also be changed to its component that contains \mathcal{P} .

⁶ This result is similar to Proposition 4.15 in [11, Chapter V], but the latter does not provide a proof.

Remark 5.20. Corollary 5.19 is equivalent to saying that if Theorem 5.13 holds globally (i.e., Ω_α can be replaced by \mathcal{M}), then the singular set \mathcal{C} is non-attractive. Theorem 5.13 holds globally, if \mathcal{M} is compact, or if $e(\xi)$ is radially unbounded (i.e., $\|e(\xi)\| \rightarrow \infty$ as $\|\xi\| \rightarrow \infty$). The radial unboundedness of $e(\xi)$ is consistent with the physical intuition, and is probably not restrictive in practice (e.g., it is true for Example 5.3, a typical case in the literature and in practice). Note that Theorem 5.13 does hold globally for all examples where the desired path is compact in this chapter (i.e., Examples 5.3, 5.11, 5.22 and all examples in Section 5.6). \triangleleft

Remark 5.21. If the singular set \mathcal{C} is non-attractive, by Definition 5.15, it is still possible that some trajectories (commencing outside \mathcal{C}) can converge to the singular set \mathcal{C} . Nevertheless, in this case, one can immediately conclude that there must be some other trajectories that do not converge to \mathcal{C} , no matter how near they start to the singular set \mathcal{C} . \triangleleft

Note that by Theorem 5.13, Corollary 5.17 and Corollary 5.19, we *cannot* conclude that trajectories converge to the desired path from *almost all* initial conditions (i.e., *almost global* convergence to \mathcal{P}). The claim about almost global convergence to the desired path can be refuted simply by an example below where the singular set is of measure *non-zero*.

Example 5.22 (\mathcal{C} of measure *non-zero*). If the singular set is of measure non-zero, one cannot expect *almost global* convergence to the desired path since every trajectory starting from the singular set will remain in that set. To construct such a case, first we introduce a smooth but non-real-analytic function (see Fig. 5.3a) $b : \mathbb{R}^2 \rightarrow \mathbb{R}$:

$$b(x, y) = \begin{cases} \exp\left(\frac{1}{1-x^2-y^2}\right) & \text{if } x^2 + y^2 > 1, \\ 0 & \text{otherwise.} \end{cases} \quad (5.24)$$

We can construct the function $\phi : \mathbb{R}^2 \rightarrow \mathbb{R}$ using (5.24) as below:

$$\phi(x, y) = 4 + (-x^2 - y^2) \cdot b(x, y). \quad (5.25)$$

The desired path $\mathcal{P} = \{(x, y) \in \mathbb{R}^2 : \phi(x, y) = 0\}$ is a circle of radius approximately 2. Moreover, the singular set \mathcal{C} of the vector field derived from ϕ is a disk of radius 1 centered at the origin (see Fig. 5.3b). In this case, almost global convergence to the desired path is not possible, since the singular set \mathcal{C} has a non-zero measure. \triangleleft

Note that the function ϕ in the example above is *not* real analytic. In fact, it is proved in [50] that when all the level functions ϕ_i are real analytic, then the singular set of the corresponding vector field is of measure zero. However, even if the level functions ϕ_i are real analytic, we still cannot conclude that the initial conditions such that trajectories converging to the singular set are of measure zero,

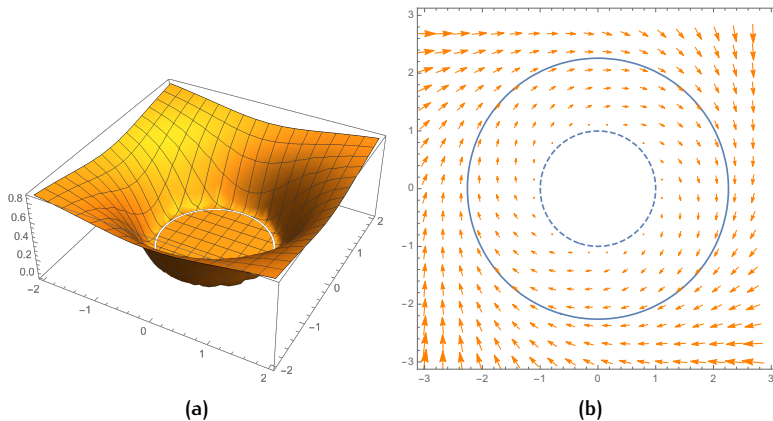


Figure 5.3: Example 5.22. (a) The graph of the smooth non-real-analytic function b in (5.24). (b) The non-real-analytic vector field of which the function ϕ is given in (5.25). The solid line is the desired path and the dashed line is the boundary of the singular set, which is the unit disk centered at the origin.

and thus almost global convergence to the desired path cannot be guaranteed. A well-known example where an equilibrium, which is obviously of measure zero, is *non-attractive* but almost all trajectories converge to it is presented in [124, p. 186].

The discussion above shows that it is generally challenging to study the domain of attraction of the desired path \mathcal{P} or the singular set \mathcal{C} : we cannot even guarantee the *almost global* convergence to the desired path by Corollary 5.17 and Corollary 5.19. However, by Theorem 5.13, if the level functions ϕ_i are known *a priori*, then one can *numerically* check whether the singular set \mathcal{C} is empty or not. If $\mathcal{C} \neq \emptyset$, it obviously follows that global convergence to the desired path \mathcal{P} is not possible. But this requires the knowledge of the singular set, hence the knowledge of the specific expression of the vector field.

It is our interest to study whether we can obtain a general result about the convergence of the desired path *without knowing the specific analytic expressions of the vector field and the singular set*. This interest is further motivated by the observation that the singular set is nonempty in many examples in the literature where the desired path is homeomorphic to the unit circle. Example 5.3 is consistent with this observation.

5.5 SINGULAR POINTS AND NON-PATH-CONVERGING TRAJECTORIES

5.5.1 Existence of singular points

The following result shows that for the whole space to be the domain of attraction of an attractor, the shapes of the whole space and the attractor should be consistent topologically, independent of the system's specific form.

Lemma 5.23. *Consider the autonomous system $\dot{x} = f(x)$, where f is Lipschitz continuous and x is defined on a smooth finite-dimensional manifold \mathcal{M} . Suppose \mathcal{L} is a compact asymptotically stable embedded submanifold of \mathcal{M} . Then \mathcal{L} is a strong deformation retract of its domain of attraction.*

Proof. Combine Theorem 5, Corollary 7 and Proposition 10 in [99]. \square

Rather than merely presenting this lemma, we list below several key steps behind this lemma, which are of theoretical interest. For convenience, the domain of attraction of \mathcal{L} is denoted by $\mathcal{A}(\mathcal{L})$.

S.1 As \mathcal{L} is a compact embedded submanifold, there exists a tubular neighborhood \mathcal{W} of \mathcal{L} which can be continuously shrunk to \mathcal{L} ; precisely, \mathcal{L} is a strong deformation retract of \mathcal{W} .

S.2 The asymptotic stability of \mathcal{L} implies the existence of a smooth Lyapunov function V on $\mathcal{A}(\mathcal{L})$ of which the time derivative \dot{V} is negative definite on $\mathcal{A}(\mathcal{L})$ [153, Theorem 3.1]. We can choose a constant $\rho > 0$ such that the sublevel set $V_\rho := \{x \in \mathcal{M} : V(x) \leq \rho\}$, which is a smooth manifold [152], is strictly contained in the tubular neighborhood⁷ \mathcal{W} . It follows from the negative definiteness of \dot{V} that the vector field f in Lemma 5.23 only crosses the boundary ∂V_ρ of the sublevel set V_ρ once, or precisely, the vector field is transverse to ∂V_ρ .

S.3 Define the *first hitting time* to be the first time instant when the system trajectory starting from $\bar{x} \in \mathcal{A}(\mathcal{L})$ reaches the sublevel set V_ρ . Then since the vector field is transverse to ∂V_ρ , it is proved that the *first hitting time* $T_\rho(\bar{x})$ is continuous with respect to $\bar{x} \in \mathcal{A}(\mathcal{L})$.

S.4 The continuity of the first hitting time implies that $\mathcal{A}(\mathcal{L})$ can be continuously shrunk to V_ρ ; precisely, V_ρ is a strong deformation retract of $\mathcal{A}(\mathcal{L})$.

⁷ Existence of ρ is guaranteed by the properties of the Lyapunov function V

S.5 The two continuous deformation processes in **S.1** and **S.4** imply that $\mathcal{A}(\mathcal{L})$ can be continuously shrunk to \mathcal{L} . Or precisely, \mathcal{L} is a strong deformation retract of $\mathcal{A}(\mathcal{L})$.⁸

Remark 5.24 (Outline of an alternative proof). We can independently derive the same result as Lemma 5.23 using the “local triviality” property [77, Chapter 10] and the Wazewski set theorem [27, Theorem 2.3]. We briefly introduce our proof technique for its theoretical interest as follows.

The desired path \mathcal{P} (i.e., equivalent to \mathcal{L} in Lemma 5.23) being a compact regular level set implies the property called “local triviality” [77, Chapter 10], which shows the “stability” of the topology of level sets near the desired path. This means that other level sets in the vicinity of the desired path look like the desired path; i.e. they are compact and homeomorphic to the desired path. Consequently, this vicinity is homeomorphic to the elliptic solid torus $\mathcal{D} \times S^1$, where $\mathcal{D} \subseteq \mathbb{R}^{n-1}$ is an ellipsoid centered at $\mathbf{0} \in \mathbb{R}^{n-1}$ and is a sublevel set of the Lyapunov function (5.19). Thus, we can indirectly study the properties of the original vector field χ in a neighborhood of the desired path by investigating the vector field χ' on this topological space: the elliptic solid torus $\mathcal{D} \times S^1$.

Then using the Lyapunov function (5.19) and its negative definite derivative, it can be shown that the vector field χ' is *transverse* to the boundary $\mathcal{S} := \partial \mathcal{D} \times S^1$ of the elliptic solid torus $\mathcal{D} \times S^1$. This implies the continuity of the *first hitting time* which is the first time instant a trajectory “outside” of the elliptic solid torus reaches the boundary \mathcal{S} . Therefore, one may imagine that the set of all converging trajectories is continuously compressed into the boundary \mathcal{S} , while every point in the boundary \mathcal{S} remains stationary during the whole continuous deformation process. This can be rigorously proved by the Wazewski set theorem [27, Theorem 2.3], where the boundary \mathcal{S} turns out to be an *exit set*, which roughly means that every trajectory starting from this boundary will *immediately exit* from it.

Moreover, as the desired path is an embedded submanifold of \mathcal{M} , it has a tubular neighborhood \mathcal{W} and this neighborhood can be continuously shrunk onto the desired path [77, Theorem 6.24, Proposition 6.25]. Combining this continuous deformation process with the other one mentioned above, it is intuitive to see that

⁸ Technically, **S.1** implies that there exists a homotopy (corresponding to a strong deformation retraction) $s : \mathcal{W} \times [0, 1] \rightarrow \mathcal{W}$ such that $s(w, 0) = w, s(w, 1) \in \mathcal{L}$ for all $w \in \mathcal{W}$ and $s(l, t) = l$ for all $l \in \mathcal{L}$ and $t \in [0, 1]$. Similarly, **S.4** implies that there exists a homotopy (corresponding to a strong deformation retraction) $h : \mathcal{A}(\mathcal{L}) \times [0, 1] \rightarrow \mathcal{A}(\mathcal{L})$ such that $h(y, 0) = y, h(y, 1) \in V_\rho$ for all $y \in \mathcal{A}(\mathcal{L})$ and $h(v, t) = v$ for all $v \in V_\rho$ and $t \in [0, 1]$. A new homotopy (corresponding to a strong deformation retraction) $r : \mathcal{A}(\mathcal{L}) \times [0, 1] \rightarrow \mathcal{A}(\mathcal{L})$ can be constructed as $r(y, t) = h(y, 2t)$ for $y \in \mathcal{A}(\mathcal{L})$ and $t \in [0, 1/2]$, and $r(y, t) = s(h(y, 1), 2t - 1)$ for $y \in \mathcal{A}(\mathcal{L})$ and $t \in (1/2, 1]$. This homotopy r shows that \mathcal{L} is indeed a strong deformation retract of $\mathcal{A}(\mathcal{L})$ [99, Theorem 4].

the desired path \mathcal{P} is a (strong) deformation retract of its domain of attraction denoted by $\mathcal{A}(\mathcal{P})$.⁹

Our proof and that of Lemma 5.23 both revolve around a) the regularity of the desired path (i.e., a compact regular level set and thus an embedded submanifold) and b) the continuity of the first hitting time (due to the transversality of the vector field to some surfaces encompassing the desired path). These two aspects turn out to be crucial in deriving the result. \triangleleft

Remark 5.25. Note that Lemma 5.23 does not hold if \mathcal{L} is not compact. In fact, the compactness of \mathcal{L} (or the desired path) is a crucial assumption in deriving the subsequent results. A counterexample is illustrated in Chapter 6 (i.e., Counterexample 1). \triangleleft

An implication of Lemma 5.23 is the following theorem:

Theorem 5.26 (Homotopy equivalence). *The domain of attraction of the desired path \mathcal{P} with respect to (5.1) is homotopy equivalent to the unit circle S^1 .*

Proof. Let $\mathcal{L} = \mathcal{P}$ in Lemma 5.23 and note that $\mathcal{P} \approx S^1$. \square

We explain the potential utility of Theorem 5.26. One benefit relies on the computability of the related topological invariants. If global convergence to the limit cycle \mathcal{P} holds, then by Theorem 5.26, the configuration space \mathcal{M} and the limit cycle \mathcal{P} are homotopy equivalent. This means that the homotopy equivalence of the configuration space \mathcal{M} and the limit cycle \mathcal{P} is a necessary condition for the global convergence. This further implies that to check if global convergence to the limit cycle \mathcal{P} is possible, we can examine the topological invariants which are invariant under homotopy equivalences. These topological invariants include the Euler characteristic [76, p. 178], homotopy groups [76, p. 208], homology/cohomology groups [76, pp. 339-355, pp. 374-378]. Some of these invariants are already known for some important topological spaces, and more are being investigated in the literature. For example, the Euler characteristic of $SO(3)$ is 2, while that of S^1 is 0. This implies that on the manifold $\mathcal{M} = SO(3)$, it is impossible to guarantee global convergence to a compact desired path $\mathcal{P} \subseteq SO(3)$ which is homeomorphic to the unit circle. In practice, this implies that, for example, a quadcopter for which the orientations are defined on $SO(3)$, cannot follow a set of desired orientations defined by $\mathcal{P} \approx S^1$, from every initial orientation.

Even though homotopy equivalent sets can look very different (compare $\mathbb{R}^2 \setminus \{0\}$ and S^1 for example), another benefit of Theorem 5.26 is that it helps one

⁹ Technically, due to the continuity of the first hitting time, we can define a continuous time function $T : \mathcal{A}(\mathcal{P}) \rightarrow \mathbb{R}$, such that $\Psi^{T(p)}(p) \in \mathcal{W}$ for every $p \in \mathcal{A}(\mathcal{P})$, where $\Psi : \mathbb{R} \times \mathcal{M} \rightarrow \mathcal{M}$ is the flow of the dynamical system (5.1). Then we can deform $\mathcal{A}(\mathcal{P})$ onto \mathcal{P} by first “squeezing” $\mathcal{A}(\mathcal{P})$ into \mathcal{W} via the homotopy $G(p, s) = \Psi^{2s-T(p)}(p)$ with $s \in [0, \frac{1}{2}]$, and then \mathcal{W} onto \mathcal{P} via the homotopy $G(p, t) = H(\Psi^{T(p)}(p), 2t - 1)$ with $t \in [\frac{1}{2}, 1]$, where H is a homotopy corresponding to the deformation retraction of \mathcal{W} onto \mathcal{P} .

obtain some intuition of how a domain of attraction looks. It also helps rule out some possibly wrong intuition that one might be misled into initially, especially when some path-converging or non-path-converging trajectories are of measure zero, and hence it is difficult, if not impossible, to be depicted by computer simulations. We will illustrate by examples in Section 5.6.

The following theorem is particularized to $\mathcal{M} = \mathbb{R}^n$.

Theorem 5.27 (Impossibility of global convergence in \mathbb{R}^n). *If the configuration space \mathcal{M} is the n -dimensional Euclidean space \mathbb{R}^n , then global convergence to the desired path \mathcal{P} is not possible. In addition, if the dichotomy convergence property (i.e., Theorem 5.13) holds globally¹⁰, then the singular set \mathcal{C} is nonempty.*

Proof. Since $\mathcal{M} = \mathbb{R}^n$ is *not* homotopy equivalent to¹¹ S^1 , the conclusion follows directly from Theorem 5.26 and the dichotomy result of Theorem 5.13. \square

A major motivation of Theorem 5.27 is the observation that in many examples in the literature [50], [63], [74], [157], the singular sets are nonempty, and hence global convergence to the desired path is simply not possible¹². But is it the case that whenever $\mathcal{P} \approx S^1$, then there is always a nonempty singular set? For the 2D case, this is true by the Poincaré-Bendixson theorem, concluding that there always exist at least one singular point of the vector field within the region enclosed by the desired path, which is a limit cycle of the autonomous systems. Nevertheless, the Poincaré-Bendixson theorem cannot be straightforwardly extended to higher-dimensional spaces, for which the conclusion is not clear, but Theorem 5.27 is able to give an affirmative answer.

It is true that if the singular set \mathcal{C} is determined to be nonempty, then global convergence to the desired path \mathcal{P} is not possible by Theorem 5.13. However, the significance of Theorem 5.27 is that it gives a more fundamental conclusion in the sense that it does not depend on the specific expressions of the level functions ϕ_i (hence the vector field χ), and avoids the possibly complicated computations of the singular set \mathcal{C} when the system dimensions are large. Most importantly, the independence of Theorem 5.27 on the level functions ϕ_i implies that even though we can choose different level functions ϕ_i to represent the same desired path \mathcal{P} , practically speaking, Theorem 5.27 simply prevents us from hoping for better performance in terms of global convergence to the desired path by trying different level functions ϕ_i .

Note that the root causes of this topological obstacle are: a) the system (5.1) is autonomous; b) the asymptotically stable desired path is homeomorphic to

¹⁰ See Remark 5.20 regarding when Theorem 5.13 globally holds.

¹¹ This can be seen from, for example, the fact that the Euler characteristic of S^1 is 0 while that of \mathbb{R}^n is 1.

¹² When the singular set is non-empty, every trajectory of (5.1) starting from the singular set will simply remain stationary in the singular set (since a singular point is an equilibrium point of (5.1)), and thus it does *not* converge to the desired path. Therefore, the *global* convergence of trajectories to the desired path is simply *not* possible.

the unit circle while $\mathcal{M} = \mathbb{R}^n$. Another implication of Theorem 5.27 is that if one must achieve a global convergence result, then the only possible approach is to change the topology of the desired path \mathcal{P} , if the autonomous system (5.1) is given. This is possible by, for example, “cutting” and “stretching” the compact desired path along an additional dimension, and thereby transforming it to an unbounded one which is homeomorphic to the real line (i.e., $\mathcal{P} \approx \mathbb{R}$). This way, at least, the topological obstruction is removed. See Chapter 9 for related results along these lines applicable in Euclidean spaces.

5.5.2 The existence of non-path-converging trajectories

Theorem 5.27 concludes that global convergence to the desired path in \mathbb{R}^n is not possible when $\mathcal{M} = \mathbb{R}^n$. Thus, it is of significant interest to show the existence of the non-path-converging trajectories, which do not converge to \mathcal{P} . A theorem identifying some of these trajectories follows; the proof involves notions such as covering spaces, lifts, fundamental groups and homology, so we refer to Chapter 7, Chapter 11 and Chapter 13 in [76] for an introduction.

Before presenting the main theorem, we first provide some preliminary lemmas and notations. The notation $H_{n-1}(\cdot)$ denotes the $(n-1)$ -dimensional homology group [76, Chapter 13], and $(\cdot)_*$ denotes the homomorphism between homology groups induced by a continuous map (\cdot) . Let $\mathcal{B}^{n-1} := \{x \in \mathbb{R}^{n-1} : \|x\| < 1\}$ be the unit open ball in \mathbb{R}^{n-1} centered at $\mathbf{0}$, and $\mathcal{B}_-^{n-1} := \mathcal{B}^{n-1} \setminus \{\mathbf{0}\}$.

Lemma 5.28. *There holds $H_{n-1}(\mathcal{B}_-^{n-1} \times \mathbb{R}) = \{0\}$.*

Proof. Since S^{n-2} is a deformation retract of \mathcal{B}_-^{n-1} , and \mathbb{R} is contractible (i.e., homotopy equivalent to a singleton), $\mathcal{B}_-^{n-1} \times \mathbb{R}$ is homotopy equivalent to $S^{n-2} \times \{x_0\}$, for a point $x_0 \in \mathbb{R}$. In addition, $S^{n-2} \times \{x_0\}$ is homotopy equivalent to S^{n-2} . Therefore, we have [76, Theorem 13.23]

$$H_{n-1}(\mathcal{B}_-^{n-1} \times \mathbb{R}) = H_{n-1}(S^{n-2}) = \{0\}.$$

□

Lemma 5.29. *Let $i_{\partial\bar{\mathcal{B}}_R} : \partial\bar{\mathcal{B}}_R \rightarrow \mathbb{R}^n \setminus \mathcal{P}$ be the inclusion map, where $\partial\bar{\mathcal{B}}_R$ denotes the boundary of a closed ball $\bar{\mathcal{B}}_R \subseteq \mathbb{R}^n$ of radius R containing the desired path \mathcal{P} . The homomorphism $i_{\partial\bar{\mathcal{B}}_R,*} : H_{n-1}(\partial\bar{\mathcal{B}}_R) \rightarrow H_{n-1}(\mathbb{R}^n \setminus \mathcal{P})$ induced by $i_{\partial\bar{\mathcal{B}}_R}$ is non-trivial¹³.*

Proof. Fix $x_0 \in \mathcal{P}$, and denote by $j_{\partial\bar{\mathcal{B}}_R}$ and $j_{\mathbb{R}^n \setminus \mathcal{P}}$ respectively the inclusions of $\partial\bar{\mathcal{B}}_R$ and $\mathbb{R}^n \setminus \mathcal{P}$ into $\mathbb{R}^n \setminus \{x_0\}$. Then

$$j_{\partial\bar{\mathcal{B}}_R} = j_{\mathbb{R}^n \setminus \mathcal{P}} \circ i_{\partial\bar{\mathcal{B}}_R}. \quad (5.26)$$

¹³ A homomorphism $h : G \rightarrow G'$ between any two groups (e.g., fundamental groups, homology groups) is called *trivial* if h maps every element in G to the identity element, denoted by 0 , in G' . The homomorphism h is called *non-trivial* if it is not trivial.

Since x_0 lies inside the ball \bar{B}_R of which the boundary is $\partial\bar{B}_R$, $\partial\bar{B}_R$ is a deformation retract of $\mathbb{R}^n \setminus \{x_0\}$ and hence $j_{\partial\bar{B}_R}$ is a homotopy equivalence between $\partial\bar{B}_R$ and $\mathbb{R}^n \setminus \{x_0\}$. Thus $j_{\partial\bar{B}_R}$ induces an isomorphism $j_{\partial\bar{B}_R,*}$ between $H_{n-1}(\partial\bar{B}_R)$ and $H_{n-1}(\mathbb{R}^n \setminus \{x_0\})$ [76, Corollary 13.9]. Since (5.26) implies [76, Proposition 13.2]

$$\begin{aligned} j_{\partial\bar{B}_R,*} : H_{n-1}(\partial\bar{B}_R) &\rightarrow H_{n-1}(\mathbb{R}^n \setminus \{x_0\}) \\ j_{\partial\bar{B}_R,*} &= j_{\mathbb{R}^n \setminus \mathcal{P},*} \circ i_{\partial\bar{B}_R,*}, \end{aligned}$$

and $H_{n-1}(\partial\bar{B}_R) \cong H_{n-1}(\mathbb{R}^n \setminus \{x_0\}) \cong \mathbb{Z}$ [76, Theorem 13.23], this implies that $i_{\partial\bar{B}_R,*}$ is non-trivial. \square

Now we are ready to state the following main theorem.

Theorem 5.30 (Existence of non-path-converging trajectories). *Suppose $n \geq 3$ for the autonomous differential equation (5.1), where the desired path $\mathcal{P} \subseteq \mathbb{R}^n$ is an embedded submanifold in \mathbb{R}^n and a (locally) asymptotically stable limit cycle. For any closed ball $\bar{B}_R \subseteq \mathbb{R}^n$ that contains \mathcal{P} (precisely, $\mathcal{P} \subseteq \text{int } \bar{B}_R$), there exists at least one trajectory of (5.1) starting from the boundary $\partial\bar{B}_R$ of the ball \bar{B}_R that does not converge to \mathcal{P} .*

Proof. **Step 1 (construct the map Ψ^T):** We prove by contradiction. Denote by $\Psi : \mathbb{R} \times \mathbb{R}^n \rightarrow \mathbb{R}^n$ the flow of (5.1); i.e. $\gamma(t) = \Psi^t(x)$ is the solution of (5.1) with the initial condition $\gamma(0) = x$. Suppose that every trajectory starting from the boundary $\partial\bar{B}_R$ of the closed ball \bar{B}_R (i.e., $\partial\bar{B}_R$ is an $(n-1)$ -dimensional sphere) converges to the limit cycle \mathcal{P} ; then for any point $x \in \partial\bar{B}_R$, there exists some $T_x > 0$ such that $\Psi^t(x) \in \mathcal{O}$ for all $t > T_x$, where \mathcal{O} is a tubular neighborhood \mathcal{O} of \mathcal{P} in \mathbb{R}^n .¹⁴ By the compactness of $\partial\bar{B}_R$ and the asymptotic stability of the limit cycle \mathcal{P} , one can show that there exists $T > 0$ such that $\Psi^T(\partial\bar{B}_R) \subseteq \mathcal{O} \setminus \mathcal{P}$.

Step 2 (rewrite Ψ^T): We can write $\Psi^T : \partial\bar{B}_R \rightarrow \mathbb{R}^n \setminus \mathcal{P}$ as the composition of two functions as below:

$$\Psi^T = i_{\mathcal{O} \setminus \mathcal{P}} \circ g_T,$$

where $g_T : \partial\bar{B}_R \rightarrow \mathcal{O} \setminus \mathcal{P}$ is simply the codomain restriction of Ψ^T , and $i_{\mathcal{O} \setminus \mathcal{P}} : \mathcal{O} \setminus \mathcal{P} \rightarrow \mathbb{R}^n \setminus \mathcal{P}$ is the inclusion map.

Step 3 (construct a covering map): Since \mathcal{P} is an embedded submanifold in \mathbb{R}^n , and \mathcal{O} is a tubular neighborhood, there exists a diffeomorphism¹⁵ β from \mathcal{O} to $\mathcal{B}^{n-1} \times \mathbb{S}^1$ such that $\beta(\mathcal{P}) = \{\mathbf{0}\} \times \mathbb{S}^1$ [77, Theorem 6.24]. Since β is a diffeomorphism between \mathcal{O} and $\mathcal{B}^{n-1} \times \mathbb{S}^1$, and $\beta(\mathcal{P}) = \{\mathbf{0}\} \times \mathbb{S}^1$, it follows

¹⁴ Since \mathcal{P} is an embedded submanifold in \mathbb{R}^n , a tubular neighborhood \mathcal{O} of \mathcal{P} always exists [77, Theorem 6.24].

¹⁵ More precisely, the tubular neighborhood \mathcal{O} being diffeomorphic to $\mathcal{B}^{n-1} \times \mathbb{S}^1$ is because the normal bundle of a loop in \mathbb{R}^n is orientable.

that $\mathcal{O} \setminus \mathcal{P}$ is diffeomorphic to $\mathcal{B}_-^{n-1} \times \mathbb{S}^1$ with a diffeomorphism $\beta' : \mathcal{O} \setminus \mathcal{P} \rightarrow \mathcal{B}_-^{n-1} \times \mathbb{S}^1$, where $\beta'(x) = \beta(x)$ for $x \in \mathcal{O} \setminus \mathcal{P}$. Therefore,

$$\begin{aligned} p : \mathcal{B}_-^{n-1} \times \mathbb{R} &\rightarrow \mathcal{O} \setminus \mathcal{P} \\ (u, \theta) &\mapsto \beta'^{-1}((u, e^{i\theta})) \end{aligned}$$

is a covering map [76, p. 278] with $\mathcal{B}_-^{n-1} \times \mathbb{R}$ being the covering space of $\mathcal{O} \setminus \mathcal{P}$.

Step 4 (lift g_T and form a contradiction): Since $\partial\bar{\mathcal{B}}_R$ is simply connected and locally path-connected for $n \geq 3$ [76, Theorem 7.20], the continuous map $g_T : \partial\bar{\mathcal{B}}_R \rightarrow \mathcal{O} \setminus \mathcal{P}$ can be lifted [76, Corollary 11.19]; that is, there exists $\tilde{g}_T : \partial\bar{\mathcal{B}}_R \rightarrow \mathcal{B}_-^{n-1} \times \mathbb{R}$ such that $g_T = p \circ \tilde{g}_T$ (see Fig. 5.4). It follows from Lemma 5.28 that $\tilde{g}_{T,*} : H_{n-1}(\partial\bar{\mathcal{B}}_R) \rightarrow H_{n-1}(\mathcal{B}_-^{n-1} \times \mathbb{R})$ is trivial. Therefore, $\Psi_*^T = i_{\mathcal{O} \setminus \mathcal{P},*} \circ p_* \circ \tilde{g}_{T,*}$ is trivial [76, Proposition 13.2]. Let $i_{\partial\bar{\mathcal{B}}_R} : \partial\bar{\mathcal{B}}_R \rightarrow \mathbb{R}^n \setminus \mathcal{P}$ be the inclusion map of $\partial\bar{\mathcal{B}}_R$ to $\mathbb{R}^n \setminus \mathcal{P}$. Since $i_{\partial\bar{\mathcal{B}}_R} : \partial\bar{\mathcal{B}}_R \rightarrow \mathbb{R}^n \setminus \mathcal{P}$ and $\Psi^T : \partial\bar{\mathcal{B}}_R \rightarrow \mathbb{R}^n \setminus \mathcal{P}$ are homotopic¹⁶, it follows that $i_{\partial\bar{\mathcal{B}}_R,*}^T = \Psi_*^T$ [76, Theorem 13.8], and hence $i_{\partial\bar{\mathcal{B}}_R,*}^T$ is trivial. However, the conclusion that $i_{\partial\bar{\mathcal{B}}_R,*}^T$ is trivial contradicts Lemma 5.29. \square

Remark 5.31 (Why require $n \geq 3$?). The reason that the theorem cannot be proved when $n = 2$ (at least following the argument for $n \geq 3$) is that the continuous map g_T cannot be lifted (i.e., there does not exist the continuous map \tilde{g}_T such that $g_T = p \circ \tilde{g}_T$). Note that $\partial\bar{\mathcal{B}}_R \approx \mathbb{S}^{n-1}$. If $n = 2$, then $\partial\bar{\mathcal{B}}_R \approx \mathbb{S}^1$, which is *not* simply connected. Then [76, Corollary 11.19] cannot be used to imply the existence of the lift \tilde{g}_T of the continuous map g_T as what we did in the proof. In fact, it can be further shown that this lift \tilde{g}_T does not exist according to the lifting criterion [76, Theorem 11.18]. This is elaborated as follows. First, the fundamental group of $\partial\bar{\mathcal{B}}_R$ is $\pi_1(\partial\bar{\mathcal{B}}_R, \rho_1) = \pi_1(\mathbb{S}^1, \rho_2) = \mathbb{Z}$ for any base points $\rho_1 \in \partial\bar{\mathcal{B}}_R$ and $\rho_2 \in \mathbb{S}^1$. Second, when $n = 2$, $\mathcal{B}_-^{n-1} \times \mathbb{R} = ((-1, 0) \cup (0, 1)) \times \mathbb{R} = ((-1, 0) \times \mathbb{R}) \cup ((0, 1) \times \mathbb{R}) := \mathcal{A}_1 \cup \mathcal{A}_2$, which consists of two disjoint contractible subspaces denoted by \mathcal{A}_1 and \mathcal{A}_2 . Therefore, the fundamental group of \mathcal{A}_1 and \mathcal{A}_2 at any of their base points is 0 in both cases. These two facts imply that the conditions of [76, Theorem 11.18] cannot be satisfied (since the homomorphism $g_{T,*}$ between corresponding fundamental groups is non-trivial while the homomorphism p_* is trivial). Therefore, there does not exist the lift \tilde{g}_T of g_T , and the subsequent proof cannot proceed. In fact, one can easily observe using an example that the theorem indeed does not hold for the case where $n = 2$ (e.g., see the first example in Section 5.6). \triangleleft

Remark 5.32. The sphere $\partial\bar{\mathcal{B}}_R$ in the theorem can be generalized to any smooth $(n-1)$ -sphere (i.e., any smooth submanifold diffeomorphic to \mathbb{S}^{n-1}). This is due to the Jordan-Brouwer Separation theorem [52, Chapter 2.5] and the Generalized Schoenflies Theorem [12, Chapter V], [18], [87]. \triangleleft

¹⁶ A homotopy between $i_{\partial\bar{\mathcal{B}}_R} : \partial\bar{\mathcal{B}}_R \rightarrow \mathbb{R}^n \setminus \mathcal{P}$ and $\Psi^T : \partial\bar{\mathcal{B}}_R \rightarrow \mathbb{R}^n \setminus \mathcal{P}$ is $G : \partial\bar{\mathcal{B}}_R \times [0, 1] \rightarrow \mathbb{R}^n \setminus \mathcal{P}$ defined by $G(x, s) = \Psi^{s,T}(x)$.

$$\begin{array}{ccc}
& \mathcal{B}_-^{n-1} \times \mathbb{R} & \\
& \searrow \bar{g}_T \quad \downarrow p & \\
\partial \bar{\mathcal{B}}_R & \xrightarrow{g_T} \mathcal{O} \setminus \mathcal{P} & \xrightarrow{i_{\mathcal{O} \setminus \mathcal{P}}} \mathbb{R}^n \setminus \mathcal{P} \\
& \curvearrowleft \Psi^T \simeq i_{\partial \bar{\mathcal{B}}_R} &
\end{array}$$

Figure 5.4: Relationships of continuous maps in Theorem 5.30. The set $\partial \bar{\mathcal{B}}_R$ is an $(n - 1)$ -dimensional sphere. The map p is a covering map, \bar{g}_T is a lift of g_T such that $g_T = p \circ \bar{g}_T$, and $\Psi^T = i_{\mathcal{O} \setminus \mathcal{P}} \circ g_T$, where $i_{\mathcal{O} \setminus \mathcal{P}}$ is an inclusion map. The map Ψ^T is homotopic to the inclusion map $i_{\partial \bar{\mathcal{B}}_R}$.

The essential idea behind the proof of Theorem 5.30 is that the ball $\bar{\mathcal{B}}_R$ cannot be continuously shrunk to a point if there are “holes” or “obstacles” in the ball’s interior. Imagine a two-dimensional sphere containing the desired path, which can be treated as a circle, and the whole space is \mathbb{R}^3 . The sphere will be continuously shrunk as its points move towards the desired path along the system’s flows. Note that the deforming sphere does not intersect with the desired path during this process since the path is a periodic orbit of the autonomous system (i.e., the desired path can be seen as an obstacle). If *all* points of the sphere are driven by the flows to converge to the path ultimately, the deforming sphere will be pulled apart into pieces, but this is impossible due to the continuity of flows. This essential idea might be utilized to show the following two conjectures.

Conjecture 5.33. *Suppose the assumptions of Theorem 5.30 hold, but the domain of the vector field becomes $\mathbb{R}^n \setminus \mathcal{H}$, where \mathcal{H} is a nonempty set. If there exists a closed ball $\bar{\mathcal{B}}_R$ such that $\mathcal{H} \cap \text{int } \bar{\mathcal{B}}_R \neq \emptyset$, then there exists at least one trajectory of (5.1) starting from the boundary of the ball $\partial \bar{\mathcal{B}}_R$ such that it does not converge to the limit cycle \mathcal{P} .*

Here the set \mathcal{H} can be regarded as a collection of holes, and the condition $\mathcal{H} \cap \text{int } \bar{\mathcal{B}}_R \neq \emptyset$ means that there is at least one hole inside the closed ball $\bar{\mathcal{B}}_R$. Furthermore, as this ball can be shrunk to be arbitrarily close to the “hole”, this indicates that in the close vicinity of the “hole”, such a non-path-converging trajectory exists. This somehow gives a way to locate where the non-path-converging trajectories originate from. In practice, this indicates the following conjecture:

Conjecture 5.34. *It is impossible for vehicles (e.g. a wheeled robot, a drone) of which the motions are governed by the autonomous system (5.1) to smoothly converge to a desired configuration (e.g., position, orientation) from every initial configuration in an environment scattered with obstacles.*

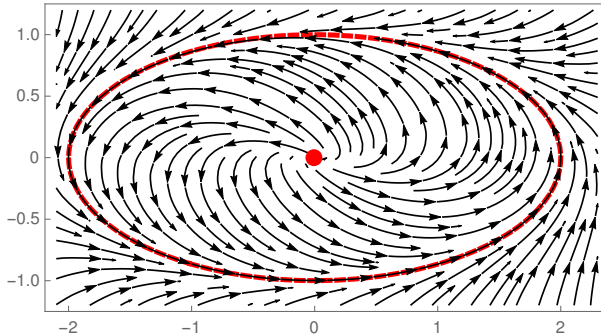


Figure 5.5: Streamlines of the first example. The solid line (red) is the desired path, and the center point (red) is the only singular point.

This is because the vehicles cannot bump into obstacles, and thus these obstacles are regarded as “holes” \mathcal{H} in the configuration space \mathcal{M} (e.g., $\mathcal{M} = \mathbb{R}^2$ for a wheeled robot moving on a plane or $\mathcal{M} = SE(3)$ for a drone flying with different poses). This is a general conjecture independent of how the configuration space looks; a similar conclusion was drawn in [68], [120] for the special case of a *sphere world*. Conjecture 5.34 is also consistent with the recent result in [17, Theorem 11], which shows that the global asymptotic stabilization of the origin using continuous controllers is not possible in environments with (bounded) obstacles.

5.6 NUMERICAL SIMULATIONS

We present simulation examples in this section to illustrate the theoretical results in Section 5.5.1. These examples are meant to display the initial conditions under which trajectories do *not* converge to the desired path. They are consistent with the claim that the domains of attraction of the desired path are indeed homotopy equivalent to the unit circle.

In the first example, we choose $\phi = x^2/4 + y^2 - 1$ and the gain is $k = 1$ in (5.3). For the 2D case, the wedge product in (5.3) is calculated by $\perp_\phi = E\phi$, where $E \in SO(2)$ is a 90° rotation matrix. It can be numerically calculated that there is only one singular point $s_{A1} = (0, 0)$. Since the eigenvalues of the Jacobian matrix of the vector field at this singular point have all positive real parts, the singular point is a source of (5.1). Therefore, one could conclude that the domain of attraction of the ellipse is $\mathcal{A}_1 := \mathbb{R}^2 \setminus s_{A1}$, and it is indeed homotopy equivalent to the unit circle (see the streamlines in Fig. 5.5).

In the second example, we choose a Cassini oval, which is characterized by $\phi = x^4 + y^4 - 2a^2(x^2 - y^2) + a^4 - b^4$, where $a = 2, b = 2.1$. The gain of the vector field (5.3) is $k = 0.1$. One could calculate that there are three singular points:

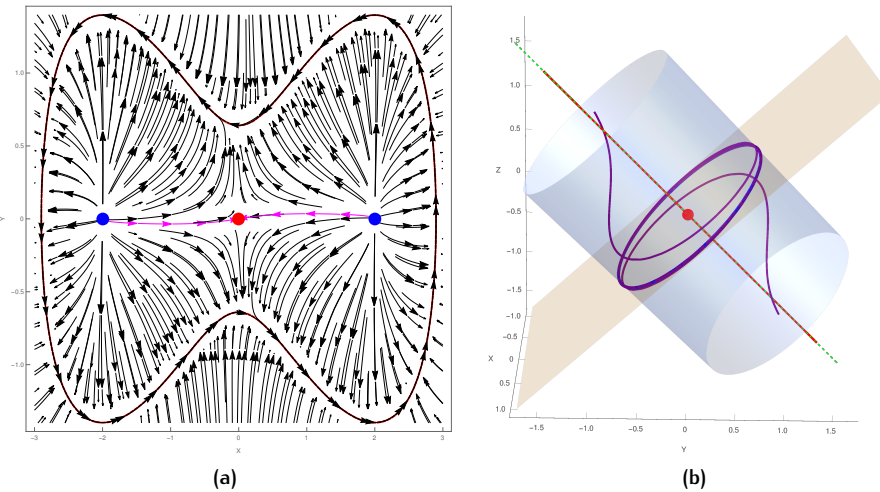


Figure 5.6: (a) Streamlines of the second example. The solid line (red) is the desired path and the three point (two blue and one red) are singular points. The magenta streamlines converge to the central singular point. (b) The 3D tilted circle (blue dashed line) generated by the intersection of a rotated (i.e., non axis-parallel) right circular cylinder and a rotated plane. The point (red) at the center is the only singular point. The dashed line (green) is the cylinder's line of symmetry and is normal to the plane. The four solid lines (two red and two purple) are trajectories of (5.1) with different initial conditions.

$s_{B1} = (0, 0), s_{B2} = (a, 0), s_{B3} = (-a, 0)$. Following the first example, one might think that the domain of attraction of this example is $\mathcal{A}_2 := \mathbb{R}^2 \setminus \{s_{B1}, s_{B2}, s_{B3}\}$, similar to the case of a circle or an ellipse. A direct computer numerical calculation may also lead one to this conclusion¹⁷. But this is incorrect by Theorem 5.26, as \mathcal{A}_2 is *not* homotopy equivalent to S^1 . In fact, by examining the eigenvalues of the Jacobian matrices at these three singular points, we find out that s_{B1} is a saddle point while s_{B2} and s_{B3} are unstable sources. By the Hartman-Grobman theorem [124, Theorem 7.3], one could conclude that there must be a “line” of points (the stable manifold of s_{B1}) starting from which the trajectories of (5.1) converge to the saddle point s_{B1} , and by Theorem 5.26, this “line” probably connects the other two singular points. In fact, after experimenting with different plotting parameters¹⁸, we find out that there indeed exists such a “line” \mathcal{L}_B (see the magenta arrows in Fig. 5.6a). Then the domain of attraction of the Cassini oval is $\mathcal{A}_2 := \mathbb{R}^2 \setminus \mathcal{L}_B \approx S^1$.

In the third example, a 3D tilted circle is the desired path, which is the intersection of a rotated (i.e., non axis-parallel) right circular cylinder and a

¹⁷ For example, by invoking `StreamPlot` in Mathematica directly.

¹⁸ We use `StreamPlot` in Mathematica and combine figures with different sampling parameters.

rotated plane described by $\phi_1 = x^2 + 0.5(y+z)^2 - 1 = 0$ and $\phi_2 = y - z = 0$ respectively (see Fig. 5.6b). The gains are chosen as $k_1 = k_2 = 1$ for the vector field (5.3). There is only one singular point at the origin $s_{C1} = (0, 0, 0)$, and there is only one eigenvalue of the Jacobian matrix with a positive real part. The line of symmetry of the cylinder, denoted by $\mathcal{L}_C := \{(0, u, -u) \in \mathbb{R}^3 : u \in \mathbb{R}\}$, is normal to the plane. The vector field evaluated at any point $p \in \mathcal{L}_C$ on this line is $\chi(p) = (0, -2y, 2y)$, where y is the second coordinate of the point. This vector $\chi(p)$ aligns with \mathcal{L}_C and points towards the singular point s_{C1} . This is consistent with Theorem 5.30, since for every ball that contains that desired path, every trajectory starting from the intersection point of the ball and the line of symmetry \mathcal{L}_C will move along \mathcal{L}_C and converge to the singular point rather than the desired path. In addition, the domain of attraction of the tilted circle is $\mathcal{A}_3 := \mathbb{R}^3 \setminus \mathcal{L}_C$, which is also homotopy equivalent to S^1 . This example is the same as that in [74]. Note that, [74] cannot claim global convergence, since the initial condition is restricted in a compact set. As shown here, only *almost global* convergence to the 3D circle can be achieved.

In the fourth example, we consider a configuration space which is *not* the Euclidean space. Specifically, we consider the example of a planar robot arm with two revolute joints, and we want to control the angles $\theta_1, \theta_2 \in S^1$ of these two revolute joints such that the end-effector of the robot arm follows some desired trajectory (see Fig. 5.7a). Therefore, the configuration space $\mathcal{M} = T^2 = S^1 \times S^1$ is a torus. We aim to let the joint angles follow the desired path $\mathcal{P} \subseteq \mathcal{M}$ in the joint space as below:

$$\mathcal{P} = \{(\theta_1, \theta_2) \in S^1 \times S^1 : \phi(\theta_1, \theta_2) = 0\}, \quad (5.27)$$

where $\phi(\theta_1, \theta_2) = \theta_1 + \theta_2 - \pi/2$. The desired path in the joint space described by these two angles corresponds to a circle trajectory of the center of the end-effector in the Cartesian space. In other words, if the joint angles θ_1 and θ_2 are controlled to follow \mathcal{P} , then it turns out that the center of the end-effector will follow a circle centered at $(0, L_2)$ with radius L_1 , where L_1 and L_2 are the link lengths of the robot arm. The configuration space \mathcal{M} and the desired path $\mathcal{P} \subseteq \mathcal{M}$ are illustrated in Fig. 5.7b. Since $\mathcal{M} = T^2$ is not homotopy equivalent to S^1 , global convergence from \mathcal{M} to the desired path $\mathcal{P} \subseteq \mathcal{M}$ is not possible from Theorem 5.26. However, one way to achieve global convergence¹⁹ is to lift the problem to the covering space [76, pp. 278-287] \mathbb{R}^2 of T^2 , and the simple-closed desired path \mathcal{P} is thereby transformed to a straight line in \mathbb{R}^2 , which is a deformation retract of \mathbb{R}^2 . Then the vector-field guided path-following problem can be solved in the space \mathbb{R}^2 . More specifically, we regard the angles in (5.27) as $(\theta_1, \theta_2) \in \mathbb{R}^2$, and the function $\phi : \mathbb{R}^2 \rightarrow \mathbb{R}$, and derive the guiding vector field using (5.3). Here, the vector field is no longer defined on T^2 but on \mathbb{R}^2 . By some computations, one can observe that there are no singular points of the vector field (5.3) in \mathbb{R}^2 , and

¹⁹ More precisely, this global convergence is considered from the covering space \mathbb{R}^2 rather than $\mathcal{M} = T^2$.

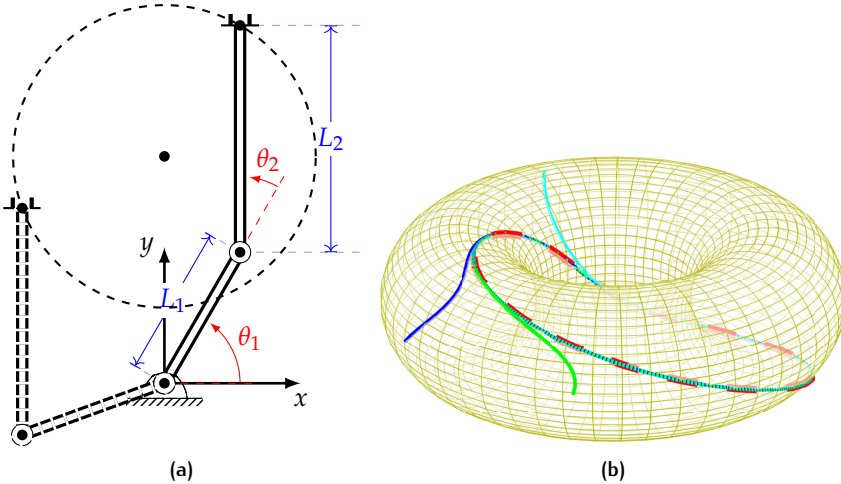


Figure 5.7: (a) A planar robot arm with two revolute joints of which the angles are denoted by θ_1 and θ_2 . The dashed line is the desired path to follow in the Cartesian space \mathbb{R}^2 , which corresponds to $\phi(\theta_1, \theta_2) = \theta_1 + \theta_2 - \pi/2 = 0$ in the joint space $\mathcal{M} = \mathbb{S}^1 \times \mathbb{S}^1$. (b) Simulations of trajectories on the torus $\mathcal{M} = \mathbb{S}^1 \times \mathbb{S}^1$. The torus $\mathcal{M} = \mathbb{S}^1 \times \mathbb{S}^1$ is transparent such that trajectories are visible. The red dashed line is the desired path $\mathcal{P} \subseteq \mathcal{M}$. The blue, green and cyan solid lines are trajectories corresponding to initial conditions $(\theta_1, \theta_2) = (0, 0), (0.3\pi, 0)$ and $(1.5\pi, 0.5\pi)$ respectively.

therefore, the global convergence from any point $(\theta_1, \theta_2) \in \mathbb{R}^2$ in the covering space to the desired path \mathcal{P} is expected. As seen from Fig. 5.7b, three integral curves of the vector field (5.3) all converge to the desired path \mathcal{P} . For more detail about the idea of “lifting” the original configuration space to achieve global convergence to the desired path in the Euclidean space, see Chapter 9.

In the fifth example, the manifold \mathcal{M} is the special orthogonal group $SO(3)$, which consists of a set of orthogonal matrices whose determinants are 1. Since $SO(3)$ is an embedded submanifold of $\mathbb{R}^{3 \times 3}$, we have $SO(3) = \{A \in \mathbb{R}^{3 \times 3} : A^\top A = I, \det A = 1\}$. Therefore, we can choose six functions in (5.10) as follows: $f_1 = A_1^\top A_2$, $f_2 = A_1^\top A_3$, $f_3 = A_2^\top A_3$, $f_4 = A_1^\top A_1 - 1$, $f_5 = A_2^\top A_2 - 1$, $f_6 = A_3^\top A_3 - 1$, and $a_i = 0$ for $i = 1, \dots, 6$, in (5.10), where A_j is the j -th column of the matrix²⁰ A , for $j = 1, 2, 3$. Note that the gradient of the function f_i , $i = 1, \dots, 6$, is a column vector consisting of the partial derivatives of f_i with

²⁰ These constraints do not rule out the possibility that $\det A = -1$, but once the initial configuration is in $SO(3)$, then the whole trajectory is always in $SO(3)$; i.e., the determinant of any matrix of the trajectory is always 1. This is due to the fact that $\{A \in O(3) : \det A = -1\}$ and $\{A \in O(3) : \det A = 1\} = SO(3)$ are disjoint.

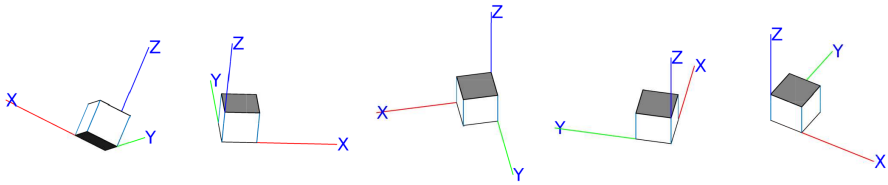


Figure 5.8: The motions of the coordinate frames, where cubes are used for better visualization. The coordinate frames at time instants 0.0, 1.4, 4.1, 6.9 and 9.6 seconds are shown from left to right.

respect to each of the nine entries of the matrix $A \in \mathbb{R}^{3 \times 3}$. We choose the desired path:

$$\begin{aligned}\mathcal{P} &= \{A \in SO(3) : \phi_1(A) = a_{13} = 0, \phi_2(A) = a_{23} = 0\} \\ &= \underbrace{\{\text{Rot}_z(\theta) : \theta \in S^1\}}_{\mathcal{P}_1} \cup \underbrace{\{\text{Rot}_x(\pi)\text{Rot}_z(\theta) : \theta \in S^1\}}_{\mathcal{P}_2},\end{aligned}\quad (5.28)$$

where a_{ij} is the ij -th entry of the matrix A , and $\text{Rot}_{\{x,y,z\}}(\theta) \in SO(3)$ is the rotation matrix encoding the rotation of θ rads about the x , y , or z -axis. Since \mathcal{P} constitutes two disjoint components \mathcal{P}_1 and \mathcal{P}_2 in (5.28), which component a trajectory converges to relies on the initial condition. We choose the initial condition to be $\xi_0 = \text{Rot}_x(\pi/4)\text{Rot}_y(-\pi/4) \in SO(3)$, and the corresponding trajectory converges to \mathcal{P}_1 . Intuitively, the trajectory in $SO(3)$ represents continuous pose transitions starting from $\text{Rot}_x(\pi/4)\text{Rot}_y(-\pi/4)$ to rotations about the z -axis of the “identity pose” $I = \text{Rot}_x(0)\text{Rot}_y(0)\text{Rot}_z(0)$ (see Fig. 5.8).

Remark 5.35. It might be elusive to design a desired path \mathcal{P} on $SO(3)$, which is the zero regular level set of the “stacked” function $\Phi := (\phi_1, \phi_2) : SO(3) \rightarrow \mathbb{R}^2$. One convenient approach is to introduce two continuous surjective functions $\mu : SO(3) \rightarrow S^2 \subseteq \mathbb{R}^3$ defined by $R \mapsto Rv$ with $v = (0, 0, 1) \in S^2 \subseteq \mathbb{R}^3$, and $\pi_{xy} : S^2 \subseteq \mathbb{R}^3 \rightarrow \mathbb{R}^2$ being the projection of the first two coordinates onto the xy -plane. One can check that μ is a submersion on $SO(3)$ and π_{xy} is a submersion on $S^2 \setminus \{(x, y, z) \in S^2 \subseteq \mathbb{R}^3 : z = 0\}$. Let $\Phi = \pi_{xy} \circ \mu$; then every point of the open disk $\{(x, y) \in \mathbb{R}^2 : x^2 + y^2 < 1\}$ is a regular point of Φ . Therefore, the desired path \mathcal{P} above is the (regular) zero-level set $\Phi^{-1}((0, 0)) = (\pi_{xy} \circ \mu)^{-1}((0, 0)) = \mu^{-1}((0, 0, 1)) \cup \mu^{-1}((0, 0, -1)) = \mathcal{P}_1 \cup \mathcal{P}_2$ in (5.28). It is of interest to investigate more complicated desired paths in $SO(3)$ (i.e., pose motions) by specifying different functions Φ . \triangleleft

5.7 CONCLUSIONS

We investigate some topological aspects of a guiding vector field defined on a general smooth Riemannian manifold for the path-following control problem, and analyze the stability and attractiveness of the desired path and the singular set. Specifically, we first generalize the widely-studied guiding vector field on the Euclidean space to that defined on a general smooth manifold such that the new guiding vector field enables asymptotic following of a desired path defined on a manifold, such as a torus for robot arm joint space control applications. Then, motivated by many examples in the literature, we propose a question regarding whether singular points always exist in a guiding vector field when the desired path is homeomorphic to the unit circle. This question is directly related to the possibility of global convergence to the desired path. Since we consider a general smooth n -dimensional Riemannian manifold \mathcal{M} , the Poincaré-Bendixson theorem is not always applicable.

To answer this question, we first derive the dichotomy convergence property of the new guiding vector field, and conduct stability and attractiveness analysis of the desired path and the singular set. Then we revisit an existing topological result and provide some interpretations and implications for the vector-field guided path-following problem. It turns out that the domain of attraction of the desired path (homeomorphic to the unit circle) is homotopy equivalent to the unit circle. For the particular case when $\mathcal{M} = \mathbb{R}^n$, we conclude that global convergence to the desired path is impossible, and singular points always exist when the dichotomy convergence property holds globally. Motivated by this impossibility result of global convergence to the desired path, we have shown the existence of non-path-converging trajectories. More specifically, we have proved that for any ball containing the desired path, there always exists at least one non-path-converging trajectory starting from the boundary of the ball. This result is related to the topological aspect of motion planning problems in obstacle-populated environments. Several numerical examples are provided to illustrate the theoretical results.

6

THE DOMAIN OF ATTRACTION OF THE DESIRED PATH IN VECTOR-FIELD GUIDED PATH FOLLOWING

In the vector-field guided path-following problem, a sufficiently smooth vector field is designed such that its integral curves converge to and propagate along a one-dimensional geometric desired path. The existence of singular points where the vector field vanishes creates a topological obstruction to global convergence to the desired path, and some topological analysis has been conducted in Chapter 5. In this chapter, we strengthen Theorem 5.26 in Chapter 5 by showing that the domain of attraction (DOA) of the desired path, which is a compact asymptotically stable one-dimensional embedded submanifold in an n -dimensional ambient manifold \mathcal{M} , is homeomorphic to $\mathbb{R}^{n-1} \times S^1$, not just homotopic equivalent to S^1 as shown in Theorem 5.26.

This chapter is based on

- W. Yao, B. Lin, B. D. O. Anderson, and M. Cao, “The domain of attraction of the desired path in vector-field guided path following,” 2021, *Submitted*.

6.1 INTRODUCTION

Despite the advantages of vector-field guided path-following algorithms, a major issue is the existence of singular points where the vector field vanishes. This issue is the motivation for the topological analysis of these algorithms, and some questions regarding the attractiveness of singular points and the desired path, the dichotomy convergence results, and the possibility of global convergence to the desired path, have been answered in Chapter 5, under the assumption that the desired path is homeomorphic to the unit circle S^1 . In particular, it has been shown in Theorem 5.26 that the domain of attraction (DOA) of the desired path, which is a compact asymptotically stable embedded submanifold, is homotopic equivalent to S^1 . This result characterizes the DOA in terms of homotopic equivalence, but homotopic equivalent objects may be distinctive in the geometric or set-theoretical sense (e.g., S^1 and $\mathbb{R}^2 \setminus \{0\}$).

Generically, the aforementioned desired path is a *compact asymptotically stable embedded* submanifold, denoted by \mathcal{A} for convenience, in an ambient finite-dimensional manifold. Some studies also characterize the DOA of the submanifold \mathcal{A} . In [11, Chapter V, Lemma 3.2], it has been shown that the intersection of an ϵ -neighborhood of \mathcal{A} and some sublevel set of a Lyapunov function is a deformation retract of the DOA of \mathcal{A} . This result has been strengthened in [10], [99], which prove that \mathcal{A} itself is actually a deformation retract of its DOA, and thus \mathcal{A} and its DOA are homotopic equivalent. In [152, Theorem 3.4], it is claimed that \mathcal{A} is diffeomorphic to a tubular neighborhood of itself. This result will be discussed later in Remark 6.16.

In this chapter, we strengthen the result in Theorem 5.26. We show that the DOA of the desired path \mathcal{P} is not just homotopic equivalent to S^1 (as shown in Theorem 5.26), but is actually homeomorphic to $\mathbb{R}^{n-1} \times S^1$, where n is the dimension of the ambient manifold \mathcal{M} . Discussion on a related result in [152, Theorem 3.4] is provided in Remark 6.16.

The remainder of this chapter is organized as follows. Section 6.2 formally introduces the problem to be treated in this chapter, along with a review of the guiding vector field on a smooth n -dimensional Riemannian manifold for path following. Then Section 6.3 provides the answer to the problem, which further characterizes the topological property of the DOA of the desired path. Finally, Section 6.4 concludes the chapter.

6.2 PROBLEM FORMULATION

In this section, we review guiding vector fields defined on an n -dimensional Riemannian manifold \mathcal{M} with the Riemannian metric denoted by g in Chapter 5, after which we formulate the problem.

6.2.1 Vector-field guided path following on Riemannian manifolds

The desired path $\mathcal{P} \subseteq \mathcal{M}$ is described as the intersection of zero-level sets of twice continuously differentiable functions $\phi_i : \mathcal{M} \rightarrow \mathbb{R}$, $i = 1, \dots, n - 1$. Namely,

$$\mathcal{P} := \{\xi \in \mathcal{M} : \phi_i(\xi) = 0, i = 1, \dots, n - 1\},$$

where the functions ϕ_i are termed *level functions* for convenience. This description of the desired path \mathcal{P} enables one to define the *path-following error* $e : \mathcal{M} \rightarrow \mathbb{R}^{n-1}$ by stacking all ϕ_i functions together; that is,

$$e(\xi) = (\phi_1(\xi), \dots, \phi_{n-1}(\xi))^\top, \quad (6.1)$$

The reason for calling it path-following error is that, using this notion, the desired path \mathcal{P} is equivalent to

$$\mathcal{P} = \{\xi \in \mathcal{M} : e(\xi) = 0\}. \quad (6.2)$$

Using the level functions ϕ_i , the guiding vector field $\chi : \mathcal{M} \rightarrow T\mathcal{M}$ defined on the manifold \mathcal{M} is

$$\chi(\xi) = \perp_\phi(\xi) - \sum_{i=1}^{n-1} k_i \phi_i(\xi) \operatorname{grad} \phi_i(\xi), \quad (6.3)$$

where k_i are positive constants, $\operatorname{grad} \phi_i(\cdot) \in T_{(\cdot)}\mathcal{M}$ are the gradient vectors of the level functions ϕ_i on the manifold \mathcal{M} , and $\perp_\phi(\cdot) \in T_{(\cdot)}\mathcal{M}$ is a generalization to the manifold \mathcal{M} of the wedge product of all the gradient vectors $\operatorname{grad} \phi_i(\cdot)$ (see Chapter 5 for more detail). The term $\perp_\phi(\xi)$ is orthogonal to each of the gradient $\operatorname{grad} \phi_i(\xi)$, the same as its counterpart defined on the Euclidean space, as stated in Lemma 5.1 in Chapter 5. The first and second terms on the right of (6.3) induce motion along the path, and motion towards the path, respectively. A point $\xi \in \mathcal{M}$ where the vector field vanishes (i.e., $\chi(\xi) = 0$) is called a *singular point*, and the set of singular points is called the *singular set*, which is defined by

$$\mathcal{C} = \{\xi \in \mathcal{M} : \chi(\xi) = 0\}.$$

6.2.2 Assumptions and problem statement

For certain manifolds \mathcal{M} and under the global dichotomy convergence condition, the existence of a singular point (or possibly a set of singular points) is unavoidable (e.g., Theorem 5.27 in Chapter 5). The following standing assumption is required. In effect, it is an assumption on the functions ϕ_i .

Assumption 6.1 (Chapter 5). There are no singular points on the desired path. More precisely, \mathcal{C} is empty or otherwise there holds $\text{dist}(\mathcal{C}, \mathcal{P}) > 0$.

Assumption 6.1 ensures the “regularity” of the desired path \mathcal{P} stated in Lemma 6.2.

Lemma 6.2 (Chapter 5, Regularity of \mathcal{P}). *The zero vector $\mathbf{0} \in \mathbb{R}^{n-1}$ is a regular value of the map e in (6.1), and hence the desired path \mathcal{P} is a C^2 embedded submanifold in \mathcal{M} .*

Given the guiding vector field $\chi : \mathcal{M} \rightarrow T\mathcal{M}$ in (6.3), one investigates the solutions to the following autonomous ordinary differential equation:

$$\dot{\xi}(t) = \chi(\xi(t)). \quad (6.4)$$

The manifold \mathcal{M} is called the *configuration space*. To use the path-following error $e(\xi(t))$ along a trajectory $\xi(t)$ of (6.4) to determine the convergence to the desired path, we need the following standing assumption.

Assumption 6.3 (Chapter 5). For any given constant $\kappa > 0$, there holds $\inf\{||e(\xi)|| : \text{dist}(\xi, \mathcal{P}) \geq \kappa\} > 0$,

To obtain the topological results later, we impose the following standing assumption as in Chapter 5:

Assumption 6.4. The desired path \mathcal{P} is homeomorphic to the unit circle S^1 (i.e., $\mathcal{P} \approx S^1$).

It is shown in Theorem 5.26 of Chapter 5 that the DOA of the desired path \mathcal{P} has the same homotopy type as the unit circle S^1 . Despite its theoretical interest and its usefulness as shown in Chapter 5, Theorem 5.26 of Chapter 5 gives a very rough impression of how the DOA may look, since two homotopy equivalent objects may be geometrically or set-theoretically very different; for example, $\mathbb{R}^2 \setminus \{0\}$ and S^1 are homotopy equivalent. Another example is $\{0\}$ and \mathbb{R}^n , for any positive number n . Suppose $\mathcal{M} = \mathbb{R}^2$, then it is unclear, for instance, if the DOA of the desired path \mathcal{P} is $\mathbb{R}^2 \setminus \{0\}$ (or \mathbb{R}^2 excluding any other point). Therefore, having a stronger notion to capture the “shape” of the DOA is highly desirable, and the problem to be solved in this chapter is to obtain such a stronger notion to replace the homotopy equivalence between the desired path and its DOA.

Observe that neither $\mathbb{R}^2 \setminus \{0\}$ and S^1 , nor $\{0\}$ and \mathbb{R}^n , are *homeomorphic*. Thus a candidate notion to consider is the homeomorphic relation between two topological objects. In the subsequent sections, we will strengthen Theorem 5.26 of Chapter 5 by showing that the DOA is homeomorphic to $\mathbb{R}^{n-1} \times S^1$, where n is the dimension of the manifold \mathcal{M} (i.e., Theorem 6.15).

6.3 FURTHER CHARACTERIZATION OF THE DOA

6.3.1 A property near a compact regular level set

There is a property holding near a *compact component*¹ of a *regular level set* (i.e., the level set of a regular value of a smooth map). In particular, when the component of some regular level set of a smooth map is compact, then locally all level sets are compact and homeomorphic to the compact component. In addition, these level sets are placed “nicely” as precisely stated in the following proposition.

Proposition 6.5. *Let $f_i : \mathcal{M} \rightarrow \mathbb{R}$, $i = 1, \dots, n - 1$, be smooth surjective functions. Suppose the smooth map $F = (f_1, \dots, f_{n-1}) : \mathcal{M} \rightarrow \mathbb{R}^{n-1}$ has a regular value $p \in \mathbb{R}^{n-1}$. If there exists a compact component \mathcal{S}_0 of $F^{-1}(p)$, then there exist some open neighborhood \mathcal{Q} of \mathcal{S}_0 in \mathcal{M} and an open neighborhood \mathcal{U} of p in \mathbb{R}^{n-1} , along with a diffeomorphism $\Gamma : \mathcal{Q} \rightarrow \mathcal{U} \times \mathcal{S}_0$ such that*

$$\pi_{\mathcal{U}} \circ \Gamma = F|_{\mathcal{Q}},$$

where $\pi_{\mathcal{U}}$ denotes the projection of the product space $\mathcal{U} \times \mathcal{S}_0$ onto the first factor \mathcal{U} , and $F|_{\mathcal{Q}}$ is the restriction of F to \mathcal{Q} .

Proof. One can check that the conditions of the Ehresmann theorem [30, p. 378] are satisfied, and thus the conclusion follows from the theorem. For a detailed argument, also see [85, Proposition 2.1]. \square

To explain Proposition 6.5, for simplicity, we assume that there is only one component of $F^{-1}(p)$ and it is compact (i.e., $\mathcal{S}_0 = F^{-1}(p)$). Then Proposition 6.5 claims that near the compact regular level set \mathcal{S}_0 (i.e., in the neighborhood \mathcal{Q}), all level sets are homeomorphic to \mathcal{S}_0 . Moreover, these level sets are placed “nicely” in a way that is explicitly expressed by the homeomorphism Γ : they are homeomorphic to $\mathcal{U} \times \mathcal{S}_0$ (see Fig. 6.1). Roughly speaking, the level sets $F^{-1}(\mathcal{U})$ in the open neighborhood \mathcal{Q} are topologically equivalent to putting copies of \mathcal{S}_0 in parallel and crossing them through by \mathcal{U} , as illustrated by a thick line in Fig. 6.1 (i.e., $\mathcal{U} \times \mathcal{S}_0$). We can think of this property as showing the “stability” of the topology of level sets near the compact regular level set \mathcal{S}_0 .

Remark 6.6. In this proposition, one can let the map F be only *twice continuously differentiable* (i.e., $F \in C^2$), and hence the map Γ can be changed to a C^2 -diffeomorphism. \triangleleft

Let $\pi_i : \mathbb{R}^n \rightarrow \mathbb{R}$ be the projection function that gives the i -th argument of a function; namely, π_i is defined by $\pi_i(x_1, \dots, x_i, \dots, x_n) = x_i$. Then one naturally has the following corollary related to the path following problem.

¹ When we talk about the components of some level set, we can regard the level set itself as a topological space with the topology inherited from the ambient space, and then the concept of *component* is the same as that in the preliminaries (i.e., Section 2.3 in Chapter 2).

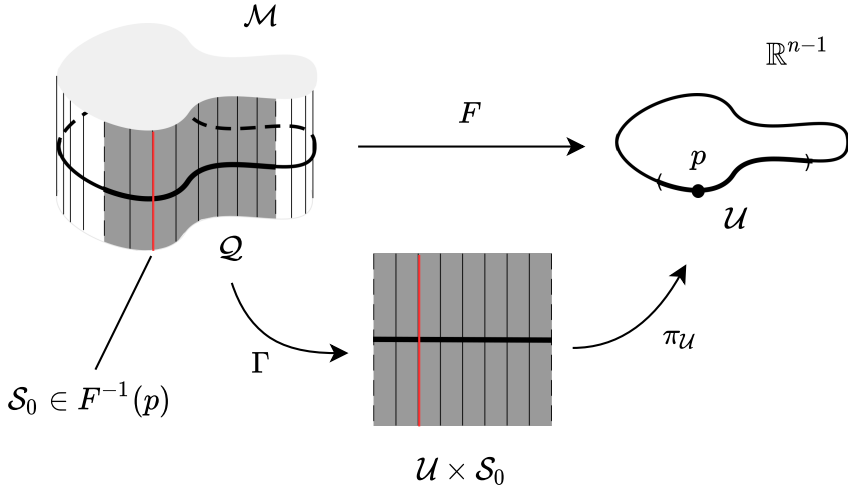


Figure 6.1: The illustration of Proposition 6.5. The red vertical line in \mathcal{M} represents S_0 , which is a compact component of the regular level set $F^{-1}(p)$, where $p \in \mathcal{U} \subseteq \mathbb{R}^{n-1}$. The shaded region is an open neighborhood denoted by \mathcal{Q} of S_0 in \mathcal{M} , and \mathcal{U} is an open neighborhood of $p \in \mathbb{R}^{n-1}$. All level sets in \mathcal{Q} are topologically equivalent to S_0 , and they are “placed nicely” in the sense that they are homeomorphic to $\mathcal{U} \times S_0$. This picture takes inspiration from [77, Fig. 10.1].

Corollary 6.7. *There is an open neighborhood \mathcal{Q} of the desired path $\mathcal{P} = e^{-1}(\mathbf{0})$ in \mathcal{M} and a C^2 -diffeomorphism Γ from \mathcal{Q} to $\mathcal{U} \times \mathbb{S}^1$, where $\mathcal{U} = e(\mathcal{Q}) \subseteq \mathbb{R}^{n-1}$, such that*

$$e|_{\mathcal{Q}} = \pi_{\mathcal{U}} \circ \Gamma. \quad (6.5)$$

Therefore, $e_i = \phi_i = \pi_i \circ \Gamma$ in \mathcal{Q} , for $i = 1, \dots, n - 1$.

Proof. From Lemma 6.2, the C^2 map $e = (\phi_1(\cdot), \dots, \phi_{n-1}(\cdot))^\top$ has a regular value $\mathbf{0} \in \mathbb{R}^{n-1}$, and the inverse image is the desired path (i.e., $\mathcal{P} := e^{-1}(\mathbf{0})$), which is assumed to be homeomorphic to the unit circle (i.e., $\mathcal{P} \approx \mathbb{S}^1$), hence compact [76, Theorem 5.27]. From Proposition 6.5 and Remark 6.6, the conclusions then follow. \square

The illustration of Corollary 6.7 is shown in Fig. 6.2. This implies that there exists a neighborhood $\mathcal{U} \subseteq \mathbb{R}^{n-1}$ of $\mathbf{0}$ such that the preimage $e^{-1}(\mathcal{U})$ “looks like” a solid torus $\mathcal{U} \times \mathbb{S}^1$ in the homeomorphic sense.

6.3.2 DOA of the desired path

We consider the autonomous system (6.4). Let $t \mapsto \Psi(t, x_0)$ be the solution to (6.4) with the initial condition $\Psi(0, x_0) = x_0$, then $\Psi : \mathbb{R}_{\geq 0} \times \mathcal{M} \rightarrow \mathcal{M}$ is a flow

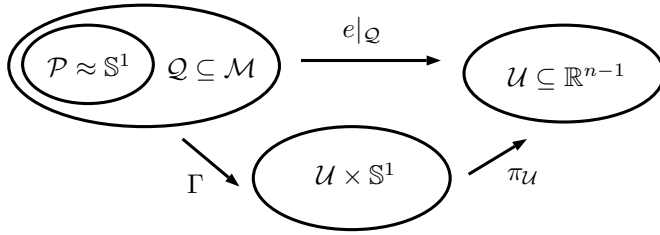


Figure 6.2: The illustration of Corollary 6.7.

[25]. We will also use $\Psi^t(x_0)$ interchangeably with $\Psi(t, x_0)$, as is standard in the literature. Without loss of generality, we can assume that the solution to (6.4) is forward complete (i.e., the solution is well-defined for $t \rightarrow \infty$), since otherwise one can replace the vector field χ by $\chi/(1 + \|\chi\|)$ without causing any difference to the topological properties of the flow that will be discussed in the sequel [25, Proposition 1.14].

Next, we define two sets \mathcal{W}° and \mathcal{W}^- of some subset $\mathcal{W} \subseteq \mathcal{M}$ below. To understand these sets intuitively, an example is presented after the definition.

Definition 6.8 ([27, Definition 2.2]). Given $\mathcal{W} \subseteq \mathcal{M}$, two sets \mathcal{W}° and \mathcal{W}^- are defined below:

$$\begin{aligned}\mathcal{W}^\circ &:= \{\gamma \in \mathcal{W} : \exists t > 0, \Psi(t, \gamma) \notin \mathcal{W}\} \\ \mathcal{W}^- &:= \{\gamma \in \mathcal{W} : \forall t > 0, \Psi([0, t], \gamma) \not\subseteq \mathcal{W}\},\end{aligned}$$

where $\not\subseteq$ means “not a subset of”. The set $\mathcal{W}^- \subseteq \mathcal{W}^\circ$ is called the *exit set* of \mathcal{W} .

Example 6.9. Suppose, with abuse of notation, we have a compact asymptotically stable invariant set $\mathcal{P} \subseteq \mathcal{M}$ (or a point when \mathcal{P} is a singleton), and its DOA is denoted by $A(\mathcal{P})$. We also assume that there is an open and precompact neighborhood $\mathcal{U} \supseteq \mathcal{P}$ of \mathcal{P} such that i) The closure of \mathcal{U} , denoted by $\bar{\mathcal{U}}$, is a (proper) subset of the DOA $A(\mathcal{P})$; ii) every trajectory starting from the boundary $\partial\mathcal{U}$ of \mathcal{U} immediately leaves the boundary and enters the neighborhood \mathcal{U} (and thus converges to \mathcal{P} subsequently). Therefore, every trajectory starting from \mathcal{U} converges to \mathcal{P} . Define $\mathcal{W} = \mathcal{M} \setminus \mathcal{U}$, which is a closed set in \mathcal{M} . Then the aforementioned boundary $\partial\mathcal{U} \subseteq \mathcal{W}$ is the *exit set* \mathcal{W}^- , since every trajectory starting from it immediately leaves the set \mathcal{W} , and thus it acts like an *exit* of \mathcal{W} . Since \mathcal{U} is a proper subset of the DOA $A(\mathcal{P})$, we define $\mathcal{W}^\circ = \mathcal{W} \cap A(\mathcal{P}) \neq \emptyset$. The set \mathcal{W}° is such that every trajectory starting from \mathcal{W}° may stay in \mathcal{W} for some time (in contrast to \mathcal{W}^- for which trajectories leave \mathcal{W} immediately) but leaves \mathcal{W} and enters \mathcal{U} eventually (see Fig. 6.3).

Through this example, the sets \mathcal{W}° and \mathcal{W}^- may be seen as a generalization of some neighborhoods of \mathcal{P} , while \mathcal{W} itself is a generalization or, better expressed, variation on the set of points in the *exterior* of the DOA of \mathcal{P} , but also actually

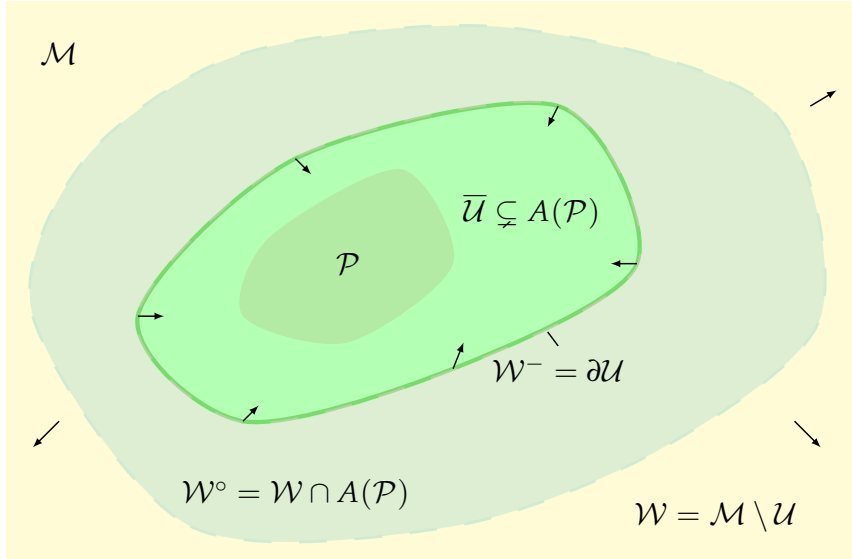


Figure 6.3: Illustration of \mathcal{W} , \mathcal{W}° and \mathcal{W}^- in \mathcal{M} . The red region (covered by green) is a compact asymptotically stable invariant set \mathcal{P} , with the DOA denoted by $A(\mathcal{P})$. The green region represents an open and precompact neighborhood \mathcal{U} of \mathcal{P} and $\overline{\mathcal{U}}$ is a proper subset of $A(\mathcal{P})$. The yellow and cyan (covered by yellow) regions represent \mathcal{W} and \mathcal{W}° respectively. The black arrows are some vectors of a vector field on \mathcal{M} . All vectors on the boundary $\partial\mathcal{U}$ are transverse to $\partial\mathcal{U}$ and point to the interior of \mathcal{U} . The exit set is $\mathcal{W}^- = \partial\mathcal{U}$, which acts like an exit of the set \mathcal{W} .

including part of that DOA. It is well known that, in general, there is no systematic way to find the DOA $A(\mathcal{P})$. Thus, in this chapter, we first find those sets $\mathcal{W}, \mathcal{W}^\circ, \mathcal{W}^-$, and then characterize the DOA by taking advantage of the physical intuition associated with these sets.

△

For simplicity, we denote by $e_{\mathcal{Q}}$ the restriction of e to \mathcal{Q} (i.e., $e_{\mathcal{Q}} := e|_{\mathcal{Q}}$), where \mathcal{Q} is defined in Corollary 6.7. In addition, we define an ellipsoid:

$$\mathcal{D} := \{x \in \mathbb{R}^{n-1} : x^\top K x < r\} \subseteq \mathbb{R}^{n-1} \quad (6.6)$$

centered at $\mathbf{0} \in \mathcal{U} = e(\mathcal{Q}) \subseteq \mathbb{R}^{n-1}$, where $K := \text{diag}\{k_1, \dots, k_{n-1}\}$ is the diagonal matrix with all the positive gains k_i , $i = 1, \dots, n-1$, and r is chosen sufficiently small such that $\overline{\mathcal{D}} \subseteq \mathcal{U}$, where $\overline{\mathcal{D}}$ denotes the closure of \mathcal{D} . Since $e_{\mathcal{Q}}^{-1}(\overline{\mathcal{D}}) \approx \overline{\mathcal{D}} \times \mathbb{S}^1$ by Corollary 6.7, $e_{\mathcal{Q}}^{-1}(\overline{\mathcal{D}})$ is an embedded submanifold with the manifold boundary [77, p. 120]

$$\mathcal{S} := e_{\mathcal{Q}}^{-1}(\partial\overline{\mathcal{D}}) \subseteq \mathcal{M}, \quad (6.7)$$

which is homeomorphic to $\partial\overline{\mathcal{D}} \times \mathbb{S}^1$. We define the set \mathcal{W} below:

$$\mathcal{W} := \mathcal{M} \setminus e_{\mathcal{Q}}^{-1}(\mathcal{D}) \subseteq \mathcal{M}. \quad (6.8)$$

With the introduction of the exit set in Definition 6.8, the next lemma identifies exactly what the exit set of \mathcal{W} is, and also shows the forward-invariance of $e_{\mathcal{Q}}^{-1}(\overline{\mathcal{D}}) \subseteq \mathcal{M}$ and $e_{\mathcal{Q}}^{-1}(\mathcal{D}) \subseteq \mathcal{M}$.

Lemma 6.10. *It holds that*

1. *The set \mathcal{S} in (6.7) is the exit set \mathcal{W}^- of \mathcal{W} ;*
2. *The sets $e_{\mathcal{Q}}^{-1}(\overline{\mathcal{D}})$ and $e_{\mathcal{Q}}^{-1}(\mathcal{D})$ are forward-invariant sets with respect to (6.4), and $\Psi^{(0,+\infty)}(\mathcal{S}) \subseteq e_{\mathcal{Q}}^{-1}(\mathcal{D})$, where $\Psi^{(0,+\infty)}(\mathcal{S}) := \{\Psi^t(p) : t \in (0, +\infty), p \in \mathcal{S}\}$.*

Proof. Proof of Claim 1): First note that

$$\begin{aligned} \langle \text{grad } \phi_i, \chi \rangle_g &\stackrel{(6.3)}{=} \left\langle \text{grad } \phi_i, \perp_{\phi}(\xi) - \sum_{j=1}^{n-1} k_j \phi_j(\xi) \text{grad } \phi_j(\xi) \right\rangle_g \\ &= \left\langle \text{grad } \phi_i, - \sum_{j=1}^{n-1} k_j \phi_j(\xi) \text{grad } \phi_j(\xi) \right\rangle_g, \end{aligned} \quad (6.9)$$

for $i = 1, \dots, n-1$, where $\langle \cdot, \cdot \rangle_g$ denotes the Riemannian metric, and we have used the orthogonality property (Lemma 5.1 in Chapter 5) in the last equation. Now we can calculate the time derivative of the path-following error e :

$$\begin{aligned} \frac{d}{dt} e(\xi(t)) &= \frac{d}{dt} \begin{bmatrix} \phi_1(\xi(t)) \\ \vdots \\ \phi_{n-1}(\xi(t)) \end{bmatrix} = \begin{bmatrix} \langle \text{grad } \phi_1, \chi \rangle_g \\ \vdots \\ \langle \text{grad } \phi_{n-1}, \chi \rangle_g \end{bmatrix} \\ &\stackrel{(6.9)}{=} \begin{bmatrix} \langle \text{grad } \phi_1, - \sum_{j=1}^{n-1} k_j \phi_j \text{grad } \phi_j \rangle_g \\ \vdots \\ \langle \text{grad } \phi_{n-1}, - \sum_{j=1}^{n-1} k_j \phi_j \text{grad } \phi_j \rangle_g \end{bmatrix}. \end{aligned} \quad (6.10)$$

We adopt the common convention in differential manifold theory that a vector field with a subscript represents the vector at the point represented by the subscript. Let χ' denote the vector field defined on $\mathcal{U} \times \mathbb{S}^1$ such that

$$\chi'_{\Gamma(p)} = \Gamma_*(\chi_p)$$

for any point $p \in \mathcal{Q}$, where Γ_* is the tangent map of Γ . Since Γ is a C^2 -diffeomorphism, one can obtain information about χ by studying χ' . Define a

function $\Pi : \mathcal{U} \times \mathbb{S}^1 \rightarrow \mathcal{U}$ by $\Pi(\cdot) := (\pi_1(\cdot), \dots, \pi_{n-1}(\cdot))^\top$, where each component function $\pi_i(\cdot)$ is a projection function. One can calculate that

$$\begin{aligned} (\Pi^\top K \Pi) \circ \Gamma(\cdot) &= \left(\sum_{i=1}^{n-1} k_i \pi_i^2(\cdot) \right) \circ \Gamma(\cdot) \\ &= \sum_{i=1}^{n-1} k_i (\pi_i^2 \circ \Gamma)(\cdot) = \sum_{i=1}^{n-1} k_i e_i^2(\cdot) = e(\cdot)^\top K e(\cdot). \end{aligned} \quad (6.11)$$

In addition, by definition of a tangent vector [77, pp. 50-55], we have

$$\begin{aligned} \chi(e^\top K e) &= \frac{d}{dt} (e(\xi(t))^\top K e(\xi(t))) \Big|_{t=0} \\ &\stackrel{(6.10)}{=} \begin{bmatrix} \langle \text{grad } \phi_1, -\sum_{j=1}^{n-1} k_j \phi_j \text{ grad } \phi_j \rangle_g \\ \vdots \\ \langle \text{grad } \phi_{n-1}, -\sum_{j=1}^{n-1} k_j \phi_j \text{ grad } \phi_j \rangle_g \end{bmatrix}^\top \begin{bmatrix} k_1 \phi_1 \\ \vdots \\ k_{n-1} \phi_{n-1} \end{bmatrix} \\ &= - \left\langle \sum_{j=1}^{n-1} k_j \phi_j \text{ grad } \phi_j, \sum_{j=1}^{n-1} k_j \phi_j \text{ grad } \phi_j \right\rangle_g \leq 0, \end{aligned} \quad (6.12)$$

where $\xi : (-\epsilon, \epsilon) \rightarrow \mathcal{Q}$ is a trajectory of (6.4) with $\xi(0) \in \Gamma^{-1}(\partial \bar{\mathcal{D}} \times \mathbb{S}^1)$ and $\dot{\xi}(0) = \chi_{\xi(0)}$. Therefore, we have

$$\chi'(\Pi^\top K \Pi) = \chi((\Pi^\top K \Pi) \circ \Gamma) \stackrel{(6.11)}{=} \chi(e^\top K e) \stackrel{(6.12)}{=} -\|l(\cdot)\|^2 \leq 0, \quad (6.13)$$

where $l(\cdot) := \sum_{j=1}^{n-1} k_j \phi_j(\cdot) \text{ grad } \phi_j(\cdot)$. Note that for any point $\xi \in \mathcal{M}$, if $\|l(\xi)\| = 0$, then either $\text{grad } \phi_j(\xi), j = 1, \dots, n-1$, are linearly dependent, or they are linearly independent, but all $\phi_j(\xi)$ equal zero. In the former case, the first term of (6.3) satisfies $\perp_\phi(\xi) = 0$, and thus $\chi(\xi) = 0$, leading to $\xi \in \mathcal{C}$. In the latter case, it is obvious that $\xi \in \mathcal{P}$. Therefore, we have

$$\chi'_{\xi}(\Pi^\top K \Pi) < 0, \quad \forall \xi \in \partial \bar{\mathcal{D}} \times \mathbb{S}^1 \quad (6.14)$$

as there are all regular points on $\Gamma^{-1}(\partial \bar{\mathcal{D}} \times \mathbb{S}^1) \subseteq \mathcal{Q} \setminus \mathcal{P}$, and

$$\chi'_{\xi}(\Pi^\top K \Pi) \leq 0, \quad \forall \xi \in \bar{\mathcal{D}} \times \mathbb{S}^1 \quad (6.15)$$

where the equality is taken only for points $\xi \in \Gamma(\mathcal{P}) \approx \{\mathbf{0}\} \times \mathbb{S}^1$.

Given an initial condition $\zeta(0) \in \mathcal{S} \subseteq \mathcal{Q}$, let $\zeta : \mathbb{R}_{\geq 0} \rightarrow \mathcal{M}$ be the solution to (6.4). Since \mathcal{Q} is an open subset in \mathcal{M} , there is some $\epsilon > 0$ such that $\zeta(t) \in \mathcal{Q}$ for $t \in (-\epsilon, \epsilon)$. Let

$$\tilde{\zeta} := \Gamma \circ \zeta|_{(-\epsilon, \epsilon)}$$

and therefore

$$\frac{d}{dt} \tilde{\zeta} = \chi' \circ \tilde{\zeta} \quad (6.16)$$

on $\mathcal{U} \times \mathbb{S}^1$ with $\tilde{\zeta}(0) \in \partial\bar{\mathcal{D}} \times \mathbb{S}^1$. According to (6.14), one has

$$\frac{d}{dt} (\Pi^\top K \Pi) \circ \tilde{\zeta}(t)|_{t=0} = \chi'(\Pi^\top K \Pi) < 0,$$

and hence by (6.15), we have $(\Pi^\top K \Pi) \circ \tilde{\zeta}(t) < r$ for any $t \in (0, \epsilon)$, where recall that r is defined in (6.6). Thus, $\tilde{\zeta}((0, \epsilon)) \subseteq \mathcal{D} \times \mathbb{S}^1$. Therefore, $\zeta([0, \epsilon)) \subseteq e_{\mathcal{Q}}^{-1}(\mathcal{D})$ and this shows that \mathcal{S} is the exit set of \mathcal{W} .

Proof of Claim 2: Suppose $\zeta(0) \in e_{\mathcal{Q}}^{-1}(\bar{\mathcal{D}})$. By (6.15) and using the same reasoning as above, we have $(\Pi^\top K \Pi) \circ \tilde{\zeta}(t) \leq r$ for any $t \in [0, \epsilon]$, and thus $\tilde{\zeta}[0, \epsilon] \subseteq \bar{\mathcal{D}} \times \mathbb{S}^1$. By the compactness of $\bar{\mathcal{D}} \times \mathbb{S}^1$, one can show that there is an extension of the solution $\tilde{\zeta}$ of (6.16) on $(-\epsilon, +\infty)$ such that $\tilde{\zeta}(0, \infty) \subseteq \mathcal{D} \times \mathbb{S}^1$ [66, Theorem 3.3]. Then due to the uniqueness of the solution to the Cauchy problem of (6.4), $\zeta = \Gamma^{-1} \circ \tilde{\zeta}$ is defined on $(-\epsilon, +\infty)$ and thus $\zeta(0, \infty) \subseteq \Gamma^{-1}(\mathcal{D} \times \mathbb{S}^1) = e_{\mathcal{Q}}^{-1}(\mathcal{D})$. This shows that $e_{\mathcal{Q}}^{-1}(\bar{\mathcal{D}})$ is an invariant set of the flow Ψ , and $\Psi^{(0, +\infty)}(\mathcal{S}) \subseteq e_{\mathcal{Q}}^{-1}(\mathcal{D})$. The same argument can be applied to the case where $\zeta(0) \in e_{\mathcal{Q}}^{-1}(\mathcal{D})$ to yield that $e_{\mathcal{Q}}^{-1}(\mathcal{D})$ is also an invariant set. \square

Observe that the vector field χ in (6.3) is transverse to \mathcal{S} in \mathcal{M} as stated below.

Lemma 6.11. *It holds that $\text{span}\{\chi_p\} \oplus T_p \mathcal{S} = T_p \mathcal{M}$ for $p \in \mathcal{S}$, where \oplus is the direct sum; that is, the vector field χ is transverse to \mathcal{S} in \mathcal{M} .*

Proof. Since \mathcal{S} is homeomorphic to $\partial\bar{\mathcal{D}} \times \mathbb{S}^1$, \mathcal{S} is an $(n - 1)$ -dimensional submanifold in \mathcal{M} . For any $p \in \mathcal{S}$, we have $e_{*p}(T_p \mathcal{S}) = T_{e(p)} \partial\bar{\mathcal{D}}$, where e_{*p} is the tangent map of e at p . Then (6.14) implies that $\chi_p \notin T_p \mathcal{S}$ for $p \in \mathcal{S}$, and hence $\text{span}\{\chi_p\} \oplus T_p \mathcal{S} = T_p \mathcal{M}$ for $p \in \mathcal{S}$; that is, the vector field χ is transverse to \mathcal{S} in \mathcal{M} . \square

The following lemma states that the flow $\Psi(\cdot, \cdot)$ of (6.4) is open and injective.

Lemma 6.12. *The flow $\Psi : \mathbb{R} \times \mathcal{S} \rightarrow \mathcal{M}$ of (6.4) is an open injection. In particular, $\Psi : (-\infty, +\infty) \times \mathcal{S} \rightarrow \Psi^{(-\infty, +\infty)}(\mathcal{S})$ is a homeomorphism.*

Proof. We first show that $\Psi(\cdot, \cdot)$ is an open map from $\mathbb{R} \times \mathcal{S}$ to \mathcal{M} . Since $\text{span}\{\chi_p\} \oplus T_p \mathcal{S} = T_p \mathcal{M}$ for any point $p \in \mathcal{S}$ by Lemma 6.11, the tangent map $\Psi_{*(0,p)}$ of the flow $\Psi(\cdot, \cdot)$ is a surjection from $T_{(0,p)}(\mathbb{R} \times \mathcal{S})$ onto $T_{\Psi(0,p)}\mathcal{M}$ for each point $(0, p) \in \mathbb{R} \times \mathcal{S}$. Therefore, $\Psi(\cdot, \cdot)$ is locally an open map from

some open neighborhood \mathcal{O} of $(0, p)$. Thus, $\Psi(\mathcal{O}) := \{\Psi^t(q) : (t, q) \in \mathcal{O}\}$ is open in \mathcal{M} . For any fixed $t_0 \in \mathbb{R}$, denote by $t_0 + \mathcal{O}$ the set $\{(t + t_0, q) : (t, q) \in \mathcal{O}\}$, which is an open neighborhood of (t_0, p) . Therefore,

$$\begin{aligned}\Psi(t_0 + \mathcal{O}) &= \{\Psi^{t_0+t}(q) = \Psi^{t_0}(\Psi^t(q)) : (t, q) \in \mathcal{O}\} \\ &= \Psi^{t_0}(\{\Psi^t(q) : (t, q) \in \mathcal{O}\}) = \Psi^{t_0}(\Psi(\mathcal{O}))\end{aligned}$$

is open since $\Psi^{t_0}(\cdot)$ is a C^2 -diffeomorphism of \mathcal{M} . Thus, $\Psi(\cdot, \cdot)$ is an open map from $\mathbb{R} \times \mathcal{S}$ to \mathcal{M} .

To prove that $\Psi(\cdot, \cdot)$ is an injection from $\mathbb{R} \times \mathcal{S}$ to \mathcal{M} , suppose $\Psi^t(p) = \Psi^{t'}(q)$ for some $p, q \in \mathcal{S}$ and $t, t' \in \mathbb{R}$. If $t = t'$, then $p = q$ due to the uniqueness of the solution to the Cauchy problem in (6.4). Now assume that $t < t'$, then $p = \Psi^{t'-t}(q)$. According to Lemma 6.10, $p \in e_Q^{-1}(\mathcal{D})$, which contradicts the condition that $p \in \mathcal{S}$. A similar contradiction arises if $t > t'$. Therefore, we have $t = t'$ and $p = q$, justifying that $\Psi(\cdot, \cdot)$ is an injection from $\mathbb{R} \times \mathcal{S}$ to \mathcal{M} .

We have proved above that the flow $\Psi : \mathbb{R} \times \mathcal{S} \rightarrow \mathcal{M}$ of (6.4) is an open injection. Now if we restrict the codomain of Ψ to its image $\Psi^{(-\infty, +\infty)}(\mathcal{S})$, then the map $\Psi : (-\infty, +\infty) \times \mathcal{S} \rightarrow \Psi^{(-\infty, +\infty)}(\mathcal{S})$ is continuous, bijective, and open, hence a homeomorphism [77, Theorem A.38 (c)]. \square

According to Definition 6.8, the set \mathcal{W}° is particularized to

$$\mathcal{W}^\circ = \{x \in \mathcal{W} : \exists t > 0, \Psi^t(x) \in e_Q^{-1}(\mathcal{D})\}. \quad (6.17)$$

Based on Lemma 6.10 and Lemma 6.12, we could now give the exact expression of the set \mathcal{W}° .

Proposition 6.13. *Let $\Psi(\cdot, \cdot)$ be the flow of (6.4). Then the set \mathcal{W}° as defined in Definition 6.8 and particularized to (6.17) is*

$$\mathcal{W}^\circ = \Psi^{(-\infty, 0]}(\mathcal{S}).$$

In addition, \mathcal{W}° is homeomorphic to $(-\infty, 0] \times \mathcal{S}$ given by the homeomorphism $\Psi^{(\cdot)}(\cdot)$, and \mathcal{W}° is open in \mathcal{W} .

Proof. We first show that $\mathcal{W}^\circ = \Psi^{(-\infty, 0]}(\mathcal{S})$. According to Definition 6.8 and (6.17), for any $x \in \mathcal{W}^\circ$, there exists some $\tau > 0$ such that $\Psi^\tau(x) \in e_Q^{-1}(\mathcal{D})$. Let

$$a := \inf\{t \in (0, \tau) : \Psi^{[t, \tau]}(x) \subseteq e_Q^{-1}(\mathcal{D})\} \geq 0,$$

and then $\Psi^a(x) \in e_Q^{-1}(\partial\bar{\mathcal{D}})$, and therefore, $x \in \Psi^{-a}(e_Q^{-1}(\partial\bar{\mathcal{D}})) = \Psi^{-a}(\mathcal{S}) \subseteq \Psi^{(-\infty, 0]}(\mathcal{S})$. Thus, $\mathcal{W}^\circ \subseteq \Psi^{(-\infty, 0]}(\mathcal{S})$. Conversely, suppose $x \in \Psi^{(-\infty, 0]}(\mathcal{S})$. Then there exists some $t \leq 0$ and $y \in \mathcal{S}$ such that $\Psi^t(y) = x$, or $y = \Psi^{-t}(x)$. Since \mathcal{S} is the exit set of \mathcal{W} by Lemma 6.10, there exists a positive constant δ such

that $\Psi^{(0,\delta)}(y) \subseteq e_Q^{-1}(\mathcal{D})$. Therefore, we have $\Psi^{-t+\delta}(x) \in e_Q^{-1}(\mathcal{D})$. In view of the definition of \mathcal{W}° in (6.17), it follows that $x \in \mathcal{W}^\circ$, hence $\Psi^{(-\infty,0]}(\mathcal{S}) \subseteq \mathcal{W}^\circ$. Combining this with the previous claim that $\mathcal{W}^\circ \subseteq \Psi^{(-\infty,0]}(\mathcal{S})$, we have $\mathcal{W}^\circ = \Psi^{(-\infty,0]}(\mathcal{S})$.

By Lemma 6.12, $\Psi : (-\infty, +\infty) \times \mathcal{S} \rightarrow \Psi^{(-\infty, +\infty)}(\mathcal{S})$ is a homeomorphism. Hence $\Psi^{(\cdot)}(\cdot)$ is a homeomorphism from $(-\infty, 0] \times \mathcal{S}$ to \mathcal{W}° .

Finally, we prove that \mathcal{W}° is open in \mathcal{W} by showing that $\mathcal{W}^\circ = \Psi^{(-\infty, +\infty)}(\mathcal{S}) \cap \mathcal{W}$. Since $e_Q^{-1}(\mathcal{D})$ is an invariant set of the flow by Lemma 6.10, $\Psi^{(0,+\infty)}(q) \subseteq e_Q^{-1}(\mathcal{D})$ for every $q \in \mathcal{S}$, and therefore, $\Psi^{(0,+\infty)}(\mathcal{S}) \cap \mathcal{W} = \emptyset$. So $\Psi^{(-\infty, +\infty)}(\mathcal{S}) \cap \mathcal{W} = \Psi^{(-\infty,0]}(\mathcal{S}) \cap \mathcal{W} = \mathcal{W}^\circ \cap \mathcal{W} = \mathcal{W}^\circ$. Since $\Psi^{(-\infty, +\infty)}(\mathcal{S})$ is open in \mathcal{M} by Lemma 6.12, \mathcal{W}° is open in \mathcal{W} . \square

Now we can characterize the “shape” of the set $e_Q^{-1}(\overline{\mathcal{D}}) \cup \mathcal{W}^\circ$, which is related to the DOA of the desired path \mathcal{P} as shown later.

Proposition 6.14. *The set $e_Q^{-1}(\overline{\mathcal{D}}) \cup \mathcal{W}^\circ$ is homeomorphic to $\mathbb{R}^{n-1} \times \mathbb{S}^1$.*

Proof. By Proposition 6.13, $(t, q) \mapsto \Psi^t(q)$ is a homeomorphism from $(-\infty, 0] \times \mathcal{S}$ to \mathcal{W}° . In addition, \mathcal{S} is homeomorphic to $\partial\overline{\mathcal{D}} \times \mathbb{S}^1$ with the homeomorphism $\Gamma^{-1}|_{\partial\overline{\mathcal{D}} \times \mathbb{S}^1}$ by Corollary 6.7. Therefore,

$$\begin{aligned} Y : (-\infty, 0] \times \partial\overline{\mathcal{D}} \times \mathbb{S}^1 &\rightarrow \mathcal{W}^\circ \\ (t, b, s) &\mapsto \Psi^t \circ \Gamma^{-1}(b, s) \end{aligned}$$

is a homeomorphism, where $\Gamma^{-1} : \overline{\mathcal{D}} \times \mathbb{S}^1 \rightarrow e_Q^{-1}(\overline{\mathcal{D}})$ is also a homeomorphism. For simplicity, define

$$\mathcal{X} := (-\infty, 0] \times \partial\overline{\mathcal{D}} \times \mathbb{S}^1 \sqcup \overline{\mathcal{D}} \times \mathbb{S}^1$$

with the disjoint union topology [76, p. 64], where \sqcup is the disjoint union. We define a new topological space \mathcal{X}/\sim , where \sim is the equivalence relation that identifies $(0, b, s)$ from $\{0\} \times \partial\overline{\mathcal{D}} \times \mathbb{S}^1$ with (b, s) from $\overline{\mathcal{D}} \times \mathbb{S}^1$. Therefore, the natural projection

$$\text{pr} : \mathcal{X} \rightarrow \mathcal{X}/\sim$$

is a quotient map [101, Chapter 2, Section 22]. Note that $e_Q^{-1}(\overline{\mathcal{D}})$ and \mathcal{W}° are subspaces of $e_Q^{-1}(\overline{\mathcal{D}}) \cup \mathcal{W}^\circ$. Therefore, the map

$$\begin{aligned} Y \sqcup \Gamma^{-1} : \mathcal{X} &\rightarrow \mathcal{W}^\circ \cup e_Q^{-1}(\overline{\mathcal{D}}) \\ (-\infty, 0] \times \partial\overline{\mathcal{D}} \times \mathbb{S}^1 &\ni (t, b, s) \mapsto Y(t, b, s) \\ \overline{\mathcal{D}} \times \mathbb{S}^1 &\ni (b, s) \mapsto \Gamma^{-1}(b, s) \end{aligned}$$

$$\begin{array}{ccc}
 \mathcal{X} & & \\
 \downarrow \text{pr} & \searrow Y \sqcup \Gamma^{-1} & \\
 \mathcal{X}/\sim & \xrightarrow[\Lambda]{} & \mathcal{W}^\circ \cup e_Q^{-1}(\bar{\mathcal{D}})
 \end{array}$$

Figure 6.4: Since pr is a quotient map and $Y \sqcup \Gamma^{-1}$ is continuous, Λ is continuous.

is continuous. By construction, there exists the unique map

$$\Lambda : \mathcal{X}/\sim \rightarrow \mathcal{W}^\circ \cup e_Q^{-1}(\bar{\mathcal{D}})$$

such that $\Lambda \circ \text{pr} = Y \sqcup \Gamma^{-1}$ (see Fig. 6.4). Due to the property of a quotient map [101, Theorem 22.2], the map Λ is continuous (see Fig. 6.4). One can check that Λ is a bijection. In addition, Λ is an open map. This is justified as follows. First, both $(-\infty, 0] \times \partial\bar{\mathcal{D}} \times \mathbb{S}^1$ and $\bar{\mathcal{D}} \times \mathbb{S}^1$ are topological manifolds with boundaries $\{0\} \times \partial\bar{\mathcal{D}} \times \mathbb{S}^1$ and $\partial\bar{\mathcal{D}} \times \mathbb{S}^1$ respectively. Note that the boundaries are homeomorphic to each other in a natural way which is given by the equivalent relation \sim ; i.e., $(0, b, s) \mapsto (b, s)$ is a natural homeomorphism. Then it follows from applying the technique of attaching manifolds together along their boundaries [76, Theorem 3.79] that \mathcal{X}/\sim is an n -manifold. Second, $\mathcal{W}^\circ \cup e_Q^{-1}(\bar{\mathcal{D}}) = \Psi^{(-\infty, +\infty)}(\mathcal{S}) \cup e_Q^{-1}(\mathcal{D})$, which is an open subset in \mathcal{M} , and hence it is also an n -manifold. Thus, Λ is a continuous injection between two (boundaryless) n -manifolds, and hence it is open [100, Theorem 36.5]. Therefore, Λ is a homeomorphism, and it remains to show that \mathcal{X}/\sim is homeomorphic to $\mathbb{R}^{n-1} \times \mathbb{S}^1$.

Note that $\mathbb{R}^{n-1} = \bar{\mathcal{D}} \cup (\mathbb{R}^{n-1} \setminus \mathcal{D})$. Define

$$\begin{aligned}
 f : (-\infty, 0] \times \partial\bar{\mathcal{D}} &\rightarrow \mathbb{R}^{n-1} \setminus \mathcal{D} \\
 (t, q) &\mapsto q - tq.
 \end{aligned}$$

It is obvious that f is a homeomorphism. Applying the same argument above, one can show that²

$$f \times \text{id}_{\mathbb{S}^1} \sqcup \text{id}_{\bar{\mathcal{D}}} \times \text{id}_{\mathbb{S}^1} : \mathcal{X} \rightarrow \mathbb{R}^{n-1} \times \mathbb{S}^1,$$

where id is the identity function, induces a homeomorphism Λ' between \mathcal{X}/\sim and $\mathbb{R}^{n-1} \times \mathbb{S}^1$ (see Fig. 6.5). \square

In the context of the vector-field guided path-following problem, we could interpret Proposition 6.14 more intuitively and leads to the following theorem.

² We explain the notation “ \times ” connecting two functions. Given any functions $f : X \rightarrow X'$ and $g : Y \rightarrow Y'$, the map $f \times g : X \times Y \rightarrow X' \times Y'$ is defined by $(f \times g)(x, y) = (f(x), g(y))$ for $x \in X$ and $y \in Y$.

$$\begin{array}{ccc}
 \mathcal{X} & & f \times \text{id}_{S^1} \sqcup \text{id}_{\overline{\mathcal{D}}} \times \text{id}_{S^1} \\
 \text{pr} \downarrow & \searrow & \\
 \mathcal{X}/\sim & \xrightarrow[\Lambda']{} & \mathbb{R}^{n-1} \times S^1
 \end{array}$$

Figure 6.5: Since pr is a quotient map and $f \times \text{id}_{S^1} \sqcup \text{id}_{\overline{\mathcal{D}}} \times \text{id}_{S^1}$ is continuous, Λ' is continuous.

Theorem 6.15. *If the desired path \mathcal{P} is homeomorphic to the unit circle S^1 , then the set of initial conditions such that trajectories of (6.4) eventually converge to the desired path \mathcal{P} is homeomorphic to $\mathbb{R}^{n-1} \times S^1$.*

Proof. One easily observes that the set $e_{\mathcal{Q}}^{-1}(\overline{\mathcal{D}}) \cup \mathcal{W}^\circ$ consists of initial conditions such that trajectories of (6.4) eventually converge to the desired path \mathcal{P} . Then the result follows immediately from Proposition 6.14. \square

Remark 6.16. In Theorem 3.4 of [152], it is claimed that the DOA of a compact or non-compact *uniformly asymptotically stable*³ submanifold \mathcal{A} of a finite-dimensional manifold \mathcal{M} is diffeomorphic to an open tubular neighborhood of \mathcal{A} . Therefore, Theorem 6.15 is consistent with this claim. However, the proof of [152, Theorem 3.4] in [152] is very brief, only indicating the method of the proof without giving much detail, while we provide detailed and thorough proofs of Theorem 6.15, along with several lemmas and propositions to offer more geometric intuition. Moreover, the strong claim of [152, Theorem 3.4] without imposing the compactness requirement on \mathcal{A} might not be accurate, as shown in Counterexample 1 below. As future work, we will develop a complete and detailed proof of [152, Theorem 3.4] with an additional assumption that \mathcal{A} is compact, and indicate why the theorem would fail if \mathcal{A} was not compact [83]. \triangleleft

Counterexample 1. Consider the manifold

$$\mathcal{M} = \mathbb{R}^2 \setminus \{(-1, 0), (1, 0)\}$$

with the subspace topology inherited from \mathbb{R}^2 . Define

$$\mathcal{A} := (-1, 1) \times \{0\} \subseteq \mathcal{M}$$

³ Let $\xi(t)$ denote a trajectory of an autonomous system. In [152], a closed set \mathcal{A} is said to be *uniformly asymptotically stable* if there exists $r > 0$ such that for every $\epsilon > 0$, there exists a time instant $T(\epsilon)$ such that $\text{dist}(\xi(0), \mathcal{A}) < r \implies \text{dist}(\xi(t), \mathcal{A}) < \epsilon$ for $t > T(\epsilon)$. Uniform asymptotic stability is stronger than *asymptotic stability*, but if \mathcal{A} is compact, then these two notions are equivalent. Since we focus on the compact case in this chapter, we do not bother to explicitly compare these two notions.

as a subspace of \mathcal{M} . One can verify that \mathcal{A} is closed in \mathcal{M} and is a submanifold of \mathcal{M} . Note that \mathcal{A} is *not* compact⁴, because the open cover $\mathcal{U}_\epsilon := \{(-1 + \epsilon, 1 - \epsilon) \times (-\epsilon, \epsilon) : \forall \epsilon > 0\}$ of \mathcal{A} does not have a finite subcover. Define a potential function $f : \mathcal{M} \rightarrow \mathbb{R}_{\geq 0}$ as below:

$$f(p) = (\text{dist}(p, \mathcal{A}))^2$$

$$= \begin{cases} y^2, & \text{if } -1 < x < 1 \\ (x-1)^2 + y^2, & \text{if } x > 1 \text{ or } x = 1, y \neq 0 \\ (x+1)^2 + y^2, & \text{if } x < -1 \text{ or } x = -1, y \neq 0, \end{cases}$$

where $p = (x, y)$ is a point in \mathcal{M} . One can verify that $f(\cdot)$ is continuously differentiable. Indeed, the partial derivatives of f with respect to x and y are:

$$\frac{\partial f}{\partial x} = \begin{cases} 0, & \text{if } -1 < x < -1 \text{ or } x = \pm 1, y \neq 0 \\ 2(x-1), & \text{if } x > 1 \\ 2(x+1), & \text{if } x < -1 \end{cases} \quad (6.18)$$

and $\frac{\partial f}{\partial y} = 2y$, respectively. Therefore, we can define the gradient system

$$\dot{p} = -\nabla f(p), \quad (6.19)$$

and it can be easily verified that \mathcal{A} is globally uniformly asymptotically stable with respect to (6.19) by using the radially unbounded Lyapunov function $V(p) = f^2(p)$. Namely, the DOA of \mathcal{A} is the manifold \mathcal{M} , which is *not* contractible. However, according to [152, Theorem 3.4], the DOA of \mathcal{A} is homeomorphic to its tubular neighborhood, but its tubular neighborhood is homeomorphic to $\mathcal{A} \times \mathbb{R}$, which is contractible. Therefore, this counterexample shows that the claim of [152, Theorem 3.4] without requiring the compactness of \mathcal{A} is not accurate. Furthermore, in this case, the DOA of \mathcal{A} is not even homotopy equivalent to itself since the fundamental group of the DOA; i.e., \mathcal{M} , is non-zero, but that of \mathcal{A} is 0 as it is contractible. \triangle

6.4 CONCLUSIONS

It has been shown in Chapter 5 that the DOA of a desired path \mathcal{P} , which is a compact asymptotically stable one-dimensional embedded submanifold under an autonomous system, is homotopic equivalent to the unit circle S^1 . However, homotopic equivalent objects may be geometrically and set-theoretically distinctive, so this characterization of the DOA sometimes may not be satisfactory. In this

⁴ A topological space \mathcal{X} is *compact* if every open cover of \mathcal{X} has a finite subcover.

chapter, we strengthen this result and show that the DOA is homeomorphic to $\mathbb{R}^{n-1} \times S^1$, where n is the dimension of the ambient manifold \mathcal{M} . We also provide an example showing that if the considered submanifold was not compact (see Remark 6.16), then its DOA is *not* even homotopy equivalent to the submanifold, not to mention Theorem 6.15.

7

REFINED DICHOTOMY CONVERGENCE IN VECTOR-FIELD GUIDED PATH-FOLLOWING ON \mathbb{R}^n

Under some broad conditions, a dichotomy convergence property in the vector-field guided path-following problem has been proved in previous chapters: the integral curves of a guiding vector field converge to either the desired path or the singular set, where the vector field becomes zero. In this chapter, we show that under the condition of real analyticity of the level functions (i.e., functions whose zero-level sets define the desired path), the convergence to the singular set (assuming it is compact) implies the convergence to a single point of the set, dependent on the initial condition. Thus, limit cycles are precluded. Numerical simulations support the theoretical results.

This chapter is based on

- W. Yao, B. Lin, B. D. O. Anderson, and M. Cao, "Refining dichotomy convergence in vector-field guided path following control," in *European Control Conference (ECC)*, 2021.

7.1 INTRODUCTION

An issue arising with the dichotomy convergence property associated with vector-field guided path-following algorithms is that generally, convergence (e.g., with respect to a metric) to a closed invariant set does not automatically imply the convergence to a single point of the set. It is known that this implication is true under some conditions for gradient flows [3], [4], while it is not yet completely clear for non-gradient flows. In particular, the guiding vector fields for path-following designed in Chapters 4, 5, 9 and 10, are not gradients of any potential functions, but as shown in [63], Chapter 4 (Proposition 4.8, Proposition 4.14) and Chapter 5 (Theorem 5.13), under some conditions, the integral curves of the vector fields (i.e., the trajectories of the autonomous differential equation where the right-hand side is the guiding vector field) have the dichotomy convergence property: they either converge to the desired path or the singular set, where the vector field becomes zero. As the desired path is a limit cycle (when the desired path is homeomorphic to the unit circle), it is obvious that trajectories do not converge to a single point in the desired path; however, it is to this point unresolved whether trajectories converging to the singular set will converge to a single point in the singular set (where, in general, the point depends on the initial condition).

In this chapter, we discuss the issue pertinent to the relationship between convergence of trajectories of a non-gradient system to a set and convergence to a single point of the set. Under the condition of real analyticity of the level functions, we obtain a refined version of the dichotomy convergence property: the convergence to the singular set entails the convergence to a single point of the set. This result not only is relevant to the specialized path-following problem, but also extends the results in [3], [4] (using proof techniques suggested by those works and appealing to the Łojasiewicz inequality [84]) to some non-gradient flows.

The rest of the chapter is organized as follows. Section 7.2 revisits (or particularizes) guiding vector fields defined on \mathbb{R}^n , for $n \geq 2$, and formulates the problem. Then the main results are presented in Section 7.3. Simulation results are reported in Section 7.4. Finally, Section 7.5 concludes the chapter.

7.2 BACKGROUND AND PROBLEM FORMULATION

7.2.1 Guiding vector fields on \mathbb{R}^n

As discussed before, in the vector-field guided path-following problem, the desired path \mathcal{P} is the intersection of the zero-level sets of sufficiently smooth functions, called *level functions*:

$$\mathcal{P} = \{\xi \in \mathbb{R}^n : \phi_i(\xi) = 0, i = 1, \dots, n - 1\}, \quad (7.1)$$

where $\phi_i : \mathbb{R}^n \rightarrow \mathbb{R}$ are twice continuously differentiable functions. The desired path in (7.1) is naturally assumed to be non-empty and one-dimensional. More assumptions are imposed in Section 7.2.2.

Recall that the guiding vector field $\chi : \mathbb{R}^2 \rightarrow \mathbb{R}^2$ for path following in the 2D case \mathbb{R}^2 is [63]:

$$\chi(\xi) = E\nabla\phi(\xi) - k\phi(\xi)\nabla\phi(\xi), \quad (7.2)$$

where $\nabla\phi$ is the gradient vector of the function ϕ , $E = \begin{bmatrix} 0 & -1 \\ 1 & 0 \end{bmatrix}$ is a 90° rotation matrix, and $k > 0$ is a constant. In higher dimensions, the vector field $\chi : \mathbb{R}^n \rightarrow \mathbb{R}^n$ for $n \geq 3$ is (see Chapter 9 for more detail):

$$\begin{aligned} \chi(\xi) &= \perp_\phi(\xi) - \sum_{i=1}^{n-1} k_i \phi_i(\xi) \nabla \phi_i(\xi) \\ &= \perp_\phi(\xi) - N(\xi) K e(\xi), \end{aligned} \quad (7.3)$$

where \perp_ϕ is the wedge product of all the gradient vectors¹ $\nabla\phi_i$ and $k_i > 0$ are constants for $i = 1, \dots, n - 1$, $N(\xi) = [\nabla\phi_1(\xi) \ \dots \ \nabla\phi_{n-1}(\xi)] \in \mathbb{R}^{n \times (n-1)}$, $K = \text{diag}\{k_1, \dots, k_{n-1}\}$ and

$$e(\xi) = (\phi_1(\xi), \dots, \phi_{n-1}(\xi)) \in \mathbb{R}^{n-1}. \quad (7.4)$$

This vector field has been treated in Chapter 4 (for $n = 3$), Chapter 5 (for Riemannian manifolds) and will be elaborated in Chapter 9 (for $n \geq 3$). Note that the vector fields in (7.2) and (7.3) are *not* gradients of any potential function. The integral curves of the vector fields; i.e., the trajectories of the autonomous system described by the differential equation $\dot{\xi}(t) = \chi(\xi(t))$ for $\xi \in \mathbb{R}^n$, converge to the desired path under some conditions, and the desired path \mathcal{P} turns out to be a limit cycle of the aforementioned autonomous system if the desired path is

¹ The sign of the wedge product depends on the order of the gradient vectors. However, this does not affect the convergence result.

homeomorphic to the unit circle. However, trajectories may also converge to the singular set \mathcal{C} defined below:

$$\mathcal{C} = \{\xi \in \mathbb{R}^n : \chi(\xi) = \mathbf{0}\}, \quad (7.5)$$

and its elements are called *singular points*. As with Chapter 4, we define the following set \mathcal{L} :

$$\mathcal{L} = \{\xi \in \mathbb{R}^n : N(\xi)Ke(\xi) = 0\}. \quad (7.6)$$

7.2.2 Assumptions

As with previous chapters, we impose the following standing assumptions.

Assumption 7.1. There are no singular points on the desired path. More precisely, \mathcal{C} is empty or otherwise there holds $\text{dist}(\mathcal{C}, \mathcal{P}) > 0$.

Assumption 7.2. For any given constant $\kappa > 0$, there holds $\inf\{||e(\xi)|| : \xi \in \mathbb{R}^n, \text{dist}(\xi, \mathcal{P}) \geq \kappa\} > 0$, where $e(\cdot)$ is defined in (7.4).

Assumption 7.3. For any given constant $\kappa > 0$, we have $\inf\{\|N(\xi)Ke(\xi)\| : \text{dist}(\xi, \mathcal{L}) \geq \kappa\} > 0$.

It has been known in the literature [63] and in Chapters 4 and 5 that the desired path is an asymptotically stable limit cycle when it is homeomorphic to the unit circle, and trajectories “spiral” and converge to the desired path but do not converge to any single point on the desired path. Nevertheless, the answer to the following question is not yet clear. When the trajectories converge to the singular set rather than the desired path, will they converge to a singular point, or can they also “spiral” towards the singular set not converging to any single point? *We only consider guiding vector fields on Euclidean spaces \mathbb{R}^n for $n \geq 2$ in this chapter.*

7.3 REFINED DICHOTOMY CONVERGENCE

In this section, we show that if a trajectory of $\dot{\xi}(t) = \chi(\xi(t))$ converges to the singular set \mathcal{C} , then under some conditions, it converges to a point in \mathcal{C} . This result depends on a property of real analytic functions, which is stated in the following lemma.

Lemma 7.4 (Łojasiewicz gradient inequality [84]). *Let $V : \mathbb{R}^n \rightarrow \mathbb{R}$ be a real analytic function on a neighborhood of $\xi^* \in \mathbb{R}^n$. Then there are constants $c > 0$ and $\mu \in [0, 1)$ such that*

$$\|\nabla V(\xi)\| \geq c|V(\xi) - V(\xi^*)|^\mu \quad (7.7)$$

in some neighborhood \mathcal{U} of ξ^ .*

Inspired by [3], [4], we have the following result.

Theorem 7.5 (Refined dichotomy convergence for \mathbb{R}^2). *Let $\chi : \mathbb{R}^2 \rightarrow \mathbb{R}^2$ be the vector field defined in (7.2), and suppose ϕ in (7.1) is real analytic and the set \mathcal{C} in (7.5) is bounded (hence compact). If a trajectory of $\dot{\xi}(t) = \chi(\xi(t))$ converges metrically to the set \mathcal{C} , then the trajectory converges to a point in \mathcal{C} .*

Proof. Given that a trajectory $\xi(t)$ converges to the set \mathcal{C} , which is bounded, the trajectory $\xi(t)$ has a limit point $\xi^* \in \mathcal{C}$. It remains to show that $\lim_{t \rightarrow \infty} \xi(t) = \xi^*$.

Define $V : \mathbb{R}^2 \rightarrow \mathbb{R}$ by $V(\xi) := \phi^2(\xi)$, where the function ϕ is defined in (7.1), then V is also real analytic. Taking the time derivative of V along the trajectory $\xi(t)$ and noting that $\nabla V = 2\phi\nabla\phi$, we have (arguments of functions are omitted for simplicity)

$$\begin{aligned}\frac{d}{dt}V &= \nabla V^\top \dot{\xi} = \nabla V^\top (E\nabla\phi - k\phi\nabla\phi) \\ &= (2\phi\nabla\phi)^\top E\nabla\phi - \frac{1}{2}k\nabla V^\top \nabla V \\ &= -\frac{1}{2}k\|\nabla V\|^2 \leq 0.\end{aligned}\tag{7.8}$$

Therefore, $V(\xi(t))$ is non-increasing along the trajectory. Since the trajectory converges to \mathcal{C} , we can choose a positive constant ϵ satisfying $\epsilon < \text{dist}(\mathcal{P}, \mathcal{C})$, and then there exists $T > 0$, such that $\text{dist}(\xi(t), \mathcal{C}) < \epsilon$ for all $t \geq T$. Let $\mathcal{S} := \{p \in \mathbb{R}^2 : \text{dist}(p, \mathcal{C}) \leq \epsilon\}$. Note that \mathcal{S} is compact (since \mathcal{C} is compact) and $\text{dist}(\mathcal{P}, \mathcal{S}) > 0$ (since $\epsilon < \text{dist}(\mathcal{P}, \mathcal{C})$). Let $m := \min_{p \in \mathcal{S}} |\phi(p)| > 0$. Therefore, for all $t \geq T$, we have

$$\begin{aligned}\|\dot{\xi}\| &= \|E\nabla\phi - k\phi\nabla\phi\| \\ &\leq \|E\nabla\phi\| + \frac{k}{2}\|\nabla V\| \\ &= \left(\frac{1}{2|\phi|} + \frac{k}{2} \right) \|\nabla V\| \\ &\leq \underbrace{\left(\frac{1}{2m} + \frac{k}{2} \right)}_{k'} \|\nabla V\|.\end{aligned}$$

This implies that, for all $t \geq T$,

$$\|\nabla V\| \geq \frac{1}{k'} \|\dot{\xi}\|. \tag{7.9}$$

Substituting (7.9) into (7.8) and using Lemma 7.4, we have

$$\begin{aligned}\frac{d}{dt}V &= -\frac{1}{2}k\|\nabla V\|^2 \\ &\leq -\frac{k}{2k'}\|\nabla V\|\|\dot{\xi}\| \\ &\leq -\frac{ck}{2k'}|V(\xi(t)) - V(\xi^*)|^\mu\|\dot{\xi}\|\end{aligned}\tag{7.10}$$

in an open neighborhood $\mathcal{U} \subseteq \mathcal{S}$ of ξ^* for some $\mu \in [0, 1)$ and $t \geq T$. Since $V(\xi(t)) > V(\xi^*) > 0$, it follows from (7.10) that

$$\begin{aligned}\frac{2k'}{ck}(V(\xi(t)) - V(\xi^*))^{-\mu}\frac{d}{dt}V &\leq -\|\dot{\xi}\| \implies \\ c'\frac{d}{dt}(V(\xi(t)) - V(\xi^*))^{1-\mu} &\leq -\|\dot{\xi}\|,\end{aligned}\tag{7.11}$$

where $c' = 2k'/((1-\mu)ck) > 0$. If t_1 and t_2 with $T \leq t_1 < t_2$ are such that $\xi(t) \in \mathcal{U}$ for all $t \in (t_1, t_2)$, then by integration of (7.11), we have

$$\begin{aligned}L_{12} &:= \int_{t_1}^{t_2} \|\dot{\xi}(t)\| dt \\ &\leq -c' \int_{t_1}^{t_2} \frac{d}{dt}(V(\xi(t)) - V(\xi^*))^{1-\mu} dt \\ &= c' \left[(V(\xi(t_1)) - V(\xi^*))^{1-\mu} - (V(\xi(t_2)) - V(\xi^*))^{1-\mu} \right] \\ &\leq c'(V(\xi(t_1)) - V(\xi^*))^{1-\mu}.\end{aligned}\tag{7.12}$$

Choose $r > 0$ such that $\mathcal{B}_r(\xi^*) \subseteq \mathcal{U}$, where $\mathcal{B}_r(\xi^*) := \{\xi \in \mathbb{R}^2 : \|\xi - \xi^*\| < r\}$. Since ξ^* is a limit point and $V(\cdot)$ is continuous, we can choose $t_1 \geq T$ sufficiently large such that $\|\xi(t_1) - \xi^*\| < r/2$ and $c'(V(\xi(t_1)) - V(\xi^*))^{1-\mu} < r/2$ in (7.12). Note that $\xi(t_1) \in \mathcal{B}_r(\xi^*)$. The trajectory $\xi(t)$ remains in $\mathcal{B}_r(\xi^*)$ after t_1 .² This shows that the trajectory $\xi(t)$ eventually enters and remains in $\mathcal{B}_r(\xi^*)$. Since r can be chosen arbitrarily small, convergence of the trajectory $\xi(t)$ to ξ^* is thus proved. \square

The same conclusion applies for the n -dimensional vector field in (7.3), but we additionally need the following lemma.

Lemma 7.6. *It holds that $\det(N^\top N) = \|\perp_\phi\|^2$, where N and \perp_ϕ are defined in (7.3).*

Proof. If $\nabla\phi_1, \dots, \nabla\phi_{n-1}$ are linearly dependent, then we have $\det(N^\top N) = \|\perp_\phi\|^2 = 0$. Now suppose $\nabla\phi_1, \dots, \nabla\phi_{n-1}$ are linearly independent. In this case,

² Suppose not, then there exists the smallest time instant $t_2 > t_1$ such that $\|\xi(t_2) - \xi^*\| = r$ and $\xi(t) \in \mathcal{U}$ for any $t \in (t_1, t_2)$. Therefore, we have $\|\xi(t_2) - \xi^*\| \leq \|\xi(t_2) - \xi(t_1)\| + \|\xi(t_1) - \xi^*\| < L_{12} + r/2 < r$, a contradiction, where L_{12} is shown in (7.12).

it follows that $\|\perp_\phi\| \neq 0$. So we can define the normalized vector $v = \perp_\phi / \|\perp_\phi\|$. Since \perp_ϕ is orthogonal to all the gradients $\nabla\phi_i, i = 1, \dots, n - 1$ (see Lemma 5.1 in Chapter 5 for more detail), we have

$$\det(N^\top N) = \det \left(\begin{bmatrix} v^\top \\ N^\top \end{bmatrix} \begin{bmatrix} v & N \end{bmatrix} \right) = \det \left(\begin{bmatrix} v^\top \\ N^\top \end{bmatrix} \right)^2.$$

According to the definition of \perp_ϕ , we have $\|\perp_\phi\| = \det \left(\begin{bmatrix} v^\top \\ N^\top \end{bmatrix} \right)$. Then it follows that $\det(N^\top N) = \|\perp_\phi\|^2$. \square

Theorem 7.7 (Refined dichotomy convergence for \mathbb{R}^n). *Let $\chi : \mathbb{R}^n \rightarrow \mathbb{R}^n$ be the vector field defined in (7.3), and suppose ϕ in (7.1) is real analytic and the set \mathcal{C} in (7.5) is bounded (hence compact). If a trajectory of $\dot{\xi}(t) = \chi(\xi(t))$ converges metrically to the set \mathcal{C} , then the trajectory converges to a point in \mathcal{C} .*

Proof. The proof is similar to that in Theorem 7.5 except for the following differences. Define $V : \mathbb{R}^n \rightarrow \mathbb{R}$ by $V(\xi) := 1/2 e^\top K e$, where $e = (\phi_1, \dots, \phi_{n-1})^\top$; then V is also real analytic. Note that

$$\nabla V(\xi) = \sum_{i=1}^{n-1} k_i \phi_i(\xi) \nabla \phi_i(\xi) = N(\xi) K e(\xi).$$

Taking the time derivative of V along the trajectory $\xi(t)$, we have

$$\begin{aligned} \frac{d}{dt} V(\xi) &= \nabla V(\xi)^\top \dot{\xi} \\ &= \nabla V(\xi)^\top (\perp_\phi(\xi) - N(\xi) K e(\xi)) \\ &= (N(\xi) K e(\xi))^\top \perp_\phi(\xi) - \|\nabla V(\xi)\|^2 \\ &= -\|\nabla V(\xi)\|^2 \leq 0, \end{aligned} \tag{7.13}$$

where we use the fact that $(N(\xi) K e(\xi))^\top \perp_\phi(\xi) = 0$ due to orthogonality. Therefore, $V(\xi(t))$ is non-increasing along the trajectory. Since the trajectory converges to \mathcal{C} , we can choose a positive constant ϵ satisfying $\epsilon < \text{dist}(\mathcal{P}, \mathcal{C})$, and then there exists $T > 0$, such that $\text{dist}(\xi(t), \mathcal{C}) < \epsilon$ for all $t \geq T$. Let $\mathcal{S} := \{p \in \mathbb{R}^n : \text{dist}(p, \mathcal{C}) \leq \epsilon\}$. Note that \mathcal{S} is compact and $\text{dist}(\mathcal{P}, \mathcal{S}) > 0$. For $t \geq T$, the trajectory $\xi(t)$ will stay in $\mathcal{S} \setminus \mathcal{C}$. Let the eigenvalues of the matrix $N(\xi)^\top N(\xi)$ evaluated at $\xi \in \mathcal{S} \setminus \mathcal{C}$ be denoted by $0 \leq \lambda_1(\xi) \leq \dots \leq \lambda_{n-1}(\xi)$. Since the gradient vectors $\nabla \phi_i(\xi), i = 1, \dots, n - 1$, are linearly independent for $\xi \in \mathcal{S} \setminus \mathcal{C}$, the eigenvalues are all positive $\lambda_i(\xi) > 0$ for $\xi \in \mathcal{S} \setminus \mathcal{C}$, and by Lemma

7.6, we have $\det(N(\xi)^\top N(\xi)) = \|\perp_\phi(\xi)\|^2 = \lambda_1(\xi) \cdots \lambda_{n-1}(\xi) > 0$ for $\xi \in \mathcal{S} \setminus \mathcal{C}$. We also have

$$\begin{aligned}\lambda_{n-1}(\xi) &= \max_{\|v\|=1} v^\top N(\xi)^\top N(\xi)v \leq \\ &\quad (\|\nabla\phi_1(\xi)\| + \cdots + \|\nabla\phi_{n-1}(\xi)\|)^2 \leq (n-1)^2\beta^2,\end{aligned}\quad (7.14)$$

where $\beta := \max_{i=1,\dots,n-1} \max_{p \in \mathcal{S}} \|\nabla\phi_i(p)\| > 0$. In addition,

$$\begin{aligned}\|N(\xi)Ke(\xi)\|^2 &= (Ke(\xi))^\top (N(\xi)^\top N(\xi))(Ke(\xi)) \geq \\ &\quad \lambda_1(\xi)\|Ke(\xi)\|^2 \geq \lambda_1(\xi)k_{\min}^2\|e(\xi)\|^2 \geq \lambda_1(\xi)k_{\min}^2\alpha,\end{aligned}\quad (7.15)$$

where $k_{\min} := \min\{k_1, \dots, k_{n-1}\}$ and $\alpha := \min_{p \in \mathcal{S}} \|e(p)\|^2 > 0$ (due to $\text{dist}(\mathcal{P}, \mathcal{S}) > 0$ and Assumption 7.2). Therefore,

$$\lambda_1(\xi) \leq \frac{1}{\alpha k_{\min}^2} \|N(\xi)Ke(\xi)\|^2. \quad (7.16)$$

Furthermore, we have

$$\|\perp_\phi(\xi)\|^2 \leq \lambda_1(\xi)\lambda_{n-1}^{n-2}(\xi) \leq \frac{((n-1)\beta)^{2(n-2)}}{\alpha k_{\min}^2} \|N(\xi)Ke(\xi)\|^2,$$

which implies

$$\|\perp_\phi(\xi)\| \leq a\|N(\xi)Ke(\xi)\|, \quad (7.17)$$

where $a = ((n-1)\beta)^{n-2}/(k_{\min}\sqrt{\alpha}) > 0$. Now, we have

$$\begin{aligned}\|\dot{\xi}\| &= \|\perp_\phi(\xi) - N(\xi)Ke(\xi)\| \\ &\leq \|\perp_\phi(\xi)\| + \|N(\xi)Ke(\xi)\| \\ &\stackrel{(7.17)}{\leq} (a+1)\|N(\xi)Ke(\xi)\| = (a+1)\|\nabla V(\xi)\|.\end{aligned}$$

The remaining parts of the proof are the same as those of Theorem 7.5. \square

Remark 7.8. It is shown in [3], [4] that single limit point convergence of a bounded solution of a gradient flow cannot be proved in general for smooth but *non-real-analytic* cost functions, whereas the real analyticity of the cost function can guarantee the single limit point convergence. Note that these results *cannot* be directly applied here since the vector fields in (7.2) and (7.3) are not gradients of any cost functions. Nevertheless, we reach the same conclusions under the conditions regarding the real-analyticity of ϕ_i . Therefore, Theorem 7.5 and Theorem 7.7 can be regarded as extensions of the results in [3], [4]. \triangleleft

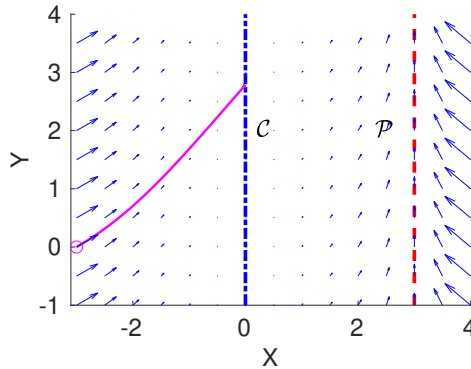


Figure 7.1: First simulation results. The real analytic ϕ function is $\phi(x, y) = x^3/3 - 9$. The dashed-dot blue and dashed red lines are the singular set \mathcal{C} and the desired path \mathcal{P} respectively. The blue arrows represent the vector field. The solid magenta curve is the trajectory starting from $(-3, 0)$. Due to the analyticity of ϕ , the trajectory converges to a point in \mathcal{C} .

7.4 SIMULATIONS

In this section, we show two simulation examples where the functions ϕ are real analytic and non-real-analytic respectively to verify Theorem 7.5.

In the first example, we choose a real analytic ϕ function: $\phi(x, y) = x^3/3 - 9$, hence $\nabla\phi = (x^2, 0)^\top$. Therefore, \mathcal{C} is the y-axis, which is unbounded, and \mathcal{P} is the vertical line $x = 3$, which is a one-dimensional embedded manifold. The vector field is $\chi(x, y) = x^2(-k\phi(x, y), 1)^\top$, and the simulation results are shown in Fig. 7.1, where the control gain is $k = 0.1$.

In the second example, we choose a non-real-analytic ϕ function, and illustrate the case where a trajectory converges to the singular set \mathcal{C} but *not* to a single point in \mathcal{C} . First, consider the following smooth bump function:

$$b(x) = \begin{cases} \exp(1/x) & \text{if } x < 0 \\ 0 & \text{if } x \geq 0 \end{cases}, \quad (7.18)$$

which is smooth but non-real-analytic. Therefore, we can construct a non-real-analytic function $\phi(x, y) = b(x)(x^3/3 - 9)$. The gradient and the vector field are:

$$\nabla\phi = \begin{cases} \left(x^2 e^{1/x} - \frac{e^{1/x}(x^3/3 - 9)}{x^2}, 0\right)^\top & \text{if } x < 0 \\ (0, 0)^\top & \text{if } x \geq 0 \end{cases},$$

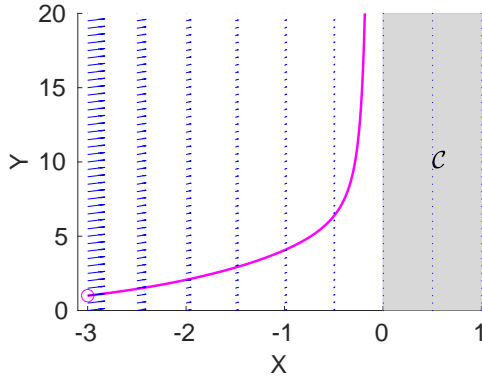


Figure 7.2: Second simulation results. The non-real-analytic ϕ function is $\phi(x, y) = b(x)(x^3/3 - 9)$, where $b(x)$ is in (7.18). The singular set \mathcal{C} is the shaded area: the right-half plane including the y -axis. The blue arrows represent the vector field. The solid magenta curve is the trajectory starting from $(-3, 1)$. In contrast to Fig. 7.1, although the trajectory converges to \mathcal{C} , it does *not* converge to any single point in \mathcal{C} .

$$\chi = \begin{cases} \left(-k e^{1/x} (x^3/3 - 9) \sigma_1, \sigma_1 \right)^\top & \text{if } x < 0 \\ (0, 0)^\top & \text{if } x \geq 0 \end{cases},$$

where $\sigma_1 = x^2 e^{1/x} - e^{1/x} (x^3/3 - 9)/x^2$. The singular set is the right-half plane $x \geq 0$. In this example, a trajectory converges to \mathcal{C} but not to a single point in \mathcal{C} , as seen in Fig. 7.2, where the control gain is $k = 1$.

7.5 CONCLUSIONS

We give a refined dichotomy convergence result for the path-following problem on \mathbb{R}^n for $n \geq 2$. In particular, we show that real analyticity of the level function leads to the refined conclusion that converging of a trajectory to a singular set implies converging to a point in this set. This is in contrast to the convergence to the desired path, where a trajectory spirals towards the set without converging to any single point of the set. Although the guiding vector field is *not* a gradient of any potential function, this result is consistent with [3], [4] where only gradient flows are considered.

Part II

APPLICATIONS WITH FORMAL GUARANTEES

8

GUIDING VECTOR FIELDS FOR FOLLOWING OCCLUDED PATHS

Accurately following a geometric desired path in a two-dimensional space is a fundamental task for many engineering systems, in particular mobile robots. When the desired path is occluded by obstacles, it is necessary and crucial to temporarily deviate from the path for obstacle/collision avoidance. In this chapter, we develop a composite guiding vector field via the use of smooth bump functions, and provide theoretical guarantees that the integral curves of the vector field can follow an arbitrary sufficiently smooth desired path and avoid collision with static and moving obstacles of arbitrary shapes. These two behaviors are *reactive* since path (re)-planning and symbolic map construction are not involved. To deal with the common deadlock problem, we introduce a switching vector field, and the Zeno behavior is excluded. We also elaborate on the extensions of our approach to higher-dimensional spaces and nonholonomic robot models. Simulations are conducted to support the theoretical results.

This chapter is based on

- W. Yao, B. Lin, B. D. O. Anderson, and M. Cao, "Guiding vector fields for following occluded paths," *IEEE Transactions on Automatic Control (TAC)*, 2021, *Under review*.
- W. Yao, B. Lin, and M. Cao, "Integrated path following and collision avoidance using a composite vector field," in *2019 IEEE 58th Conference on Decision and Control (CDC)*, IEEE, 2019, pp. 250–255.

8.1 INTRODUCTION

When the desired path is *occluded* by obstacles, a robot needs to *deviate* from the desired path to avoid colliding with the obstacles, and then *return* to the desired path to continue the path-following task. We clarify the meanings of “occlusion by obstacles” and “deviation”. Usually, path-following algorithms are designed based on a predefined desired path taking no account of obstacles. Then notice is taken of (initially) unforeseen obstacles, with a view to designing a modification to the original algorithms; the modified algorithm then takes trajectories around the obstacle and return to the original desired path having passed the obstacle. This is normally achieved one obstacle at a time, and some extension to moving obstacles is possible [73], [128], [139], [151], [173]. Without considering the path-following requirement, there exist many obstacle/collision-avoidance algorithms in the field of motion planning, such as the Artificial Potential Field (APF) method [67], the navigation function method [68], [112], [120], the Dynamic Window (DW) method [41] and the Vector Field Histogram (VFH) method [14]. These approaches usually require a global map including obstacles to allow planning of a feasible path, and extensions of some of these approaches also allow only local information of obstacles [132, Chapter 6]. However, these collision-avoidance/path-planning algorithms alone are not automatically compatible with path-following algorithms. This is because a starting point and a destination point are required in collision-avoidance algorithms to plan a feasible path or determine possible moving directions between these two points, while they are not required in path-following algorithms for which a desired path is explicitly specified. In particular, vector-field guided path-following algorithms usually enable trajectories from *almost all* starting points in the workspace to converge to and propagate along the desired path, rather than from only one predefined starting point and converging to a single destination point [63], [74], [165].

Only a few existing studies integrate path-following algorithms and collision-avoidance algorithms. An approach is proposed in [139] to deform slightly the desired path such that the obstacle-avoidance behavior is realized at the cost of compromising the path-following accuracy. However, only experimental studies using wheeled robots in an environment scattered with unforeseen static and moving obstacles are provided, whereas the theoretical analysis is limited. In [128], the idea of locally deforming the desired path is adopted, and a force field is also utilized to realize path-following and collision-avoidance functionalities simultaneously. This approach is computationally efficient, as experimentally verified with a ground vehicle moving in an unknown environment populated with dynamic obstacles. Nevertheless, since only straight lines are considered as desired paths between adjacent waypoints, this approach can be restrictive in some applications, such as satellites circulating along orbits. In [92], a switching guidance system with a path-following mode and a collision-avoidance mode for

an unmanned surface vessel is designed. The system is effective if the desired paths and obstacles have some typical geometric shapes, such as straight lines and circles, and positions and velocities of obstacles are provided. However, this approach can be challenging to apply if non-circular obstacles are considered. The two-mode switching methodology is also adopted in [150], where the authors develop the constant avoidance-angle reactive collision-avoidance algorithm and combine it with pure-pursuit or line-of-sight path-following algorithms. Although mathematical analysis is conducted for a sparse scenario with locally sensed circular obstacles, there is no theoretical guarantee of the effectiveness of the algorithm in an environment with many obstacles of non-circular shapes. Another unified framework integrating both path following and collision avoidance is proposed in [73], where the authors combine the Deformable Virtual Zone (DVZ) method and the Lyapunov backstepping design. The DVZ method renders the collision-avoidance behavior *reactive*, as only proximity information about obstacles is used. However, there is an inherent limitation since the path-following controller and the collision-avoidance controller may generate antagonistic control commands. A heuristic switching mechanism is thereby introduced to address this issue, but the corresponding rigorous mathematical analysis and formal guarantees are limited.

Some studies focus on creating, modifying, or combining vector fields to realize both path-following and collision-avoidance behaviors. In [173], given accurate information of static obstacles, two vector fields, one for path following and the other for collision avoidance, are combined with weights determined by a decay function such that the adverse effects caused by the overlapping of two vector fields can be mitigated. Different decay functions are numerically evaluated, but there is no theoretical guarantee for collision avoidance or path following. This approach is further developed in [151] to ensure minimal deviation from the desired path during the obstacle-avoidance process, where the locations and sizes of static circular obstacles are known. The paper also proposes a numerical solution to detect singular points generated by the weighted sum of two vector fields. Nevertheless, only circular desired paths and circular obstacles are considered in the study. In [110], a family of 2D vector fields is suitably blended to yield almost global feedback motion plans provided that the global information of the environment populated with static circular obstacles is given. This approach can steer a unicycle robot to a desired configuration, but it is not always suitable for path-following tasks where the repetitive motion of traversing along a path is required.

8.1.1 Contributions

This chapter proposes a general and unified framework in the first instance in \mathbb{R}^2 using a *composite guiding vector field* to enable trajectories to follow any sufficiently

smooth desired paths occluded by static or moving obstacles of arbitrary shapes. The guiding vector field is suitable to use in practical situations where obstacles are detected by onboard sensors during the movement of a vehicle. Namely, a vehicle does not need to know the global information about obstacles before it follows a desired path, but rather it obtains in real time information about the existence, shapes and velocities of obstacles locally. The composite guiding vector field is obtained by *smoothly* combining two vector fields, one for path following and the other for *reactive* collision avoidance, via bump functions. The use of bump functions reduces the undesirable effects of integrating two vector fields (c.f. [173]). To avoid trajectories getting stuck in a region, we also introduce a switching mechanism with detailed theoretical analysis. Some discussions on extending the composite guiding vector field to any higher-dimensional spaces and considering robot models other than the single integrator model are also provided.

The main contributions of this chapter develop the following advantages of the proposed approach:

1) Our approach is general and flexible. The desired path and the boundaries of the obstacles are any sufficiently smooth one-dimensional manifolds. Therefore, they are either homeomorphic to the unit circle or the real line¹, and thereby the common convexity assumption is dropped [112]. In addition, the construction of the composite vector field does not involve any specific geometric relationships between the robot, the desired path, and the obstacles. Thus, the composite vector field applies to general cases;

2) The collision-avoidance behavior in this approach is *reactive* in the sense that obstacles are assumed unpredictable, and that the guiding vector field acts as a feedback control command *directly* to the system without the often time-consuming process of path (re)-planning or creation of global symbolic maps. More specifically, since our approach does not fall into the traditional *path-planning* category, we do not require the global knowledge about obstacles in the design phase of the algorithm. Instead, local information is sufficient: whenever a new obstacle is encountered, the composite vector field is easily updated by adding a new component (see Remark 8.14), without compromising the original theoretical guarantees for the path-following and collision-avoidance behaviors. This enables real-time autonomous robot navigation and motion control without knowing the global map. When moving obstacles are considered, we allow measurement errors of the obstacles' velocities, and provide some robustness guarantees involving the time-varying guiding vector field (see Remark 8.34);

3) Our analysis is based on nonlinear systems theory, and there are rigorous theoretical guarantees for both path-following and collision-avoidance motions, which are often absent in the related literature as mentioned above. In particular, we prove that there is no Zeno phenomenon in our proposed switching mecha-

¹ An example of the latter sort of obstacle could be a river or a coastline.

nism (see Theorem 8.30), which is introduced to deal with the common deadlock situation;

4) Our composite vector field can be naturally extended to any higher-dimensional spaces, including 3D Euclidean space². Spaces with dimensions higher than three correspond to abstract configuration spaces, such as robot arm joint spaces. Thus, the composite vector field is, for instance, directly applicable in the low-level control of robot arms in the joint space.

In contrast to these advantages mentioned above, we also prove a general result showing a common limitation of combining two vector fields (see Lemma 8.20). We regard this result as another contribution since it gives a theoretical explanation of the common phenomenon that singular points exist when two vector fields are blended, regardless of what decay functions (or bump functions) one uses to mitigate the overlapping effects. This result can be regarded as a counterpart of the well-known limitation of motion-planning algorithms based on the negative gradient of a potential/navigation function [68], [120], both issues being fundamentally topological. Note, though, that our settings and approach are fundamentally different from those based on a potential/navigation function. For example, our composite vector field is not the (negative) gradient of any potential/navigation function, and we do not require a destination point to which trajectories converge. We also do not restrict consideration to a compact workspace (c.f. [68], [120]). One consequence of these differences is that the limitation of our approach can sometimes be removed (see Remark 8.21), and thereby, perhaps surprisingly, global convergence of trajectories to the desired path with the collision-avoidance guarantee is possible (see Remark 8.21).

8.1.2 Chapter structure

The remainder of this chapter is organized as follows. Section 8.2 formulates the problem. In Section 8.3, the systematic construction of the composite vector field is elaborated. Then Section 8.4 presents the convergence results of the integral curves of the composite vector field. Section 8.5 introduces the switching mechanism to deal with the deadlock problem and replaces some difficult technical conditions in Theorem 8.24. Three extensions of our approach are discussed in Section 8.6, and simulation results are illustrated in Section 8.7. Finally, Section 8.8 concludes the chapter.

² In 2D, the desired path and the obstacle boundaries are one-dimensional. However, in the ambient 3D space, the desired path is still one-dimensional but the obstacle boundaries need to be two-dimensional. See Section 8.6.2 for more details.

8.2 PROBLEM FORMULATION

In this section, we introduce related notations, essential assumptions and formulate the problem.

8.2.1 Preliminaries

A *discrete set* \mathcal{A} in \mathbb{R}^n is a set consisting of only isolated points; that is, for every point $p \in \mathcal{A}$, there exists an open neighborhood $\mathcal{U}_p \subseteq \mathbb{R}^n$ of p , such that $\mathcal{U}_p \cap \mathcal{A} = \{p\}$. A discrete set is at most countable (i.e., finite or countably infinite). A function $f : \Omega \subseteq \mathbb{R}^m \rightarrow \mathbb{R}^n$ is bounded away from zero in Ω if there exists a real number $c > 0$, such that $\|f(x)\| > c$ for all $x \in \Omega$.

8.2.2 Desired paths

The desired path $\mathcal{P} \subseteq \mathbb{R}^2$ is defined by

$$\mathcal{P} = \{\xi \in \mathbb{R}^2 : \phi(\xi) = 0\}, \quad (8.1)$$

which is the zero-level set of the twice continuously differentiable function $\phi : \mathbb{R}^2 \rightarrow \mathbb{R}$. This description of the desired path \mathcal{P} does not require any parametrization, and it is common in vector-field guided path-following algorithms [24], [28], [36], [50], [89], [98], [156], [157]. In addition, one can naturally assume that \mathcal{P} is a one-dimensional connected submanifold in \mathbb{R}^2 . Thus, \mathcal{P} is either homeomorphic to a circle if it is compact, or the real line \mathbb{R} otherwise [76, Theorem 5.27]. One can use the value $|\phi(\xi)|$ at a point $\xi \in \mathbb{R}^2$ to crudely approximate the distance $\text{dist}(\xi, \mathcal{P})$ between a point $\xi \in \mathbb{R}^2$ and the path \mathcal{P} under a mild assumption shown later (i.e. Assumption 8.7). For simplicity, we call $\phi(\xi)$ the (signed) *path-following error* at a point $\xi \in \mathbb{R}^2$.

8.2.3 Obstacles, reactive areas and repulsive areas

At each time instant $t \geq 0$, we consider a finite set of obstacles $\mathcal{O}_{\text{all}}^t = \{\mathcal{O}_i^t \subseteq \mathbb{R}^2 : i \in \mathcal{I}\}$, where m is the total number of obstacles and $\mathcal{I} = \{1, 2, \dots, m\}$. We assume that the obstacles are of finite sizes at every time instant³:

Assumption 8.1. At any time instant $t \geq 0$, the set \mathcal{O}_i^t is bounded for any $i \in \mathcal{I}$.

³ Obstacles can have infinite sizes as well; i.e., at any/some time instant $t \geq 0$, the set \mathcal{O}_i^t is unbounded. This is useful, for example, when one wants to restrict a vehicle's movement within a compact space, so the obstacle is the unbounded space beyond this compact space. However, if this unbounded obstacle occludes the desired path (i.e., $\mathcal{O}_i^t \cap \mathcal{P} \neq \emptyset$), then a trajectory might not be able to return to the desired path, and the magnitude of the path-following error can grow infinitely large. To avoid this undesirable consequence and for simplicity, we do not consider unbounded obstacles in this chapter.

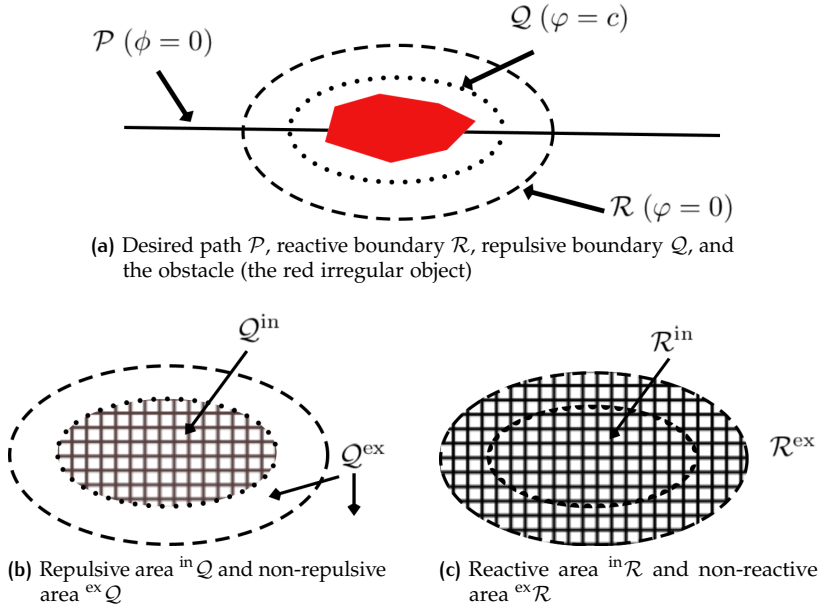


Figure 8.1: Illustrations of concepts.

We do not deal with the specific form of the obstacles $\mathcal{O}_{\text{all}}^t$, but we define some “boundaries” to enclose each obstacle (or to enclose a collection of obstacles if they are very close to each other) such that avoiding collision with the obstacles is simplified to avoiding collision with these boundaries regardless of the possibly complicated geometric shapes of the obstacles. Specifically, fixing t , we define the *reactive boundary* \mathcal{R}_i^t and the *repulsive boundary* \mathcal{Q}_i^t around the obstacle \mathcal{O}_i^t as follows:

$$\mathcal{R}_i^t = \{\xi \in \mathbb{R}^2 : \varphi_i(\xi, t) = 0\}, \quad (8.2)$$

$$\mathcal{Q}_i^t = \{\xi \in \mathbb{R}^2 : \varphi_i(\xi, t) = c_i\}, \quad (8.3)$$

where $\varphi_i : \mathbb{R}^2 \times \mathbb{R} \rightarrow \mathbb{R}$ is a twice continuously differentiable function and $c_i \neq 0$ is a constant. The smoothness of the function φ_i with respect to t represents the smooth motion of an obstacle. The definitions (8.2) and (8.3) are similar to (8.1) for simplicity. By Assumption 8.1, \mathcal{R}_i^t and \mathcal{Q}_i^t are compact. We also assume that at each time instant $t \geq 0$, the boundaries \mathcal{R}_i^t and \mathcal{Q}_i^t are one-dimensional connected submanifolds in \mathbb{R}^2 . The reactive boundary \mathcal{R}_i^t decomposes the plane into the “interior”: the bounded open subset denoted by ${}^{\text{in}}\mathcal{R}_i^t$, and the “exterior”: the unbounded open subset denoted by ${}^{\text{ex}}\mathcal{R}_i^t$, and there holds $\mathcal{R}_i^t = \partial {}^{\text{in}}\mathcal{R}_i^t = \partial {}^{\text{ex}}\mathcal{R}_i^t$ [51, Section VI.52], where $\partial(\cdot)$ denotes the boundary of a set (\cdot) . For convenience, we call ${}^{\text{in}}\mathcal{R}_i^t$ the (*open*) *reactive area* and ${}^{\text{ex}}\mathcal{R}_i^t$ the (*open*) *non-reactive area*. Similarly,

for the repulsive boundary \mathcal{Q}_i^t , we define the *(open) repulsive area* ${}^{\text{in}}\mathcal{Q}_i^t$ and the *(open) non-repulsive area* ${}^{\text{ex}}\mathcal{Q}_i^t$, and there holds $\mathcal{Q}_i^t = \partial {}^{\text{in}}\mathcal{Q}_i^t = \partial {}^{\text{ex}}\mathcal{Q}_i^t$ (see Fig. 8.1). We simply replace “open” by “closed” to refer to the closure of these sets (e.g. $\overline{{}^{\text{in}}\mathcal{R}_i^t}$ is the *closed reactive area*, where $\overline{(\cdot)}$ denotes the closure of a set). Intuitively, the reactive area ${}^{\text{in}}\mathcal{R}_i^t$ is the area where the robot can sense the obstacles and needs to be reactive to obstacles, and the repulsive area ${}^{\text{in}}\mathcal{Q}_i^t$ is the “dangerous” area where the robot is forbidden to enter. We make the following intuitively reasonable standing assumptions:

Assumption 8.2. There holds $\mathcal{O}_i^t \subseteq {}^{\text{in}}\mathcal{Q}_i^t \subseteq {}^{\text{in}}\mathcal{R}_i^t$ and $\text{dist}(\mathcal{Q}_i^t, \mathcal{R}_i^t) > 0$ for all $t \geq 0$.

Assumption 8.3. There holds $\mathcal{P} \not\subseteq \overline{\bigcup_{i \in \mathcal{I}} {}^{\text{in}}\mathcal{R}_i^t}$ for all $t \geq 0$.

Assumption 8.4. There holds $\text{dist}({}^{\text{in}}\mathcal{R}_i^t, {}^{\text{in}}\mathcal{R}_j^t) > 0$ for all $i \neq j \in \mathcal{I}$ and $t \geq 0$.

Assumption 8.2 stipulates the relative positioning of the obstacles, the reactive boundary, and the repulsive boundary. Assumption 8.3 means that the desired path cannot be fully covered by obstacles; otherwise, path following is meaningless. Assumption 8.4 implies that any two obstacles are sufficiently far away such that any two reactive areas are disjoint⁴.

8.2.4 Problem formulation

When there are no obstacles, the vector field guided path following (VF-PF) problem, as defined in Problem 1.1, requires one to design a vector field such that the integral curves of the vector field will converge to and propagate along the desired path defined in (8.1). If there are obstacles on/near the desired path, the vector field needs to be modified to meet additional requirements, leading to the problem of Vector-Field guided Path-Following with Collision-Avoidance (VF-CAPF):

Definition 8.5 (VF-CAPF Problem). Design a continuously differentiable vector field $\chi : \mathbb{R} \times \mathbb{R}^2 \rightarrow \mathbb{R}^2$ for $\dot{\xi}(t) = \chi(t, \xi(t))$ such that:

1. (Path-following). In the absence of obstacles, the vector field χ solves the VF-PF problem.
2. (Repulsive ${}^{\text{in}}\mathcal{Q}_i^t$). If $\xi(0) \notin \bigcup_{i \in \mathcal{I}} \overline{{}^{\text{in}}\mathcal{Q}_i^0}$, then $\xi(t) \notin \bigcup_{i \in \mathcal{I}} \overline{{}^{\text{in}}\mathcal{Q}_i^t}$ for $t \geq 0$.⁵

⁴ If two reactive areas overlap, one can regard the corresponding two obstacles as one big (disconnected) obstacle and define a bigger reactive area.

⁵ Since the closed repulsive areas are “dangerous”, it is naturally assumed that the initial conditions do not include these areas. Nevertheless, as shown later, our approach can still guarantee that any trajectory starting from the closed repulsive areas will leave eventually (see Corollary 8.17 and the first simulation example in Section 8.7).

3. (Bounded Path-following Error). There exists $M > 0$ such that the path-following error satisfies $|\phi(\xi(t))| \leq M$ for $t \geq 0$. Moreover, for any connected time interval $\Xi \subseteq \mathbb{R}$ satisfying $\xi(t) \notin \bigcup_{i \in \mathcal{I}} \overline{\text{in} \mathcal{R}_i^t}$ for $t \in \Xi$, the absolute path-following error $|\phi(\xi(t))|$ is strictly decreasing over Ξ .
4. (Penetrable $\overline{\text{in} \mathcal{R}_i^t}$). Fix $i \in \mathcal{I}$, and consider trajectories $\xi(\cdot)$ starting from almost all initial conditions. If there exists $t_1 > 0$ such that $\xi(t_1) \in \overline{\text{in} \mathcal{R}_i^{t_1}}$, then there exists another (possibly non-unique) time instant $t_2 > t_1$ such that $\xi(t_2) \notin \overline{\text{in} \mathcal{R}_i^{t_2}}$. In addition, the trajectory cannot cross the reactive boundary \mathcal{R}_i^t infinitely fast; i.e., $\inf\{t_2 - t_1 : t_2 > t_1, \xi(t_2) \notin \overline{\text{in} \mathcal{R}_i^{t_2}}\} > 0$.

Remark 8.6. Objective 2 ensures that trajectories do not collide with obstacles. As obstacles might be right on the desired path, Objective 3 requires that the magnitude of the path-following error should be at least bounded by some constant. In addition, the magnitude of the path-following error should be decreasing along a trajectory if no obstacles are nearby. Objective 4 prevents trajectories starting from almost all initial points from staying in a reactive area forever such that the repetitive motion of following the desired path is possible (i.e., a reactive area is always penetrable). “Almost all” means the set of initial points of trajectories that cannot leave the reactive area forms a zero-measure set. Moreover, Objective 4 also requires that the Zeno phenomenon [82] cannot occur. \triangleleft

For simplicity, we consider *static* obstacles first (in Sections 8.3, 8.4 and 8.5). Therefore, the superscript t in the notations are removed, and the vector field $\chi : \mathbb{R}^2 \rightarrow \mathbb{R}^2$ becomes time-invariant. The extension to moving obstacles and the time-varying vector field $\chi : \mathbb{R} \times \mathbb{R}^2 \rightarrow \mathbb{R}^2$ will be deferred until Section 8.6.

8.3 COMPOSITE VECTOR FIELD

8.3.1 Path-following vector field and reactive vector field

The basic task of vector-field guided path-following problem is designing a vector field that guides a robot to move towards and circulate along the desired path. From the definitions of the desired path in (8.1) and the reactive boundary in (8.2), using the approach in [63], we can define the corresponding *vector fields* $\chi_{\mathcal{P}}, \chi_{\mathcal{R}_i} : \mathbb{R}^2 \rightarrow \mathbb{R}^2$ associated with \mathcal{P} and \mathcal{R}_i by

$$\chi_{\mathcal{P}}(\xi) = \gamma_0 E \nabla \phi(\xi) - k_p \phi(\xi) \nabla \phi(\xi), \quad (8.4)$$

$$\chi_{\mathcal{R}_i}(\xi) = \gamma_i E \nabla \varphi_i(\xi) - k_{r_i} \varphi_i(\xi) \nabla \varphi_i(\xi), \quad i \in \mathcal{I} \quad (8.5)$$

where $\gamma_i \in \{1, -1\}$, $i \in \{0\} \cup \mathcal{I}$ determines the propagation direction along the desired path or the reactive boundaries, $E = \begin{bmatrix} 0 & -1 \\ 1 & 0 \end{bmatrix}$ is the 90° rotation matrix and k_p, k_{r_i} are positive gains. The latter term of each equation above is a signed gradient, and guides integral curves to converge towards the desired path or the reactive boundaries, whereas the first term is perpendicular to the gradient and provides a propagation speed along the desired path or the reactive boundaries. For simplicity and without loss of generality, we assume $\gamma_i = 1$ for all $i \in \{0\} \cup \mathcal{I}$ throughout the subsequent theoretical development by default.

We call $\chi_{\mathcal{P}}$ the *path-following vector field* and $\chi_{\mathcal{R}_i}$ the *reactive vector field*. The singular set of the vector fields $\chi_{\mathcal{P}}$ and $\chi_{\mathcal{R}_i}$ are denoted by $\mathcal{C}_{\mathcal{P}}$ and $\mathcal{C}_{\mathcal{R}_i}$ respectively and defined below:

$$\begin{aligned}\mathcal{C}_{\mathcal{P}} &= \{\xi \in \mathbb{R}^2 : \chi_{\mathcal{P}}(\xi) = 0\} = \{\xi \in \mathbb{R}^2 : \nabla \phi(\xi) = 0\}, \\ \mathcal{C}_{\mathcal{R}_i} &= \{\xi \in \mathbb{R}^2 : \chi_{\mathcal{R}_i}(\xi) = 0\} = \{\xi \in \mathbb{R}^2 : \nabla \varphi_i(\xi) = 0\}.\end{aligned}$$

Each point is called a *singular point*, where the corresponding vector field vanishes. In this case, the singular points happen to be the *critical points* of ϕ or φ_i , but this is not true for vector fields defined in other higher-dimensional (Euclidean) spaces (see Chapters 4, 5 or 9). Since \mathcal{P} , \mathcal{R}_i and \mathcal{Q}_i are one-dimensional connected submanifolds in \mathbb{R}^2 , 0 is a regular value for ϕ and φ_i , and c_i is another regular value for φ_i [77, p. 105]. Therefore, there are no singular points on \mathcal{P} , \mathcal{R}_i and \mathcal{Q}_i ; i.e., $\mathcal{P} \cap \mathcal{C}_{\mathcal{P}} = \emptyset$, $\mathcal{R}_i \cap \mathcal{C}_{\mathcal{R}_i} = \emptyset$ and $\mathcal{Q}_i \cap \mathcal{C}_{\mathcal{R}_i} = \emptyset$.

8.3.2 Behavior with a single vector field

Let $\chi = \chi_{\mathcal{P}}$ or $\chi = \chi_{\mathcal{R}_i}$, and we consider the following autonomous differential equation:

$$\dot{\xi}(t) = \chi(\xi(t)). \quad (8.6)$$

Given an initial condition $\xi(0) \in \mathbb{R}^2$, the existence and uniqueness of solutions to the above differential equation is guaranteed, as $\chi(\xi)$ is continuously differentiable with respect to ξ (see Theorem 2.1). Taking $\chi = \chi_{\mathcal{P}}$ as an example, it is proved in [63, Lemma 2] that a trajectory $\xi(t)$ converges to either the desired path \mathcal{P} or the singular set $\mathcal{C}_{\mathcal{P}}$ under the following assumption:

Assumption 8.7 ([63]). For any $\kappa > 0$, there holds $\inf\{|\phi(\xi)| : \text{dist}(\xi, \mathcal{P}) \geq \kappa\} > 0$. Similarly, for any $\kappa > 0$, there holds $\inf\{\|\nabla \phi(\xi)\| : \text{dist}(\xi, \mathcal{C}_{\mathcal{P}}) \geq \kappa\} > 0$.

Note that corresponding to the same desired path \mathcal{P} , there is an infinite number of choices⁶ of the function ϕ in (8.1). This assumption restricts one to choose a

6 For example, if $\mathcal{P} = \phi^{-1}(0)$, then one can define $\tilde{\phi}(\cdot) = \phi(\cdot)\Lambda(\cdot)$, where $\Lambda : \mathbb{R} \rightarrow \mathbb{R}$ and $\Lambda(p) \neq 0$ for any $p \notin \mathcal{P} = \phi^{-1}(0)$. A trivial choice of $\Lambda(\cdot)$ is any non-zero constant function. Therefore, $\mathcal{P} = \phi^{-1}(0) = \tilde{\phi}^{-1}(0)$ and $\tilde{\phi}$ is another function to characterize the same desired path \mathcal{P} .

“valid” function ϕ such that when $|\phi(\xi(t))| \rightarrow 0$ as $t \rightarrow \infty$ along an infinitely-extendable trajectory $\xi(t)$, then $\text{dist}(\xi(t), \mathcal{P}) \rightarrow 0$ as $t \rightarrow \infty$ (guaranteed by the first part of the assumption), and when $\|\nabla\phi(\xi(t))\| \rightarrow 0$ as $t \rightarrow \infty$ then $\text{dist}(\xi(t), \mathcal{C}_{\mathcal{P}}) \rightarrow 0$ as $t \rightarrow \infty$ (guaranteed by the second part of the assumption). The assumption holds for all the examples presented later in this chapter. Under this assumption, we have the following important *dichotomy convergence* lemma.

Lemma 8.8 (Dichotomy convergence, [63]). *Under Assumption 8.7, let $\chi_{\mathcal{P}} : \mathbb{R}^2 \rightarrow \mathbb{R}^2$ be the vector field associated with the one-dimensional connected submanifold \mathcal{P} described by (8.1). Given an initial condition $\xi(0) \in \mathbb{R}^2$, any trajectory of $\dot{\xi}(t) = \chi_{\mathcal{P}}(\xi(t))$ converges either to \mathcal{P} or the singular set $\mathcal{C}_{\mathcal{P}}$ as $t \rightarrow t^*$, where $t^* \leq \infty$.*

Remark 8.9 (Time-invariant scaling). The dichotomy convergence lemma continues to hold up to a time-invariant positive scaling (e.g., the normalization) of the vector field, such that the orientation of each vector of $\chi_{\mathcal{P}}$ is not modified [25, Proposition 1.14]. \triangleleft

In the scenario of path following, the convergence of trajectories to the singular set $\mathcal{C}_{\mathcal{P}}$ is not desirable, and therefore, it is important to know how large the set of initial points of trajectories converging to $\mathcal{C}_{\mathcal{P}}$ is. A related result (Corollary 5.19 in Chapter 5) shows that, under some conditions, the singular set $\mathcal{C}_{\mathcal{P}}$ is non-attractive; that is, there does not exist an open neighborhood \mathcal{U} of $\mathcal{C}_{\mathcal{P}}$ such that every trajectory starting from \mathcal{U} converges to the singular set $\mathcal{C}_{\mathcal{P}}$. However, the non-attractiveness of $\mathcal{C}_{\mathcal{P}}$ does not exclude the possibility that some trajectories still converge to $\mathcal{C}_{\mathcal{P}}$; neither does it imply that the set of initial conditions of trajectories converging to $\mathcal{C}_{\mathcal{P}}$ is of measure zero. We use the notation $\mathcal{W}(\mathcal{C}_{\mathcal{P}})$ to represent the set of initial conditions for trajectories of (8.6) to asymptotically converge to the singular set $\mathcal{C}_{\mathcal{P}}$. Precisely,

$$\mathcal{W}(\mathcal{C}_{\mathcal{P}}) := \{\xi_0 \in \mathbb{R}^n : \xi(0) = \xi_0, \text{dist}(\xi(t), \mathcal{C}_{\mathcal{P}}) \rightarrow 0 \text{ as } t \rightarrow \infty\}.$$

If $\mathcal{C}_{\mathcal{P}}$ consists of only one point denoted by c , which is also an equilibrium of (8.6), then we define $\mathcal{W}(c) := \mathcal{W}(\mathcal{C}_{\mathcal{P}})$, which is referred to as the *local inset* of c [124, p. 39]. If the singular set $\mathcal{C}_{\mathcal{P}}$ is discrete or the function ϕ is real analytic, a trajectory converging to $\mathcal{C}_{\mathcal{P}}$ actually converges to a single point in $\mathcal{C}_{\mathcal{P}}$, and therefore, $\mathcal{W}(\mathcal{C}_{\mathcal{P}}) = \bigcup_{c \in \mathcal{C}_{\mathcal{P}}} \mathcal{W}(c)$ (see Theorems 7.5 and 7.7). For any point $c \in \mathcal{C}_{\mathcal{P}}$, the Hessian matrix at this point is denoted by $H_{\phi}(c) := \nabla^2\phi(c)$, which is a symmetric matrix since $\phi \in C^2$. Now we state the following result regarding how “large” the set of initial conditions which render trajectories converging to the singular set $\mathcal{C}_{\mathcal{P}}$.

Lemma 8.10. *Suppose the singular set $\mathcal{C}_{\mathcal{P}}$ is discrete. If the matrix $\phi(c)H_{\phi}(c)$ has at least one negative eigenvalue for every point $c \in \mathcal{C}_{\mathcal{P}}$, then $\mathcal{W}(\mathcal{C}_{\mathcal{P}}) = \bigcup_{c \in \mathcal{C}_{\mathcal{P}}} \mathcal{W}(c)$ is a set of measure zero. If $\phi(c)H_{\phi}(c)$ has all negative eigenvalues for every point $c \in \mathcal{C}_{\mathcal{P}}$, then $\mathcal{W}(\mathcal{C}_{\mathcal{P}}) = \mathcal{C}_{\mathcal{P}}$.*

Proof. It is proved in [63, Lemma 3 and Corollary 1] that if $\phi(c)H_\phi(c)$ has at least one negative eigenvalue for $c \in \mathcal{C}_P$, then $\mu(\mathcal{W}(c)) = 0$, where μ is the Lebesgue measure. Since \mathcal{C}_P is discrete, it is at most countable. By the non-negativity and subadditivity properties of the Lebesgue measure, $0 \leq \mu(\mathcal{W}(\mathcal{C}_P)) = \mu(\bigcup_{c \in \mathcal{C}_P} \mathcal{W}(c)) \leq \sum_{c \in \mathcal{C}_P} \mu(\mathcal{W}(c)) = 0$. Therefore, $\mathcal{W}(\mathcal{C}_P)$ is of measure zero. The last statement of the lemma is due to Lemma 3 and Corollary 1 in [63]. \square

Remark 8.11. If the Hessian matrix $H_\phi(c)$ of a critical point $c \in \mathcal{C}_P$ is non-singular, this critical point is called *non-degenerate*. If every critical point $c \in \mathcal{C}_P$ of ϕ is non-degenerate, then ϕ is a *Morse function* [86, Definition 1.14]. If ϕ is a Morse function, then every critical point in \mathcal{C}_P is isolated [86, Corollary 1.12], and thus the singular set \mathcal{C}_P is discrete. Since almost all smooth functions are Morse functions⁷, the condition of \mathcal{C}_P being discrete is not conservative. In many practical examples, the set \mathcal{C}_P is even finite⁸ [50], [63], [74], [157]. In particular, if ϕ is a Morse function and $\nabla\phi(\xi) \neq 0$ when $\|\xi\|$ is sufficiently large, then \mathcal{C}_P is finite. \triangleleft

Note that Lemma 8.8 and Lemma 8.10 still hold if P , ϕ , H_ϕ , χ_P , and \mathcal{C}_P are replaced by \mathcal{R}_i , φ_i , H_{φ_i} , $\chi_{\mathcal{R}_i}$, and $\mathcal{C}_{\mathcal{R}_i}$ respectively.

8.3.3 Smooth zero-in and zero-out functions

In preparation for studying the simultaneous effects of two vector fields, we will introduce some special functions to “blend” different vector fields, which is inspired by the following result.

Lemma 8.12 (Existence of smooth bump functions, [77, Proposition 2.25]). *Given a nonempty open subset $B \subseteq \mathbb{R}^n$ and a nonempty closed subset $A \subseteq \mathbb{R}^n$ such that $A \subseteq B$, there exists a smooth (i.e., infinitely differentiable) function $\sqcap : \mathbb{R}^n \rightarrow \mathbb{R}$ such that $\sqcap(x) \equiv 1$ for $x \in A$, $0 \leq \sqcap(x) \leq 1$ for $x \in B \setminus A$ and $\sqcap(x) \equiv 0$ for $x \in \mathbb{R}^n \setminus B$.*

The function \sqcap in Lemma 8.12 is a *smooth bump function*, which is a smooth real-valued function that attains 1 on a compact set and attains zero beyond an *open neighborhood* of that set [77, pp. 40-47]. It is obvious that there also exists an “inverted” bump function $\sqcup : \mathbb{R}^n \rightarrow \mathbb{R}$ which attains 0 on a compact set and attains 1 beyond an *open neighborhood* of that set (e.g., $\sqcup = 1 - \sqcap$). These functions are ideal to “blend” different vector fields by keeping or removing some parts of the vector field to possibly reduce the undesirable effects of overlapping, while the original smoothness of the vector fields is still maintained. We have the following corollary.

⁷ Precisely, Morse functions form an open, dense subset of the space of smooth functions [56, Chapter 6, Theorem 1.2].

⁸ When ϕ is real analytic, it has been proved in [50] that \mathcal{C}_P is of measure zero, which roughly indicates that \mathcal{C}_P is not very “large”. Nevertheless, in general, it is possible that \mathcal{C}_P is not discrete or bounded, but these examples seem quite artificial (see Chapters 3 and 5).

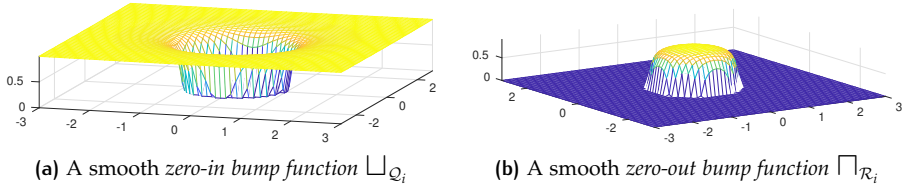


Figure 8.2: Illustration of smooth zero-in and zero-out bump functions.

Corollary 8.13. For any reactive boundary \mathcal{R}_i in (8.2) and repulsive boundary \mathcal{Q}_i in (8.3), $i \in \mathcal{I}$, there exist smooth functions $\sqcup_{\mathcal{Q}_i}, \sqcap_{\mathcal{R}_i} : \mathbb{R}^2 \rightarrow [0, \infty)$ defined below:

$$\sqcup_{\mathcal{Q}_i}(\xi) = \begin{cases} 0 & \xi \in \overline{\text{in } \mathcal{Q}_i} \\ S_i(\xi) & \xi \in \text{ex } \mathcal{Q}_i \cap \text{in } \mathcal{R}_i, \\ 1 & \xi \in \overline{\text{ex } \mathcal{R}_i} \end{cases} \quad \sqcap_{\mathcal{R}_i}(\xi) = \begin{cases} 1 & \xi \in \overline{\text{in } \mathcal{Q}_i} \\ Z_i(\xi) & \xi \in \text{ex } \mathcal{Q}_i \cap \text{in } \mathcal{R}_i, \\ 0 & \xi \in \overline{\text{ex } \mathcal{R}_i} \end{cases} \quad (8.7)$$

where $S_i : \text{ex } \mathcal{Q}_i \cap \text{in } \mathcal{R}_i \rightarrow (0, 1)$ and $Z_i : \text{ex } \mathcal{Q}_i \cap \text{in } \mathcal{R}_i \rightarrow (0, 1)$ are smooth functions.

Intuitively, we call $\sqcup_{\mathcal{Q}_i}$ a *smooth zero-in function* with respect to \mathcal{Q}_i and $\sqcap_{\mathcal{R}_i}$ a *smooth zero-out function* with respect to \mathcal{R}_i (see Fig. 8.2). Since $\sqcup_{\mathcal{Q}_i}$ is smooth, it is evident that $S_i(\xi)$ vanishes smoothly to 0 as ξ approaches \mathcal{Q}_i , and smoothly approaches value 1 as ξ approaches \mathcal{R}_i , and the converse applies for $Z_i(\xi)$. One can similarly define the smooth zero-out function $\sqcap_{\mathcal{Q}_i}(\xi)$ for \mathcal{Q}_i and the smooth zero-in function $\sqcup_{\mathcal{R}_i}$ for \mathcal{R}_i , but it is not necessary for the construction of a composite vector field to be discussed later.

8.3.4 Composite vector field

We use smooth zero-in and zero-out functions to “blend” different vector fields and obtain the composite vector field $\chi_c : \mathcal{D} \subseteq \mathbb{R}^2 \rightarrow \mathbb{R}^2$ as follows:

$$\chi_c(\xi) = \left(\prod_{i \in \mathcal{I}} \sqcup_{\mathcal{Q}_i}(\xi) \right) \hat{\chi}_{\mathcal{P}}(\xi) + \sum_{i \in \mathcal{I}} (\sqcap_{\mathcal{R}_i}(\xi) \hat{\chi}_{\mathcal{R}_i}(\xi)), \quad (8.8)$$

where $\hat{(\cdot)}$ is the normalization notation (i.e., $\hat{v} = v/\|v\|$ for a non-zero vector $v \in \mathbb{R}^n$), and $\mathcal{D} = \mathbb{R}^2 \setminus (\bigcup_i \mathcal{C}_{\mathcal{R}_i} \cup \mathcal{C}_{\mathcal{P}})$ is the domain on which the composite vector field is well-defined. Under Assumption 8.4, (8.8) is equivalent to:

$$\chi_c(\xi) \stackrel{(8.7)}{=} \begin{cases} \hat{\chi}_{\mathcal{R}_i}(\xi) & \xi \in \overline{\text{in } \mathcal{Q}_i} \cap \mathcal{D} \\ S_i(\xi)\hat{\chi}_{\mathcal{P}}(\xi) + Z_i(\xi)\hat{\chi}_{\mathcal{R}_i}(\xi) & \xi \in \overline{\text{ex } \mathcal{Q}_i} \cap \overline{\text{in } \mathcal{R}_i} \cap \mathcal{D} \\ \hat{\chi}_{\mathcal{P}}(\xi) & \xi \in \mathcal{D} \setminus (\bigcup_{k \in \mathcal{I}} \overline{\text{in } \mathcal{R}_k}), \end{cases} \quad (8.9)$$

for each $i \in \mathcal{I}$. From (8.9), one observes that only the reactive vector field $\chi_{\mathcal{R}_i}$ is active in the corresponding closed repulsive areas $\overline{\text{in } \mathcal{Q}_i}$, and only the path-following vector field $\chi_{\mathcal{P}}$ is active in the union of the closed non-reactive areas $\bigcup_{i \in \mathcal{I}} \overline{\text{ex } \mathcal{R}_i}$, whereas both the path-following vector field $\chi_{\mathcal{P}}$ and the reactive vector field $\chi_{\mathcal{R}}$ are active in the intersection of the reactive area and the non-repulsive area; namely, $\mathcal{M}_i := \overline{\text{ex } \mathcal{Q}_i} \cap \overline{\text{in } \mathcal{R}_i}$, called the *(open) mixed area* for convenience. The closure of this area $\overline{\mathcal{M}_i}$ is called the *closed mixed area*. Note that the composite vector field χ_c is not “mixed” on the reactive and repulsive boundaries. We consider the following system:

$$\dot{\xi}(t) = \chi_c(\xi(t)), \quad \xi(0) \in \mathcal{D}. \quad (8.10)$$

Due to the continuous differentiability of the right-hand-side, the existence and uniqueness of solutions is guaranteed (see Theorem 2.1). We define the *composite singular set*:

$$\mathcal{C}_c := \{\xi \in \mathcal{D} : \chi_c(\xi) = 0\}, \quad (8.11)$$

which contains all the equilibria of (8.10). Note that this set may contain some singular points in $\bigcup_i \mathcal{C}_{\mathcal{R}_i} \cup \mathcal{C}_{\mathcal{P}}$, and also new singular points due to the blending of the two vector fields in the union of the mixed area $\bigcup_i \mathcal{M}_i$.

Remark 8.14 (Local information). In practice, only locally sensed obstacles need to be considered for the computation of the composite vector field χ_c . From the compact expression in (8.8), it seems necessary to know *all* the obstacles in the workspace, but this is not true if one observes the expanded form in (8.9). When a trajectory enters a reactive area, meaning that a robot can detect an obstacle, the composite vector field χ_c in (8.9) only depends on the current reactive vector field $\chi_{\mathcal{R}_i}$ and the path-following vector field $\chi_{\mathcal{P}}$ but *not* on the knowledge of other obstacles. \triangleleft

8.4 ANALYSIS OF THE COMPOSITE VECTOR FIELD

Under Assumption 8.4 and in view of (8.9), different reactive vector fields $\chi_{\mathcal{R}_i}$ do not overlap. Therefore, without loss of generality, we only consider the case of one obstacle; i.e., the index set \mathcal{I} is a singleton. Thus, the subscripts i are removed from the notations in this section for simplicity. We also assume that the obstacle is sufficiently close to the desired path (precisely, ${}^{\text{in}}\mathcal{R} \cap \mathcal{P} \neq \emptyset$) such that collision avoidance is necessary. Now, the composite vector field (8.9) simplifies to

$$\chi_c(\xi) = \begin{cases} \hat{\chi}_{\mathcal{R}}(\xi) & \xi \in \overline{{}^{\text{in}}\mathcal{Q}} \cap \mathcal{D} \\ S(\xi)\hat{\chi}_{\mathcal{P}}(\xi) + Z(\xi)\hat{\chi}_{\mathcal{R}}(\xi) & \xi \in {}^{\text{ex}}\mathcal{Q} \cap {}^{\text{in}}\mathcal{R} \cap \mathcal{D} \\ \hat{\chi}_{\mathcal{P}}(\xi) & \xi \in \overline{{}^{\text{ex}}\mathcal{R}} \cap \mathcal{D}, \end{cases} \quad (8.12)$$

where $\mathcal{D} = \mathbb{R}^2 \setminus (\mathcal{C}_{\mathcal{R}} \cup \mathcal{C}_{\mathcal{P}})$. An intuitive illustration is shown in Fig. 8.3. Before presenting the first result, we define the repulsiveness of a set below.

Definition 8.15 (Repulsiveness of sets). A nonempty set $\mathcal{A} \subseteq \mathbb{R}^2$ is *repulsive* with respect to the dynamics $\dot{\xi} = f(\xi)$, where $f : \mathbb{R}^2 \rightarrow \mathbb{R}^2$ is Lipschitz continuous, if for each point $\xi_0 \in \mathcal{A}$, there exists $T > 0$, such that the trajectory $\xi(t)$ with the initial condition $\xi(0) = \xi_0$ satisfies $\xi(t) \notin \mathcal{A}$ for $t \geq T$. If this holds for almost every point in \mathcal{A} except for a set of measure zero, then \mathcal{A} is called *almost repulsive*. Namely, \mathcal{A} is *almost repulsive* if there exists a subset $\mathcal{B} \subseteq \mathcal{A}$ of measure zero such that $\mathcal{A} \setminus \mathcal{B}$ is repulsive.

The following lemma states the positive invariance property of the nonrepulsive area ${}^{\text{ex}}\mathcal{Q}$. Namely, for all $\xi(0) \in {}^{\text{ex}}\mathcal{Q}$, it follows that $\xi(t) \in {}^{\text{ex}}\mathcal{Q}$ for $t \geq 0$.

Lemma 8.16 (Positive invariance of ${}^{\text{ex}}\mathcal{Q}$). *If $\mathcal{W}(\mathcal{C}_{\mathcal{R}}) \cap \mathcal{Q} = \emptyset$, then the nonrepulsive area ${}^{\text{ex}}\mathcal{Q}$ is positively invariant with respect to (8.10).*

Proof. We prove this by contradiction. Suppose ${}^{\text{ex}}\mathcal{Q}$ is not positively invariant, then there exists $\xi(0) \in {}^{\text{ex}}\mathcal{Q}$ and $T > 0$ such that $\xi(T) \in \mathcal{Q}$. Note that in the closed repulsive area $\overline{{}^{\text{in}}\mathcal{Q}}$, the differential equation is simplified to $\dot{\xi} = \hat{\chi}_{\mathcal{R}}(\xi)$. Also note that the trajectory will leave \mathcal{Q} later; otherwise, this implies \mathcal{Q} contains a periodic orbit and thus contradicts Lemma 8.8. Therefore, there exists some time instant $T' > T$ such that $\xi(T') \notin \mathcal{Q}$. Next, we prove that the trajectory cannot go into the interior ${}^{\text{in}}\mathcal{Q}$. Suppose, on the contrary, $\xi(T') \in {}^{\text{in}}\mathcal{Q}$. Since $\mathcal{W}(\mathcal{C}_{\mathcal{R}}) \cap \mathcal{Q} = \emptyset$, the trajectory will not converge to $\mathcal{C}_{\mathcal{R}}$. Therefore, the trajectory will reach the boundary \mathcal{Q} again at some time instant $T'' > T'$; otherwise, again there is a contradiction of Lemma 8.8. Hence, on the time interval $\Xi := [T, T'']$, $\xi(t) \in \overline{{}^{\text{in}}\mathcal{Q}}$, and $\xi(T), \xi(T'') \in \mathcal{Q}$. For convenience, we denote the segment of trajectory $\xi(t)$ over Ξ by $\xi(\Xi) := \{\xi(t) \in \mathbb{R}^2 : t \in \Xi\}$, which is the image of the time interval Ξ under ξ . Since $\xi(\Xi)$ is closed and $\xi(\Xi) \subseteq \overline{{}^{\text{in}}\mathcal{Q}}$, the segment of

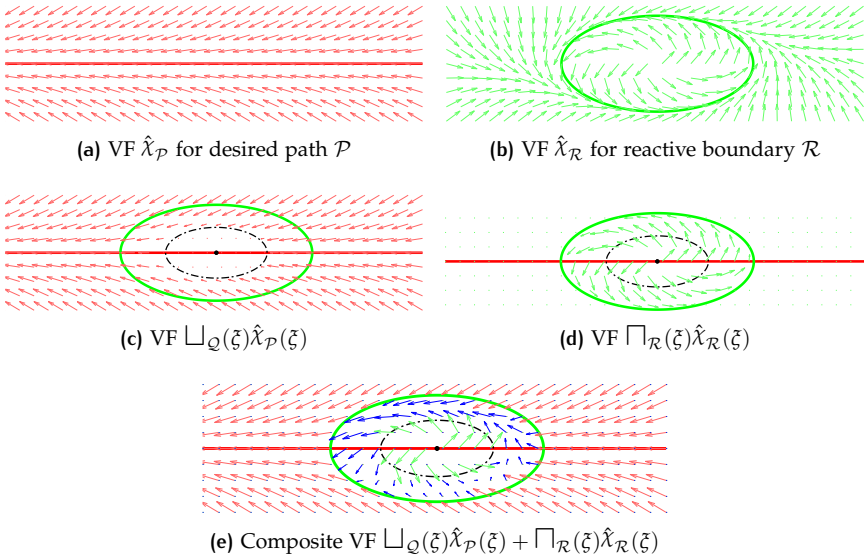


Figure 8.3: Construction of the composite vector field χ_c in (8.12). Each arrow in the subfigures represents a vector of the corresponding vector field evaluated at the position of the *tail* of the arrow. In (e), the green arrows belong to the reactive vector field χ_R and are all in $\overline{\text{in} \mathcal{Q}}$. The red arrows belong to the path-following vector field χ_P and are all in $\overline{\text{ex} \mathcal{R}}$. The blue arrows belong to the weighted sum of χ_P and χ_R and are all in the mixed area $\mathcal{M} = \text{ex} \mathcal{Q} \cap \text{in} \mathcal{R}$.

trajectory $\xi(\Xi)$ is compact in \mathbb{R}^2 . For what follows, we consider the trajectory over the time interval Ξ . Again, note that the differential equation (8.10) is simplified to $\dot{\xi} = \hat{\chi}_R(\xi)$ over this time interval. Choose the Lyapunov function candidate $V(\varphi(\xi)) = \varphi^2(\xi)/2$, then

$$\frac{d}{dt} V(\varphi(\xi)) = -k_r \frac{Z(\xi)}{\|\chi_R(\xi)\|} \varphi^2(\xi) \|\nabla \varphi(\xi)\|^2. \quad (8.13)$$

Due to the uniqueness of solutions and $\mathcal{W}(\mathcal{C}_{\mathcal{R}_i}) \cap \mathcal{Q} = \emptyset$, we have $\frac{d}{dt} V(\varphi(\xi(t))) < 0$ for $t \in \Xi$. However, the fact that $\xi(T), \xi(T'') \in \mathcal{Q}$ contradicts the strict decreasing property of $V(\xi(t))$ for $t \in \Xi$ (on the repulsive boundary \mathcal{Q} , φ attains the same value). The contradiction implies that the trajectory cannot go from the boundary \mathcal{Q} to the interior $\text{in} \mathcal{Q}$. Furthermore, the strict decreasing property of $V(\xi(t))$ also proves the repulsiveness of the boundary \mathcal{Q} ; more precisely, for every $\xi(0) \in \mathcal{Q}$, we have $\xi(t) \notin \mathcal{Q}$ for all $t > 0$. Combining the previous arguments with the uniqueness of solutions shows that once the trajectory starts from the non-repulsive area $\text{ex} \mathcal{Q}$, it will never reach the repulsive boundary \mathcal{Q} .

or the repulsive area $\text{in} \mathcal{Q}$. Thus the non-repulsive area $\text{ex} \mathcal{Q}$ is indeed positively invariant. \square

The almost repulsiveness of the closed repulsive area $\overline{\text{in} \mathcal{Q}}$ is stated in the following corollary.

Corollary 8.17 (Almost repulsiveness of $\overline{\text{in} \mathcal{Q}}$). *The set $\overline{\text{in} \mathcal{Q}} \setminus \mathcal{W}(\mathcal{C}_{\mathcal{R}})$ is repulsive. If the assumptions of Lemma 8.10 hold⁹, then $\overline{\text{in} \mathcal{Q}}$ is almost repulsive.*

Proof. We need to show that if $\xi(0) \in \overline{\text{in} \mathcal{Q}} \setminus \mathcal{W}(\mathcal{C}_{\mathcal{R}})$, then there exists $T > 0$, such that $\xi(t) \notin \overline{\text{in} \mathcal{Q}} \setminus \mathcal{W}(\mathcal{C}_{\mathcal{R}})$ for $t \geq T$. Since $\xi(0) \in \overline{\text{in} \mathcal{Q}} \setminus \mathcal{W}(\mathcal{C}_{\mathcal{R}})$, we can use the same argument as in Lemma 8.16 and conclude that there exists a time instant T , such that $\xi(T) \in \text{ex} \mathcal{Q}$. Due to the positive invariance of $\text{ex} \mathcal{Q}$, $\xi(t) \notin \overline{\text{in} \mathcal{Q}} \setminus \mathcal{W}(\mathcal{C}_{\mathcal{R}})$ for $t \geq T$. If the assumptions of Lemma 8.10 hold, then the local inset $\mathcal{W}(\mathcal{C}_{\mathcal{R}})$ is of measure zero, so $\overline{\text{in} \mathcal{Q}}$ is almost repulsive by Definition 8.15. \square

The following lemma states that the absolute path-following error $|\phi(\xi(t))|$ is indeed bounded.

Lemma 8.18 (Bounded path-following error). *If $\mathcal{C}_{\mathcal{P}}$ is bounded, then the absolute path-following error $|\phi(\xi(t))|$ of any trajectory $\xi(t)$ of (8.10) is bounded.*

Proof. Suppose a trajectory of (8.10) is defined on the time interval $\mathcal{T} = [0, T_f]$, where $T_f \leq \infty$. We want to prove that there exists a positive finite constant M such that $|\phi(\xi(t))| \leq M$ for all $t \in \mathcal{T}$. First, it is obvious that the absolute path-following error $|\phi(\cdot)| : \mathbb{R}^2 \rightarrow \mathbb{R}$ is continuous. Depending on where a trajectory $\xi(t)$ lies, three cases are discussed.

Case 1: Suppose the trajectory $\xi(t)$ always lies in the closed reactive area $\overline{\text{in} \mathcal{R}}$, then $|\phi(\xi(t))|$ attain its maximum value on the compact set $\overline{\text{in} \mathcal{R}}$. Namely, $|\phi(\xi(t))| \leq M_1$ for all $t \in \mathcal{T}$, where $M_1 = \max_{p \in \overline{\text{in} \mathcal{R}}} |\phi(p)|$.

Case 2: Suppose the trajectory $\xi(t)$ always lies in the closed non-reactive area $\overline{\text{ex} \mathcal{R}}$, then the differential equation (8.10) is reduced to $\dot{\xi} = \hat{\chi}_{\mathcal{P}}(\xi)$. By Lemma 8.8, the trajectory either converges to the desired path \mathcal{P} or the singular set $\mathcal{C}_{\mathcal{P}}$. a) Suppose the trajectory $\xi(t)$ converges to the desired path \mathcal{P} as $t \rightarrow T_f$; that is, $|\phi(\xi(t))| \rightarrow 0$ as $t \rightarrow T_f$. Then, fixing $\epsilon > 0$ such that $|\phi(\xi(0))| > \epsilon$, there exists $0 < T' < T_f$, such that $|\phi(\xi(t))| < \epsilon$ for $t > T'$. Let $\gamma := \max_{0 \leq t \leq T'} |\phi(\xi(t))|$, then the magnitude of the path-following error is bounded by $\max\{\epsilon, \gamma\} = \gamma = |\phi(\xi(0))|$, where the last equality is due to the decreasing property of the Lyapunov function $V = 1/2 \phi^2(\xi)$, which will be elaborated in **Case 3** later. b) If the trajectory $\xi(t)$ converges to the set $\mathcal{C}_{\mathcal{P}}$ (it is naturally assumed that $\mathcal{C}_{\mathcal{P}} \subseteq \overline{\text{ex} \mathcal{R}}$, otherwise it is trivial), then there exists $0 < T'' < T_f$, such that $\text{dist}(\xi(t), \mathcal{C}_{\mathcal{P}}) < \epsilon$ for $t > T''$. It follows that $\xi(t) \in \mathcal{C}'_{\mathcal{P}} := \{p \in \mathbb{R}^2 : \text{dist}(p, \mathcal{C}_{\mathcal{P}}) \leq \epsilon\}$ for $t > T''$.

⁹ In this case, replace $\mathcal{P}, \phi, \chi_{\mathcal{P}}$, and $\mathcal{C}_{\mathcal{P}}$ with $\mathcal{R}, \varphi, \chi_{\mathcal{R}}$, and $\mathcal{C}_{\mathcal{R}}$ respectively in the lemma.

Since \mathcal{C}_P is bounded (hence compact), the set \mathcal{C}'_P is compact. Therefore, we can let $\beta := \max_{x \in \mathcal{C}'_P} |\phi(x)|$. Let $\alpha := \max_{0 \leq t \leq T''} |\phi(\xi(t))|$, then the magnitude of the path-following error is bounded by $\max\{\alpha, \beta\}$. Overall, in both sub-cases a) and b), the magnitude of the path-following error $|\phi(\xi(t))|$ is bounded by $M_2 := \max\{\gamma, \alpha, \beta\}$.

Case 3: Suppose the trajectory lies alternately in $\overline{\text{ex}\mathcal{R}}$ and $\overline{\text{in}\mathcal{R}}$. First, we suppose $\xi(0) \in \overline{\text{in}\mathcal{R}}$. Denote all maximal connected closed intervals by $\rho_j \subseteq \mathcal{T}, j = 1, 2, \dots$, such that $\xi(t) \in \overline{\text{in}\mathcal{R}}$ for $t \in \rho_j$. Similarly, denote all maximal connected closed intervals by $\delta_k \subseteq \mathcal{T}, k = 1, 2, \dots$, such that $\xi(t) \in \overline{\text{ex}\mathcal{R}}$ for $t \in \delta_k$. For $t \in \bigcup_j \rho_j$, it follows that $|\phi(\xi(t))| \leq M_1$ according to **Case 1**. Therefore, we only need to consider the time intervals δ_k over which the trajectory is in the closed non-reactive area $\overline{\text{ex}\mathcal{R}}$. For convenience, the minimum value in δ_k is denoted by δ_k^1 (i.e., the first time instant). As **Case 2**, the differential equation (8.10) is reduced to $\dot{\xi} = \hat{\chi}_P(\xi)$. If $\mathcal{W}(\mathcal{C}_P) \cap \mathcal{R} = \emptyset$, given $\xi(\delta_k^1) \in \mathcal{R}$, the trajectory will not converge to any points in \mathcal{C}_P . Using the Lyapunov function candidate $V(\phi(\xi)) = 1/2 \phi^2(\xi)$ and taking the time derivative, one obtains

$$\frac{d}{dt} V(\phi(\xi)) = -k_p \frac{S(\xi)}{\|\chi_P(\xi)\|} \phi^2(\xi) \|\nabla \phi(\xi)\|^2.$$

This shows that $V(\phi(\xi(t)))$, hence $|\phi(\xi(t))|$ is decreasing as t increases. Therefore, for each time interval δ_k , $|\phi(\xi(t))|$ attains its maximum value $\max_{t \in \delta_k} |\phi(\xi(t))| = |\phi(\xi(\delta_k^1))| \leq M_3$, where $M_3 := \max_{p \in \mathcal{R}} |\phi(p)|$ (maximum attainable due to the compactness of the boundary \mathcal{R}). Therefore, for all $t \in \bigcup_k \delta_k$, $|\phi(\xi(t))| \leq M_3 \leq M_1$. Now we suppose $\xi(0) \in \overline{\text{ex}\mathcal{R}}$, then using the same analysis as before, it can be easily concluded that for all $t \in \bigcup_k \delta_k$, $|\phi(\xi(t))| \leq \max\{M_1, d_0\}$, where $d_0 = |\phi(\xi(0))|$. If the trajectory converges to the singular set \mathcal{C}_P , then using the same analysis discussed in **Case 2**, the absolute path-following error $|\phi(\xi(t))|$ is bounded by $\max\{\alpha, \beta\}$. Overall, the magnitude of the path-following error $|\phi(\xi(t))|$ is bounded by $M_3 := \max\{M_1, \alpha, \beta\}$. To sum up, the magnitude of the path-following error $|\phi(\xi(t))|$ is bounded by $M := \max\{M_1, \alpha, \beta, \gamma\}$. \square

Remark 8.19. Suppose the trajectory does not converge to the singular set \mathcal{C}_P , then it is interesting to note that the upper bound M of the absolute path-following error $|\phi(\xi(t))|$ is only related to the initial error $\gamma = |\phi(\xi(0))|$ and the largest error between the reactive area $\overline{\text{in}\mathcal{R}}$ and the desired path P (i.e., $M_1 = \max_{p \in \overline{\text{in}\mathcal{R}}} |\phi(p)|$). Thus this upper bound can be reduced by starting a trajectory near the desired path or shrinking the reactive area. \triangleleft

In the sequel, the properties of the mixed area $\mathcal{M} = \text{ex}\mathcal{Q} \cap \overline{\text{in}\mathcal{R}}$ will be investigated. First it can be shown that the closed mixed area $\overline{\mathcal{M}}$ is not positively invariant. Since $P \not\subseteq \overline{\text{in}\mathcal{R}}$, there exists at least one vector on the reactive boundary which points from the boundary to the desired path. More precisely, there exists

$p \in \mathcal{R}$ such that $\chi_c(p) = a(p)\hat{\chi}_{\mathcal{P}}(p)$ is not in the tangent cone¹⁰ of the closed mixed area $\overline{\mathcal{M}}$. By the Nagumo's theorem (see Theorem 2.13), the closed mixed area $\overline{\mathcal{M}}$ is not positively invariant. Thus there exists at least one point $\xi_0 \in \overline{\mathcal{M}}$ and $T > 0$, such that the trajectory at time T satisfies $\xi(T) \notin \overline{\mathcal{M}}$. However, the non-positive-invariance property of the closed mixed area is not sufficient to guarantee that any trajectory will not be trapped in this area. In fact, the next lemma demonstrates a limitation of combining two vector fields.

Lemma 8.20 (A common limitation). *If $\mathcal{C}_{\mathcal{P}} \cap {}^{\text{in}}\mathcal{R} = \emptyset$, then there is at least one saddle point of (8.10) in the mixed area \mathcal{M} .*

Proof. Note that on the repulsive boundary \mathcal{Q} , the vector field is simplified to

$$\hat{\chi}_{\mathcal{R}}(\xi) = \frac{\sqrt{k_r^2 c^2 + 1}}{\|\chi_{\mathcal{R}}\|} \cdot \underbrace{\frac{1}{\sqrt{k_r^2 c^2 + 1}} (E - k_r c I)}_F \nabla \varphi, \quad (8.14)$$

where $I \in \mathbb{R}^{2 \times 2}$ is the identity matrix and $F \in SO(2)$ is a rotation matrix. Therefore, the (Poincaré) index (see Definition 2.16) of the boundary \mathcal{Q} is 1 since the vector $\hat{\chi}_{\mathcal{R}}(\xi)$ rotates an angle of 2π counterclockwise when a point ξ traverses the boundary \mathcal{Q} in the counterclockwise direction (this also implies that there is at least one equilibrium point in ${}^{\text{in}}\mathcal{Q}$). On the reactive boundary \mathcal{R} , the vector field is simplified to $\hat{\chi}_{\mathcal{P}}(\xi)$. Now imagine that the whole plane is filled with only $\hat{\chi}_{\mathcal{P}}(\xi)$, given $\mathcal{C}_{\mathcal{P}} \cap {}^{\text{in}}\mathcal{R} = \emptyset$, the index of the reactive boundary \mathcal{R} is 0. Since the vector field remains the same on \mathcal{R} for the composite vector field χ_c , the index of \mathcal{R} is still 0. As the composite vector field χ_c is still continuous, we can conclude by the index theorem (see Theorem 2.17) that there must exist at least one saddle point in the mixed area \mathcal{M} . This is justified as follows. By the index theorem, the index of a saddle point is -1 , and the index of a node or a focus or a center is 1. Denote the number of saddle points in the repulsive area ${}^{\text{in}}\mathcal{Q}$ and the mixed area \mathcal{M} by $a_1 \geq 0$ and $a_2 \geq 0$, respectively, and denote the total number of nodes, foci and centers in the repulsive area ${}^{\text{in}}\mathcal{Q}$ and the mixed area \mathcal{M} by $b_1 \geq 0$ and $b_2 \geq 0$, respectively. Since the index of the repulsive boundary \mathcal{Q} is 1, we have $-a_1 + b_1 = 1$. Similarly, since the index of the reactive boundary \mathcal{R} is 0, we have $-a_1 + b_1 - a_2 + b_2 = 0$, which implies that $a_2 = b_2 + 1 \geq 1$. Therefore, at least one saddle point exists in \mathcal{M} . \square

Remark 8.21. We impose the condition $\mathcal{C}_{\mathcal{P}} \cap {}^{\text{in}}\mathcal{R} = \emptyset$ here because this condition holds in many practical examples. For example, when the desired path is a straight line characterized by $\phi(x, y) = y$, then $\mathcal{C}_{\mathcal{P}} = \emptyset$ and the condition $\mathcal{C}_{\mathcal{P}} \cap {}^{\text{in}}\mathcal{R} = \emptyset$ automatically holds. This condition is also satisfied for all examples

¹⁰ The tangent cone to a closed set $\mathcal{A} \subseteq \mathbb{R}^2$ at a point $x \in \mathbb{R}^2$ is defined as $\mathcal{T}_{\mathcal{A}}(x) = \{v \in \mathbb{R}^2 : \liminf_{h \rightarrow 0} \text{dist}(x + hv, \mathcal{A})/h = 0\}$.

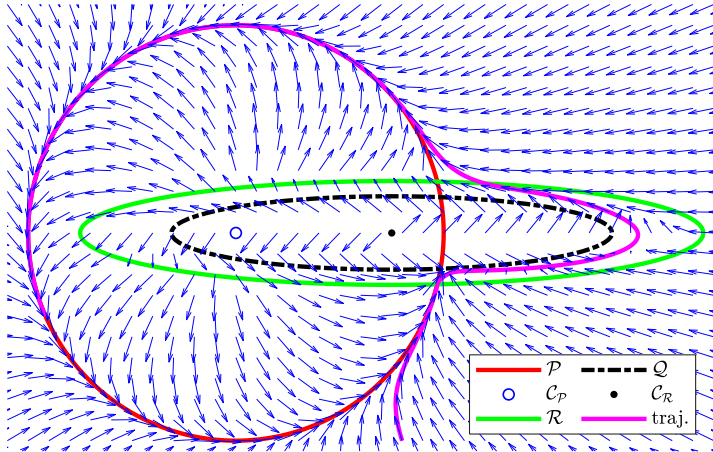


Figure 8.4: In this example, the reactive area ${}^{\text{in}}\mathcal{R}$ is enlarged such that $\mathcal{C}_P \cap {}^{\text{in}}\mathcal{R} \neq \emptyset$, and thereby Lemma 8.20 does not hold. Numerical calculation shows no equilibria in the mixed area \mathcal{M} , and thus $\mathcal{C}_c = \emptyset$ in (8.11).

in Section 8.7. Moreover, the number of saddle points is exactly one more than the total number of nodes, foci and centers in the mixed area as shown in the proof. This is a topological limitation of the composite vector field regardless of the specific form of the reactive boundary, the repulsive boundary and the zero-in and zero-out functions (i.e., the choice of $S(\xi)$ and $Z(\xi)$). The best we can hope for is that there is only one saddle point in the mixed area, and thus trajectories starting from almost all initial conditions will *not* be attracted to the saddle point. However, note that if $\mathcal{C}_P \cap {}^{\text{in}}\mathcal{R} \neq \emptyset$, then it is possible that there are no equilibria in the mixed area \mathcal{M} (see Fig. 8.4), and thus this limitation can be removed. This is perhaps surprising since a similar limitation *always* exists in traditional motion planning algorithms based on potential functions or navigation functions [68], [120] \triangleleft

In the path-following problem (without obstacles), it is desirable that there are no singular points (i.e., $\mathcal{C}_P = \emptyset$) such that global convergence to the desired path is guaranteed by Lemma 8.8. In contrast, as implied by Lemma 8.20, the emptiness of the singular set \mathcal{C}_P is not desirable when there are obstacles, since the condition $\mathcal{C}_P \cap {}^{\text{in}}\mathcal{R} = \emptyset$ of Lemma 8.20 holds automatically, implying the existence of a saddle point in \mathcal{M} .

We will prove that almost all initial points give rise to trajectories leaving the closed mixed area $\overline{\mathcal{M}}$ after some time. The following definition explains what is meant by trajectories leaving a set.

Definition 8.22. A trajectory $\xi : \mathbb{R} \rightarrow \mathbb{R}^2$ leaves a nonempty set $\mathcal{A} \subseteq \mathbb{R}^2$ if there exists $t_1 > t_0$ such that $\xi(t_0) \in \mathcal{A}$ and $\xi(t_1) \notin \mathcal{A}$.

The definition implies that whether a trajectory will enter the set \mathcal{A} again (and remain or not remain there) is irrelevant. We present the following lemma.

Lemma 8.23 (Leaving $\overline{\mathcal{M}}$). *Suppose $\mathcal{C}_P \cap {}^{in}\mathcal{R} = \emptyset$ and there is only one equilibrium point (i.e., a saddle point) $c_0 \in \mathcal{C}_c$ in the mixed area \mathcal{M} . Furthermore, suppose there exists a trajectory $\xi(t)$ starting from the repulsive boundary \mathcal{Q} and reaching the reactive boundary \mathcal{R} , then trajectories starting from almost all initial points in the closed mixed area $\overline{\mathcal{M}}$ will leave $\overline{\mathcal{M}}$.*

Proof. From Lemma 8.20, the only equilibrium in the mixed area \mathcal{M} is a saddle point. Thus the initial conditions of trajectories that converge to the saddle point form a set of measure zero. Since the index of the saddle point is -1 , there are no closed orbits around it. Closed orbits could only be possible when they surround the repulsive area ${}^{in}\mathcal{Q}$. However, since there is a trajectory moving from the repulsive boundary \mathcal{Q} to the reactive boundary \mathcal{R} , such closed orbits cannot exist, as there would be violation of the uniqueness of solutions (see Theorem 2.1). Therefore, trajectories starting from almost all initial points in the closed mixed area $\overline{\mathcal{M}}$ will leave $\overline{\mathcal{M}}$ by the Poincaré-Bendixson theorem (see Theorem 2.15). \square

We are now ready to present the main theorem.

Theorem 8.24. *The VF-CAPF problem with the vector field in (8.8) is solved if the following conditions hold simultaneously:*

- C.1** $\mathcal{W}(\mathcal{C}_R) \cap \mathcal{Q} = \emptyset$, \mathcal{C}_P is bounded, and the initial condition $\xi(0) \notin \mathcal{W}(\mathcal{C}_P)$;
- C.2** $\mathcal{C}_P \cap {}^{in}\mathcal{R} = \emptyset$ and there is only one equilibrium $c_0 \in \mathcal{C}_c$ in the mixed area \mathcal{M} ;
- C.3** There exists a trajectory $\xi(t)$ starting from the repulsive boundary \mathcal{Q} and reaching the reactive boundary \mathcal{R} .

Proof. If there are no obstacles and given that $\xi(0) \notin \mathcal{W}(\mathcal{C}_P)$, then due to Lemma 8.8, the first control objective of the VF-CAPF problem is achieved. Given that $\mathcal{W}(\mathcal{C}_R) \cap \mathcal{Q} = \emptyset$, Lemma 8.16 and Corollary 8.17 imply that the second control objective of the VF-CAPF problem in Definition 8.5 is fulfilled. Since \mathcal{C}_P is bounded, Lemma 8.18 shows that the magnitude of the path-following error is bounded, and the third control objective is met. Next, under conditions **C.2** and **C.3**, Lemma 8.23 shows that almost all initial points in the closed mixed area $\overline{\mathcal{M}}$ give rise to trajectories leaving $\overline{\mathcal{M}}$. Due to the uniqueness of solutions, the vector field degenerates to the normalized path-following vector field $\chi_c = \hat{\chi}_P$ once the trajectory leaves the reactive area. Then the trajectory will follow the desired path until it possibly returns to the reactive area again. Since $S(\xi)$ and $Z(\xi)$ are bounded, the norm of the composite vector field $\|\chi_c\|$ is finite. Therefore, the time difference between two consecutive time instants $\Delta t_r > 0$ of entry from the non-reactive area into the reactive area cannot be infinitely small. Thus the fourth control objective is accomplished. \square

Remark 8.25. The technical results in this section still hold if one replaces the normalized vector fields $\hat{\chi}_{\mathcal{P}}$ and $\hat{\chi}_{\mathcal{R}_i}$ with the original ones $\chi_{\mathcal{P}}$ and $\chi_{\mathcal{R}_i}$ in (8.8); i.e., (8.8) is changed to $\chi_c(\xi) = (\prod_{i \in \mathcal{I}} \sqcup_{Q_i}(\xi)) \chi_{\mathcal{P}}(\xi) + \sum_{i \in \mathcal{I}} (\sqcap_{\mathcal{R}_i}(\xi) \chi_{\mathcal{R}_i}(\xi))$. This is because the core technical proofs rely on the Lyapunov analysis of the vector fields $\chi_{\mathcal{P}}$ or $\chi_{\mathcal{R}_i}$ separately. The proofs of the results for the new composite vector field with the original vector fields $\chi_{\mathcal{P}}$ and $\chi_{\mathcal{R}_i}$ are almost the same except for minor changes; e.g., (8.13) and (8.14) need to be multiplied by $\|\chi_{\mathcal{R}}\|$ without affecting the subsequent technical development. \triangleleft

The local insets $\mathcal{W}(\mathcal{C}_{\mathcal{R}})$ and $\mathcal{W}(\mathcal{C}_{\mathcal{P}})$ in Condition C.1 can be numerically calculated¹¹. Fortunately, the calculation can be avoided for some typical desired paths or boundaries, such as circles or ellipses, since the local insets are the same as the singular sets. More generally, sufficient conditions to avoid the calculation of $\mathcal{W}(\cdot)$ are given in Corollary 8.26, which results from combining Lemma 8.10 and Theorem 8.24.

Corollary 8.26. Suppose the singular sets $\mathcal{C}_{\mathcal{P}}$ and $\mathcal{C}_{\mathcal{R}}$ are discrete, $\phi(p)H_{\phi}(p)$ and $\varphi(q)H_{\varphi}(q)$ have all negative eigenvalues for every point $p \in \mathcal{C}_{\mathcal{P}}, q \in \mathcal{C}_{\mathcal{R}}$. The VF-CAPF problem with the vector field in (8.8) is solved if the conditions in Theorem 8.24 hold, where $\mathcal{W}(\mathcal{C}_{\mathcal{R}}) = \mathcal{C}_{\mathcal{R}}$ and $\mathcal{W}(\mathcal{C}_{\mathcal{P}}) = \mathcal{C}_{\mathcal{P}}$.

Remark 8.27. Conditions C.2 and C.3 in Theorem 8.24 might probably hold in practice, even though they are difficult to verify in theory. Condition C.2 might be satisfied by changing some design choices: a) the function ϕ characterizing the desired path \mathcal{P} ; b) the function φ and the constant c characterizing the repulsive boundary \mathcal{Q} and reactive boundary \mathcal{R} , and c) the functions $S(\cdot)$ and $Z(\cdot)$ in the smooth zero-in and zero-out functions. Condition C.3 is not conservative because the existence of only one such trajectory is sufficient, but it is challenging to verify analytically. This condition is employed here to eliminate the possibilities of limit cycles in the mixed area, ensuring that trajectories can eventually leave the mixed area. Note that the proof of existence and non-existence of limit cycles in general is a challenging problem in nonlinear systems theory. There are only a few available tools, such as the Poincaré-Bendixson theorem, the Bendixson criterion and index theory [66, Lemma 2.1-2.3], [149, Chapter 9]. These tools might be used to verify condition C.3. \triangleleft

The main disadvantages of the composite vector field approach discussed above are: a) Conditions C.2 and C.3 are difficult to check; b) In many cases, the limitation revealed in Lemma 8.20 exists. However, Conditions C.2 and C.3 are crucial to avoid the well-known phenomenon called *deadlock*, but few algorithms in the literature provide a theoretical guarantee to avoid it [171]. Nevertheless, we will use a *switching vector field* in Section 8.5 to replace these two conditions with easily-verifiable ones and also remove the limitation in Lemma 8.20.

¹¹ For instance, if the singular points are hyperbolic, then the local insets are manifolds [124, Theorem 7.6] that can be numerically computed via the graph transform method or the Lyapunov-Perron method [149, Chapter 3.5], [97], [109]

8.5 SWITCHING VECTOR FIELD

To replace the two conditions mentioned earlier and deal with undesirable equilibria in the mixed area, we introduce a switching vector field and prove that this switching vector field can solve the VF-CAPF problem.

Singular points in the mixed area \mathcal{M} appear where the components $S(\xi)\hat{\chi}_P(\xi)$ and $Z(\xi)\hat{\chi}_R(\xi)$ in (8.7) cancel each other. Specifically, this happens only if $S(\xi) = Z(\xi)$. Namely, the extra singular points (should they exist) belong to the following set

$$\mathcal{E} = \{\xi \in \mathbb{R}^2 : S(\xi) = Z(\xi)\}. \quad (8.15)$$

This set \mathcal{E} is nonempty since the functions $S(\cdot), Z(\cdot)$ are continuous, and $S(\cdot)$ decreases to 0 “radially inwardly” towards the repulsive boundary \mathcal{Q} , whereas $Z(\cdot)$ decreases to 0 “radially outwardly” towards the reactive boundary \mathcal{R} . In addition, \mathcal{E} is compact and $\mathcal{E} \subsetneq \mathcal{M}$; i.e., this set does not intersect the reactive boundary \mathcal{R} or the repulsive boundary \mathcal{Q} . The functions $S(\cdot)$ and $Z(\cdot)$ are flexible design choices and characterize the set \mathcal{E} . For simplicity of analysis, the functions $S(\cdot)$ and $Z(\cdot)$ are designed such that the set \mathcal{E} only contains “rings”. More precisely, the set \mathcal{E} constitutes a finite number of one-dimensional compact connected submanifolds in \mathbb{R}^2 . In Section 8.7, we illustrate how to design these functions.

The closed ϵ -neighborhood \mathcal{E}^ϵ of the set \mathcal{E} is $\mathcal{E}^\epsilon = \{\xi \in \mathcal{M} : \text{dist}(\xi, \mathcal{E}) \leq \epsilon\}$, where $\epsilon > 0$. Due to the compactness of \mathcal{E} and \mathcal{R} , and $\mathcal{E} \cap \mathcal{R} = \emptyset$, one can always choose an $\epsilon > 0$ sufficiently small such that¹² $\text{dist}(\mathcal{E}^\epsilon, \mathcal{R}) > 0$. The basic idea is that if a trajectory enters \mathcal{E}^ϵ , then it will possibly be attracted to a stable equilibrium in \mathcal{M} . Nevertheless, we can then switch to another vector field such that this possibility is excluded. This new vector field is designed as a “perturbed” version of the reactive vector field in the sense that it is induced by a slightly enlarged reactive boundary, as introduced in the sequel. The existence of an enlarged reactive boundary is guaranteed by the following lemma.

Lemma 8.28. *Given φ and \mathcal{R} in (8.2), there exists a constant $\delta \neq 0$ such that $\mathcal{R}_\delta := \varphi^{-1}(\delta) = \{\xi \in \mathbb{R}^2 : \varphi(\xi) = \delta\}$ is a one-dimensional compact connected submanifold in \mathbb{R}^2 , also satisfying $\text{dist}(\mathcal{R}, \mathcal{R}_\delta) > 0$ and ${}^{in}\mathcal{R} \subseteq {}^{in}\mathcal{R}_\delta$, where ${}^{in}\mathcal{R}_\delta$ is the perturbed reactive area defined analogously to ${}^{in}\mathcal{R}$.*

Proof. From Section 8.2, one knows that 0 is a regular value of φ , and $\mathcal{R} = \varphi^{-1}(0)$ is a one-dimensional compact connected submanifold in \mathbb{R}^2 (i.e., $\varphi^{-1}(0)$ is homeomorphic to \mathbb{S}^1). By the Ehresmann theorem [30, p. 378], which can be regarded as a generalization of the Morse theorem [106, Theorem 2.6], there exists an open interval \mathcal{I} of 0 such that $\varphi^{-1}(\mathcal{I})$ is homeomorphic to $\mathcal{I} \times \varphi^{-1}(0)$, given by a homeomorphism denoted by Γ , such that $\pi_{\mathcal{I}} \circ \Gamma = \varphi|_{\varphi^{-1}(\mathcal{I})}$, where

¹² Since $\text{dist}(\mathcal{E}, \mathcal{R}) := \delta > 0$, one can, for instance, choose $\epsilon = \delta/2$ such that $\text{dist}(\mathcal{E}^\epsilon, \mathcal{R}) > 0$, according to [136, Chapter 1, Lemma 3.1].

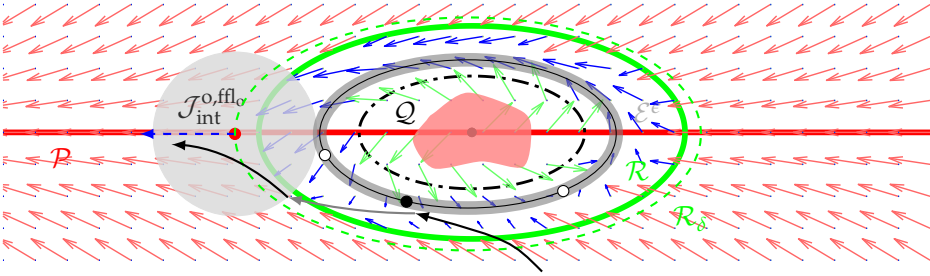


Figure 8.5: Notations for the switching vector field (8.17). The pink irregular shape is the obstacle. The dot-dashed black line is the repulsive boundary \mathcal{Q} . The solid black line is \mathcal{E} and the shaded area around \mathcal{E} is ϵ -neighborhood \mathcal{E}^ϵ . Two white points on the solid line \mathcal{E} are saddle points, and the black point is a stable equilibrium of (8.10). The solid green line and dashed green line are the reactive boundary \mathcal{R} and the perturbed reactive boundary \mathcal{R}_δ , respectively. The red horizontal solid line is the desired path \mathcal{P} . The red point is an intersection point between \mathcal{R}_δ and \mathcal{P} , where a blue arrow represents the outward-pointing normal of \mathcal{R}_δ . The gray disk symbolizes the set $\mathcal{J}_{\text{int}}^{0,ffl}$ in (8.16). Three arrows compose a trajectory starting from beyond the reactive area, where the black and gray arrows correspond to $\sigma = 1$ and $\sigma = 2$ respectively.

$\pi_{\mathcal{I}}$ is the projection onto the first factor. Therefore, for any $q \in \mathcal{I}$, the level curve $\varphi^{-1}(q)$ is homeomorphic to $\mathcal{R} = \varphi^{-1}(0)$; namely, $\varphi^{-1}(q)$ is a one-dimensional compact connected submanifold in \mathbb{R}^2 for any $q \in \mathcal{I}$, and thus $\text{dist}(\mathcal{R}, \mathcal{R}_q) > 0$ for any $q \in \mathcal{I}$, where $\mathcal{R}_q := \varphi^{-1}(q)$. Moreover, choose an $\alpha \in \mathcal{I}$ such that $\alpha \neq 0$ and $-\alpha \in \mathcal{I}$. Let $\delta = \alpha$. If ${}^{\text{in}}\mathcal{R} \subseteq {}^{\text{in}}\mathcal{R}_\delta$ is satisfied, then the proof is complete; otherwise, we choose $\delta = -\alpha$. \square

Remark 8.29. This lemma means that the shape of the level set $\varphi^{-1}(\delta)$ is similar to the zero-level set $\varphi^{-1}(0) = \mathcal{R}$. More precisely, $\varphi^{-1}(\delta)$ is homeomorphic to the reactive boundary \mathcal{R} . For example, suppose the reactive boundary enclosing an obstacle is an ellipse, characterized by $\varphi = x^2/a^2 + y^2/b^2 - 1 = 0$, where $a, b \neq 0$ are constants. All the level sets $\varphi^{-1}(k)$ for $k > -1$ are ellipses of different sizes. \triangleleft

Note that the only difference in the definition of \mathcal{R}_δ from that in (8.2) is the constant δ . Therefore, we can similarly derive a *perturbed reactive vector field* $\chi_{\mathcal{R}_\delta}$ by replacing the level function φ with $\varphi^\delta := \varphi - \delta$ in (8.5). This notation also implies that $\varphi^0 = \varphi$. Accordingly, we define the singular set $\mathcal{C}_{\mathcal{R}_\delta}$ corresponding to this perturbed reactive vector field $\chi_{\mathcal{R}_\delta}$ as $\mathcal{C}_{\mathcal{R}_\delta} := \{\xi \in \mathbb{R}^2 : \chi_{\mathcal{R}_\delta}(\xi) = 0\} = \{\xi \in \mathbb{R}^2 : \nabla \varphi^\delta(\xi) = 0\}$. Since $\varphi^\delta = \varphi - \delta \implies \nabla \varphi^\delta = \nabla \varphi$, it turns out that

the singular set for the perturbed reactive vector field is the same as that for the reactive vector field; i.e.,

$$\mathcal{C}_{\mathcal{R}_\delta} = \mathcal{C}_{\mathcal{R}}.$$

We define $\mathcal{J}_{\text{int}} := \mathcal{R}_\delta \cap \mathcal{P} \neq \emptyset$, which is the set of all intersection points between the perturbed reactive boundary \mathcal{R}_δ and the desired path \mathcal{P} . For simplicity, we assume that this set \mathcal{J}_{int} is finite, as otherwise, one can choose a different perturbed reactive boundary \mathcal{R}_δ such that this assumption holds. The *outward-pointing normal* [141] of the perturbed reactive boundary \mathcal{R}_δ at a point $q \in \mathcal{R}_\delta$, denoted by $N_0(q) \in \mathbb{S}^1 \subseteq \mathbb{R}^2$, is an outward-pointing unit vector perpendicular to \mathcal{R}_δ at $q \in \mathcal{R}_\delta$. Now we can define the set of points where the path-following vector field $\chi_{\mathcal{P}}$ points towards a similar direction to the outward-pointing normal of \mathcal{R}_δ at the intersection points: $\mathcal{J}_{\text{int}}^o := \{\xi \in \mathcal{J}_{\text{int}} : \hat{\chi}_{\mathcal{P}}(\xi)^\top N_0(\xi) > 0\}$, which is a finite set. Starting from any point of this set, the integral curves of the path-following vector field will be “driven out” of the perturbed reactive area ${}^{\text{in}}\mathcal{R}_\delta$. Due to the continuity of $\hat{\chi}_{\mathcal{P}}$ and the finiteness of $\mathcal{J}_{\text{int}}^o$, one can choose an $\epsilon_o > 0$ sufficiently small such that for every two distinct intersection points $q_i, q_j \in \mathcal{J}_{\text{int}}^o$, their closed ϵ_o -neighborhoods are disjoint (i.e., $q_i^{\epsilon_o} \cap q_j^{\epsilon_o} = \emptyset$, where $q_i^{\epsilon_o} := \{\xi \in \mathbb{R}^2 : \text{dist}(\xi, q_i) \leq \epsilon_o\}$ and $q_j^{\epsilon_o}$ is defined similarly), and in each of these ϵ_o -neighborhood, $\hat{\chi}_{\mathcal{P}}$ points towards a similar direction to the outward-pointing normal at the corresponding intersection point; namely, $\forall q \in \mathcal{J}_{\text{int}}^o$ and $\forall \xi \in q^{\epsilon_o}$, there holds $\hat{\chi}_{\mathcal{P}}(\xi)^\top N_0(q) > 0$. We define the union of these ϵ_o -neighborhoods to be

$$\mathcal{J}_{\text{int}}^{o,\text{ffl}_o} := \bigcup_{q \in \mathcal{J}_{\text{int}}^o} q^{\epsilon_o}. \quad (8.16)$$

See Fig. 8.5 for the introduced new concepts.

Now we consider the following switching system

$$\dot{\xi}(t) = \chi_{\sigma(t)}(\xi(t)), \quad (8.17)$$

where $\sigma : [0, \infty) \rightarrow \{1, 2\}$ is the *switching signal*¹³, of which the discrete transitions depend on its previous discrete state $\lim_{\tau \rightarrow t^-} \sigma(\tau)$ and the continuous state $\xi(t)$ at time t , as shown in Fig. 8.6. More precisely, $\sigma(t) = 1$ if $\lim_{\tau \rightarrow t^-} \sigma(\tau) = 2$ and $\xi(t) \in {}^{\text{ex}}\mathcal{R} \cap \mathcal{J}_{\text{int}}^{o,\text{ffl}_o}$, and the right-hand side of (8.17) becomes the composite vector field $\chi_1 = \chi_c$; $\sigma(t) = 2$ if $\lim_{\tau \rightarrow t^-} \sigma(\tau) = 1$ and $\xi(t) \in \mathcal{E}^e$, and the right-hand side of (8.17) becomes the perturbed reactive vector field $\chi_2 = \chi_{\mathcal{R}_\delta}$; otherwise, the switching signal retains the previous value: $\sigma(t) = \lim_{\tau \rightarrow t^-} \sigma(\tau)$. Solutions to (8.17) are interpreted *in the sense of Carathéodory* [82, p. 10]; that is, a

¹³ A switching signal is a piecewise constant function which attains a constant value between any two consecutive *switching times* (i.e., the discontinuities), and the number of switching times is finite on every bounded time interval [82, p. 6].

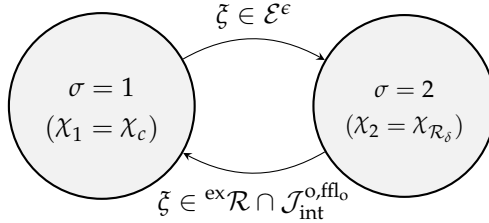


Figure 8.6: The discrete transitions of the switching signal σ in (8.17).

solution to (8.17) is an absolutely continuous function $\xi : [0, \infty) \rightarrow \mathbb{R}^n$ satisfying $\xi(t) = \xi(t_0) + \int_{t_0}^t \chi(\tau, \xi(\tau)) d\tau$, where $\chi(\tau, \xi(\tau))$ in the integral is adapted from the right-hand side of (8.17) to show its explicit dependence on time t due to the switching signal $\sigma(t)$. The solution is piecewise differentiable and satisfies the differential equation (8.17) almost everywhere.

Recall that Conditions **C.2** and **C.3** in Theorem 8.24 are used to prevent trajectories from converging to an attractive equilibrium in $\mathcal{C}_c \subseteq \mathcal{M}$ and from converging to a closed orbit in \mathcal{M} respectively. Namely, the common objective is to prevent trajectories from getting stuck in the mixed area \mathcal{M} . Using the switching vector field $\chi_{\sigma(t)}$, we can replace these two conditions with more verifiable ones in the following theorem.

Theorem 8.30. Suppose the functions $S(\cdot)$ and $Z(\cdot)$ in (8.7) are chosen such that the set \mathcal{E} in (8.15) is a one-dimensional connected manifold¹⁴. Consider the switching system (8.17), the VF-CAPF problem is solved if the following conditions hold simultaneously:

C.1 Condition **C.1** in Theorem 8.24; i.e., $\mathcal{W}(\mathcal{C}_{\mathcal{R}}) \cap \mathcal{Q} = \emptyset$, $\mathcal{C}_{\mathcal{P}}$ is bounded, and the initial condition $\xi(0) \notin \mathcal{W}(\mathcal{C}_{\mathcal{P}})$;

C.2 $\mathcal{W}(\mathcal{C}_{\mathcal{R}_{\delta}}) \cap \mathcal{E}^{\epsilon} = \emptyset$;

C.3 The initial conditions $\xi(0) \notin {}^{in}\mathcal{R}$ and $\sigma(0) = 1$.

In particular, the Zeno behavior does not occur.

Proof. Step 1: We first show that trajectories of (8.17) will not converge to any equilibrium points in \mathcal{E} . Precisely, trajectories of (8.17) will not converge to the set $\mathcal{S} := \mathcal{C}_c \cap \mathcal{E} = \mathcal{C}_c \cap \mathcal{E}^{\epsilon}$, where \mathcal{C}_c defined in (8.11) is the set of singular points of the composite vector field χ_c , which happens to be the set of equilibrium points of (8.17) when $\sigma = 1$. Note that the perturbed reactive vector field $\chi_{\mathcal{R}_{\delta}}$ is activated only if $\xi(t) \in \mathcal{E}^{\epsilon}$, but given condition **C.2** and the dichotomy convergence property (Lemma 8.8), trajectories of $\dot{\xi} = \chi_2(\xi) = \chi_{\mathcal{R}_{\delta}}(\xi)$ will not converge to \mathcal{S} . Therefore, it suffices to consider only the case $\sigma = 1$. Suppose there exists

¹⁴ Roughly speaking, \mathcal{E} is (the trace) of a simple closed curve.

a trajectory $\xi(t)$ of (8.17), where $\chi_{\sigma=1} = \chi_c$, converging to \mathcal{S} ; then there exists a time instant $T_1 \geq 0$ such that $\xi(T_1) \in \mathcal{E}^\epsilon$. In this case, the system switches to $\dot{\xi} = \chi_{\mathcal{R}_\delta}(\xi)$. However, as mentioned before, the trajectory will then converge to the perturbed reactive boundary \mathcal{R}_δ if no switching happened afterward. In particular, there exists $T_2 > T_1$ such that $\xi(T_2) \in \mathcal{R}$. Since $\text{dist}(\mathcal{E}, \mathcal{R}) > 0$, this implies that the trajectory cannot converge to \mathcal{S} .

Step 2: Now we show that there are no closed orbits in the reactive area ${}^{\text{in}}\mathcal{R}$ (given condition **C.3**). Using similar arguments as before, it suffices to investigate only the case when $\sigma = 1$ and the switching system (8.17) becomes $\dot{\xi} = \chi_c(\xi)$. As shown in the proof of Lemma 8.20, the index of the reactive boundary \mathcal{R} is 0. Since there are no equilibrium points between the reactive boundary \mathcal{R} and \mathcal{E} (precisely, ${}^{\text{in}}\mathcal{R} \cap {}^{\text{ex}}\mathcal{E}$, where ${}^{\text{ex}}\mathcal{E}$ is defined analogously to ${}^{\text{ex}}\mathcal{R}$), any closed orbit starting between the reactive boundary \mathcal{R} and \mathcal{E} must intersect \mathcal{E}^ϵ to enclose equilibria such that its index becomes 1 [66, Lemma 2.3]. Therefore, any trajectory corresponding to a closed orbit must intersect \mathcal{E}^ϵ , but then the vector field switches to $\chi_{\mathcal{R}_\delta}$. Therefore, there cannot be closed orbits in the reactive area ${}^{\text{in}}\mathcal{R}$.

Step 3: Now we show that trajectories will eventually leave the closed reactive area ${}^{\text{in}}\mathcal{R}$. *Step 1* has proved that any trajectories cannot converge to the set \mathcal{E} , since any such trajectories would be driven to move to the reactive boundary \mathcal{R} by the perturbed reactive vector field $\chi_{\sigma=2} = \chi_{\mathcal{R}_\delta}$. If the switching signal does not change to $\sigma = 1$, then the trajectory will converge to the perturbed reactive boundary \mathcal{R}_δ according to condition **C.2** and the dichotomy convergence property in Lemma 8.8. Since the switching signal only switches to $\sigma = 1$ if $\xi(t) \in {}^{\text{ex}}\mathcal{R} \cap \mathcal{J}_{\text{int}}^{\text{o,ffl}_0}$, this implies that the trajectory will eventually leave the closed reactive area ${}^{\text{in}}\mathcal{R}$. Moreover, once the condition $\xi(T) \in {}^{\text{ex}}\mathcal{R} \cap \mathcal{J}_{\text{int}}^{\text{o,ffl}_0}$ is satisfied at some time T , the vector field becomes $\chi_{\sigma=1} = \chi_c = \hat{\chi}_{\mathcal{P}}$. Due to the property of the set $\mathcal{J}_{\text{int}}^{\text{o,ffl}_0}$ in (8.16), the trajectory will eventually leave the perturbed reactive boundary \mathcal{R}_δ .

Step 4: Finally, we show that the Zeno behavior cannot occur. Let $d := \text{dist}(\mathcal{E}^\epsilon, \mathcal{R}) > 0$, and $v_m := \max_{\xi \in \overline{\mathcal{M}}} \{\chi_{\sigma=1}, \chi_{\sigma=2}\} < \infty$. Therefore, the duration Δt between any two switching time instants is lower bounded by $d/v_m > 0$, thus excluding the Zeno behavior. \square

Remark 8.31. One can observe that in this switching approach, the composite vector field χ_c degenerates to the normalized path-following vector field $\hat{\chi}_{\mathcal{P}}$, and the switching happens between $\hat{\chi}_{\mathcal{P}}$ and $\chi_{\mathcal{R}_\delta}$. Thus the design of the composite vector field seems redundant. However, the switching mechanism is only introduced to solve the deadlock problem. Once there is no such problem, then a composite vector field is more efficient as it can avoid the non-smooth and possible tortuous motion caused by the switching of different vector fields. \triangleleft

Similarly to Corollary 8.26, the following corollary facilitates the verification of the conditions in Theorem 8.30. Note that since $\varphi^\delta = \varphi - \delta$, the Hessian matrices satisfy $H_\varphi(\cdot) = H_{\varphi^\delta}(\cdot)$.

Corollary 8.32. *Consider the switching system (8.17) and suppose the singular sets \mathcal{C}_P and $\mathcal{C}_R = \mathcal{C}_{R_\delta}$ are discrete. If $\varphi(p)H_\varphi(p)$, $\varphi(q)H_\varphi(q)$ and $\varphi^\delta(q)H_\varphi(q)$ have all negative eigenvalues¹⁵ for every point $p \in \mathcal{C}_P$ and $q \in \mathcal{C}_R$, where $\varphi^\delta := \varphi - \delta$, then the VF-CAPF problem is solved if conditions in Theorem 8.30 hold, where $\mathcal{W}(\mathcal{C}_R) = \mathcal{W}(\mathcal{C}_{R_\delta}) = \mathcal{C}_R$ and $\mathcal{W}(\mathcal{C}_P) = \mathcal{C}_P$.*

8.6 DISCUSSIONS

8.6.1 Moving obstacles

In this section, we will re-design the reactive vector field $\chi'_R : \mathbb{R} \times \mathbb{R}^2 \rightarrow \mathbb{R}^2$ to include the “motion information” of obstacles, and thus obtain a new composite time-varying vector field $\chi'_c : \mathbb{R} \times \mathbb{R}^2 \rightarrow \mathbb{R}^2$. Note that since the desired path is still static, the path-following vector field $\chi_P : \mathbb{R}^2 \rightarrow \mathbb{R}^2$ remains unchanged. Also note that since the new reactive vector field χ'_R is time-varying (i.e., explicitly time-dependent), the normalization factor $1/\|\chi'_R\|$ of χ'_R is also time-varying, and thereby the phase portrait of $\hat{\chi}'_R$ is possibly different from that of the original vector field χ'_R (c.f., Remark 8.9). For this reason, we do not use normalized vector fields in (8.8), but retreat to

$$\chi'_c(t, \xi) = \left(\prod_{i \in \mathcal{I}} \sqcup_{Q_i}(\xi) \right) \chi_P(\xi) + \sum_{i \in \mathcal{I}} \left(\sqcap_{R_i}(t, \xi) \chi'_{R_i}(t, \xi) \right), \quad (8.18)$$

where we note that χ_P and χ'_{R_i} are not normalized. As mentioned in Section 8.2, we require that the motion of obstacles is sufficiently smooth in the sense that the function $\varphi_i(t, \xi)$, which is related to the reactive boundary of the i -th obstacle, is twice continuously differentiable in t . Again by Assumption 8.4, it is sufficient to consider only one moving obstacle.

To ensure the previous results still hold for the new reactive vector field (hence the new composite vector field), we use a Lyapunov analysis to derive the new vector field χ'_R . Specifically, we add an additional time-varying term to the original reactive vector field (8.5) as follows:

$$\chi'_R(t, \xi) = E \nabla \varphi(t, \xi) - k_r \varphi(t, \xi) \nabla \varphi(t, \xi) + \omega(t, \xi), \quad (8.19)$$

¹⁵ If $|\delta|$ is sufficiently small (i.e., $|\delta| \approx 0$), then the signs of eigenvalues of $\varphi(q)H_\varphi(q)$ and $\varphi^\delta(q)H_\varphi(q)$ for every point $q \in \mathcal{C}_R$ are the same. Therefore, one does not need to check the condition related to $\varphi^\delta(q)H_\varphi(q)$.

where $\nabla\varphi(t, \xi) := \frac{\partial\varphi(t, \xi)}{\partial\xi} \in \mathbb{R}^2$ and $\omega : \mathbb{R}_+ \times \mathbb{R}^2 \rightarrow \mathbb{R}^2$ is an additional term to be determined. We choose the Lyapunov function candidate $V(t, \xi) = \frac{1}{2}k\varphi^2(t, \xi)$, where k is a positive constant. Now we have

$$\begin{aligned}\frac{d}{dt}V(t, \xi) &= \frac{dV}{d\varphi}\nabla\varphi(t, \xi)^\top \dot{\xi} + \frac{dV}{d\varphi}\frac{\partial\varphi}{\partial t} \\ &\stackrel{(8.19)}{=} k\varphi\nabla\varphi^\top \chi'_{\mathcal{R}} + k\varphi\frac{\partial\varphi}{\partial t} \\ &= -kk_r\varphi^2\|\nabla\varphi\|^2 + k\varphi\left(\nabla\varphi^\top \omega + \frac{\partial\varphi}{\partial t}\right),\end{aligned}\quad (8.20)$$

where the second equation uses the equality $\dot{\xi} = \chi'_{\mathcal{R}}$ as we only consider the new reactive vector field $\chi'_{\mathcal{R}}$ now and conduct the Lyapunov analysis. Now let ω be chosen as

$$\omega = \frac{1}{\|\nabla\varphi\|^2} \left(-\frac{\partial\varphi}{\partial t} - l\varphi \right) \nabla\varphi,\quad (8.21)$$

where l is a positive constant. Substituting (8.21) into (8.20), we have $\frac{d}{dt}V(t, \xi) = -kk_r\varphi^2\|\nabla\varphi\|^2 - kl\varphi^2 \leq -2lV$. Therefore, by Theorem 4.9 in [66], the integral curves of the new reactive vector field in (8.19) will (globally) uniformly exponentially converge to the time-varying reactive boundary \mathcal{R} characterized by $\varphi(t, \xi) = 0$.

We have shown above that the new reactive vector field $\chi'_{\mathcal{R}}$ can still guide trajectories to converge to the reactive boundary \mathcal{R} , which is time-varying now due to the motion of the obstacle. Therefore, by combining (8.18), (8.19) and (8.21), we obtain a new composite vector field χ'_c , which is time-varying. The previous results still hold for this new composite vector field χ'_c , for which the proofs are almost the same (see Remark 8.25).

Remark 8.33. Note that to ensure the additional term ω in (8.21) is well defined, it is required that $\|\nabla\varphi\| \neq 0$. Fortunately, it is shown in Theorem 4.9 that this requirement is always satisfied locally for bounded paths. In other words, there exists a positive constant α such that the gradient $\nabla\varphi$ is non-zero in the reactive boundary's neighborhood $\mathcal{E}_\alpha := \{\xi \in \mathbb{R}^2 : |\varphi(\xi)| \leq \alpha\}$. For unbounded paths, it is required that $\|E\nabla\varphi\|$, or equivalently $\|\nabla\varphi\|$, is bounded away from zero on \mathcal{R} , and there exists a positive constant β such that $\|\nabla\varphi\|$ is upper-bounded in $\mathcal{E}_\beta := \{\xi \in \mathbb{R}^2 : |\varphi(\xi)| \leq \beta\}$ (see Theorem 4.15). \triangleleft

Remark 8.34 (Robustness). In practice, one might expect that the time derivative information $\frac{\partial\varphi}{\partial t}$ in (8.21) is contaminated by measurement error. Fortunately, the exponential convergence property mentioned above provides some robustness against this error. It turns out that we can still reduce the value of the Lyapunov function V to an arbitrarily small positive value by increasing the gain l in (8.21). This is justified as follows. Let the gain $l > 1/2 + \epsilon$, where $\epsilon > 0$ is a constant. Suppose some time-varying measurement error $\rho(t, \xi) \in \mathbb{R}$ is added

to the information of the time derivative $\frac{\partial \varphi}{\partial t}$. Therefore, (8.21) is perturbed as $\omega = \frac{1}{\|\nabla \varphi\|^2} \left(-\frac{\partial \varphi}{\partial t} + \rho - l\varphi \right) \nabla \varphi$, and (8.20) is changed to

$$\frac{d}{dt} V(t, \xi) = -kk_r \varphi^2 \|\nabla \varphi\|^2 - kl\varphi^2 + k\rho\varphi \quad (8.22)$$

$$\leq -\left(l - \frac{1}{2}\right)k\varphi^2 + \frac{1}{2}k\rho^2 \quad (8.23)$$

$$\leq -\epsilon k\varphi^2, \quad \forall |\varphi| \geq \alpha(|\rho|) > 0, \quad (8.24)$$

where (8.23) has used the fact that $\rho\varphi \leq \rho^2/2 + \varphi^2/2$, and $\alpha(|\rho|) = \frac{1}{\sqrt{2l-2\epsilon-1}}|\rho|$ is a class κ function. Therefore, by Theorem 4.9 in [66], the system $\dot{\xi}(t) = \chi'_{\mathcal{R}}(t, \xi)$, where $\chi'_{\mathcal{R}}(t, \xi)$ is in (8.19), is input-to-state stable (ISS) with respect to the measurement error ρ . If the measurement error is uniformly bounded $|\rho(\cdot)| < \rho_b$, where $\rho_0 > 0$ is a constant, this implies that by choosing $l > 1/2 + \epsilon$, the value of the Lyapunov function V will eventually decrease to within $V = k\varphi^2/2 \leq \frac{k\rho_b^2}{2(2l-2\epsilon-1)}$. By choosing a large ϵ , the decreasing rate of V is greater as observed from (8.24). Furthermore, one may assume that the measurement error is vanishing in the sense that $|\rho| \leq \beta|\varphi|$, where $\beta > 0$ is a constant. In this case, by choosing $l > \beta$, the Lyapunov function value V will decrease (globally) uniformly exponentially to 0. This is justified using the same argument as before. Namely, from (8.22), we have $\frac{d}{dt} V(t, \xi) = -kk_r \varphi^2 \|\nabla \varphi\|^2 - kl\varphi^2 + k\rho\varphi \leq -(l - \beta)k\varphi^2 = -2(l - \beta)V$, and then we can employ Theorem 4.9 in [66] to obtain the robustness result. \triangleleft

8.6.2 Higher-dimensional spaces

One of the advantages of using the composite vector field is its natural extension to any higher-dimensional spaces, since the path-following and reactive vector fields on higher-dimensional spaces have been studied in the literature (see Chapters 4 and 9 and [50]). We take the 3D case as an example. In \mathbb{R}^3 , a desired path \mathcal{P} is usually described by the intersection of two surfaces defined by the zero-level sets of ϕ_1 and ϕ_2 respectively, where $\phi_1, \phi_2 : \mathbb{R}^3 \rightarrow \mathbb{R}$ are twice continuously differentiable. Namely, the description in (8.1) is extended to $\mathcal{P} = \{\xi \in \mathbb{R}^3 : \phi_1(\xi) = 0, \phi_2(\xi) = 0\}$, and the path-following vector field becomes

$$\chi_{\mathcal{P}}(\xi) = \nabla \phi_1(\xi) \times \nabla \phi_2(\xi) - \sum_{i=1}^2 k_i \phi_i(\xi) \nabla \phi_i(\xi), \quad (8.25)$$

where k_i are positive constants. As for obstacles in 3D, the corresponding repulsive and reactive boundaries are naturally extended to be *repulsive surfaces* and *reactive surfaces* to avoid collision from all directions in 3D. Similarly, these two

surfaces can be defined respectively as the c -level surface and zero-level surface of a C^2 function $\varphi : \mathbb{R}^3 \rightarrow \mathbb{R}$. Similar to (8.25), the reactive vector field χ_R can be defined as

$$\chi_R(\xi) = \nabla \varphi(\xi) \times v - k_r \varphi(\xi) \nabla \varphi(\xi), \quad (8.26)$$

where $v \in \mathbb{R}^3$ is a constant vector indicating how to bypass the obstacle on the reactive surface $\varphi^{-1}(0)$. The 3D composite vector field is attained by substituting χ_P and χ_R in (8.8) by their 3D counterparts in (8.25) and (8.26) respectively. The extension to higher-dimensional spaces \mathbb{R}^n , where $n > 3$, is straightforward by using higher-dimensional vector fields in [50] or in Chapter 9. However, although the physical intuition is clear, the rigorous analysis in higher-dimensional spaces using dynamical systems theory is challenging; especially, the Poincaré-Bendixson theorem is no longer applicable for analysis. Exploring the provision of rigorous underpinnings will be left for future work, while a numerical simulation example in \mathbb{R}^3 is shown in Section 8.7.

8.6.3 Complicated robot models

To solve the VF-CAPF problem is to design a vector field $\chi : \mathbb{R}^2 \rightarrow \mathbb{R}^2$ such that its integral curves (that is, trajectories of the ODE $\dot{\xi}(t) = \chi(\xi)$, where $\xi \in \mathbb{R}^2$) fulfill the control objectives. In robotics, the ODE implies that the robot model is the single-integrator model:

$$\dot{\xi}(t) = u(t), \quad (8.27)$$

where $\xi(t) = (x(t), y(t))$ represents the position of the robot at time t , and u is the control input, which is designed to be the vector field (i.e., $u(t) = \chi(\xi(t))$), taking the robot position $\xi(t)$ as the feedback signal. Therefore, the vector field indicates the desired velocity (or orientation) $\chi(\xi)$ at position $\xi \in \mathbb{R}^2$. In general, the vector field provides a *high-level guidance* layer for the robot motion. The low-level control is usually implemented by other control techniques, of which the performance is usually assumed sufficiently well achieved such that one can abstract away the low-level control layer [63], [111], [165]. Moreover, it has been shown in [91] that it is usually sufficient to consider the single-integrator model (8.27), and then employ the paper's methodology to deal with constraints imposed by vehicle shapes, kinematics, etc. The methodology is based on transformations that generate a zone around a robot to account for these constraints. Regarding the approach presented in this chapter, one can enlarge the repulsive or reactive boundaries to consider different robot models. Nevertheless, for more complicated robot models, control laws based on vector fields have been derived for differential-drive robots, fixed-wing aircraft, quadrotors, etc. (see [50], [63], [118], Chapters 4, 5, 10). We provide two examples of dealing with 2D and 3D Dubins car models in Section 8.7.

8.7 SIMULATIONS

8.7.1 Smooth zero-in and zero-out functions

Given the function φ and a constant c as in (8.3), we define two *smooth* functions:

$$f_1(\xi) = \begin{cases} 0 & \xi \in \{\varphi(\xi) \leq c\} \\ \exp\left(\frac{l_1}{c - \varphi(\xi)}\right) & \xi \in \{\varphi(\xi) > c\}, \end{cases} \quad (8.28)$$

$$f_2(\xi) = \begin{cases} \exp\left(\frac{l_2}{\varphi(\xi)}\right) & \xi \in \{\varphi(\xi) < 0\} \\ 0 & \xi \in \{\varphi(\xi) \geq 0\}, \end{cases} \quad (8.29)$$

where $l_1 > 0, l_2 > 0$ are used to change the decaying or increasing rate. Throughout this section, the zero-in and zero-out bump functions are designed as

$$\sqcup_{\mathcal{Q}}(\xi) = \frac{f_1(\xi)}{f_1(\xi) + f_2(\xi)}, \quad \sqcap_{\mathcal{R}}(\xi) = \frac{f_2(\xi)}{f_1(\xi) + f_2(\xi)}. \quad (8.30)$$

One can verify that the denominators of the above bump functions are always positive, and the functions satisfy the conditions in Corollary 8.13. In addition, thanks to this design, the set \mathcal{E} in (8.15) is simply the $l_2 c / (l_1 + l_2)$ -level set of φ ; i.e.,

$$\mathcal{E} = \varphi^{-1}\left(\frac{l_2}{l_1 + l_2}c\right).$$

8.7.2 2D composite vector field

In this simulation example, the desired path is a circle described by the function canonically chosen as $\phi(x, y) = x^2 + y^2 - R^2 = 0$, where $R > 0$ is the radius. According to Lemma 8.10, one can conclude that $\mathcal{C}_{\mathcal{P}} = \mathcal{W}(\mathcal{C}_{\mathcal{P}}) = \{(0, 0)\}$. Six obstacles are placed either directly on the desired path, or very close to it (see Fig. 8.7). Depending on the shapes of the obstacles, some reactive boundaries are described by rotated ellipses: $\varphi(x, y) = ((x - o_x) \cos \beta + (y - o_y) \sin \beta)^2 / a^2 + ((x - o_x) \sin \beta - (y - o_y) \cos \beta)^2 / b^2 - 1 = 0$, where $a, b > 0$ and β is the rotation angle about the center of the ellipse (o_x, o_y) . The singular sets and the corresponding insets are simply $\mathcal{C}_{\mathcal{R}} = \mathcal{W}(\mathcal{C}_{\mathcal{R}}) = \{(o_x, o_y)\}$. Two obstacles are enclosed by one reactive boundary which is modeled by a Cassini oval described by $\varphi(x, y) = [(x - 0.9)^2 + (y - 2)^2][(x + 0.9)^2 + (y - 2)^2] - 0.9 = 0$, and we have $\mathcal{C}_{\mathcal{R}} = \mathcal{W}(\mathcal{C}_{\mathcal{R}}) = \{(\pm 0.9, 2)\}$ for this reactive boundary. Since the functions ϕ and φ chosen for circles, ellipses and Cassini ovals are common in practice, we call them *canonical functions* for simplicity.

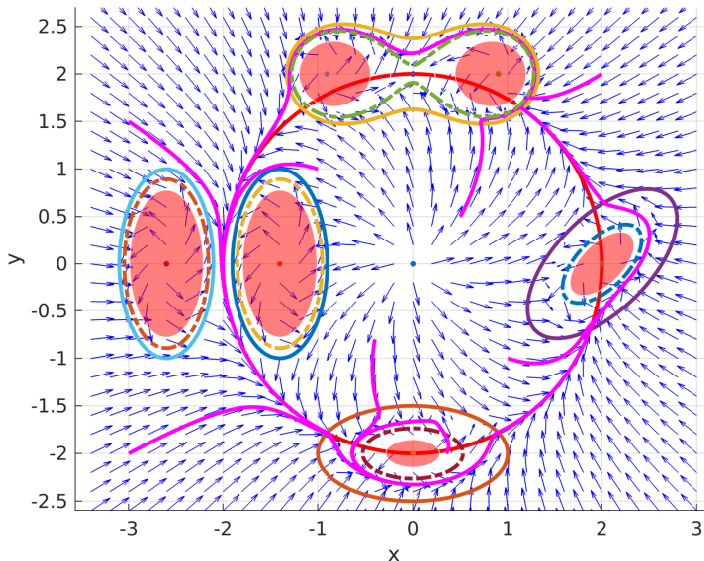


Figure 8.7: Simulation I. The red curve (partly covered by the pink curve) is the desired path. The red transparent shapes are obstacles, the solid closed curves enclosing them are the reactive boundaries and the dashed lines are the repulsive boundaries. The pink curves are trajectories starting from eight different positions. One of the initial point is in the repulsive area.

As shown in Fig. 8.7, starting from eight different positions, $(1, -1)$, $(2, 2)$, $(-1, 1)$, $(-3, 1.5)$, $(-3, -2)$, $(0.35, -2)$, $(0.5, 0.5)$ and $(-0.4, -0.8)$, all trajectories successfully follow the desired path and bypass the obstacles without entering the repulsive areas (except when starting from the repulsive area). Note that the trajectories smoothly pass the narrow passage surrounded by two vertical ellipses, while the vanilla artificial potential field method can hardly achieve this [69]. Also, note that this method is effective even though the Cassini oval is *not* convex. By numerical calculations, we find that there is only one saddle point in \mathcal{E} in each reactive area. Therefore, as verified by the simulation, no trajectories are attracted to stable points in \mathcal{E} , so the switching vector field is not employed.

8.7.3 Switching vector field to overcome the deadlock

In this simulation, we use one obstacle for simplicity. The corresponding reactive boundary is described by $\varphi = 2x^4 + 2(y+1)^4 - 3x^2(y+1)^2 - 2 = 0$, which is represented as the solid green curve in Fig. 8.8. This rather unusual boundary is used to illustrate the generality of our approach to obstacles of various shapes. The desired path is an ellipse described by $\phi = x^2/9 + y^2 - 1 = 0$. The constant c is -1.5 for the repulsive boundary in (8.3), and the gains for the vector fields are

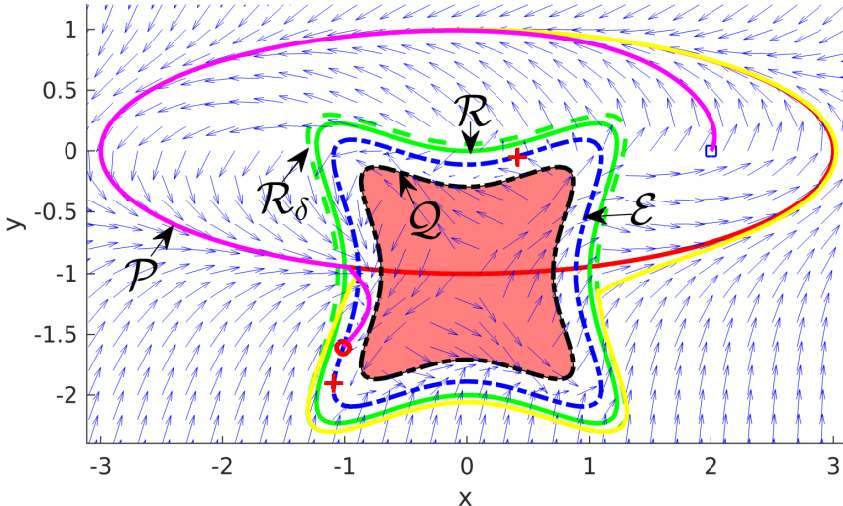


Figure 8.8: Simulation II. The red transparent area represents an obstacle. Two red crosses represent two saddle points and the red small circle represent the stable equilibrium in \mathcal{E} . The magenta curve is a trajectory of (8.8) starting from $(2, 0)$. It is attracted to the stable equilibrium and get stuck in the reactive area. This deadlock behavior does not occur when the trajectory (yellow curve) is generated by the switching vector field.

$k_p = 1$ and $k_r = 0.4$ in (8.4) and (8.5) respectively. One can numerically calculate three equilibria in \mathcal{E} : two saddle points and one stable equilibrium. Therefore, a trajectory of the composite vector field will be attracted to the stable equilibria and thus get stuck in the mixed area. However, the switching vector field in (8.17) can resolve this issue. The set \mathcal{E}^ϵ is approximated using the level set value; that is, $\mathcal{E}^\epsilon \approx \{\xi \in \mathbb{R}^2 : |\varphi(\xi) - l_2 c / (l_1 + l_2)| \leq \epsilon\}$, where we choose $l_1 = l_2 = \epsilon = 0.1$. See Fig. 8.8 for the simulation results. Instead of using switching vector fields, another possible solution is to eliminate stable equilibria using the approach introduced in Chapter 9, given that the parametrization of a deformed desired path to bypass obstacles is known.

8.7.4 Moving obstacles and 2D Dubins car model

In this simulation, an obstacle is moving at a constant speed, and thereby the reactive boundary is a moving ellipse. The function $\varphi(t, x, y)$ is $\varphi = (x + 5 - v_{\text{obs}}t)^2/a^2 + y^2/b^2 - 1$, where $a = 2$, $b = 1$, and $v_{\text{obs}} = 0.5$ is the constant speed of the obstacle along the positive x-axis. The desired path is a sinusoidal curve described by $\phi(x, y) = y - \sin(x) = 0$. Using the composite vector field, where the reactive vector field is given by (8.19), trajectories can bypass the moving

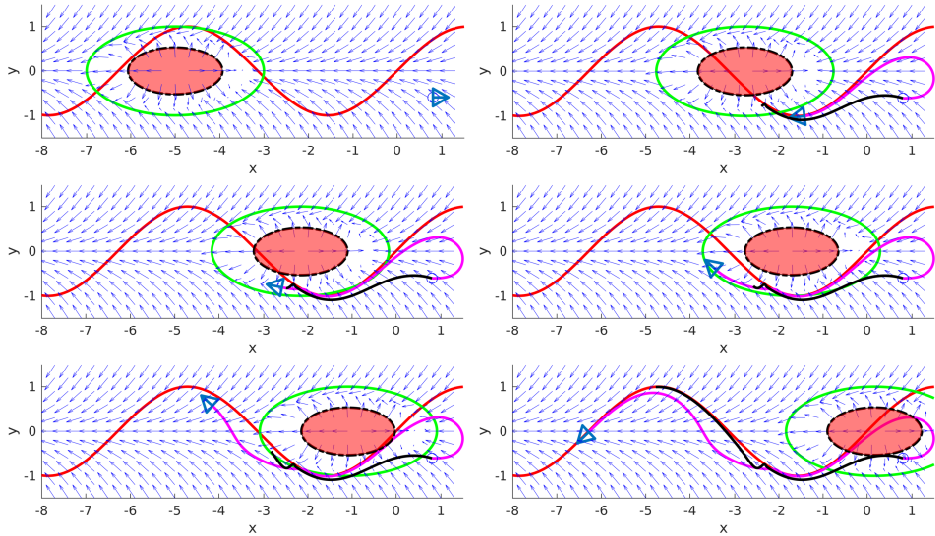


Figure 8.9: Simulation III with a moving obstacle at $t = 0\text{s}, 4.47\text{s}, 5.67\text{s}, 6.57\text{s}, 7.82\text{s}$ and 10.32s respectively from left to right, top to bottom. The red curve is the desired path, and the red elliptic shape is the moving obstacle. The repulsive boundary and the reactive boundary are represented by the dashed black line and the solid green line, respectively. The black curve is the trajectory of the single-integrator model starting from $(0.8, -0.6)$, whereas the magenta curve is the trajectory of the 2D Dubins car model with speed $s = 1$ and initial conditions $(x_0, y_0, \theta_0) = (0.8, -0.6, 0)$. The triangles represent the poses of the robot at different time instants. The results show that the two trajectories bypass the obstacle and then follow the desired path.

obstacle and follow the desired path afterward. To illustrate at the same time the applicability of the composite vector field for robot models other than the single-integrator model, we consider the following 2D Dubins car model:

$$\dot{x} = s \cos \theta \quad \dot{y} = s \sin \theta \quad \dot{\theta} = u_\theta, \quad (8.31)$$

where (x, y) is the robot's position in \mathbb{R}^2 , $\theta \in [0, 2\pi]$ is the robot's orientation, u_θ is the control input and s is the constant speed. We follow Theorem 4.24 to design the control input u_θ . See Fig. 8.9 for the simulation results.

8.7.5 3D composite vector field and 3D Dubins car model

In this simulation, a 3D static obstacle modeled by a solid ball occupies a planar desired path shown in Fig. 8.10. Since the desired path is a planar curve, we simply choose $\phi_1(x, y, z) = z$, and $\phi_2(x, y, z)$ is obtained by using radial-basis

functions to interpolate several sample points [50]. Specifically, we assume that $\phi_2(q) = -1 + \sum_{k=1}^N \omega_k f(\|q - q^{(k)}\|)$, where $q = (x, y, z) \in \mathbb{R}^3$ is the function input, $q^{(k)} \in \mathbb{R}^3$ are N sample points on the desired path, where $N > 1$, ω_k are N unknown parameters to be calculated and $f : \mathbb{R}_{\geq 0} \rightarrow \mathbb{R}$ is a radial-basis function. The parameters ω_k are determined by N constraints: $\phi_2(q^{(k)}) = 0$ for $k = 1, \dots, N$. If the sample points $q^{(k)}$ are chosen such that the Gram matrix $G = [g_{ij}] \in \mathbb{R}^{N \times N}$, where $g_{ij} = f(\|q^{(i)} - q^{(j)}\|)$, is non-singular, then the parameters are uniquely determined by $\omega = G^{-1}\mathbf{1}_N$, where $\omega = (\omega_1, \dots, \omega_N)^\top$ and $\mathbf{1}_N \in \mathbb{R}^N$ is a column vector with all ones. In this example, we choose the radial-basis function $f(r) = r^2 \ln(r+1)$ and six sample points $q^{(k)}$: $(1.5, 0), (1.5, 2.6), (-0.75, 1.3), (-3, 0), (-0.75, -1.3), (1.5, -2.6)$. The corresponding parameter vector is $w = (-0.048, 0.035, -0.048, 0.035, -0.048, 0.035)$. The resulting 3D path-following vector field χ_P is calculated from (8.25). For the reactive surface, we choose $\varphi(x, y, z) = (x + 2.8)^2 + y^2 + z^2 - 1$ and $v = (1, 0, 0)^\top$ to create the 3D reactive vector field in (8.26). The gains for the vector fields are $k_1 = 5, k_2 = 2$ and $k_r = 2$. We choose $c = -0.72$ for the repulsive surface; i.e., $\mathcal{Q} = \varphi^{-1}(c)$. The zero-in and zero-out bump functions are the same as (8.30) with $l_1 = l_2 = 0.1$. We also consider the following 3D Dubins car model:

$$\dot{x} = s \cos \theta \quad \dot{y} = s \sin \theta \quad \dot{\theta} = u_\theta \quad \dot{z} = u_z, \quad (8.32)$$

where (x, y, z) is the robot's position in \mathbb{R}^3 , $\theta \in [0, 2\pi]$ is the robot's orientation, u_θ and u_z are the control inputs, and s is the constant speed. We follow Theorem 4.24 to design the control inputs u_θ and u_z . See Fig. 8.10 for the results.

8.8 CONCLUSIONS

We consider the problem, initially in \mathbb{R}^2 , of following an arbitrary desired path occluded by a finite number of static or moving obstacles of arbitrary shapes. This problem, called the VF-CAPF problem, is different from the traditional motion planning problem with obstacles because no starting point and destination point are necessary to calculate a feasible path. We design a composite vector field to solve this problem. To address the issue of motions being “trapped” at a stable equilibrium, we propose a switching mechanism involving two vector fields. The path-following and obstacle-avoidance behaviors are provably guaranteed to be effective. Three extensions of our approach are discussed, taking into account moving obstacles with measured velocities, vector fields on higher-dimensional spaces, and nonholonomic robot models. Various numerical simulations support the theoretical results.

Our approach using the composite vector field or switching vector field has many advantages; e.g., a) Rigorous theoretical guarantees are provided, which

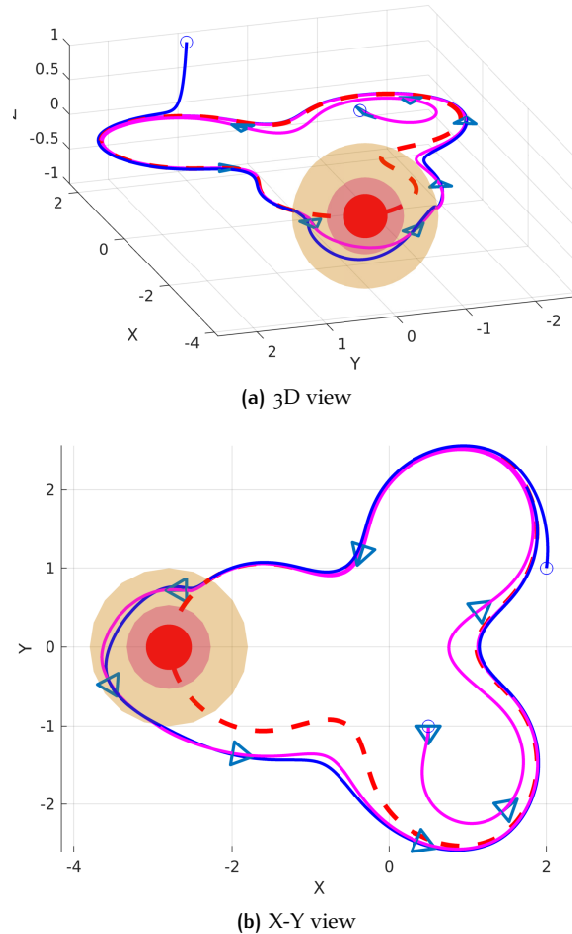


Figure 8.10: Simulation IV. The solid red ball is the obstacle, and the magenta and orange surfaces are the *repulsive surface* and the *reactive surface* respectively. The blue curve is the trajectory starting at $(2, 1, 1)$ corresponding to the single-integrator model, whereas the magenta curve is the trajectory with the initial condition $(x_0, y_0, z_0, \theta_0) = (0.5, -1, 0.3, -\pi/2)$ corresponding to the 3D Dubins car model, where the speed is $s = 1$. The triangles represent the poses of the robot at different time instants.

are usually absent in the literature; b) The collision-avoidance behavior is reactive, since the trajectory is guided directly by the vector field, and thereby the time-consuming operations, such as path re-planning or the creation of a symbolic map, are not required. The vector field is updated easily by adding a new term once a new obstacle is encountered. c) The composite vector field can be naturally extended to spaces of arbitrary dimensions. d) The shapes of the desired path and the obstacles are very general; e.g., convexity and no specific geometric relationships are required. However, there are also some disadvantages; for instance, the theoretical analysis for the high-dimensional case is challenging, and the switching vector field possibly renders trajectories tortuous and complicated.

9

A SINGULARITY-FREE GUIDING VECTOR FIELD FOR ROBOT NAVIGATION

In robot navigation tasks, such as UAV highway traffic monitoring, it is important for a mobile robot to follow a specified desired path. However, most of the existing path-following algorithms cannot guarantee global convergence to desired paths or enable following self-intersecting desired paths due to the existence of singular points where algorithms return unreliable or even no solutions. One typical example arises in *vector-field guided path-following* (VF-PF) algorithms. These algorithms are based on a vector field, and the singular points are exactly where the vector field becomes zero. Conventional VF-PF algorithms generate a vector field of the same dimensions as those of the space where the desired path lives. In this chapter, we show that it is mathematically *impossible* for conventional VF-PF algorithms to achieve global convergence to desired paths that are *self-intersecting* or even just *simple closed* (precisely, homeomorphic to the unit circle). Motivated by this new impossibility result, we propose a novel method to transform self-intersecting or simple closed desired paths to *non-self-intersecting* and *unbounded* (precisely, homeomorphic to the real line) counterparts in a *higher-dimensional* space. Corresponding to this new desired path, we construct a singularity-free guiding vector field on a higher-dimensional space. The integral curves of this new guiding vector field is thus exploited to enable global convergence to the higher-dimensional desired path, and therefore, the projection of the integral curves on a lower-dimensional subspace converge to the physical (lower-dimensional) desired path. Rigorous theoretical analysis is carried out for the theoretical results using dynamical systems theory. In addition, we show both by theoretical analysis and numerical simulations that our proposed method is an extension combining conventional VF-PF algorithms and trajectory tracking algorithms. Finally, to show the practical value of our proposed approach for complex engineering systems, we conduct outdoor experiments with a fixed-wing airplane in windy environment to follow both 2D and 3D desired paths.

This chapter is based on

- W. Yao, H. G. de Marina, B. Lin, and M. Cao, "Singularity-free guiding vector field for robot navigation," *IEEE Transactions on Robotics (TRO)*, vol. 37, no. 4, 2021.
- W. Yao, H. G. de Marina, and M. Cao, "Vector field guided path following control: Singularity elimination and global convergence," in *2020 59th IEEE Conference on Decision and Control (CDC)*, IEEE, 2020, pp. 1543–1549.

9.1 INTRODUCTION

Although the VF-PF algorithms are intuitive and easy to implement, the rigorous analysis remains nontrivial for general desired paths [31], [63], [156], [157]. Significant difficulty in the analysis and application of the VF-PF algorithms arises when there are singular points¹ in the vector field (see Fig. 9.1a and Fig. 9.1b). In such a case, the convergence of trajectories to the desired path cannot be guaranteed globally, and the normalization of the vector field at those points is not well-defined [50], [63], [156], [157]. In [50], it is assumed that these singular points are repulsive to simplify the analysis, while this assumption is dropped in [63] for a planar desired path and in Chapter 4 for a desired path in 3D. However, to the best of our knowledge, few efforts have been made on dealing with singular points directly or on eliminating them effectively. Recently, [119] presents a simple treatment of the singular point: the robot does not change its course inside a ball centered at the singular point. Under some conditions, the Lyapunov function evaluated at the exit point is proved to be smaller than that at the entry point.

Related to the existence of singular points, one of the challenges for the VF-PF navigation problem is to follow a self-intersecting desired path. Many existing VF-PF algorithms (e.g., [50], [63], [74], [104], [156]) fail to fulfill this task. This is rooted in the fact that the vector field degenerates to zero at the crossing points of a self-intersecting desired path, leading to a zero guidance signal, and thus a robot can get stuck on the desired path (see Fig. 9.1b). Due to the existence of singular points on the desired path, some effective VF-PF algorithms such as [63], [156], [157] become invalid simply because the assumptions are violated in this case. In fact, this task is also challenging for other existing path-following methods, since in the vicinity of the crossing points, many methods are “ill-defined”. For example, the line-of-sight (LOS) method [40] is not applicable as there is not a unique projection point in the vicinity of the intersection of the desired path. Indeed, many existing path-following algorithms either focus on simple desired paths such as circles or straight lines [104], [137], [172], or only deal with desired paths that are sufficiently smooth [50], [63], [156], [157]. One might retreat to the virtual-target path-following algorithm [134]. In this method, a virtual target has its own dynamics travelling on the desired path; thus the path-following navigation problem is implicitly converted to a target tracking problem. Although through this conversion, it is possible for a robot to follow a self-intersecting desired path, this method is inherently a tracking approach, and thus may inherit the performance limitations mentioned before, such as limited path-following accuracy.

Another challenging task arising from the VF-PF methods is the description of the desired path, which is crucial for the derivation of the vector field. For

¹ A point where a vector field becomes zero is called a *singular point* of the vector field [77, p. 219].

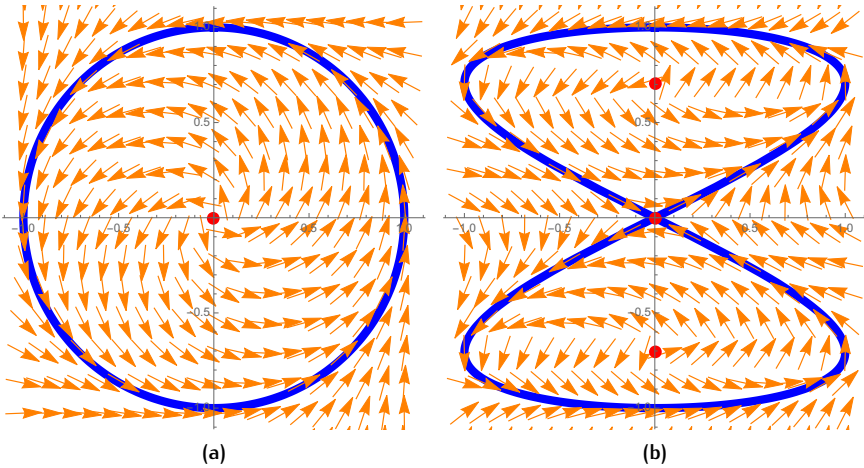


Figure 9.1: The *normalized* vector fields [63] for a circle path described by $\phi(x,y) = x^2 + y^2 - 1 = 0$ in (a) and a figure “8” path described by $\phi(x,y) = x^2 - 4y^2(1 - y^2) = 0$ in (b). The red points are the singular points of the (un-normalized) vector fields.

generality, the desired path is usually determined by the intersection of several hyper-surfaces represented by the zero-level sets of some implicit functions [50], [63], [119], [127], [156], [157]. For planar desired paths, for example, the implicit function of a star curve might be as complicated as that in [81], while for desired paths in a higher-dimensional space, it is counter-intuitive to create hyper-surfaces such that the intersection is precisely the desired path, such as a helix. On the other hand, many geometric curves are described by parametric equations [35] rather than implicit functions. It is possible to transform the parametric equations to implicit functions and then derive the vector field, but this might not always be feasible and is computationally expensive. The restrictive characterization of the desired path limits the applicability of VF-PF algorithms to some extent.

In this chapter, we improve the VF-PF methodology in the sense that we address the aforementioned three issues: the existence of singular points, the obstacle of dealing with self-intersecting paths, and the difficulty of representing a generic desired path. Specifically, based on the design of guiding vector fields in Chapter 4, we use an intuitive idea to eliminate singular points of the vector field so that global convergence to the desired path, even if self-intersecting, is guaranteed. The general idea is to extend the dimensions of the vector field and eliminate singular points simultaneously. This procedure naturally leads to a simple way to transform the descriptions of desired paths from parameterized forms to the intersection of several hyper-surfaces, which are required in creating a guiding vector field.

It is important to clarify the terminology used throughout this chapter. In many VF-PF algorithms, the desired path is a geometric object which is not necessarily parameterized. In a precise mathematical language, we assume that the desired path is a *one-dimensional connected differential manifold*. Therefore, we can generally classify desired paths into two categories: those homeomorphic to the unit circle S^1 if they are compact, and those homeomorphic to the real line \mathbb{R} otherwise [76, Theorem 5.27]. This assumption is not a restriction, since many desired paths in practice, such as a circle, an ellipse, a Cassini oval, a spline and a straight line, satisfy this assumption. For ease of exposition, we refer to those desired paths homeomorphic to the unit circle as *simple closed* desired paths, and those homeomorphic to the real line as *unbounded* desired paths. Note that *self-intersecting* paths do not satisfy this assumption. Nevertheless, we will introduce in the sequel how to *transform* a self-intersecting physical desired path to a non-self-intersecting and unbounded higher-dimensional desired path such that the assumption holds to apply our algorithm.

9.1.1 Contributions

Firstly, we show by rigorous topological analysis that guiding vector fields with the same dimension as the desired path (e.g., [63], [81], [89], [157]) cannot guarantee the global convergence to a simple closed or self-intersecting desired path (see Theorem 9.11 in Section 9.3). With the dichotomy of convergence discussed in the chapter, this implies that singular points of the vector field *always exist* for a *simple closed* or *self-intersecting* desired path regardless of which hypersurfaces one uses to characterize the desired path. This explains why many VF-PF algorithms in the literature cannot guarantee global convergence in the Euclidean space to a simple closed desired path. We note that excluding singular points is important in practice (e.g., for fixed-wing aircraft guidance and navigation) since degenerated or pathological solutions of system dynamics can be safely avoided. Therefore, this topological obstacle is the primary motivation of the subsequent theoretical development including the introduction of extended dynamics (see Section 9.4) and the creation of singularity-free guiding vector fields (see Section 9.5).

Secondly, due to the aforementioned topological obstruction, we improve the existing VF-PF algorithms such that *all* singular points are removed, and global convergence of trajectories to the desired path is rigorously guaranteed (see Section 9.4 and Section 9.5). We overcome this topological obstruction by changing the topology of the desired paths. Specifically, we transform a physical *simple closed* or *self-intersecting* desired path to a new *unbounded* and *non-self-intersecting* desired path in a *higher-dimensional space*. We then derive the corresponding guiding vector field on this higher-dimensional space, which is guaranteed to have *no* singular points.

Thirdly, our proposed method to create this new singularity-free guiding vector field is proved to enjoy several appealing features (see Section 9.5.2). For example, we provide theoretical guarantees for global exponential convergence of trajectories of system dynamics to the desired path. In addition, the new system dynamics with the singularity-free guiding vector field is robust against perturbation, such as noisy position measurements (see Feature 3 in Section 9.5.2). Moreover, using our proposed method, it becomes straightforward to represent hyper-surfaces of which the intersection is the new higher-dimensional desired path, as long as a parametrization of the physical (lower-dimensional) desired path is available (see Feature 2 in Section 9.5.2).

Last but not least, we successfully conduct experiments using a fixed-wing aircraft to verify the effectiveness of our proposed VF-PF algorithm in 3D (see Section 9.6), in addition to the experiment with an e-puck robot [94] in our previous preliminary work [164]. This verifies the practical significance of our proposed method for highly complex autonomous vehicles. We also discuss and conclude that our proposed VF-PF algorithm combines and extends features of the conventional VF-PF algorithms and trajectory tracking algorithms (see Section 9.7). While we do not claim that our proposed new singularity-free guiding vector field is always superior than traditional trajectory tracking algorithms in every application scenario (such as quadcopter attitude tracking), we emphasize that it significantly improves conventional VF-PF algorithms by providing a global solution and enabling the path-following behavior of complicated or unconventional desired paths (e.g., a self-intersecting Lissajous curve). This is imperative and irreplaceable in applications such as fixed-wing aircraft guidance and navigation where convergence to and propagation along a desired path from *every* initial position is required.

The remainder of this chapter is organized as follows. Section 9.2 introduces conventional guiding vector fields for path following. In Section 9.3, a theorem about the impossibility of global convergence to simple closed or self-intersecting desired paths using the conventional VF-PF algorithm is elaborated. This is the main motivation for the design of higher-dimensional guiding vector fields, which will be utilized in Section 9.4 through *extended dynamics*. Based on the previous sections, the construction approach of *singularity-free* guiding vector fields is presented in Section 9.5. In addition, several appealing features of this method are highlighted in this section. Then experiments with a fixed-wing aircraft are conducted to validate the theoretical results in Section 9.6. Following this, Section 9.7 discusses how our proposed approach can be viewed as a combined extension of VF-PF algorithms and trajectory tracking algorithms. Finally, Section 9.9 concludes the chapter.

9.2 GUIDING VECTOR FIELDS FOR PATH FOLLOWING

In this section, we introduce the vector-field guided path-following (VF-PF) navigation problem and the guiding vector fields. The VF-PF navigation problem in \mathbb{R}^n is the same as Problem 1.1, except that \mathcal{M} is changed to \mathbb{R}^n . For completeness of this chapter, we still state the problem as follows.

Problem 9.1 (VF-PF navigation problem in \mathbb{R}^n). Given a desired path $\mathcal{P} \subseteq \mathbb{R}^n$ defined in (9.1), the VF-PF navigation problem is to design a continuously differentiable vector field $\chi : \mathbb{R}^n \rightarrow \mathbb{R}^n$ for the differential equation $\dot{\xi}(t) = \chi(\xi(t))$ such that the two conditions below are satisfied:

- 1) There exists a neighborhood $\mathcal{D} \subseteq \mathbb{R}^n$ of the desired path \mathcal{P} such that for all initial conditions $\xi(0) \in \mathcal{D}$, the distance $\text{dist}(\xi(t), \mathcal{P})$ between the trajectory $\xi(t)$ and the desired path \mathcal{P} approaches zero as time $t \rightarrow \infty$; that is, $\lim_{t \rightarrow \infty} \text{dist}(\xi(t), \mathcal{P}) = 0$;
- 2) If a trajectory starts from the desired path, then the trajectory stays on the path for $t \geq 0$ (i.e., $\xi(0) \in \mathcal{P} \implies \xi(t) \in \mathcal{P}$ for all $t \geq 0$). In addition, the vector field on the desired path is non-zero (i.e., $0 \notin \chi(\mathcal{P})$).

In this chapter, we only investigate the guiding vector field on the Euclidean space \mathbb{R}^n .

9.2.1 Guiding vector fields on \mathbb{R}^n

Suppose a desired path in the n -dimensional Euclidean space is described by the intersection of $(n - 1)$ hypersurfaces; i.e.,

$$\mathcal{P} = \{\xi \in \mathbb{R}^n : \phi_i(\xi) = 0, i = 1, \dots, n - 1\}, \quad (9.1)$$

where $\phi_i : \mathbb{R}^n \rightarrow \mathbb{R}$, $i = 1, \dots, n - 1$, are of differentiability class C^2 . It is naturally assumed that \mathcal{P} in (9.1) is *nonempty* and *connected*. We further require the regularity of the desired path as shown later in Assumption 9.5. For better understanding, $\phi_i(\cdot) = 0$ can be regarded as $(n - 1)$ constraints, resulting in a one degree-of-freedom desired path.

Remark 9.2. Topologically, the desired path \mathcal{P} itself is one-dimensional, independent of the dimensions of the Euclidean space where it lives. However, with slight abuse of terminology and for convenience, the desired path \mathcal{P} is called an *n-D (or nD) desired path* if it lives in the n -dimensional Euclidean space \mathbb{R}^n and *not* in any lower-dimensional subspace $\mathcal{W} \subseteq \mathbb{R}^n$ (i.e., the *smallest subspace* the desired path lives in). For example, a planar desired path might be defined in the three-dimensional Euclidean space \mathbb{R}^3 , but we only consider the two-dimensional subspace $\mathcal{W} \subseteq \mathbb{R}^2$ where it is contained, and it is thus natural to call it a 2D (or 2-D) desired path rather than a 3D (or 3-D) desired path. Sometimes, for simplic-

ity, we refer to a tangent vector field on the n -dimensional Euclidean space \mathbb{R}^n as an *n -dimensional vector field*, and we say that *this vector field is n -dimensional*. \triangleleft

The vector field $\chi : \mathbb{R}^n \rightarrow \mathbb{R}^n$ is designed as below:

$$\chi = \wedge(\nabla\phi_1, \dots, \nabla\phi_{n-1}) - \sum_{i=1}^{n-1} k_i \phi_i \nabla\phi_i, \quad (9.2)$$

where $\nabla\phi_i$ is the gradient of ϕ_i , $k_i > 0$ are constant gains, and $\wedge : \mathbb{R}^n \times \dots \times \mathbb{R}^n \rightarrow \mathbb{R}^n$ is the wedge product. In particular, let $p_i = (p_{i1}, \dots, p_{in})^\top \in \mathbb{R}^n$, $i = 1, \dots, n-1$, and $b_j \in \mathbb{R}^n$ be the standard basis column vector with the j th component being 1 and the other components being 0. Then an intuitive *formal expression* for $\wedge(p_1, \dots, p_{n-1})$ is

$$\wedge(p_1, \dots, p_{n-1}) = \begin{vmatrix} b_1 & b_2 & \cdots & b_n \\ p_{11} & p_{12} & \cdots & p_{1n} \\ \vdots & \vdots & \ddots & \vdots \\ p_{n-1,1} & p_{n-1,2} & \cdots & p_{n-1,n} \end{vmatrix}. \quad (9.3)$$

In other words, $\wedge(p_1, \dots, p_{n-1})$ is obtained by the cofactor expansion along the first row of (9.3), where b_i should initially be regarded as scalars, and in the final evaluation replaced by the basis vectors [42, pp. 241-242].

To simplify the notations, we define a matrix $N(\xi) = (\nabla\phi_1(\xi), \dots, \nabla\phi_{n-1}(\xi)) \in \mathbb{R}^{n \times (n-1)}$, a positive definite gain matrix $K = \text{diag}\{k_1, \dots, k_{n-1}\} \in \mathbb{R}^{(n-1) \times (n-1)}$ and a C^2 function $e : \mathbb{R}^n \rightarrow \mathbb{R}^{n-1}$ by stacking ϕ_i ; that is,

$$e(\xi) = (\phi_1(\xi), \dots, \phi_{n-1}(\xi))^\top \in \mathbb{R}^{n-1}. \quad (9.4)$$

In addition, we define $\perp_\phi : \mathbb{R}^n \rightarrow \mathbb{R}^n$ by $\xi \in \mathbb{R}^n \mapsto \times(\nabla\phi_1(\xi), \dots, \nabla\phi_{n-1}(\xi))$. Therefore, the vector field (9.2) can be compactly written as

$$\chi(\xi) = \perp_\phi(\xi) - N(\xi)Ke(\xi). \quad (9.5)$$

Using this notation, the desired path is equivalent to

$$\mathcal{P} = \{\xi \in \mathbb{R}^n : e(\xi) = 0\}. \quad (9.6)$$

We call $e(\xi)$ the *path-following error* or simply *error* between the point $\xi \in \mathbb{R}^n$ and the desired path \mathcal{P} .

Remark 9.3. As mentioned in Sections 1.1.4 and 1.1.5 in Chapter 1, many vector fields in the literature can be seen as *variants* of the vector field in (9.2). Note that we do *not* consider time-varying gains or components in the vector field as

[50], [74] do. For one thing, this simplifies the structure of the vector field and facilitates the practical implementation; for another, this clarifies the topological property of these vector fields as studied in Section 9.3. For convenience, we refer to these (time-invariant) vector fields in the literature as *conventional vector fields*. \triangleleft

9.2.2 Assumptions

To justify using the norm of the path-following error $\|e(\cdot)\|$ instead of $\text{dist}(\cdot, \mathcal{P})$, we need some assumptions that are easily satisfied in practice (see Chapter 3). To this end, we define two sets. The *singular set* consisting of singular points of a vector field is defined as below:

$$\mathcal{C} = \{\xi \in \mathbb{R}^n : \chi(\xi) = 0\}. \quad (9.7)$$

Another related set is

$$\mathcal{H} = \{\xi \in \mathbb{R}^n : N(\xi)Ke(\xi) = 0\}. \quad (9.8)$$

It can be proved that $\mathcal{H} = \mathcal{P} \cup \mathcal{C}$.

Lemma 9.4. *It holds that $\mathcal{H} = \mathcal{P} \cup \mathcal{C}$.*

Proof. First, it is easy to see that for any point $\xi \in \mathcal{P} \cup \mathcal{C}$, we have $\xi \in \mathcal{H}$, thus $\mathcal{P} \cup \mathcal{C} \subseteq \mathcal{H}$. Second, for any point $\xi' \in \mathcal{H}$, it follows that $N(\xi')Ke(\xi') = \sum_{i=1}^{n-1} k_i \phi_i(\xi') \nabla \phi_i(\xi') = 0$. If $e(\xi') = 0$, then $\xi' \in \mathcal{P}$. If $e(\xi') \neq 0$, then the former equation implies that $\nabla \phi_i(\xi')$, $i = 1, \dots, n-1$, are linearly dependent (recalling that $k_i > 0$); hence the first term of the vector field becomes zero (i.e., $\perp_\phi(\xi) = 0$). Since $\xi' \in \mathcal{H}$, the second term of the vector field is also zero, thus the vector field $\chi(\xi') = 0$ and $\xi' \in \mathcal{C}$. The reasoning shows that $\mathcal{H} \subseteq \mathcal{P} \cup \mathcal{C}$. Combining $\mathcal{P} \cup \mathcal{C} \subseteq \mathcal{H}$ and $\mathcal{H} \subseteq \mathcal{P} \cup \mathcal{C}$, it is indeed true that $\mathcal{H} = \mathcal{P} \cup \mathcal{C}$. \square

As with Chapter 7, we propose the following standard assumptions.

Assumption 9.5. There are no singular points on the desired path. More precisely, \mathcal{C} is empty or otherwise there holds $\text{dist}(\mathcal{C}, \mathcal{P}) > 0$.

Assumption 9.6. In view of (9.6), as the norm of the path-following error $\|e(\xi)\|$ approaches zero, the trajectory $\xi(t)$ approaches the desired path \mathcal{P} . Similarly, in view of (9.8), as the “error” $\|N(\xi)Ke(\xi)\|$ approaches zero, the trajectory $\xi(t)$ approaches the set \mathcal{H} .

Due to Assumption 9.5, Lemma 5.7 holds here. Namely, the zero vector $\mathbf{0} \in \mathbb{R}^{n-1}$ is a regular value of the C^2 function e in (9.4), and hence the desired path \mathcal{P} is a C^2 embedded submanifold in \mathbb{R}^n .

Remark 9.7. Henceforth the “regularity” of the desired path is guaranteed; namely, the desired path \mathcal{P} is assumed to be a one-dimensional connected manifold, which can generally be classified into those homeomorphic to the unit circle if they are compact, and those homeomorphic to the real line otherwise [76, Theorem 5.27]. Thus throughout the chapter, we use the notions of *simple closed desired paths* and *desired paths homeomorphic to the unit circle* interchangeably. The same applies to *unbounded desired paths* and *desired paths homeomorphic to the real line*. Note that self-intersecting desired paths do not satisfy Assumption 9.5, as shown later in Proposition 9.8, but we will propose a method in Section 9.5 to transform them into unbounded and non-self-intersecting desired paths, which are then homeomorphic to the real line \mathbb{R} . \triangleleft

9.3 ISSUES ON THE GLOBAL CONVERGENCE TO DESIRED PATHS

In this section, we show that, under some conditions, it is not possible to guarantee global convergence to desired paths using the existing VF-PF algorithms as introduced in Section 9.2. More specifically, given a desired path $\mathcal{P} \subseteq \mathbb{R}^n$ as described in (9.1), we investigate solutions (trajectories) of the autonomous ordinary differential equation:

$$\dot{\xi}(t) = \chi(\xi(t)), \quad (9.9)$$

where χ is defined in (9.5). We consider the cases of self-intersecting and simple closed desired paths respectively.

We first show that the crossing points of a self-intersecting desired path \mathcal{P} are singular points of the corresponding vector field χ in (9.2).

Proposition 9.8. *If the desired path \mathcal{P} in (9.1) is self-intersecting, then the crossing points of the desired path are singular points of the vector field χ in (9.2).*

Proof. Since $c \in \mathcal{P}$ is a crossing point, we have $e(c) = 0$, and thus the vector field at the crossing point is simplified to $\chi(c) = \perp_\phi(c)$ in view of (9.5). Next we show that the gradients at the crossing point $\nabla\phi_i(c)$ are linearly dependent, and hence $\chi(c) = 0$. Suppose, on the contrary, the gradients are not linearly dependent. Then we can use the implicit function theorem [49] to conclude that there is a unique curve in a neighborhood of c satisfying $e(\xi) = 0$, where $\xi \in \mathbb{R}^n$. But this contradicts the fact that \mathcal{P} is self-intersecting. Therefore, the gradients at the crossing point are indeed linearly dependent. \square

Remark 9.9. This proposition shows that $0 \in \chi(\mathcal{P})$ when \mathcal{P} is a self-intersecting desired path, and therefore, the VF-PF navigation problem (Problem 9.8) cannot

be addressed as the second requirement about $0 \notin \chi(\mathcal{P})$ is always violated. Note that Assumption 9.5 does not hold in this case, but we will propose in the sequel an approach to transform a self-intersecting desired path such that Assumption 9.5 holds. \triangleleft

In Fig. 9.1b, for example, the 2D desired path resembling the figure “8” is self-intersecting. It can be numerically calculated that the vector field at the crossing point is zero. This is intuitive in the sense that there is no “preference” for the vector at this point to point to either the left or right portion of the desired path, leaving the only option of zero.

Now we consider simple closed desired paths. In the planar case, due to the Poincaré-Bendixson theorem (see Theorem 2.15), there is at least one singular point of the 2D vector field in the region enclosed by the simple closed desired path. Thus we can conclude that global convergence to a simple closed *planar* desired path is not possible. However, this conclusion cannot be trivially generalized to the higher-dimensional case since the Poincaré-Bendixson theorem is restricted to the planar case. Nevertheless, we can still reach this conclusion with some topological analysis.

Proposition 9.10. *If an n-D desired path $\mathcal{P} \subseteq \mathbb{R}^n$ described by (9.1) is simple closed, under the dynamics (9.9) where the guiding vector field $\chi : \mathbb{R}^n \rightarrow \mathbb{R}^n$ is in (9.2), then it is not possible to guarantee the global convergence of trajectories of (9.9) to the desired path \mathcal{P} ; precisely, the domain of attraction of \mathcal{P} cannot be \mathbb{R}^n .*

Proof. This is a direct consequence of Theorem 5.27 in Chapter 5. An alternative proof particularized to the \mathbb{R}^n case is provided in Section 9.8. \square

Based on Proposition 9.8 and Proposition 9.10, we can reach the following key statement about the impossibility of global convergence to some desired paths.

Theorem 9.11 (Impossibility of global convergence). *If an n-D desired path $\mathcal{P} \subseteq \mathbb{R}^n$ described by (9.1) is simple closed or self-intersecting, then it is not possible to guarantee the global convergence to the desired path with respect to the dynamics in (9.9) with the n-dimensional guiding vector field χ in (9.2); more precisely, the domain of attraction of \mathcal{P} cannot be \mathbb{R}^n .*

Proof. If the desired path \mathcal{P} is self-intersecting, then by Proposition 9.8, there is at least one singular point on the desired path. Obviously, the path-following problem formulated by Problem 9.1 cannot be solved. If the desired path \mathcal{P} is simple closed, then the global convergence to the desired path is impossible by Proposition 9.10. \square

Remark 9.12. We note that the topological obstacle to global convergence to the desired path roots in two aspects: i) the geometry of the desired path: being either simple closed or self-intersecting; ii) the time-invariance property of the vector field. Note that a state-dependent positive scaling (e.g., the normalization)

of vector fields does not affect the topological properties of interest (i.e., the phase portrait, or the convergent results) [25, Proposition 1.14]. \triangleleft

To overcome this topological obstacle and let Assumption 9.5 be satisfied even for self-intersecting desired paths, we propose a new idea in the sequel to construct unbounded and non-self-intersecting desired paths from the originally simple closed or self-intersecting desired paths by “cutting” and “stretching” them in a higher-dimensional space. Indeed, such a higher-dimensional desired path will codify or contain information about the (lower-dimensional) physical desired path. Based on the proposed higher-dimensional desired paths, we can derive a guiding vector field on this higher-dimensional space and show that its singular set is empty. However, to take advantage of the new guiding vector field, we need to *transform* (or *project* in the linear transformation case) its integral curves into a lower-dimensional subspace that contains the information of the physical desired path. The details of transformation into another space will be discussed in Section 9.4, and the detailed construction of a singularity-free guiding vector field on a higher-dimensional space will be presented in Section 9.5.

9.4 EXTENDED DYNAMICS AND CONVERGENCE RESULTS

In this section and the subsequent sections, we consider an m -dimensional Euclidean space \mathbb{R}^m , where $m > n$. The reason is self-evident as the chapter develops, but it is not necessary to bother with this difference now. To proceed, we introduce the *extended dynamics* and derive related convergence results. The extended dynamics relates to a *transformation operator* defined as follows:

Definition 9.13. A transformation operator is a function $G_l : \mathbb{R}^m \rightarrow \mathbb{R}^m$ which is twice continuously differentiable and *globally Lipschitz continuous* with the Lipschitz constant l .

One can observe that the corresponding Jacobian matrix function of a transformation operator $DG_l = \partial G_l / \partial x : \mathbb{R}^m \rightarrow \mathbb{R}^{m \times m}$ is locally Lipschitz continuous, where x is the argument of G_l . The transformation operator is able to transform a space into another space (or subspace). One example is a *linear transformation operator* defined by $G_l(x) = Ax$, where A is a non-zero matrix, called the *matrix representation* [140, Remark 6.1.15] of this particular linear transformation operator G_l . Now we introduce the extended dynamics as follows.

Lemma 9.14 (Extended dynamics). *Let $\chi : \mathcal{D} \subseteq \mathbb{R}^m \rightarrow \mathbb{R}^m$ be a vector field that is locally Lipschitz continuous. Given an initial condition $\xi(0) = \xi_0 \in \mathcal{D}$, suppose that $\xi(t)$ is the unique solution to the differential equation $\dot{\xi}(t) = \chi(\xi(t))$, then $(\xi(t), {}^{\text{trs}}\xi(t)) \in$*

\mathbb{R}^{2m} , where ${}^{\text{trs}}\xi(t) := G_l(\xi(t))$ and G_l is a transformation operator, is the unique solution to the following initial value problem:

$$\begin{cases} \dot{\xi}(t) = \chi(\xi(t)) & \xi(0) = \xi_0 \\ {}^{\text{trs}}\dot{\xi}(t) = \mathbf{D}G_l(\xi(t)) \cdot \chi(\xi(t)) & {}^{\text{trs}}\xi(0) = G_l(\xi_0). \end{cases} \quad (9.10)$$

Moreover, if the trajectory $\xi(t)$ asymptotically converges to some set $\mathcal{A} \neq \emptyset \subseteq \mathbb{R}^m$, then ${}^{\text{trs}}\xi(t)$ asymptotically converges to the transformed set

$${}^{\text{trs}}\mathcal{A} := G_l(\mathcal{A}) = \{p \in \mathbb{R}^m : p = G_l(q), q \in \mathcal{A}\}.$$

Proof. Due to the twice continuous differentiability of the transformation operator G_l , the corresponding Jacobian matrix function $\mathbf{D}G_l = \partial G_l / \partial x : \mathbb{R}^m \rightarrow \mathbb{R}^{m \times m}$ is locally Lipschitz continuous, where x is the argument of G_l . Therefore, the product of the vector field χ and the Jacobian $\mathbf{D}G_l$ are also locally Lipschitz continuous. It follows that $(\xi(t), {}^{\text{trs}}\xi(t)) \in \mathbb{R}^{2m}$, where ${}^{\text{trs}}\xi(t) = G_l(\xi(t))$, is the unique solution to (9.10) [25]. Recall that l is the (global) Lipschitz constant of G_l . Fix t , then

$$\begin{aligned} \text{dist}({}^{\text{trs}}\xi(t), {}^{\text{trs}}\mathcal{A}) &= \inf\{\|{}^{\text{trs}}\xi(t) - p\| : p \in {}^{\text{trs}}\mathcal{A}\} \\ &= \inf\{\|G_l(\xi(t)) - G_l(q)\| : q \in \mathcal{A}\} \\ &\leq \inf\{l\|\xi(t) - q\| : q \in \mathcal{A}\} \\ &= l \cdot \text{dist}(\xi(t), \mathcal{A}). \end{aligned}$$

Since $\xi(t)$ asymptotically converges to \mathcal{A} , we have $\text{dist}(\xi(t), \mathcal{A}) \rightarrow 0$ as $t \rightarrow \infty$. In other words, for any $\epsilon > 0$, there exists a $T > 0$, such that for all $t \geq T$, $\text{dist}(\xi(t), \mathcal{A}) < \epsilon/l$; hence $\text{dist}({}^{\text{trs}}\xi(t), {}^{\text{trs}}\mathcal{A}) \leq l \cdot \text{dist}(\xi(t), \mathcal{A}) < \epsilon$. Therefore, $\text{dist}({}^{\text{trs}}\xi(t), {}^{\text{trs}}\mathcal{A}) \rightarrow 0$ as $t \rightarrow \infty$. Thus the transformed solution ${}^{\text{trs}}\xi(t)$ asymptotically converges to the transformed set ${}^{\text{trs}}\mathcal{A}$. \square

We call the ordinary differential equation with the initial condition in (9.10) the *extended dynamics*. Correspondingly, ${}^{\text{trs}}\xi(t) := G_l(\xi(t))$ is called the *transformed solution* or *transformed trajectory* of (9.10). Before presenting Corollary 9.16 related to the VF-PF navigation problem, we first define the *transformed desired path* and the *transformed singular set*.

Definition 9.15. The *transformed desired path* ${}^{\text{trs}}\mathcal{P}$ of $\mathcal{P} \subseteq \mathbb{R}^m$ in (9.6) and the *transformed singular set* ${}^{\text{trs}}\mathcal{C}$ of $\mathcal{C} \subseteq \mathbb{R}^m$ in (9.7) are defined below:

$${}^{\text{trs}}\mathcal{P} := G_l(\mathcal{P}) = \{p \in \mathbb{R}^m : p = G_l(q), q \in \mathcal{P}\} \quad (9.11)$$

$${}^{\text{trs}}\mathcal{C} := G_l(\mathcal{C}) = \{p \in \mathbb{R}^m : p = G_l(q), q \in \mathcal{C}\}. \quad (9.12)$$

In some practical applications, it is desirable to scale the vector field to have a specified constant length. This is useful if a robot takes the vector field as the control input directly and is required to move at a constant speed. In this case, the properties of the integral curves of the scaled vector field are stated in the corollary below. Recall that the solution $x(t)$ to an initial value problem $\dot{x} = f(x)$, $x(0) = x_0$, where $f(x)$ is sufficiently smooth, is not always possible to be prolonged to infinity. In other words, the solution might only be well-defined in a finite time interval $[0, t^*)$, where $t^* < \infty$ [25]. The time instant t^* is called the maximal prolonged time of the solution.

Corollary 9.16. *Suppose the desired path \mathcal{P} in (9.6) is unbounded (i.e., $\mathcal{P} \approx \mathbb{R}$). Let $\chi : \mathcal{D} \subseteq \mathbb{R}^m \rightarrow \mathbb{R}^m$ be the vector field defined in (9.2). Suppose $\xi(t)$ is the unique solution to the initial value problem $\dot{\xi}(t) = s\hat{\chi}(\xi(t))$, $\xi(0) = \xi_0 \notin \mathcal{C}$, where $s > 0$ is a constant and $\hat{\cdot}$ is the normalization operator. Consider the following dynamics*

$$\begin{cases} \dot{\xi}(t) = s\hat{\chi}(\xi(t)) & \xi(0) = \xi_0 \notin \mathcal{C} \\ {}^{\text{trs}}\dot{\xi}(t) = \mathbf{D}G_l \cdot s\hat{\chi}(\xi(t)) & {}^{\text{trs}}\xi(0) = G_l(\xi_0), \end{cases} \quad (9.13)$$

where G_l is a transformation operator. Suppose $t^* \leq \infty$ is the maximal prolonged time of the transformed solution ${}^{\text{trs}}\xi(t)$ to (9.13). Then ${}^{\text{trs}}\xi(t)$ asymptotically converges to the transformed desired path ${}^{\text{trs}}\mathcal{P}$ in (9.11) as $t \rightarrow \infty$ or the transformed singular set ${}^{\text{trs}}\mathcal{C}$ in (9.12) as $t \rightarrow t^*$.

Proof. First consider the differential equation $\dot{\xi} = \chi(\xi)$. Using the same Lyapunov function candidate as (9.25) and the argument in the proof of Proposition 9.10, we have $\dot{V}(e) \leq 0$. In addition, the norm of the first term of the scaled vector field $s\hat{\chi}(\xi)$ is $s\|\perp_\phi\|/\|\chi\|$, and it is obviously upper bounded in \mathbb{R}^m . Since the new vector field $s\hat{\chi}(\xi)$ differs from the actual vector field $\chi(\xi)$ only by the magnitude of each vector, the two differential equations $\dot{\xi} = \chi(\xi)$ and $\dot{\xi} = s\hat{\chi}(\xi)$ have the same phase portrait in $\mathbb{R}^m \setminus \mathcal{C}$ [25, Proposition 1.14]. Therefore, from the dichotomy convergence result proved in Proposition 4.14, the solution to $\dot{\xi} = s\hat{\chi}(\xi)$ will converge to either \mathcal{P} or \mathcal{C} for initial conditions $\xi(0) \in \mathbb{R}^m \setminus \mathcal{C}$.

Note that if the maximal prolonged time is $t^* < \infty$, then the solution to $\dot{\xi} = s\hat{\chi}(\xi)$ must converge to the singular set \mathcal{C} . This is shown by contradiction. Since $\|\dot{\xi}\| = s < \infty$, $\xi^* := \lim_{t \rightarrow t^*} \xi(t) = \xi(0) + \int_0^{t^*} \dot{\xi}(t) dt$ exists. Suppose $\chi(\xi^*) \neq 0$, then we can define the solution at $t = t^*$, then it can be further prolonged to $t^* + \epsilon$ for some $\epsilon > 0$, contradicting that t^* is the maximal prolonged time. This shows that $\chi(\xi^*) = 0$ and thus the solution converges to \mathcal{C} .

Finally, suppose $\xi(t)$ is the unique solution to the initial value problem $\dot{\xi}(t) = s\hat{\chi}(\xi(t))$, $\xi(0) = \xi_0$, then by Lemma 9.14, $(\xi(t), {}^{\text{trs}}\xi(t))$ is the solution to (9.13). Therefore, the transformed trajectory ${}^{\text{trs}}\xi(t)$ asymptotically converges to the transformed desired path ${}^{\text{trs}}\mathcal{P}$ as $t \rightarrow \infty$ or the transformed singular set ${}^{\text{trs}}\mathcal{C}$ as $t \rightarrow t^*$. \square

Remark 9.17. Due to the normalization of the vector field in (9.13), the right-hand side of the differential equation is not well defined at singular points of the vector field. Therefore, if the transformed singular set ${}^{\text{trs}}\mathcal{C}$ is bounded, then the maximal interval to which the transformed trajectory ${}^{\text{trs}}\xi(t)$ can be prolonged is only finite when the transformed trajectory ${}^{\text{trs}}\xi(t)$ is converging to ${}^{\text{trs}}\mathcal{C}$. This happens when the initial value $\xi(0)$ is in the invariant manifold of the singular set \mathcal{C} . \triangleleft

The previous lemma states that the *transformed trajectory* converges to either the *transformed desired path* or the *transformed singular set* for initial conditions ${}^{\text{trs}}\xi(0) \in \mathbb{R}^m \setminus G_l(\mathcal{C})$, while the latter case is undesirable. A preferable situation is where the (transformed) singular set is empty. Moreover, as indicated by Theorem 9.11, to seek for global convergence, the only possibility is to consider unbounded and non-self-intersecting desired paths (i.e., $\mathcal{P} \approx \mathbb{R}$). Therefore, we reach the following corollary.

Corollary 9.18 (Global convergence to ${}^{\text{trs}}\mathcal{P}$). *Suppose the desired path \mathcal{P} in (9.11) is unbounded (i.e., $\mathcal{P} \approx \mathbb{R}$). If $\mathcal{C} = \emptyset$ (equivalently, ${}^{\text{trs}}\mathcal{C} = \emptyset$), then the transformed trajectory ${}^{\text{trs}}\xi(t)$ of (9.13) globally asymptotically converges to the transformed desired path ${}^{\text{trs}}\mathcal{P}$ as $t \rightarrow \infty$ in the sense that the initial condition $\xi(0)$ (and hence ${}^{\text{trs}}\xi(0)$) can be arbitrarily chosen in \mathbb{R}^m .*

As will be shown later, only the second differential equation of (9.10) or (9.13) is relevant to the physical robotic system. This corollary thus motivates us to design a (higher-dimensional) vector field such that the singular set is empty, in which case global convergence to the (transformed) desired path is guaranteed. In the next section, we will introduce an intuitive idea to “cut” and “stretch” a possibly simple closed or self-intersecting physical desired path and create a higher-dimensional singularity-free vector field.

9.5 HIGH-DIMENSIONAL SINGULARITY-FREE GUIDING VECTOR FIELDS

In this section, we explain how to implicitly construct an unbounded desired path from the physical desired path (possibly simple closed or self-intersecting) together with a higher-dimensional guiding vector field without any singular points (a.k.a, singularity-free guiding vector field).

For simplicity, we restrict the transformation operator $G_l : \mathbb{R}^m \rightarrow \mathbb{R}^m$ to a linear one defined by $G_l(x) = P_a x$, where $P_a \in \mathbb{R}^{m \times m}$ is a non-zero matrix defined by

$$P_a = I - \hat{a}\hat{a}^\top, \quad (9.14)$$

where I is the identity matrix of suitable dimensions and $\hat{a} = a/\|a\| \in \mathbb{R}^m$ is a normalized non-zero vector. In this case, G_l is actually a linear transformation

that projects an arbitrary vector to the hyperplane orthogonal to the given non-zero vector a , and P_a is the matrix representation of G_l . One can observe that the linear transformation G_l is globally Lipschitz continuous with the Lipschitz constant $l = \|P_a\| = 1$, where $\|\cdot\|$ is the induced matrix two-norm. In addition, the Jacobian is simply $DG_l = P_a$.

Before formulating the problem in the sequel, we define the *coordinate projection function* $\pi_{(1,\dots,n)} : \mathbb{R}^m \rightarrow \mathbb{R}^n$ as

$$\pi_{(1,\dots,n)}(x_1, \dots, x_n, \dots, x_m) = (x_1, \dots, x_n),$$

where $m > n$. In other words, the coordinate projection function $\pi_{(1,\dots,n)}$ takes only the first n components of an m -dimensional vector and generates a lower-dimensional one.

Problem 9.19. Given an n -D physical desired path² ${}^{phy}\mathcal{P}$ in \mathbb{R}^n , we aim to find an m -D desired path ${}^{hgh}\mathcal{P}$ in \mathbb{R}^m , where $m > n$, which satisfies the following conditions:

- 1) There exist functions $\phi_i(\cdot)$, $i = 1, \dots, m - 1$, such that ${}^{hgh}\mathcal{P}$ is described by (9.1);
- 2) The singular set ${}^{hgh}\mathcal{C}$ of the *higher-dimensional* vector field ${}^{hgh}\chi : \mathbb{R}^m \rightarrow \mathbb{R}^m$ in (9.2) corresponding to ${}^{hgh}\mathcal{P}$ is empty;
- 3) There exists a transformation operator $G_l : \mathbb{R}^m \rightarrow \mathbb{R}^m$ such that $\pi_{(1,\dots,n)}({}^{trs}\mathcal{P}) = {}^{phy}\mathcal{P}$, where the transformed desired path ${}^{trs}\mathcal{P} = G_l({}^{hgh}\mathcal{P})$.

Remark 9.20. It is important to distinguish among the *physical desired path* ${}^{phy}\mathcal{P}$, the *higher-dimensional desired path* ${}^{hgh}\mathcal{P}$ and the *transformed desired path* ${}^{trs}\mathcal{P}$. A major difference is the dimensions of their ambient space; that is, ${}^{phy}\mathcal{P} \subseteq \mathbb{R}^n$, while ${}^{hgh}\mathcal{P}, {}^{trs}\mathcal{P} \subseteq \mathbb{R}^m$ and $m > n$. Although the higher-dimensional desired path ${}^{hgh}\mathcal{P}$ and the transformed desired path ${}^{trs}\mathcal{P}$ both live in \mathbb{R}^m , the transformed desired path ${}^{trs}\mathcal{P}$ lives in a subspace $\mathcal{W} \subseteq \mathbb{R}^m$ probably with $\dim(\mathcal{W}) < m$ since ${}^{trs}\mathcal{P} = G_l({}^{hgh}\mathcal{P})$. Indeed, for the case of a linear transformation operator in (9.14), the transformed desired path ${}^{trs}\mathcal{P} = P_a({}^{hgh}\mathcal{P})$ lives in the orthogonal complement subspace \mathcal{W} of the linear space spanned by the vector a (i.e., $\text{span}\{a\}$), and $\dim(\mathcal{W}) = m - 1 < m$. \triangleleft

Next, we propose the solution to Problem 9.19 in Section 9.5.1. Having found the higher-dimensional desired path ${}^{hgh}\mathcal{P}$, then we can directly derive the corresponding vector field ${}^{hgh}\chi$ defined on \mathbb{R}^m by (9.2). Some features of the approach illustrated in Section 9.5.1 are highlighted in Section 9.5.2.

² Recall the notion of an n -D desired path in Remark 9.2.

9.5.1 Construction of a singularity-free guiding vector field

Suppose an n -D physical path ${}^{\text{phy}}\mathcal{P}$ is parameterized by

$$x_1 = f_1(w), \dots, x_n = f_n(w), \quad (9.15)$$

where $w \in \mathbb{R}$ is the parameter of the desired path and $f_i \in C^2$, $i = 1, \dots, n$. We can simply let

$$\phi_1(\xi) = x_1 - f_1(w), \dots, \phi_n(\xi) = x_n - f_n(w), \quad (9.16)$$

where $\xi = (x_1, \dots, x_n, w)$ has an additional coordinate w now and is an m -dimensional vector, where $m = n + 1$. So the m -D desired path is

$${}^{\text{hgh}}\mathcal{P} = \{\xi = (x_1, \dots, x_n, w) \in \mathbb{R}^m : \phi_i(\xi) = 0, i = 1, \dots, n\}. \quad (9.17)$$

Thus the first requirement of Problem 9.19 is met. Intuitively, the new higher-dimensional desired path ${}^{\text{hgh}}\mathcal{P}$ is obtained by “cutting” and “stretching” the n -D desired path ${}^{\text{phy}}\mathcal{P}$ along the additional virtual w -axis (see Fig. 9.7). From the higher-dimensional desired path ${}^{\text{hgh}}\mathcal{P} \subseteq \mathbb{R}^m$ in (9.17), we obtain the corresponding guiding vector field on the higher-dimensional space \mathbb{R}^m by (9.2):

$${}^{\text{hgh}}\chi = \perp_{\phi} - \sum_{i=1}^n k_i \phi_i \nabla \phi_i.$$

It can be calculated that $\nabla \phi_i = (0, \dots, 1, \dots, -f'_i(w))^{\top}$ for $i = 1, \dots, n$, where $f'_i(w) := \frac{df_i(w)}{dw}$ and 1 is the i -th component of the gradient vector. Therefore,

$$\perp_{\phi} = (-1)^n (f'_1(w), \dots, f'_n(w), 1)^{\top} \in \mathbb{R}^m = \mathbb{R}^{n+1}.$$

It is interesting that the m -th coordinate of this vector is a constant $(-1)^n$ regardless of the specific parametric form of the desired path. This means that $\|\perp_{\phi}(\xi)\| \neq 0$ for $\xi \in \mathbb{R}^m$ globally. From Lemma 5.1, we know that the propagation term \perp_{ϕ} of the vector field is always linearly independent from the convergence term $\sum_{i=1}^n k_i \phi_i \nabla \phi_i$ unless they are zero vectors. However, as we have shown that $\|\perp_{\phi}\| \neq 0$ in \mathbb{R}^m globally, this reveals the appealing property that the vector field ${}^{\text{hgh}}\chi(\xi) \neq 0$ for any point $\xi \in \mathbb{R}^m$, implying that there are no singular points in the higher-dimensional space \mathbb{R}^m ; i.e., ${}^{\text{hgh}}\mathcal{C} = \emptyset$. Thus, the second requirement of Problem 9.19 (as well as a related condition in Corollary 9.18) is satisfied.

To let the third requirement of Problem 9.19 be satisfied, we retreat to a linear transformation operator with a matrix representation P_a . One of the simplest linear transformation operators corresponds to $a = b_{n+1} \in \mathbb{R}^m$, which is a

standard basis column vector with the $(n+1)$ -th component being 1 and the other components being 0. This is used to transform an m -dimensional space to an n -dimensional subspace by “zeroing” the last coordinate. Specifically, we let $a = b_{n+1}$, then the matrix representation of the linear transformation operator is $P_a = \begin{bmatrix} I_{n \times n} & \mathbf{0} \\ \mathbf{0} & 0 \end{bmatrix}$, where $\mathbf{0}$ are zero vectors of suitable dimensions. Observe that the n -D desired path ${}^{\text{phy}}\mathcal{P} \subseteq \mathbb{R}^n$ is the orthogonal projection of the higher-dimensional desired path ${}^{\text{hgh}}\mathcal{P} \subseteq \mathbb{R}^m$ on the plane where $w = 0$; i.e.,

$$\pi_{(1,\dots,n)}({}^{\text{hgh}}\mathcal{P}) = \pi_{(1,\dots,n)}({}^{\text{trs}}\mathcal{P}) = {}^{\text{phy}}\mathcal{P}.$$

Therefore, the third requirement of Problem 9.19 is also satisfied. By the construction in (9.17), the higher-dimensional desired path ${}^{\text{hgh}}\mathcal{P} \subseteq \mathbb{R}^m$ satisfying all the conditions in Problem 9.19 is thus found. Ultimately, we can take advantage of the new “well-behaved” guiding vector field ${}^{\text{hgh}}\chi \in \mathbb{R}^m$ derived from ${}^{\text{hgh}}\mathcal{P} \subseteq \mathbb{R}^m$ as mentioned above. This result is formally stated in the following theorem.

Theorem 9.21. *Suppose an n -D physical desired path ${}^{\text{phy}}\mathcal{P} \subseteq \mathbb{R}^n$ is parameterized by (9.15). If ϕ_1, \dots, ϕ_n are chosen as in (9.16), then there are no singular points in the corresponding guiding vector field ${}^{\text{hgh}}\chi : \mathbb{R}^{n+1} \rightarrow \mathbb{R}^{n+1}$ defined on the $(n+1)$ -dimensional space \mathbb{R}^{n+1} . Let $a = b_{n+1}$ for the linear transformation operator P_a . Suppose the transformed trajectory of the extended dynamics (9.13) is ${}^{\text{trs}}\xi(t) := (x_1(t), \dots, x_n(t), w(t))^\top$. Then the projected transformed trajectory*

$$\text{Prj}\xi(t) := \pi_{(1,\dots,n)}({}^{\text{trs}}\xi(t)) = (x_1(t), \dots, x_n(t))^\top$$

globally asymptotically converges to the physical desired path ${}^{\text{phy}}\mathcal{P}$ as $t \rightarrow \infty$.

Proof. By (9.2) and (9.16), the guiding vector field on the $(n+1)$ -dimensional space \mathbb{R}^{n+1} is

$${}^{\text{hgh}}\chi(x_1, \dots, x_n, w) = \begin{bmatrix} (-1)^n f'_1(w) - k_1 \phi_1 \\ \vdots \\ (-1)^n f'_n(w) - k_n \phi_n \\ (-1)^n + \sum_{i=1}^n k_i \phi_i f'_i(w) \end{bmatrix}. \quad (9.18)$$

As discussed before, the singular set ${}^{\text{hgh}}\mathcal{C} = \emptyset$. According to Corollary 9.18, ${}^{\text{trs}}\xi(t)$ globally asymptotically converges to the transformed desired path ${}^{\text{trs}}\mathcal{P} = G_l({}^{\text{hgh}}\mathcal{P}) = P_a({}^{\text{hgh}}\mathcal{P})$ as $t \rightarrow \infty$. Since $a^\top {}^{\text{trs}}\xi = a^\top P_a \xi = 0$, the $(n+1)$ -th coordinate $w(t)$ of the transformed trajectory ${}^{\text{trs}}\xi(t)$ is equal to 0, meaning that the transformed trajectory ${}^{\text{trs}}\xi(t)$ lies in the subspace $\mathcal{W} := \{(x_1, \dots, x_{n+1}) \in \mathbb{R}^n : x_{n+1} = 0\}$. Therefore, the projected transformed trajec-

tory $\text{Prj} \xi(t) = \pi_{(1, \dots, n)}(\text{trs} \xi(t))$ globally asymptotically converges to the physical desired path $\text{phy}\mathcal{P}$. \square

Remark 9.22. Note that the proof of convergence to the physical desired path $\text{phy}\mathcal{P}$ is indirect. The norm of the path-following error $\|e(\cdot)\| = \|(\phi_1(\cdot), \dots, \phi_n(\cdot))\|$ captures the distance to the higher-dimensional desired path $\text{hgh}\mathcal{P}$, taking into account the additional coordinate w as well. It is shown first that in the higher-dimensional space \mathbb{R}^{n+1} , the norm of the path-following error $\|e(\cdot)\|$ approaches zero asymptotically. Then the convergence to the transformed desired path $\text{trs}\mathcal{P}$ is obtained from Corollary 9.16 (or Corollary 9.18). Due to the special choice of the linear transformation operator P_a , where $a = b_{n+1}$, the transformed desired path $\text{trs}\mathcal{P}$ is “almost” the same as the physical desired path $\text{phy}\mathcal{P}$, except that it has an additional but constant coordinate $w(t) \equiv 0$. \triangleleft

We have shown that, by extending the vector field from \mathbb{R}^n to \mathbb{R}^{n+1} , the new guiding vector field does not have any singular points. Therefore, by using the extended dynamics, the convergence to the physical desired path is guaranteed globally. When $n > 3$, this case corresponds to some configuration spaces, such as the robot arm joint space in a smooth manifold embedded in \mathbb{R}^n . See Chapter 5 for more details.

9.5.2 Features of the approach

There are several intriguing features of our proposed approach discussed above in Section 9.5.1. These features are summarized below. For ease of narration and without loss of generality, we take the case of a 2D physical desired path $\text{phy}\mathcal{P} \subseteq \mathbb{R}^2$ for discussion (i.e., $n = 2$).

Feature 1. The corresponding higher-dimensional desired path $\text{hgh}\mathcal{P} = \{\xi \in \mathbb{R}^{2+1} : \phi_1(\xi) = 0, \phi_2(\xi) = 0\}$ is not self-intersecting. This is due to the fact that a crossing point must be a singular point (see Proposition 9.8), but we have shown that there are no singular points in the higher-dimensional guiding vector field. In fact, the parameter of the desired path w in (9.15) is implicitly transformed to an additional coordinate of the higher-dimensional desired path. Thus the physical planar desired path $\text{phy}\mathcal{P}$ is “cut” and “stretched” into the three-dimensional Euclidean space, and becomes unbounded and non-self-intersecting along the additional dimension (see Fig. 9.7). The significance of this feature is that even a self-intersecting physical desired path $\text{phy}\mathcal{P}$ described by (9.15) can be successfully followed by using the new singularity-free guiding vector field, which in fact corresponds to a non-self-intersecting “stretched” desired path $\text{hgh}\mathcal{P}$.

Feature 2. This approach facilitates the expression of hypersurfaces characterized by implicit functions ϕ_i . Usually, a parameterized form of the desired path is more readily available than the hypersurfaces of which the intersection is the desired path. Therefore, given the parameterized form in (9.15), we do not need to convert

them into $\phi(x, y) = 0$ and derive the corresponding 2D vector field. Instead, by simply defining two ϕ functions as in (9.16), we obtain a singularity-free vector field ${}^{\text{hgh}}\chi$ defined on \mathbb{R}^{2+1} .

Feature 3. One only needs to examine the boundedness of $|f'_i(z)|$, $i = 1, 2$, in the vicinity of the higher-dimensional desired path ${}^{\text{hgh}}\mathcal{P}$ to guarantee both the property of local exponential vanishing of the norm of the path-following error $\|e\|$ and the property of robustness against disturbance of the system dynamics (9.9), while these properties usually require more conditions to be satisfied for general vector fields (see Chapter 4).

Feature 4. Only Assumption 9.6 is required. Since the new guiding vector field does not have any singular points, the other assumption, Assumption 9.5, is vacuously true. This is independent of the specific parametrizations of the desired path in (9.15).

Feature 5. The additional virtual coordinate can be used to realize scalable distributed multi-robot coordinated path-following navigation by adding a consensus term (see Chapter 10).

9.6 EXPERIMENTS WITH AN AUTONOMOUS AIRCRAFT

In this section, we demonstrate the effectiveness of our path-following approach with an autonomous fixed-wing aircraft. In particular, we verify the tracking of both 2D and 3D self-intersecting desired paths. All the related software has been developed within the open-source project for autopilots *Paparazzi* [47]. The codes only require the corresponding parametric equations to implement other desired paths³.

9.6.1 The autonomous aircraft and airfield

For the experiments, we use one Opterra as shown in Fig. 9.2. Two *elevons* actuate the aircraft at the wings and one motor acts in pushing the configuration. The vehicle's electronics consists of the autopilot *Apogee*, an Ublox GPS receptor, a Futaba receiver, and a X-Bee S1 radio modem. The Apogee's core is an STM32F4 microcontroller where our algorithm runs with a fixed frequency of 50Hz, and all the relevant data are logged in an SD card at 100Hz. The ground segment consists of a standard laptop with another X-Bee S1 radio modem to monitor the telemetry and a Futaba transmitter in case of taking over manual control of the vehicle. The flights took place on July 18, 2020, in Ciudad Real (Spain) with GPS

³ https://github.com/noether/paparazzi/tree/gvf_advanced/sw/airborne/modules/guidance/gvf_parametric.

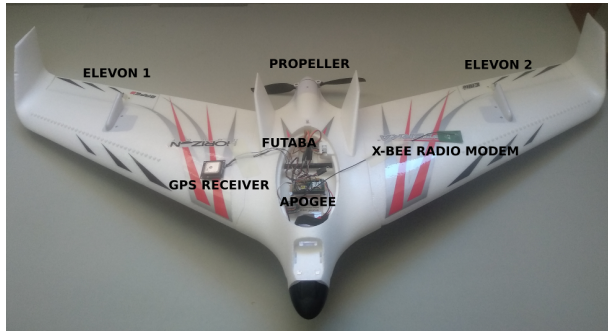


Figure 9.2: Autonomous Opterra 1.2m equipped with Paparazzi's Apogee autopilot. The airframe is built by E-Flite / Horizon Hobby company.

coordinates $(39.184535, -4.020797)$ degrees. The weather forecast reported 36°C and a South wind of 14 km/h .

9.6.2 Aircraft's guidance system design

We employ a decoupled vertical and horizontal model for setting the aircraft's guiding reference signals. In particular, accounting for the nonholonomic lateral constraint of the aircraft, we consider the following unicycle model

$$\dot{x} = v \cos \theta \quad \dot{y} = v \sin \theta \quad \dot{\theta} = u_{\theta} \quad \dot{z} = u_z, \quad (9.19)$$

where (x, y, z) is the 3D position, θ is the heading angle on the XY plane, v is the ground speed, u_{θ} is the angular velocity control/guiding signal to change the heading, and u_z is the guiding signal for the climbing velocity. We will show how to design the guiding signals u_{θ} and u_z , which are injected into the control system of the aircraft that deals with the nontrivial couplings of the lateral and vertical modes. Particularly, u_{θ} is tracked by banking the aircraft depending on the current speed v and the *pitch* angle to achieve a *coordinated turn*, and u_z is tracked by controlling the pitch angle and the propulsion to vary the lift and the vertical component of the pushed force coming from the propeller⁴. The experiments will show that our algorithm is compatible with the model (9.19) and the low-level controller employed in Paparazzi for a fixed-wing aircraft.

Note that the wind has a noticeable impact on the ground speed of the aircraft. Nevertheless, as the experimental results indicate, such a wind speed does not impact the intended performance of the algorithm. In practice, we consider θ as the heading angle (given by the velocity vector), not the attitude *yaw* angle. If there is no wind, both angles are the same in our setup. When we consider

⁴ We leave the reader to check the details of the employed low-level controllers at http://wiki.paparazziuav.org/wiki/Control_Loops.

the heading instead of the yaw for the model (9.19), the aircraft compensates the lateral wind by *crabbing* such that aerodynamic angle *sideslip* is almost zero.⁵

For following 3D paths (including 2D paths at a constant altitude), we will employ a higher-dimensional 4D vector field. The generalized 4D velocity vector of the aircraft is defined as $\dot{\xi} = (\dot{x}, \dot{y}, \dot{z}, \dot{w})^\top$, where (\dot{x}, \dot{y}) is the actual ground velocity of the aircraft, \dot{z} is the vertical speed, and \dot{w} is the velocity in the additional coordinate to be determined. Now we present the control algorithm design; that is, the design of u_θ and u_z in (9.19) with the following proposition:

Proposition 9.23. *Suppose the 3D physical desired path ${}^{\text{phy}}\mathcal{P} \subseteq \mathbb{R}^3$ to follow is parameterized by (9.15). Then a corresponding 4D vector field $\chi : \mathbb{R}^4 \rightarrow \mathbb{R}^4$ can be constructed by Theorem 9.21. Assume that the vector field satisfies $\chi_1(\xi)^2 + \chi_2(\xi)^2 \neq 0$ for $\xi \in \mathbb{R}^4$, where χ_i denotes the i -th entry of χ . Consider the model (9.19), and let the dynamics of the additional coordinate w be*

$$\dot{w} = \frac{v\chi_4}{\sqrt{\chi_1^2 + \chi_2^2}}. \quad (9.20)$$

Let the angular velocity control input u_θ and the climbing velocity input u_z be

$$u_\theta = \underbrace{\left(\frac{-1}{\|\chi^p\|} \hat{\chi}^p \top E J(\chi^p) \dot{\xi} \right)}_{:= \dot{\theta}_d} - k_\theta \hat{h} \top E \hat{\chi}^p, \quad (9.21a)$$

$$u_z = \frac{v\chi_3}{\sqrt{\chi_1^2 + \chi_2^2}}, \quad (9.21b)$$

where $k_\theta > 0$ is a gain constant, $h = (\cos \theta, \sin \theta)^\top$, $E = \begin{bmatrix} 0 & -1 \\ 1 & 0 \end{bmatrix}$, $\chi^p = (\hat{\chi}_1, \hat{\chi}_2)^\top$ and $J(\chi^p)$ is the Jacobian matrix of χ^p with respect to the generalized position $\xi = (x, y, z, w)$ and $\dot{\xi} = (\dot{x}, \dot{y}, \dot{z}, \dot{w})^\top$ is the generalized velocity. Let the angle difference directed from $\hat{\chi}^p$ to \hat{h} be denoted by $\beta \in (-\pi, \pi]$. If the initial angle difference satisfies $\beta(0) \in (-\pi, \pi)$, then it will vanish asymptotically (i.e., $\beta(t) \rightarrow 0$). Furthermore, the actual robot trajectory $(x(t), y(t), z(t))$ will converge to the physical desired path ${}^{\text{phy}}\mathcal{P}$ asymptotically as $t \rightarrow \infty$.

Proof. Let

$$\chi' := \frac{1}{\sqrt{\chi_1^2 + \chi_2^2}} \chi$$

⁵ Crabbing happens when the inertial velocity makes an angle with the nose heading due to wind. Slipping happens when the aerodynamic velocity vector makes an angle (sideslip) with the body ZX plane. Slipping is (almost) always undesirable because it degrades aerodynamic performance. Crabbing is not an issue for the aircraft.

be the scaled 4D vector field. We aim to let the generalized robot velocity $\dot{\xi} = (\dot{x}, \dot{y}, \dot{z}, \dot{w})^\top$ eventually align with and point towards the same direction as the scaled vector field. Specifically, let the orientation error be defined by

$$e_{ori}(t) = \dot{\xi} - v\chi' \stackrel{(9.20),(9.21b)}{=} v \begin{bmatrix} \cos \theta - \chi'_1 \\ \sin \theta - \chi'_2 \\ 0 \\ 0 \end{bmatrix} = \begin{bmatrix} h - g \\ \mathbf{0} \end{bmatrix} \in \mathbb{R}^4,$$

where $h = (\cos \theta, \sin \theta)^\top$ and $g = (\chi'_1, \chi'_2)^\top$. It is obvious that $e_{ori} \rightarrow 0$ if and only if $h - g \rightarrow 0$. Therefore, it suffices to show that the orientation of h asymptotically aligns with that of g . Note that

$$\hat{\chi}^p = \frac{1}{\sqrt{\hat{\chi}_1^2 + \hat{\chi}_2^2}} \begin{bmatrix} \hat{\chi}_1 \\ \hat{\chi}_2 \end{bmatrix} = \frac{1}{\sqrt{\chi_1^2 + \chi_2^2}} \begin{bmatrix} \chi_1 \\ \chi_2 \end{bmatrix} = g$$

and $\hat{h} = h$. Therefore, we can define a new orientation error as $e_{or} := \hat{h} - \hat{\chi}^p \in \mathbb{R}^2$. Choose the Lyapunov function candidate $V = 1/2 e_{or}^\top e_{or}$ and its time derivative is

$$\begin{aligned} \dot{V} &= \dot{e}_{or}^\top e_{or} = (\dot{\theta} E \hat{h} - \dot{\theta}_d E \hat{\chi}^p)^\top (\hat{h} - \hat{\chi}^p) \\ &= (\dot{\theta} - \dot{\theta}_d) \hat{h}^\top E \hat{\chi}^p \stackrel{(9.21a)}{=} -k_\theta (\hat{h}^\top E \hat{\chi}^p)^2, \end{aligned} \quad (9.22)$$

which is negative semi-definite. The second equation makes use of the identities: $\dot{\hat{h}} = \dot{\theta} E \hat{h}$ and $\dot{\hat{\chi}}^p = \dot{\theta}_d E \hat{\chi}^p$, where $\dot{\theta}_d$ is defined in (9.21a). The third equation is derived by exploiting the facts that $E^\top = -E$ and $a^\top E a = 0$ for any vector $a \in \mathbb{R}^2$. Note that $\dot{V} = 0$ if and only if the angle difference between \hat{h} and $\hat{\chi}^p$ is $\beta = 0$ or $\beta = \pi$. Since it is assumed that the initial angle difference $\beta(t=0) \neq \pi$, it follows that $\dot{V}(t=0) < 0$, and thus there exists a sufficiently small $\epsilon > 0$ such that $V(t=\epsilon) < V(t=0)$. It can be shown by contradiction that $|\beta(t)|$ is monotonically decreasing with respect to time t ⁶. By (9.22), one observes that $|\beta(t)|$ and $V(t)$ tends to 0, implying that the generalized velocity $\dot{\xi}$ will converge asymptotically to the scaled vector field $v\chi'$. Note that the integral curves of the state-dependent positive scaled vector field χ' has the same convergence results as those for the original vector field χ [25, Proposition 1.14]. Therefore, the generalized trajectory $(x(t), y(t), z(t), w(t))$ will converge to the higher-dimensional desired path ${}^{hgh}\mathcal{P}$ in (9.17). From Theorem 9.21, the actual

6 Suppose there exist $0 < t_1 < t_2$ such that $|\beta(t_1)| < |\beta(t_2)|$. It can be calculated that $V(t) = 1 - \cos \beta(t)$, and thus $V(t_1) < V(t_2)$, contradicting the decreasing property of \dot{V} . Thus $|\beta(t)|$ is indeed monotonically decreasing.

robot trajectory (i.e., the projected transformed trajectory) $(x(t), y(t), z(t))$ will converge to the physical desired path ${}^{\text{phy}}\mathcal{P}$ asymptotically as $t \rightarrow \infty$. \square

We set our aircraft to fly at a constant airspeed (around $12m/s$) and a constant altitude; therefore, we have a bounded speed v (estimated onboard with an Inertial Navigation System) when we account for the wind. For tracking 3D paths, the aircraft will nose down or change the propeller's revolutions per minute (r.p.m.); nevertheless, the airspeed is also bounded between $9m/s$ and $16m/s$. Note that both ground and airspeed are not control/guiding signals; therefore, we do not face any saturation problems regarding these variables.

9.6.3 Accommodating the guidance to the aircraft's dynamics

An arbitrary function $\phi_i(\cdot)$ in (9.16), which depends on a specific parametrization $f_i(\cdot)$, may result in a highly sensitive coordinate w . This can lead to considerable vibrations of the guidance signals, due to noisy sensor readings or disturbances of the position, that cannot be tracked effectively by the aircraft.

We propose two approaches, which can be combined to mitigate this practical effect. The first one is to re-parameterize the equations for the 3D desired path ${}^{\text{phy}}\mathcal{P}$; this does not affect the convergence result. Suppose ${}^{\text{phy}}\mathcal{P}$ is re-parameterized by

$$x = f_1(g(w)), \quad y = f_2(g(w)), \quad z = f_3(g(w)),$$

where $g : \mathbb{R} \rightarrow \mathbb{R}$ is a smooth bijection with non-zero derivative (i.e., $\frac{dg}{dw}(w) \neq 0$ for all $w \in \mathbb{R}$). A simple example of g is $g(w) = \beta w$, where β is a positive constant. This is adopted for the experiments. Let ϕ_1 , ϕ_2 , and ϕ_3 be chosen as in (9.16), then the first term of the higher-dimensional vector field becomes (for simplicity, the arguments are omitted)

$$\wedge(\nabla\phi_1, \nabla\phi_2, \nabla\phi_3) = -\left(\frac{df_1}{dg} \frac{dg}{dw}, \frac{df_2}{dg} \frac{dg}{dw}, \frac{df_3}{dg} \frac{dg}{dw}, 1\right)^{\top}.$$

To reduce the effect of the “virtual speed” from the fourth coordinate of the equation above, the “gain” $\frac{dg}{dw}$ can be chosen large such that $(\frac{df_1}{dg} \cdot \frac{dg}{dw})^2 + (\frac{df_2}{dg} \cdot \frac{dg}{dw})^2 + (\frac{df_3}{dg} \cdot \frac{dg}{dw})^2 \gg 1$, which implies that

$$\|\nabla\phi_1 \times \nabla\phi_2 \times \nabla\phi_3\| \approx \left| \frac{dg}{dw} \right| \sqrt{(\frac{df_1}{dg})^2 + (\frac{df_2}{dg})^2 + (\frac{df_3}{dg})^2}.$$

However, from the analytic expression of the vector field

$$\chi = \begin{bmatrix} -\frac{dg}{dw} \cdot \frac{df_1}{dg} - k_1\phi_1 \\ -\frac{dg}{dw} \cdot \frac{df_2}{dg} - k_2\phi_2 \\ -\frac{dg}{dw} \cdot \frac{df_3}{dg} - k_3\phi_3 \\ -1 + \frac{dg}{dw} \left(k_1\phi_1 \frac{df_1}{dg} + k_2\phi_2 \frac{df_2}{dg} + k_3\phi_3 \frac{df_3}{dg} \right) \end{bmatrix},$$

one observes that, when $\|(\phi_1, \phi_2, \phi_3)\|$ is large, (i.e., the aircraft is far from the desired path), the additional coordinate of the vector has also been enlarged approximately by a factor of $\frac{dg}{dw}$. Thus, the "gain" $|\frac{dg}{dw}|$ should not be chosen too large.

The second approach is to scale down the functions ϕ_i . That is, the equations (9.16) are changed to

$$\tilde{\phi}_i(x, y, z, w) = L\phi_i, i = 1, 2, 3,$$

where $L \in (0, 1)$. The corresponding 3D vector field is thus changed to

$$\tilde{\chi} = L \begin{bmatrix} -L^2 \frac{df_1}{dw} - k_1\phi_1 \\ -L^2 \frac{df_2}{dw} - k_2\phi_2 \\ -L^2 \frac{df_3}{dw} - k_3\phi_3 \\ -L^2 + k_1\phi_1 \frac{df_1}{dw} + k_2\phi_2 \frac{df_2}{dw} + k_3\phi_3 \frac{df_3}{dw} \end{bmatrix}.$$

The new guiding vector field is scaled down; thus, it helps to lower the sensitivity of the additional coordinate w .

9.6.4 The 2D trefoil curve

We start with following a 2D self-intersecting desired path, the trefoil curve, at a constant altitude $z_0 = 50m$ over the ground level. The parametric equations of the trefoil curve are given by

$$\begin{aligned} f_1(w) &= \cos(\beta w \omega_1)(a \cos(\beta w \omega_2) + b) \\ f_2(w) &= \sin(\beta w \omega_1)(a \cos(\beta w \omega_2) + b) \\ f_3(w) &= 0, \end{aligned}$$

where we have set $\beta = \frac{dg}{dw} = 0.45$ (the "gain" introduced in Section 9.6.3), $\omega_1 = 0.02$, $\omega_2 = 0.03$, $a = 80$, and $b = 160$. In order to fit into the available flying

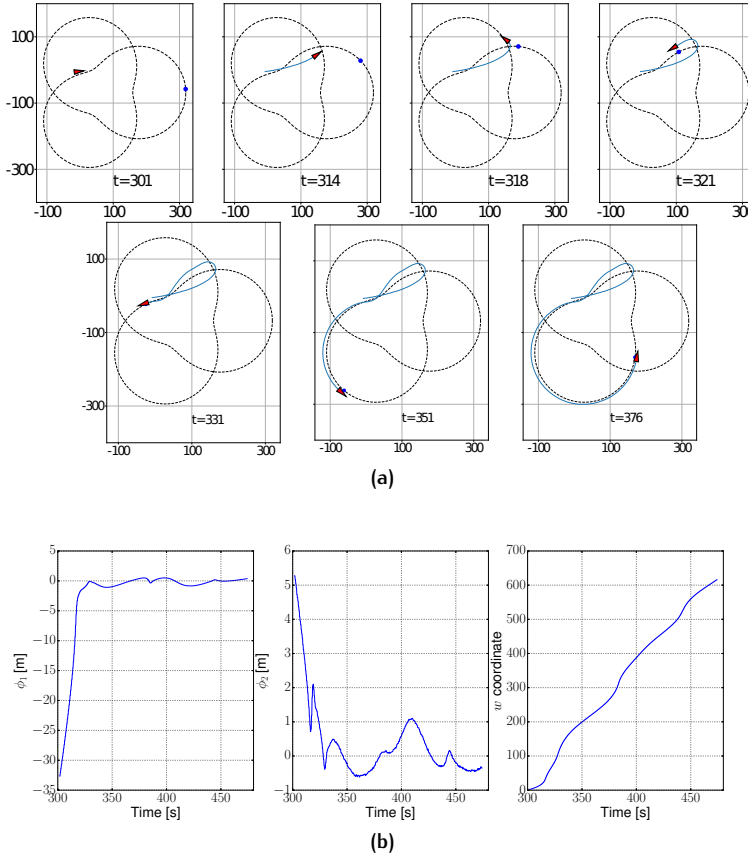


Figure 9.3: Flight results I. (a) illustrate the trajectories of the aircraft, which flies at a constant altitude of 50 meters. The blue dot, representing $(f_1(w), f_2(w))$, moves forward but *waits* for the aircraft at time $t = 321$. Afterward, the aircraft converges to the desired path as the first two plots in (b) indicate with ϕ_1 and ϕ_2 fluctuating around 0. The third plot in (b) shows the evolution of the virtual coordinate w , of which the grow rate varies as it is in the closed-loop with the aircraft's position to facilitate the path convergence.

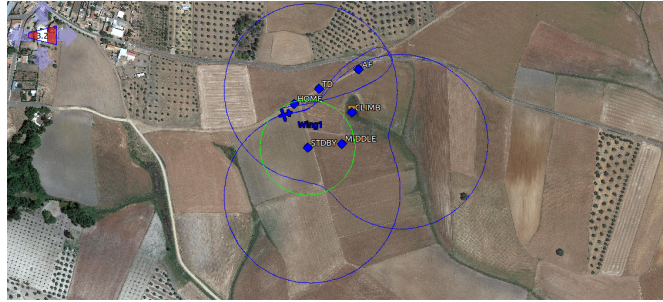


Figure 9.4: The screenshot of the ground control station corresponding to Fig. 9.3. The green circle is the *stand-by* trajectory before the aircraft starts following the trefoil curve. The blue line is the 2D trajectory of the aircraft.

space, these parametric equations have been rotated by α and shifted adequately by (x_o, y_o) in the autopilot; i.e.,

$$\begin{aligned} f_1^*(w) &= \cos(\alpha)f_1(w) - \sin(\alpha)f_2(w) + x_o \\ f_2^*(w) &= \sin(\alpha)f_1(w) + \cos(\alpha)f_2(w) + y_o \\ f_3^*(w) &= f_3(w) + z_o. \end{aligned}$$

Note that the same affine transformation must be done for both f_i' and f_i'' (needed for the Jacobian of χ as we will see shortly). In particular, for the presented flight, we set $x_o = 79$, $y_o = -68.10$ and $z_o = 50$ meters and $\alpha = 0$. We set the scaling factor $L = 0.1$ for the construction of $\tilde{\phi}_i$ as in Section 9.6.3, and we choose the gains $k_1 = k_2 = k_3 = 0.002$. We finally set $k_\theta = 1$ for the control/guidance signal u_θ in Proposition 9.23.

Note that for computing all the control signals (9.21), we need $f_i(w)$ and their derivatives $f_i'(w)$ and $f_i''(w)$ with respect to w . For the sake of completeness, we provide the Jacobian $J(\chi^p)$ in (9.21a) which is given by

$$J(\chi^p) = FJ(\hat{\chi}) = F(I - \hat{\chi}\hat{\chi}^\top)J(\chi)/\|\chi\|,$$

where $F = \begin{bmatrix} 1 & 0 & 0 \\ 0 & 1 & 0 \\ 0 & 0 & 0 \end{bmatrix}$, and $J(\chi)$ is shown below

$$J(\chi) =$$

$$L \begin{bmatrix} -k_1 L & 0 & 0 & -f_1''(\beta w)L^2\beta^2 + k_1\beta Lf_1'(\beta w) \\ 0 & -k_2 L & 0 & -f_2''(\beta w)L^2\beta^2 + k_2\beta Lf_2'(\beta w) \\ 0 & 0 & -k_3 L & -f_3''(\beta w)L^2\beta^2 + k_3\beta Lf_3'(\beta w) \\ k_1\beta Lf_1'(\beta w) & k_2\beta Lf_2'(\beta w) & k_3\beta Lf_3'(\beta w) & \beta^2 \sum_{i=1}^3 [k_i\phi_i f_i''(\beta w) - k_i L f_i'^2(\beta w)] \end{bmatrix}$$

The flight results for the trefoil curve are shown in Figure 9.3.

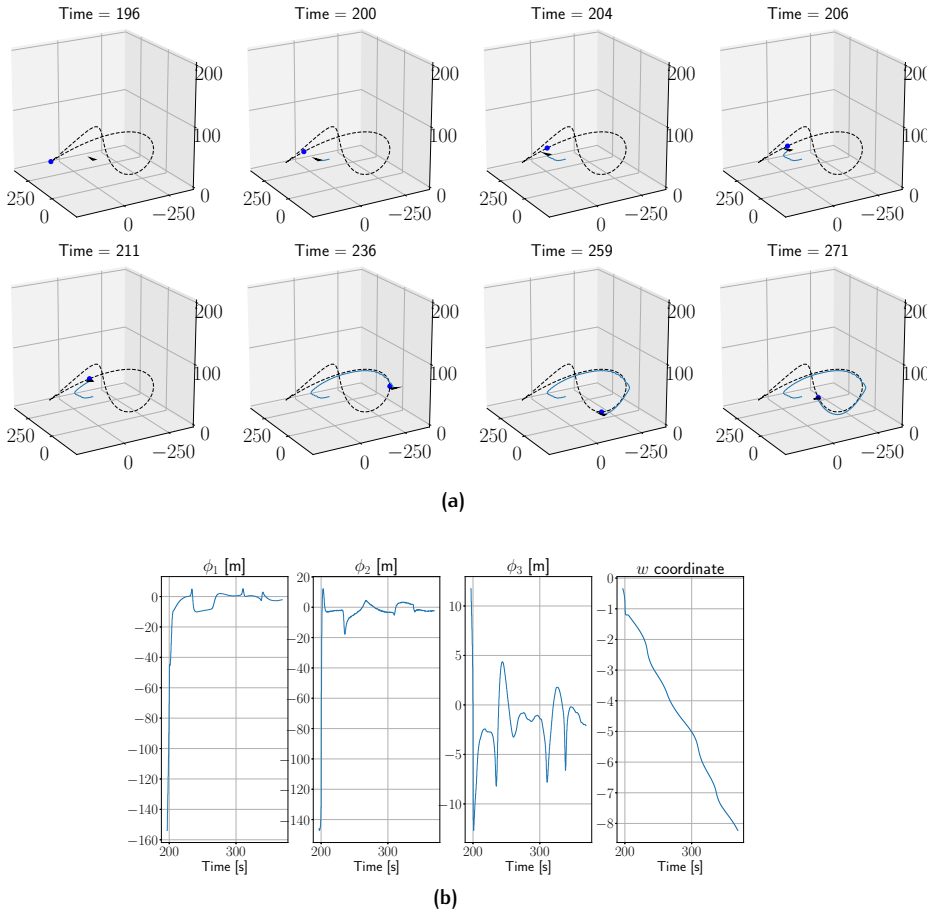


Figure 9.5: Flight results II. (a) illustrates the trajectories of the aircraft. The blue dot, representing $(f_1(w), f_2(w), f_3(w))$, moves forward quickly but *waits* for the aircraft at time $t = 204$. This quick movement is due to the fast variation of w in the beginning (see the fourth plot in (b)). Afterward, the vehicle converges to the desired path as the first three plots in (b) indicate with ϕ_1, ϕ_2 , and ϕ_3 fluctuating around 0. The aircraft has been trimmed to fly at a constant altitude, but the desired path requires the vehicle to track a sinusoidal ascending/descending trajectory, and any disturbance (e.g., unsteady wind) makes the aircraft sensitive to track accurately a climbing/descending speed. In addition, the Lissajous curve demands aggressive turnings slightly beyond the capabilities of the aircraft when the aircraft descends and achieves the maximum speed. The fourth plot in (b) shows the evolution of the virtual coordinate w , of which the grow rate varies as it is in the closed-loop with the aircraft's position to facilitate the path convergence.

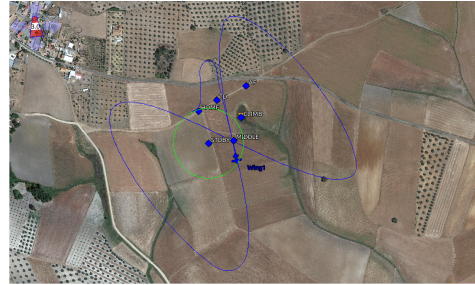


Figure 9.6: The screenshot of the ground control station corresponding to Fig. 9.5. The green circle is the *stand-by* trajectory before the aircraft starts following the Lissajous curve. The blue line is the 2D trajectory of the aircraft. In particular, the aircraft passes by the *middle waypoint* corresponding to the highest point of the desired path.

9.6.5 The 3D Lissajous curve

We consider the 3D Lissajous curve described as below:

$$\begin{aligned} f_1(w) &= c_x \cos(\beta w \omega_x + d_x) \\ f_2(w) &= c_y \cos(\beta w \omega_y + d_y) \\ f_3(w) &= c_z \cos(\beta w \omega_z + d_z), \end{aligned}$$

where we have set $\beta = \frac{dg}{dw} = 0.01$, $\omega_x = 1$, $\omega_y = \omega_z = 2$, $c_x = c_y = 225$, $c_z = -20$, $d_x = d_z = 0$, and $d_y = \pi/2$. This selection of parameters gives us an *eight-shaped* desired path that is bent along the vertical axis. As with the trefoil curve, we have added an affine transformation of $f_i(w)$, $f'_i(w)$ and $f''_i(w)$ in the autopilot to fit the Lissajous curve into the available flying space. In particular, we have set $x_0 = 79$, $y_0 = -68.10$, $z_0 = 50$, $\alpha = 0.66$. Finally, for the construction of $\tilde{\phi}_i$, we have chosen $L = 0.1$, $k_1 = k_2 = 0.002$ and $k_3 = 0.0025$. We finally set $k_\theta = 1$ for the control/guiding signal u_θ in Proposition 9.23. We show the flight results in Figure 9.5.

9.7 DISCUSSION: PATH FOLLOWING OR TRAJECTORY TRACKING?

In this section, we show that our proposed higher-dimensional VF-PF algorithm is an extension that combines elements from both conventional VF-PF algorithms (e.g., [63], see Remark 9.3) and trajectory tracking algorithms (e.g., [131, p. 506]). While our generated guiding vector field is the standard output for the path-

following approach, we will argue that our algorithm can also be seen as a fair extension of a trajectory tracking approach. Therefore, our algorithm, to some extent, combines and extends elements from both approaches. For ease of explanation and without loss of generality, we restrict our focus to a physical planar desired path in \mathbb{R}^2 ; that is, ${}^{\text{phy}}\mathcal{P} \subseteq \mathbb{R}^2$.

Compared to trajectory tracking algorithms, a similarity exists in the sense that the additional coordinate w in the proposed VF-PF algorithms acts like the time variable in trajectory tracking algorithms. However, our approach is an extension in the sense that the time-like variable is in fact state-dependent. In trajectory tracking algorithms, a desired trajectory $(x_d(t), y_d(t))$ is given. Then, at any time instant t , the algorithm aims to decrease the distance to the *desired trajectory point* $(x_d(t), y_d(t))$, which moves as time t advances. Note that the dynamics of the *desired trajectory point* $(x_d(t), y_d(t))$ is *open-loop* in the sense that it does not depend on the current states of the robot, but only depends on time t . From (9.16), if we let $\phi_i = 0$, $i = 1, 2$, then we may call the point $(f_1(w(\xi(t))), f_2(w(\xi(t))))$ the *guiding point*, since it always stays on the desired path and may be regarded as the counterpart of the *desired trajectory point* in trajectory tracking algorithms. But as we will show later, the *guiding point* is essentially different from the *desired trajectory point*. Note that the *guiding point* $(f_1(w(\xi(t))), f_2(w(\xi(t))))$ in our VF-PF algorithm depends on the evolution of the additional coordinate $w(\xi(t))$, of which the dynamics is state-dependent as shown in (9.20). This might be roughly regarded as a *closed-loop* version of the *desired trajectory point*. An intuitive consequence of this difference is that the *desired trajectory point* $(x_d(t), y_d(t))$ in trajectory tracking algorithms always moves *unidirectionally* along the desired trajectory as t monotonically increases, while the *guiding point* can move *bidirectionally* along the desired path, subject to the current state (i.e., the robot position). In fact, when the initial position of the *guiding point* $(f_1(w(\xi(0))), f_2(w(\xi(0))))$ is far from the initial position of the robot, the *guiding point* “proactively” moves towards the robot along the desired path to accelerate the path-following process. This feature, along with better robustness against perturbation in some cases, are experimentally studied in our previous work [164, Section VII]. To illustrate this closed-loop feature more intuitively, after the robot has successfully followed the desired path, we manually move the robot far away from the desired path and keep it stationary (to mimic the situation of erroneous localization and operation failure of the robot). As is clear in the supplementary video⁷, although the robot is kept stationary, the guiding point $(f_1(w(\xi(t))), f_2(w(\xi(t))))$ can still move in the reverse direction to approach the robot along the desired path such that the norm of the path-following error decreases, and the guiding point eventually stops at some place on the desired path. After that, the guiding point does not move until the robot is released to move again.

⁷ http://tiny.cc/video_tr021yao

In existing VF-PF algorithms, a two-dimensional vector field on \mathbb{R}^2 is created for guiding the robot movement (see Remark 9.3). However, as we aim to create a higher-dimensional (i.e., three-dimensional) vector field, our approach can be roughly regarded as utilizing an infinite number of layers of projected two-dimensional vector fields, and thus might be seen as a *dynamic* two-dimensional vector field. The dynamic property is due to the dynamics of the additional coordinate w . For example, consider a circular desired path parameterized by

$$x = f_1(w) = \cos(4w) \quad y = f_2(w) = \sin(4w),$$

where $w \in \mathbb{R}$ is the parameter. In conventional VF-PF algorithms, a 2D vector field can be created, as shown in Fig. 9.1a, but there exists a singular point at the center of the circle. Nevertheless, using our approach, we can generate a singularity-free 3D vector field, as illustrated in Fig. 9.7. For clarity of visualization, we plot the 3D vectors, which originate from three planes where the w values are 0, 0.6, and 1.4, respectively. For each value of the additional coordinate w , we can obtain a projected 2D vector field, as shown in Fig. 9.8. Therefore, we can observe that these 2D vector fields change dynamically as w varies. As a result of the dynamics of w , the *guiding point* ($f_1(w(\xi(t))), f_2(w(\xi(t)))$) moves along the 2D desired path (not necessarily unidirectionally). Again, we note that this point is *not* the same as the *desired trajectory point* in trajectory tracking algorithms since the integral curves of the 2D vector field do not converge to this point, as can be seen graphically from Fig. 9.8 or analytically from the expression of the vector field in (9.5): the second term leads to convergence to the *guiding point*, while the first term “deviates” this convergence, since it controls the propagation along the *higher-dimensional* desired path.

In many existing VF-PF algorithms, the desired path is usually not parameterized but is described by the intersection of hyper-surfaces, while the latter case might be restrictive in describing more complicated desired paths. However, our approach enables the possibility to use a parameterized desired path directly in the design of a higher-dimensional vector field. Our approach thus extends the flexibility of conventional VF-PF algorithms. The desired path can now be described by either the intersection of hyper-surfaces or parameterized functions. In the latter case, the parametric equations can be easily converted using (9.15), (9.16) and (9.17) and leads to a higher-dimensional desired path and singularity-free guiding vector field. Theoretically, the parametrization is not instrumental, since it is only utilized to derive the expressions of functions ϕ_i , of which the zero-level sets are interpreted as hyper-surfaces. The subsequent derivation of the vector field is based on ϕ_i , independent of the specific parametrization of the desired path.

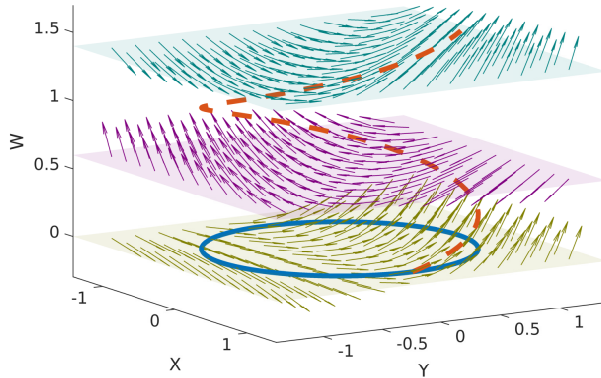


Figure 9.7: Three layers of the 3D vector field corresponding to a circle. The solid line is the 2D desired path while the dashed line is the corresponding 3D (unbounded) desired path. Three layers of the 3D vector field evaluated at $w = 0, 0.6, 1.4$ respectively are illustrated.

9.8 AN ALTERNATIVE PROOF

In this section, we give an alternative proof of Proposition 9.10. Given an autonomous differential equation $\dot{x}(t) = f(x(t))$, where f is continuously differentiable in x , and let $t \mapsto \Psi(t, x_0)$ be the solution to the differential equation with the initial condition $\Psi(0, x_0) = x_0$, then Ψ is a flow [25]. In the literature, the notation $\Psi^t(x_0)$, which is adopted in the sequel, is often used in place of $\Psi(t, x_0)$. To assist the proof of Proposition 9.10, we state a more general result in the following lemma regarding any time-invariant autonomous system that admits a (locally) asymptotically stable limit cycle. Note that similar to the definition of Lyapunov stability of an equilibrium point [66, Chapter 4], a limit cycle \mathcal{L} is (locally) asymptotically stable if for every neighborhood $\mathcal{U} \supseteq \mathcal{L}$ of the limit cycle \mathcal{L} , there exists a *smaller* neighborhood $\mathcal{V} \subseteq \mathcal{U}$, such that every trajectory starting from \mathcal{V} always stays within \mathcal{U} and \mathcal{L} is locally attractive.

Lemma 9.24 (Asymptotically stable limit cycles are not GAS). *Consider an autonomous differential equation $\dot{x}(t) = f(x(t))$, where $f : \mathbb{R}^n \rightarrow \mathbb{R}^n$ is continuously differentiable in x . Suppose there is a (locally) asymptotically stable limit cycle $\mathcal{L} \subseteq \mathbb{R}^n$, then global convergence of trajectories to the limit cycle is not possible; namely, the domain of attraction of the limit cycle cannot be \mathbb{R}^n . In other words, the limit cycle cannot be globally asymptotically stable (GAS) in \mathbb{R}^n .*

Proof. We prove by contradiction: Suppose that global convergence to the limit cycle \mathcal{L} holds. Since the limit cycle is compact, it is an embedded submanifold in \mathbb{R}^n [77, Proposition 5.21]. So we can take a tubular neighborhood $\mathcal{O} \supseteq \mathcal{L}$ of the limit cycle [77, Theorem 6.24]. Then due to the asymptotic stability of the

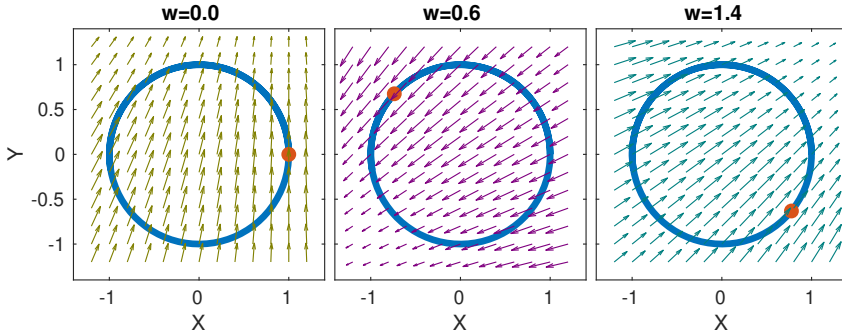


Figure 9.8: The projected 2D vector field corresponding to $w = 0, 0.6, 1.4$ respectively. The solid line is the projected 2D desired path. The solid dots represent the guiding point $(\cos(4w), \sin(4w))$.

limit cycle, there exists a smaller neighborhood $\mathcal{U} \subseteq \mathcal{O}$ of the limit cycle such that every trajectory starting from \mathcal{U} will remain within the tubular neighborhood \mathcal{O} perpetually. Since the limit cycle is compact, we can find a closed ball $\bar{\mathcal{B}} \subseteq \mathbb{R}^n$ centered at $\mathbf{0} \in \mathbb{R}^n$ sufficiently large such that the limit cycle lies in its interior (i.e., $\mathcal{L} \subseteq \bar{\mathcal{B}}$). Due to the global convergence assumption, for any point $w \in \bar{\mathcal{B}}$, there exists a time instant $T_w > 0$ such that $\Psi^{T_w}(w) \in \mathcal{U}$, where Ψ denotes the flow of the differential equation $\dot{x} = f(x)$. Due to the continuous dependence on initial conditions [66, Theorem 3.5], there exists an open set $\mathcal{V}_w \ni w$, such that $\Psi^{T_w}(\mathcal{V}_w) \subseteq \mathcal{U}$. Therefore, according to the uniqueness of solutions to the differential equation (see Theorem 2.1) and the asymptotic stability discussed before, we further have $\Psi^t(\mathcal{V}_w) \subseteq \mathcal{O}$ for all $t \geq T_w$. Thus, for every point $w \in \bar{\mathcal{B}}$, we can associate an open set \mathcal{V}_w and a time instant T_w as discussed before. Since $\mathcal{D} := \{\mathcal{V}_w \subseteq \mathbb{R}^n : w \in \bar{\mathcal{B}}\}$ is an open cover of the compact ball $\bar{\mathcal{B}}$, there exists a finite number of points $w_i \in \bar{\mathcal{B}}, i = 1, \dots, k$, and $\mathcal{V}_{w_i} \in \mathcal{D}$, such that $\bigcup_{i=1}^k \mathcal{V}_{w_i} \supseteq \bar{\mathcal{B}}$ [140, Theorem 1.5.8]. Thus, we can take $T > \max_{i=1, \dots, k} \{T_{w_i}\}$, and therefore, we have $\Psi^T(\mathcal{B}) \subseteq \mathcal{O}$.

Let $r : \mathcal{O} \rightarrow \mathcal{L}$ be a retraction⁸ of \mathcal{O} onto \mathcal{L} ; i.e., $r \circ i_{\mathcal{L}} = \text{id}_{\mathcal{L}}$, where $i_{\mathcal{L}} : \mathcal{L} \rightarrow \mathcal{O}$ is the inclusion map of \mathcal{L} in \mathcal{O} and id is the identity map. Now let $i'_{\mathcal{L}} : \mathcal{L} \rightarrow \bar{\mathcal{B}}$ be another inclusion map, and note that for any $t \in \mathbb{R}$, $\Psi^t(\cdot)$ is a diffeomorphism of \mathcal{L} [25, p. 13]. Then it is easy to check that $\text{id}_{\mathcal{L}} = \Psi^{-T} \circ r \circ \Psi^T \circ i'_{\mathcal{L}}$, where we view Ψ^T as a map from $\bar{\mathcal{B}}$ to \mathcal{O} and Ψ^{-T} a map from \mathcal{L} to \mathcal{L} . It is conventional to use $(\cdot)_*$ and $\pi_1(\cdot)$ to denote the homomorphism and the fundamental group respectively. Then

$$\begin{aligned} (\text{id}_{\mathcal{L}})_* &= (\Psi^{-T} \circ r \circ \Psi^T \circ i'_{\mathcal{L}})_* \\ &= (\Psi^{-T})_* \circ (r)_* \circ (\Psi^T)_* \circ (i'_{\mathcal{L}})_*, \end{aligned} \tag{9.23}$$

⁸ The existence of r is guaranteed by Proposition 6.25 in [77].

where $(\text{id}_{\mathcal{L}})_* : \pi_1(\mathcal{L}) \rightarrow \pi_1(\mathcal{L})$, $(i'_{\mathcal{L}})_* : \pi_1(\mathcal{L}) \rightarrow \pi_1(\overline{\mathcal{B}})$, $(\Psi^T)_* : \pi_1(\overline{\mathcal{B}}) \rightarrow \pi_1(\mathcal{O})$, $r_* : \pi_1(\mathcal{O}) \rightarrow \pi_1(\mathcal{L})$ and $(\Psi^{-T})_* : \pi_1(\mathcal{L}) \rightarrow \pi_1(\mathcal{L})$ are the homomorphisms of fundamental groups induced by the corresponding maps [77, Proposition A.64, A.65]. Since $\overline{\mathcal{B}}$ is contractible and $\pi_1(\overline{\mathcal{B}}) \cong \{0\}$, where \cong denotes the isomorphic relation, both $(i'_{\mathcal{L}})_*$ and $(\Psi^T)_*$ are zero morphisms, and so is the composition $(\Psi^{-T})_* \circ (r)_* \circ (\Psi^T)_* \circ (i'_{\mathcal{L}})_*$. But this contradicts with the left-hand side of (9.23), where $(\text{id}_{\mathcal{L}})_*$ is the identity map (and an isomorphism) of $\pi_1(\mathcal{L}) \cong \mathbb{Z}$. The contradiction implies that global convergence is not possible. \square

Based on Lemma 9.24, we can prove Proposition 9.10.

Proof of Proposition 9.10. We consider the autonomous systems (9.9). Without loss of generality, we assume that the flow of (9.9) is complete, since otherwise we can replace the vector field χ by $\chi/(1 + \|\chi\|)$ without changing the phase portrait [25, Proposition 1.14].

Given $\alpha > 0$, we define a neighborhood of the desired path \mathcal{P} by

$$\mathcal{E}_\alpha = \{\xi \in \mathbb{R}^n : \|e(\xi)\| < \alpha\}. \quad (9.24)$$

Therefore, the value of $\|e(\cdot)\|$ encodes the *distance* to the desired path in view of the definition of \mathcal{P} in (9.6). From Lemma 5.1, we have $N^\top \chi = N^\top (\perp_\phi - NKe) = -N^\top NKe$. We define a Lyapunov function candidate

$$V(e) = \frac{1}{2} e^\top K e, \quad (9.25)$$

and take the time derivative of it, obtaining

$$\begin{aligned} \dot{V}(e) &= \frac{1}{2} (\dot{e}^\top K e + e^\top K \dot{e}) \\ &= \frac{1}{2} (\chi^\top NKe + e^\top KN^\top \chi) \\ &= -e^\top Qe = -\|NKe\|^2 \leq 0, \end{aligned} \quad (9.26)$$

where the $(n-1) \times (n-1)$ matrix

$$Q(\xi) = K^\top N^\top(\xi) N(\xi) K \quad (9.27)$$

is positive semidefinite. Based on the LaSalle's invariance principle (Theorem 2.6), one can show that the desired path \mathcal{P} is the limit cycle of (9.9) by construction, and that \mathcal{P} is Lyapunov stable. The claim then easily follows from Lemma 9.24. \square

9.9 CONCLUSIONS

In this chapter, we first show that the integral curves of a time-invariant continuously differential vector field as in (9.2) cannot guarantee global converge to desired paths which are simple closed (i.e., homeomorphic to the unit circle) or self-intersecting. Motivated by this general topological result, we propose a novel approach to create unbounded desired paths from simple closed or self-intersecting ones, and construct a singularity-free higher-dimensional guiding vector field. One of the advantages of this approach is that global convergence to the desired paths, which can be even self-intersecting, is now rigorously guaranteed. This is achieved by the introduction of a transformation operator and the extended dynamics. Another advantage is that, given a parameterized desired path, we can easily describe the hyper-surfaces as the zero-level set of some implicit functions, and then the proposed vector field on a higher-dimensional space can be directly constructed. This increases the applicability of conventional VF-PF algorithms. In addition, we highlight five features of our approach, with rigorous theoretic guarantees. We also show that our approach is a combined extension of both conventional VF-PF algorithms and trajectory tracking algorithms. Finally, we conduct outdoor experiments with a fixed-wing aircraft under wind perturbation to validate the theoretical results and demonstrate the practical effectiveness for complex robotic systems.

10

GUIDING VECTOR FIELDS FOR MULTI-ROBOT COORDINATED NAVIGATION

Tasks requiring repetitive execution, such as environmental monitoring and area patrolling, are more efficiently accomplished by a group of coordinated robots, which are equipped onboard with path-following navigation algorithms. Among these algorithms, those based on guiding vector fields have been shown to achieve outstanding performance, but most of them are designed for the navigation of one single robot.

In this chapter, we propose coordinating guiding vector fields for the distributed motion coordination and navigation of a group of an arbitrary number of robots on different desired paths or surfaces. The motion coordination is realized implicitly by controlling additional virtual coordinates integrated with the original guiding vector field, and these virtual coordinates turn out to be the parameters defining the desired paths or surfaces. Therefore, after motion coordination is quantified by desired parametric displacements, rigorous mathematical guarantees underpinned by dynamical systems theory and Lyapunov theory are provided for the effective distributed motion coordination and navigation of robots on paths or surfaces from all initial positions. A control algorithm is further derived from the coordinating guiding vector field for a Dubins-car-like model with actuation saturation.

Our algorithm excels in its flexibility to deal with a wide range of paths and surfaces, its distributed and scalable nature and its low cost in communication and computation, among others. Extensive simulations and fixed-wing aircraft outdoor experiments validate the effectiveness and robustness of our algorithm.

This chapter is based on

- W. Yao, H. G. de Marina, Z. Sun, and M. Cao, “Distributed coordinated path following using guiding vector fields,” in *IEEE International Conference on Robotics and Automation (ICRA)*, 2021.
- W. Yao, H. G. de Marina, Z. Sun, and M. Cao, “Guiding vector fields for multi-robot coordinated navigation,” 2021, *Submitted*.

10.1 INTRODUCTION

Compared with a single robot, a multi-robot system is usually more efficient in accomplishing tasks associated with vast areas or volumes, such as environmental monitoring and area patrolling. Nevertheless, to reliably and systematically coordinate robots in a large multi-robot system without a central nexus is one of the grand challenges in robotics [155]. A fundamental question of this challenge is how to design a mechanism such that multiple robots are able to accurately follow possibly different desired paths and coordinate their motions in a distributed fashion, with the resulting formation satisfying some geometric or parametric constraints. In this chapter, we propose a coordinating guiding vector field with virtual dimensions to guide an arbitrary number of robots to realize motion coordination on possibly different desired paths or surfaces in a distributed way through local information exchange. The proposed guiding vector field has many appealing features such as ensuring rigorous guarantees of motion coordination and path/surface convergence.

10.1.1 Related work

Single-robot path-following capability is fundamental in mobile robotics applications, and many algorithms have been proposed and widely studied [137]. It is concluded by numerical simulations in [137] that those algorithms based on guiding vector fields achieve relatively high path-following accuracy while they require less control effort, compared with several other tested algorithms, such as LQR-based ones [115] and nonlinear guidance laws (NLGL) [111]. This conclusion is experimentally supported by [22]. Despite the performance advantages, these vector field guided path-following algorithms are mostly designed for a single robot, while the extension for a multi-robot system is relatively less studied. In fact, to the best of our knowledge, there are only a few studies exploiting a guiding vector field for distributed multi-robot motion coordination. In [32], the guiding vector field proposed in [63] is combined with a distributed algorithm to dynamically change the radii of circular paths such that multiple fixed-wing aircraft flying at a constant speed can eventually follow the same circular path and keep pre-defined inter-robot distances. A different guiding vector field is derived in [102] based on various potential functions for multiple robots to move on common paths such as a circle or a straight line. Another work [114] presents a distributed control law for a number of robots to circulate a closed curve described in a specific form in 3D.

Without employing a guiding vector field, various algorithms are proposed in the literature for multi-robot coordinated path-following. A virtual structure is utilized in [48] for multiple robots to coordinate their motions while they follow predefined paths. As each robot needs to broadcast its states and reference

trajectories to other robots, the communication overhead increases as the number of robots increases. A theoretical study is illustrated in [169] considering planar simple closed curves and unit-speed particles. In [123], the desired motion coordination among robots are generated by a linear exo-system, and an output-regulation controller is implemented on some robots while others are controlled through local interactions. Many other works study multi-robot distributed path-following on planar simple desired paths (e.g., a straight line), such as [20], [23], [38], [117], [148]. The papers [95], [96] design distributed controllers for robots characterized by the single-integrator or double-integrator model such that they can generate 2D desired geometric patterns composed of simple closed curves or circulate a 2D closed curve.

Circular formation control and circumnavigation control, which have been extensively studied, can be regarded as specialized cases of multi-robot coordinated path-following control. In the circular formation control problem, robots are required to distribute along a circle and maintain some desired arc distances using local interactions [60], [125], [135], [138], [144], [145]. Motivated by some specific applications, such as entrapment of a hostile target, an additional requirement for all robots to move persistently along the circle is imposed in a circumnavigation control problem [34], [39], [43], [129], [163], [170]. Nevertheless, as clear from their problem formulations, these studies only take into account circular paths mostly in a 2D plane. Although it is possible to extend these studies to consider other closed paths, this might require some continuous transformation between paths, which is a nontrivial task in general.

10.1.2 Contributions

We propose a coordinating guiding vector field for a multi-robot system to achieve global convergence to desired paths or surfaces while their motions are coordinated in a distributed way via local communication. Based on the coordinating guiding vector field, a saturated control algorithm is then designed for a nonholonomic Dubins-car-like model. Specifically, we consider desired paths and surfaces defined as parametric equations such that the motion coordination among robots can be quantified by relative parametric differences. Starting from the guiding vector field for single-robot path following [50], [63], we then consider multiple robots following different desired paths or maneuvering on different surfaces, where the robot motions are coordinated by the coordinating guiding vector fields that are extended with virtual coordinates and coupled via a consensus term [108]. The consensus term is related to virtual coordinates of neighboring robots encoded in an undirected communication graph. These new guiding vector fields implicitly and effectively control the *relative parametric separation* among robots.

Our approach is appealing in several aspects: 1) There are rigorous mathematical guarantees on the global convergence of robots' trajectories converging to the desired paths or surfaces and achieving the motion coordination. 2) Our approach can deal with complex paths, such as self-intersecting, non-closed, and non-convex ones in an n -dimensional configuration space, and applicable for arbitrary surfaces described by parametric equations. The approach can also be naturally extended for higher-dimensional manifolds (e.g., a cube). 3) Given a fixed communication frequency, the communication cost is low, since every two neighboring robots only need to receive and transmit the virtual coordinates, of which the number is equal to that of the path or surface parameters. The approach is also computationally cheap and is suitable for real-time applications since online optimization is not required. 4) The approach is distributed and scalable, so the number of robots can be arbitrarily large. 5) The effectiveness of our algorithm is verified by simulations with a large multi-robot system and by outdoor experiments with real fixed-wing aircraft. Thus, our algorithm is robust against wind perturbation, localization inaccuracy and actuator saturation. 6) We also demonstrate that our algorithm is promising in applications such as area or volume coverage tasks by exploiting a 2D or 3D Lissajous curve with *irrational coefficients*.

The remainder of this chapter is organized as follows. Section 10.2 introduces the preliminaries on graph theory and guiding vector fields for path following. Then Section 10.3 elaborates on how to extend the guiding vector field for multi-robot distributed motion coordination and navigation on desired paths. The theoretical results are further extended to deal with coordinated maneuvering on parametric surfaces in Section 10.4. We also discuss how the coordinating guiding vector field can be seamlessly integrated with a safety barrier certificate to address the collision issue in Section 10.5. Next, we consider a realistic robot model for fixed-wing aircraft and derive a control law from the coordinating guiding vector field in Section 10.6. Moreover, extensive simulation examples and experiments with fixed-wing aircraft are carried out in Section 10.7. Finally, Section 10.8 concludes the chapter.

10.2 PRELIMINARIES

10.2.1 Notations

The set of integers $\{m \in \mathbb{Z} : i \leq m \leq j\}$ is denoted by \mathbb{Z}_i^j . We use boldface for a vector $v \in \mathbb{R}^n$, and its j -th entry is denoted by v_j for $j \in \mathbb{Z}_1^n$. Consider a system consisting of N robots. Any quantity associated with the i -th robot is symbolized by the superscript $(\cdot)^{[i]}$. For example, the notation $u^{[i]} \in \mathbb{R}^n$ denotes a vector associated with the i -th robot for $i \in \mathbb{Z}_1^N$, and the j -th entry of it is denoted by $u_j^{[i]}$.

for $j \in \mathbb{Z}_1^n$ (note that $u_j^{[i]}$ is not boldfaced since it is a scalar). The notation $\text{diag}\{\cdot\}$ denotes a diagonal (block) matrix obtained by putting vectors or matrices on the diagonal. If \mathcal{A} is a finite set, then $|\mathcal{A}|$ denotes its cardinality (i.e., the number of elements in the set).

10.2.2 Graph theory

This subsection is based on [88]. A finite, undirected *graph* (or *graph* for short) is a set-theoretic object $\mathcal{G} = (\mathcal{V}, \mathcal{E})$, where the *vertex set* $\mathcal{V} := \{1, \dots, N\}$ contains a finite set of elements, called *vertices*, and the *edge set* \mathcal{E} is a subset of $\mathcal{V} \times \mathcal{V}$, of which the elements are denoted by (i, j) , representing the *adjacent* relationship between vertices i and j for $i, j \in \mathcal{V}$. The k -th edge is denoted by $\mathcal{E}_k = (\mathcal{E}_k^{\text{head}}, \mathcal{E}_k^{\text{tail}})$, where $\mathcal{E}_k^{\text{head}} \in \mathcal{V}$ and $\mathcal{E}_k^{\text{tail}} \in \mathcal{V}$ are the *head* and *tail* of the edge, respectively. The set of neighboring robots of robot i is denoted by $\mathcal{N}_i := \{j \in \mathcal{V} : (i, j) \in \mathcal{E}\}$. The graph \mathcal{G} is *connected* if there is a path between any pair of vertices in \mathcal{V} . The *adjacency matrix* $A(\mathcal{G})$ of the undirected graph \mathcal{G} is the symmetric $N \times N$ matrix encoding the adjacency relationships of vertices; that is, $[A(\mathcal{G})]_{ij} = 1$ if $(i, j) \in \mathcal{E}$ and $[A(\mathcal{G})]_{ij} = 0$ otherwise. The *Laplacian matrix* $L(\mathcal{G})$ of \mathcal{G} is the $N \times N$ matrix defined by $[L(\mathcal{G})]_{ij} = -a_{ij}$ for $i \neq j$ and $[L(\mathcal{G})]_{ii} = \sum_{k=1}^N a_{ik}$ for $i \in \mathbb{Z}_1^N$, where a_{ij} is the ij -th entry of the adjacency matrix. For an undirected graph, we define the elements of the incidence matrix $B \in \mathbb{R}^{|\mathcal{V}| \times |\mathcal{E}|}$ by $b_{ik} = +1$ if $i = \mathcal{E}_k^{\text{tail}}$, $b_{ik} = -1$ if $i = \mathcal{E}_k^{\text{head}}$, and $b_{ik} = 0$ otherwise. The N -cycle graph $C_N = (\{1, \dots, N\}, \mathcal{E}_C)$ is the graph where the edge set \mathcal{E}_C contains edges (i, j) with $i - j = \pm 1 \pmod N$.

10.2.3 Guiding vector field with a virtual coordinate for a single robot

Guiding vector fields with virtual coordinates for robot navigation enjoy many features, such as guaranteeing global convergence to the desired path and enabling self-intersected desired path following (see Chapter 9). We present here a brief introduction. Suppose the desired path ${}^{\text{phy}}\mathcal{P}$ is parameterized by

$$x_1 = f_1(w), \dots, x_n = f_n(w),$$

where x_j is the j -th coordinate, $w \in \mathbb{R}$ is the parameter of the path and f_j is twice continuously differentiable (i.e., $f_j \in C^2$), for $j \in \mathbb{Z}_1^n$. To derive a corresponding guiding vector field for the desired path, we need to describe the desired path as the intersection of n hyper-surfaces [50], [63], [74], [157]. To this end, taking w as an additional argument, we define n level functions $\phi_j : \mathbb{R}^{n+1} \rightarrow \mathbb{R}$ as follows: $\phi_1(\xi) = x_1 - f_1(w), \dots, \phi_n(\xi) = x_n - f_n(w)$, where $\xi = (x_1, \dots, x_n, w) \in \mathbb{R}^{n+1}$ is the generalized coordinate with an additional (virtual) coordinate w . Therefore,

the desired path with an additional coordinate is the intersection of the hyper-surfaces described by the zero-level set of these functions; that is,

$${}^{\text{high}}\mathcal{P} := \{\xi \in \mathbb{R}^{n+1} : \phi_j(\xi) = 0, j \in \mathbb{Z}_1^n\}.$$

The projection of the higher-dimensional ${}^{\text{high}}\mathcal{P}$ onto the hyper-plane spanned by the first n coordinates is the original desired path ${}^{\text{phy}}\mathcal{P}$, so we can use the higher-dimensional guiding vector field $\chi : \mathbb{R}^{n+1} \rightarrow \mathbb{R}^{n+1}$ corresponding to ${}^{\text{high}}\mathcal{P}$ to follow the original desired path ${}^{\text{phy}}\mathcal{P}$ by using a projection technique (see Chapter 9), where the vector field χ is defined by

$$\chi(\xi) = \times(\nabla\phi_1, \dots, \nabla\phi_n) - \sum_{j=1}^n k_j \phi_j \nabla\phi_j, \quad (10.1)$$

where $\nabla\phi_j \in \mathbb{R}^{n+1}$ is the gradient of ϕ_j with respect to its generalized coordinate ξ , k_j are positive gains, and the first term is the wedge product [45, Chapter 7.2] of all the gradients $\nabla\phi_j \in \mathbb{R}^{n+1}, j \in \mathbb{Z}_1^n$ (it degenerates to the cross product if $n = 2$). The physical interpretation of the vector field χ is clear: the second term $-\sum_{j=1}^n k_j \phi_j \nabla\phi_j$ is a weighted sum of all the gradients, which guides the trajectory towards the intersection of the hyper-surfaces (i.e., the desired path), while the first term $\times(\nabla\phi_1, \dots, \nabla\phi_n)$, being orthogonal to all the gradients $\nabla\phi_j$ [45, Proposition 7.2.1], provides a propagation direction along the desired path.

10.3 DISTRIBUTED MOTION COORDINATION ON DESIRED PATHS

In Chapter 9, the higher-dimensional guiding vector field in (10.1) is proved to possess no singular points where the vector field becomes zero, thanks to the additional dimension (i.e., the additional virtual coordinate w). However, like many of other current studies (e.g., [50], [74], [104]), the vector field is used for the guidance of only *one single* robot. We aim to extend the vector field to include a *coordination component* and achieve motion coordination among multiple robots. Since the additional virtual coordinate w not only helps eliminate singular points, but also acts as the path parameter, one idea is to utilize the virtual coordinate w to coordinate the robots' motions. Thus, the question is:

General Question: Suppose there are N robots, where $N > 1$, and the communication topology is described by an undirected graph $\mathcal{G} = (\mathcal{V}, \mathcal{E})$, where $\mathcal{V} = \{1, \dots, N\}$ represent these N robots; if $(i, j) \in \mathcal{E}$, then information can flow between Robot i and Robot j . Based on the higher-dimensional vector field in (10.1), how to design an extra *coordination mechanism* using the virtual coordinates

$w^{[i]}, i \in \mathbb{Z}_1^N$, such that 1) Each robot can follow their desired paths; 2) All robots can coordinate their motions by controlling the virtual coordinates $w^{[i]}, i \in \mathbb{Z}_1^N$, via *local* information exchange among neighboring robots?

The extra coordination mechanism and the precise meaning of motion coordination will become clear in the sequel, where a mathematical problem formulation based on dynamical systems theory is presented.

10.3.1 Mathematical problem formulation

Suppose the i -th robot is required to follow a path in \mathbb{R}^n , parameterized by n parametric equations:

$$x_1^{[i]} = f_1^{[i]}(w^{[i]}) \quad \dots \quad x_n^{[i]} = f_n^{[i]}(w^{[i]}), \quad (10.2)$$

where $x_j^{[i]}$ is the j -th coordinate, $f_j^{[i]} \in C^2$ is the j -th parametric function for the i -th robot, $i \in \mathbb{Z}_1^N, j \in \mathbb{Z}_1^n$, and $w^{[i]}$ is the parameter of the desired path. To derive the path-following guiding vector field, we use the parameter $w^{[i]}$ as an additional virtual coordinate, and the higher-dimensional desired path is described by

$$\mathcal{P}^{[i]} := \{\xi^{[i]} \in \mathbb{R}^{n+1} : \phi_1^{[i]}(\xi^{[i]}) = 0, \dots, \phi_n^{[i]}(\xi^{[i]}) = 0\},$$

where $\xi^{[i]} := (x_1^{[i]}, \dots, x_n^{[i]}, w^{[i]}) \in \mathbb{R}^{n+1}$ denotes the *generalized coordinate* of the i -th robot. Note that the $(n+1)$ -th entry of $\xi^{[i]}$ is the additional virtual coordinate $w^{[i]}$. The level functions are

$$\phi_j^{[i]}(x_1^{[i]}, \dots, x_n^{[i]}, w^{[i]}) = x_j^{[i]} - f_j^{[i]}(w^{[i]})$$

for $i \in \mathbb{Z}_1^N$ and $j \in \mathbb{Z}_1^n$. We define

$$\Phi^{[i]}(\xi^{[i]}) := (\phi_1^{[i]}(\xi^{[i]}), \dots, \phi_n^{[i]}(\xi^{[i]}))^\top \in \mathbb{R}^n.$$

Observe that $\xi^{[i]} \in \mathcal{P}^{[i]}$ if and only if $\|\Phi^{[i]}(\xi^{[i]})\| = 0$. Therefore, we can use $\Phi^{[i]}(\xi^{[i]})$ to quantify the distance to the desired path $\mathcal{P}^{[i]}$. In the context of path following, we call $\Phi^{[i]}(\xi^{[i]})$ the *path-following error* to $\mathcal{P}^{[i]}$. The aim is to design guiding controllers such that the norm $\|\Phi^{[i]}(\xi^{[i]})\|$ converges to zero

eventually. By combining (10.1) and (10.2), we obtain the analytic expression of the *path-following guiding vector field* $\mathbf{pf}\chi^{[i]} : \mathbb{R}^{n+1} \rightarrow \mathbb{R}^{n+1}$ for the i -th robot:

$$\mathbf{pf}\chi^{[i]}(\xi^{[i]}) = \begin{bmatrix} (-1)^n f_1^{[i]'}(w^{[i]}) - k_1^{[i]} \phi_1^{[i]}(\xi^{[i]}) \\ \vdots \\ (-1)^n f_n^{[i]'}(w^{[i]}) - k_n^{[i]} \phi_n^{[i]}(\xi^{[i]}) \\ (-1)^n + \sum_{l=1}^n k_l^{[i]} \phi_l^{[i]}(\xi^{[i]}) f_l^{[i]'}(w^{[i]}) \end{bmatrix} \quad (10.3)$$

for $i \in \mathbb{Z}_1^N$, where $k_j^{[i]} > 0$ are constant gains, and $f_j^{[i]'}'$ are the derivatives of $f_j^{[i]}$ with respect to the argument $w^{[i]} \in \mathbb{R}$.

To achieve coordination in $w^{[i]}$, thus indirectly coordinate the positions of robots, we introduce a new concept: a *coordination component*. The coordination component $\mathbf{cr}\chi^{[i]} : \mathbb{R} \times \mathbb{R}^N \rightarrow \mathbb{R}^{n+1}$ for the i -th robot, $i \in \mathbb{Z}_1^N$, is:

$$\mathbf{cr}\chi^{[i]}(t, w) = (0, \dots, 0, c^{[i]}(t, w))^\top \in \mathbb{R}^{n+1}, \quad (10.4)$$

where $w = (w^{[1]}, \dots, w^{[N]})^\top$, and $c^{[i]} : \mathbb{R} \times \mathbb{R}^N \rightarrow \mathbb{R}$ is called the *coordination function* to be designed later¹, which enables coordination among robots through the local interactions via the neighboring virtual coordinates $w^{[j]}$ for $j \in \mathcal{N}_i$. Specifically, we want the virtual coordinates of multiple robots $w^{[i]}(t) - w^{[j]}(t)$ to converge to $\Delta^{[i,j]}(t)$ for $(i, j) \in \mathcal{E}$, where $\Delta^{[i,j]}(t) \in \mathbb{R}$ are real-valued continuously differentiable functions, representing the desired differences between $w^{[i]}(t)$ and $w^{[j]}(t)$ at time t , satisfying $\Delta^{[i,j]}(t) = -\Delta^{[j,i]}(t)$. It is naturally assumed that $\Delta^{[i,j]}(t)$ are chosen appropriately such that the resulting formation is feasible² at any time $t \geq 0$.

We design the i -th *coordinating guiding vector field* $\mathfrak{X}^{[i]} : \mathbb{R} \times \mathbb{R}^{n+1+N} \rightarrow \mathbb{R}^{n+1}$ to be the weighted sum of the path-following vector field $\mathbf{pf}\chi^{[i]}$ and the coordination component $\mathbf{cr}\chi^{[i]}$ as below:

$$\mathfrak{X}^{[i]}(t, \xi^{[i]}, w) = \mathbf{pf}\chi^{[i]}(\xi^{[i]}) + k_c \mathbf{cr}\chi^{[i]}(t, w), \quad (10.5)$$

where $k_c > 0$ is a parameter to adjust the contribution of $\mathbf{pf}\chi^{[i]}$ and $\mathbf{cr}\chi^{[i]}$ to $\mathfrak{X}^{[i]}$. With a larger value of k_c , the motion coordination is achieved faster. The coordinating guiding vector field $\mathfrak{X}^{[i]}$ represents the desired moving direction for Robot i , guiding the robot's motion. Thus it is imperative to study the

¹ Although the argument of the coordination function $c^{[i]}(\cdot, \cdot)$ contains all the virtual coordinates $w^{[j]}$, $j \in \mathbb{Z}_1^N$, we do not require the knowledge of all virtual coordinates, but only those of the neighbors $w^{[j]}$ for $j \in \mathcal{N}_i$ as shown later.

² If the communication topology does not contain any cycles, then arbitrary values of the desired parametric differences $\Delta^{[i,j]}$ are feasible as long as $\Delta^{[i,j]} = -\Delta^{[j,i]}$ is satisfied for $i, j \in \mathbb{Z}_1^N$; otherwise, one needs to examine the feasibility of the resulting formation.

guidance result, or precisely, the convergence results of the integral curves of the vector field $\mathfrak{X}^{[i]}$ for $i \in \mathbb{Z}_1^N$. Precisely, we stack all the robot states as a vector $\xi := (\xi^{[1]^\top}, \dots, \xi^{[N]^\top})^\top \in \mathbb{R}^{(n+1)N}$ and stack all the coordinating guiding vector fields as $\mathfrak{X}(t, \xi) := (\mathfrak{X}^{[1]^\top}, \dots, \mathfrak{X}^{[N]^\top})^\top \in \mathbb{R}^{(n+1)N}$. We study the integral curves of $\mathfrak{X}(t, \xi)$; that is, the trajectories or solutions to the differential equation

$$\dot{\xi} = \mathfrak{X}(t, \xi) \quad (10.6)$$

given an initial condition $\xi_0 \in \mathbb{R}^{(n+1)N}$ at $t = t_0 \geq 0$. Note that if the coordination function $c^{[i]}(t, w)$ in (10.4) is time-invariant, it is not explicitly dependent on time t , and we can simply rewrite it to $c^{[i]}(w)$. In this case, the system (10.6) can be rewritten as $\dot{\xi} = \mathfrak{X}(\xi)$, which is an autonomous system; otherwise, it is a non-autonomous system [66, Chapter 1], which is more difficult to analyze as we will show later. Now we can formally formulate the problem as follows:

Problem 10.1 (Multi-robot path following). Design the coordinating guiding vector field $\mathfrak{X}^{[i]}$ in (10.5) for $i \in \mathbb{Z}_1^N$, such that the trajectories of (10.6), given an initial condition $\xi_0 \in \mathbb{R}^{(n+1)N}$ at $t = t_0 \geq 0$, fulfill the following two control objectives:

1. **(Path Following)** Robot i 's path-following error to its desired path $\mathcal{P}^{[i]}$ converges to zero asymptotically for $i \in \mathbb{Z}_1^N$. That is, $\|\Phi^{[i]}(\xi^{[i]}(t))\| \rightarrow 0$ as $t \rightarrow \infty$ for $i \in \mathbb{Z}_1^N$.
2. **(Motion Coordination)** Each robot's motion is coordinated distributedly subject to the communication graph \mathcal{G} (i.e., Robot i can communicate with Robot j if and only if $(i, j) \in \mathcal{E}$) such that their additional virtual coordinates satisfy $w^{[i]}(t) - w^{[j]}(t) - \Delta^{[i,j]}(t) \rightarrow 0$ as $t \rightarrow \infty$ for $(i, j) \in \mathcal{E}$.

Given the path-following vector field in (10.3), we will design the coordination function $c^{[i]}(\cdot)$ later such that it coordinates the robots' motion but do not affect the path-following performance. We propose the following mild standing assumption:

Assumption 10.2. The communication graph $\mathcal{G} = (\mathcal{V}, \mathcal{E})$ is undirected and connected.

Assumption 10.2 implies that if $(i, j) \in \mathcal{E}$, then Robot i and Robot j can share information bidirectionally, and no robot is isolated from the multi-robot system (e.g., a cycle graph satisfies this assumption).

10.3.2 Time-invariant and time-varying coordination components and convergence analysis

Observe that the coordination of the virtual coordinates directly affects the coordination of the positions of the robots implicitly, since the virtual coordinate corresponds to the parameter of a desired path. Motivated by this observation, we will design both time-invariant coordination component $c^{[i]}(\mathbf{w})$ and time-varying coordination component $c^{[i]}(t, \mathbf{w})$ in (10.4) in this subsection, and analyze the trajectories of (10.6), which is an autonomous system in the former case and a non-autonomous system in the latter case.

10.3.2.1 Time-invariant coordination component

Given the desired path $\mathcal{P}^{[i]}$, we can design the *desired parametric differences* $\Delta^{[i,j]}$ starting from a particular *reference configuration*³ $\mathbf{w}^* := (w^{[1]*}, \dots, w^{[N]*})^\top$. Hence, $\Delta^* = D^\top \mathbf{w}^*$ is the stacked vector of $\Delta^{[i,j]}$, $(i, j) \in \mathcal{E}$, where $D \in \mathbb{R}^{N \times |\mathcal{E}|}$ is an incidence matrix obtained by assigning arbitrary orientations to the edges of the undirected graph⁴ [88, p. 23]. Now we propose to employ the following consensus control algorithm [116, p. 25]:

$$c^{[i]} = - \sum_{j \in \mathcal{N}_i} (w^{[i]} - w^{[j]} - \Delta^{[i,j]}), \quad \forall i \in \mathbb{Z}_1^N. \quad (10.7)$$

Equation (10.7) can be rewritten in a compact form as

$$\mathbf{c}(\mathbf{w}) = -L(\mathbf{w} - \mathbf{w}^*) = -L\tilde{\mathbf{w}}, \quad (10.8)$$

where $\mathbf{c}(\mathbf{w}) = (c^{[1]}(\mathbf{w}), \dots, c^{[N]}(\mathbf{w}))^\top$, $L = L(\mathcal{G})$ is the Laplacian matrix and

$$\tilde{\mathbf{w}} = \mathbf{w} - \mathbf{w}^*.$$

Combining (10.3), (10.4), (10.5) and (10.7), we attain the coordinating guiding vector field $\mathfrak{X}^{[i]}$ for $i \in \mathbb{Z}_1^N$. The vector field $\mathfrak{X}^{[i]}$ only takes as inputs Robot i 's own states and its neighbors' virtual coordinates $w^{[j]}$ for $j \in \mathcal{N}_i$.

Remark 10.3. From (10.4), (10.5) and (10.7), one observes that neighboring information exchange only happens in the coordination component $c^{[i]}(\cdot)$. Notably, the communication burden is low: Robot i transmits only a scalar $w^{[i]}$ to the neighboring Robot $j \in \mathcal{N}_i$. \triangleleft

³ Note that \mathbf{w}^* is not known by the robots. Instead, Robot i is only aware of the desired parametric differences relative to its neighbors (i.e., $\Delta^{[i,j]}$ for $j \in \mathcal{N}_i$).

⁴ Different assignments of the edges' orientations of the undirected graph only affect the signs of each entry in an incidence matrix D , while the desired relative parametric differences are still the same among robots. In addition, the Laplacian matrix $L = DD^\top$ introduced later remains the same independent of the orientation assignment.

10.3.2.2 Convergence analysis for the time-invariant case

The convergence analysis of trajectories to (10.6) is nontrivial given that the right-hand side of (10.6) is *not* a gradient of any potential function, since the path-following vector field in (10.1) contains a wedge product of all the gradients. In this subsection, we show that the coordinating guiding vector field (10.5) enables multiple robots to follow their desired paths while they are coordinated by the virtual coordinates such that $w^{[i]}(t) - w^{[j]}(t)$ converges to $\Delta^{[i,j]}$ for $(i, j) \in \mathcal{E}$ as $t \rightarrow \infty$. For simplicity, we first consider Robot i , and most of the function arguments are ignored henceforth unless ambiguity arises. We define

$$K^{[i]} := \text{diag}\{k_1^{[i]}, \dots, k_n^{[i]}\}$$

$$\mathbf{f}^{[i]}'(w^{[i]}) := (f_1^{[i]}'(w^{[i]}), \dots, f_n^{[i]}'(w^{[i]}))^\top.$$

Then one can calculate that

$$\nabla \phi_j^{[i]\top} \mathbf{p}^f \chi^{[i]} = \begin{bmatrix} 0 \\ \vdots \\ 1 \\ \vdots \\ 0 \\ -f_j^{[i]}'(w^{[i]}) \end{bmatrix}^\top \begin{bmatrix} (-1)^n f_1^{[i]}'(w^{[i]}) - k_j^{[i]} \phi_1^{[i]} \\ \vdots \\ (-1)^n f_n^{[i]}'(w^{[i]}) - k_n^{[i]} \phi_n^{[i]} \\ (-1)^n + \sum_{l=1}^n k_l^{[i]} \phi_l^{[i]} f_l^{[i]}'(w^{[i]}) \end{bmatrix}$$

$$= -k_j^{[i]} \phi_j^{[i]} - f_j^{[i]}'(w^{[i]}) \cdot [\mathbf{f}^{[i]}'(w^{[i]})^\top K^{[i]} \Phi^{[i]}]$$

for $j \in \mathbb{Z}_1^n$, where 1 is at the j -th entry of $\nabla \phi_j^{[i]}$. Therefore, we have

$$\begin{bmatrix} \nabla \phi_1^{[i]\top} \mathbf{p}^f \chi^{[i]} \\ \vdots \\ \nabla \phi_n^{[i]\top} \mathbf{p}^f \chi^{[i]} \end{bmatrix} = -K^{[i]} \Phi^{[i]} - \mathbf{f}^{[i]}'(w^{[i]}) \mathbf{f}^{[i]}'(w^{[i]})^\top K^{[i]} \Phi^{[i]}. \quad (10.9)$$

We can also calculate that

$$\begin{bmatrix} \nabla \phi_1^{[i]\top} \text{cr} \chi^{[i]}(w) \\ \vdots \\ \nabla \phi_n^{[i]\top} \text{cr} \chi^{[i]}(w) \end{bmatrix} = -c^{[i]}(w) \begin{bmatrix} f_1^{[i]}'(w^{[i]}) \\ \vdots \\ f_n^{[i]}'(w^{[i]}) \end{bmatrix} = -c^{[i]}(w) \mathbf{f}^{[i]}'(w^{[i]}). \quad (10.10)$$

Therefore,

$$\dot{\Phi}^{[i]} = \frac{d}{dt} \begin{bmatrix} \phi_1^{[i]} \\ \vdots \\ \phi_n^{[i]} \end{bmatrix} = \begin{bmatrix} \nabla \phi_1^{[i]^\top} \text{pf} \chi^{[i]} + k_c \nabla \phi_1^{[i]^\top} \text{cr} \chi^{[i]}(\mathbf{w}) \\ \vdots \\ \nabla \phi_n^{[i]^\top} \text{pf} \chi^{[i]} + k_c \nabla \phi_n^{[i]^\top} \text{cr} \chi^{[i]}(\mathbf{w}) \end{bmatrix}$$

$$\stackrel{(10.9),(10.10)}{=} -K^{[i]} \Phi^{[i]} - f^{[i]'}(w^{[i]}) f^{[i]'}(w^{[i]})^\top K^{[i]} \Phi^{[i]} - k_c c^{[i]}(\mathbf{w}) f^{[i]'}(w^{[i]}). \quad (10.11)$$

Now we consider all robots. We define

$$\mathfrak{F} := \text{diag}\{f^{[1]'}, \dots, f^{[N]'}\} \in \mathbb{R}^{nN \times N}$$

$$K := \text{diag}\{K^{[1]}, \dots, K^{[N]}\} \in \mathbb{R}^{nN \times nN}$$

$$\Phi := (\Phi^{[1]^\top}, \dots, \Phi^{[N]^\top})^\top \in \mathbb{R}^{nN}.$$

Then according to (10.11), we have

$$\dot{\Phi} = \begin{bmatrix} -K^{[1]} \Phi^{[1]} - f^{[1]'}(w^{[1]}) f^{[1]'}(w^{[1]})^\top K^{[1]} \Phi^{[1]} - k_c c^{[1]}(\mathbf{w}) f^{[1]'}(w^{[1]}) \\ \vdots \\ -K^{[N]} \Phi^{[N]} - f^{[N]'}(w^{[N]}) f^{[N]'}(w^{[N]})^\top K^{[N]} \Phi^{[N]} - k_c c^{[N]}(\mathbf{w}) f^{[N]'}(w^{[N]}) \end{bmatrix}$$

$$= -K\Phi - \mathfrak{F}\mathfrak{F}^\top K\Phi - k_c \mathfrak{F}c(\mathbf{w}). \quad (10.12)$$

One can also calculate that

$$\dot{w}^{[i]} = \begin{bmatrix} 0 & \dots & 0 & 1 \end{bmatrix} (\text{pf} \chi^{[i]}(\xi^{[i]}) + k_c \text{cr} \chi^{[i]}(\xi^{[i]}))$$

$$= (-1)^n + f^{[i]'}(w^{[i]})^\top K^{[i]} \Phi^{[i]}(\xi^{[i]}) + k_c c^{[i]}(\mathbf{w}). \quad (10.13)$$

By $\tilde{w} := \mathbf{w} - \mathbf{w}^*$, there holds

$$\dot{\tilde{w}} = \dot{w} = (-1)^n \mathbf{1} + \mathfrak{F}^\top K\Phi + k_c c(\mathbf{w}), \quad (10.14)$$

where $\mathbf{1} \in \mathbb{R}^N$ is a vector consisting of all ones. The Laplacian matrix can be factorized as $L = DD^\top$, where $D \in \mathbb{R}^{N \times |\mathcal{E}|}$ is the incidence matrix. We define the *composite error vector* e to be

$$e = (\Phi^\top, (D^\top \tilde{w})^\top)^\top \in \mathbb{R}^{nN+|\mathcal{E}|}$$

and the composite gain matrix to be

$$\mathfrak{K} = \text{diag}\{K, k_c I_{|\mathcal{E}|}\} \in \mathbb{R}^{(nN+|\mathcal{E}|) \times (nN+|\mathcal{E}|)},$$

where $I_{|\mathcal{E}|}$ is the $|\mathcal{E}|\text{-by-}|\mathcal{E}|$ identity matrix. Therefore, from (10.8), (10.12) and (10.14), and noting that $D^\top \mathbf{1} = \mathbf{0}$, we have the following composite error dynamics:

$$\dot{\mathbf{e}} = \begin{bmatrix} \dot{\Phi} \\ D^\top \tilde{\mathbf{w}} \end{bmatrix} = \begin{bmatrix} -K\Phi - \mathfrak{F}\mathfrak{F}^\top K\Phi + k_c \mathfrak{F} L \tilde{\mathbf{w}} \\ D^\top \mathfrak{F}^\top K\Phi - k_c D^\top L \tilde{\mathbf{w}} \end{bmatrix}. \quad (10.15)$$

With the error dynamics, one needs to prove that $\mathbf{e}(t) \rightarrow \mathbf{0}$ as $t \rightarrow \infty$ to show the effectiveness of the coordinating guiding vector field $\mathfrak{X}^{[i]}$. This result is formally stated below under the following practical assumption:

Assumption 10.4. The first and second derivatives of $f_j^{[i]}(\cdot)$ in (10.2) are bounded for all $i \in \mathbb{Z}_1^N, j \in \mathbb{Z}_1^n$.

Theorem 10.5 (Time-invariant coordination). *Under Assumptions 10.2 and 10.4, and given constant desired parametric differences $\Delta^{[i,j]}$ for $(i, j) \in \mathcal{E}$, the coordinating guiding vector fields $\mathfrak{X}^{[i]}$ for $i \in \mathbb{Z}_1^N$ designed by combining (10.3), (10.4), (10.5) and (10.7) solve Problem 10.1 globally in the sense that the aggregate initial state $\xi_0 \in \mathbb{R}^{(n+1) \times N}$ can be arbitrary.*

Proof. Consider the following Lyapunov function candidate

$$V(\mathbf{e}) = \frac{1}{2} \mathbf{e}^\top \mathfrak{K} \mathbf{e} = \frac{1}{2} \left(\Phi^\top K \Phi + k_c \tilde{\mathbf{w}}^\top L \tilde{\mathbf{w}} \right), \quad (10.16)$$

of which the time derivative satisfies

$$\begin{aligned} \dot{V}(\mathbf{e}) &= \dot{\mathbf{e}}^\top \mathfrak{K} \mathbf{e} \\ &\stackrel{(10.15)}{=} \begin{bmatrix} -K\Phi - \mathfrak{F}\mathfrak{F}^\top K\Phi + k_c \mathfrak{F} L \tilde{\mathbf{w}} \\ D^\top \mathfrak{F}^\top K\Phi - k_c D^\top L \tilde{\mathbf{w}} \end{bmatrix}^\top \begin{bmatrix} K & \\ & k_c I_{|\mathcal{E}|} \end{bmatrix} \begin{bmatrix} \Phi \\ D^\top \tilde{\mathbf{w}} \end{bmatrix} \\ &= -\|K\Phi\|^2 - \|\mathfrak{F}^\top K\Phi\|^2 + k_c (\mathfrak{F} L \tilde{\mathbf{w}})^\top K\Phi + k_c (\mathfrak{F}^\top K\Phi)^\top L \tilde{\mathbf{w}} - k_c^2 \|L \tilde{\mathbf{w}}\|^2 \\ &= -\|K\Phi\|^2 - \|\mathfrak{F}^\top K\Phi\|^2 + 2k_c (\mathfrak{F}^\top K\Phi)^\top (L \tilde{\mathbf{w}}) - k_c^2 \|L \tilde{\mathbf{w}}\|^2 \\ &= -\|K\Phi\|^2 - \|\mathfrak{F}^\top K\Phi - k_c L \tilde{\mathbf{w}}\|^2 \\ &\leq -\|K\Phi\|^2 \leq 0. \end{aligned} \quad (10.17) \quad (10.18)$$

From (10.18), we know that \dot{V} is negative semi-definite. It follows from the LaSalle's invariance principle (Theorem 2.6) that the trajectories of (10.6) will converge to the largest invariant set \mathcal{A} in

$$\mathcal{B} := \{\mathbf{e} : \dot{V}(\mathbf{e}) = 0\} = \{\mathbf{e} : \Phi = \mathbf{0}\}.$$

By checking (10.15), we can conclude that the largest invariant set \mathcal{A} in \mathcal{B} corresponds to having $D^\top L\tilde{w} = D^\top DD^\top \tilde{w} = 0$, which implies $D^\top \tilde{w} = 0$ as we will show now. Since $D^\top DD^\top \tilde{w} = 0$, it follows that $D^\top \tilde{w}$ is in the null space of $D^\top D$, which is the null space of D . In addition, $D^\top \tilde{w}$ is in the range space of D^\top , which is orthogonal to the null space of D . To sum up, $D^\top \tilde{w}$ is both contained in and orthogonal to the null space of D . This implies that $D^\top \tilde{w} = \mathbf{0}$. Therefore, the largest invariant set \mathcal{A} in \mathcal{B} is

$$\mathcal{A} = \{e : \Phi = \mathbf{0}, D^\top \tilde{w} = \mathbf{0}\}.$$

This implies that $\|\Phi^{[i]}\| \rightarrow 0$ for all $i \in \mathbb{Z}_1^N$ and $(w^{[i]}(t) - w^{[j]}(t)) - \Delta^{[i,j]} \rightarrow \mathbf{0}$ for $(i, j) \in \mathcal{E}$ as $t \rightarrow \infty$. Namely, all robots' path-following errors vanish asymptotically, and the differences of neighboring virtual coordinates \tilde{w} converge to the desired relative states Δ^* , and thus the coordinated motion is achieved. Note that (10.16) is positive (except when $e = \mathbf{0}$) and radially unbounded in e (i.e., $V(e) \rightarrow \infty$ as $\|e\| \rightarrow \infty$), and its time derivative is negative semi-definite regardless of the magnitude of e . Hence, the vanishing of the composite error e is global regardless of the initial aggregate state ξ_0 . \square

10.3.2.3 Time-varying coordination component

In practice, one might want to have time-dependent desired parametric differences $\Delta^{[i,j]}(t)$ such that the inter-robot distances dynamically adapt to the environment [163]. To this end, we define the continuously differentiable *reference states* $\delta^{[i]} : \mathbb{R}_{\geq 0} \rightarrow \mathbb{R}$ for $i \in \mathbb{Z}_1^N$ such that the desired virtual coordinate difference $\Delta^{[i,j]}(t) = \delta^{[i]}(t) - \delta^{[j]}(t)$. It is obvious that $\Delta^{[i,j]}(t) = -\Delta^{[j,i]}(t)$. Therefore, we employ the following time-varying consensus control algorithm [116, p. 25]:

$$c^{[i]}(t, w) = \frac{\dot{\delta}^{[i]}(t)}{k_c} - \sum_{j \in \mathcal{N}_i} (w^{[i]}(t) - w^{[j]}(t) - \Delta^{[i,j]}(t)). \quad (10.19)$$

The quantity $\dot{\delta}^{[i]}(t)$ in (10.19) is a feed-forward term to "inform" the changing rate of the time-varying reference state, and this quantity is indispensable since the coordination objective is now time-varying. The gain $1/k_c$ will be canceled out in the subsequent theoretical derivation. Combining (10.3), (10.4), (10.5) and (10.19), we attain the coordinating guiding vector field $\mathfrak{X}^{[i]}$ for $i \in \mathbb{Z}_1^N$. The vector field $\mathfrak{X}^{[i]}$ takes as inputs Robot i 's own states, its neighbors' virtual coordinates $w^{[j]}$ for $j \in \mathcal{N}_i$, the time-varying desired difference $\Delta^{[i,j]}(t)$, and the time derivative of its reference state $\dot{\delta}^{[i]}(t)$. Note that Remark 10.3 still applies here.

10.3.2.4 Convergence analysis for the time-varying case

The analysis of the convergence of trajectories of (10.6) is more difficult. This is not only because the right-hand side of (10.6) is *not* a gradient of any potential function as mentioned before, but also because (10.6) is nonlinear and non-autonomous (as the reference states $\delta^{[i]}(t)$ are explicitly time-dependent). Nevertheless, using different analysis tools, we can still obtain the same conclusion as Theorem 10.5. Namely, we show that the coordinating guiding vector field (10.5) enables multiple robots to follow their desired paths while they are coordinated by the virtual coordinates such that $w^{[i]}(t) - w^{[j]}(t)$ converges to $\Delta^{[i,j]}(t)$ for $(i, j) \in \mathcal{E}$.

For convenience of subsequent theoretical analysis, we define $\tilde{w}_\delta^{[i]}(t)$ as the difference between the virtual coordinate $w^{[i]}(t)$ and the reference state $\delta^{[i]}(t)$; that is, $\tilde{w}_\delta^{[i]}(t) := w^{[i]}(t) - \delta^{[i]}(t)$. Observe that the coordination control objective $w^{[i]}(t) - w^{[j]}(t) \rightarrow \Delta^{[i,j]}(t)$ is equivalent to that $\tilde{w}_\delta^{[i]} - \tilde{w}_\delta^{[j]} \rightarrow 0$ for $(i, j) \in \mathcal{E}$, which implies that the new states $\tilde{w}_\delta^{[i]}, i \in \mathbb{Z}_1^N$, reach consensus eventually. Therefore, Equation (10.19) can be rewritten as below:

$$c^{[i]}(t, \mathbf{w}) = \frac{\dot{\delta}^{[i]}(t)}{k_c} - \sum_{j \in \mathcal{N}_i} (\tilde{w}_\delta^{[i]}(t) - \tilde{w}_\delta^{[j]}(t)), \quad (10.20)$$

For notational simplicity, we stack $\tilde{w}_\delta^{[i]}$ and $\delta^{[i]}$ in two column vectors respectively: $\tilde{\mathbf{w}}_\delta := (\tilde{w}_\delta^{[1]}, \dots, \tilde{w}_\delta^{[N]})^\top$ and $\delta := (\delta^{[1]}, \dots, \delta^{[N]})^\top$; hence,

$$\tilde{\mathbf{w}}_\delta(t) = \mathbf{w}(t) - \delta(t).$$

Therefore, (10.20) can be further simplified as below:

$$c(t, \mathbf{w}) = \dot{\delta}(t)/k_c - L\tilde{\mathbf{w}}_\delta(t), \quad (10.21)$$

where $c(t, \mathbf{w}) = (c^{[1]}(t, \mathbf{w}), \dots, c^{[N]}(t, \mathbf{w}))^\top$ and $L = L(\mathcal{G})$ is the Laplacian matrix. Thanks to the simplification, the convergence analysis becomes similar to that of the time-invariant case in Section 10.3.2.2. Therefore, we use the same notations as before, and the calculations are similar except for formula related to the time-dependent reference states $\delta(t)$. In particular, (10.14) is replaced by the following:

$$\begin{aligned} \dot{\tilde{\mathbf{w}}}_\delta &= \dot{\mathbf{w}} - \dot{\delta} \stackrel{(10.21)}{=} [(-1)^n \mathbf{1} + \mathfrak{F}^\top K \Phi + k_c(\dot{\delta}/k_c - L\tilde{\mathbf{w}}_\delta(t))] - \dot{\delta} \\ &= [(-1)^n \mathbf{1} + \mathfrak{F}^\top K \Phi - k_c L \tilde{\mathbf{w}}_\delta(t) + \dot{\delta}] - \dot{\delta} \\ &= (-1)^n \mathbf{1} + \mathfrak{F}^\top K \Phi - k_c L \tilde{\mathbf{w}}_\delta, \end{aligned} \quad (10.22)$$

where note that the first term $\dot{\delta}/k_c$ in (10.21) has been canceled out, and thus (10.22) is the same as the time-invariant case in (10.14) except that $\tilde{w}_\delta(t) = w(t) - \delta(t)$ contains the term $\delta(t)$ that is time-dependent. We need different analysis tools for the non-autonomous system (10.6) due to (10.21). Specifically, we will employ the LaSalle's invariance principle for *non-autonomous* systems (i.e., Theorem 2.8) and Barbalat's lemma (i.e, Lemma 2.7) for the analysis. We impose the following reasonable assumption for the time-varying reference states:

Assumption 10.6. The time derivatives of the reference states $\dot{\delta}^{[i]}(t)$ are bounded at any time instant $t \geq 0$ for all $i \in \mathbb{Z}_1^N$.

We have the following theorem:

Theorem 10.7 (Time-varying coordination). *Under Assumptions 10.2, 10.4 and 10.6, and given time-dependent desired parametric differences $\Delta^{[i,j]}(t)$ for $(i, j) \in \mathcal{E}$, the coordinating guiding vector fields $\mathfrak{X}^{[i]}$ for $i \in \mathbb{Z}_1^N$ designed by combining (10.3), (10.4), (10.5) and (10.19) solve Problem 10.1 globally in the sense that the aggregate initial state $\xi \in \mathbb{R}^{(n+1) \times N}$ can be arbitrary.*

Proof. We define a similar composite error vector

$$\mathbf{e}_\delta = (\Phi^\top, (D^\top \tilde{w}_\delta)^\top)^\top \in \mathbb{R}^{nN+|\mathcal{E}|}$$

and the composite error dynamics is

$$\dot{\mathbf{e}}_\delta = \begin{bmatrix} \dot{\Phi} \\ D^\top \dot{\tilde{w}}_\delta \end{bmatrix} = \begin{bmatrix} -K\Phi - \mathfrak{F}\mathfrak{F}^\top K\Phi + k_c \mathfrak{F} L \tilde{w}_\delta \\ D^\top \mathfrak{F}^\top K\Phi - k_c D^\top L \tilde{w}_\delta \end{bmatrix}. \quad (10.23)$$

We use the Lyapunov function candidate $V = \frac{1}{2} \mathbf{e}_\delta^\top \mathfrak{K} \mathbf{e}_\delta$, and taking the time derivative of V , we have:

$$\begin{aligned} \dot{V}(\mathbf{e}_\delta) &= \dot{\mathbf{e}}_\delta^\top \mathfrak{K} \mathbf{e}_\delta \\ &\stackrel{(10.23)}{=} -\|K\Phi\|^2 - \|\mathfrak{F}^\top K\Phi\|^2 + 2k_c (\mathfrak{F}^\top K\Phi)^\top (L \tilde{w}_\delta) - k_c^2 \|L \tilde{w}_\delta\|^2 \end{aligned} \quad (10.24)$$

$$\leq -\|K\Phi\|^2 \leq 0, \quad (10.25)$$

Equation (10.25) means that \dot{V} is negative semi-definite. The system (10.6) is non-autonomous due to the time-varying term (10.21) in the coordinating guiding vector fields $\mathfrak{X}^{[i]}$ for $i \in \mathbb{Z}_1^N$. Therefore, we use the LaSalle's invariance principle for *non-autonomous* systems (i.e., Theorem 2.8) to conclude that $\|K\Phi\|^2 \rightarrow 0$ as $t \rightarrow \infty$, hence $\|\Phi^{[i]}\| \rightarrow 0$ as $t \rightarrow \infty$ for all $i \in \mathbb{Z}_1^N$; i.e., all robots' path-following errors vanish asymptotically. Moreover, the quadratic form of the Lyapunov function V implies that V is radially unbounded with respect to $\|\mathbf{e}_\delta\|$ (i.e., $V(\mathbf{e}_\delta) \rightarrow \infty$ as $\|\mathbf{e}_\delta\| \rightarrow \infty$), and thus the convergence holds globally: the norm of the initial path-following error $\|\mathbf{e}_\delta(0)\|$ can be arbitrarily large.

To prove the convergence of the second term $D^\top \tilde{w}_\delta$ of the composite error vector, we use Barbalat's lemma (i.e., Lemma 2.7). Firstly, (10.25) shows that $\dot{V} \leq 0$, hence $V(t) \leq V(0)$ for $t \geq 0$. This implies that the composite error e_δ is bounded, and thus Φ and $D^\top \tilde{w}_\delta$ are all bounded. Due to Assumption 10.4, one can verify that \dot{e}_δ in (10.23) is also bounded, and thus $\dot{\Phi}$ and $D^\top \dot{\tilde{w}}_\delta$ are bounded as well. Next, we show that the second-order time derivative \ddot{V} is bounded. One can calculate that $\ddot{V} = \ddot{e}_\delta^\top \mathcal{K} e_\delta + \dot{e}_\delta^\top \mathcal{K} \dot{e}_\delta$. It is obvious that the second term of \ddot{V} is bounded, so we only need to show that \ddot{e}_δ is bounded. We have

$$\ddot{e}_\delta = \begin{bmatrix} -K\dot{\Phi} - \dot{\mathfrak{F}}\dot{\mathfrak{F}}^\top K\Phi - \mathfrak{F}(\dot{\mathfrak{F}}^\top K\Phi + \mathfrak{F}^\top K\dot{\Phi}) + k_c \dot{\mathfrak{F}} L \tilde{w}_\delta + k_c \mathfrak{F} L \dot{\tilde{w}}_\delta \\ D^\top (\dot{\mathfrak{F}}^\top K\Phi + \mathfrak{F}^\top K\dot{\Phi}) - k_c D^\top L \dot{\tilde{w}}_\delta \end{bmatrix},$$

where $\dot{\mathfrak{F}} = \text{diag}\{\dot{\mathfrak{F}}^{[1]}(w^{[1]}), \dots, \dot{\mathfrak{F}}^{[N]}(w^{[N]})\}$ with

$$\dot{\mathfrak{F}}^{[i]}(w^{[i]}) = (f_1^{[i]''}(w^{[i]}), \dots, f_n^{[i]''}(w^{[i]}))^\top \dot{w}^{[i]}$$

for $i \in \mathbb{Z}_1^N$. Since $\Phi, D^\top \tilde{w}_\delta, \dot{\Phi}, D^\top \dot{\tilde{w}}_\delta$ are all bounded, and by (10.22), Assumptions 10.4 and 10.6, we have that \ddot{e}_δ is indeed bounded. Therefore, \ddot{V} is bounded, and thus \dot{V} is uniformly continuous in time t . By invoking Lemma 4.3 in [133], we have that $\dot{V}(e_\delta) \rightarrow 0$ as $t \rightarrow \infty$. Equivalently, $\dot{e}_\delta^\top \mathcal{K} e_\delta \rightarrow 0$ as $t \rightarrow \infty$. Since the argument above shows that $\|\Phi\| \rightarrow 0$ as $t \rightarrow \infty$, from (10.24) and the boundedness of \mathfrak{F} and $D^\top \tilde{w}_\delta$, we thus have $L \tilde{w}_\delta \rightarrow 0$ as $t \rightarrow \infty$. Furthermore, by Assumption 10.2, $L \tilde{w}_\delta \rightarrow 0$ as $t \rightarrow \infty$ implies that $\tilde{w}_\delta^{[i]} - \tilde{w}_\delta^{[j]} \rightarrow 0$ for all $i, j \in \mathbb{Z}_1^N$ [116, Corollarylyry 2.5]. This further implies that $w^{[i]}(t) - w^{[j]}(t) \rightarrow \Delta^{[i,j]}(t)$. Therefore, the differences in the virtual coordinates $w^{[i]}$ of all robots converge to the desired value, and thus the coordinated motion can be achieved. As in the proof of Theorem 10.5, the global convergence property is attained due to the radial unboundedness of the Lyapunov function V with respect to $\|e_\delta\|$. \square

10.4 DISTRIBUTED COORDINATED MANEUVERING ON SURFACES

In this section, we extend the previous results such that N robots can converge to (possibly different) two-dimensional *surfaces* (e.g., spheres), while they maneuver and coordinate their motions according to some parameters of the surfaces. It is clear in the previous sections what is meant by following a (one-dimensional) desired path, but it is perhaps unclear what is meant by coordinated motion on (two-dimensional) surfaces. Therefore, we first clarify the meaning of coordinated motion on surfaces in Section 10.4.1, and then mathematically formulate the

problem in Section 10.4.2, and derive the coordinating guiding vector field and conduct the convergence analysis in Section 10.4.3.

10.4.1 Coordinated motion in a desired set

10.4.1.1 Single robot trajectories in a desired set

For simplicity, we first study trajectories of *one* robot within a *desired set* of any dimensions. Suppose the desired set is in the following parametric form:

$$x_1 = f_1(w_1, \dots, w_k), \dots, x_n = f_n(w_1, \dots, w_k), \quad (10.26)$$

where $w_1, \dots, w_k \in \mathbb{R}$ are k parameters, $n \in \mathbb{N}$ is the dimension of the ambient Euclidean space (mainly $n \in \{2, 3\}$ for applications with mobile robots), $f_j, j \in \mathbb{Z}_1^n$, are twice continuously differentiable functions (i.e., $f_j \in C^2$). Precisely, the desired set described by (10.26) is $\mathcal{M} := \{(x_1, \dots, x_n) \in \mathbb{R}^n : (10.26), w_j \in \mathbb{R}, j \in \mathbb{Z}_1^k\}$. In particular, generically, if $k = 1$, then $\mathcal{M} = \mathcal{P}$ is a desired path, which is one-dimensional (or roughly speaking, it has one degree of freedom), while if $k = 2$, then \mathcal{M} is a two-dimensional surface. The k parameters $w_j, j \in \mathbb{Z}_1^k$, can be used as coordinates to localize a point in \mathcal{M} . Therefore, one can represent the position of a robot in \mathcal{M} by a k -tuple denoted by $(w_1, \dots, w_k)_\mathcal{M}$ in the parameter space. This chapter mainly focuses on parametric paths and surfaces (i.e., $k = 1$ or $k = 2$), but the generalization to $k > 2$ is obvious after we elaborate on the case of $k = 2$ in this section.

Typically, if $k = 1$, then \mathcal{M} is a desired path, denoted by \mathcal{P} . It is clear that if a robot starts from the position $(w_1)_\mathcal{M}$ in \mathcal{P} , then its trajectory (subject to directions) coincides with the desired path \mathcal{P} , and how fast the trajectory propagates along the desired path is determined by the time derivative $\dot{w}_1 \in \mathbb{R}$ along the robot trajectory. If $k = 2$, then \mathcal{M} is a surface, denoted by \mathcal{S} . If a robot starts from the position $(w_1, w_2)_\mathcal{M}$ in \mathcal{S} , it is the ratio between the different velocities \dot{w}_1 and \dot{w}_2 that determines the eventual trajectory of the robot in \mathcal{S} . An example is shown as follows.

Example 10.8. Suppose the desired set \mathcal{M} is the sphere parameterized as below:

$$\mathcal{S}_{\text{sph}} := \begin{cases} x_1 &= \cos(w_1) \cos(w_2) \\ x_2 &= \cos(w_1) \sin(w_2) \\ x_3 &= \sin(w_1) \end{cases}. \quad (10.27)$$

If $\dot{w}_1 = 0$ and $\dot{w}_2 \neq 0$, then the robot's trajectory is parallel to the sphere's equator starting from a point in \mathcal{S}_{sph} . \triangleleft

We will show later that our proposed coordinating guiding vector field allows one to set the values of \dot{w}_j for $j \in \mathbb{Z}_1^k$, so we can guarantee that a robot moves as expected within \mathcal{M} .

10.4.1.2 Coordinated motion of multiple robots

Now we consider N robots, where $N > 1$. The coordinated motion among multiple robots is characterized by the predefined desired geometric or parametric differences $\Delta_{(\cdot)}^{[i,j]}$, $i \neq j \in \mathbb{Z}_1^N$, between neighboring robots, for which the neighboring relationships are encoded in an undirected communication graph. Note that the subscript in $\Delta_{(\cdot)}^{[i,j]}$ specifies which parameter of the desired set is considered (in the case of one parameter as in the previous section, this subscript is omitted for simplicity).

In the previous section, we only consider one parameter (i.e., $k = 1$) w_1 to be communicated among robots. In this case, these robots exhibit behavior of *chasing each other* on one-dimensional desired paths $\mathcal{P}^{[i]}$. Dealing with a desired set \mathcal{M} with $k > 1$ gives us more freedom for the coordinated motion of robots. For simplicity, we consider the case of $k = 2$ (i.e., the desired set \mathcal{M} is a two-dimensional surface), in the following example.

Example 10.9. In this example, two robots coordinate their motions in the desired set: the sphere described by (10.27). Specifically, we require that the difference between each of the two parameters, $w_1^{[1]}$ and $w_2^{[1]}$, of Robot 1, and each of those of Robot 2, $w_1^{[2]}$ and $w_2^{[2]}$, is $-\pi$. Namely, the desired parametric differences are $\Delta_1^{[1,2]} = \Delta_2^{[1,2]} = -\pi$. We also require that, at the steady state, they move at specific parametric speeds. The desired speeds in the first and the second parameter are $\dot{w}_1^* = 0$ and $\dot{w}_2^* = 1$, respectively in the first scenario, and $\dot{w}_1^* = \dot{w}_2^* = 1$ in the second scenario for both robots. We use the coordinating guiding vector field that will be introduced later to produce the simulation results shown in Fig. 10.1. Note that in Fig. 10.1b, during the steady state, the Euclidean distance between two neighboring robots is not constant, but their geodesic distance, which is equal to the absolute value of the desired parametric difference $|\Delta^{[\cdot,\cdot]}|$, remain constant. \triangleleft

In the next subsection, we formally define the problem of motion coordination of robots on surfaces, and provide the technical detail of the coordinating guiding vector field for surface navigation as employed in Example 10.9.

10.4.2 Mathematical problem formulation

In previous sections, the i -th robot is required to follow a one-dimensional desired path, which is parameterized by one parameter $w^{[i]}$. In contrast, to converge to a two-dimensional surface, we need to use two parameters denoted by $w_1^{[i]}$ and

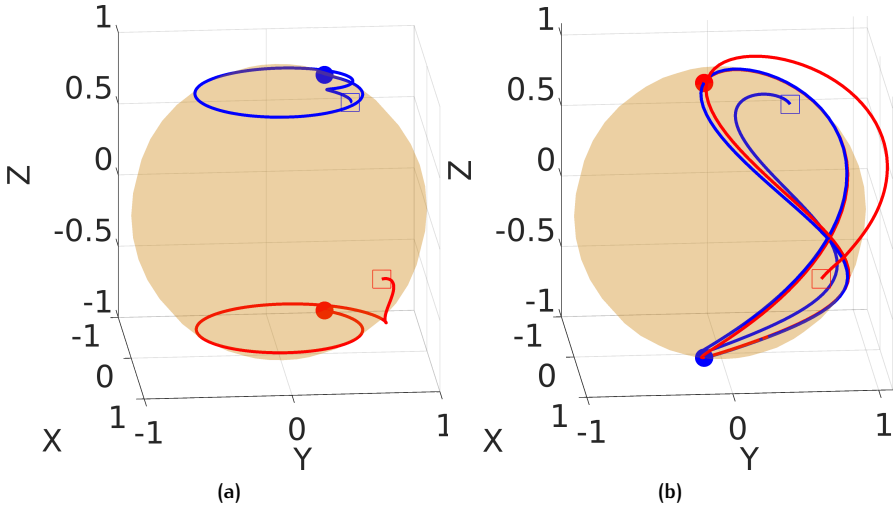


Figure 10.1: Simulation results of two robots coordinating their motions on the sphere described by (10.27). The blue and red dots represent Robot 1 and 2, respectively, and the square symbols represent the initial positions. The desired parametric differences are $\Delta_1^{[1,2]} = \Delta_2^{[1,2]} = -\pi$. (a) The desired parametric speeds are $\dot{w}_1^* = 0$ and $\dot{w}_2^* = 1$ for both robots. (b) The desired parametric speeds are $\dot{w}_1^* = \dot{w}_2^* = 1$ for both robots.

$w_2^{[i]}$, respectively. Specifically, suppose the i -th robot is required to converge to a two-dimensional surface $\mathcal{S}^{[i]} \subseteq \mathbb{R}^n$, which is parameterized by n parametric equations:

$$x_1^{[i]} = f_1^{[i]}(w_1^{[i]}, w_2^{[i]}) \quad \dots \quad x_n^{[i]} = f_n^{[i]}(w_1^{[i]}, w_2^{[i]}), \quad (10.28)$$

where $x_j^{[i]}$ is the j -th coordinate, $f_j^{[i]} \in C^2$ is the j -th parametric function for the i -th robot, for $i \in \mathbb{Z}_1^N, j \in \mathbb{Z}_1^n$, and $w_1^{[i]}, w_2^{[i]}$ are two parameters of the surface. To derive the corresponding guiding vector field, we use the parameters $w_1^{[i]}$ and $w_2^{[i]}$ as two additional virtual coordinates, and the surface $\mathcal{S}^{[i]}$ is described by

$$\mathcal{S}^{[i]} := \{\xi^{[i]} \in \mathbb{R}^{n+2} : \phi_1^{[i]}(\xi^{[i]}) = 0, \dots, \phi_n^{[i]}(\xi^{[i]}) = 0\},$$

where $\xi^{[i]} := (x_1^{[i]}, \dots, x_n^{[i]}, w_1^{[i]}, w_2^{[i]}) \in \mathbb{R}^{n+2}$ denotes the *generalized coordinate* of the i -th robot. Note that the $(n+1)$ -th and the $(n+2)$ -th entries of $\xi^{[i]}$ are the additional virtual coordinates $w_1^{[i]}$ and $w_2^{[i]}$, respectively. The functions $\phi_j^{[i]}$ are

$$\phi_j^{[i]}(x_1^{[i]}, \dots, x_n^{[i]}, w_1^{[i]}, w_2^{[i]}) = x_j^{[i]} - f_j^{[i]}(w_1^{[i]}, w_2^{[i]})$$

for $i \in \mathbb{Z}_1^N$ and $j \in \mathbb{Z}_1^n$. We define

$$\Phi^{[i]}(\xi^{[i]}) := (\phi_1^{[i]}(\xi^{[i]}), \dots, \phi_n^{[i]}(\xi^{[i]}))^\top \in \mathbb{R}^n.$$

Observe that $\xi^{[i]} \in \mathcal{S}^{[i]}$ if and only if $\|\Phi^{[i]}(\xi^{[i]})\| = 0$. Therefore, we can similarly use $\Phi^{[i]}(\xi^{[i]})$, called the *surface-convergence error*, to quantify the distance to the desired surface $\mathcal{S}^{[i]}$.

We use the same structure as the guiding vector field discussed before. However, since the dimensions of the states become $n+2$, the original wedge product is not well-defined. Therefore, we need to introduce an *extra vector* $v = (v_1, \dots, v_{n+2})^\top \in \mathbb{R}^{n+2}$ into the wedge product. Specifically, the new guiding vector field $s^f\chi^{[i]} : \mathbb{R}^{n+2} \rightarrow \mathbb{R}^{n+2}$ corresponding to the surface $\mathcal{S}^{[i]}$, called the *surface-navigation vector field*, is

$$s^f\chi^{[i]}(\xi^{[i]}) = \wedge(\nabla\phi_1^{[i]}(\xi^{[i]}), \dots, \nabla\phi_n^{[i]}(\xi^{[i]}), v) - \sum_{j=1}^n k_j^{[i]} \phi_j^{[i]}(\xi^{[i]}) \nabla\phi_j^{[i]}(\xi^{[i]}), \quad (10.29)$$

For simplicity, we choose $v_1 = \dots = v_n \equiv 0$ while v_{n+1}, v_{n+2} can be zero or non-zero values. One can expand (10.29) and attain the detailed expression as shown below:

$$s^f\chi^{[i]}(\xi^{[i]}) = (-1)^n \begin{bmatrix} v_{n+2}\partial_{w_1}f_1^{[i]} - v_{n+1}\partial_{w_2}f_1^{[i]} \\ \vdots \\ v_{n+2}\partial_{w_1}f_n^{[i]} - v_{n+1}\partial_{w_2}f_n^{[i]} \\ v_{n+2} \\ -v_{n+1} \end{bmatrix} + \begin{bmatrix} -k_1^{[i]}\phi_1^{[i]} \\ \vdots \\ -k_n^{[i]}\phi_n^{[i]} \\ \sum_{j=1}^n k_j^{[i]}\phi_j^{[i]}\partial_{w_1}f_j^{[i]} \\ \sum_{j=1}^n k_j^{[i]}\phi_j^{[i]}\partial_{w_2}f_j^{[i]} \end{bmatrix}, \quad (10.30)$$

where $\partial_{w_1}f_j^{[i]} := \frac{\partial f_j^{[i]}}{\partial w_1^{[i]}}$ and $\partial_{w_2}f_j^{[i]} := \frac{\partial f_j^{[i]}}{\partial w_2^{[i]}}$ for $i \in \mathbb{Z}_1^N$ and $j \in \mathbb{Z}_1^n$.

To achieve coordination in $w_1^{[i]}$ and $w_2^{[i]}$, thus indirectly coordinate the positions of robots, we similarly introduce two *coordination components* ${}^{cr}\chi_1^{[i]}, {}^{cr}\chi_2^{[i]} : \mathbb{R} \times \mathbb{R}^N \rightarrow \mathbb{R}^{n+2}$ for the i -th robot, $i \in \mathbb{Z}_1^N$:

$${}^{cr}\chi_1^{[i]}(t, \mathbf{w}_1^{[\cdot]}) = (0, \dots, 0, c_1^{[i]}(t, \mathbf{w}_1^{[\cdot]}), 0)^\top, \quad (10.31a)$$

$${}^{cr}\chi_2^{[i]}(t, \mathbf{w}_2^{[\cdot]}) = (0, \dots, 0, 0, c_2^{[i]}(t, \mathbf{w}_2^{[\cdot]}))^\top, \quad (10.31b)$$

where $\mathbf{w}_1^{[\cdot]} = (w_1^{[1]}, \dots, w_1^{[N]})^\top$, $\mathbf{w}_2^{[\cdot]} = (w_2^{[1]}, \dots, w_2^{[N]})^\top$, and $c_1^{[i]}, c_2^{[i]} : \mathbb{R} \times \mathbb{R}^N \rightarrow \mathbb{R}$ are the *coordination functions* to be designed later⁵, which enables coordination among robots through the local interactions via the *neighboring* virtual coordinates $w_1^{[j]}$ and $w_2^{[j]}$ for $j \in \mathcal{N}_i$. Specifically, we want the virtual coordinates of multiple robots $w_1^{[i]}(t) - w_1^{[j]}(t)$ and $w_2^{[i]}(t) - w_2^{[j]}(t)$ to converge to $\Delta_1^{[i,j]}(t)$ and $\Delta_2^{[i,j]}(t)$ for $(i, j) \in \mathcal{E}$, where $\Delta_1^{[i,j]}(t), \Delta_2^{[i,j]}(t) \in \mathbb{R}$ are real-valued continuously differentiable functions, representing the desired differences between $w_1^{[i]}(t)$ and $w_1^{[j]}(t)$ at time t and satisfying $\Delta_1^{[i,j]}(t) = -\Delta_1^{[j,i]}(t)$ and $\Delta_2^{[i,j]}(t) = -\Delta_2^{[j,i]}(t)$. It is naturally assumed that $\Delta_1^{[i,j]}(t)$ and $\Delta_2^{[i,j]}(t)$ are chosen appropriately such that the resulting formation is feasible at any time $t \geq 0$.

We design the i -th *coordinating guiding vector field* $\mathfrak{X}^{[i]} : \mathbb{R} \times \mathbb{R}^{n+2N} \rightarrow \mathbb{R}^{n+2}$ to be the weighted sum of the surface-navigation vector field ${}^{\text{sf}}\chi^{[i]}$ and the coordination components ${}^{\text{cr}}\chi_1^{[i]}$ and ${}^{\text{cr}}\chi_2^{[i]}$ as below:

$$\mathfrak{X}^{[i]}(t, \xi^{[i]}, \mathbf{w}_1^{[\cdot]}, \mathbf{w}_2^{[\cdot]}) = {}^{\text{sf}}\chi^{[i]}(\xi^{[i]}) + k_{c1} {}^{\text{cr}}\chi_1^{[i]}(t, \mathbf{w}_1^{[\cdot]}) + k_{c2} {}^{\text{cr}}\chi_2^{[i]}(t, \mathbf{w}_2^{[\cdot]}), \quad (10.32)$$

where $k_{c1}, k_{c2} > 0$ are parameters to adjust the contribution of ${}^{\text{sf}}\chi^{[i]}$, ${}^{\text{cr}}\chi_1^{[i]}$ and ${}^{\text{cr}}\chi_2^{[i]}$ to $\mathfrak{X}^{[i]}$.

We stack all the robot states as a vector $\xi := (\xi^{[1]\top}, \dots, \xi^{[N]\top})^\top \in \mathbb{R}^{(n+2)N}$ and stack all the coordinating guiding vector fields as $\mathfrak{X}(t, \xi) := (\mathfrak{X}^{[1]\top}, \dots, \mathfrak{X}^{[N]\top})^\top \in \mathbb{R}^{(n+2)N}$. Now we need to investigate the integral curves of $\mathfrak{X}(t, \xi)$; i.e., the trajectories of the differential equation: $\dot{\xi} = \mathfrak{X}(t, \xi)$, given an initial condition $\xi_0 \in \mathbb{R}^{(n+2)N}$ at $t = t_0 \geq 0$. For simplicity, we assume that the coordination functions $c_1^{[i]}(t, \mathbf{w}_1^{[\cdot]})$ and $c_2^{[i]}(t, \mathbf{w}_2^{[\cdot]})$ in (10.31) are time-invariant, and v is a constant vector. Therefore, the system (10.33) is an autonomous system:

$$\dot{\xi} = \mathfrak{X}(\xi). \quad (10.33)$$

Now we can formally formulate the problem.

Problem 10.10 (Multi-robot surface navigation). Design the coordinating guiding vector field $\mathfrak{X}^{[i]}$ in (10.32) for $i \in \mathbb{Z}_1^N$, such that the trajectories of (10.33), given an initial condition $\xi_0 \in \mathbb{R}^{(n+2)N}$ at $t = t_0 \geq 0$, fulfill the following control objectives:

1. **(Surface convergence)** Robot i 's surface-convergence errors tend to zero asymptotically for $i \in \mathbb{Z}_1^N$. Namely, $\|\Phi^{[i]}(\xi^{[i]}(t))\| \rightarrow 0$ as $t \rightarrow \infty$ for $i \in \mathbb{Z}_1^N$.

⁵ As the first footnote, we do not require the knowledge of all virtual coordinates, but only those of the neighbors $w_1^{[j]}$ or $w_2^{[j]}$ for $j \in \mathcal{N}_i$.

2. **(Motion coordination)** Each robot's motion is coordinated distributedly subject to the communication graph \mathcal{G} (i.e., Robot i can communicate with Robot j if and only if $(i, j) \in \mathcal{E}$) such that their additional virtual coordinates satisfy $w_1^{[i]}(t) - w_1^{[j]}(t) - \Delta_1^{[i,j]} \rightarrow 0$ and $w_2^{[i]}(t) - w_2^{[j]}(t) - \Delta_2^{[i,j]} \rightarrow 0$ as $t \rightarrow \infty$ for $(i, j) \in \mathcal{E}$.
3. **(Surface maneuvering)** Given desired parametric speeds $\dot{w}_1^* \in \mathbb{R}$ and $\dot{w}_2^* \in \mathbb{R}$, the robot motion can achieve these speeds in the sense that $\dot{w}_1^{[i]}(t) \rightarrow \dot{w}_1^*$ and $\dot{w}_2^{[i]}(t) \rightarrow \dot{w}_2^*$ as $t \rightarrow \infty$ for $i \in \mathbb{Z}_1^N$.

Given the surface-navigation vector field in (10.30), we will design the coordination function $c_1^{[i]}(\cdot), c_2^{[i]}(\cdot)$ later.

10.4.3 Time-invariant coordination component

In this subsection, we will design time-invariant coordination components $c_1^{[i]}(\mathbf{w}_1^{[\cdot]})$ and $c_2^{[i]}(\mathbf{w}_2^{[\cdot]})$, and analyze the trajectories of (10.33), which is an autonomous system.

10.4.3.1 Coordination component

Given the desired surface $\mathcal{S}^{[i]}$, we can design the desired parametric differences $\Delta_1^{[i,j]}$ and $\Delta_2^{[i,j]}$ starting from particular reference configurations $\mathbf{w}_1^* := (\mathbf{w}_1^{[1]*}, \dots, \mathbf{w}_1^{[N]*})^\top$ and $\mathbf{w}_2^* := (\mathbf{w}_2^{[1]*}, \dots, \mathbf{w}_2^{[N]*})^\top$. Hence, $\Delta_1^* = D^\top \mathbf{w}_1^* \in \mathbb{R}^{|\mathcal{E}|}$ and $\Delta_2^* = D^\top \mathbf{w}_2^* \in \mathbb{R}^{|\mathcal{E}|}$ are the stacked vectors of $\Delta_1^{[i,j]}, \Delta_2^{[i,j]}, (i, j) \in \mathcal{E}$, respectively, where $D \in \mathbb{R}^{N \times |\mathcal{E}|}$ is an incidence matrix [88, p. 23]. We employ the following consensus control algorithm:

$$c_1^{[i]} = - \sum_{j \in \mathcal{N}_i} (w_1^{[i]} - w_1^{[j]} - \Delta_1^{[i,j]}), \quad (10.34a)$$

$$c_2^{[i]} = - \sum_{j \in \mathcal{N}_i} (w_2^{[i]} - w_2^{[j]} - \Delta_2^{[i,j]}), \quad (10.34b)$$

for $i \in \mathbb{Z}_1^N$. Equations (10.34) can be rewritten compactly as

$$\mathbf{c}_1^{[\cdot]}(\mathbf{w}_1^{[\cdot]}) = -L(\mathbf{w}_1^{[\cdot]} - \mathbf{w}_1^*) = -L\tilde{\mathbf{w}}_1^{[\cdot]}, \quad (10.35a)$$

$$\mathbf{c}_2^{[\cdot]}(\mathbf{w}_2^{[\cdot]}) = -L(\mathbf{w}_2^{[\cdot]} - \mathbf{w}_2^*) = -L\tilde{\mathbf{w}}_2^{[\cdot]}, \quad (10.35b)$$

where $\mathbf{c}_j^{[\cdot]}(\mathbf{w}_j^{[\cdot]}) = (c_j^{[1]}(\mathbf{w}_j^{[\cdot]}), \dots, c_j^{[N]}(\mathbf{w}_j^{[\cdot]}))^\top$ for $j = 1, 2$, $L = L(\mathcal{G})$ is the Laplacian matrix and

$$\tilde{\mathbf{w}}_1^{[\cdot]} = \mathbf{w}_1^{[\cdot]} - \mathbf{w}_1^*, \quad \tilde{\mathbf{w}}_2^{[\cdot]} = \mathbf{w}_2^{[\cdot]} - \mathbf{w}_2^*.$$

Combining (10.30), (10.31), (10.32) and (10.34), we attain the coordinating guiding vector field $\mathfrak{X}^{[i]}$ for $i \in \mathbb{Z}_1^N$. The vector field $\mathfrak{X}^{[i]}$ only takes as inputs Robot i 's own states and its neighbors' virtual coordinates $w_1^{[j]}, w_2^{[j]}$ for $j \in \mathcal{N}_i$.

Remark 10.11. As in Remark 10.3, from (10.31), (10.32) and (10.34), one observes that neighboring information exchange only involves the coordination components $c_1^{[i]}, c_2^{[i]}$, and Robot i transmits only two scalars $w_1^{[i]}, w_2^{[i]}$ to the neighboring Robot $j \in \mathcal{N}_i$. \triangleleft

10.4.3.2 Convergence analysis

In this subsection, we show that the coordinating guiding vector field (10.32) enables multiple robots to follow their desired paths while they are coordinated by the virtual coordinates such that $w_1^{[i]}(t) - w_1^{[j]}(t)$ converges to $\Delta_1^{[i,j]}$, and $w_2^{[i]}(t) - w_2^{[j]}(t)$ converges to $\Delta_2^{[i,j]}$ for $(i, j) \in \mathcal{E}$ as $t \rightarrow \infty$. To achieve motion coordination on a surface, we impose the following reasonable assumption:

Assumption 10.12. The first derivatives $\partial_{w_1} f_j^{[i]}(\cdot) := \frac{\partial f_j^{[i]}}{\partial w_1^{[i]}}$, $\partial_{w_2} f_j^{[i]}(\cdot) := \frac{\partial f_j^{[i]}}{\partial w_2^{[i]}}$, and the second derivatives $\partial_{w_1}^2 f_j^{[i]}(\cdot)$, $\partial_{w_1}^2 f_j^{[i]}(\cdot)$, $\partial_{w_2}^2 f_j^{[i]}(\cdot)$, $\partial_{w_2}^2 f_j^{[i]}(\cdot)$, where $\partial_{w_k}^{w_l} f_j^{[i]}(\cdot) := \frac{\partial^2 f_j^{[i]}}{\partial w_l^{[i]} \partial w_k^{[i]}}$ for $k, l \in \{1, 2\}$, are bounded for all $i \in \mathbb{Z}_1^N, j \in \mathbb{Z}_1^n$.

Now we can reach the following theorem:

Theorem 10.13 (Motion coordination on surfaces). *Under Assumptions 10.2 and 10.12, and given constant desired parametric differences $\Delta_1^{[i,j]}, \Delta_2^{[i,j]}$ for $(i, j) \in \mathcal{E}$, the coordinating guiding vector fields $\mathfrak{X}^{[i]}$ for $i \in \mathbb{Z}_1^N$ designed by combining (10.30), (10.31), (10.32) and (10.35), and choosing*

$$v = (-1)^{n+1}(0, \dots, 0, \dot{w}_2^*, -\dot{w}_1^*)$$

in (10.29), solve Problem 10.10 globally in the sense that the aggregate initial state $\xi_0 \in \mathbb{R}^{(n+2) \times N}$ can be arbitrary.

Proof. For simplicity, we first consider Robot i , and most of the function arguments are ignored henceforth unless ambiguity arises. We define

$$\begin{aligned} K^{[i]} &:= \text{diag}\{k_1^{[i]}, \dots, k_n^{[i]}\} \in \mathbb{R}^{n \times n}, \\ \partial_{w_1} f^{[i]}(\cdot) &:= (\partial_{w_1} f_1^{[i]}(w_1^{[i]}, w_2^{[i]}), \dots, \partial_{w_1} f_n^{[i]}(w_1^{[i]}, w_2^{[i]}))^\top, \\ \partial_{w_2} f^{[i]}(\cdot) &:= (\partial_{w_2} f_1^{[i]}(w_1^{[i]}, w_2^{[i]}), \dots, \partial_{w_2} f_n^{[i]}(w_1^{[i]}, w_2^{[i]}))^\top. \end{aligned}$$

Then one can calculate that

$$\begin{aligned} \nabla \phi_j^{[i]^\top} \text{sf} \chi^{[i]} &\stackrel{(10.30)}{=} \begin{bmatrix} 0 \\ \vdots \\ 1 \\ \vdots \\ 0 \\ -\partial_{w_1} f_j^{[i]} \\ -\partial_{w_2} f_j^{[i]} \end{bmatrix}^\top \left(\wedge(\nabla \phi_1^{[i]}, \dots, \nabla \phi_n^{[i]}, v) + \begin{bmatrix} -k_1^{[i]} \phi_1^{[i]} \\ \vdots \\ -k_n^{[i]} \phi_n^{[i]} \\ \sum_{j=1}^n k_j^{[i]} \phi_j^{[i]} \partial_{w_1} f_j^{[i]} \\ \sum_{j=1}^n k_j^{[i]} \phi_j^{[i]} \partial_{w_2} f_j^{[i]} \end{bmatrix} \right) \\ &= -k_j^{[i]} \phi_j^{[i]} - \partial_{w_1} f_j^{[i]} \cdot [\partial_{w_1} f^{[i]^\top} K^{[i]} \Phi^{[i]}] - \partial_{w_2} f_j^{[i]} \cdot [\partial_{w_2} f^{[i]^\top} K^{[i]} \Phi^{[i]}] \end{aligned}$$

for $j \in \mathbb{Z}_1^N$, where 1 is at the j -th entry of $\nabla \phi_j^{[i]}$. Therefore, we have

$$\begin{bmatrix} \nabla \phi_1^{[i]^\top} \text{sf} \chi^{[i]} \\ \vdots \\ \nabla \phi_n^{[i]^\top} \text{sf} \chi^{[i]} \end{bmatrix} = -K^{[i]} \Phi^{[i]} - \partial_{w_1} f^{[i]^\top} \cdot [\partial_{w_1} f^{[i]^\top} K^{[i]} \Phi^{[i]}] - \partial_{w_2} f^{[i]^\top} \cdot [\partial_{w_2} f^{[i]^\top} K^{[i]} \Phi^{[i]}]. \quad (10.36)$$

We can also calculate that

$$\begin{bmatrix} \nabla \phi_1^{[i]^\top} \text{cr} \chi_1^{[i]}(w) \\ \vdots \\ \nabla \phi_n^{[i]^\top} \text{cr} \chi_1^{[i]}(w) \end{bmatrix} = -c_1^{[i]}(w) \begin{bmatrix} \partial_{w_1} f_1^{[i]} \\ \vdots \\ \partial_{w_1} f_n^{[i]} \end{bmatrix} = -c_1^{[i]}(w) \partial_{w_1} f^{[i]}(w). \quad (10.37)$$

The same calculation applies for $\text{cr} \chi_2^{[i]}$. Therefore,

$$\begin{aligned} \dot{\Phi}^{[i]} &= \frac{d}{dt} (\phi_1^{[i]}, \dots, \phi_n^{[i]})^\top \\ &= \begin{bmatrix} \nabla \phi_1^{[i]^\top} \text{sf} \chi^{[i]} + k_{c1} \nabla \phi_1^{[i]^\top} \text{cr} \chi_1^{[i]} + k_{c2} \nabla \phi_1^{[i]^\top} \text{cr} \chi_2^{[i]} \\ \vdots \\ \nabla \phi_n^{[i]^\top} \text{sf} \chi^{[i]} + k_{c1} \nabla \phi_n^{[i]^\top} \text{cr} \chi_1^{[i]} + k_{c2} \nabla \phi_n^{[i]^\top} \text{cr} \chi_2^{[i]} \end{bmatrix} \\ &\stackrel{(10.36), (10.37)}{=} -K^{[i]} \Phi^{[i]} - \partial_{w_1} f^{[i]^\top} \partial_{w_1} f^{[i]^\top} K^{[i]} \Phi^{[i]} - \partial_{w_2} f^{[i]^\top} \partial_{w_2} f^{[i]^\top} K^{[i]} \Phi^{[i]} \\ &\quad - k_{c1} c_1^{[i]}(w) \partial_{w_1} f^{[i]}(w) - k_{c2} c_2^{[i]}(w) \partial_{w_2} f^{[i]}(w). \end{aligned} \quad (10.38)$$

for $i \in \mathbb{Z}_1^N$. Now we consider all robots. We define

$$\begin{aligned}\mathfrak{F}_1 &:= \text{diag}\{\partial_{w_1} f^{[1]}, \dots, \partial_{w_1} f^{[N]}\} \in \mathbb{R}^{nN \times N} \\ \mathfrak{F}_2 &:= \text{diag}\{\partial_{w_2} f^{[1]}, \dots, \partial_{w_2} f^{[N]}\} \in \mathbb{R}^{nN \times N} \\ K &:= \text{diag}\{K^{[1]}, \dots, K^{[N]}\} \in \mathbb{R}^{nN \times nN} \\ \Phi &:= (\Phi^{[1]^\top}, \dots, \Phi^{[N]^\top})^\top \in \mathbb{R}^{nN}.\end{aligned}$$

Then we have the following equation:

$$\begin{aligned}\Phi &= \begin{bmatrix} -K^{[1]}\Phi^{[1]} - \partial_{w_1} f^{[1]}\partial_{w_1} f^{[1]^\top} K^{[1]}\Phi^{[1]} - \partial_{w_2} f^{[1]}\partial_{w_2} f^{[1]^\top} K^{[1]}\Phi^{[1]} \\ -k_{c1}c_1^{[1]}(w)\partial_{w_1} f^{[1]}(w) - k_{c2}c_2^{[1]}(w)\partial_{w_2} f^{[1]}(w) \\ \vdots \\ -K^{[N]}\Phi^{[N]} - \partial_{w_1} f^{[N]}\partial_{w_1} f^{[N]^\top} K^{[N]}\Phi^{[N]} - \partial_{w_2} f^{[N]}\partial_{w_2} f^{[N]^\top} K^{[N]}\Phi^{[N]} \\ -k_{c1}c_1^{[N]}(w)\partial_{w_1} f^{[N]}(w) - k_{c2}c_2^{[N]}(w)\partial_{w_2} f^{[N]}(w) \end{bmatrix} \\ &= -K\Phi - \mathfrak{F}_1\mathfrak{F}_1^\top K\Phi - \mathfrak{F}_2\mathfrak{F}_2^\top K\Phi - k_{c1}\mathfrak{F}_1 c_1^{[\cdot]}(w) - k_{c2}\mathfrak{F}_2 c_2^{[\cdot]}(w). \quad (10.39)\end{aligned}$$

One can also calculate that

$$\begin{aligned}\dot{w}_1^{[i]} &= [0 \ \dots \ 0 \ 1 \ 0] (\mathbf{s}f\chi^{[i]} + k_{c1}\mathbf{cr}\chi_1^{[i]} + k_{c2}\mathbf{cr}\chi_2^{[i]}) \\ &= (-1)^n v_{n+2} + \partial_{w_1} f^{[i]^\top} K^{[i]}\Phi^{[i]}(\xi^{[i]}) + k_{c1}c_1^{[i]}, \\ \dot{w}_2^{[i]} &= [0 \ \dots \ 0 \ 0 \ 1] (\mathbf{s}f\chi^{[i]} + k_{c1}\mathbf{cr}\chi_1^{[i]} + k_{c2}\mathbf{cr}\chi_2^{[i]}) \\ &= (-1)^{n+1} v_{n+1} + \partial_{w_2} f^{[i]^\top} K^{[i]}\Phi^{[i]}(\xi^{[i]}) + k_{c2}c_2^{[i]}. \quad (10.40)\end{aligned}$$

By $\tilde{w} := w - w^*$, there holds

$$\dot{\tilde{w}}_1^{[\cdot]} = \dot{w}_1^{[\cdot]} = (-1)^n v_{n+2} \mathbf{1} + \mathfrak{F}_1^\top K\Phi + k_{c1}c_1^{[\cdot]}, \quad (10.41)$$

$$\dot{\tilde{w}}_2^{[\cdot]} = \dot{w}_2^{[\cdot]} = (-1)^{n+1} v_{n+1} \mathbf{1} + \mathfrak{F}_2^\top K\Phi + k_{c2}c_2^{[\cdot]}. \quad (10.42)$$

The Laplacian matrix can be factorized as $L = DD^\top$. We define the *composite error vector* e to be

$$e = (\Phi^\top, (D^\top \tilde{w}_1^{[\cdot]})^\top, (D^\top \tilde{w}_2^{[\cdot]})^\top)^\top \in \mathbb{R}^{nN+2|\mathcal{E}|}$$

and the composite gain matrix to be

$$\mathfrak{K} = \text{diag}\{K, k_{c1}I_{|\mathcal{E}|}, k_{c2}I_{|\mathcal{E}|}\} \in \mathbb{R}^{(nN+2|\mathcal{E}|) \times (nN+2|\mathcal{E}|)}.$$

Therefore, from (10.35), (10.39) and (10.41), and noting that $D^\top \mathbf{1} = \mathbf{0}$, we have the following composite error dynamics:

$$\dot{\mathbf{e}} = \begin{bmatrix} \dot{\Phi} \\ D^\top \tilde{\mathbf{w}}_1^{[\cdot]} \\ D^\top \tilde{\mathbf{w}}_2^{[\cdot]} \end{bmatrix} = \begin{bmatrix} -K\Phi - \mathfrak{F}_1 \mathfrak{F}_1^\top K\Phi - \mathfrak{F}_2 \mathfrak{F}_2^\top K\Phi + k_{c1} \mathfrak{F}_1 L \tilde{\mathbf{w}}_1^{[\cdot]} + k_{c2} \mathfrak{F}_2 L \tilde{\mathbf{w}}_2^{[\cdot]} \\ D^\top \mathfrak{F}_1^\top K\Phi - k_{c1} D^\top L \tilde{\mathbf{w}}_1^{[\cdot]} \\ D^\top \mathfrak{F}_2^\top K\Phi - k_{c2} D^\top L \tilde{\mathbf{w}}_2^{[\cdot]} \end{bmatrix}. \quad (10.43)$$

Consider the following Lyapunov function candidate

$$V(\mathbf{e}) = \frac{1}{2} \mathbf{e}^\top \mathcal{K} \mathbf{e} = \frac{1}{2} \left(\Phi^\top K \Phi + k_{c1} \tilde{\mathbf{w}}_1^{[\cdot] \top} L \tilde{\mathbf{w}}_1^{[\cdot]} + k_{c2} \tilde{\mathbf{w}}_2^{[\cdot] \top} L \tilde{\mathbf{w}}_2^{[\cdot]} \right), \quad (10.44)$$

of which the time derivative satisfies

$$\begin{aligned} \dot{V}(\mathbf{e}) &= \dot{\mathbf{e}}^\top \mathcal{K} \mathbf{e} \\ &\stackrel{(10.43)}{=} \begin{bmatrix} -K\Phi - \mathfrak{F}_1 \mathfrak{F}_1^\top K\Phi - \mathfrak{F}_2 \mathfrak{F}_2^\top K\Phi + k_{c1} \mathfrak{F}_1 L \tilde{\mathbf{w}}_1^{[\cdot]} + k_{c2} \mathfrak{F}_2 L \tilde{\mathbf{w}}_2^{[\cdot]} \\ D^\top \mathfrak{F}_1^\top K\Phi - k_{c1} D^\top L \tilde{\mathbf{w}}_1^{[\cdot]} \\ D^\top \mathfrak{F}_2^\top K\Phi - k_{c2} D^\top L \tilde{\mathbf{w}}_2^{[\cdot]} \end{bmatrix}^\top \\ &\quad \begin{bmatrix} K & & \\ & k_{c1} I_{|\mathcal{E}|} & \\ & & k_{c2} I_{|\mathcal{E}|} \end{bmatrix} \begin{bmatrix} \Phi \\ D^\top \tilde{\mathbf{w}}_1^{[\cdot]} \\ D^\top \tilde{\mathbf{w}}_2^{[\cdot]} \end{bmatrix} \end{aligned} \quad (10.45)$$

$$\begin{aligned} &= -\|K\Phi\|^2 - \|\mathfrak{F}_1^\top K\Phi\|^2 - \|\mathfrak{F}_2^\top K\Phi\|^2 + k_{c1} (\mathfrak{F}_1 L \tilde{\mathbf{w}}_1^{[\cdot]})^\top K\Phi \\ &\quad + k_{c2} (\mathfrak{F}_2 L \tilde{\mathbf{w}}_2^{[\cdot]})^\top K\Phi + k_{c1} (\mathfrak{F}_1^\top K\Phi)^\top L \tilde{\mathbf{w}}_1^{[\cdot]} - k_{c1}^2 \|L \tilde{\mathbf{w}}_1^{[\cdot]}\|^2 \\ &\quad + k_{c2} (\mathfrak{F}_2^\top K\Phi)^\top L \tilde{\mathbf{w}}_2^{[\cdot]} - k_{c2}^2 \|L \tilde{\mathbf{w}}_2^{[\cdot]}\|^2 \end{aligned} \quad (10.46)$$

$$\begin{aligned} &= -\|K\Phi\|^2 - \|\mathfrak{F}_1^\top K\Phi\|^2 - \|\mathfrak{F}_2^\top K\Phi\|^2 + 2k_{c1} (\mathfrak{F}_1^\top K\Phi)^\top (L \tilde{\mathbf{w}}_1^{[\cdot]}) \\ &\quad + 2k_{c2} (\mathfrak{F}_2^\top K\Phi)^\top (L \tilde{\mathbf{w}}_2^{[\cdot]}) - k_{c1}^2 \|L \tilde{\mathbf{w}}_1^{[\cdot]}\|^2 - k_{c2}^2 \|L \tilde{\mathbf{w}}_2^{[\cdot]}\|^2 \end{aligned} \quad (10.47)$$

$$\begin{aligned} &= -\|K\Phi\|^2 - \|\mathfrak{F}_1^\top K\Phi - k_{c1} L \tilde{\mathbf{w}}_1^{[\cdot]}\|^2 - \|\mathfrak{F}_2^\top K\Phi - k_{c2} L \tilde{\mathbf{w}}_2^{[\cdot]}\|^2 \\ &\leq -\|K\Phi\|^2 \leq 0. \end{aligned} \quad (10.48)$$

From (10.48), we know that \dot{V} is negative semi-definite. We use the LaSalle's invariance principle (i.e., Theorem 2.8) to conclude that $\|K\Phi\|^2 \rightarrow 0$ as $t \rightarrow \infty$, hence $\|\Phi^{[i]}\| \rightarrow 0$ as $t \rightarrow \infty$ for all $i \in \mathbb{Z}_1^N$; i.e., all robots' path-following errors vanish asymptotically. Moreover, the quadratic form of the Lyapunov function V implies that V is radially unbounded with respect to $\|\mathbf{e}\|$ (i.e., $V(\mathbf{e}) \rightarrow \infty$ as $\|\mathbf{e}\| \rightarrow \infty$), and thus the convergence holds globally: the norm of the initial path-following error $\|\mathbf{e}(0)\|$ can be arbitrarily large.

To prove the convergence of the second and third term $D^\top \tilde{w}_1^{[\cdot]}, D^\top \tilde{w}_2^{[\cdot]}$ of the composite error vector, we use Barbata's lemma (i.e., Lemma 2.7). Firstly, (10.48) shows that $\dot{V} \leq 0$, hence $V(t) \leq V(0)$ for $t \geq 0$. This implies that the composite error e is bounded, and thus Φ and $D^\top \tilde{w}_1^{[\cdot]}, D^\top \tilde{w}_2^{[\cdot]}$ are all bounded. Due to Assumption 10.12, one can verify that \dot{e} in (10.43) is also bounded, and thus $\dot{\Phi}, D^\top \tilde{w}_1^{[\cdot]}, D^\top \tilde{w}_2^{[\cdot]}$ are bounded as well. Next, we show that the second-order time derivative \ddot{V} is bounded. One can calculate that $\ddot{V} = \dot{e}^\top \mathcal{K} e + \dot{e}^\top \mathcal{K} \dot{e}$. It is obvious that the second term of \ddot{V} is bounded, so we only need to show that \dot{e} is bounded. We have

$$\ddot{e} = \begin{bmatrix} \ddot{e}_1 \\ D^\top (\hat{\mathfrak{F}}_1^\top K\Phi + \mathfrak{F}_1^\top K\dot{\Phi}) - k_{c1} D^\top L \dot{\tilde{w}}_1^{[\cdot]} \\ D^\top (\hat{\mathfrak{F}}_2^\top K\Phi + \mathfrak{F}_2^\top K\dot{\Phi}) - k_{c2} D^\top L \dot{\tilde{w}}_2^{[\cdot]} \end{bmatrix},$$

where

$$\begin{aligned} \ddot{e}_1 &= -K\dot{\Phi} - \hat{\mathfrak{F}}_1 \mathfrak{F}_1^\top K\Phi - \mathfrak{F}_1(\hat{\mathfrak{F}}_1^\top K\Phi + \mathfrak{F}_1^\top K\dot{\Phi}) + k_{c1} \hat{\mathfrak{F}}_1 L \tilde{w}_1^{[\cdot]} + k_{c1} \mathfrak{F}_1 L \dot{\tilde{w}}_1^{[\cdot]} \\ &\quad - \hat{\mathfrak{F}}_2 \mathfrak{F}_2^\top K\Phi - \mathfrak{F}_2(\hat{\mathfrak{F}}_2^\top K\Phi + \mathfrak{F}_2^\top K\dot{\Phi}) + k_{c2} \hat{\mathfrak{F}}_2 L \tilde{w}_2^{[\cdot]} + k_{c2} \mathfrak{F}_2 L \dot{\tilde{w}}_2^{[\cdot]}, \end{aligned}$$

and $\hat{\mathfrak{F}}_1 = \text{diag}\{\frac{d}{dt} \partial_{w_1} f_1^{[1]}, \dots, \frac{d}{dt} \partial_{w_1} f_1^{[N]}\}$ with

$$\frac{d}{dt} \partial_{w_1} f_1^{[i]} = \begin{bmatrix} \partial_{w_1}^1 f_1^{[i]} & \partial_{w_1}^2 f_1^{[i]} \\ \vdots & \vdots \\ \partial_{w_1}^n f_1^{[i]} & \partial_{w_1}^{n+1} f_1^{[i]} \end{bmatrix} \begin{bmatrix} \tilde{w}_1^{[i]} \\ \tilde{w}_2^{[i]} \end{bmatrix}$$

for $i \in \mathbb{Z}_1^N$. Since $\Phi, D^\top \tilde{w}_1^{[\cdot]}, D^\top \tilde{w}_2^{[\cdot]}, \dot{\Phi}, D^\top \dot{\tilde{w}}_1^{[\cdot]}, D^\top \dot{\tilde{w}}_2^{[\cdot]}$ are all bounded, and by (10.40) and Assumption 10.12, we have that $\hat{\mathfrak{F}}_1, \hat{\mathfrak{F}}_2$ are bounded, hence \ddot{e} is indeed bounded. Therefore, \dot{V} is bounded, and thus \dot{V} is uniformly continuous in time t . By invoking Lemma 4.3 in [133], we have that $\dot{V}(e) \rightarrow 0$ as $t \rightarrow \infty$. Equivalently, $\dot{e}^\top \mathcal{K} e \rightarrow 0$ as $t \rightarrow \infty$. Since the argument above shows that $\|\Phi\| \rightarrow 0$ as $t \rightarrow \infty$, from (10.47) and the boundedness of $\hat{\mathfrak{F}}_1, \hat{\mathfrak{F}}_2, D^\top \tilde{w}_1^{[\cdot]}, D^\top \tilde{w}_2^{[\cdot]}$, we thus have $L \tilde{w}_1^{[\cdot]} \rightarrow 0$ and $L \tilde{w}_2^{[\cdot]} \rightarrow 0$ as $t \rightarrow \infty$. Furthermore, by Assumption 10.2, $L \dot{\tilde{w}}_1^{[\cdot]} \rightarrow 0$ and $L \dot{\tilde{w}}_2^{[\cdot]} \rightarrow 0$ as $t \rightarrow \infty$ imply that $\tilde{w}_1^{[i]} - \tilde{w}_1^{[j]} \rightarrow 0$ and $\tilde{w}_2^{[i]} - \tilde{w}_2^{[j]} \rightarrow 0$ for all $i, j \in \mathbb{Z}_1^N$ [116, Corollary 2.5]. This further implies that $w_1^{[i]}(t) - w_1^{[j]}(t) \rightarrow \Delta_1^{[i,j]}(t)$ and $w_2^{[i]}(t) - w_2^{[j]}(t) \rightarrow \Delta_2^{[i,j]}(t)$. Therefore, the differences in the virtual coordinates $w_1^{[i]}$ and $w_2^{[i]}$ of all robots converge to the desired value, and thus the coordinated motion can be achieved. As in the proof of Theorem 10.5, the global convergence property is attained due to the radial unboundedness of the Lyapunov function V with respect to $\|e\|$.

Using the fact that $\lim_{t \rightarrow \infty} K\Phi = \mathbf{0}$, $\lim_{t \rightarrow \infty} L\tilde{\mathbf{w}}_1^{[\cdot]} = \mathbf{0}$ and $\lim_{t \rightarrow \infty} L\tilde{\mathbf{w}}_1^{[\cdot]} = \mathbf{0}$, we have

$$\begin{aligned} \lim_{t \rightarrow \infty} \mathbf{w}_1^{[i]} &= \lim_{t \rightarrow \infty} \begin{bmatrix} 0 & \dots & 1 & 0 \end{bmatrix} \mathfrak{X}^{[i]}(t, \xi^{[i]}, \mathbf{w}_1^{[\cdot]}, \mathbf{w}_2^{[\cdot]}) \\ &= \lim_{t \rightarrow \infty} \begin{bmatrix} 0 & \dots & 1 & 0 \end{bmatrix} \left({}^{\text{sf}}\chi^{[i]}(\xi^{[i]}) + k_{c1} {}^{\text{cr}}\chi_1^{[i]}(t, \mathbf{w}_1^{[\cdot]}) + k_{c2} {}^{\text{cr}}\chi_2^{[i]}(t, \mathbf{w}_2^{[\cdot]}) \right) \\ &= \lim_{t \rightarrow \infty} \begin{bmatrix} 0 & \dots & 1 & 0 \end{bmatrix} \left({}^{\text{sf}}\chi^{[i]}(\xi^{[i]}) \right) \\ &\stackrel{(10.30)}{=} \lim_{t \rightarrow \infty} \left(\begin{bmatrix} 0 & \dots & 1 & 0 \end{bmatrix} \begin{bmatrix} (-1)^n(v_{n+2}\partial_{w_1}f_1^{[i]} - v_{n+1}\partial_{w_2}f_1^{[i]}) \\ \vdots \\ (-1)^n(v_{n+2}\partial_{w_1}f_n^{[i]} - v_{n+1}\partial_{w_2}f_n^{[i]}) \\ (-1)^n v_{n+2} \\ (-1)^{n+1} v_{n+1} \end{bmatrix} \right) \\ &= (-1)^n(-1)^n \dot{\mathbf{w}}_1^* = \dot{\mathbf{w}}_1^*. \end{aligned}$$

Similarly, we have $\lim_{t \rightarrow \infty} \dot{\mathbf{w}}_2^{[i]} = \dot{\mathbf{w}}_2^*$. Therefore, the desired motion on the surface described in Problem 10.10 can be achieved. \square

Remark 10.14. We can also design time-varying coordination components in the same way as (10.19), and the analysis is almost the same except for the use of more complicated notations. Moreover, the above analysis can be further extended for more parameters. For example, to define motion coordination confined in a three-dimensional manifold (e.g., a cube) rather than a surface, one may choose three parameters $w_i, i = 1, 2, 3$. The design methodology and analysis techniques for the two-parameter case can be directly adopted for this case with more cumbersome notations. In addition, if one uses $m \geq 2$ parameters, then one also needs to choose $m - 1$ extra vectors v_1, \dots, v_{m-1} as what has been shown in (10.29) such that the wedge produce is well-defined. The detailed theoretical development is similar to the two-parameter case and thus omitted. \triangleleft

10.5 EXTENDING THE VECTOR FIELD TO INCORPORATE COLLISION AVOIDANCE

The focus of our work is the introduction and rigorous analysis of coordinating guiding vector fields for following paths or navigating surfaces with motion coordination as discussed above. However, to demonstrate the flexibility and practicality of our approach, in this section, we briefly explain how our proposed approach can incorporate existing collision avoidance algorithms [147]. For example, we can modify the *nominal* guiding vector field (10.5) in a minimally invasive way using *safety barrier certificates* [146], [147]. Without loss of generality,

we only consider the coordinating guiding vector field for path following. Namely, the number of parameters is 1, and thus there is only one virtual coordinate for each robot.

For $i \neq j$, $i, j \in \mathbb{Z}_1^N$, we define a function

$$\mathfrak{h}_{ij}(\xi^{[i]}, \xi^{[j]}) = \|P(\xi^{[i]} - \xi^{[j]})\|^2 - R^2,$$

where $R > 0$ is the safe distance, P is the projection matrix $P = I - \begin{bmatrix} \mathbf{0} & \mathbf{0} \\ \mathbf{0} & 1 \end{bmatrix} \in \mathbb{R}^{(n+1) \times (n+1)}$ and I is the $(n+1)$ -by- $(n+1)$ identity matrix. The function \mathfrak{h}_{ij} reflects whether two robots keep a safe distance. Therefore, we can define the *safe set* \mathfrak{S} :

$$\mathfrak{S} = \{(\xi^{[1]}\top, \dots, \xi^{[N]}\top)\top \in \mathbb{R}^{(n+1)N} : \mathfrak{h}_{ij}(\xi^{[i]}, \xi^{[j]}) \geq 0, \forall i \neq j\}. \quad (10.49)$$

Using \mathfrak{h}_{ij} , we can define a barrier function [6]:

$$B_{ij}(\xi^{[i]}, \xi^{[j]}) := \frac{1}{\mathfrak{h}_{ij}(\xi^{[i]}, \xi^{[j]})} \quad (10.50)$$

for $i \neq j$, $i, j \in \mathbb{Z}_1^N$. We want to modify the *nominal vector field* $\mathfrak{X}^{[i]}$ such that the new vector field denoted by $\check{\mathfrak{X}}^{[i]}$ also enables collision-avoidance, which is encoded in the safety barrier certificate [146], [147]. Specifically, the new vector field $\check{\mathfrak{X}}^{[i]}$ is obtained by minimizing $\sum_{i=1}^N \|\check{\mathfrak{X}}^{[i]} - \mathfrak{X}^{[i]}\|^2 / 2$ subject to the constraint $\dot{B}_{ij} \leq \alpha / B_{ij}$ where $\alpha > 0$ is a constant, for $j < i$ and $i, j \in \mathbb{Z}_1^N$. Using (10.50) and the equivalence $\dot{B}_{ij} = -\dot{\mathfrak{h}}_{ij} / \mathfrak{h}_{ij}^2 = -[2(\xi^{[i]} - \xi^{[j]})^\top P^\top (\check{\mathfrak{X}}^{[i]} - \check{\mathfrak{X}}^{[j]})] / \mathfrak{h}_{ij}^2$, the constraint $\dot{B}_{ij} \leq \alpha / B_{ij}$ can be rewritten as

$$(\xi^{[j]} - \xi^{[i]})^\top P^\top \check{\mathfrak{X}}^{[i]} + (\xi^{[i]} - \xi^{[j]})^\top P^\top \check{\mathfrak{X}}^{[j]} \leq \frac{\alpha}{2} \mathfrak{h}_{ij}^3. \quad (10.51)$$

Therefore, the new vector field $\check{\mathfrak{X}} := (\check{\mathfrak{X}}^{[1]}\top, \dots, \check{\mathfrak{X}}^{[N]}\top)\top \in \mathbb{R}^{(n+1)N}$ is calculated by the quadratic program below:

$$\begin{aligned} \min_{\check{\mathfrak{X}} \in \mathbb{R}^{(n+1)N}} \quad & \frac{1}{2} \sum_{i=1}^N \|\check{\mathfrak{X}}^{[i]} - \mathfrak{X}^{[i]}\|^2 \\ \text{s.t.} \quad & (10.51), \quad \forall j \in \mathcal{D}_i, \end{aligned} \quad (10.52)$$

where \mathcal{D}_i is the set of robots within distance R with respect to Robot i ; i.e., $\mathcal{D}_i := \{j \in \mathbb{Z}_1^N : \mathfrak{h}_{ij} \leq 0, j \neq i\}$. Note that the definition of \mathcal{D}_i is based on geographical distances and it is different from the neighborhood \mathcal{N}_i , which is based on a communication graph \mathcal{G} . If Robot i keeps a safe distance to all other

robots (i.e., $\mathfrak{h}_{ij} \geq 0$ for all $j \neq i$), then the new vector field $\check{\mathfrak{X}}^{[i]}$ is the same as the original one $\mathfrak{X}^{[i]}$. In addition, since the virtual coordinate is not considered in the constraint (10.51), there always holds $\mathfrak{X}_{n+1}^{[i]} = \check{\mathfrak{X}}_{n+1}^{[i]}$ for $i \in \mathbb{Z}_1^N$. Note that this optimization problem is *centralized* in the sense that it requires the positions and the nominal vector fields of *all* robots. We can change it to the following *distributed* version:

$$\begin{aligned} & \min_{\check{\mathfrak{X}}^{[i]} \in \mathbb{R}^{n+1}} \frac{1}{2} \|\check{\mathfrak{X}}^{[i]} - \mathfrak{X}^{[i]}\|^2 \\ & \text{s.t. } (\zeta^{[j]} - \zeta^{[i]})^\top P^\top \check{\mathfrak{X}}^{[i]} \leq \frac{\alpha}{4} \mathfrak{h}_{ij}^3, \quad \forall j \in \mathcal{D}_i \end{aligned} \quad (10.53)$$

for each robot $i \in \mathbb{Z}_1^N$. In this optimization problem, Robot i only needs to measure⁶ the positions $p^{[j]} = P\zeta^{[j]}$ of nearby robots for $j \in \mathcal{D}_i$, and does *not* need to obtain other robots' nominal vector field $\mathfrak{X}^{[j]}$, which is only possible via communication (rather than measurement). If all the constraints in (10.53) are satisfied, so are those in (10.52). Therefore, a feasible solution of (10.53) is also a feasible solution of (10.52). Assume that the initial positions of robots are in the safe set \mathfrak{S} , then it is guaranteed that all the robots will always be in the safe set \mathfrak{S} [6], [146], [147], and one observes that the quadratic program (10.53) is always feasible, since $\check{\mathfrak{X}}^{[i]} = \mathbf{0}$ remains a trivial solution. This implies that a robot can always keep stationary (i.e., $\dot{p}^{[i]} = P\check{\mathfrak{X}}^{[i]} = \mathbf{0}$) to maintain a safe distance to other robots even if the nominal vector field $\mathfrak{X}^{[i]}$ attempted to drive the robot to move closer to others. The quadratic program (10.53) can be rewritten into the following standard form

$$\begin{aligned} & \min_{\check{\mathfrak{X}}^{[i]} \in \mathbb{R}^{n+1}} \frac{1}{2} \check{\mathfrak{X}}^{[i]^\top} \check{\mathfrak{X}}^{[i]} + f^\top \check{\mathfrak{X}}^{[i]} \\ & \text{s.t. } A\check{\mathfrak{X}}^{[i]} \leq b, \end{aligned} \quad (10.54)$$

where the inequality is entrywise, and $f = -\mathfrak{X}^{[i]}$. The matrix $A \in \mathbb{R}^{|\mathcal{D}_i| \times (n+1)}$ and the vector $b \in \mathbb{R}^{|\mathcal{D}_i|}$, where the j -th row of A is $A_{j,:} = (\zeta^{[j]} - \zeta^{[i]})^\top P^\top$, and the j -entry of b is $b_j = \alpha \mathfrak{h}_{ij}^3 / 4$, for $j \in \mathcal{D}_i$. Note that the last column of A is a zero vector.

⁶ In practice, the measurement is always inaccurate. However, the robustness property of control barrier functions against perturbation [154] mitigate the consequence of inaccurate measurement.

10.6 SATURATED CONTROLLER FOR A DUBINS-CAR-LIKE MODEL

If a robot's dynamics can be approximately modeled by the single-integrator model, then the coordinating guiding vector field in (10.5) can be used directly as the velocity input to the robot. For the unicycle model, one can use feedback linearization to transform it into the single-integrator model [168] to utilize the guiding vector field directly. However, we will design a controller for a model resembling a unicycle traveling at a constant speed (i.e., the Dubins-car model) without using the feedback linearization technique. Note that the control algorithm design idea in this section is applicable to robot models whose motions are characterized by the robot's orientations, such as the car-like model and the underwater glider model [130]. These models (approximately) represent many different robotic systems in reality, thus the design methodology is widely applicable.

Different from the unicycle model, which allows backwards or stationary motion, we use the following Dubins-car-like 3D model that describes fixed-wing aircraft dynamics:

$$\dot{p}_1^{[i]} = v \cos \theta^{[i]}, \quad \dot{p}_2^{[i]} = v \sin \theta^{[i]}, \quad \dot{p}_3^{[i]} = u_z^{[i]}, \quad \dot{\theta}^{[i]} = u_\theta^{[i]}, \quad (10.55)$$

where v is a constant airspeed, $(p_1^{[i]}, p_2^{[i]}, p_3^{[i]})^\top \in \mathbb{R}^3$ is the position of the i -th aircraft's center of mass, $\theta^{[i]}$ is the yaw angle, and $u_z^{[i]}$ and $u_\theta^{[i]}$ are two control inputs to be designed. Since the essential role of a guiding vector field is to provide the desired yaw angle to guide the flight of a fixed-wing aircraft, the core idea behind the control algorithm design is to align the aircraft's flying direction with that given by the guiding vector field. Without loss of generality, we assume that there is only one parameter (i.e., we consider path following rather than surface navigation). Therefore, the coordinating guiding vector field has an additional coordinate, and thus one needs to add an additional virtual coordinate $p_4^{[i]}$ such that the aircraft's generalized position is $(p_1^{[i]}, p_2^{[i]}, p_3^{[i]}, p_4^{[i]}) \in \mathbb{R}^4$. Correspondingly, its generalized velocity is $(\dot{p}_1^{[i]}, \dot{p}_2^{[i]}, \dot{p}_3^{[i]}, \dot{p}_4^{[i]}) = (v \cos \theta^{[i]}, v \sin \theta^{[i]}, u_z^{[i]}, \dot{p}_4^{[i]})$, where $\dot{p}_4^{[i]}$ is virtual, acting as an extra design freedom. To align the aircraft heading $v(\cos \theta^{[i]}, \sin \theta^{[i]})$ with the counterpart of the coordinating guiding vector field $\mathfrak{X}^{[i]}$, we need to "partially normalize" the vector field $\mathfrak{X}^{[i]}$ such that its first two entries form a vector of the same length as v ; that is,

$$v\mathfrak{X}^{[i]} := v\mathfrak{X}^{[i]} / \sqrt{\mathfrak{X}_1^{[i]2} + \mathfrak{X}_2^{[i]2}}.$$

Subsequently, we need to design the yaw angular control input $u_\theta^{[i]}$ such that the aircraft heading $v(\cos \theta^{[i]}, \sin \theta^{[i]})$ gradually aligns with the vector formed by the first two entries of $v\bar{\mathfrak{X}}^{[i]}$ (i.e., $v(\bar{\mathfrak{X}}^{[i]}_1, \bar{\mathfrak{X}}^{[i]}_2)$). For the last two entries of the generalized velocity $(\dot{p}_1^{[i]}, \dot{p}_2^{[i]}, \dot{p}_3^{[i]}, \dot{p}_4^{[i]})$, one can simply equate them with those of the “partially normalized” vector field $v\bar{\mathfrak{X}}^{[i]}$ respectively:

$$\begin{aligned}\dot{p}_3^{[i]} &= u_z^{[i]} = v\bar{\mathfrak{X}}_3^{[i]} / \sqrt{\bar{\mathfrak{X}}_1^{[i]2} + \bar{\mathfrak{X}}_2^{[i]2}} \\ \dot{p}_4^{[i]} &= v\bar{\mathfrak{X}}_4^{[i]} / \sqrt{\bar{\mathfrak{X}}_1^{[i]2} + \bar{\mathfrak{X}}_2^{[i]2}}.\end{aligned}\quad (10.56)$$

This control algorithm design method in Chapter 9 and [119] is extended here to handle the issue with the actuator saturation in the yaw angular control input $u_\theta^{[i]}$ as described below. First, we define the saturation function $\text{Sat}_a^b : \mathbb{R} \rightarrow \mathbb{R}$ by $\text{Sat}_a^b(x) = x$ for $x \in [a, b]$, $\text{Sat}_a^b(x) = a$ for $x \in (-\infty, a)$ and $\text{Sat}_a^b(x) = b$ for $x \in (b, \infty)$, where $a, b \in \mathbb{R}, a < b$ are some constants. Although the saturation function Sat_a^b is not differentiable, it is Lipschitz continuous. For convenience, we call the time interval when $\text{Sat}_a^b(x(t)) = b$ the *upper saturation period*, and the time interval when $\text{Sat}_a^b(x(t)) = a$ the *lower saturation period*. We use the notation \bar{v} to denote the normalization of a vector v (i.e., $\bar{v} = v / \|v\|$). We also define

$$\bar{\mathfrak{X}}_p^{[i]} = (\bar{\mathfrak{X}}_1^{[i]}, \bar{\mathfrak{X}}_2^{[i]})^\top,\quad (10.57)$$

which is the vector formed by the first two entries of the normalized vector field $\bar{\mathfrak{X}}^{[i]}$. Therefore, $\bar{\mathfrak{X}}_p^{[i]}$ represents the orientation given by the vector field $\bar{\mathfrak{X}}^{[i]}$. In addition, one can easily calculate that $\bar{\mathfrak{X}}_p^{[i]} = (\bar{\mathfrak{X}}_1^{[i]}, \bar{\mathfrak{X}}_2^{[i]})$.

Suppose we are given 3D physical desired paths ${}^{\text{phy}}\mathcal{P}^{[i]} \subseteq \mathbb{R}^3$ parameterized by (10.2), and the coordinating guiding vector field $\bar{\mathfrak{X}}^{[i]} : \mathbb{R}^{3+N} \rightarrow \mathbb{R}^{3+1}$ in (10.5). We denote the orientation of the aircraft by $\bar{h}^{[i]} = \bar{h}^{[i]} = (\cos \theta^{[i]}, \sin \theta^{[i]})^\top$, the (signed) angle difference directed from $\bar{\mathfrak{X}}_p^{[i]}$ to $\bar{h}^{[i]}$ by $\sigma^{[i]} \in (-\pi, \pi]$ and define the rotation matrix $E = \begin{bmatrix} 0 & -1 \\ 1 & 0 \end{bmatrix}$. The following theorem states that the aircraft’s orientation $\bar{h}^{[i]}$ will converge to that of the vector field $\bar{\mathfrak{X}}_p^{[i]}$ asymptotically (i.e., $\sigma^{[i]}$ converges to zero).

Theorem 10.15. *Assume that the vector field satisfies $\bar{\mathfrak{X}}_1^{[i]}(\xi^{[i]})^2 + \bar{\mathfrak{X}}_2^{[i]}(\xi^{[i]})^2 > \gamma > 0$ for $\xi^{[i]} \in \mathbb{R}^{3+1}, i \in \mathbb{Z}_1^N$, where γ is a positive constant. Let the angular velocity control input $u_\theta^{[i]}$ in model (10.55) be*

$$\dot{\theta}^{[i]} = u_\theta^{[i]} = \text{Sat}_a^b(\dot{\theta}_d^{[i]} - k_\theta \bar{h}^{[i]^\top} E \bar{\mathfrak{X}}_p^{[i]}),\quad (10.58)$$

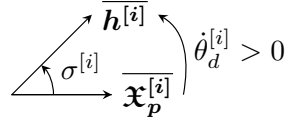


Figure 10.2: The signed angle $\sigma^{[i]}$.

where

$$\dot{\theta}_d^{[i]} = -\bar{\mathfrak{X}}_p^{[i]\top} E \dot{\mathfrak{X}}_p^{[i]} / \|\bar{\mathfrak{X}}_p^{[i]}\|, \quad (10.59)$$

$k_\theta > 0$ is a constant, and $a < 0$, $b > 0$ are constants for the saturation function Sat_a^b . If the angle difference $\sigma^{[i]}$ satisfies the following conditions:

1. The initial angle difference $\sigma^{[i]}(t=0) \neq \pi$;
2. $\sigma^{[i]}(t) \in [0, \pi]$ during the upper saturation period, and $\sigma^{[i]}(t) \in (-\pi, 0]$ during the lower saturation period,

then $\sigma^{[i]}$ will vanish asymptotically (i.e., $\sigma^{[i]}(t) \rightarrow 0$).

Proof. Since $\mathfrak{X}_1^{[i]}(\xi^{[i]})^2 + \mathfrak{X}_2^{[i]}(\xi^{[i]})^2 > \gamma > 0$ by assumption, the control inputs in (10.56) are continuously differentiable, and thus Lipschitz continuous. One can show that the yaw angular control input in (10.58) is also Lipschitz continuous. Therefore, the control inputs guarantee that the solution to the dynamical system in (10.55) exists and is unique (see Theorem 2.1). We define the orientation error by $e_o^{[i]} := \bar{h}^{[i]} - \bar{\mathfrak{X}}_p^{[i]}$ and the Lyapunov-like function $V = e_o^{[i]\top} e_o^{[i]} / 2$. The time derivative of V is

$$\dot{V} = \dot{e}_o^{[i]\top} e_o^{[i]} = (\theta^{[i]} - \dot{\theta}_d^{[i]}) \bar{h}^{[i]\top} E \bar{\mathfrak{X}}_p^{[i]} \quad (10.60)$$

$$\stackrel{(10.58)}{=} (\text{Sat}_a^b(\dot{\theta}_d^{[i]} - k_\theta \bar{h}^{[i]\top} E \bar{\mathfrak{X}}_p^{[i]}) - \dot{\theta}_d^{[i]}) \bar{h}^{[i]\top} E \bar{\mathfrak{X}}_p^{[i]}, \quad (10.61)$$

where $\dot{\theta}_d^{[i]}$ is shown right below (10.58), and (10.60) utilizes the identities $\dot{\bar{h}}^{[i]} = \dot{\theta}_d^{[i]} E \bar{h}^{[i]}$ and $\dot{\bar{\mathfrak{X}}_p^{[i]}} = \dot{\theta}_d^{[i]} E \bar{\mathfrak{X}}_p^{[i]}$ (see Chapter 9). If the angular control input is not saturated, then (10.61) is simplified to $\dot{V} = -k_\theta (\bar{h}^{[i]\top} E \bar{\mathfrak{X}}_p^{[i]})^2 \leq 0$, and $\dot{V} = 0$ if and only if the angle difference between $\bar{h}^{[i]}$ and $\bar{\mathfrak{X}}_p^{[i]}$ is $\sigma^{[i]} = 0$ or $\sigma^{[i]} = \pi$. Note that $\bar{h}^{[i]\top} E \bar{\mathfrak{X}}_p^{[i]} = \sin \sigma^{[i]}$. Therefore, during the upper saturation period when $\dot{\theta}_d^{[i]} - k_\theta \bar{h}^{[i]\top} E \bar{\mathfrak{X}}_p^{[i]} > b$, we have $\sigma^{[i]}(t) > 0 \implies \bar{h}^{[i]\top} E \bar{\mathfrak{X}}_p^{[i]} > 0 \implies \dot{V} = (b - \dot{\theta}_d^{[i]}) \bar{h}^{[i]\top} E \bar{\mathfrak{X}}_p^{[i]} < -k_\theta (\bar{h}^{[i]\top} E \bar{\mathfrak{X}}_p^{[i]})^2 \leq 0$. Similarly, during the lower saturation period, we have $\dot{V} = (a - \dot{\theta}_d^{[i]}) \bar{h}^{[i]\top} E \bar{\mathfrak{X}}_p^{[i]} < -k_\theta (\bar{h}^{[i]\top} E \bar{\mathfrak{X}}_p^{[i]})^2 \leq 0$.

(since now $\overline{\mathbf{h}^{[i]}}^\top E \overline{\mathfrak{X}_p^{[i]}} < 0$). Therefore, V is always decreasing in all three cases, and thereby the absolute value of the angle difference $|\sigma^{[i]}|$ is decreasing. Note that $V = 0$ if and only if $\overline{\mathbf{h}^{[i]}} = \overline{\mathfrak{X}_p^{[i]}}$, or equivalently $\sigma^{[i]} = 0$. In addition, $\sigma^{[i]}(t=0) \neq \pi$, hence $\dot{V}(t=0) \neq 0$. Using the Lyapunov argument [66, Theorem 4.1], it follows that $V(t)$ converges to 0 as $t \rightarrow \infty$; equivalently, $\sigma^{[i]}(t)$ converges to 0 as $t \rightarrow \infty$. \square

Remark 10.16. The quantity $\dot{\mathfrak{X}}_p^{[i]}$ in (10.59) can be calculated by

$$\dot{\mathfrak{X}}_p^{[i]} = J(\mathfrak{X}_p^{[i]})\dot{\zeta}^{[i]}, \quad (10.62)$$

where $J(\mathfrak{X}_p^{[i]}) \in \mathbb{R}^{2 \times (3+N)}$ is the Jacobian matrix of $\mathfrak{X}_p^{[i]}$ with respect to the generalized position $\zeta^{[i]} = (\xi^{[i-w]^\top}, \mathbf{w}^\top)^\top = (x_1^{[i]}, x_2^{[i]}, x_3^{[i]}, \mathbf{w}^\top)^\top \in \mathbb{R}^{3+N}$, with $\xi^{[i-w]}$ representing the vector obtained by deleting the last entry (i.e., the virtual coordinate $w^{[i]}$) of $\zeta^{[i]} \in \mathbb{R}^{n+1}$. In addition, we can simplify the computation of the Jacobian $\mathfrak{X}_p^{[i]}$ to

$$\begin{aligned} J(\mathfrak{X}_p^{[i]}) &= FJ(\overline{\mathfrak{X}^{[i]}}) = F(I - \overline{\mathfrak{X}^{[i]}} \overline{\mathfrak{X}^{[i]}}^\top)J(\mathfrak{X}^{[i]})/\|\mathfrak{X}^{[i]}\| \\ &= F(I - \overline{\mathfrak{X}^{[i]}} \overline{\mathfrak{X}^{[i]}}^\top)J(\mathbf{p}^f \chi^{[i]} + k_c \mathbf{c}^r \chi^{[i]})/\|\mathfrak{X}^{[i]}\| \\ &= F(I - \overline{\mathfrak{X}^{[i]}} \overline{\mathfrak{X}^{[i]}}^\top)(J(\mathbf{p}^f \chi^{[i]}) + k_c J(\mathbf{c}^r \chi^{[i]}))/\|\mathfrak{X}^{[i]}\|, \end{aligned}$$

where $F = \begin{bmatrix} 1 & 0 & 0 & 0 \\ 0 & 1 & 0 & 0 \end{bmatrix}$ and the Jacobians $J(\mathbf{p}^f \chi^{[i]})$ and $J(\mathbf{c}^r \chi^{[i]})$ are shown in (10.63) and (10.64), respectively (\mathbf{b}_i is the basis vector with the i -th entry being 1).

$$J(\mathbf{p}^f \chi^{[i]}) = \left[\begin{array}{cccc|c} -k_1^{[i]} & 0 & 0 & \cdots & \mathbf{0}_{4 \times (i-1)} \\ 0 & -k_2^{[i]} & 0 & \cdots & \\ 0 & 0 & -k_3^{[i]} & \cdots & \\ k_1^{[i]} f_1^{[i]}'(w^{[i]}) & k_2^{[i]} f_2^{[i]}'(w^{[i]}) & k_3^{[i]} f_3^{[i]}'(w^{[i]}) & \cdots & \\ \vdash & -f_1^{[i]''}(w^{[i]}) + k_1^{[i]} f_1^{[i]}'(w^{[i]}) & \vdash & \vdash & \mathbf{0}_{4 \times (N-i)} \\ \vdash & -f_2^{[i]''}(w^{[i]}) + k_2^{[i]} f_2^{[i]}'(w^{[i]}) & \vdash & \vdash & \\ \vdash & -f_3^{[i]''}(w^{[i]}) + k_3^{[i]} f_3^{[i]}'(w^{[i]}) & \vdash & \vdash & \\ \vdash & \sum_{j=1}^3 [k_j^{[i]} \phi_j^{[i]} f_j^{[i]''}(w^{[i]}) - k_j^{[i]} f_j^{[i]'}(w^{[i]})]^2 & \vdash & \vdash & \end{array} \right]. \quad (10.63)$$

$$\begin{aligned}
J(\text{cr}\chi^{[i]}) &= \begin{bmatrix} \mathbf{0}_{3 \times 3} & \mathbf{0}_{3 \times N} \\ \frac{\partial c^{[i]}(\mathbf{w})}{\partial \xi^{[i-w]}} & \frac{\partial c^{[i]}(\mathbf{w})}{\partial \mathbf{w}} \end{bmatrix} \\
&= \begin{bmatrix} \mathbf{0}_{4 \times 3} & \mathbf{0}_{3 \times N} \\ a_{i1} \cdots a_{i(i-1)} & -\sum_{j=1}^N a_{ij} \quad a_{i(i+1)} \cdots a_{iN} \end{bmatrix} = \begin{bmatrix} \mathbf{0}_{4 \times 3} & \mathbf{0}_{3 \times N} \\ -\mathbf{b}_i^\top L & \end{bmatrix}. \tag{10.64}
\end{aligned}$$

Although (10.62) contains states $\dot{w}^{[j]}$ from all robots, we emphasize that *each robot only needs the information $w^{[j]}$ and $\dot{w}^{[j]}$ from its neighbors (i.e., $j \in \mathcal{N}_i$), and thus the control algorithm is distributed*. This is because in (10.64), those terms a_{ij} become zero if j is not a neighbor of the i -th robot, and thereby the corresponding information $w^{[j]}$ and $\dot{w}^{[j]}$ is *not* required by the i -th robot. In the case of a cycle communication graph, each robot only needs the information of $w^{[j]}$ and $\dot{w}^{[j]}$ from its *two* neighbors, regardless of the size of the multi-robot system. \triangleleft

Remark 10.17 (Interpretation of Condition 2). In the proof of the theorem, it has been shown that

$$\dot{\overline{\mathfrak{X}}_p^{[i]}} = \dot{\theta}_d^{[i]} E \overline{\mathfrak{X}}_p^{[i]}.$$

Since $E \overline{\mathfrak{X}}_p^{[i]}$ is orthogonal to $\overline{\mathfrak{X}}_p^{[i]}$, the quantity $\dot{\theta}_d^{[i]}$ in (10.58) encodes how fast the vector field changes its orientation along the trajectory of the aircraft (i.e., $\dot{\theta}_d^{[i]}$ is the *change rate of the vector field orientation*). Since $\overline{\mathbf{h}^{[i]}}^\top E \overline{\mathfrak{X}}_p^{[i]} \leq 1$ in (10.58), saturation may happen due to the possibly large magnitude of the term $\dot{\theta}_d^{[i]}$. If upper saturation happens at $t = t_0$, the change rate of the vector field orientation $\dot{\theta}_d^{[i]}$ demands a faster change than the aircraft can achieve; therefore, if $\sigma^{[i]}(t_0) > 0$, then the vector field orientation encoded by $\overline{\mathfrak{X}}_p^{[i]}$ will “chase” the aircraft orientation vector $\overline{\mathbf{h}^{[i]}}$ such that the angle difference $\sigma^{[i]}(t)$ is decreasing (see Fig. 10.2). Thus as long as $\sigma^{[i]}(t_0) > 0$, the Lyapunov function V is still decreasing. However, if the saturation lasts for a long time such that $\overline{\mathfrak{X}}_p^{[i]}$ overtakes the aircraft orientation vector $\overline{\mathbf{h}^{[i]}}$, the angle $\sigma^{[i]}(t)$ will become negative and violate Condition 2 in Theorem 10.15, thus the decreasing property of the Lyapunov function V is not necessarily guaranteed; in this case, $\dot{V} > -k_\theta \left(\overline{\mathbf{h}^{[i]}}^\top E \overline{\mathfrak{X}}_p^{[i]} \right)^2$,

so \dot{V} may be negative or positive. Therefore, although Condition 2 in Theorem 10.15 might be difficult to check in practice, it conveys the core message that the saturation, albeit allowed, should not last for a long time. However, this condition is only sufficient (not necessary), while in practice, violating this condition does not immediately entail instability of the algorithm. As the aircraft is guided by the vector field, the

aircraft can re-orient its heading towards the desired path even if it temporarily deviates from the desired path due to saturation or other constraints (such as path curvature), as long as the change rate of the vector field orientation $\dot{\theta}_d^{[i]}$ does not saturate the control input persistently. The subsequent fixed-wing aircraft experiment verifies the effectiveness of the control law. \triangleleft

Nevertheless, we can remove Condition 2 in Theorem 10.15 by imposing an upper bound on the magnitude of $\dot{\theta}_d^{[i]}$, as shown in Corollary 10.18.

Corollary 10.18. *Suppose there exists a positive constant d satisfying $d < \min\{-a, b\}$, where a, b are the threshold values of the saturation function $\text{Sat}_a^b(\cdot)$ in Theorem 10.15 (note that $a < 0$), such that the change rate of the vector field orientation $|\dot{\theta}_d^{[i]}| \leq d$. Let $\bar{k}_\theta := \min\{-a - d, b - d\}$, which is positive. If the positive gain k_θ in (10.58) is chosen within the range $(0, \bar{k}_\theta)$, then the angle difference $\sigma^{[i]}$ converges to 0 without requiring Condition 2 in Theorem 10.15.*

Proof. Given that $k_\theta \in (0, \bar{k}_\theta)$, one can calculate that $\max\{\dot{\theta}_d^{[i]} - k_\theta \overline{\mathbf{h}^{[i]}}^\top E \overline{\mathfrak{X}_p^{[i]}}\} = d + k_\theta < b$ and $\min\{\dot{\theta}_d^{[i]} - k_\theta \overline{\mathbf{h}^{[i]}}^\top E \overline{\mathfrak{X}_p^{[i]}}\} = -d - k_\theta > a$. Therefore, saturation never happens and thus Condition 2 in Theorem 10.15 can be neglected. \square

To reduce the magnitude of $\dot{\theta}_d^{[i]}$ and avoid possible saturation, one can scale down the path parameter in the parametric functions in (10.2) (e.g. by changing $f_j^{[i]}(w^{[i]})$ to $f_j^{[i]}(\beta w^{[i]})$, where $0 < \beta < 1$), or choose another desired path with a smaller curvature. Another approach to avoid input saturation is to add an additional constraint $|u_\theta^{[i]}| \leq \min\{|a|, |b|\}$ in the quadratic program in Section 10.5.

10.7 SIMULATIONS AND EXPERIMENTS

10.7.1 Simulations

In all simulations, the communication topology is a *cycle graph*, and thus each robot is only allowed to communicate with its two adjacent neighbors. For example, Robot 2 can only transmit its virtual coordinate $w^{[2]}$ to and receive the virtual coordinates $w^{[1]}$ and $w^{[3]}$ from Robot 1 and Robot 3. Note that due to this simple communication graph, both the communication load and the computation load for each robot is much lower than that in the centralized scenario.

In the first simulation, we let $N = 50$ robots follow a 3D (i.e., $n = 3$) *self-intersected bent “∞”-shaped curve* parameterized by $x_1^{[i]} = 15 \sin(2w^{[i]})$, $x_2^{[i]} = 30 \sin(w^{[i]}) \sqrt{0.5(1 - 0.5 \sin^2(w^{[i]}))}$ and $x_3^{[i]} = 5 + 5 \cos(2w^{[i]}) - 2$ for $i \in \mathbb{Z}_1^N$. The period of this closed curve is $T = 2\pi$ and the desired differences between

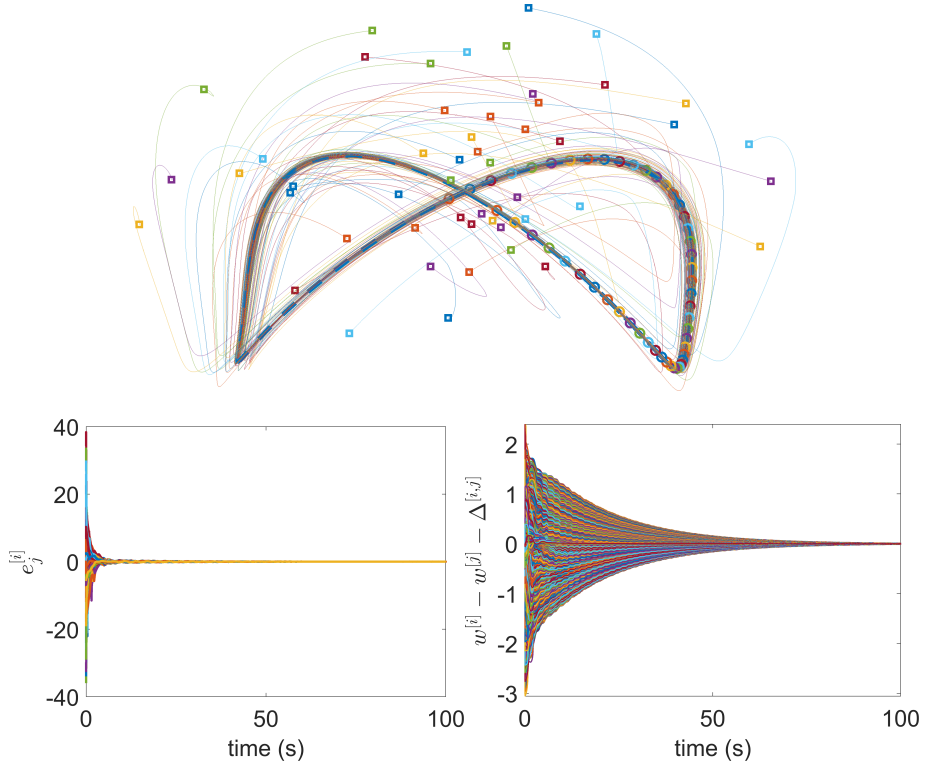


Figure 10.3: The first simulation results. On top, the trajectories of robots, where squares and circles symbolize the trajectories' initial and final positions respectively. On the bottom left, the path-following errors $e_j^{[i]}$ for $i \in \mathbb{Z}_1^N$ and $j \in \mathbb{Z}_1^n$. On the bottom right, the coordination error $w^{[i]} - w^{[j]} - \Delta^{[i,j]}$ for $i, j \in \mathbb{Z}_1^N, i < j$.

two adjacent robots' virtual coordinates are $T/(2N)$. We construct the desired parametric differences $\Delta^{[i,j]}$ from the reference $w^{[i]*} = (i-1)T/(2N)$ for $i \in \mathbb{Z}_1^N$. The control gains for the coordinating vector field are: $k_1^{[i]} = k_2^{[i]} = k_3^{[i]} = 1, k_c = 300$ for $i \in \mathbb{Z}_1^N$, where k_c is large to accelerate the motion coordination. As shown in Fig. 10.3, all robots follow the “∞”-shaped path successfully and keep desired positions (in terms of $w^{[i]}$) between each other. The path-following errors and the coordination errors converge to zero eventually.

In the second simulation, we aim to show that our algorithm is also applicable to path-following control of complicated and *open* curves (i.e., aperiodic curve), and demonstrate its potential application to volume coverage in 3D [16]. To this end, we choose a 3D Lissajous curve (i.e., $n = 3$) with *irrational* coefficients, of which the parametric equations are $x_1^{[i]} = \cos(n_x w^{[i]}) + m_x$, $x_2^{[i]} = \cos(n_y w^{[i]}) + m_y$ and $x_3^{[i]} = \cos(n_z w^{[i]}) + m_z$ for $i \in \mathbb{Z}_1^N$, and the coefficients are chosen as

$n_x = \sqrt{2}, n_y = 4.1, n_z = 7.1, m_x = 0.1, m_y = 0.7, m_z = 0$. This is an open curve bounded in a cube (as n_x is irrational). Therefore, it is ideal for a volume coverage task. To clearly illustrate this idea, we choose $N = 3$ robots and simulate for 100 seconds. The control gains for the coordinating guiding vector field are: $k_1^{[i]} = k_2^{[i]} = k_3^{[i]} = k_c = 1$ for $i \in \mathbb{Z}_1^N$. We construct the desired parametric differences $\Delta^{[i,j]}$ from the references $w^{[i]*}(t) = (i-1)2\pi/N$, for $i \in \mathbb{Z}_1^N$. Since the Lissajous curve will fill the whole cube as the path parameter $w^{[i]}$ varies from 0 to infinity, for illustration purpose, we only plot part of the desired path where $w^{[i]} \in [0, 30\pi]$ (see the magenta curve in Fig. 10.4). As seen in Fig. 10.4, the three robots tend to cover the whole volume of the unit cube, and the path-following errors and coordination errors are almost zero after 20 seconds.

In the third simulation, we show how different robots can follow different desired paths while they still coordinate their motions to form some formation shapes. We let $N = 21$ robots follow three different paths, where the first seven robots follow a large circle of radius $a > 0$ parameterized by $x_1^{[i]} = a \cos w^{[i]}, x_2^{[i]} = a \sin w^{[i]}$ for $i = 1, \dots, 7$, the last seven robots follow a small circle of radius $0 < b < a$ parameterized by $x_1^{[i]} = b \cos w^{[i]}, x_2^{[i]} = b \sin w^{[i]}$ for $i = 15, \dots, 21$, and the remaining seven robots follow an ellipse with a semimajor axis a and a semiminor axis b , parameterized by $x_1^{[i]} = a \cos w^{[i]}, x_2^{[i]} = b \sin w^{[i]}$ for $i = 8, \dots, 14$. These three paths are concentric (see Fig. 10.5). The robots are coordinated in a distributed way such that they are equally separated in the path parameter $w^{[i]}$; in other words, we construct the desired parametric differences $\Delta^{[i,j]}$ from the references $w^{[i]*}(t) = (i-1)2\pi/N$, for $i \in \mathbb{Z}_1^N$. Other parameters are chosen as $a = 10, b = 5, k_1^{[i]} = k_2^{[i]} = 1, k_c = 100$ for $i \in \mathbb{Z}_1^N$. An interesting feature is that during the steady-state, these robots will not overlap with each other, since overlapping happens if any two of the robots' virtual coordinates are equal, while the distributed coordination guarantees that the adjacent neighbors satisfy $|w^{[i]} - w^{[j]}| = 2\pi/N$, where i and j are any neighboring indices. These robots successfully generate varying formation shapes: they cluster in different parts of the three desired paths. After 40 seconds, the path-following errors and the coordination errors are almost 0.

In the fourth simulation, we show how multiple robots converge to a torus and form a desired pattern while they maneuver on the torus. Specifically, we manually select $N = 67$ reference points $(w_1^{[i]*}, w_2^{[i]*}), i \in \mathbb{Z}_1^N$ such that they form a pattern resembling the four letters "ICRA". Then based on these reference points, one can calculate the desired parametric differences $\Delta_1^*, \Delta_2^* \in \mathbb{R}^{67}$. Note that Robot i only needs to know the desired parametric differences with respect to its neighbors; i.e., $\Delta_1^{[i,j]}, \Delta_2^{[i,j]}$ for $j \in \mathcal{N}_i$. These 67 robots are required to converge to a torus of which the parametric equations are $x_1^{[i]} = (2 + \cos w_1^{[i]}) \cos w_2^{[i]}, x_2^{[i]} = (2 + \cos w_1^{[i]}) \sin w_2^{[i]}, x_3^{[i]} = \sin w_1^{[i]}$ for $i \in \mathbb{Z}_1^N$ (hence $n = 3$ in Theorem 10.13).

They are also required to maneuver on the torus in the sense that $\dot{w}_1^* = \dot{w}_2^* = -1$. By Theorem 10.13, the extra vector v is thus chosen as $v = (0, 0, 0, -1, 1)$. Other parameters are chosen as $k_1^{[i]} = k_2^{[i]} = 1, k_c = 10$ for $i \in \mathbb{Z}_1^N$. The simulation results are shown in Fig. 10.6.

10.7.2 Experiments with multiple fixed-wing aircraft

In this experiment, two autonomous fixed-wing aircraft (i.e., Autonomous Opterra 1.2m) are employed to validate Theorem 10.15. The aircraft are equipped with open-source software/hardware components developed from *Paparazzi* [47]. The codes related to the proposed algorithm are in [26]. We choose the following 3D Lissajous curve $f_1^{[i]}(w) = 225 \cos(w^{[i]}), f_2^{[i]}(w^{[i]}) = 225 \cos(2w^{[i]} + \pi/2), f_3^{[i]}(w^{[i]}) = -20 \cos(2w^{[i]})$, for $i = 1, 2$, which is a bent “∞”-shaped path. The mission requires both aircraft to have $\Delta^{[1,2]} = \Delta^{[2,1]} = 0$; i.e., to fly in a tight formation. The overlapping at steady state is avoided by biasing the GPS measurement of one aircraft by a constant distance of one meter in the horizontal plane; i.e., when the aircraft achieve $\Delta^{[1,2]} = \Delta^{[2,1]} = 0$, they are displaced physically. We choose $k_1^{[i]} = k_2^{[i]} = 0.002, k_3^{[i]} = 0.0025, k_c = 0.01, k_\theta = 1$, for $i = 1, 2$, and the communication frequency is 10 Hz. In the experiment, the weather forecast reported 14 degrees Celsius and a South wind of 10 km/h. In Figure 10.7, the telemetry shows that both aircraft converge to fly together and follow the path. The experiment shows that once an aircraft flies far ahead of its partner, the algorithm guides the airplane to deviate from the curve to travel more distances to “wait” for its partner. Nevertheless, these deviations from the desired path are within the order of one or two meters (see Figure 10.8).

Note that the employed aircraft do *not* control their ground speeds. In fact, they have a reference signal in their throttle to keep a safe airspeed, and the aircraft increase/decrease such a reference to ascend/descend. A traditional trajectory tracking algorithm would *force* the aircraft to track an *open-loop* point $(f_1^{[i]}(t), f_2^{[i]}(t), f_3^{[i]}(t))$; i.e., it requires controlling the airspeed/ground speed of the aircraft. Such a requirement is demanding if the aircraft are not equipped with the required sensors or actuators (e.g., spoilers/flaps), and the wind always affects the speed of the airplane. By contrast, our guidance algorithm is free from such a requirement since the parameter w is in *closed-loop* with the aircraft state, and thereby adapting automatically to the position and velocity of the aircraft.

10.8 CONCLUSIONS

In this chapter, we address the problem of multi-robot coordinated navigation using a new guiding vector field. The proposed approach enables an arbitrary

number of robots to follow or navigate possibly different desired paths or surfaces and achieve motion coordination in a distributed way. Specifically, we derive time-invariant and time-varying coordinating guiding vector fields to rigorously guarantee the convergence and motion coordination on desired paths or surfaces from all initial positions (i.e., global convergence). This is achieved by exploiting the higher-dimensional guiding vector field with path or surface parameters as virtual coordinates, and employing distributed consensus algorithms to render the virtual coordinate differences (i.e., parametric differences) converging to the pre-specified desired ones in a multi-robot system. Based on the coordinating guiding vector field, a control law is designed for a nonholonomic Dubins-car-like robot model, which takes into account the actuation saturation. Moreover, we also elaborate on how to effectively integrate the coordinating guiding vector field with a safety barrier certificate to realize collision avoidance among robots. Extensive simulation examples verify the effectiveness of our approach and showcase possible practical applications. Furthermore, we conduct outdoor experiments with multiple fixed-wing aircraft to demonstrate our algorithm's practical value including its robustness against wind perturbation, actuation saturation, etc. There are many fascinating features of our approach as outlined in Section 10.1.2.

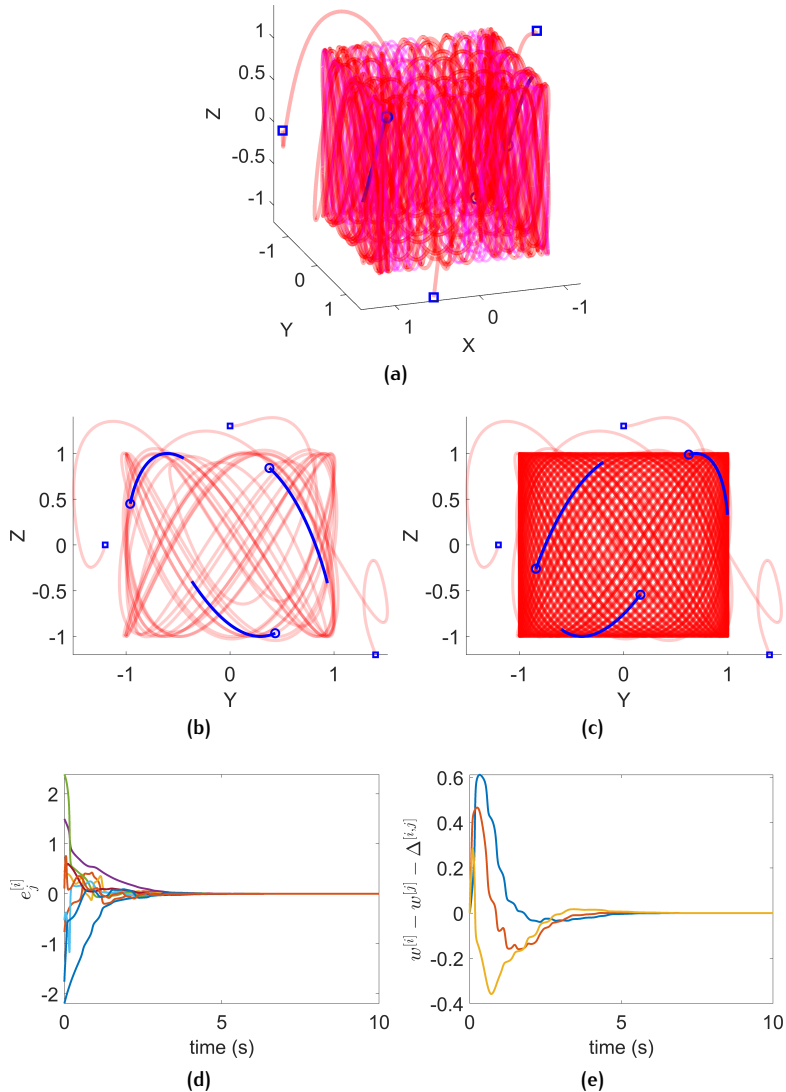


Figure 10.4: The second simulation results. Squares and circles symbolize trajectories' initial and final positions, and the solid blue lines are the trajectories during the last 30 time steps. (a) The trajectories of three robots follow an open Lissajous curve with irrational coefficients. The magenta curve represents part of the Lissajous curve. (b) and (c) correspond to the Y-Z side views of the trajectories at time 9.4 and 76.8 seconds, respectively. (d) The path-following errors $e_j^{[i]}$ for $i \in \mathbb{Z}_1^N$ and $j \in \mathbb{Z}_1^n$. (e) The coordination error $w^{[i]} - w^{[j]} - \Delta^{[i,j]}$ for $i, j \in \mathbb{Z}_1^N, i < j$. Only 10 seconds of data are shown for clarity in (d) and (e).

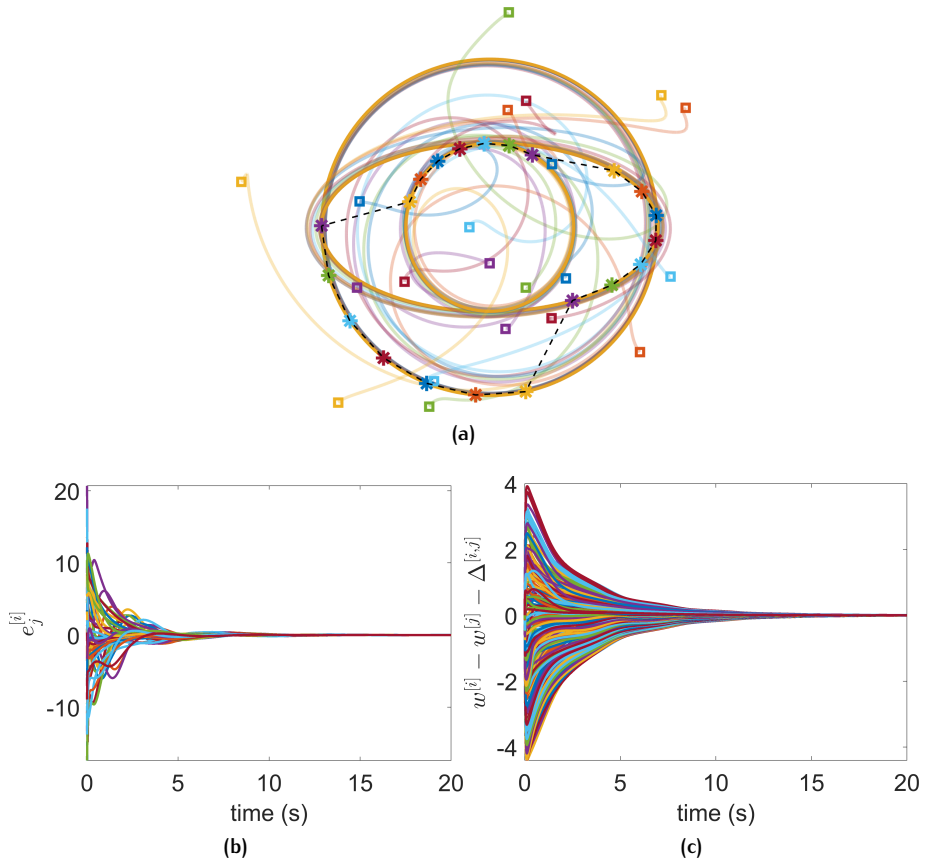


Figure 10.5: The third simulation results. (a) The trajectories of robots, where squares and * symbolize the trajectories' initial and final positions respectively. The dashed black line shows the communication links between robots (i.e., a cycle graph). (b) The path-following errors $e_j^{[i]}$ for $i \in \mathbb{Z}_1^N$ and $j \in \mathbb{Z}_1^n$. (c) The coordination error $w^{[i]} - w^{[j]} - \Delta^{[i,j]}$ for $i, j \in \mathbb{Z}_1^N, i < j$. Only 20 seconds of data are shown for clarity in (b) and (c).

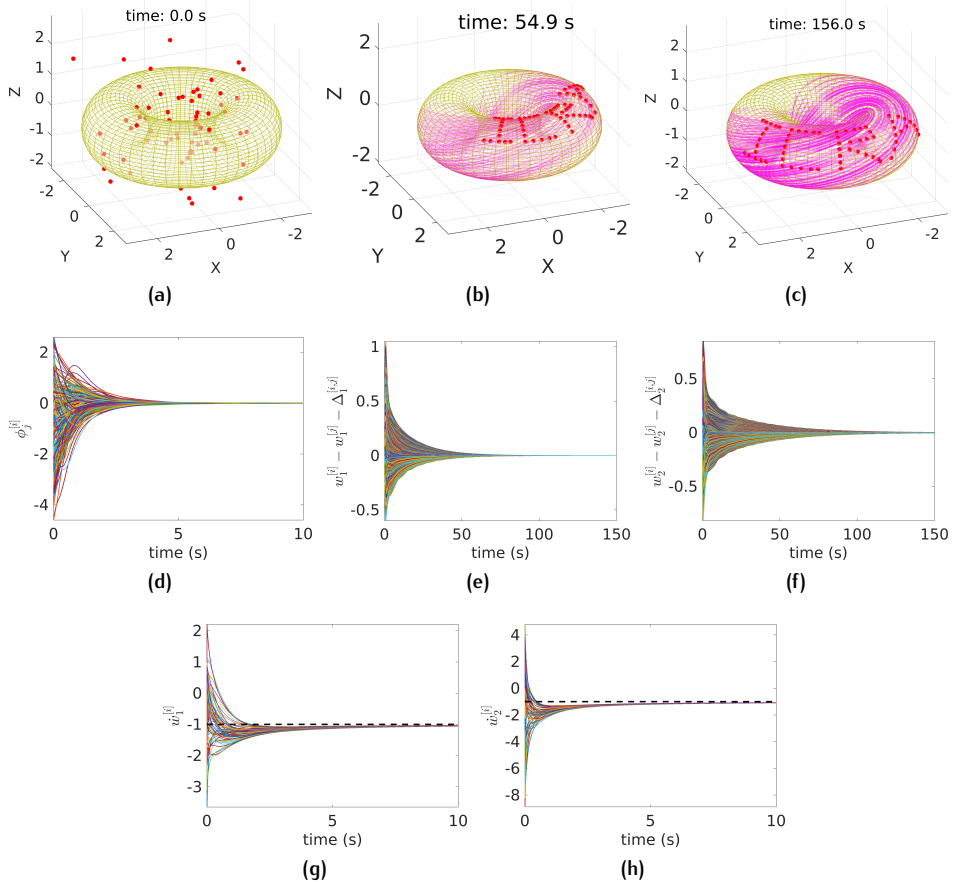


Figure 10.6: The fourth simulation results. (a)-(c) Sixty-seven robots, represented by red dots, converge to and maneuver on a torus while they form the pattern “ICRA” at different time instants. The magenta curves are the trajectories of different robots. (d) The surface-convergence errors $\phi_j^{[i]}$ for $i \in \mathbb{Z}_1^N$ and $j \in \mathbb{Z}_1^n$ converge to zero eventually. Only 10 seconds of data are shown for clarity. (e)-(f) The coordination errors $w_1^{[i]} - w_1^{[j]} - \Delta_1^{[i,j]}$ and $w_2^{[i]} - w_2^{[j]} - \Delta_2^{[i,j]}$ for the two parameters for $i, j \in \mathbb{Z}_1^N, i < j$ converge to zero eventually. (g)-(h) The parametric velocities $\dot{w}_1^{[i]}$ and $\dot{w}_2^{[i]}$ converge to the desired values $\dot{w}_1^* = \dot{w}_2^* = -1$ denoted by black dashed lines. Only 10 seconds of data are shown for clarity.

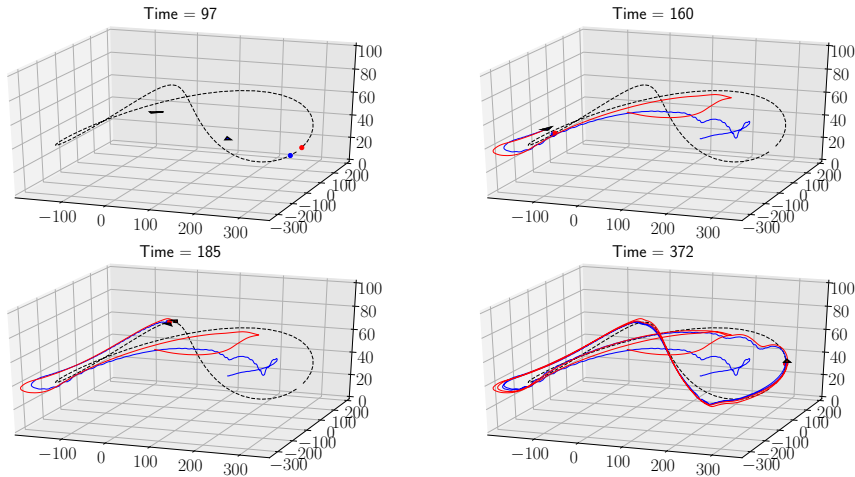


Figure 10.7: Two aircraft (blue and red trajectories) fly together and follow a 3D bent “∞”-shaped path. Although the subfigures show that the aircraft’s positions are overlapped, in reality, the same position corresponds to two different ones since the aircraft’s GPS receptors are biased with respect to each other by one meter in the XY plane.

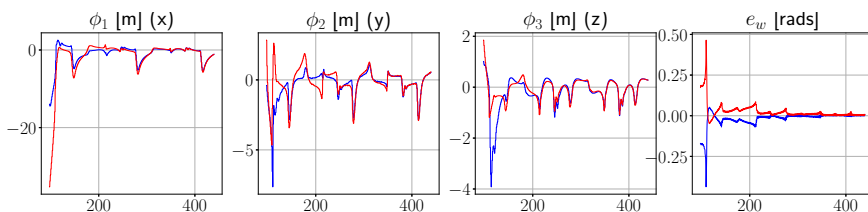


Figure 10.8: Path-following errors (in XYZ) of the two aircraft (blue and red) to the desired 3D path, and errors with respect to the desired $\Delta w = 0$. The horizontal axes denote time in seconds.

11

CONCLUSIONS AND FUTURE RESEARCH

This thesis presents extensive theoretical results and applications of guiding vector fields for robot motion control.

From the theoretical perspective, we study a sequence of interrelated topics, which include the relationship between the vanishing of the level value and the convergence of trajectories to the zero-level set, the attractiveness and stability properties of the desired path and singular sets, the robustness of the guiding vector field, the domain of attraction of the desired path, the existence of singular points of the guiding vector field and the existence of trajectories not converging to the desired path.

From the application perspective, we show several results including how to integrate path following and collision avoidance using smooth bump functions, how to create a singularity-free guiding vector field for robot navigation, and how to coordinate an arbitrary number of robots in a distributed way such that they maneuver and maintain predefined parametric distances. All these applications are supported by rigorous mathematical guarantees and verified in various simulation settings and real-robot experiments.

In what follows we summarize the main contributions of each chapter of this thesis and provide some recommendations for future research.

11.1 CONCLUSIONS

Part I of the thesis includes Chapter 3 to Chapter 7, and this part introduces the theoretical foundation of vector-field guided path-following algorithms.

In Chapter 3, motivated by the fact that the desired path is described by the zero-level set of a sufficiently smooth function, we study the problem regarding whether the vanishing of the level value implies the convergence of trajectories of an autonomous system to the zero-level set. We show that in general, this implication does not hold unless some additional conditions identified in this thesis were imposed. These conditions serve as the standing assumptions for the subsequent theoretical development. Note that this result is independent of the vector-field guided path-following problem, since in many control problems, the target set of interest is the zero-level set of a Lyapunov function.

In Chapter 4, we specifically focus on the 3D guiding vector field, and show the asymptotic and exponential convergence of the path-following error for both bounded and unbounded desired paths. We also prove the local input-to-state (ISS) stability of the error dynamics, which is then utilized for the control algorithm design for a fixed-wing aircraft model. Note that the analysis techniques for the 3D guiding vector field can be straightforwardly extended for higher-dimensional guiding vector fields.

Chapter 5 and Chapter 6 focus on some topological aspects of the vector-field guided path-following algorithms. Specifically, we generalize the guiding vector fields on Euclidean spaces to those defined on a general smooth Riemannian manifold \mathcal{M} . These guiding vector fields are imperative in control on manifolds, such as robot arm control in joint spaces. We study the autonomous system $\dot{\xi}(t) = \chi(\xi(t))$, where χ is the guiding vector field defined on \mathcal{M} . In particular, under the assumption that the desired path is compact (i.e., homeomorphic to the unit circle S^1), we analyze the stability and attractiveness of the desired path and the singular set. It turns out that in this general case, the desired path is still asymptotically stable and the singular set is non-attractive under some conditions. In addition, we show that global convergence of trajectories to the desired path in the Euclidean space \mathbb{R}^n is *not* possible, and singular points always exist. This is a consequence of the more general result: the domain of attraction of the compact desired path is homotopy equivalent to the unit circle S^1 . Chapter 6 then strengthens this result and shows that the domain of attraction is homeomorphic to $\mathbb{R}^{n-1} \times S^1$, where n is the dimension of the ambient manifold \mathcal{M} . We also show in Chapter 5 the existence of trajectories diverging away from the desired path. Specifically, we consider the Euclidean space \mathbb{R}^n , where $n \geq 3$, and prove that for any ball containing the desired path, there always exists at least one trajectory starting from the boundary of the ball that does not converge to the desired path.

In Chapter 7, we refine the dichotomy convergence property of trajectories in the vector-field guided path-following problem. It has been shown in previous chapters that trajectories either converge to the desired path or the singular set, but it is of interest to ask the question whether trajectories converging to the singular set actually converge to a single point of the set. We show that if the level functions are real analytic, then the answer to the previous question is affirmative.

Part II of the thesis includes Chapters 8, 9 and 10, and this part focuses on various applications of the vector-field guided path-following algorithms.

In Chapter 8, we consider the practical scenario where the desired path is occluded by a finite number of static or moving obstacles of arbitrary shapes. We design a new guiding vector field by combining two guiding vector fields via smooth bump functions to achieve both the tasks of path following and collision avoidance. A switching vector field is also proposed to deal with the issue of undesirable singular points where a trajectory is trapped. The path-following and obstacle-avoidance capabilities are provably guaranteed to be effective.

Chapter 9 is motivated by the impossibility result of global convergence of trajectories to a self-intersecting or compact desired path (precisely, homeomorphic to the unit circle S^1), as elaborated in Chapter 5 and Chapter 6. Since this impossibility result is inherent in the topology of the desired path, we then propose an approach to change the topology of the desired path by “cutting” and “stretching” it to become homeomorphic to the real line \mathbb{R} . We further prove that this transformation gives rise to a higher-dimensional guiding vector field that has no singular points in the whole Euclidean space, and we prove that trajectories from all initial conditions will converge to the desired path, even if it is self-intersecting. This approach requires a parametric equation of the desired path, and the global convergence is rigorously guaranteed by the introduction of a transformation operator and the extended dynamics. Five features of our approach are highlighted in Chapter 9 and we demonstrate that our approach is a combined extension of both conventional vector-field guided path-following algorithms and trajectory tracking algorithms. Experiments with fixed-wing aircraft under wind perturbation validate the theoretical results and showcase its practical effectiveness.

Chapter 10 shifts the focus from a single-robot in previous chapters to a multi-robot system. In this chapter, we extend the higher-dimensional singularity-free guiding vector field proposed in Chapter 9 to address the problem of multi-robot coordinated navigation on different desired paths or surfaces. We utilize the additional virtual dimension of the singularity-free guiding vector field, and apply a consensus algorithm to this additional dimension. Since the additional dimension is closely related to the parameters of the desired paths or surfaces, by controlling this dimension via local interactions of neighboring robots, the robots’ motions are coordinated implicitly such that they can follow the desired paths or surfaces and maintain predefined parametric distances between each other. As a result, time-invariant and time-varying coordinating guiding vector fields are derived and motion coordination from all initial positions is guaranteed. Based on the coordinating guiding vector field, a control algorithm for a nonholonomic Dubins-car-like model, taking into account input saturation, is designed. Extensive simulation examples and experiments verify the theoretical results.

11.2 FUTURE RESEARCH

In this section, we elaborate on the limitations of our work in this thesis, and recommend some possible future research problems.

In Chapters 4, 8, 9 and 10, a control algorithm is designed for a unicycle robot model or a Dubins car model based on guiding vector fields. The design principles are the same: steer the heading of the robot such that it eventually

aligns with the heading given by the guiding vector field. This control algorithm design principle is simple and effective for kinematics models of which the motion is essentially characterized by the heading. However, it is our future work to design effective control algorithms for more complicated robot kinematics or even dynamics models, such as those corresponding to underactuated marine vessels in [9]. As preliminary results, two more control design examples are shown in Appendix A.

In Chapters 5 and 6, the topological analysis is conducted only for *compact* asymptotically stable desired paths. Although we have shown that the two results, Lemma 5.23 and Theorem 6.15, related to the domain of attraction of the desired paths, do not hold for non-compact desired paths, it is interesting but probably challenging to characterize the domain of attraction for non-compact desired paths.

In Chapter 7, it is shown that if the level function is real analytic, then convergence of trajectories to the singular set is equivalent to convergence to a single point in the set (i.e., Theorems 7.5 and 7.7). However, this result is proved for guiding vector fields on the Euclidean space \mathbb{R}^n , while it is unclear if this conclusion still holds for guiding vector fields defined on a general Riemannian manifold \mathcal{M} in Chapters 5 and 6, and it is of theoretical interest to find out the answer. We anticipate that a major theoretical difficulty is probably due to the use of a partition of unity [77, Chapter 2] for the manifold. A partition of unity involves non-real analytic functions, which can violate the real analyticity condition.

In Chapter 8, the problem of path-following with collision-avoidance is considered in a 2D space. Although a practical approach is indicated for the higher-dimensional spaces, the rigorous mathematical guarantees are not provided. To provide the guarantees would probably be challenging due to the fact that the behavior of nonlinear systems in higher-dimensional spaces can be very complicated (e.g., even leading to chaos).

It has been shown that the additional virtual coordinates in Chapters 9 and 10 lead to many advantages of the path-following algorithms, such as guarantees of global convergence to the desired path. However, in practice, if the parameters of the path-following algorithms are not properly chosen, the virtual coordinates can change very fast. This would result in demanding control commands for a real aircraft, and may lead to control saturation. It would be of practical interest to improve the algorithm by limiting the change rate of the virtual coordinate, or to introduce an automatic-tuning method for the parameters.

In Chapter 10, we only consider undirected and fixed communication graphs among robots, but it is of practical and theoretical interest to take into account directed and changing communication graphs. Additionally, communication of the virtual coordinates among agents is necessary, while it is unclear how the coordination can be achieved by using only relative measurements of some physical quantities without explicit communication. For some simple desired paths, such

as a circle, it is possible to estimate the virtual coordinates of neighboring robots by measuring the relative positions without explicit communication, but for more complicated paths, such as a Lissajous path, the estimation might be challenging.

In this thesis, we only focus on those guiding vector fields consisting of propagation terms and convergence terms with specific forms shown in (1.2), (4.2), (9.2) and (5.6). It would be of interest to study guiding vector fields of other forms, such as those reviewed in Sections 1.1.4 and 1.1.5. In particular, it would be of theoretical interest to study the topological properties of guiding vector fields with time-varying terms when the desired path depends on time (e.g., [50], [74]). In addition, in Chapter 5, when we define a desired path on an n -dimensional smooth Riemannian manifold, we still use the functions $(\phi_1, \dots, \phi_{n-1})^\top : \mathcal{M} \rightarrow \mathbb{R}^{n-1}$. This could be a restriction. A more general form is to change the codomain of $(\phi_1, \dots, \phi_{n-1})^\top$ to an $(n-1)$ -dimensional smooth manifolds \mathcal{N} . Consequently, the design of the guiding vector field becomes more flexible. We are currently conducting further investigation regarding this aspect.

Note that the VF-PF algorithms studied in this thesis are designed for the problem formulation in Problem 1.1. If the desired path is changed from a one-dimensional manifold to a trajectory (i.e., a function of time), then one can use many existing trajectory tracking algorithms [46], [75], [103] to address the path-following problem if the image of the trajectory is the same as the desired path. Similarly, if one can find an exo-system such that the reference output corresponds to the desired path, then one can also utilize many existing output regulation algorithms [57], [58], [61]. Therefore, it would be of interest to study how to design a trajectory or an exo-system corresponding to a given (geometric) desired path.

Part III
APPENDIX

A

CONTROL ALGORITHMS FOR A 3D UAV MODEL AND A DYNAMICS MODEL

Our proposed guiding vector field method can still be applied to more complex models, such as a 3D UAV model (Section A.1) and a dynamic aircraft model (Section A.2).

A.1 3D UAV MODEL

Consider a nonholonomic 3D UAV model [81], [8, Eq. (9.7)] as follows:

$$\dot{x}(t) = v_a(t) \cos \psi(t) \cos \gamma(t) \quad (\text{A.1a})$$

$$\dot{y}(t) = v_a(t) \sin \psi(t) \cos \gamma(t) \quad (\text{A.1b})$$

$$\dot{z}(t) = v_a(t) \sin \gamma(t) \quad (\text{A.1c})$$

$$\dot{\gamma}(t) = w_\gamma(t) \quad (\text{A.1d})$$

$$\dot{\psi}(t) = w_\psi(t), \quad (\text{A.1e})$$

where (x, y, z) is the UAV's position, and γ and ψ are the pitch angle and the yaw angle, respectively. The components of the control input $u(t) = (v_a(t), w_\gamma(t), w_\psi(t))^\top$ correspond to the airspeed, the pitch angular speed and the yaw angular speed, respectively. The model (A.1) can be written in an input-affine form as follows:

$$\begin{bmatrix} \dot{x}(t) \\ \dot{y}(t) \\ \dot{z}(t) \\ \dot{\gamma}(t) \\ \dot{\psi}(t) \end{bmatrix} = \begin{bmatrix} \cos \gamma(t) \cos \psi(t) & 0 & 0 \\ \cos \gamma(t) \sin \psi(t) & 0 & 0 \\ \sin \gamma(t) & 0 & 0 \\ 0 & 1 & 0 \\ 0 & 0 & 1 \end{bmatrix} \begin{bmatrix} v_a(t) \\ w_\gamma(t) \\ w_\psi(t) \end{bmatrix} \underbrace{u(t)}_{\text{u(t)}}. \quad (\text{A.2})$$

Consider the point $(L, 0, 0)^\top$ in the traditionally defined UAV body frame, where $L \neq 0$, and redefine the system output as

$$\begin{aligned} x_L(t) &= x(t) + L \cos \psi(t) \cos \gamma(t) \\ y_L(t) &= y(t) + L \sin \psi(t) \cos \gamma(t) \\ z_L(t) &= z(t) + L \sin \gamma(t). \end{aligned} \quad (\text{A.3})$$

Therefore,

$$\begin{bmatrix} \dot{x}_L(t) \\ \dot{y}_L(t) \\ \dot{z}_L(t) \end{bmatrix} = \underbrace{\begin{bmatrix} \cos \gamma(t) \cos \psi(t) & -L \sin \gamma(t) \cos \psi(t) & -L \cos \gamma(t) \sin \psi(t) \\ \cos \gamma(t) \sin \psi(t) & -L \sin \gamma(t) \sin \psi(t) & L \cos \gamma(t) \cos \psi(t) \\ \sin \gamma(t) & L \cos \gamma(t) & 0 \end{bmatrix}}_{M(\gamma, \psi)} \underbrace{\begin{bmatrix} v_a(t) \\ w_\gamma(t) \\ w_\psi(t) \end{bmatrix}}_{u(t)}. \quad (\text{A.4})$$

Assume that the UAV is not allowed to fly vertically; i.e., the pitch angle $\gamma \neq \pm\pi/2$. Then $\det M(\gamma, \psi) = -L^2 \cos \gamma \neq 0$. Therefore, after introducing the new control input $u_L(t) = (\dot{x}_L(t), \dot{y}_L(t), \dot{z}_L(t))^\top$, we can rewrite (A.4) as

$$u(t) = M(\gamma, \psi)^{-1} u_L(t) = \begin{bmatrix} \cos \gamma(t) \cos \psi(t) & \cos \gamma(t) \sin \psi(t) & \sin \gamma(t) \\ -\frac{\sin \gamma(t) \cos \psi(t)}{L} & -\frac{\sin \gamma(t) \sin \psi(t)}{L} & \frac{\cos \gamma(t)}{L} \\ -\frac{\sin \psi(t)}{L \cos \gamma(t)} & \frac{\cos \psi(t)}{L \cos \gamma(t)} & 0 \end{bmatrix} u_L(t). \quad (\text{A.5})$$

Let $u_L(t) = \chi(\xi_L(t))$, where $\chi(\cdot)$ is the vector field in (4.2) in Chapter 4, and $\xi_L(t) = (x_L, y_L, z_L)$ in (A.3). Thus, the control input is

$$u(t) = \begin{bmatrix} v_a(t) \\ w_\gamma(t) \\ w_\psi(t) \end{bmatrix} = \begin{bmatrix} \cos \gamma(t) \cos \psi(t) & \cos \gamma(t) \sin \psi(t) & \sin \gamma(t) \\ -\frac{\sin \gamma(t) \cos \psi(t)}{L} & -\frac{\sin \gamma(t) \sin \psi(t)}{L} & \frac{\cos \gamma(t)}{L} \\ -\frac{\sin \psi(t)}{L \cos \gamma(t)} & \frac{\cos \psi(t)}{L \cos \gamma(t)} & 0 \end{bmatrix} \chi(\xi_L(t)). \quad (\text{A.6})$$

Combining (A.2) and (A.6), we obtain the following closed-loop kinematics:

$$\begin{bmatrix} \dot{x} \\ \dot{y} \\ \dot{z} \\ \dot{\gamma} \\ \dot{\psi} \end{bmatrix} = \begin{bmatrix} \cos^2 \gamma \cos^2 \psi & \cos^2 \gamma \cos \psi \sin \psi & \cos \gamma \sin \gamma \cos \psi \\ \cos^2 \gamma \cos \psi \sin \psi & \cos^2 \gamma \sin^2 \psi & \cos \gamma \sin \gamma \sin \psi \\ \cos \gamma \sin \gamma \cos \psi & \cos \gamma \sin \gamma \sin \psi & \sin^2 \gamma \\ -\frac{\sin \gamma \cos \psi}{L} & -\frac{\sin \gamma \sin \psi}{L} & \frac{\cos \gamma}{L} \\ -\frac{\sin \psi}{L \cos \gamma} & \frac{\cos \psi}{L \cos \gamma} & 0 \end{bmatrix} \chi(\xi_L(t)),$$

where $\xi_L(t) = (x_L, y_L, z_L)$ is shown in (A.3). Using this control law (A.6), we can enable the point $(L, 0, 0)^\top$ in the UAV body frame to follow the desired path; the

idea of the control law design is the same as using feedback linearization for a unicycle robot model. We use the same helix as the second example of Chapter 4 as the desired path and simulate the effects of the control algorithm (A.6) (see Fig. A.1).

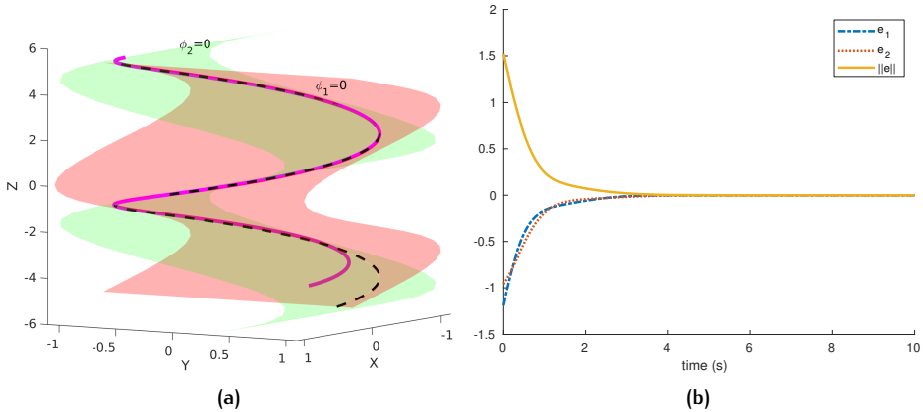


Figure A.1: (a) The trajectory (pink curve) $\xi_L(t) = (x_L, y_L, z_L)$ converges to the helix. (b) The path-following errors converge to zero.

A.2 A CONTROL ALGORITHM DESIGN EXAMPLE FOR A DYNAMICS MODEL

The proposed guiding vector field method may still be applied to more complex models, such as dynamic aircraft models, in an ad hoc manner. For example, we

consider the dynamic aircraft model given in the classical textbook [8, Eq. (9.24)] as follows (for simplicity, the time t is omitted):

$$\dot{x} = v_a \cos \psi \cos \gamma \quad (\text{A.7a})$$

$$\dot{y} = v_a \sin \psi \cos \gamma \quad (\text{A.7b})$$

$$\dot{z} = v_a \sin \gamma \quad (\text{A.7c})$$

$$\dot{v}_a = \frac{F_{\text{thrust}}}{m} - \frac{F_{\text{drag}}}{m} - g \sin \gamma \quad (\text{A.7d})$$

$$\dot{\psi} = \frac{F_{\text{lift}}}{m v_a} \frac{\sin \phi}{\cos \gamma} \quad (\text{A.7e})$$

$$\dot{\gamma} = \frac{F_{\text{lift}}}{m v_a} \cos \phi - \frac{g}{v_a} \cos \gamma \quad (\text{A.7f})$$

$$F_{\text{lift}} = \frac{1}{2} \rho v_a^2 S C_L \quad (\text{A.7g})$$

$$F_{\text{drag}} = \frac{1}{2} \rho v_a^2 S (C_{D0} + K C_L^2), \quad (\text{A.7h})$$

where the control inputs are thrust, lift coefficient, and bank angle ($F_{\text{thrust}}, C_L, \phi$)[⊤]. The variables x, y, z, v_a, ψ and γ have the same meanings as in Section A.1. The constants m and g denote the mass and gravity constant, respectively. Lift force F_{lift} and drag force F_{drag} are expressed in (A.7g) and (A.7h), respectively, where K is the induced drag factor determined by aerodynamic efficiency, C_{D0} is the zero-lift drag coefficient, S is the platform area of the UAV wing and ρ is the air density. Comparing (A.7) with (A.1), one observes that a possible control solution is to let the previous control input (A.6) be the desired kinematics control input in this model. Specifically, we add a superscript d to represent the *desired values* and rewrite (A.6) as

$$u^d(t) = \begin{bmatrix} v_a^d(t) \\ w_\gamma^d(t) \\ w_\psi^d(t) \end{bmatrix} = \begin{bmatrix} \cos \gamma(t) \cos \psi(t) & \cos \gamma(t) \sin \psi(t) & \sin \gamma(t) \\ -\frac{\sin \gamma(t) \cos \psi(t)}{L} & -\frac{\sin \gamma(t) \sin \psi(t)}{L} & \frac{\cos \gamma(t)}{L} \\ -\frac{\sin \psi(t)}{L \cos \gamma(t)} & \frac{\cos \psi(t)}{L \cos \gamma(t)} & 0 \end{bmatrix} \chi(\xi_L(t)), \quad (\text{A.8})$$

where $\xi_L = (x_L, y_L, z_L)^{\top}$ is shown in (A.3). Thus, in view of (A.7d), (A.7e) and (A.7f), it is desirable that

$$\dot{v}_a = f(v_a^d, v_a) \quad (\text{A.9a})$$

$$\dot{\psi} = \omega_\psi^d \quad (\text{A.9b})$$

$$\dot{\gamma} = \omega_\gamma^d \quad (\text{A.9c})$$

where $f(v_a^d, v_a)$ is a continuously differentiable function such that $v_a \rightarrow v_a^d$ as $t \rightarrow \infty$. Suppose that the desired airspeed v_a^d changes slowly, then we can let

$$f(v_a^d, v_a) = K_v(v_a^d - v_a), \quad (\text{A.10})$$

where K_v is a positive gain. Relating (A.7d), (A.7e), (A.7f), (A.9a), (A.9b), (A.9c) and (A.10), we obtain the following equations

$$\begin{aligned} \frac{F_{\text{thrust}}}{m} - \frac{F_{\text{drag}}}{m} - g \sin \gamma &= K_v(v_a^d - v_a) \\ \frac{F_{\text{lift}}}{m v_a} \frac{\sin \phi}{\cos \gamma} &= \omega_\psi^d \\ \frac{F_{\text{lift}}}{m v_a} \cos \phi - \frac{g}{v_a} \cos \gamma &= \omega_\gamma^d. \end{aligned}$$

Solving the equation, one obtains the lift coefficient as follows:

$$C_L = \frac{2m}{\rho v_a S} \sqrt{(\omega_\psi^d \cos \gamma)^2 + (g \cos \gamma / v_a + \omega_\gamma^d)^2}. \quad (\text{A.11})$$

The thrust is

$$\begin{aligned} F_{\text{thrust}} &= F_{\text{drag}} + mg \sin \gamma + K_v(v_a^d - v_a) \\ &= \frac{1}{2} \rho v_a^2 S (C_{D0} + K C_L^2) + mg \sin \gamma + K_v(v_a^d - v_a), \end{aligned} \quad (\text{A.12})$$

where C_L is computed by (A.11). The bank angle is

$$\phi = \text{atan2}(\phi_s, \phi_c), \quad (\text{A.13})$$

where atan2 is the four-quadrant inverse tangent function and

$$\phi_s = \frac{2\omega_\psi^d m v_a \cos \gamma}{\rho v_a^2 S C_L} \quad \phi_c = \frac{2m v_a (g \cos \gamma / v_a + \omega_\gamma^d)}{\rho v_a^2 S C_L}$$

with C_L computed by (A.11). Therefore, the dynamic control input $u_{\text{dyn}} = (F_{\text{thrust}}, C_L, \phi)^\top$ is attained.

BIBLIOGRAPHY

- [1] *A giant subsea snake robot*, Accessed on 26.06.2021. [Online]. Available: <https://www.oceannews.com/news/science-technology/a-giant-subsea-snake-robot>.
- [2] *AI robots to patrol India borders soon, prototype to come in December*, Accessed on 26.06.2021. [Online]. Available: <https://www.businesstoday.in/technology/news/story/ai-robots-to-patrol-india-borders-prototype-to-come-in-december-194617-2019-05-02>.
- [3] P.-A. Absil and K. Kurdyka, "On the stable equilibrium points of gradient systems," *Systems & control letters*, vol. 55, no. 7, pp. 573–577, 2006.
- [4] P.-A. Absil, R. Mahony, and B. Andrews, "Convergence of the iterates of descent methods for analytic cost functions," *SIAM Journal on Optimization*, vol. 16, no. 2, pp. 531–547, 2005.
- [5] A. P. Aguiar, J. P. Hespanha, and P. V. Kokotović, "Performance limitations in reference tracking and path following for nonlinear systems," *Automatica*, vol. 44, no. 3, pp. 598–610, 2008.
- [6] A. D. Ames, X. Xu, J. W. Grizzle, and P. Tabuada, "Control barrier function based quadratic programs for safety critical systems," *IEEE Transactions on Automatic Control*, vol. 62, no. 8, pp. 3861–3876, 2016.
- [7] S. Axler, *Linear algebra done right*. Springer, 2015.
- [8] R. W. Beard and T. W. McLain, *Small unmanned aircraft: Theory and practice*. Princeton university press, 2012.
- [9] D. Belleter, M. A. Maghenem, C. Paliotta, and K. Y. Pettersen, "Observer based path following for underactuated marine vessels in the presence of ocean currents: A global approach," *Automatica*, vol. 100, pp. 123–134, 2019.
- [10] E. Bernauau, E. Moulay, P. Coirault, and Q. Hui, "Topological properties for compact stable attractors in \mathbb{R}^n ," in *2019 Proceedings of the Conference on Control and its Applications*, SIAM, 2019, pp. 15–21.
- [11] N. P. Bhatia and G. P. Szegö, *Stability theory of dynamical systems*. Springer Science & Business Media, 2002.
- [12] R. H. Bing, *The geometric topology of 3-manifolds*. American Mathematical Soc., 1983, vol. 40.
- [13] F. Blanchini and S. Miani, *Set-theoretic methods in control*. Springer, 2008.

- [14] J. Borenstein and Y. Koren, "The vector field histogram-fast obstacle avoidance for mobile robots," *IEEE transactions on robotics and automation*, vol. 7, no. 3, pp. 278–288, 1991.
- [15] E. Borhaug, A. Pavlov, and K. Y. Pettersen, "Integral LOS control for path following of underactuated marine surface vessels in the presence of constant ocean currents," in *47th IEEE Conference on Decision and Control*, IEEE, 2008, pp. 4984–4991.
- [16] A. Borkar, A. Sinha, L. Vachhani, and H. Arya, "Collision-free trajectory planning on lissajous curves for repeated multi-agent coverage and target detection," in *2016 IEEE/RSJ International Conference on Intelligent Robots and Systems (IROS)*, IEEE, 2016, pp. 1417–1422.
- [17] P. Braun and C. Kellett, "On (the existence of) Control Lyapunov Barrier Functions," 2017. [Online]. Available: https://epub.uni-bayreuth.de/3522/1/CLBFs_submission_pbraun.pdf.
- [18] M. Brown, "A proof of the generalized schoenflies theorem," *Bulletin of the American Mathematical Society*, vol. 66, no. 2, pp. 74–76, 1960.
- [19] F. Bullo and A. D. Lewis, *Geometric control of mechanical systems: modeling, analysis, and design for simple mechanical control systems*. Springer, 2019, vol. 49.
- [20] M. Burger, A. Pavlov, E. Borhaug, and K. Y. Pettersen, "Straight line path following for formations of underactuated surface vessels under influence of constant ocean currents," in *2009 American Control Conference*, IEEE, 2009, pp. 3065–3070.
- [21] W. Caharija, K. Y. Pettersen, M. Bibuli, P. Calado, E. Zereik, J. Braga, J. T. Gravdahl, A. J. Sørensen, M. Milovanović, and G. Bruzzone, "Integral line-of-sight guidance and control of underactuated marine vehicles: Theory, simulations, and experiments," *IEEE Transactions on Control Systems Technology*, vol. 24, no. 5, pp. 1623–1642, 2016.
- [22] W. Caharija, K. Y. Pettersen, P. Calado, and J. Braga, "A comparison between the ILOS guidance and the vector field guidance," *IFAC-PapersOnLine*, vol. 48, no. 16, pp. 89–94, 2015.
- [23] H. Chen, Y. Cong, X. Wang, X. Xu, and L. Shen, "Coordinated path-following control of fixed-wing unmanned aerial vehicles," *IEEE Transactions on Systems, Man, and Cybernetics: Systems*, 2021.
- [24] Y.-Y. Chen and Y.-P. Tian, "A curve extension design for coordinated path following control of unicycles along given convex loops," *International Journal of Control*, vol. 84, no. 10, pp. 1729–1745, 2011.
- [25] C. Chicone, *Ordinary differential equations with applications*. Springer Science & Business Media, 2006, vol. 34.

- [26] *Code repository for this paper*, 2020. [Online]. Available: https://github.com/noether/paparazzi/tree/gvf_param_multi/sw/airborne/modules/guidance/gvf_parametric.
- [27] C. C. Conley, *Isolated invariant sets and the Morse index*, 38. American Mathematical Soc., 1978.
- [28] L. Consolini, M. Maggiore, C. Nielsen, and M. Tosques, “Path following for the PVTOL aircraft,” *Automatica*, vol. 46, no. 8, pp. 1284–1296, 2010.
- [29] G. Conte, S. Duranti, and T. Merz, “Dynamic 3D path following for an autonomous helicopter,” *IFAC Proceedings Volumes*, vol. 37, no. 8, pp. 472–477, 2004.
- [30] R. H. Cushman and L. M. Bates, *Global aspects of classical integrable systems*. Springer, 1997, vol. 94.
- [31] H. G. De Marina, Y. A. Kapitanyuk, M. Bronz, G. Hattenberger, and M. Cao, “Guidance algorithm for smooth trajectory tracking of a fixed wing UAV flying in wind flows,” in *2017 IEEE International Conference on Robotics and Automation (ICRA)*, IEEE, 2017, pp. 5740–5745.
- [32] H. G. De Marina, Z. Sun, M. Bronz, and G. Hattenberger, “Circular formation control of fixed-wing UAVs with constant speeds,” in *2017 IEEE/RSJ International Conference on Intelligent Robots and Systems (IROS)*, IEEE, 2017, pp. 5298–5303.
- [33] M. Deghat, B. D. Anderson, and Z. Lin, “Combined flocking and distance-based shape control of multi-agent formations,” *IEEE Transactions on Automatic Control*, vol. 61, no. 7, pp. 1824–1837, 2015.
- [34] M. Deghat, I. Shames, B. D. Anderson, and C. Yu, “Localization and circumnavigation of a slowly moving target using bearing measurements,” *IEEE Transactions on Automatic Control*, vol. 59, no. 8, pp. 2182–2188, 2014. doi: [10.1109/TAC.2014.2299011](https://doi.org/10.1109/TAC.2014.2299011).
- [35] M. P. Do Carmo, *Differential Geometry of Curves and Surfaces: Revised and Updated Second Edition*. Courier Dover Publications, 2016.
- [36] K. D. Do, “Global output-feedback path-following control of unicycle-type mobile robots: A level curve approach,” *Robotics and Autonomous Systems*, vol. 74, pp. 229–242, 2015.
- [37] K. D. Do, Z.-P. Jiang, and J Pan, “Robust adaptive path following of underactuated ships,” *Automatica*, vol. 40, no. 6, pp. 929–944, 2004.
- [38] A. Doosthoseini and C. Nielsen, “Coordinated path following for unicycles: A nested invariant sets approach,” *Automatica*, vol. 60, pp. 17–29, 2015.
- [39] J. Fonseca, J. Wei, K. H. Johansson, and T. A. Johansen, “Cooperative decentralised circumnavigation with application to algal bloom tracking,” in *2019 IEEE/RSJ International Conference on Intelligent Robots and Systems (IROS)*, 2019, pp. 3276–3281. doi: [10.1109/IROS40897.2019.8967632](https://doi.org/10.1109/IROS40897.2019.8967632).

- [40] T. I. Fossen, M. Breivik, and R. Skjetne, "Line-of-sight path following of underactuated marine craft," *IFAC Proceedings Volumes*, vol. 36, no. 21, pp. 211–216, 2003.
- [41] D. Fox, W. Burgard, and S. Thrun, "The dynamic window approach to collision avoidance," *IEEE Robotics & Automation Magazine*, vol. 4, no. 1, pp. 23–33, 1997.
- [42] J. B. Fraleigh and A. B. Raymond, "Linear algebra 3rd ed," *Reading: Addison Wesley*, 1995.
- [43] A. Franchi, P. Stegagno, and G. Oriolo, "Decentralized multi-robot encirclement of a 3D target with guaranteed collision avoidance," *Autonomous Robots*, vol. 40, no. 2, pp. 245–265, 2016.
- [44] E. W. Frew and D. Lawrence, "Tracking dynamic star curves using guidance vector fields," *Journal of Guidance, Control, and Dynamics*, vol. 40, no. 6, pp. 1488–1495, 2017.
- [45] A. Galbis and M. Maestre, *Vector analysis versus vector calculus*. Springer Science & Business Media, 2012.
- [46] W.-Y. Gan, D.-Q. Zhu, W.-L. Xu, and B. Sun, "Survey of trajectory tracking control of autonomous underwater vehicles," *Journal of marine science and technology*, vol. 25, no. 6, p. 13, 2017.
- [47] B. Gati, "Open source autopilot for academic research-the paparazzi system," in *2013 American Control Conference*, IEEE, 2013, pp. 1478–1481.
- [48] J. Ghommam, H. Mehrjerdi, M. Saad, and F. Mnif, "Formation path following control of unicycle-type mobile robots," *Robotics and Autonomous Systems*, vol. 58, no. 5, pp. 727–736, 2010.
- [49] M. Giaquinta and G. Modica, *Mathematical analysis: an introduction to functions of several variables*. Springer Science & Business Media, 2010.
- [50] V. M. Goncalves, L. C. A. Pimenta, C. A. Maia, B. C. O. Dutra, and G. A. S. Pereira, "Vector fields for robot navigation along time-varying curves in n -dimensions," *IEEE Transactions on Robotics*, vol. 26, no. 4, pp. 647–659, Aug. 2010, ISSN: 1552-3098. DOI: 10.1109/TRO.2010.2053077.
- [51] T. Gowers, J. Barrow-Green, and I. Leader, *The Princeton companion to mathematics*. Princeton University Press, 2010.
- [52] V. Guillemin and A. Pollack, *Differential topology*. American Mathematical Soc., 2010, vol. 370.
- [53] W. M. Haddad and V. Chellaboina, *Nonlinear dynamical systems and control: a Lyapunov-based approach*. Princeton university press, 2011.
- [54] W. Hahn, *Stability of motion*. Springer, 1967, vol. 138.
- [55] U. Helmke and J. B. Moore, *Optimization and dynamical systems*. Springer Science & Business Media, 2012.

- [56] M. W. Hirsch, *Differential topology*. Springer Science & Business Media, 2012, vol. 33.
- [57] J. Huang, *Nonlinear output regulation: theory and applications*. SIAM, 2004.
- [58] J. Huang and Z. Chen, "A general framework for tackling the output regulation problem," *IEEE Transactions on Automatic Control*, vol. 49, no. 12, pp. 2203–2218, 2004.
- [59] A. Iggidr, B. Kalitine, and R. Oubtib, "Semidefinite Lyapunov functions stability and stabilization," *Mathematics of Control, Signals and Systems*, vol. 9, no. 2, pp. 95–106, 1996.
- [60] M. Iqbal, S.-i. Azuma, J. Leth, and T. D. Ngo, "Circular and concentric formation of kinematic unicycles," in *2019 IEEE International Conference on Robotics and Automation (ICRA)*, IEEE, 2019, pp. 1–6.
- [61] A. Isidori and C. I. Byrnes, "Output regulation of nonlinear systems," *IEEE transactions on Automatic Control*, vol. 35, no. 2, pp. 131–140, 1990.
- [62] F. Jones, *Lebesgue integration on Euclidean space*. Jones & Bartlett Learning, 2001.
- [63] Y. A. Kapitanyuk, A. V. Proskurnikov, and M. Cao, "A guiding vector-field algorithm for path-following control of nonholonomic mobile robots," *IEEE Transactions on Control Systems Technology*, vol. 26, no. 4, pp. 1372–1385, Jul. 2018, ISSN: 1063-6536. doi: [10.1109/TCST.2017.2705059](https://doi.org/10.1109/TCST.2017.2705059).
- [64] Y. A. Kapitanyuk, S. A. Chepinskii, and A. A. Kapitonov, "Geometric path following control of a rigid body based on the stabilization of sets," *IFAC Proceedings Volumes*, vol. 47, no. 3, pp. 7342–7347, 2014.
- [65] Y. A. Kapitanyuk, H. G. de Marina, A. V. Proskurnikov, and M. Cao, "Guiding vector field algorithm for a moving path following problem," *IFAC-PapersOnLine*, vol. 50, no. 1, pp. 6983–6988, 2017.
- [66] H. Khalil, *Nonlinear Systems*, Third. Prentice Hall, 2002.
- [67] O. Khatib, "Real-time obstacle avoidance for manipulators and mobile robots," *The International Journal of Robotics Research*, vol. 5, no. 1, pp. 90–98, Mar. 1986.
- [68] D. E. Koditschek and E. Rimon, "Robot navigation functions on manifolds with boundary," *Advances in applied mathematics*, vol. 11, no. 4, pp. 412–442, 1990.
- [69] Y. Koren and J. Borenstein, "Potential field methods and their inherent limitations for mobile robot navigation," in *Proceedings. 1991 IEEE International Conference on Robotics and Automation*, IEEE, 1991, pp. 1398–1404.
- [70] S. M. LaValle, *Planning algorithms*. Cambridge university press, 2006.

- [71] S. Lacroix, G. Roberts, E. Benard, M. Bronz, F. Burnet, E. Bouhoubeiny, J.-P. Condomines, C. Doll, G. Hattenberger, F. Lamraoui, *et al.*, “Fleets of enduring drones to probe atmospheric phenomena with clouds,” in *EGU General Assembly Conference Abstracts*, vol. 18, 2016.
- [72] K. Łakomy and M. M. Michałek, “The VFO path-following kinematic controller for robotic vehicles moving in a 3D space,” in *Robot Motion and Control (RoMoCo), 2017 11th International Workshop on*, IEEE, 2017, pp. 263–268.
- [73] L. Lapierre, R. Zapata, and P. Lepinay, “Combined path-following and obstacle avoidance control of a wheeled robot,” *The International Journal of Robotics Research*, vol. 26, no. 4, pp. 361–375, 2007.
- [74] D. A. Lawrence, E. W. Frew, and W. J. Pisano, “Lyapunov vector fields for autonomous unmanned aircraft flight control,” *Journal of Guidance, Control, and Dynamics*, vol. 31, no. 5, pp. 1220–1229, 2008.
- [75] H. Lee and H. J. Kim, “Trajectory tracking control of multirotors from modelling to experiments: A survey,” *International Journal of Control, Automation and Systems*, vol. 15, no. 1, pp. 281–292, 2017.
- [76] J. M. Lee, *Introduction to topological manifolds: Second Edition*. Springer Science & Business Media, 2010, vol. 202.
- [77] ——, *Introduction to Smooth Manifolds: Second Edition*, ser. Graduate texts in mathematics. Springer, 2015, ISBN: 9787510098833.
- [78] ——, *Introduction to Riemannian manifolds: Second Edition*. Springer, 2018.
- [79] S. Lee, A. Cho, and C. Kee, “Integrated waypoint path generation and following of an unmanned aerial vehicle,” *Aircraft Engineering and Aerospace Technology*, 2010.
- [80] Z. Li, J. Sun, and S. Oh, “Design, analysis and experimental validation of a robust nonlinear path following controller for marine surface vessels,” *Automatica*, vol. 45, no. 7, pp. 1649–1658, 2009.
- [81] Y. Liang and Y. Jia, “Combined vector field approach for 2D and 3D arbitrary twice differentiable curved path following with constrained UAVs,” *Journal of Intelligent & Robotic Systems*, vol. 83, no. 1, pp. 133–160, 2016.
- [82] D. Liberzon, *Switching in systems and control*. Springer Science & Business Media, 2003.
- [83] B. Lin, W. Yao, and M. Cao, “On Wilson’s theorem about domains of attraction and tubular neighborhoods,” 2021, Under preparation. [Online]. Available: http://tiny.cc/lin_wilson.
- [84] S. Łojasiewicz, “Sur la géométrie semi-et sous-analytique,” in *Annales de l’institut Fourier*, vol. 43, 1993, pp. 1575–1595.

- [85] O. Lukina, F. Takens, and H. Broer, "Global properties of integrable hamiltonian systems," *Regular and Chaotic Dynamics*, vol. 13, no. 6, pp. 602–644, 2008.
- [86] Y. Matsumoto, *An introduction to Morse theory*. American Mathematical Soc., 2002, vol. 208.
- [87] B. Mazur, "On embeddings of spheres," *Bulletin of the American Mathematical Society*, vol. 65, no. 2, pp. 59–65, 1959.
- [88] M. Mesbahi and M. Egerstedt, *Graph theoretic methods in multiagent networks*. Princeton University Press, 2010, vol. 33.
- [89] M. M. Michałek and T. Gawron, "VFO path following control with guarantees of positionally constrained transients for unicycle-like robots with constrained control input," *Journal of Intelligent & Robotic Systems*, vol. 89, no. 1-2, pp. 191–210, 2018.
- [90] M. Michalek and K. Kozłowski, "Vector-field-orientation feedback control method for a differentially driven vehicle," *IEEE Transactions on Control Systems Technology*, vol. 18, no. 1, pp. 45–65, 2010.
- [91] J. Minguez and L. Montano, "Extending collision avoidance methods to consider the vehicle shape, kinematics, and dynamics of a mobile robot," *IEEE Transactions on Robotics*, vol. 25, no. 2, pp. 367–381, 2009.
- [92] S. Moe and K. Y. Pettersen, "Set-based line-of-sight (LOS) path following with collision avoidance for underactuated unmanned surface vessel," in *2016 24th Mediterranean Conference on Control and Automation (MED)*, IEEE, 2016, pp. 402–409.
- [93] S. Moe, K. Y. Pettersen, T. I. Fossen, and J. T. Gravdahl, "Line-of-sight curved path following for underactuated USVs and AUVs in the horizontal plane under the influence of ocean currents," in *2016 24th Mediterranean Conference on Control and Automation (MED)*, IEEE, 2016, pp. 38–45.
- [94] F. Mondada, M. Bonani, X. Raemy, J. Pugh, C. Cianci, A. Klaptocz, S. Magnenat, J.-C. Zufferey, D. Floreano, and A. Martinoli, "The e-puck, a robot designed for education in engineering," in *Proceedings of the 9th conference on autonomous robot systems and competitions*, IPCB: Instituto Politécnico de Castelo Branco, vol. 1, 2009, pp. 59–65.
- [95] A. H. Mong-ying and V. Kumar, "Pattern generation with multiple robots," in *2006 IEEE International Conference on Robotics and Automation (ICRA)*, IEEE, 2006, pp. 2442–2447.
- [96] A. H. Mong-ying, S. Loizou, and V. Kumar, "Stabilization of multiple robots on stable orbits via local sensing," in *2007 IEEE International Conference on Robotics and Automation (ICRA)*, IEEE, 2007, pp. 2312–2317.

- [97] G. Moore and E. Hubert, "Algorithms for constructing stable manifolds of stationary solutions," *IMA journal of numerical analysis*, vol. 19, no. 3, pp. 375–424, 1999.
- [98] A. Morro, A. Sgorbissa, and R. Zaccaria, "Path following for unicycle robots with an arbitrary path curvature," *IEEE Transactions on Robotics*, vol. 27, no. 5, pp. 1016–1023, 2011.
- [99] E. Moulay and S. P. Bhat, "Topological properties of asymptotically stable sets," *Nonlinear Analysis: Theory, Methods & Applications*, vol. 73, no. 4, pp. 1093–1097, 2010.
- [100] J. R. Munkres, *Elements of algebraic topology*. CRC Press, 2018.
- [101] J. Munkres, *Topology: Pearson New International Edition*, Second. Pearson Education Limited, 2013, ISBN: 9781292036786.
- [102] K. Nakai and K. Uchiyama, "Vector fields for UAV guidance using potential function method for formation flight," in *AIAA Guidance, Navigation, and Control (GNC) Conference*, 2013, p. 4626.
- [103] T. P. Nascimento, C. E. Dórea, and L. M. G. Gonçalves, "Nonholonomic mobile robots' trajectory tracking model predictive control: A survey," *Robotica*, vol. 36, no. 5, pp. 676–696, 2018.
- [104] D. R. Nelson, D. B. Barber, T. W. McLain, and R. W. Beard, "Vector field path following for miniature air vehicles," *IEEE Transactions on Robotics*, vol. 23, no. 3, pp. 519–529, 2007.
- [105] *New coalition to shape the urban airspace of european cities*, Accessed on 26.06.2021. [Online]. Available: <https://insideunmannedsystems.com/new-coalition-to-shape-the-urban-airspace-of-european-cities/>.
- [106] L. Nicolaescu, *An invitation to Morse theory*. Springer Science & Business Media, 2011.
- [107] H. Nijmeijer and A. Van der Schaft, *Nonlinear dynamical control systems*. Springer, 1990, vol. 175.
- [108] R. Olfati-Saber, J. A. Fax, and R. M. Murray, "Consensus and cooperation in networked multi-agent systems," *Proc. IEEE*, vol. 95, no. 1, pp. 215–233, 2007.
- [109] H. Osinga, "Computing invariant manifolds: Variations on graph transform," PhD thesis, University of Groningen, 1996.
- [110] D. Panagou, "Motion planning and collision avoidance using navigation vector fields," in *2014 IEEE International Conference on Robotics and Automation (ICRA)*, IEEE, 2014, pp. 2513–2518.
- [111] S. Park, J. Deyst, and J. P. How, "Performance and Lyapunov stability of a nonlinear path following guidance method," *Journal of Guidance, Control, and Dynamics*, vol. 30, no. 6, pp. 1718–1728, 2007.

- [112] S. Paternain, D. E. Koditschek, and A. Ribeiro, "Navigation functions for convex potentials in a space with convex obstacles," *IEEE Transactions on Automatic Control*, vol. 63, no. 9, pp. 2944–2959, 2017.
- [113] W. F. Phillips, *Mechanics of flight*. John Wiley & Sons, 2004.
- [114] L. C. Pimenta, G. A. Pereira, M. M. Gonçalves, N. Michael, M. Turpin, and V. Kumar, "Decentralized controllers for perimeter surveillance with teams of aerial robots," *Advanced Robotics*, vol. 27, no. 9, pp. 697–709, 2013.
- [115] A. Ratnoo, P. Sujit, and M. Kothari, "Adaptive optimal path following for high wind flights," *IFAC Proceedings Volumes*, vol. 44, no. 1, pp. 12985–12990, 2011.
- [116] W. Ren and R. W. Beard, *Distributed consensus in multi-vehicle cooperative control*, 2. Springer, 2008, vol. 27.
- [117] L. A. V. Reyes and H. G. Tanner, "Flocking, formation control, and path following for a group of mobile robots," *IEEE Transactions on Control Systems Technology*, vol. 23, no. 4, pp. 1268–1282, 2015.
- [118] A. M. Rezende, V. M. Gonçalves, A. H. Nunes, and L. C. Pimenta, "Robust quadcopter control with artificial vector fields," in *2020 IEEE International Conference on Robotics and Automation (ICRA)*, IEEE, 2020, pp. 6381–6387.
- [119] A. M. Rezende, V. M. Gonçalves, G. V. Raffo, and L. C. Pimenta, "Robust fixed-wing UAV guidance with circulating artificial vector fields," in *2018 IEEE/RSJ International Conference on Intelligent Robots and Systems (IROS)*, IEEE, 2018, pp. 5892–5899.
- [120] E. Rimon and D. E. Koditschek, "Exact robot navigation using artificial potential functions," *IEEE Transactions on Robotics and Automation*, vol. 8, no. 5, pp. 501–518, 1992. doi: [10.1109/70.163777](https://doi.org/10.1109/70.163777).
- [121] B. Rubí, R. Pérez, and B. Morcego, "A survey of path following control strategies for UAVs focused on quadrotors," *Journal of Intelligent & Robotic Systems*, pp. 1–25, 2019.
- [122] R. Rysdyk, "UAV path following for constant line-of-sight," in *2nd AIAA "Unmanned Unlimited" Conf. and Workshop & Exhibit*, 2003, p. 6626.
- [123] L. Sabattini, C. Secchi, M. Cocetti, A. Levratti, and C. Fantuzzi, "Implementation of coordinated complex dynamic behaviors in multirobot systems," *IEEE Transactions on Robotics*, vol. 31, no. 4, pp. 1018–1032, 2015.
- [124] S. Sastry, *Nonlinear systems: analysis, stability, and control*. Springer Science & Business Media, 2013, vol. 10.
- [125] R. Sepulchre, D. A. Paley, and N. E. Leonard, "Stabilization of planar collective motion: All-to-all communication," *IEEE Transactions on Automatic Control*, vol. 52, no. 5, pp. 811–824, 2007.

- [126] M. M. Seron, J. H. Braslavsky, P. V. Kokotovic, and D. Q. Mayne, "Feedback limitations in nonlinear systems: From bode integrals to cheap control," *IEEE Transactions on Automatic Control*, vol. 44, no. 4, pp. 829–833, 1999.
- [127] A. Sgorbissa and R. Zaccaria, "3D path following with no bounds on the path curvature through surface intersection," in *2010 IEEE/RSJ International Conference on Intelligent Robots and Systems (IROS)*, IEEE, 2010, pp. 4029–4035.
- [128] ——, "Integrated obstacle avoidance and path following through a feedback control law," *Journal of Intelligent & Robotic Systems*, vol. 72, no. 3-4, pp. 409–428, 2013.
- [129] I. Shames, S. Dasgupta, B. Fidan, and B. D. O. Anderson, "Circumnavigation using distance measurements under slow drift," *IEEE Transactions on Automatic Control*, vol. 57, no. 4, pp. 889–903, 2011.
- [130] B. Siciliano and O. Khatib, *Springer Handbook of Robotics*. Secaucus, NJ, USA: Springer-Verlag New York, Inc., 2007, ISBN: 354023957X.
- [131] B. Siciliano, L. Sciavicco, L. Villani, and G. Oriolo, *Robotics: modelling, planning and control*. Springer Science & Business Media, 2010.
- [132] R. Siegwart, I. R. Nourbakhsh, and D. Scaramuzza, *Introduction to autonomous mobile robots*. MIT press, 2011.
- [133] J.-J. E. Slotine, W. Li, et al., *Applied nonlinear control*, 1. Prentice hall Englewood Cliffs, NJ, 1991, vol. 199.
- [134] D. Soetanto, L. Lapierre, and A. Pascoal, "Adaptive, non-singular path-following control of dynamic wheeled robots," in *42nd IEEE Conference on Decision and Control*, IEEE, vol. 2, 2003, pp. 1765–1770.
- [135] D. St-Onge, C. Pincioli, and G. Beltrame, "Circle formation with computation-free robots shows emergent behavioural structure," in *2018 IEEE/RSJ International Conference on Intelligent Robots and Systems (IROS)*, IEEE, 2018, pp. 5344–5349.
- [136] E. M. Stein and R. Shakarchi, *Real Analysis: Measure Theory, Integration, And Hilbert Spaces*. Princeton University Press, 2009.
- [137] P. B. Sujit, S. Saripalli, and J. B. Sousa, "Unmanned aerial vehicle path following: A survey and analysis of algorithms for fixed-wing unmanned aerial vehicles," *IEEE Control Systems*, vol. 34, no. 1, pp. 42–59, Feb. 2014, ISSN: 1066-033X. DOI: 10.1109/MCS.2013.2287568.
- [138] Z. Sun, H. G. de Marina, G. S. Seyboth, B. D. O. Anderson, and C. Yu, "Circular formation control of multiple unicycle-type agents with nonidentical constant speeds," *IEEE Transactions on Control Systems Technology*, vol. 27, no. 1, pp. 192–205, 2018.

- [139] M. H. Tanveer, C. T. Recchiuto, and A. Sgorbissa, "Analysis of path following and obstacle avoidance for multiple wheeled robots in a shared workspace," *Robotica*, vol. 37, no. 1, pp. 80–108, 2019.
- [140] T. Tao, *Analysis II*, Third, ser. Texts and Readings in Mathematics. Springer, Singapore, 2016. doi: <https://doi.org/10.1007/978-981-10-1804-6>.
- [141] K. Tapp, *Differential geometry of curves and surfaces*. Springer, 2016.
- [142] M. Vidyasagar, *Nonlinear systems analysis*. SIAM, 2002, vol. 42.
- [143] C. Wang, W. Xia, and G. Xie, "Limit-cycle-based design of formation control for mobile agents," *IEEE Transactions on Automatic Control*, 2019.
- [144] C. Wang, G. Xie, and M. Cao, "Forming circle formations of anonymous mobile agents with order preservation," *IEEE Transactions on Automatic Control*, vol. 58, no. 12, pp. 3248–3254, 2013.
- [145] ——, "Controlling anonymous mobile agents with unidirectional locomotion to form formations on a circle," *Automatica*, vol. 50, no. 4, pp. 1100–1108, 2014.
- [146] L. Wang, A. D. Ames, and M. Egerstedt, "Safe certificate-based maneuvers for teams of quadrotors using differential flatness," in *2017 IEEE International Conference on Robotics and Automation (ICRA)*, IEEE, 2017, pp. 3293–3298.
- [147] ——, "Safety barrier certificates for collisions-free multirobot systems," *IEEE Transactions on Robotics*, vol. 33, no. 3, pp. 661–674, 2017.
- [148] Y. Wang, D. Wang, and S. Zhu, "Cooperative moving path following for multiple fixed-wing unmanned aerial vehicles with speed constraints," *Automatica*, vol. 100, pp. 82–89, 2019.
- [149] S. Wiggins, *Introduction to applied nonlinear dynamical systems and chaos*, Second. Springer Science & Business Media, 2003.
- [150] M. S. Wiig, K. Y. Pettersen, and T. R. Krogstad, "Collision avoidance for underactuated marine vehicles using the constant avoidance angle algorithm," *IEEE Transactions on Control Systems Technology*, vol. 28, no. 3, pp. 951–966, 2019.
- [151] J. P. Wilhelm and G. Clem, "Vector field UAV guidance for path following and obstacle avoidance with minimal deviation," *Journal of Guidance, Control, and Dynamics*, vol. 42, no. 8, pp. 1848–1856, 2019.
- [152] F Wilson Jr, "The structure of the level surfaces of a Lyapunov function," *Journal of Differential Equations*, vol. 3, no. 3, pp. 323–329, 1967.
- [153] F. W. Wilson, "Smoothing derivatives of functions and applications," *Transactions of the American Mathematical Society*, vol. 139, pp. 413–428, 1969.

- [154] X. Xu, P. Tabuada, J. W. Grizzle, and A. D. Ames, "Robustness of control barrier functions for safety critical control," *IFAC-PapersOnLine*, vol. 48, no. 27, pp. 54–61, 2015.
- [155] G.-Z. Yang, J. Bellingham, P. E. Dupont, P. Fischer, L. Floridi, R. Full, N. Jacobstein, V. Kumar, M. McNutt, R. Merrifield, *et al.*, "The grand challenges of science robotics," *Science Robotics*, vol. 3, no. 14, eaar7650, 2018.
- [156] W. Yao and M. Cao, "Path following control in 3D using a vector field," *Automatica*, vol. 117, p. 108957, 2020, ISSN: 0005-1098. doi: <https://doi.org/10.1016/j.automatica.2020.108957>.
- [157] W. Yao, Y. A. Kapitanyuk, and M. Cao, "Robotic path following in 3D using a guiding vector field," in *2018 IEEE Conference on Decision and Control (CDC)*, IEEE, 2018, pp. 4475–4480.
- [158] W. Yao, B. Lin, B. D. O. Anderson, and M. Cao, "Domain of attraction of compact asymptotically stable regular manifolds in vector-field guided path following," *IEEE Transactions on Automatic Control (TAC)*, 2021, To be submitted.
- [159] ——, "Guiding vector fields for following occluded paths," *IEEE Transactions on Automatic Control (TAC)*, 2021, Under review.
- [160] ——, "Refining dichotomy convergence in vector-field guided path following control," in *European Control Conference (ECC)*, To appear, 2021. [Online]. Available: http://tiny.cc/yao_ecc21.
- [161] ——, "Topological analysis of vector-field guided path following on manifolds," *IEEE Transactions on Automatic Control*, 2021, Conditionally accepted. [Online]. Available: http://tiny.cc/yao_topo.
- [162] W. Yao, B. Lin, and M. Cao, "Integrated path following and collision avoidance using a composite vector field," in *2019 IEEE 58th Conference on Decision and Control (CDC)*, IEEE, 2019, pp. 250–255.
- [163] W. Yao, H. Lu, Z. Zeng, J. Xiao, and Z. Zheng, "Distributed static and dynamic circumnavigation control with arbitrary spacings for a heterogeneous multi-robot system," *Journal of Intelligent & Robotic Systems*, vol. 94, no. 3-4, pp. 883–905, 2019.
- [164] W. Yao, H. G. de Marina, and M. Cao, "Vector field guided path following control: Singularity elimination and global convergence," in *2020 59th IEEE Conference on Decision and Control (CDC)*, IEEE, 2020, pp. 1543–1549.
- [165] W. Yao, H. G. de Marina, B. Lin, and M. Cao, "Singularity-free guiding vector field for robot navigation," *IEEE Transactions on Robotics*, vol. 37, no. 4, 2021.

- [166] W. Yao, H. G. de Marina, Z. Sun, and M. Cao, "Distributed coordinated path following using guiding vector fields," in *IEEE International Conference on Robotics and Automation (ICRA)*, To appear, arXiv preprint arXiv:2103.12372, 2021.
- [167] ——, "Guiding vector fields for multi-robot coordinated navigation," *IEEE Transactions on Robotics*, 2021, To be submitted.
- [168] X. Yun and Y. Yamamoto, "On feedback linearization of mobile robots," Department of Computer and Information Science, University of Pennsylvania, technical report, 1992.
- [169] F. Zhang and N. E. Leonard, "Coordinated patterns of unit speed particles on a closed curve," *Systems & control letters*, vol. 56, no. 6, pp. 397–407, 2007.
- [170] R. Zheng and D. Sun, "Circumnavigation by a mobile robot using bearing measurements.,," in *2014 IEEE/RSJ International Conference on Intelligent Robots and Systems (IROS)*, 2014, pp. 4643–4648.
- [171] D. Zhou, Z. Wang, S. Bandyopadhyay, and M. Schwager, "Fast, on-line collision avoidance for dynamic vehicles using buffered voronoi cells," *IEEE Robotics and Automation Letters*, vol. 2, no. 2, pp. 1047–1054, 2017.
- [172] S. Zhu, D. Wang, and C. B. Low, "Ground target tracking using UAV with input constraints," *Journal of Intelligent & Robotic Systems*, vol. 69, no. 1, pp. 417–429, Jan. 2013, ISSN: 1573-0409. DOI: 10.1007/s10846-012-9737-y.
- [173] Y. Zhu, T. Moleski, and J. Wilhelm, "Evaluation of decay functions for vector field based obstacle avoidance," in *AIAA Scitech 2019 Forum*, 2019, p. 1058.

SUMMARY

Using a designed vector field to guide robots to follow a given geometric desired path has found a range of practical applications, such as underwater pipeline inspection, warehouse navigation and highway traffic monitoring. It is thus in great need to build a rigorous theory to guide practical implementations with formal guarantees. It is even so when multiple robots are required to follow predefined desired paths or maneuver on surfaces and coordinate their motions to efficiently accomplish repetitive and laborious tasks.

In this thesis, we propose and study a specific class of vector field, called *guiding vector fields*, on the Euclidean space and a general Riemannian manifold, for single-robot and multi-robot path following and motion coordination. A guiding vector field is generally composed of two terms: a convergence term which enables the integral curves of the vector field to converge to the desired path, and a propagation term which is tangent to the desired path such that propagation along the desired path is ensured. The guiding vector field is completely determined (up to positive coefficients) by a number of twice continuously differentiable real-value functions (called *level functions*). The intersection of the zero-level sets of these level functions is the desired path to be followed. Since the guiding vector field is not the gradient of any potential function, and also due to the existence of *singular points* where the vector field vanishes, the theoretical analysis becomes challenging. Therefore, in Part I of the thesis, we derive extensive theoretical results. And then in Part II, we elaborate on how to utilize guiding vector fields with variations in practical applications.

In Part I, first, motivated by the observation that the desired path is the intersection of the zero-level sets of level functions, we study the relationship between the values of the level functions, called the *level values*, and the convergence of the integral curves of the vector field to the desired path. It turns out that even when the level values along an integral curve converge to zero, the integral curve itself may not converge to the desired path. We then provide some necessary assumptions that are adopted throughout the thesis to guarantee that the vanishing of the level values along the integral curve indeed entails the convergence of the integral curve to the desired path. These assumptions facilitate the subsequent analysis as we only need to study the convergence result of the level values. We also strengthen the existing dichotomy convergence result which states that the integral curves either (locally) converge to the desired path or the singular set (i.e., the set of all singular points). We show that real analyticity of the level functions is a sufficient condition to reach the refined conclusion that convergence to a singular set implies convergence to a single point of the set.

Next, we study the autonomous system where the right-hand side is a guiding vector field defined on the n -dimensional Euclidean space \mathbb{R}^n or a general smooth Riemannian manifold \mathcal{M} . Specifically, we show the exponential convergence of path-following errors in the vicinity of the desired path, and the local input-to-state stability (ISS) of the path-following error dynamics when the guiding vector field is on the 3D Euclidean space. These results can be straightforwardly applied to guiding vector fields defined on higher-dimensional Euclidean spaces. In addition, the local ISS property justifies the effectiveness of the control algorithm design principle used for many robot kinematics models, such as the unicycle model. We then generalize the guiding vector field from a Euclidean space to a general smooth Riemannian manifold. The generalized guiding vector field is imperative for path-following in some abstract configuration space (e.g., robot arm joint space). We show that the dichotomy convergence result and the asymptotic stability of desired paths still hold. We then turn to the special case where the desired path is homeomorphic to the unit circle S^1 and study the guiding vector field from a topological viewpoint. We prove that the existence of singular points is inherent in the topology of the desired path in Euclidean spaces. Especially, in \mathbb{R}^n , where $n \geq 3$, there always exists a trajectory that starts from the boundary of any ball containing the desired path and does not converge to the desired path. Moreover, in the general n -dimensional Riemannian manifold case, the domain of attraction of the desired path is homeomorphic to $\mathbb{R}^{n-1} \times S^1$.

In Part II, we develop variations of guiding vector fields, and demonstrate their use in three practical applications: path following with obstacle avoidance, desired path global convergence and multi-robot motion coordination. In the first application, we consider the practical situation where the desired path is partly occupied by a finite number of static or moving obstacles. We use a smooth bump function to combine two guiding vector fields, one for path following and the other for collision avoidance. We show that additional singular points appear in many cases even though the combined guiding vector field is still sufficiently smooth. Nevertheless, we provide theoretical conditions and a switching mechanism such that the path-following and obstacle-avoidance behaviors are guaranteed to be effective. This approach is reactive and general, hence suitable for real-time applications and can deal with obstacles of arbitrary shapes. In the second application, motivated by the topological analysis (in particular, the existence of singular points) of guiding vector fields in Part I, we propose a novel idea to transform the topology of the desired path such that the bounded or self-intersecting desired paths become unbounded and non-self-intersecting (precisely, homeomorphic to the real line \mathbb{R}). This approach leads to a singularity-free higher-dimensional guiding vector field that can guarantee global convergence of trajectories to the desired path. The additional dimension corresponds to a virtual coordinate that represents the parameter of the desired path. In the last application, we exploit this additional dimension of the singularity-free guiding vector field to enable the distributed motion coordination and navigation of a

group of an arbitrary number of robots on different desired paths or surfaces. The resulting algorithm is distributed, scalable, and low-cost in communication and computation. All these applications have formal guarantees and are also supported by extensive simulation examples and real experiments with fixed-wing aircraft.

SAMENVATTING

Het gebruik van een beoogd vectorveld dat de robots leidt om een geometrisch gewenst pad te volgen is terug te vinden in een scala aan praktische toepassingen, waaronder inspectie aan onderwater pijplijnen, navigatie in magazijnen en verkeersmonitoring op snelwegen. Het is hiervoor noodzakelijk om een nauwgezette theorie te ontwikkelen welke formele garanties kan bieden voor praktische implementaties. Het is nog meer van belang wanneer van meerdere robots wordt verlangd om aangewezen paden te volgen of om op specifieke oppervlaktes te manoeuvreren; hierbij coördineren ze hun eigen bewegingen opdat ze herhalende en arbeidsintensieve taken kunnen volbrengen.

Dit proefschrift gaat over een specifieke klasse van vectorvelden, namelijk de guiding vectorvelden. We bestuderen deze vectorvelden in een Euclidische ruimte en een algemeen Riemannian manifold voor padvolgning en bewegingscoördinatie van een enkele robot alsook van een groep robots. Het guiding vectorveld bestaat doorgaans uit twee delen, te weten een convergentie deel welke het mogelijk maakt dat de integraalkrommen van de vectorveld convergeren naar het gewenste pad en een *propagatie* deel welke raakt aan het gewenste pad opdat de verplaatsing langs het gewenste pad wordt gewaarborgd. Het guiding vectorveld kan volledig worden beschreven tot op de positieve coefficiënten) door tweemaal continu differentieerbaar reële functies (genaamd niveaufuncties). De doorsnede van de nul-niveauverzamelingen van deze niveaufuncties is het gewenste pad welke wordt gevuld. De theoretische analyse zit vol uitdagingen mede doordat de guiding vectorvelden geen gradiënt zijn van een potentiaal functie alsmede door de aanwezigheid van *singuliere* punten waar het vectorveld verdwijnt. We zullen daarom in Deel I van dit proefschrift richten op het verkrijgen van uitgebreide theoretische resultaten. In Deel II zullen we nader ingaan op het gebruik van guiding vectorvelden in de praktische toepassingen.

In Deel I bestuderen we eerst de relatie tussen de waarden van de niveaufuncties, de zogenaamde niveauwaarden, en de convergentie van de integraalkrommen van de vectorvelden naar het gewenste pad. De reden voor deze studie is gebaseerd op het inzicht dat het gewenste pad de doorsnede is van de nul niveauverzamelingen van de niveaufuncties. Het blijkt dat zelfs wanneer de niveauwaarden langs een integraalkromme naar nul convergeert, dit niet impliceert dat de desbetreffende integraalkromme convergeert naar het gewenste pad. We geven enkele noodzakelijke aannames welke gebruikt worden door het hele proefschrift om te garanderen dat de verdwijning van de niveauwaarden langs de integraalkromme inderdaad leidt tot convergentie van de integraalkromme naar

het gewenste pad. Deze aannames dragen bij in de navolgende analyse gezien we alleen de convergentie van de niveauwaarden hoeven na te gaan.

Hierna bestuderen we autonome systemen waarbij het guiding vectorveld, gedefinieerd in de n -dimensionele Euclidische ruimte \mathbb{R}^n of een algemeen glad Riemannian manifold \mathcal{M} , is te vinden aan de rechterhand. In het bijzonder tonen we de exponentiële convergentie van de fout aan, in de buurt van het gewenste pad, en de lokale input-to-state stabiliteit (ISS) van het systeem welke de fout beschrijft voor guiding vectorvelden die zich in een 3D Euclidische ruimte bevinden. Deze resultaten kunnen eenvoudig worden toegepast voor guiding vectorvelden in hoger-dimensionele Euclidische ruimtes. Daarnaast, rechtvaardigt de lokale ISS eigenschap de effectiviteit van het regelontwerp welke gebruikt wordt voor veel kinematische robot modellen, waaronder het eenwieler model. Dit principe is ook gebruikt in dit proefschrift. We hebben hierna het guiding vectorveld gegeneraliseerd van een Euclidische ruimte naar een algemeen glad Riemannian manifold. Het gegeneraliseerde guiding vectorveld is cruciaal voor padvolgning in sommige abstracte ruimte configuraties. (bijvoorbeeld, robot arm joint ruimte). We tonen aan dat het dichotome convergentie resultaat en de asymptotische stabiliteit van de gewenste paden nog steeds van toepassing zijn. We vervolgen de analyse met het speciale geval waarbij het gewenste pad homeomorf is tot de eenheidscirkel S^1 en bestuderen de guiding vectorvelden vanuit een topologische invalshoek. We tonen aan dat de aanwezigheid van singuliere punten inherent is aan de topologie van het gewenste pad in Euclidische ruimte. Met name in \mathbb{R}^n , waarbij $n \geq 3$, bestaat er altijd een baan welke start aan de rand van elke bal welke het gewenste pad bevat, maar toch niet convergeert naar het gewenste pad. Bovendien, in het algemene n -dimensionele Riemannian manifold geval is het domein van aantrekking van het gewenste pad homeomorphic tot $\mathbb{R}^{n-1} \times S^1$.

In Deel II ontwikkelen we variaties van de guiding vectorvelden en demonstreren het gebruik hiervan in drie praktische toepassingen, namelijk padvolgning waarbij hindernissen worden vermeden, globale convergentie tot het gewenste pad en bewegingscoördinatie van een groep robots. In de eerste toepassing beschouwen we een praktische situatie waarbij het gewenste pad gedeeltelijk is bezet door een aantal statische of bewegende hindernissen. We gebruiken een gladde bump functie om twee guiding vectorvelden te combineren, eentje voor padvolgning en het andere voor het vermijden van botsingen. We tonen aan dat er in veel gevallen singuliere punten bijkomen alhoewel het samengevoegde guiding vectorveld voldoende glad is. Desalniettemin verstrekken we theoretische voorwaarden en een switch mechanisme zodat het padvolgende en hindernis vermijdende gedrag gegarandeerd effectief zijn. Deze aanpak is reactief en algemeen, en daarom te gebruiken in real-time toepassingen en kan omgaan met obstakels van willekeurige vormen. In de tweede toepassing, welke een gevolg is van de topologische analyse en vooral de aanwezigheid van singuliere punten van de guiding vectorvelden in Deel I, stellen we een innovatief idee voor om de topologie van het gewenste pad te transformeren zodat de begrensde of zichzelf

snijdende paden onbegrensd worden en zichzelf niet meer snijden (om precies te zijn, (homeomorf) tot de reële lijn \mathbb{R}). Deze aanpak leidt tot een singulier-vrije hoger-dimensionele guiding vectorveld dat globale convergentie van de banen tot de gewenste paden kunnen garanderen. De additionele dimensie correspondeert met een virtuele coördinaat die de parameter van het gewenste pad weergeeft. In de laatste toepassing benutten we de additionele dimensie van dit singulier-vrije guiding vectorveld om de gedistribueerde bewegingscoördinatie en navigatie van een groep robots van willekeurige grootte op verschillende gewenste paden of oppervlaktes mogelijk te maken. Het resulterende algoritme is gedistribueerd, schaalbaar en is goedkoop in communicatie en berekening. Al deze toepassingen hebben formele garanties en worden ondersteund door uitgebreide simulatie voorbeelden en experimenten met een fixed-wing vliegtuig.